

Hunting for Warped Extra Dimensions via Loop-Induced Processes

Dissertation

zur Erlangung des Grades “Doktor der Naturwissenschaften”
am Fachbereich Physik, Mathematik und Informatik
der Johannes Gutenberg-Universität
in Mainz

Christoph Schmell
geboren in Bad Kreuznach

Mainz, 2014

Erster Gutachter:

Zweiter Gutachter:

Datum der mündlichen Prüfung: 01. Dezember 2014

Dissertation an der Universität Mainz (D77)

JOHANNES GUTENBERG-UNIVERSITY OF MAINZ

Abstract

Theoretical High Energy Group (THEP)
Institute of Physics

Doctor rerum naturalium

by Christoph Schmall

This thesis is on loop-induced processes in theories with warped extra dimensions where the fermions and gauge bosons are allowed to propagate in the bulk, while the Higgs sector is localized on or near the infra-red brane. These so-called Randall-Sundrum (RS) models have the potential to simultaneously explain the hierarchy problem and address the question of what causes the large hierarchies in the fermion sector of the Standard Model (SM). The Kaluza-Klein (KK) excitations of the bulk fields can significantly affect the loop-level processes considered in this thesis and, hence, could indirectly indicate the existence of warped extra dimensions.

The analytical part of this thesis deals with the detailed calculation of three loop-induced processes in the RS models in question: the Higgs production process via gluon fusion, the Higgs decay into two photons, and the flavor-changing neutral current $b \rightarrow s\gamma$. A comprehensive, five-dimensional (5D) analysis will show that the amplitudes of the Higgs processes can be expressed in terms of integrals over 5D propagators with the Higgs-boson profile along the extra dimension, which can be used for arbitrary models with a compact extra dimension. To this end, both the boson and fermion propagators in a warped 5D background, valid to all orders in the expansion in v^2/M_{KK}^2 , are derived. It will be shown that the seemingly contradictory results for the gluon fusion amplitude in the literature can be traced back to two distinguishable, not smoothly-connected incarnations of the RS model.

The investigation of the $b \rightarrow s\gamma$ transition is performed in the KK decomposed theory. It will be argued that summing up the entire KK tower leads to a finite result, which can be well approximated by a closed, analytical expression.

In the phenomenological part of this thesis, the analytic results of all relevant Higgs couplings in the RS models in question are compared with current and in particular future sensitivities of the Large Hadron Collider (LHC) and the planned International Linear Collider. The latest LHC Higgs data is then used to exclude significant portions of the parameter space of each RS scenario. The analysis will demonstrate that especially the loop-induced Higgs couplings are sensitive to KK particles of the custodial RS model with masses in the multi tera-electronvolt range.

Finally, the effect of the RS model on three flavor observables associated with the $b \rightarrow s\gamma$ transition are examined. In particular, we study the branching ratio of the inclusive decay $\bar{B} \rightarrow X_s\gamma$, the time-dependent CP asymmetry $S_{K^*\gamma}$ in the decay $\bar{B} \rightarrow \bar{K}^*\gamma$, and the photon polarization parameter in the decay $\bar{B} \rightarrow \bar{K}_1\gamma$. It will be shown that the latter two processes are especially sensitive to the RS corrections considered in this work, which could be probed at future precision experiments.

Zusammenfassung

Gegenstand dieser Arbeit ist die Behandlung Schleifen-induzierter Prozesse in Theorien mit gekrümmten Extradimensionen. Diese sogenannten Randall-Sundrum (RS)-Modelle sind besonders attraktive Erweiterungen des Standardmodells (SM), da sie sowohl für das Hierarchieproblem im Eichsektor als auch für die Hierarchien im Flavorsektor Erklärungen liefern können. Die Arbeit fokussiert sich auf RS-Modelle mit Fermionen und Bosonen im Bulk und einem Higgs-Sektor auf bzw. nahe der Infrarot-Brane. Die Kaluza-Klein (KK)-Anregungen der Bulkfelder können signifikant zu den in dieser Arbeit behandelten Schleifen-induzierten Prozessen beitragen und daher indirekt auf die Existenz von gekrümmten Extradimensionen schließen lassen.

Der analytische Teil dieser Arbeit befasst sich mit der detaillierten Berechnung von drei Schleifen-induzierten Prozessen in o.g. RS-Modellen: dem Higgs-Produktionsprozess über Gluonfusion, dem Higgszerfall in zwei Photonen und dem Flavor ändernden neutralen Strom $b \rightarrow s\gamma$. Eine ausführliche, fünfdimensionale (5D) Analyse wird zeigen, dass die Amplituden der Higgsprozesse als Integrale über 5D Propagatoren mit dem Higgsprofil entlang der kompakten Extradimension ausgedrückt werden können. Zu diesem Zweck werden die 5D Boson- und Fermionpropagatoren in einem gekrümmten 5D Hintergrund hergeleitet, wobei der Fermionpropagator erstmals mit der exakten Abhängigkeit von den Yukawa-Matrizen und der vollen drei-Generationen-Flavorstruktur berechnet wird. Ein wichtiges Ergebnis dieser Arbeit ist, dass die sich widersprechenden Resultate in der Literatur durch zwei sich unterscheidende, nicht stetig ineinander überführbare Versionen des RS-Modells erklärt werden können.

Der $b \rightarrow s\gamma$ Übergang enthält zwei unendliche KK-Summen und wird deshalb gesondert behandelt. Es wird argumentiert, dass die Summation über alle KK-Moden zu einem endlichen Ergebnis führt, für das ein approximativer Ausdruck hergeleitet wird.

Im phänomenologischen Teil der Arbeit werden die Voraussagen für alle wichtigen Higgskopplungen sowohl mit den gegenwärtigen als auch den zukünftigen Sensitivitäten des Large Hadron Collider (LHC) und dem geplanten International Linear Collider verglichen. Die neuesten Higgs-Daten des LHC werden dazu verwendet um signifikante Regionen des Parameterraums jedes RS-Szenarios auszuschließen. Die Analyse wird zeigen, dass die Higgskopplungen sensitiv auf KK-Teilchen sind, deren Massen bis in den multi-Teraelektronenvolt-Bereich reichen.

Abschließend werden die Auswirkungen des RS-Modells auf drei auf $b \rightarrow s\gamma$ basierenden Flavor-Observablen untersucht. Speziell wird auf das Verzweigungsverhältnis des inklusiven Zerfalls $\bar{B} \rightarrow X_s\gamma$, die zeitabhängige CP-Asymmetrie $S_{K^*\gamma}$ im Zerfall $\bar{B} \rightarrow \bar{K}^*\gamma$ und auf die Polarisation des Photons im Zerfall $\bar{B} \rightarrow \bar{K}_1\gamma$ eingegangen. Es wird gezeigt, dass die letzteren beiden Prozesse sensitiv auf die in der Arbeit gefundenen RS Korrekturen sind, was durch zukünftige, sehr genaue Messungen einen Hinweis auf die Existenz von gekrümmten Extradimensionen geben könnte.

Contents

Acknowledgements	vii
Preface	ix
1 The Standard Model, Known Shortcomings, and Possible Extensions	1
1.1 The Standard Model of Elementary Particle Physics	1
1.2 Problems of the Standard Model and the Need for New Physics	6
1.3 New Physics Models beyond Extra Dimensions	11
1.3.1 Supersymmetry	12
1.3.2 Composite Higgs Models	15
1.3.3 Froggatt-Nielsen Models	19
1.4 Models with Extra Dimensions	21
1.4.1 First Appearance: Nordström, Kaluza, Klein	21
1.4.2 Generic Features of Extra-Dimensional Models	23
1.4.3 Flat Extra Dimensions	28
1.4.4 Warped Extra Dimensions	33
2 Models with Warped Extra Dimensions	39
2.1 Brane-Localized and Bulk-Higgs Scenarios	39
2.2 The Minimal Randall-Sundrum Model	41
2.2.1 The Gauge Sector	42
2.2.2 The Matter Sector	52
2.2.3 Fermion Hierarchies and the RS-GIM Mechanism	61
2.2.4 Compatibility with Electroweak Precision Tests	69
2.3 The Custodial Randall-Sundrum Model	72
2.3.1 The Gauge Sector	72
2.3.2 The Matter Sector	79
2.3.3 Compatibility with Electroweak Precision Tests	83
3 Warped 5D Propagators	87
3.1 Boson Propagators	88
3.1.1 Scalar Boson Propagator	88
3.1.2 Gauge-Boson Propagator	89
3.2 Fermion Propagators	98
3.2.1 Differential Equations and Boundary Conditions	99
3.2.2 Derivation of the Propagator Functions	100
3.2.3 Determination of the Coefficient Functions and Final Results . . .	104
3.2.4 The Special Case of the Brane-Localized Higgs Scenario	107

4	Loop Calculations in Warped Extra Dimensions	113
4.1	Higgs Production via Gluon Fusion	113
4.1.1	Preliminaries	114
4.1.2	5D Analysis of the Gluon Fusion Amplitude	116
4.1.3	Analysis of the Loop Amplitude	119
4.1.4	Impact of Higher-Dimensional $ \Phi ^2(G_{\mu\nu}^a)^2$ Operators	129
4.1.5	Extension to the RS Model with Custodial Symmetry	132
4.2	Higgs Decay into Two Photons	135
4.2.1	Preliminaries	135
4.2.2	5D Analysis of the $h \rightarrow \gamma\gamma$ Amplitude	136
4.2.3	Extension to the RS Model with Custodial Symmetry	143
4.3	The Flavor-Changing Neutral Current $b \rightarrow s\gamma$	146
4.3.1	Preliminaries	146
4.3.2	Calculation of the $b \rightarrow s\gamma$ Amplitude	149
4.3.3	Analysis of the Radiative Wilson Coefficients	152
4.3.4	Renormalization Group Evolution and Final Results	163
5	Phenomenological Implications	167
5.1	Higgs Physics in Warped Extra Dimensions	167
5.1.1	Higgs Production and Decay via W, Z Bosons	169
5.1.2	Higgs Couplings in RS Models	176
5.1.3	Numerical Analysis of the Higgs Couplings	180
5.1.4	Analysis of the Signal Rates: $h \rightarrow b\bar{b}, \tau^+\tau^-, WW^*, ZZ^*, \gamma\gamma$	186
5.2	$\bar{B} \rightarrow X_s\gamma$ Decays in Warped Extra Dimensions	198
5.2.1	The Branching Ratio $\bar{B} \rightarrow X_s\gamma$	198
5.2.2	The Time-Dependent CP Asymmetry in $\bar{B} \rightarrow \bar{K}^*\gamma$	199
5.2.3	The Photon Polarization Parameter λ_γ	201
	Conclusions	203
A	Compendium of Results for the Propagator Functions	207
B	The Yukawa Perturbativity Bound	209
B.1	NDA Estimates	209
B.2	Calculation Using the Exact 5D Fermion Propagator	211
C	Feynman Rules in the 4D Effective Theory	215
D	Results for the $b \rightarrow s\gamma$ and $b \rightarrow sg$ Amplitudes	217
	Bibliography	234

Acknowledgements

First of all, I would like to express my gratitude to my advisor for his support and guidance during my time as a diploma and Ph.D. student. It has been a pleasure to work with and to learn from him. I would also like to thank him and all other responsible persons of the graduate school *Symmetry Breaking in Fundamental Interactions* for giving me the opportunity to make great experiences abroad, either by attendances of summer schools or by giving talks at renowned places all around the world.

Furthermore, I would like to thank all members of the growing THEP working group for the great atmosphere, the interesting and amusing conversations, a lot of proof-reading, and for helping me with all kinds of physics-related and physics-unrelated problems.

I would like to thank my girlfriend for her support and understanding during the past stressful weeks and months, and, foremost, just for being the loveliest person in the world.

I dedicate this thesis to my parents, who have supported me, both emotionally and financially, throughout my life. Thank you for always being there for me - no matter how, no matter when, and no matter where.

Preface

In the field of particle physics, almost all phenomena can be explained by the Standard Model (SM) of Elementary Particle Physics. During the past decades it has passed numerous precision tests up to energies in the tera-electronvolt (TeV) range and after the discovery of the last missing particle, the Higgs boson, at the Large Hadron Collider (LHC) in summer 2012, its predicted particle content has been verified. Nevertheless, there are still some unanswered questions and unexplained phenomena that the SM does not address. For this reason, it cannot be regarded as the ultimate theory of nature and must be replaced by a more fundamental theory at some high energy scale. The SM would then emerge as a low-energy limit of this ultra-violet (UV) completion. The situation is analogous to the familiar case of classical mechanics, which must be modified to incorporate Einstein's theory of relativity in order to explain e.g. the precession of the perihelion of Mercury to high precision.

Among numerous possible extensions of the SM, models with warped extra dimensions provide a promising alternative to more popular models of *new physics*, such as supersymmetry. These so-called Randall-Sundrum (RS) models can address the gauge hierarchy problem and, moreover, give an explanation for the hierarchical structure in the SM quark masses and mixing angles. A clear indication for models with warped extra dimensions would be the *direct* detection via production of several very massive copies of the known SM particles with equidistant mass differences, the so-called Kaluza-Klein (KK) modes. However, as of today, the LHC has not detected any KK excitations yet and electroweak precision measurements indicate that they could be out of reach of the LHC. One is therefore urged to consider the *indirect* detection of new particles via verification of deviations from the SM predictions for certain observables, such as decay rates, branching ratios, charge-parity (CP) asymmetries, etc. The main focus of the thesis at hand is on whether one could probe models with warped extra dimensions via precise measurements of observables in the Higgs and the flavor sector, which are loop-suppressed in the SM and therefore allow for significant effects from the infinitely many KK excitations.

This thesis is structured as follows: In the first chapter, both the success and the shortcomings of the SM, the currently most accurate theory in particle physics, are recalled. Some of the most popular extensions of the SM are introduced, where special attention is given to their possible explanations for the hierarchy problem and the flavor structure of the SM.

Chapter 2 then introduces the versions of the RS model which this thesis focuses on. It will be distinguished between the *minimal* RS model, based on the SM gauge group, and the *custodial* RS model, based on an enlarged bulk symmetry, as well as models with a brane-localized and (narrow) bulk-Higgs sector. It will be explained in detail how RS models can generate the hierarchies in the quark sector before examining their compatibility with available electroweak precision data. We will show that the minimal RS model is disfavored, while the RS model with custodial protection remains consistent.

In order to investigate loop-level processes in an elegant way, both the warped five-dimensional (5D) boson and fermion propagators in the mixed momentum-position representation, which implicitly sum over the entire tower of KK excitations, will be calculated in Chapter 3. Closed expressions for the gauge-boson propagator in the minimal and custodial RS model will be derived, which are valid to all orders in the expansion in v^2/M_{KK}^2 . For the first time, we will calculate the 5D fermion propagator with the exact dependence on the Yukawa matrices and the full three-generation flavor structure, which will be an important tool for future loop-level calculations in theories with a warped extra dimension.

Chapters 4 and 5 form the core of this thesis. The first part of Chapter 4 deals with the detailed calculation of loop-induced processes in the Higgs sector, namely the Higgs production process via gluon fusion and the Higgs decay into two photons, in both the minimal and the custodial RS model. A detailed 5D analysis will show that both amplitudes can be expressed in terms of integrals over the 5D propagator including the contributions of the SM quarks and the full dependence on the Higgs-boson mass. These expressions can be used for arbitrary models with a compact extra dimension as long as one succeeds in deriving the respective 5D propagators. Using the explicit results for the 5D propagators, we will show that in the case of the fermion contribution to the loop-induced Higgs processes, the seemingly contradictory results in the literature can be traced back to the fact that a scalar sector localized on the IR brane cannot be considered as a limit of a more and more localized bulk field. The second part of Chapter 4 discusses the flavor-changing neutral current $b \rightarrow s\gamma$, which, as opposed to the Higgs processes, involves two infinite towers of KK modes, and thus demands for a different treatment. We will investigate the gauge-invariance of the gauge-boson contributions in the effective four-dimensional (4D) decomposed theory and argue that summing up the entire tower of KK modes leads to a finite result, which can be approximated by a simple analytic expression valid at leading order in the expansion in v^2/M_{KK}^2 .

Phenomenological implications of the results derived in the Chapter 4 will be discussed in Chapter 5. In order to compare the predictions with experimental data, the results for all flavor-diagonal Higgs couplings in the RS models in question are summarized and compared with future sensitivities of the LHC and the planned International Linear Collider (ILC). Moreover, the cross sections for Higgs production via Higgsstrahlung and vector-boson fusion, as well as the decay rates of the Higgs boson into pairs of electroweak gauge bosons, are calculated. Subsequently, the RS predictions on the signal rates of the most important Higgs processes $pp \rightarrow h \rightarrow b\bar{b}$, $\tau^+\tau^-$, WW^* , ZZ^* , $\gamma\gamma$ will be checked for compatibility with the latest LHC Higgs data. We will deduce bounds on the relevant parameters of the RS models from all processes. Finally, we will investigate the RS corrections to three flavor observables associated with the $b \rightarrow s\gamma$ transition, namely the branching ratio of the inclusive decay $\bar{B} \rightarrow X_s\gamma$, the time-dependent CP asymmetry $S_{K^*\gamma}$ in the decay $\bar{B} \rightarrow \bar{K}^*\gamma$, and the photon polarization parameter λ_γ in the decay $\bar{B} \rightarrow \bar{K}_1\gamma$. The latter two in particular turn out to receive significant corrections and could in fact allow for a discovery of warped extra dimensions to be made at future precision experiments.

The main results of this thesis will be summarized in a final section giving our outlook and conclusions.

Chapter 1

The Standard Model, Known Shortcomings, and Possible Extensions

This chapter is meant to explain the quite vague statements at the beginning of the preface in more detail.¹ A short review of the SM will be given in Section 1.1, before we discuss its shortcomings and the need for *physics beyond the SM* (BSM) in Section 1.2. A special focus will be put on two hierarchy problems. Possible extensions of the SM are then presented in Section 1.3, which deals with models based on the ordinary Minkowski space-time, and Section 1.4, which focuses on models with extra dimensions.

1.1 The Standard Model of Elementary Particle Physics

The SM has been established as the most accurate theory in particle physics to date. It combines three of the four fundamental forces of nature and can, in principle, be valid up to the Planck scale $M_{\text{Pl}} = \sqrt{\hbar c/G} \approx 1.2209 \times 10^{19} \text{ GeV}$, where gravity becomes strong and cannot be disregarded any more.² The rise of the SM dates back to the development of the Glashow-Weinberg-Salam theory [6–8] in the 1960s, which combined the weak and electromagnetic force. The strong interactions including the discovery of asymptotic freedom were then supplemented in the 1970s [9–12]. Further remarkable events in the history of the SM were, amongst others, the detection of several predicted particles like the Z boson [13], the third-generation quarks [14–16] and, last but not least, the Higgs boson [17, 18]. It would go beyond the scope of this thesis to list all of the achieved milestones, but it should be stressed that the SM has been tested at the quantum level and succeeded in explaining a wide variety of experimental results. Therefore, it is worthwhile to briefly recapitulate the structure of the SM.³

¹It is assumed that the reader is familiar with the concepts of quantum field (and gauge) theories as well as renormalization-group (RG) evolution. Recommendable introductions to these subjects can be found in e.g. [1–3] and [4, 5], respectively.

²Here, c is the speed of light in a vacuum, \hbar is the reduced Planck constant, and G is the gravitational constant. From now on, natural units $c = \hbar = 1$ will be used in this thesis.

³More detailed reviews of the SM can be found e.g. in [1, 19].

	fermions, spin-1/2	bosons, spin-1	boson, spin-0
colorless	$\nu_e \quad \nu_\mu \quad \nu_\tau$ $e \quad \mu \quad \tau$	γ Z W^\pm	h
colorful	$u \quad c \quad t$ $d \quad s \quad b$	g	

TABLE 1.1: Particle content of the SM. Shown are the mass eigenstates after the electroweak symmetry is broken. The fermion masses increase from left to right.

There is a strong experimental evidence that the SM gauge group is

$$\mathcal{G}_{\text{SM}} = SU(3)_c \times SU(2)_L \times U(1)_Y, \quad (1.1)$$

and the associated gauge bosons are the gluons (the mediators of the *strong* $SU(3)_c$ interactions) and $W^{1,2,3}$ and B bosons (the mediators of the *electroweak* $SU(2)_L \times U(1)_Y$ interactions). The above gauge symmetry together with the requirements of Poincaré invariance, unitarity, causality, stability, and renormalizability (proven by 't Hooft and Veltman [20]) completely determines the SM Lagrangian, which can be summarized as

$$\mathcal{L}_{\text{SM}} = \mathcal{L}_{\text{ferm}} + \mathcal{L}_{\mathcal{G},W,B} + \mathcal{L}_{\text{Higgs}} + \mathcal{L}_{\text{Yukawa}} + \mathcal{L}_{\text{GF}} + \mathcal{L}_{\text{FP}}. \quad (1.2)$$

As the individual terms essentially have the same structure as the Lagrangian focused on in Section 2.2, where we will consider the SM in an enlarged space-time with an additional spatial dimension, it will be refrained from going into too much detail here. Nevertheless, we shall briefly discuss what will subsequently be important.

The particle content of the SM is shown in Table 1.1, which distinguishes between fermions (spin-1/2 particles) and bosons (Higgs boson, spin-0; gauge bosons, spin-1).⁴ The fermions can be split into two classes, the *colorful* quarks and the *colorless* leptons, meaning that the former (latter) couple to the strong-interaction sector of the SM. Moreover, the fermions are grouped into three generations which share the same quantum numbers, but differ in their masses. Table 1.1 has to be regarded as qualitative in the sense that it does not distinguish between the left-handed and right-handed components of the 4D Dirac fermions, which can be obtained with the help of the projection operators $P_{L,R} = (1 \mp \gamma_5)/2$. In fact, the SM is a *chiral* theory, i.e. the particles of different handedness, or *chirality*, transform differently under the SM gauge group \mathcal{G}_{SM} . While the left-handed fermions $f_L \equiv P_L f$ transform as a doublet under $SU(2)_L$,

$$Q_L = \begin{pmatrix} u_L \\ d_L \end{pmatrix}, \quad L_L = \begin{pmatrix} \nu_{eL} \\ e_L \end{pmatrix}, \quad (1.3)$$

the right-handed ones $f_R \equiv P_R f$ are $SU(2)_L$ singlets

$$u_R, \quad d_R, \quad e_R. \quad (1.4)$$

The right-handed neutrino transforms as a singlet under the entire SM gauge group and is hence not included in the Lagrangian. This discussion makes it easy to understand

⁴The particles depicted here are the *mass eigenstates*, see below.

the structure of the term $\mathcal{L}_{\text{ferm}}$. It contains the kinetic terms for all fermion fields,

$$\mathcal{L}_{\text{ferm}} = \sum_{\Psi} \bar{\Psi} i \not{D} \Psi, \quad \Psi \in \{Q_L, u_R, d_R, L_L, e_R\}, \quad (1.5)$$

where $\not{D} \equiv \gamma^\mu D_\mu$. The covariant derivative D_μ (of a fermion field in the fundamental representation) is given by⁵

$$D_\mu = \partial_\mu - ig_s G_\mu^a \frac{t^a}{2} - ig W_\mu^i \frac{\sigma^i}{2} - ig' B_\mu Y, \quad (1.6)$$

where g_s , g , and g' are the coupling constants of the $SU(3)_c$, $SU(2)_L$, and $U(1)_Y$ subgroups, respectively, and the associated generators are given by the Gell-Mann matrices t^a ($a = 1, 2, \dots, 8$), the Pauli matrices σ^i ($i = 1, 2, 3$), and Y . Note that the fields $\Psi \equiv \Psi_j$ ($j = 1, 2, 3$) are 3-vectors in generation space. The fact that there is more than one generation in the SM allows for different bases of quark eigenstates.⁶ The kinetic terms in $\mathcal{L}_{\text{ferm}}$ are usually written in a basis, where the covariant derivative is diagonal. This basis is called interaction basis and is not the basis which determines the propagation of the fields, i.e. the mass basis, see below.

Similarly, the term $\mathcal{L}_{\mathcal{G},\mathcal{W},\mathcal{B}}$ represents the kinetic terms of the gauge bosons G_μ^a , W_μ^i , and B_μ ,

$$\mathcal{L}_{\mathcal{G},\mathcal{W},\mathcal{B}} = -\frac{1}{4} \mathcal{G}_{\mu\nu}^a \mathcal{G}^{a,\mu\nu} - \frac{1}{4} W_{\mu\nu}^i W^{i,\mu\nu} - \frac{1}{4} B_{\mu\nu} B^{\mu\nu}, \quad (1.7)$$

where the field strength tensors of the gauge fields written in the interaction basis read

$$\begin{aligned} \mathcal{G}_{\mu\nu}^a &= \partial_\mu \mathcal{G}_\nu^a - \partial_\nu \mathcal{G}_\mu^a + g_s f^{abc} \mathcal{G}_\mu^b \mathcal{G}_\nu^c, & a, b, c &= 1, 2, \dots, 8, \\ W_{\mu\nu}^i &= \partial_\mu W_\nu^i - \partial_\nu W_\mu^i + g \epsilon^{ijk} W_\mu^j W_\nu^k, & i, j, k &= 1, 2, 3, \\ B_{\mu\nu} &= \partial_\mu B_\nu - \partial_\nu B_\mu. \end{aligned} \quad (1.8)$$

The tensors f^{abc} and ϵ^{ijk} are the structure constants of the two non-abelian subgroups. The gauge-fixing and the Faddeev-Popov ghost Lagrangians, \mathcal{L}_{GF} and \mathcal{L}_{FP} , are crucial for a proper implementation of the gauge sector and will not be relevant for the further discussion in this section.

So far, no mass terms for the fermions and gauge bosons have been included. Indeed, they are forbidden by the gauge principle. For this reason, one introduces a scalar $SU(2)_L$ doublet Φ , the famous Higgs field, whose most general Lagrangian is given by

$$\mathcal{L}_{\text{Higgs}} = (D_\mu \Phi)^\dagger (D^\mu \Phi) - V(\Phi), \quad (1.9)$$

where the potential can be written as

$$V(\Phi) = -\mu^2 \Phi^\dagger \Phi + \lambda (\Phi^\dagger \Phi)^2. \quad (1.10)$$

Assuming the dimensionful parameter to be positive ($\mu^2 > 0$), the scalar field acquires a non-trivial vacuum expectation value (vev) $\langle \Phi \rangle = v > 0$, which in turn breaks the electroweak symmetry via the symmetry breaking pattern $SU(2)_L \times U(1)_Y \rightarrow U(1)_{\text{em}}$.

⁵If not stated otherwise, the sum over double indices is implicit.

⁶Assuming that neutrinos are massless, there is no such distinction in the lepton sector. However, as verified by the neutrino oscillation experiments, see e.g. [21], there are at least two massive neutrinos, so that a similar discussion also holds for the leptons. We will, however, focus on the quark sector, since the class of models this thesis is based on can explain the mixing in the quark sector, see Chapter 2.

This *electroweak symmetry breaking* (EWSB) gives masses to the matter and gauge fields. To see this, we expand the Higgs doublet around this minimum via

$$\Phi(x) = \frac{1}{\sqrt{2}} \begin{pmatrix} -i\sqrt{2}\varphi^+(x) \\ v + h(x) + i\varphi^3(x) \end{pmatrix}, \quad (1.11)$$

where the scalars φ^\pm and φ^3 represent the three Goldstone bosons associated with the symmetry breaking in question. They can be identified with the longitudinal degrees of freedom of the massive W^\pm and Z bosons. The scalar h denotes the physical Higgs boson, which is necessary to unitarize WW scattering.⁷ It is now not difficult to comprehend that the kinetic term of the Higgs $|D_\mu\Phi|^2$ gives rise to masses to the gauge bosons. The physical Higgs boson h also acquires a mass after EWSB. The radiative corrections to this mass are the origin of the *gauge hierarchy problem*, which will be discussed extensively in the next subsection. The fermion masses are generated by means of the Yukawa interactions

$$\mathcal{L}_{\text{Yukawa}} = -\bar{Q}_L\Phi\mathbf{Y}_d d_R - \bar{Q}_L\tilde{\Phi}\mathbf{Y}_u u_R - \bar{L}_L\Phi\mathbf{Y}_e e_R + \text{h.c.}, \quad (1.12)$$

where $\tilde{\Phi} \equiv i\sigma^2\Phi^\dagger$ and the quantities \mathbf{Y}_f ($f = u, d, e$) represent the non-diagonal, complex 3×3 Yukawa matrices in the interactions basis. In order to end up in the physical basis of propagating mass eigenstates shown in Table 1.1, we diagonalize these terms by bi-unitary transformations

$$\frac{v}{\sqrt{2}}\mathbf{Y}_u = \mathbf{U}_u \text{diag}(m_u, m_c, m_t) \mathbf{W}_u^\dagger, \quad (1.13)$$

and analogously for the down-type quarks and the charged leptons. The mass eigenstates can then be obtained after the rotations $f_L^{\text{mass}} \equiv \mathbf{U}_f^\dagger f_L$ and $f_R^{\text{mass}} \equiv \mathbf{W}_f^\dagger f_R$. Since the matrices \mathbf{U} and \mathbf{W} are unitary, all interactions in the lepton sector and all neutral-current interactions in the quarks sector, i.e. the couplings to the neutral gauge bosons g, γ, Z , are not affected by this rotation. The quark couplings to the W bosons, however, become

$$\mathcal{L}_{W\bar{q}q'} = \frac{g}{\sqrt{2}} \bar{u}_L \gamma^\mu W_\mu^+ \mathbf{V}_{\text{CKM}} d_L + \text{h.c.}, \quad (1.14)$$

where the matrix

$$\mathbf{V}_{\text{CKM}} \equiv \mathbf{U}_u^\dagger \mathbf{U}_d \quad (1.15)$$

is the Cabibbo-Kobayashi-Maskawa (CKM) matrix [23, 24]. We see that, while flavor mixing is not possible in neutral currents (at tree level), it is possible in the charged electroweak interactions.

The structure of the SM Lagrangian, in particular the gauge-boson couplings to fermions and the mixing in the flavor sector have been verified convincingly. Any deviation from the SM would have been seen by the precise measurements performed at the Large Electron Positron Collider (LEP) at CERN. The experimental results for the *electroweak precision (pseudo) observables* [25] are summarized in Figure 1.1,⁸ which shows the deviations of the measurements from the SM predictions in standard deviations, the so-called pull. We see that all observables are compatible with the SM. Only the decay rate of the process $Z \rightarrow b\bar{b}$ normalized to the full hadronic decay rate, $R_b^0 = \Gamma_Z^{b\bar{b}}/\Gamma_Z^{\text{had}}$,

⁷In fact, the physical Higgs particle h is not required for the generation of the gauge boson masses, which could also be implemented by means of a general non-linear sigma model, as explained in e.g. [22].

⁸It is assumed that the reader is familiar with the list of electroweak precision (pseudo) observables shown in Figure 1.1. A detailed explanation for each observable is provided e.g. in [26].

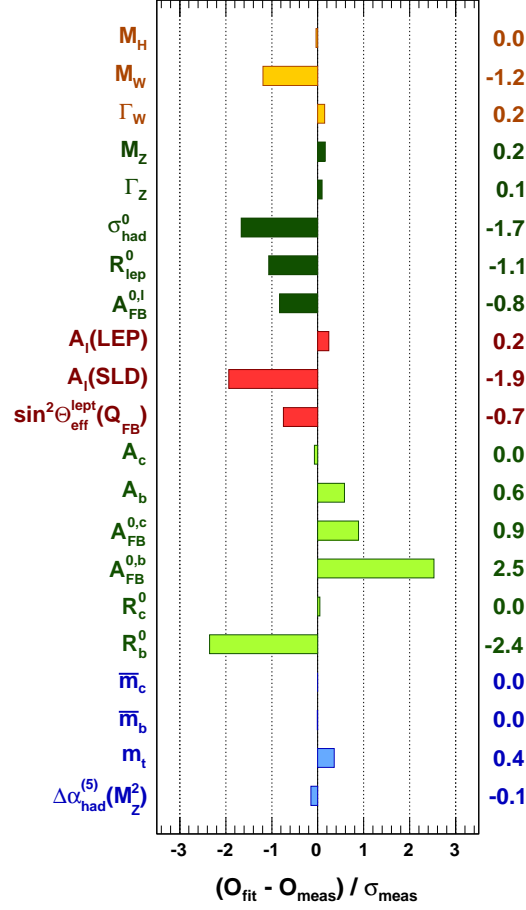


FIGURE 1.1: List of electroweak precision observables published by the GFitter group after the discovery of the Higgs boson [27]. A definition of all observables can be found in [26]. Shown are the deviations of the measurements from the SM predictions in standard deviations.

and the forward-backward asymmetry of the same decay, $A_{\text{FB}}^{b\bar{b}}$, deviate by more than two 2σ from the SM prediction. Both of them are sensitive to vertex corrections. Since the remaining observables agree within 2σ with the SM, the electroweak gauge-boson propagators should only get corrections, defined (in the W -boson case) via

$$\frac{-i}{p^2 - g^2 \Pi(p^2)/2} \left(\eta_{\mu\nu} - \frac{p_\mu p_\nu}{p^2} \right), \quad (1.16)$$

that do not spoil the SM prediction too much. Peskin and Takeuchi developed a way to parametrize possible deviations from the gauge-boson propagators by the three *oblique parameters* [28, 29]

$$\begin{aligned} S &= \frac{4s_w^2 c_w^2}{\alpha} \left[\Pi'_{ZZ}(0) + \frac{s_w^2 - c_w^2}{s_w c_w} \Pi'_{Z\gamma}(0) - \Pi'_{\gamma\gamma}(0) \right], \\ T &= \frac{1}{\alpha c_w^2 m_Z^2} \left[\Pi_{WW}(0) - c_w^2 \Pi_{ZZ}(0) - 2c_w s_w \Pi_{Z\gamma}(0) - s_w^2 \Pi_{\gamma\gamma}(0) \right], \\ U &= \frac{4s_w^2}{\alpha} \left[\Pi'_{WW}(0) - c_w^2 \Pi'_{ZZ}(0) - 2s_w c_w \Pi'_{Z\gamma}(0) - s_w^2 \Pi'_{\gamma\gamma}(0) \right], \end{aligned} \quad (1.17)$$

where $s_w \equiv \sin \theta_w = g'/\sqrt{g^2 + g'^2}$ and $c_w \equiv \cos \theta_w = g/\sqrt{g^2 + g'^2}$ are the sine and cosine of the Weinberg angle θ_w , respectively, and $\alpha \equiv e^2/4\pi$ denotes the fine-structure constant. The parameters are defined in such a way that they describe the shifts relative to the SM values, hence $S = T = U = 0$ in the SM by construction. The best fit to the experimental input values after the discovery of the Higgs leads to [27] (assuming $U = 0$)⁹

$$\begin{aligned} S_{\text{exp}} &= 0.05 \pm 0.09, \\ T_{\text{exp}} &= 0.08 \pm 0.07, \end{aligned} \quad \rho = \begin{pmatrix} 1.00 & 0.91 \\ 0.91 & 1.00 \end{pmatrix}, \quad (1.18)$$

in which ρ denotes the correlation matrix. We see that the past and current measurements verify the SM convincingly. Consequentially and importantly for the rest of this chapter, the electroweak precision measurements put severe constraints on UV completions of the SM. The question now arises why one expects the LHC to find particles that do not belong to the particle content of the SM. This is the subject of the next subsection.

1.2 Problems of the Standard Model and the Need for New Physics

There are several indications that the SM cannot be valid to arbitrary high energy scales. Discussing all of them would go beyond the scope of this thesis, but some chosen problems should be mentioned to motivate the search for BSM physics. On the one hand, there is experimental evidence based on some unexplained observations, which makes the SM fall short of being a complete theory of fundamental interactions. Especially phenomena in cosmology require new physics (NP): The SM neither incorporates the full theory of gravitation as described by Einstein's general relativity (GR), nor does it give an explanation for the accelerating expansion of the universe (as possibly described by dark energy, see [30] for a review), nor does it provide any viable dark matter (DM) candidate [31] that is compatible with all current cosmological observations. Furthermore, the CP violating phases in the CKM matrix do not provide enough CP violation for a baryon asymmetry which in turn is crucial for baryogenesis.¹⁰ Finally, in order to correctly describe the neutrino oscillations [21], which are a consequence of finite masses of at least two neutrino flavors, one may need to introduce an additional neutrino which is not incorporated in the SM. These observations alone justify the point of view that the SM cannot be a theory that is valid up to arbitrary high scales. On the other hand, it is also desirable from the theoretical standpoint to have physics beyond the SM. The stability bound of the Higgs potential, for example, indicates that the vacuum could only be metastable [33], and the unification of the strong and electroweak interactions is only almost accomplished in the SM. Furthermore, there are even more fundamental questions, such as: Why are there three fermion generations? What drives the mass term in the Higgs potential negative?

Due to all these open questions, the SM cannot be considered as a consistent theory up to arbitrary high energies, although its feature of being renormalizable would indicate that. It rather has to be seen as an effective field theory (EFT) valid up to a certain

⁹We assume $U = 0$, since Randall-Sundrum models do not contribute to the U parameter, as we will see in Chapter 2. For $U \equiv 0$, the experimental values for the S and T parameters are slightly larger [27].

¹⁰Although the SM is principally able to fulfill the necessary Sakharov criteria [32] (C violation, CP violation, baryon-number non-conservation, and interactions out of thermal equilibrium), the CP violation on the SM is orders of magnitude too small to account for the observed baryon asymmetry.

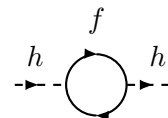
energy scale Λ_{UV} , where it is replaced by a UV completion, i.e. a more fundamental theory. As a consequence of this, the SM Lagrangian can be written as part of an effective Lagrangian

$$\mathcal{L}_{\text{eff}} = c_0 \Lambda_{\text{UV}}^4 + c_{\Phi^2} \Lambda_{\text{UV}}^2 \Phi^\dagger \Phi - \lambda (\Phi^\dagger \Phi)^2 + \mathcal{L}_{\text{gauge}}^{(4)} + \mathcal{L}_{\text{matter}}^{(4)} + \frac{\mathcal{L}^{(5)}}{\Lambda_{\text{UV}}} + \frac{\mathcal{L}^{(6)}}{\Lambda_{\text{UV}}^2} + \dots, \quad (1.19)$$

where c_0 , c_{Φ^2} , and λ are dimensionless constants, $\mathcal{L}_{\text{gauge}}^{(4)}$ includes the gauge interactions as well as the gauge-fixing and Faddeev-Popov ghost Lagrangian, while $\mathcal{L}_{\text{matter}}^{(4)}$ comprises the fermion kinetic terms as well as the Yukawa interactions. The superscripts of the operators denote their mass dimensions and the ellipses stand for operators of dimension 7 or higher.¹¹ These operators are suppressed for low-energy processes by $(E/\Lambda_{\text{UV}})^n$, where E is the typical energy scale of the process, and are therefore called *irrelevant* operators of the EFT. Dimension-four operators are *marginal*, while the ones with dimension three or lower are referred to as *relevant*. Indeed, the (cosmological) constant and the Higgs mass term are relevant in the sense that they are sensitive to the UV cutoff scale of the theory, and the latter gives rise to the gauge hierarchy problem. We will encounter another hierarchy problem when dwelling on the flavor sector of the SM. Both the gauge and the *flavor (hierarchy) problem* shall be discussed in the following, since the theory that this thesis is based on can tackle both of them, as we will see in Subsection 1.4.4 and particularly in Chapter 2.

The Gauge Hierarchy Problem

The gauge hierarchy problem is often stated as the problem of the huge radiative corrections to the bare Higgs mass, where the integration over the loop-momentum is bounded from above by a hard-momentum cutoff Λ :



$$\Rightarrow \delta m_h^2 = \frac{3\lambda_f^2}{8\pi^2} \left[-\Lambda^2 + 6m_f^2 \log \left(\frac{\Lambda}{m_f} \right) - 2m_f^2 \right].$$

Sometimes, it is then argued that this quadratic dependence on Λ is only an artifact of using the hard-momentum regularization, while in dimensional regularization the loop integral would only be logarithmically sensitive to the loop-momentum cutoff. However, this argument is due to a lack of the understanding of the (Wilsonian) renormalization group (RG), which shall be explained in the following.¹² Let us consider the general action built of local interactions O_i in d dimensions [36]

$$S = \int d^d x \sum_i g_i O_i = \int d^d x \sum_i \frac{c_i}{\Lambda^{\delta_i - d}} O_i, \quad (1.20)$$

where $c_i = \Lambda^{\delta_i - d} g_i$ with the characteristic scale of the system Λ is the dimensionless $\mathcal{O}(1)$ coupling, called Wilson coefficient, and δ_i is the mass dimension of the operator

¹¹Operators of mass dimension 1 and 3 are not gauge-invariant and thus do not appear in (1.19). The only gauge-invariant dimension-five operator is given by $1/\Lambda_{\text{UV}} (L_L \Phi)^T \boldsymbol{\lambda} (L_L \Phi)$, which gives (after EWSB) a Majorana mass term for the left-handed neutrinos $m_\nu \sim v^2/\Lambda_{\text{UV}}$. This term could arise from a UV completion of the SM via the see-saw mechanism, for a review see [34].

¹²This discussion is based on Ian Low's lecture at the TASI summer school 2013 [35].

O_i . Using dimensional analysis, we can now estimate the contribution from a given operator O_i in a scattering process at the energy scale E as $(E/\Lambda)^{\delta_i-d}$. In the case of the Higgs boson, where $O_{\Phi^2} = \Phi^\dagger\Phi$ and $g_{\Phi^2} = -\mu^2$, this means that if the cutoff scale is $\Lambda = M_{\text{Planck}} \sim 10^{19}$ GeV and the energy $E \sim 100$ GeV, the natural size of the Higgs mass term will then be

$$\mu^2 \sim c_{\Phi^2} \times \frac{(10^{19} \text{ GeV})^2}{(100 \text{ GeV})^2} \times (100 \text{ GeV})^2, \quad (1.21)$$

where we have assumed a typical scale of the low-energy theory of 100 GeV (i.e. the electroweak scale) on the right-hand side. That is, to arrive at a light mass for the Higgs boson, the value for the dimensionless coupling at the cutoff scale has to be extremely tiny, $c_{\Phi^2} \sim (10^{-17})^2$. This is the hierarchy or *fine-tuning* problem of the Higgs mass and is regarded as unnatural. In this context, it is worthwhile to recapitulate the concept of naturalness. The strongest naturalness criterion is Dirac's naturalness condition that all dimensionless coefficients are of order one and the dimensionful parameters are of the same order of magnitude [37, 38]. A weaker criterion is given by 't Hooft saying that small parameters are natural if setting a small parameter to zero enhances the symmetry of the theory [39]. Technical naturalness is yet a weaker requirement. It does not require all parameters to be of the same order, it only implies that none of the parameters receive radiative corrections that significantly exceed its magnitude. We see that the coefficient of the Higgs mass operator is not even technically natural and calls for an explanation around the TeV scale.¹³ At this point, it should be mentioned that we would arrive at the same conclusion if we considered the aforementioned one-loop corrections to the bare Higgs mass. In the case of dimensional regularization, the bare Higgs mass is quadratically dependent on the mass m_f of the heavy fermions running in the loop. These particles are assumed to have masses of order of the cutoff scale Λ , so the fine-tuning problem also appears in this regularization procedure (although the dependence on the loop-momentum cutoff is logarithmically divergent).

So far this has just been dimensional analysis. A more precise prediction on how the couplings depend on ("run" with) the energy is given by the RG equation

$$\frac{d}{d \log p} c_{\Phi^2}(p^2) = [-2 + \gamma_{\Phi^2}(g_i)] c_{\Phi^2}(p^2), \quad (1.22)$$

which includes all loop-induced effects to the couplings. The *anomalous dimensions* $\gamma_{\Phi^2}(g_i)$ may depend on all couplings, which run and in turn depend on $\log p$. In the vicinity of a fixed point ($\beta_{g_i} = dg_i/d \log p = 0$), however, the couplings $\{g_i\}$ become constant $\{g_i^*\}$ and the solution for the RG equation is given by

$$c_{\Phi^2}(p^2) = c_{\Phi^2}(\Lambda^2) \left(\frac{\Lambda}{p}\right)^{2-\gamma_{\Phi^2}(g_i^*)}. \quad (1.23)$$

Provided that $\gamma_{\Phi^2}(g_i^*) \ll 1$, the parameters c_{Φ^2} at different energy scales are related to each other quadratically. The hierarchy problem can now be formulated in terms of criticality. Figure 1.2 shows the phase diagram of EWSB [41]. In order to arrive at a

¹³Even more severe is the problem of the cosmological constant, which is indirectly measured at $(10^{-12} \text{ GeV})^4/\Lambda^4$ [40]. Thus, either the UV completion sets in at the meV scale or a fine-tuning of hundreds of orders of magnitude is necessary if one assumes $\Lambda = M_{\text{Pl}}$. Since the cosmological constant is not directly relevant for the physics of the SM, this problem will, however, be ignored and we will focus on solving the fine-tuning problem of the Higgs sector in the following.

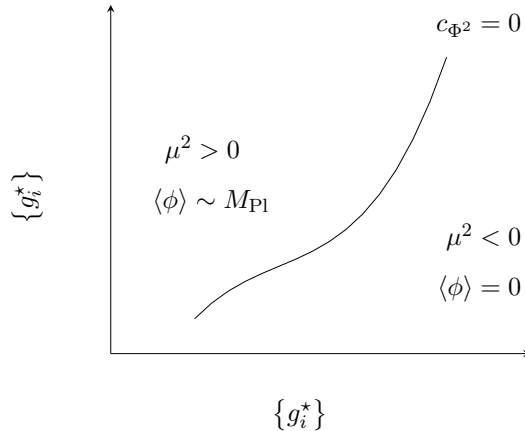


FIGURE 1.2: Phase diagram of electroweak symmetry breaking [35, 41].

Higgs vev around the electroweak scale ($c_{\Phi^2}(v^2) \approx \mathcal{O}(1)$), we have to sit extremely close to the critical line, where $c_{\Phi^2}(\Lambda^2) = 0$. There are three possible explanations for that:

1. The critical line is a locus of enhanced symmetry, which essentially forces us to sit on top of the critical line. There are only two known possibilities of such symmetries. The first one is a bosonic symmetry, namely a (spontaneously) broken global symmetry. Just like the pion, the Higgs could be a composite *Pseudo Nambu-Goldstone boson* (PNGB) of a strongly-coupled sector.¹⁴ The second one is a fermionic symmetry, i.e. *supersymmetry*. We will come back to both possibilities in the subsequent section.
2. The anomalous dimension is not $\gamma_{\Phi^2}(g_i^*) \ll 1$, but $\gamma_{\Phi^2}(g_i^*) \sim \mathcal{O}(1)$. This leads to a very slow running of the mass parameter and implies that there should be an approximate conformal invariance [43, 44]. In this scenario, since the running is slow, we do not need to sit close to the critical line to obtain a Higgs mass of 126 GeV.
3. The third possibility is to accept fine-tuning, which is not completely absent in EFTs. An example can be found in the effective description of the nucleon-nucleon scattering below the pion threshold, which is basically described by contact interaction terms between the nucleons [45]. The cutoff of this effective theory should be around the pion mass $m_\pi \approx 140$ MeV or in some cases around the QCD scale $\Lambda_{\text{UV}} \approx 1$ GeV. It turns out, however, that the inverse s -channel scattering length of protons and neutrons is measured to be $1/a_s \approx 10$ MeV, implying a fine-tuning of at least 1%. In this case, the UV completion is known, but as of today, there is no explanation for this hierarchy of scales, except for the theory being fine-tuned.

Although the third possibility cannot be disregarded completely, there are good reasons to believe that naturalness wants to tell us that something is around the corner, i.e. that some NP sets in around the TeV scale. Indeed, there are two examples in particle physics, where naturalness could have been used to successfully predict the existence of new particles:

¹⁴The Higgs could also be the fifth component of a 5D gauge field. However, by the AdS/CFT correspondence [42] this scenario is the dual description of a composite PNGB Higgs, see e.g. [22].

The first one deals with the self-energy of the electron, which is proportional to the inverse radius of the electron radius, $r_e < 10^{-18}$ m,¹⁵ and should give the electron a mass of around $m_e \sim e/r_e \sim 100$ GeV. This is much larger than the measured electron mass of 0.511 MeV. The resolution is to introduce the positron, i.e. a new particle with the same mass but opposite electric charge [48]. The creation of an e^+e^- pair out of the vacuum at the distance scale of the Bohr radius r_e cancels the infinite self-energy of the electron. The cancellation of every electron in the universe is guaranteed by a new symmetry called chiral symmetry. In this case, naturalness could have predicted both new degrees of freedom and a new symmetry principle to cancel the linear divergence in the electron mass, ending up with an only log-divergent mass $\delta m_e \sim m_e \log \Lambda/m_e$, which is controlled by the symmetry breaking parameter m_e (note that for $m_e \rightarrow 0$ the chiral symmetry is restored). Hence, the critical line is a locus of enhanced symmetry and a large cutoff is possible without much fine-tuning.

The second example is the discovery of the already-mentioned spin-0 (pseudo) scalar mesons, the pions, in low-energy QCD. Their masses of $m_\pi \approx 140$ MeV are only natural if new degrees of freedom exist at or below the scale $\Lambda_{\text{new}} \sim 4\pi m_\pi \sim 1$ GeV. As it turned out, the ρ mesons have masses of around $m_\rho \approx 750$ MeV and the QCD scale is $\Lambda_{\text{QCD}} \approx 1$ GeV, where the chiral symmetry in the light quark sector gets spontaneously broken. As a result, the pions are PNGBs of this broken symmetry and are thus much lighter than m_ρ and Λ_{QCD} . This will be dwelled on in Section 1.3.2, where we will discuss the possibility of the Higgs being a PNGB of a spontaneously broken global symmetry.

The scalar nature of the Higgs boson in the SM causes a completely analogous problem. Interactions of the Higgs with the massive gauge bosons, top quarks, and itself create a self-energy that is quadratically sensitive to the UV cutoff scale. In order to explain the naturalness of the light Higgs mass, new particles or new symmetries are required at the TeV scale, which is one of the reasons why the LHC was built. It should be emphasized that this is an important difference to other problems of the SM, which could be cured by NP setting in much above the TeV scale.¹⁶

The Flavor (Hierarchy) Problem

The downside of New Physics at the TeV scale is that it would immediately cause some trouble with flavor observables. As we have seen in Section 1.1, the fermion couplings to the neutral gauge bosons are flavor diagonal at tree level, so that flavor-changing neutral currents (FCNCs) are loop-suppressed in the SM. As a matter of fact, they are additionally suppressed due to the Glashow-Iliopoulos-Maiani (GIM) mechanism [49], which essentially states that in the case of equal quark masses the unitarity of the CKM matrix enforces FCNCs to vanish, even at loop-level.¹⁷ Higher-dimensional operators, such as the last terms in (1.19), can, however, lead to tree-level FCNCs and thus to large modifications of the SM predictions for rare meson decays or neutral meson mixing, for example. Since no deviations have been detected so far, the current measurements

¹⁵The upper bound on the size of the electron can be deduced by the measurements of its anomalous magnetic moment [46, 47].

¹⁶There is also another hint on new physics at the TeV scale, the so-called *WIMP miracle*. In a nutshell, it states that a weakly-interacting massive particle (WIMP) with a mass of around the TeV scale could be responsible for the correct abundance of dark matter in the universe today.

¹⁷This can be traced back to the fact that all SM interactions are invariant under a full $U(3)^5$ flavor symmetry, which is only broken by the Yukawa couplings.

set lower limits on the NP physics scale Λ_{UV} . The strongest bounds¹⁸ come from the K^0 - \bar{K}^0 -mixing resulting in a lower bound of

$$\Lambda_{UV} \gtrsim 10^4 - 10^5 \text{ TeV}. \quad (1.24)$$

Thus, although a model could have a good solution for the gauge hierarchy problem, the bounds from FCNCs immediately pushes the scale at which it is realized to much higher energy scales. Consequentially, a viable model addressing the hierarchy problem must at least explain why the Wilson coefficients shown in (1.20) are sufficiently small not to be in conflict with the data. Ideally, the same mechanism should explain why the Yukawa couplings have a hierarchical structure, which is put in by hand in the SM. Although the Yukawa matrices cannot be measured, since many parameters are not physical, they give rise to the large hierarchies in the quark masses and the CKM matrix. Concretely, the mass ratios read [50]

$$m_u : m_c : m_t \approx 1 : 500 : 100000, \quad m_d : m_s : m_b \approx 1 : 20 : 1000, \quad (1.25)$$

and the CKM mixing matrix (1.26) can be written in the Wolfenstein parametrization as

$$\mathbf{V}_{\text{CKM}} = \begin{pmatrix} 1 - \frac{\lambda^2}{2} & \lambda & A\lambda^3(\bar{\rho} - i\bar{\eta}) \\ -\lambda & 1 - \frac{\lambda^2}{2} & A\lambda^2 \\ A\lambda^3(1 - \bar{\rho} - i\bar{\eta}) & -A\lambda^2 & 1 \end{pmatrix}, \quad (1.26)$$

where the parameters are given by

$$\lambda = \frac{|V_{us}|}{\sqrt{|V_{ud}|^2 + |V_{us}|^2}}, \quad A = \frac{1}{\lambda} \left| \frac{V_{cb}}{V_{us}} \right|, \quad \bar{\rho} - i\bar{\eta} = -\frac{V_{ud}^* V_{ub}}{V_{cd}^* V_{cb}}. \quad (1.27)$$

While A , $\bar{\rho}$, and $\bar{\eta}$ are $\mathcal{O}(1)$ numbers, the parameter $\lambda \approx 0.23$ is small. The Wolfenstein parametrization explicitly shows the diagonal-dominant, hierarchical structure of the CKM matrix, which is not explained within the SM. While this is - just like the gauge hierarchy problem - no problem from the phenomenological point of view, it is unsatisfactory to have no explanation for these hierarchies in the fermion sector.

In the rest of this chapter, I want to present some of the current theories that address at least one of the two hierarchy problems in question. While explaining each of these BSM scenarios in detail would go beyond the scope of this thesis, it is worthwhile to give a short overview on the idea and the set-up of the most popular theories. We will also point out their compatibility with the electroweak precision tests, in particular the S and T parameters, and show some typical signals at the LHC.

1.3 New Physics Models beyond Extra Dimensions

We begin our discussion of some of the currently most popular NP models based on the ordinary Minkowski space-time with the unambiguous extension of the Poincaré group before we will then turn to the possibility of the Higgs to be a composite state. While these models mainly address the gauge hierarchy problem, we will also discuss a model whose main objective is to explain the hierarchies in the flavor sector.

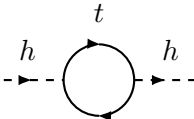
¹⁸We will concentrate on the quark sector from now on, although flavor violation is even more phenomenologically constrained in the lepton sector [50].

1.3.1 Supersymmetry

The most popular way to reduce the large corrections to the Higgs mass is given by supersymmetry (SUSY).¹⁹ Its origin can be traced back to the famous theorem of Coleman and Mandula, which basically states that under certain assumptions - such as analyticity and non-triviality of the S -matrix as well as the presence of a mass gap - the most general symmetry of the S -matrix in a local quantum fields theory is a direct product of the Poincaré group and an internal symmetry group [53].²⁰ However, this theorem included a loophole, which was pointed out by Haag, Lopuszanski, and Sohnius [55]: Coleman and Mandula implicitly assumed that the symmetry generators had to be bosonic, which was sufficient for the immediate purposes but missed the possibility of supersymmetry, the only possible extension of the Poincaré group.

In a nutshell, supersymmetry assigns each bosonic degree of freedom a fermionic one and vice versa. In the lowest SUSY, there is only a minimal number of fermions and bosons in a multiplet, the so-called supermultiplet. In particular, in the minimal version of the supersymmetric extension of the SM, the minimal supersymmetric SM (MSSM) [56], there is exactly one SUSY partner for each SM degree of freedom, which has been shown in Table 1.1: The fermionic partners of the SM gauge bosons are Majorana fermions and are called gauginos, whereas the partners of the chiral SM Weyl fermions $f_{L,R}$ are complex scalars called sfermions $\tilde{f}_{L,R}$, e.g. stops \tilde{t}_R and \tilde{t}_L , or staus $\tilde{\tau}_R$ and $\tilde{\tau}_L$. Note that the subscripts R and L do not denote the chirality of the scalars, but rather refer to the chirality of the corresponding SM Weyl fermions. In contrast to the gauge bosons and fermions, the Higgs sector has to be enlarged already in the MSSM. This is for two reasons: Firstly, a second Higgs doublet is necessary for a gauge-invariant Yukawa term for the up-type quarks and secondly, it is crucial to cancel anomalies from the Higgsinos. Consequentially, the MSSM includes two Higgs doublets (with opposite hypercharges) having four degrees of freedom each, where three of them are eaten by the gauge bosons and represent their longitudinal degrees of freedom. This in turn means that there are five physical degrees of freedom left over. Two of them are charged (H^\pm), one is a pseudoscalar (A), and two of them are scalars (h, H), where the lighter one can be identified with the 126 GeV resonance detected at the LHC. The superpartners of the scalar Higgses are called Higgsinos.

The supersymmetric origin of the theory ensures that the quantum corrections to the Higgs boson mass vanish (if SUSY is exactly realized). To see this, we consider the contribution of the top quark with mass m_t and Yukawa coupling y_t , whose contribution to the Higgs mass reads

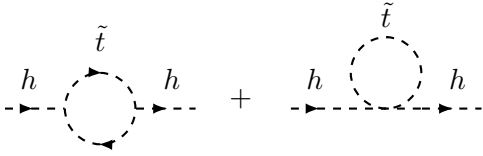


$$\rightarrow \Delta m_h^2|_{\text{top}} = \frac{3\lambda_t^2}{8\pi^2} \left[-\Lambda^2 + 6m_t^2 \log \left(\frac{\Lambda}{m_t} \right) - 2m_t^2 \right].$$

On the other hand, the contribution of its scalar superpartners, the stops, is found to be

¹⁹Thorough discussions of the theory of supersymmetry can be found e.g. in [51, 52].

²⁰This paper played an important role at that time, since it could rule out a class of ideas in which the spin and flavor group were unified in $SU(6)$ [54].



$$\rightarrow \Delta m_h^2|_{\text{stops}} = \frac{3\lambda_{\tilde{t}}}{8\pi^2} \left[-\Lambda^2 + 2M_{\tilde{t}}^2 \log \left(\frac{\Lambda}{M_{\tilde{t}}} \right) \right] - \frac{3\lambda_{\tilde{t}}^2 v^2}{8\pi^2} \left[-1 + 2 \log \left(\frac{\Lambda}{M_{\tilde{t}}} \right) \right]. \quad (1.28)$$

The condition that the coupling constants are related, $\lambda_{\tilde{t}}^2 = -\lambda_{\tilde{t}}$, is required by SUSY. Thus, after adding up the two contributions, all quadratical divergences vanish and only the logarithmical divergencies remain. If SUSY is exactly realized, then also the particle masses are the same, $M_{\tilde{t}}^2 = m_{\tilde{t}}^2$ and there are no divergencies in the limit $v \rightarrow 0$. In fact, since SUSY is a symmetry of the quantum theory, all masses are not renormalized at any order in perturbation theory [57]. Another nice feature of the MSSM is that the running of the gauge couplings will lead to a gauge-coupling unification at scale $\Lambda_{\text{GUT}} \approx 10^{16}$ GeV. This can be a strong hint of a grand unified theory (GUT), where the three gauge interactions at low energies emerge from a single gauge group at Λ_{GUT} . Furthermore, the MSSM provides a viable candidate for dark matter. Since SUSY does not forbid terms giving rise to baryon- and lepton-number violating tree-level processes, such as proton decay, one has to introduce the so-called R -parity [58]. Essentially, this symmetry forbids Feynman vertices which include only one superpartner. As a nice outcome of this rather ad-hoc imposed discrete symmetry is that the lightest supersymmetric particle (LSP) is stable and thus represents a perfect DM candidate.²¹ Despite these appealing features, the MSSM has several issues:

SUSY has to be broken in nature, since otherwise the sparticles, which have the same masses as their SM partners, would have already been detected experimentally. It turns out that it is not possible to incorporate SUSY breaking with only the MSSM content due to the supertrace theorem [62]. More generally, this theorem rules out the possibility of constructing simple models in which supersymmetry breaking is communicated to ordinary supermultiplets by tree-level renormalizable couplings. For this reason one needs a *hidden sector*, in which SUSY gets broken by the vev $\langle \mathcal{F} \rangle$ of the SUSY breaking field \mathcal{F} at a scale Λ , and some kind of *messenger sector*, which communicates the SUSY breaking to the MSSM. In the spirit of effective field theory, one includes all gauge and Lorentz invariant SUSY breaking terms, which are essentially bilinear and trilinear terms, built out of the sparticle fields, with dimensionful couplings. These (mass) couplings are usually given by

$$m_{\text{SUSY}} \sim \frac{\langle \mathcal{F} \rangle}{\Lambda}, \quad (1.29)$$

and should be in the TeV range in order to avoid another gauge hierarchy problem. While the MSSM without the SUSY breaking terms has as many parameters as the SM, the soft SUSY-breaking terms introduce 105 masses, phases, and mixing angles in the MSSM Lagrangian that cannot be rotated away by redefining the phases and flavor basis for the quark and lepton supermultiplets and consequentially have no counterpart in the ordinary SM. Thus, in principle, supersymmetry breaking (as opposed to supersymmetry itself) appears to introduce a tremendous arbitrariness in the Lagrangian. Assuming the new parameters to be generic $\mathcal{O}(1)$ numbers to circumvent fine-tuning, these terms lead to too large contributions to FCNCs and one has to assume the SUSY breaking terms to be flavor diagonal. However, there is no reason, except for the phenomenological one,

²¹There are, however, less restrictive solutions, e.g. imposing lepton-baryon number conservation as a global symmetry [59] or minimal flavor violation [60, 61].

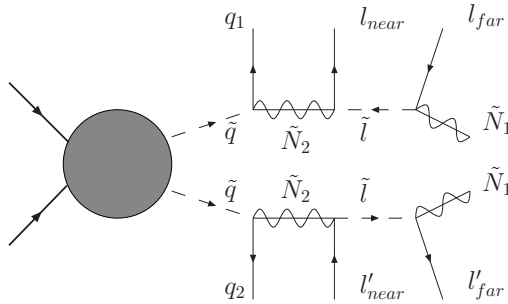


FIGURE 1.3: Typical decay chain in supersymmetric theories shown in [81]. The squarks (sleptons) are denoted by \tilde{q} (\tilde{l}) while $\tilde{N}_{1,2}$ denote the neutralinos, i.e. the mass eigenstates of mixing of the neutral gauginos and Higgsinos. The neutralino \tilde{N}_1 is the stable LSP and gives rise to missing energy in the detectors.

why this strong constraint should be imposed. Especially in models where the SUSY breaking is mediated by gravity, so-called *gravity-mediated* SUSY breaking or *mSUGRA* models [63–68], the requirement of flavor diagonality has only a phenomenological, but no theoretical foundation. *Gauge-mediated* SUSY-breaking models, on the other hand, could explain this, since the SUSY-breaking is mediated by the flavor-diagonal gauge interactions [69–75], see [76] for a nice review. It should be mentioned that despite the above disadvantages of the SUSY-breaking terms, they imply another interesting feature: If the SUSY breaking scale is large enough, RG running can turn the Higgs mass parameter negative, triggering EWSB. This is known as radiative symmetry breaking [77].

Another problem is the so-called μ *problem* of supersymmetric theories. The only term in the MSSM superpotential that has a positive mass dimension is the μ -term. The determination of the minimum of the Higgs potential and demanding for a non-zero vev that triggers EWSB imply constraints on the μ -parameter to be in the order of the SUSY-breaking scale. However, there is no reason the μ -parameter should be assumed to be in that range right from the beginning. If there is no further explanation, it should rather be at the order of the UV cutoff of the MSSM, just like the SM Higgs mass parameter. This would cause another hierarchy problem and SUSY would not have brought noticeable improvement. However, since the mass parameters in SUSY theories do not renormalize, the situation is much better than in the SM. The mass parameter would be technically natural according to the discussion below (1.21). Nevertheless, it is an open question of what sets the scale for the μ parameter of the MSSM.

Finally, the first run of LHC has not detected any light SUSY partners yet, although the light Higgs mass would require that. Typical SUSY searches look for jets (and leptons) plus missing energy, where the missing energy stems from the LSP, which stands at the end of a chain of subsequent decays of supersymmetric particles. Figure 1.3 shows an example for such a decay chain. Assuming the SUSY partners to be approximately degenerate, the current measurements push the lower bound on squark and slepton masses to the several hundred GeV (depending on the specific scenario) [78, 79], i.e. right below the TeV scale, where NP should appear in order not to reintroduce a hierarchy problem. Therefore, today’s point of view about SUSY is such that Higgsinos, stops, and the gluino should not be too far above the weak scale, while the rest of the SUSY spectrum, including the squarks of the first two generations, can be heavier and beyond the current LHC reach, see e.g. [80]. It will be interesting to observe whether (natural) SUSY will survive the second run of LHC.

1.3.2 Composite Higgs Models

In this section, we want to understand how the Higgs can emerge as a (composite) Pseudo Nambu-Goldstone boson of a strongly-coupled sector. For this purpose, it is crucial to understand the concept of *technicolor* theories, which will therefore be introduced first. In the context of composite models, it is also possible that the SM fermions are *partially composite*. This will be touched on in this subsection as well.

Technicolor Theories

Technicolor (TC) theories make use of the fact that, at the scale Λ_{QCD} , where the QCD confinement sets in, the quark condensate $\langle q\bar{q} \rangle = \langle q_L\bar{q}_R \rangle + \langle q_R\bar{q}_L \rangle$ gains a non-zero vev which in turn breaks the electroweak symmetry, even if no SM Higgs scalar was realized in nature. The electroweak symmetry is broken in the right pattern, since the quark condensate has the same charges as the SM Higgs doublet. The starting point is the Lagrangian (1.5), which shows that the kinetic terms for the fermions are invariant under a global $SU(2)_L \times SU(2)_R \times U(1)_B$ transformation.²² This chiral (and baryon-number) symmetry is broken down to $SU(2)_V \times U(1)_B$ by the quark condensate, giving rise to three massless Goldstone bosons, according to the Nambu-Goldstone theorem. These Goldstone bosons can be identified with the well-known pions. Only the $SU(2)_L \times U(1)_Y$ subgroup of the full global symmetry is gauged giving rise to the electroweak symmetry. As the QCD vacuum breaks the electroweak symmetry, the pions are eaten to give masses to the electroweak gauge bosons [22]. To see this, one can derive the effects of the conserved weak currents on the gauge-boson propagators. One finds that for a pion decay constant f_π , $SU(2)_L$ coupling constant g , and the Weinberg angle θ_w , the electroweak gauge bosons would gain masses of [82]

$$m_W = \frac{gf_\pi}{2} \approx 28 \text{ MeV}, \quad m_Z = \frac{gf_\pi}{2\cos\theta_w} \approx 32 \text{ MeV}, \quad (1.30)$$

which are, however, far below the experimentally measured values. Nevertheless, it led Weinberg [83] and Susskind [84] to propose the first TC models. Being upscaled versions of QCD, they were based on two flavors of so-called *techniquarks*, transforming in the fundamental representation of the TC gauge group $\mathcal{G}_{\text{TC}} = SU(N_{\text{TC}})$. The left-handed (right-handed) components have to transform as a doublet (singlet) under the $SU(2)_L$ gauge group in order to form a techniquark condensate that breaks the electroweak symmetry. The β -function of the new gauge group \mathcal{G}_{TC} behaves just like its QCD analog, with the only difference that the coupling becomes strong at the scale

$$\Lambda_{\text{TC}} = \sqrt{\frac{3}{N_{\text{TC}}}} \frac{f_\pi^{\text{TC}}}{f_\pi} \Lambda_{\text{QCD}} \sim 4\pi f_\pi^{\text{TC}}, \quad (1.31)$$

where f_π^{TC} is the equivalent of the pion constant, and is required to have a value $f_\pi^{\text{TC}} \approx v$ in order to give the experimentally measured gauge-boson masses. The advantage of TC theories, or in general of theories where EWSB is achieved by a strong sector, is that the hierarchy between the electroweak and the Planck scale is explained by dimensional transmutation: The scale (1.31) is generated dynamically as the scale at which the TC coupling gets strong.

²²We will concentrate on the simplified case of one generation (i.e. two flavors) here. Moreover, we will not consider the axial $U(1)$ that is broken by quantum effects, even in the chiral limit.

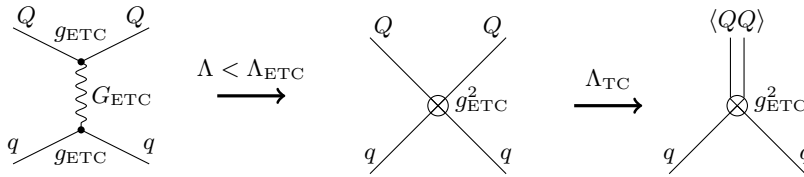


FIGURE 1.4: Visualization of the generation of mass terms in ETC theories. Both TC and SM quarks couple to the ETC gauge boson G_{ETC} which is integrated out at the scale Λ_{ETC} . The TC quarks then condense at the scale Λ_{TC} and give rise to the mass term for the SM quarks.

However, QCD-like TC models lead to predictions that are in conflict with experimental data, e.g. too large corrections to the electroweak S parameter. *Naive dimensional analysis* (NDA) [85] suggests that contribution from the technifermions gives rise to $S \sim N_{\text{TC}} N_D / \pi$, where N_D denotes the number of technidoublets. This means, even for minimal TC theories (with N_{TC}, N_D small), the contribution is $S \sim 1$ which is far above the experimental measured value (1.17). Another shortcoming of TC theories is that the EWSB is only communicated to the boson, but not to the fermion sector. For the generation of the latter's masses, it is necessary to enlarge the gauge group to $\mathcal{G}_{\text{ETC}} \supset \mathcal{G}_{\text{TC}}$. Both the SM and TC fermions must transform under the same representation so that the ETC gauge bosons G_{ETC} can couple to both of them [86, 87]. These models are referred to as *extended technicolor* (ETC) theories. After integrating out the heavy degrees of freedom at some scale $\Lambda_{\text{ETC}} > \Lambda_{\text{TC}}$, the coupling between the SM quarks (q) and techniquarks (Q) is given by

$$\mathcal{L}_{\text{int}} = g_{\text{ETC}}^2 \frac{(\bar{Q}Q)(\bar{q}q)}{\Lambda_{\text{ETC}}^2}, \quad (1.32)$$

where g_{ETC} is the \mathcal{G}_{ETC} gauge coupling. Once the TC fermions condense at a lower scale Λ_{TC} , a mass term is generated for the SM fermions

$$\frac{g_{\text{ETC}}^2}{\Lambda_{\text{ETC}}^2} \langle \bar{Q}Q \rangle \bar{q}q \quad \rightarrow \quad m_q \sim \Lambda_{\text{TC}} \left(\frac{\Lambda_{\text{TC}}}{\Lambda_{\text{ETC}}} \right)^2. \quad (1.33)$$

This is depicted in Figure 1.4. In principle, the hierarchies between the three generations can be generated by a cascade of breakings of the extended symmetry at different scales $\Lambda_1 > \Lambda_2 > \Lambda_3$. Note that Λ_{ETC} is set by the requirement that Λ_{TC} has to be of the order of the EW scale and if one uses the quark masses as an input (and assuming $g_{\text{ETC}} \sim \mathcal{O}(1)$), Λ_{ETC} should not be too large, since otherwise the heavy quark mass could not be generated. However, the same exchange of ETC gauge fields leading to the four-fermion interaction (1.32) also generates operators $(\bar{q}q)^2 / \Lambda_{\text{ETC}}^2$ giving rise to various FCNC processes. As explained in Section 1.2, the bounds from $K\bar{K}$ mixing and rare meson decays, for example, require at least $\Lambda_{\text{ETC}} \gtrsim 10^4$ TeV. Thus, there is a tension between avoiding too fast FCNCs and generating large enough quark masses, especially the mass of the top quark.

This problem can be solved by theories which do not behave like QCD, i.e. where asymptotic freedom does not arise until a scale much greater than Λ_{TC} [88–93]. The idea is that the β -function of the ETC gauge group becomes approximately conformal above Λ_{TC} . As already used in (1.23) the corresponding radiative corrections would give rise to a power-law enhancement factor $(\Lambda_{\text{ETC}}/\Lambda_{\text{TC}})^\gamma$, where γ is the anomalous dimension.

Yang-Mills theories with this behavior are called *walking*, as the couplings runs slowly for a large range of scales. Due to these radiative corrections, the corresponding *walking technicolor* theories allow for fermion masses

$$m_q \sim \Lambda_{\text{TC}} \left(\frac{\Lambda_{\text{TC}}}{\Lambda_{\text{ETC}}} \right)^{2-\gamma}, \quad (1.34)$$

which ameliorates the FCNC problem, since now the scale Λ_{ETC} can be increased. However, the anomalous dimension is bounded from above by $\gamma < 1$,²³ so that one still requires some amount of fine-tuning to explain the top quark mass. However a more severe problem with (extended) TC theories is that they are *higgsless* theories, i.e. their spectrum does not contain a sharp scalar resonance such as the one discovered at the LHC. In walking TC theories, there is a candidate that could be narrow and even lighter than those from TC, but they are still heavier than the boson found at the LHC [94].²⁴ It is therefore reasonable to look for other versions of composite models which include a light scalar particle in the spectrum.

Composite Higgs

After this short introduction to models with a composite sector, we now turn to the models combining the idea of a light scalar particle and composite models. In the eighties, Georgi and Kaplan pointed out that the Higgs boson can be naturally lighter than other composite resonances if it emerges as a Pseudo Nambu-Goldstone boson of an enlarged global symmetry of the strong sector [98, 99]. We can understand the idea with the help of the minimal composite Higgs model [100, 101]. In this model, the SM fermions and gauge bosons are assumed external fields to a strong sector with composites resonances and are considered as *elementary*. The composite sector has a global symmetry $SO(5) \times U(1)_X$, which is dynamically broken down to $SO(4) \times U(1)_X$ at an energy scale f . The subgroup $SO(4) \sim SU(2)_R \times SU(2)_L$ includes the electroweak gauge group of the SM so that the hypercharge is given by $Q_Y = T_R^3 + Q_X$. The four Goldstone bosons that emerge from the breaking $SO(5) \rightarrow SO(4)$ can be identified with the four degrees of freedom of the Higgs doublet transforming as a fundamental of $SO(4)$ or, equivalently, as a complex doublet of $SU(2)_L$. Since the Goldstone modes transform under gauge transformations as $\varphi_i(x) \rightarrow \varphi_i(x) + \alpha(x)$, where α is the gauge parameter, a Higgs potential cannot be not generated at tree-level. Loops of SM fermions and gauge bosons, on the other hand, generate a Higgs potential which breaks the electroweak gauge group $SU(2)_L \times U(1)_Y \subset SO(4)$.²⁵ In this context, the electroweak scale v is dynamically generated and can be smaller than the scale f , which distinguishes them from TC theories, where no such separation of scales exists, and which sets the scale of the heavy resonances of the strong sector.

An important imprint of PNGB models and the generated Higgs potential is that the Higgs couplings are modified compared to the SM. In the above scenario, one finds [22]

$$g_{VVh} = g_{VVh}^{\text{SM}} \sqrt{1 - \xi}, \quad g_{VVhh} = g_{VVhh}^{\text{SM}} (1 - 2\xi), \quad (1.35)$$

²³This bound can be derived by an analysis of the Schwinger-Dyson equation, see e.g. [43].

²⁴In walking TC theories, there is a PNGB connected to the breaking of the conformal symmetry, the so-called dilaton [95], which has the same quantum numbers as the SM Higgs boson, but has significantly different self-coupling [96, 97].

²⁵In order to arrive at a non-zero Higgs vev, one needs a massive fermion in the loop. In this sense, the heavy top quark was a blessing for composite Higgs models. See [100] for a detailed discussion.

where $\xi = v^2/f^2$. Note that for $f \rightarrow \infty$ we recover the SM Higgs couplings, since the effects of the heavy resonances decouple. More interesting is the case of ξ being large enough to give considerable deviations from the SM predictions. It must, however, be small enough such that the model can pass the electroweak precision tests. After including tree-level as well as loop-level corrections to the S and T parameters, one finds $\xi = v^2/f^2 \lesssim 0.1$ [22], which is a natural separation of scales. There are stronger constraints from CP-violating and FCNC processes if the EWSB is communicated to fermions via the same mechanism as in ETC. Assuming $\Lambda_{UV} \gtrsim f \gg v$, one would have to pay the price of fine-tuning the parameter ξ to be very small. This in turn would reintroduce the fine-tuning problem again. This will be addressed in the next paragraph.

Although the gap between v and f can be explained, the former still suffers from radiative corrections. This is the motivation for the so-called *collective symmetry breaking*, which is realized in a class of models called *little Higgs* [102]. In these models the global symmetry is larger than necessary to accommodate the four Goldstone bosons that can be identified with the scalar degrees of freedom of the Higgs. Since the electroweak gauge group is enlarged as well, there are additional gauge bosons which become heavy by eating the additional Goldstone bosons. If now either the SM gauge bosons or the additional bosons couple to the Higgs there is a leftover global symmetry, which ensures that the Higgs remains massless. If both couple to the Higgs, the latter acquires a mass, which is only logarithmically divergent, see [103] for further details.

Partial Compositeness

We will now come back to the issue of the too large contributions to CP-violating and FCNC processes. Milder experimental constraints than in ETC-type models can be achieved by some different mechanism that can transmit EWSB to the SM fermions. Instead of the coupling (1.32), one assumes a linear coupling between a composite operator and the SM fermions (again transmitted by ETC gauge bosons that are integrated out at scale Λ_{ETC}), e.g.

$$a \frac{\bar{q} Q \bar{Q} Q}{\Lambda_{ETC}^2}, \quad (1.36)$$

where the composite state $Q\bar{Q}Q$ must have the same quantum numbers under the SM gauge group as the quark to which it couples. Assuming a walking behavior of the *technibaryon* condensate $\langle Q\bar{Q}Q \rangle \sim B$ leads to the Lagrangian

$$\mathcal{L} \ni \Delta_L \bar{q}_L B_R + \Delta_L \bar{q}_R B_L^c - m_B \bar{B} B - m_{B^c} \bar{B}^c B^c, \quad (1.37)$$

where the mass mixing parameters are given by

$$\Delta_L \equiv a_L \Lambda_{ETC} \left(\frac{\Lambda_{TC}}{\Lambda_{ETC}} \right)^{3-\gamma_L}, \quad \Delta_R \equiv a_R \Lambda_{ETC} \left(\frac{\Lambda_{TC}}{\Lambda_{ETC}} \right)^{3-\gamma_R}. \quad (1.38)$$

Upon diagonalization of the mass terms, by the rotation

$$\begin{pmatrix} q_L \\ B_L \end{pmatrix} = \begin{pmatrix} \cos \varphi_L & -\sin \varphi_L \\ \sin \varphi_L & \cos \varphi_L \end{pmatrix} \begin{pmatrix} \psi_L \\ \chi_L \end{pmatrix}, \quad \tan \varphi_L = \frac{\Delta_L}{m_B}, \quad (1.39)$$

and similarly for the right-handed fermions, the massless Weyl fermions $\psi_{L,R}$ can be identified with the massless SM fermions before EWSB and Dirac fermions of mass $m_\chi^2 = m_B^2 + \Delta_L^2$. Note that the SM quarks are now admixtures of elementary and

composite fermions, where the elementary (composite) component is proportional to $\cos \varphi_A$ ($\sin \varphi_A$),

$$\psi_A = \cos \varphi_A q_A + \sin \varphi_A B_A, \quad A = L, R. \quad (1.40)$$

This is the reason why these models are referred to as models with *partial compositeness*. After EWSB, the massless fermions $\psi_{L,R}$ get their masses through mixing with the TC condensate Φ via the Yukawa terms

$$\begin{array}{c} \Phi \\ | \\ \hline B_R^c \quad B_L \end{array} \quad \bar{B}_L \lambda \Phi B_R^c + \text{h.c.}, \quad (1.41)$$

whose size is controlled by the mixing angles (and thus by the anomalous dimensions of the composite technibaryon),

$$\begin{array}{c} \Phi \\ | \\ \hline q_R \quad B_R^c \quad B_L \quad q_L \\ \hline \sin \varphi_R \quad \sin \varphi_L \end{array} \quad Y_\psi = \sin \varphi_L \lambda \sin \varphi_R. \quad (1.42)$$

Each Yukawa coupling can thus be generated by the fundamental $\mathcal{O}(1)$ parameter λ and the choice of the anomalous dimensions $\gamma_{L,R}$ of the composite operators B, B^c are such that the angles and consequently the (effective) Yukawa coupling is small enough. Thus, in contrast to ordinary WTC models, one can assume $\Lambda_{\text{ETC}} \sim M_{\text{Pl}}$ without having a problem of generating the large top-quark mass.

Interestingly, the concept of partial compositeness also leads to a suppression of FCNCs, which could be induced by the couplings

$$\mathcal{L} \ni g \left(\bar{B}_i \gamma_\mu \rho^\mu B_i + \bar{B}_i^c \gamma_\mu \rho^\mu B_i^c \right), \quad (1.43)$$

where ρ^μ are bosonic technicolor resonances. Rewriting this with the help of (1.39) leads to

$$\mathcal{L} \ni (g_L)_{ij} \bar{\psi}_L^i \gamma_\mu \rho^\mu \psi_L^j + (g_R)_{ij} \bar{\psi}_R^i \gamma_\mu \rho^\mu \psi_R^j, \quad (1.44)$$

where

$$\mathbf{g}_L = g \begin{pmatrix} \sin^2 \varphi_{u_L} & & \\ & \sin^2 \varphi_{c_L} & \\ & & \sin^2 \varphi_{t_L} \end{pmatrix}, \quad \mathbf{g}_R = g \begin{pmatrix} \sin^2 \varphi_{u_R} & & \\ & \sin^2 \varphi_{c_R} & \\ & & \sin^2 \varphi_{t_R} \end{pmatrix}. \quad (1.45)$$

As these couplings are non-universal, they give rise to FCNCs when going into a basis, in which the Yukawa matrices are diagonal. However, the degree of flavor violation is given by the mixing angles, which are small for the light fermions, so that FCNCs are always suppressed in models with partial compositeness. We will examine this further in Section 2.2.3, since Randall-Sundrum models with bulk fermions also display this characteristic.

1.3.3 Froggatt-Nielsen Models

With the goal to explain the hierarchies in the fermion sector, Froggatt and Nielsen [104] proposed a model without Yukawa terms. The idea is such that the left- and right-handed components of the SM quark fields have different charges under an abelian symmetry

group $U(1)_F$, the flavor symmetry group. The Yukawa terms are then generated by

$$\left(\frac{\phi}{\Lambda_{\text{Fl}}}\right)^n \bar{Q}_L \Phi q_R, \quad (1.46)$$

where the scalar field Φ is called a *flavon* and is assumed to be charged under the flavor group. In contrast, the Higgs field Φ is assumed to be neutral. Note that the term (1.46) can be generated like a Majorana mass term by integrating out a heavy fermion at scale Λ_{Fl} . Once the flavon takes on a vev

$$\frac{\langle\phi\rangle}{\Lambda_{\text{Fl}}} \sim \lambda, \quad (1.47)$$

the Yukawa terms get the structure

$$Y_{ij} = g_{ij} \lambda^{a_i - b_j}, \quad (1.48)$$

where $a_i > 0$ and $b_j < 0$ are the flavor charges of the left- and right-handed quarks, respectively, and g_{ij} are $\mathcal{O}(1)$ factors.²⁶ With the proper choice of the charges a_i and b_j , one obtains the correct pattern of the Yukawa matrices which leads to the correct mass spectrum via (2.106) and from that the hierarchical structure of CKM matrix, see [105] for more details. The rotation matrices U_q and W_q will be explicitly shown in Section 2.2.3.

Note that the Froggatt-Nielsen mechanism serves for a whole class of models, with a different source for the small parameter λ . For example, the models with partial composite fermions, which have been introduced in the previous section, lead to the Yukawas (1.42), where the smallness is due to the small anomalous dimensions in (1.38). Another example is given by models with warped extra dimensions, see Section 1.4.4. In this case, we find for the light quarks

$$Y_{ij} = g_{ij} \epsilon^{c_i - c_j}, \quad (1.49)$$

where $c_{i,j}$ are $\mathcal{O}(1)$ bulk mass parameters localizing the 5D quark profiles along the extra dimensions, g_{ij} are the fundamental Yukawa couplings, and $\epsilon \approx \Lambda_{\text{IR}}/\Lambda_{\text{UV}}$ is roughly the ratio of the TeV and the Planck scale.

A problem of Froggatt-Nielsen models based of abelian symmetries is that the relatively low flavor scale Λ_{Fl} cannot avoid large contributions to FCNCs, which spoils the good agreement with experimental data. A way out is given by *non-abelian* flavor symmetries, i.e. symmetries based on (a discrete subgroup of) the flavor symmetry $U(3)_Q \times U(3)_u \times U(3)_d$, but they are also problematic with a low flavor scale, see e.g. [105]. A way out is to impose a flavor structure of the NP sector, that respects the flavor symmetry of the SM (i.e. it is flavor blind), without further motivation. This is called minimal flavor violation (MFV) and was first mentioned in [106]. In practice, that means that any new flavor structure can be constructed only by insertions of SM Yukawa matrices, so that after rotating the corresponding fields into the mass eigenbasis no flavor-changing couplings are generated. The concept of MFV is very popular and it used in many NP models which do address the flavor problem inherently (e.g. SUSY).

²⁶Note that in (1.48) and the following equivalent formulas, no summation over double indices is implied.

1.4 Models with Extra Dimensions

An interesting alternative to models explaining the gauge hierarchy problem by symmetries is given by models with extra dimensions. As these models form the main part of this thesis, the following discussion will be somewhat more detailed than that of the previous sections. Starting with a short description of the first appearance of extra dimensions in theoretical physics, we will continue with the general set-up of extra-dimensional theories and focus on some issues these theories cannot get rid of. Finally, three specific models are presented where in the subsequent chapter particular attention will be paid to the models with warped extra dimensions. This section is based on several recommendable reviews of extra dimensions [107–111].

1.4.1 First Appearance: Nordström, Kaluza, Klein

The very first idea of extra dimensions came up in 1914, when Nordström observed that extending the Maxwell theory to five dimensions, written in terms of a 5-vector A_M , contained the 4-vector A_μ , which could be identified with the electromagnetic vector potential, plus a 4D scalar obeying the field equations for his own proposed scalar theory of gravity [112]. However, two years later Einstein formulated his GR, which turned out to be the correct description of gravity and Nordström's idea became obsolete. With the aim to combine Einstein's GR and Maxwell's theory of electromagnetism, Kaluza and Klein introduced a model that extended Einstein's GR to 4+1 dimensions [113, 114]. The additional fifth dimension was assumed to be tiny and compact, which could explain why it had not been discovered. This so-called *Kaluza-Klein* (KK) theory achieved to unify electromagnetism and gravity, the only two forces known at that time. Although the KK theory turned out not to be the correct description of nature, it is worth presenting the original model, since we will encounter some important features of models with extra dimensions.

The starting point is the 5D Einstein-Hilbert action in flat space,

$$S_5 = \int d^5x \left\{ -\frac{1}{2} M_5^3 \sqrt{G} \mathcal{R}_5[G] \right\}, \quad (1.50)$$

where M_5 is the five-dimensional Planck scale, \mathcal{R}_5 denotes the Ricci scalar, and G is the determinant of the 5D metric parametrized as

$$G^{MN} = \begin{pmatrix} \bar{g}^{\mu\nu} & \bar{A}^\mu \\ \bar{A}^{\mu T} & \bar{g}^{55} \end{pmatrix}. \quad (1.51)$$

Here and in the following the Latin (Greek) indices $M, N = 0, 1, 2, 3, 5$ ($\mu, \nu = 0, 1, 2, 3$) correspond to the 5D (4D) space-time coordinates. The field $\bar{g}^{\mu\nu}$ is a symmetric tensor and represents the 4D metric. The field \bar{A}^μ denotes the part of the 5D metric, where one index points into the fifth dimension, while the remaining one points into four dimensions. For an observer who is ignorant to the extra dimension this field is a 4-vector, i.e. it transforms under Lorentz transformations accordingly. Analogous considerations can be done for the field \bar{g}_{55} which is a scalar from the 4D point of view. Since its vev measures the size of the extra dimension, this field is called radion. Using the above metric it is straightforward to evaluate the 5D action (1.50), but it is more convenient

to parametrize the metric as

$$G^{MN} = \begin{pmatrix} \varphi^{-\frac{1}{3}} (g^{\mu\nu} - \varphi A^\mu A^\nu) & -\varphi^{\frac{2}{3}} A^\mu \\ -\varphi^{\frac{2}{3}} A^\mu T & -\varphi^{\frac{2}{3}} \end{pmatrix}, \quad (1.52)$$

which will become more obvious below. An important difference in models with one or more extra dimensions is the fact that fields are not only dependent on the coordinate of the Minkowski space-time ($x \equiv x^\mu$), but also on the position in the extra dimension, labeled by x_5 for the time being.²⁷ In other words, the 4D field $A_\mu(x)$ for instance is replaced by

$$A_\mu(x) \rightarrow A_\mu(x, x_5) = \sum_n^\infty A_\mu^{(n)}(x) \chi_n^A(x_5), \quad (1.53)$$

where we have already used that, from the 4D point of view, the compactness of the extra dimension gives rise to an infinite tower of massive *KK modes* $A_\mu^{(n)}$, whose localization in the extra dimension depends on the wave-functions or *profiles* χ_n^A . The masses of the KK modes increase with larger n . This is in analogy to the infinitely many energy states of a quantum-mechanical particle in a finite volume, where the energy levels of the particle are inverse proportional to the size of the box. What happens here is that the momentum in the compactified extra dimension is quantized, where the discretized momenta correspond to the masses of the KK modes. Under the assumption that the length of the extra dimension is of the Planck length $l_{\text{Pl}} \equiv M_{\text{Pl}}^{-1}$, the masses scale like $m_n \sim n/l_{\text{Pl}}$ and clearly decouple from the theory, whereas the massless *zero modes* $A_\mu^{(0)}$ remain. Inserting the zero modes of the metric (1.52) into (1.50) and dropping the superscripts we arrive at the Einstein-Hilbert action

$$S_5^0 = -\frac{1}{2}(2\pi R)M_5^3 \int d^4x \sqrt{g} \left[\mathcal{R}_4[g] + \frac{1}{4}\varphi F_{\mu\nu} F^{\mu\nu} - \frac{1}{6} \frac{(\partial_\mu \varphi)(\partial^\mu \varphi)}{\varphi^2} \right]. \quad (1.54)$$

It is now easy to identify the ingredients of the resulting action. The field $F_{\mu\nu} = \partial_\mu A_\nu - \partial_\nu A_\mu$ is the well-known electromagnetic field strength tensor of a $U(1)$ gauge field. After defining $M_{\text{Pl}}^2 \equiv 2\pi R M_5^3$ the action for the 4D metric $g^{\mu\nu}$ describes GR, i.e. the action of the graviton. What is left is the scalar field φ which can be redefined via $\varphi = \exp[\sqrt{6}r(x)/M_{\text{Pl}}]$ in order to arrive at a canonically normalized kinetic term. Its coupling to the kinetic term of the gauge bosons indicates that the radion has the same coupling as a dilaton field. Once it acquires a vev $\langle r \rangle$, we can identify

$$e^{\sqrt{6}\frac{\langle r \rangle}{M_{\text{Pl}}}} \leftrightarrow \frac{1}{e^2}, \quad (1.55)$$

where e on the right-hand side denotes the electric charge. Thus, this theory describes the unification of 4D general relativity and 4D electromagnetism, starting from 5D gravity. Although seeming to be very promising, this theory turned out not to be the correct description of nature. This is not least because of the discovery of the remaining fundamental forces and the establishment of the SM. Nevertheless, this example highlighted that extra-dimensional models are suitable candidates for a UV completion of the SM, since they have the potential to unify the fundamental forces.²⁸ However, the models that are focused on in the following will not have goal of unification, but their major objective is the explanation of the hierarchy problems of the SM and to have the SM as

²⁷We will concentrate on only one additional extra dimension in the following.

²⁸In fact, non-abelian fields can arise from space-times of higher dimensionality, when appropriately compactified [111].

a low-energy limit. Before we focus on them, it is worthwhile pointing out some generic features of extra-dimensional models.

1.4.2 Generic Features of Extra-Dimensional Models

As explained at the beginning of this chapter, the SM has to be regarded as an EFT and is also valid up to a certain energy scale Λ_{UV} , where it has to be replaced by a more fundamental theory, e.g. by a theory based on extra dimensions. On the other hand also the latter theories have to be considered as EFT's due to an intrinsic cutoff. This can be understood with the help of a dimensional analysis of a generic theory in D (flat) dimensions

$$S_d = \int d^d x \left\{ -\frac{1}{4g_d^2} F_{MN} F^{MN} + i\bar{\Psi} \not{D} \Psi + |D_M \Phi|^2 + y_d \Phi \bar{\Psi} \Psi + \dots \right\}, \quad (1.56)$$

where $D_M = \partial_M - iA_M$ implies that the mass dimension of the gauge field is $[A_M] = 1$ so that $[F_{MN}] = 2$ and $[g_d^2] = 4 - d$. So, for $d > 4$ the coupling constant has a negative mass dimension and provides an intrinsic scale for the theory. An analogous discussion holds for the Yukawa coupling y_d having a mass dimension of $[y_d] = (4 - d)/2$. This has an important consequence: Using NDA one can estimate the 1-loop correction to the Yukawa coupling [111]

$$\delta y_d = \frac{1}{l_d} \frac{2y_d^3}{d-4} \Lambda^{d-5}, \quad d > 4 \quad (1.57)$$

where a hard-momentum cutoff Λ has been used as a regulator²⁹ and l_d is the d -dimensional loop factor

$$\frac{1}{l_d} \equiv \frac{\Omega_d}{2(2\pi)^d} = \frac{1}{(4\pi)^{d/2} \Gamma(d/2)} = \begin{cases} \frac{1}{16\pi^2} & \text{for } d = 4 \\ \frac{1}{24\pi^3} & \text{for } d = 5 \end{cases}, \quad (1.58)$$

with the d -dimensional solid angle Ω_d . The power-law dependence on the UV cutoff indicates that certain observables are, strictly speaking, incalculable. One could argue that one could absorb the divergences in physical quantities as always done in the SM. The difference is that in extra-dimensional models (like in all non-renormalizable theories) the effects of the higher-dimensional operators *after* renormalization scale like $(E/\Lambda_{\text{UV}})^n$, where E is the typical energy of a process and Λ_{UV} is the UV cutoff scale of the theory. As already mentioned above, the importance of these operators is negligible for processes at low energies and only a finite number of operators is relevant. For energies around the cutoff, however, details of the UV completion become important, which manifests itself in two aspects. The first one is that higher-dimensional operators can contribute equally at tree level, while the second one states that loop-level effects contribute equally and become as big as the corresponding tree-level contributions of a given process, see [111] for further discussion.

The important lesson of this discussion is that one should be aware of the fact that higher-dimensional theories have an intrinsic cutoff Λ_{UV} and that observables can be very sensitive to the physics at and above Λ_{UV} . If this is the case they are incalculable within the extra-dimensional model and it is necessary to include the corresponding

²⁹If one uses a Pauli-Villiar regulator, the result would differ by an $\mathcal{O}(1)$ factor. For example, for $d = 5$ one finds a Pauli-Villiar cutoff Λ_{PV} which is related to the hard-momentum cutoff by $2\Lambda = \pi\Lambda_{\text{PV}}$ [111]. Thus, there is some uncertainty where the new physics is to be expected.

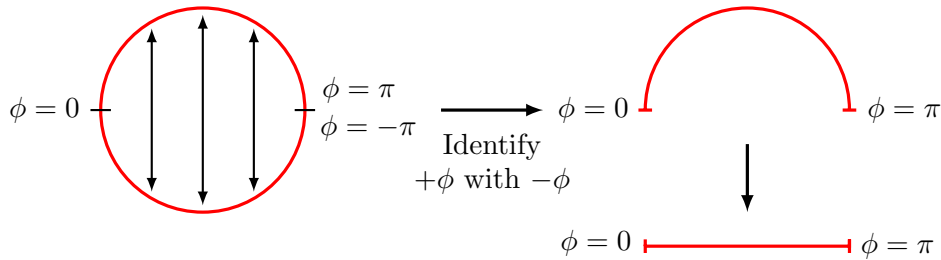


FIGURE 1.5: Visualization of an orbifold [115].

higher-dimensional operators, whose coefficients have to be determined by experiment. Also keep in mind that in order to obtain a reliable result only the KK modes below the cutoff are allowed to contribute, in particular in loop-induced processes. This will become important in Section 4.1, where we will explicitly study a process that is (naively) sensitive to the UV physics.

The previous discussion also highlights a possible application to particle physics concerning the hierarchy problem. If the extra dimensions would predict particles at the TeV scale, this would be a good reason why a cutoff could exist near that scale. If one discovered an extra-dimensional structure at the TeV scale experimentally, one would be forced to accept the existence of a cutoff not far above. In this case, the large hierarchy problem of the SM would become less urgent to be solved: The priority would rather be to understand the *little hierarchy* between the electroweak scale and the cutoff associated with the extra-dimensional physics. Hence, generic extra-dimensional models can be considered as motivated by the hierarchy problem, provided the compactification scale is near the TeV scale. Note that the situation is similar to the SUSY solution to the hierarchy problem, with the superpartners having masses of around a TeV.

Set-Up for Theories with One Compact Extra Dimension

We will specialize on the set-up of models based on one compact extra dimension, which will be useful for the understanding of the subsequent sections. Intuitively, the extra dimension would be chosen to be a conventional circle. However, it is more convenient to consider a so-called S^1/Z_2 orbifold, illustrated in Figure 1.5. This is a circle of radius r , where the points (parametrized by $\phi \in [-\pi, \pi]$) that are related by the Z_2 symmetry

$$(x^\mu, \phi) \leftrightarrow (x^\mu, -\phi) \quad (1.59)$$

are identified. The magnitude of the radius r can vary and will be specified later. The 5D action is required to be invariant under these Z_2 transformations Z . The fields themselves need not to be identified at ϕ and $-\phi$, but can differ by the eigenvalues of Z ,

$$\Phi(x, -\phi) = Z\Phi(x, \phi) = \pm\Phi(x, \phi), \quad (1.60)$$

due to $Z^2 = \text{id}$. The functions belonging to the eigenvalue $+1$ (-1) are called even (odd) functions under the Z_2 parity. Note that the Z_2 -odd functions must vanish on the orbifold *fixed points* $\phi = 0, \pm\pi$. This important feature of orbifolds is crucial to obtain a low-energy spectrum of the fermions that is compatible with the SM, see below. The fixed points are often used to provide support for *3-branes*, i.e. submanifolds with three spatial and one time dimension, on which 4D fields can be defined. The region between the boundaries is called *bulk*. To summarize, an S^1/Z_2 orbifold is effectively an interval

parametrized by $\phi \in [0, \pi]$, possibly bounded by branes, which together with the Z_2 eigenvalues of the fields contain the whole information. For the bulk 5D metric we choose an ansatz that respects 4D Lorentz symmetry,

$$ds^2 = G_{MN} dx^M dx^N = e^{-2\sigma(\phi)} \eta_{\mu\nu} dx^\mu dx^\nu - r^2 d\phi^2, \quad (1.61)$$

where throughout this thesis the Minkowski metric will be used in the convention $\eta_{\mu\nu} = \text{diag}(1, -1, -1, -1)$. The function $\sigma(\phi)$ gives information about how the geometry of the space varies in the fifth dimension. One can always define ϕ in such a way that $\sigma(0) = 0$, which we will assume from now on. The specific models introduced below will be distinguished according to the specific form of the function $\sigma(\phi)$. If $\sigma(\phi) = \text{const}$, we say the space is *flat*, otherwise the space is called *warped*.

The general proceeding in 5D theories is the following: Starting from a 5D action like (1.56), where the fifth dimension $x_5 = r\phi \in [-r\pi, r\pi]$ is now compactified, one derives the *equations of motion* (EOMs), which are differential equations the bulk fields need to obey, and the associated *boundary conditions* (BCs) by making use of the variational principle, i.e. requiring that $\delta S_5 = 0$. The variation of the action can then be written in the generic form

$$\delta S_5 = \int d^5x \delta\Phi (\mathcal{D}\Phi) + \int d^4x \delta\Phi (\mathcal{B}\Phi)|_{0,\pi}, \quad (1.62)$$

where Φ stands for any bulk field and \mathcal{D} and \mathcal{B} are differential operators. The idea now is to require both terms to vanish separately. The first term then leads to the equations of motion $\mathcal{D}\Phi = 0$. The second one determines the boundary conditions $\delta\Phi|_{0,\pi} = 0$ or $\mathcal{B}\Phi|_{0,\pi} = 0$, which the solutions to the EOMs have to satisfy. Note that the boundary terms originating from the orthogonal directions x are zero, since the fields Φ are assumed to vanish for $x^\mu \rightarrow \pm\infty$. Provided with the EOMs and BCs for the 5D fields we then make use of the KK decompositions of the form

$$\Phi(x, \phi) = \frac{e^{c_\Phi \sigma(\phi)}}{\sqrt{r}} \sum_n^\infty \Phi^{(n)}(x) \chi_n^\Phi(\phi), \quad (1.63)$$

where the factor $1/\sqrt{r}$ has been pulled out to arrive at the proper mass dimension for the KK modes $\Phi^{(n)}$. The factor $e^{c_\Phi \sigma(\phi)}$ (with a properly chosen constant c_Φ) cancels terms stemming from the 5D metric and thus ensures that the profiles $\chi_n^\Phi(\phi)$ can be interpreted as the localization of the KK modes along the extra dimension with respect to a flat metric. The profiles themselves obey the orthonormalization condition

$$\int_0^\pi d\phi e^{d_\Phi} \chi_n^\Phi(\phi) \chi_m^\Phi(\phi) = \delta_{nm}, \quad (1.64)$$

where d_Φ again depends on the specific field. Inserting the KK decomposition into the EOMs and BCs for the 5D fields can give rise to the corresponding conditions on the profiles, which will be derived for general $\sigma(\phi)$. Details about the derivations and explicit calculations can be found e.g. in the reviews [110, 111]. In the following sections, we will only work with the results, but we need to comment on some important features of extra dimensions:

- The orbifold construction (or, in general, the boundary conditions) can be used to remove unwanted degrees of freedom from the low-energy limit which is required for the SM to be compatible with the current measurements. Since the differential

operator \mathcal{D} is (essentially) a derivative on the field,³⁰ assigning fields with Z_2 -odd parity obeying *Dirichlet* (D) BCs

$$\Phi|_{\phi=0,\pi} = 0 \quad (1.65)$$

leads to a solution to the EOMs with $\Phi^{(0)} = \text{const} \equiv 0$ (once the KK decomposition has been inserted). This means that there is no massless zero mode in the theory. In contrast, fields obeying *Neumann* (N) BCs

$$\partial_\phi \Phi|_{\phi=0,\pi} = 0 \quad (1.66)$$

provide a zero mode $\Phi^{(0)} \equiv c$, where the constant c is determined by the normalization condition (1.64). Note that fields with at least one Dirichlet BCs lack a zero mode, as well.

- In general, couplings do not only depend on the coupling constant, but moreover on the so-called *overlap integrals*

$$\int_0^\pi d\phi e^{-b\sigma(\phi)} \chi_n^{\Phi_1}(\phi) \chi_m^{\Phi_2}(\phi) \chi_k^{\Phi_3}(\phi), \quad (1.67)$$

which give information about the strength of the interaction of the involved particles. Again, the constant b depends on the three involved particle species, see e.g. (1.76). Overlap integrals always appear in interactions of three or more KK-decomposed 5D fields and are important quantities for the following chapters.

- The treatment of fermions in extra dimensions requires further comments. For their description we first need a generalization of the gamma matrices. Since the Lorentz generators in five dimensions can be written as

$$M^{ab} \equiv \frac{i}{2} [\gamma^a, \gamma^b], \quad a, b \in \{0, 1, 2, 3, 5\} \quad (1.68)$$

as long as the 5D gamma matrices fulfill the Clifford algebra

$$\{\gamma^a, \gamma^b\} = 2\eta^{ab}, \quad (1.69)$$

we need to find the fifth gamma matrix obeying (1.69). A possible choice turns out to be

$$\gamma^a = \{\gamma^\mu, -i\gamma_5\}, \quad \mu \in \{0, 1, 2, 3\} \quad (1.70)$$

where the matrices γ^μ are the Dirac matrices and $\gamma_5 = i\gamma_0\gamma_1\gamma_2\gamma_3$. Recall that in four dimensions we can decompose the Dirac spinor in left- and right-handed Weyl spinors and furnish each of them with different quantum numbers like in the SM. In theories with an odd number of dimensions, however, the Dirac spinor representation is not reducible and an analogous decomposition is not possible. This can be understood by the fact that the matrix γ_5 that is used for the creation of left- and right-handed spinors via the projectors $P_{L,R} \equiv (1 \mp \gamma_5)/2$, is essentially the product of all 4D gamma matrices. Trying to build a corresponding matrix for chiralities in five dimensions we see that the product $i\gamma_0\gamma_1\gamma_2\gamma_3\gamma_5$ is the identity matrix and thus cannot be used to construct projection operators. Consequently, fermions in five or in any other odd number of extra dimensions

³⁰We will encounter various examples for this in the subsequent chapter.

are Dirac fermions. In order to arrive at the low-energy spectrum that contains the chiral SM fermions, we therefore need the orbifold construction (including the BCs) introduced above. Furthermore, in order to write down a Lorentz invariant action in a warped background, we define a tangent space in terms of the *vielbein* and the *spin connection*. The kinetic term for fermions can then be written as

$$\mathcal{L}_{\text{kin}}^{\text{ferm}} = r \int_{-\pi}^{\pi} d\phi \left\{ E_a^M \left[\frac{i}{2} \bar{Q} \gamma^a \left(\partial_M - \overleftarrow{\partial}_M \right) Q + \frac{\omega_{bcM}}{8} \bar{Q} \{ \gamma^a, \sigma^{bc} \} Q \right] - m \text{sgn}(\phi) \bar{Q} Q \right\}, \quad (1.71)$$

where E_a^M denotes the 5D vielbein,

$$G^{MN} = E_a^M E_b^N \eta^{ab}, \quad (1.72)$$

which becomes $E_a^M = \text{diag}(e^\sigma, e^\sigma, e^\sigma, e^\sigma, 1/r)$ in our background. The spin connection ω_{bcM} turns out to give no contribution to the action, see e.g. [111]. Note that the sign in front of the mass term is due to Z_2 parity assignments.

We now turn back to the importance of the orbifold construction. It can be shown that the variation of the 5D action (1.71) with respect to Ψ gives rise to two possibilities for the boundary conditions³¹

$$\begin{aligned} (N) &\equiv \Psi_R|_{0,\pi} = 0 \quad \rightarrow \quad \frac{1}{r} \partial_\phi \Psi_L|_{0,\pi} = (2\sigma' - m_\Psi) \Psi_L|_{0,\pi}, \\ (D) &\equiv \Psi_L|_{0,\pi} = 0 \quad \rightarrow \quad \frac{1}{r} \partial_\phi \Psi_R|_{0,\pi} = (2\sigma' + m_\Psi) \Psi_R|_{0,\pi}. \end{aligned} \quad (1.73)$$

This explicitly shows that compactification on an orbifold necessarily allows for BCs that distinguish the two chiralities, which will enable us to embed the SM structure. Both the Z_2 -even and Z_2 -odd functions can satisfy (N, N) , (N, D) , (D, N) , or (D, D) BCs. This fact can be used to construct the low-energy spectrum of the SM. As an example, consider the $SU(2)_L$ doublet fields $Q(x, \phi)$, which contain both chiralities $Q_L(x, \phi)$ and $Q_R(x, \phi)$. As the SM only contains left-handed doublets, it is appropriate to assign the left-handed components with a positive Z_2 parity and (N, N) BCs. According to (1.73), the right-handed components must then obey (D, D) BCs and thus cannot possess a zero mode. While at the zero-mode level the additional degrees of freedom have been removed, at the massive KK levels the number of degrees of freedom is doubled. Thus, instead of one, each fermion has two KK modes per KK level.

- A similar statement can be made for the gauge bosons. Amongst others, they are the two interesting possibilities

$$(N) \equiv \partial_\phi A_\mu|_{0,\pi} = 0, \quad A_5|_{0,\pi} = 0. \quad (1.74)$$

$$(D) \equiv A_\mu|_{0,\pi} = 0, \quad \partial_\phi [e^{2\sigma} A_5]|_{0,\pi} = 0. \quad (1.75)$$

We observe that, similar to the fermion case, the boundary conditions for A_μ and A_5 are correlated and we can again have arbitrary assignments for the BCs.

For (N, N) BCs, $\chi_0^A(\phi) = 1$ is always a solution for $m_0 = 0$. In this case, one finds $\chi_0^5(\phi) = 0$ so that no longitudinal polarization for the zero mode is provided and it remains massless. The fact that the zero mode is flat is closely related

³¹The ‘‘Neumann’’ BCs on the right-hand side are actually of mixed type, unless σ' and m_Ψ are zero.

to gauge invariance, and the necessary universality of the gauge interactions. If it was not flat, the non-trivial localizations of fermions or scalars would allow us to adjust their gauge couplings in an arbitrary way. As it happens, the overlap integrals arising from the gauge vertices have the form

$$\int_0^\pi d\phi \chi_0^A(\phi) \chi_n^\Psi(\phi) \chi_m^\Psi(\phi). \quad (1.76)$$

For a flat gauge-boson profile, this always reduce to the fermion orthonormality condition (1.64) (with $d_\Psi = 0$), so that the corresponding 4D gauge interactions are indeed universal. In contrast, the gauge invariance is broken at the massive KK level. For these modes, the fifth component acts as a Goldstone boson which is eaten to give the KK modes their masses. Thus, the physical massive KK spectrum consists only of massive spin-1 fields (with three physical polarizations each), and there are no massive physical scalars. Such massive gauge fields can and do have non-trivial profiles, so that their interactions with fermions or scalars can depend on the details of those fields.

For the (D, D) BCs, there is no massless spin-1 gauge boson, but there is a scalar with profile $\chi_0^5(\phi) \sim e^{2\sigma(\phi)}$. In the so-called gauge-Higgs unification models [116, 117], this spin-0 particle can be identified with the Higgs boson. Notice again that the profile of such a 4D scalar zero mode is fixed and no adjustable parameters to control its localization.

We are now furnished with everything that is needed to write down explicit extra-dimensional models. In the following, we will concentrate on the cases of flat and warped extra dimensions. Assuming symmetries that are compatible with the SM symmetries, we will specify the field content and look into the possible couplings of the KK particles to the zero modes, representing the SM fields, and to each other. The models will also be checked for consistency with current data, e.g. electroweak precision constraints or direct collider bounds.

1.4.3 Flat Extra Dimensions

The simplest extra-dimensional theories are given by models with flat extra dimensions, for which $\sigma(\phi) \equiv 0$ and the EOMs and BCs become very simple. In the following, we will first study a model that contains more than one extra dimension, the so-called ADD model. For this model, the previous discussion about theories with one additional extra dimension does not hold. The latter will become useful for Universal Extra Dimensions models, which can also have more than one dimension, but we will focus on the special case of one dimension here.

Arkani-Hamed, Dimopoulos, Dvali (ADD)

In 1998, Arkani-Hamed, Dimopoulos, and Dvali (ADD) invented a model with the goal to give an explanation to the hierarchy problem [118]. The idea was that gravitational forces had never been tested below 0.1 mm. One possibility for deviations from the $1/r$ behavior of Newton's potential could be due to additional compact spatial dimensions if gravity is allowed to propagate in the extra dimensions and feels the extra volume. These considerations support the following set-up: The space-time includes n additional extra

dimensions, all of them of size $\sim R$ for simplicity, compactified on an n -dimensional manifold with volume $\sim R^n$. While gravity is allowed to propagate in the bulk, all SM fields are assumed to reside on a 3-brane. Consequentially, only the graviton is accompanied by a finite tower of KK particles, which can be looked for in collider experiments. One may ask how this set-up can solve the hierarchy problem. As we deal with a theory of gravity in $d = 4 + n$ dimensions, Gauss' law leads to the gravitational potential for distances $r \ll R$

$$V(r) \sim -\frac{1}{M_d^{n+2}} \frac{1}{r^{n+1}}, \quad (r \ll R), \quad (1.77)$$

where M_d the fundamental Planck scale in d dimensions. For distances much larger than the size of the extra dimensions, $r \gg R$, the structure of the additional dimensions cannot be resolved and one observes the usual $1/r$ behavior

$$V(r) \sim -\frac{1}{M_d^{n+2} R^n} \frac{1}{r}, \quad (r \gg R). \quad (1.78)$$

An observer in four dimensions, who is ignorant to the existence of extra dimensions, would identify Newton's potential in four dimensions, so the effective 4D Planck scale can be written in terms of the fundamental quantities as

$$M_{\text{Pl}}^2 \equiv M_d^{n+2} R^n. \quad (1.79)$$

Hence, the reason for the huge effective 4D Planck mass and consequently the weakness of the gravitational interaction is due to the propagation of gravity into the extra dimensions and is attributed to the number of extra dimensions. The fundamental d -dimensional Planck scale, which sets the cutoff for the theory due to the relevance of gravity, is assumed to be

$$M_d \sim M_{\text{EW}} \quad (1.80)$$

or slightly larger, say in the TeV energy range. Therefore, quantum corrections to the Higgs mass have a cutoff at that scale and the hierarchy problem would vanish. The question now arises as to how many extra dimensions are required to obey (1.80). Let us focus on three cases (assuming $M_d = 1 \text{ TeV}$):

- $\underline{d = 5}$: In this case the radius of the extra dimension has to be $R \sim 10^{13} \text{ m}$, which would result in modifications of gravity at the scale of the solar system. Clearly, such a scenario can be ruled out.
- $\underline{d = 6}$: For two extra dimensions the radius has to be $R \sim 10^{-4} \text{ m}$, which can be accessed by gravitational experiments. Nowadays, gravitational precision measurements can probe these scales and one finds $R \leq 44 \mu\text{m}$ [119]. This scenario seems to be ruled out, either. However, one can relax the above value for the fundamental energy scale and assume e.g. $M_d \gtrsim 7 \text{ TeV}$, which would result in a radius that is below the current experimental bound. Although this relative high cutoff scale would introduce another hierarchy, the situation would still be much better than in the SM. There are, however, strong bounds from astrophysics that exclude this scenario as well.
- $\underline{d \geq 7}$: For three and more dimensions, the size of the extra dimensions cannot be examined by gravitational tests, but rather by e.g. collider or astrophysical experiments.

Before we present the current bounds from these experiments, we dwell on some shortcomings of theories with large extra dimensions. The first one is the question of why the extra dimensions are so much larger than their natural size M_d^{-1} ,

$$\frac{R}{(M_d)^{-1}} = \left[\frac{M_{\text{Pl}}}{M_d} \right]^{\frac{2}{n}}. \quad (1.81)$$

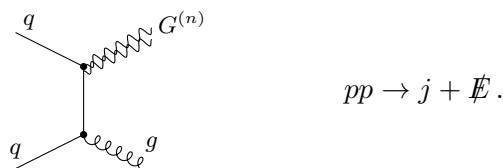
which seems to be just a reintroduction of the hierarchy problem. Nevertheless, the situation is slightly better, because there is no problem of the radiative instability of the large separation between two fundamental scales any more, similar to the μ problem in supersymmetric theories. Note that taking the limit $n \rightarrow \infty$ could circumvent this problem, since in this set-up the fundamental Planck scale just needs to be infinitesimally larger than M_{EW} to arrive at the large effective Planck scale (1.79).

Another issue of a relatively low energy cutoff is that higher-dimensional operators giving rise to FCNCs are not sufficiently suppressed. In other words, the flavor problem is not addressed in these models. Like in SUSY, one can introduce additional gauge symmetries (e.g. baryon- or lepton-number conservation). Another possibility is to allow the fermion fields to propagate in the bulk and to adjust their localization appropriately. This is the so-called *fat brane* or *split fermion* scenario, in which the couplings between the different fermion fields may be suppressed due to a small overlap of the profiles induced on the brane [120]. The same mechanism can explain the flavor problem in RS models, as we will see in the subsequent section.

Let us finally consider the current experimental bounds on large extra dimensions. The mass of the k^{th} KK mode of the graviton is $m_k \sim k/R$, where the mass differences are given by the inverse radius

$$\Delta m \sim \frac{1}{R} \sim M_d \left(\frac{M_d}{M_{\text{Pl}}} \right)^{\frac{2}{n}} \sim 10^{12 - \frac{32}{n}} \text{ eV}. \quad (1.82)$$

For $n = 4$ ($n = 6$) the mass spacing is ~ 0.01 MeV (~ 0.01 GeV), which gives rise to the interesting feature of an almost continuum spectrum of graviton states given that the number of extra dimensions is not too large. Hence, one can expect to find signals of plenty of KK modes at colliders. Since gravity couples to all particles, the KK gravitons can decay into all SM fields with universal strength $\sim M_{\text{Pl}}^{-1}$ and, consequently, any single graviton is negligible. Only summing up the complete tower leads to an observable effect. Due to the weakness of the coupling between SM particles and KK gravitons, the KK lifetime is large and the would-be stable KK gravitons can escape the detectors if produced at an accelerator. The final state is thus characterized by missing energy. As in generic dark matter searches, a characteristic signal at the LHC is then a mono-jet plus missing energy³²



The current LHC measurements require [122]

$$M_6 > 4.37 \text{ TeV}, \quad (1.83)$$

³²More details on collider signatures of large extra dimensions can be found in [121].

which disfavors a natural solution for the hierarchy problem. The most stringent bounds, however, come from astrophysics, in particular supernova collapses. In these collapses, the gravitational energy is carried away by neutrinos. Clearly, the KK gravitons can also carry away energy leading to a faster cooling. As the measured flux of neutrinos is in agreement with the theoretical predictions, bounds on the fundamental Planck scale can be derived [123]

$$M_6 \geq 50 \text{ TeV}, \quad M_7 \geq 4 \text{ TeV}, \quad M_8 \geq 1 \text{ TeV}. \quad (1.84)$$

We see that these results exclude the possibility of the ADD model to address the hierarchy model for the scenario $n = 2$ (without much fine-tuning). On the other hand, scenarios with a larger number of dimensions are still possible.

Universal Extra Dimensions (UED)

One quickly realized that the most straightforward way to build a theory in more than four dimensions is to put all SM fields into a flat space-time with N additional dimensions. These classes of models are called *Universal Extra Dimension* (UED) models [124] and have some remarkable features. Although these models can have several extra dimensions, we focus on the minimal version of UED models with one additional spatial dimension. In this case, since the radius is $r \approx (1 \text{ TeV})^{-1}$ in order to be compatible with the electroweak precision data [125], the fundamental cutoff has to be $M_5 \sim 10^{15} \text{ GeV}$. As a consequence, the hierarchy problem is not addressed in UED models with one additional spatial dimension.

Due to the fact that $\sigma(\phi) = 0$, it turns out that the EOMs reduce to

$$\left[\frac{1}{r^2} \partial_\phi^2 + (m_n^2 - m_5^2) \right] \chi_n(\phi) = 0, \quad (1.85)$$

where the 5D mass m_5 can only be non-zero for scalar bosons and fermions, whereas gauge invariance requires $m_5 = 0$ for gauge bosons. Applying Neumann BCs for the fields whose zero modes represent the SM fields, while all remaining ones, such as the right-handed fermion $SU(2)_L$ doublets and the fifth component of the 5D gauge fields, obey Dirichlet BCs, we find the solutions

$$\chi_n(\phi) = \sqrt{2} \cos(\tilde{m}_n r \phi), \quad (1.86)$$

with the mass eigenvalues $\tilde{m}_n = \sqrt{n^2/r^2 - m_5^2}$. The solutions obeying Dirichlet BCs are sines. Sines and cosines are very special in the sense that they lead to certain selection rules. In fact, it can be shown that this selection rule can be generalized to

$$n_1 \pm n_2 \pm \dots \pm n_N = 0 \quad (1.87)$$

for an interaction of N particles. These selection rules have the important consequence that at tree-level KK states can only be pair produced as indicated by the left diagram in Figure 1.6. However, at one-loop the selection rule allows the production of a single KK particle with e.g. $n = 2$, shown in the right diagram in Figure 1.6. The fact that single KK modes cannot be produced at tree level can be traced back to the invariance of the 5D theory under the transformations [111]

$$\Phi_n \rightarrow (-1)^n \Phi_n, \quad (1.88)$$

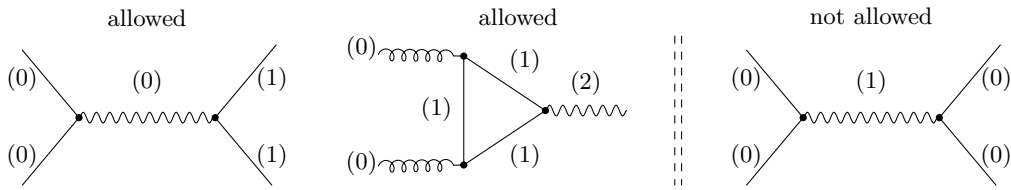


FIGURE 1.6: (Not) Allowed processes in UED models shown on the left (right). Note that at tree-level KK states can only be pair produced, whereas the production of one KK particle is possible at one-loop order.

where Φ stands for any bulk field. This symmetry, called *KK parity*, is a space-time symmetry and follows from the invariance under a reflection about the middle of the interval π :

$$\Phi(x, \phi) \rightarrow (\pm)\Phi(x, \pi - \phi), \quad (1.89)$$

where the sign depends on the specific type of field.³³ It is an exact symmetry and the resulting selection rule is responsible for the loop-suppression of single KK-mode production (for an even KK number). Note that the KK parity also ensures that the lightest KK particle cannot decay into SM particles and is therefore stable. Even though the KK masses of all particle species are degenerate at tree-level, the physical spectrum is non-degenerate once radiative corrections to the masses are taken into account. The *lightest KK particle* (LKP) turns out to be the KK photon, while the KK gluon is the heaviest, similar to the spectrum in the MSSM [126]. As pointed out in [127], a 600 GeV KK photon could explain the relic abundance of dark matter in the universe and is therefore an ideal DM candidate.³⁴ For these masses, the electroweak precision measurements [125, 130] and the FCNCs bounds [131, 132] are satisfied as well. One may ask what the current bounds from collider searches are. Due to the split particle spectrum, the KK modes can undergo a cascade of decays, similar to SUSY, where the sparticles are replaced by the KK modes of the respective SM particles, see [133] for a detailed overview of the possible decay chains. Note that the similarity between the MSSM and mUED is not accidental, since SUSY can be thought of as a theory with additional (non-commutating) dimensions. One could discriminate the two models if one detected the second photon KK mode $\gamma^{(2)}$ via the decay into two hard leptons or via a study of the charge asymmetry in the lepton-jet invariant mass distributions from a particular cascade, see [134] for further details. The current limit from direct searches is [135]

$$r^{-1} > 1.41 \text{ TeV}, \quad (1.90)$$

which stems from the search after three soft leptons, jets, and missing energy. We wrap up this discussion of universal extra dimensions with the current limit from indirect Higgs searches, see Section 5.1, which gives $r^{-1} > 500 \text{ GeV}$ [136].

³³Moreover, there is a γ_5 matrix in the case of a fermion field, see [111].

³⁴It is reported in [127] that the Wilkinson Microwave Anisotropy Probe (WMAP) observations [128, 129] impose an upper bound on the KK photon mass of 1.6 TeV.

1.4.4 Warped Extra Dimensions

We now turn to the case of warped extra dimensions which offer an elegant way to address the hierarchies of the SM by means of a non-trivial geometry in a slice of the five-dimensional AdS₅ space. As before, the extra dimension is assumed to be an S^1/Z_2 orbifold, with the parametrization $\phi \in [-\pi, \pi]$. Two branes are localized on the orbifold fixed-points $\phi = 0$, referred to as the *Planck* or *UV brane* and $|\phi| = \pi$, referred to as the *TeV* or *IR brane*. The meaning of these names will become clear later on. The size r and curvature k of the extra dimension are assumed to be of Planck size, $k \sim 1/r \sim M_{\text{Pl}}$. In the above parametrization, the function $\sigma(\phi)$ is $\sigma(\phi) = kr|\phi|$, so that the metric reads

$$ds^2 = G_{MN} dx^M dx^N = e^{-2kr|\phi|} \eta_{\mu\nu} dx^\mu dx^\nu - r^2 d\phi^2, \quad (1.91)$$

which is not invariant under the transformations (1.89). Consequentially, there is no LKP and this in turn means that there are no viable DM candidates in theories with one warped extra dimension (if no further discrete symmetry is imposed).

The metric (1.91) can be derived with the help of Einstein's equations [115]. In the original RS set-up, only gravity is allowed to propagate in the bulk and the general action in a slice of AdS₅ can be written as

$$S = S_{\text{bulk}} + S_{\text{UV}} + S_{\text{IR}}, \quad (1.92)$$

with

$$\begin{aligned} S_{\text{bulk}} &= \int d^4x \int_{-\pi}^{\pi} d\phi \sqrt{G} \left\{ -\Lambda - 2M^3 r \right\}, \\ S_{\text{UV}} &= \int d^4x \sqrt{-g_{\text{UV}}} \left\{ \mathcal{L}_{\text{UV}} - V_{\text{UV}} \right\}, \\ S_{\text{IR}} &= \int d^4x \sqrt{-g_{\text{IR}}} \left\{ \mathcal{L}_{\text{IR}} - V_{\text{IR}} \right\}, \end{aligned} \quad (1.93)$$

where Λ is the 5D cosmological constant and M is the fundamental scale of the theory. The Lagrangians $\mathcal{L}_{\text{UV,IR}}$ define the 4D theories on the AdS boundaries, e.g. $\mathcal{L}_{\text{IR}} = \mathcal{L}_{\text{SM}}$ and $\mathcal{L}_{\text{UV}} = 0$ if the SM is confined on the IR brane. The *vacuum energies* $V_{\text{UV,IR}}$ on the branes, so-called *brane tensions*, are needed to allow for a non-trivial metric, as we will see below. The induced 4D metrics are given by the 5D metric evaluated at the boundaries

$$g_{\text{UV}}^{\mu\nu}(x) = G^{\mu\nu}(x, \phi = 0), \quad g_{\text{IR}}^{\mu\nu}(x) = G^{\mu\nu}(x, \phi = \pi). \quad (1.94)$$

In order to solve the Einstein's equations that follow from the above set-up, one inserts the metric (1.91) and finds [115]

$$k = \sqrt{\frac{-\Lambda}{24M^3}}, \quad V_{\text{UV}} = -V_{\text{IR}} = 24M^3 k. \quad (1.95)$$

Note that there is no reason for this coincidence except for the stabilization for the set-up and the requirement for a flat brane metric. The situation is similar to the cosmological constant problem in the SM. The compactification radius is not set by this relation but once it takes on its value, the set-up remains stable. The radius itself is the 55-component of the metric tensor and can be fixed via a Goldberger-Wise mechanism [137], in which interaction with a bulk scalar induce a potential for this field, see [138] for details. The above set-up can now be used to solve the hierarchy problem.

Solution to the Hierarchy Problems

Warped extra dimensions turned out to be an excellent possibility to solve the hierarchy problems of the SM. Having the complete SM including the Higgs confined on the IR brane, one could not only explain, why the Higgs mass receives small contributions, but also why it is so small compared to the Planck scale. To understand this, let us have a look at the Higgs Lagrangian that is fixed on the IR brane

$$S_{\text{Higgs}} = \int d^4x r \int_{-\pi}^{\pi} d\phi \mathcal{L}_{\text{Higgs}}, \quad \mathcal{L}_{\text{Higgs}} = \delta(|\phi| - \pi) \frac{\sqrt{G}}{r} \left\{ G^{\mu\nu} (D_\mu \Phi)^\dagger D_\nu \Phi - V(\Phi) \right\}, \quad (1.96)$$

where the 5D Higgs potential can be parametrized as

$$V(\Phi) = \frac{\lambda_5}{2} \left(\Phi^\dagger \Phi - \frac{v_5^2}{2} \right)^2. \quad (1.97)$$

The subscripts indicate that the parameters are the fundamental input parameters of the 5D theory. While λ_5 is dimensionless and is thus assumed to be of $\mathcal{O}(1)$, the 5D vev v_5 is assumed to be of the order of the Planck scale M_{Pl} like all dimensionful parameters in the theory. Inserting the 5D metric (1.61) and redefining the Higgs field via $\Phi(x) \rightarrow e^{kr\pi} \Phi(x)$ in order to arrive at a canonically normalized kinetic term, we find that the action can be written as

$$S_{\text{Higgs}} = \int d^4x \sqrt{-g_{\text{IR}}} \left\{ g_{\text{IR}}^{\mu\nu} (D_\mu \Phi)^\dagger D_\nu \Phi - \frac{\lambda_5}{2} \left(\Phi^\dagger \Phi - e^{-2kr\pi} \frac{v_5^2}{2} \right)^2 \right\}, \quad (1.98)$$

where g_{IR} is the induced metric on the IR brane, defined in (1.94). Something remarkable has been happened here: The warp factor $e^{-kr\pi}$ has been moved in front of the 5D vev v_5 and reduces the effective vev in the 4D theory to

$$v = e^{-kr\pi} v_5. \quad (1.99)$$

This so-called *warping* of the vev holds for any dimensionful parameter in the theory (note that the dimensionless parameter λ_5 remains unaffected) and is depicted in Figure 1.7. In particular the 5D Higgs mass is reduced to $m_h = e^{-kr\pi} m_{h,5}$. Starting with Higgs mass of around $m_{h,5} \lesssim k \lesssim M_{\text{Pl}}$, one would arrive at a natural value for $m_h \sim \mathcal{O}(M_{\text{EW}})$ with a modest tuning

$$L \equiv kr\pi \approx 37, \quad (1.100)$$

where the parameter L is referred to as the *volume* of the RS space. The fact that the 5D Higgs mass is somewhat below the curvature and the Planck scale is due to the fact that these two scales define the masses of the KK excitations and the UV cutoff of the theory as will be explained below. We now see the effect of the non-trivial geometry (1.91) we have started with. Although all dimensionful parameters of the 5D theory are of $\mathcal{O}(M_{\text{Pl}})$, the warp factor gives rise to a mass of the IR-localized Higgs of the $\mathcal{O}(M_{\text{EW}})$. The warping also ensures that the quantum corrections to the Higgs mass are under control: As has been explained in detail in Section 1.4.2 RS models are effective field theories defined with an intrinsic cutoff that is chosen to be $\Lambda_{\text{UV}} \sim M_{\text{Pl}}$. At this energy scale, the theories have to be replaced by a more fundamental theory that provides a description of quantum gravity. Like all energies scale, this cutoff now depends on the

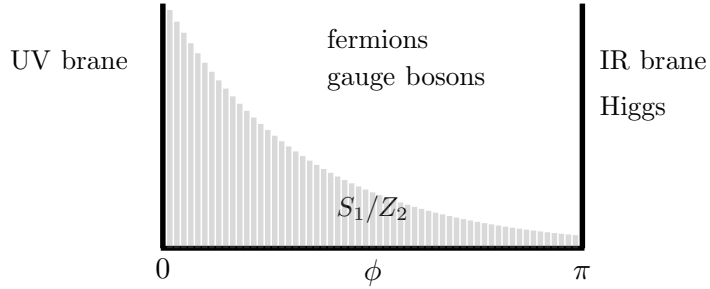


FIGURE 1.7: Illustration of the Randall-Sundrum set-up. While all other fields are allowed to propagate in the bulk, the Higgs is assumed to be localized on the IR brane. The effect of the warp factor on dimensionful parameters is indicated by the gray lines.

position in the extra dimension [139–143]

$$\Lambda_{\text{UV}}(\phi) \sim e^{-\sigma(\phi)} M_{\text{Pl}}. \quad (1.101)$$

In loop calculations this position-dependent scale sets the cutoff for the 4D (euclidean) loop momentum $p_E^2 \equiv -p^2$ on which the cutoff should be imposed [144]. Thus, confining the SM on the IR brane just gives contributions to the Higgs mass that are quadratically dependent on the warped Planck scale at $\phi = \pi$

$$\Lambda_{\text{TeV}} \equiv e^{-kr\pi} M_{\text{Pl}} = \epsilon M_{\text{Pl}} = \mathcal{O}(\text{several TeV}). \quad (1.102)$$

Consequently, there are no huge radiative corrections to the Higgs mass. As we will see below, it turned out to be convenient to allow all SM fields but the Higgs to propagate in the bulk. One may wonder how the fact of having bulk fields in the theory affects the previous discussion. In this case, the position-dependent cutoff is associated with every vertex of a Feynman diagram. This can be thought of as modeling the effect of a form factor, which accounts for the impact of quantum gravity on energy scales above the effective Planck scale at that point. In general, the coordinates ϕ_i of the vertices are integrated over the entire bulk ($0 \leq \phi_i \leq \pi$), and therefore the cutoff values vary between the TeV scale and the fundamental Planck scale.³⁵ In one-loop diagrams containing the Higgs boson, such as the Higgs self-energy diagram discussed in Section 1.3.1, the situation simplifies considerably, since in that case [144]

$$\begin{array}{c}
 \phi_1 \quad \phi_2 \\
 \circ \quad \circ \\
 \leftarrow \quad \rightarrow \\
 \text{---} \bullet \text{---} \text{---} \bullet \text{---} \text{---} \\
 \leftarrow \quad \rightarrow \\
 \circ \quad \circ \\
 \phi_1 \quad \phi_2
 \end{array}
 \quad p_E \leq \min \{ \Lambda_{\text{UV}}(\phi_1), \Lambda_{\text{UV}}(\phi_2) \} = \Lambda_{\text{TeV}}. \quad (1.103)$$

Hence, the above conclusion also holds true in the case of bulk fermions and gauge bosons. Note that the Higgs mass dependence on Λ_{TeV} , which is at least one order above M_{EW} , leads to the already mentioned little hierarchy problem which turns out to be more severe than in other possible extensions of the SM model. With the help of NDA one can estimate the one-loop correction to the Higgs mass [145]

$$\delta m_h^2 \sim \frac{\Lambda_{\text{UV}}^2(\pi)}{16\pi^2} \frac{\Lambda_{\text{UV}}^2(\pi)}{M_{\text{KK}}^2}, \quad (1.104)$$

³⁵This effect makes gauge-coupling unification possible in warped extra-dimension models [139–143].

which shows that the mass is sensitive to the cutoff to the fourth power. Thus, some fine-tuning is necessary in minimal RS models. The situation is, however, still better than in the SM, since at least the large hierarchy problem is solved.

As already mentioned above, in their original paper [115] Randall and Sundrum proposed to confine all SM field on the IR brane. One quickly realized that this leads to serious problems, since the fundamental cutoff scale is not large enough to suppress higher-dimensional operators (induced, for example, via an exchange of KK gravitons) that could lead to dangerous FCNCs or proton decay. In order to solve this, one puts all fields except for this Higgs into the bulk. Performing the steps explained in the previous section, one then finds that due to the warping the solutions for the profiles of the KK modes are Bessel instead of trigonometric functions and that the zero-mode profiles are given by (see e.g. [110])

$$\begin{aligned}
 \text{Scalars:} & \quad \chi_0^\Phi(\phi) \sim e^{(1 \pm \sqrt{4+c^2})kr|\phi|}, \\
 \text{Fermions:} & \quad \chi_0^{L,R}(\phi) \sim e^{(\frac{1}{2} \pm c_{L,R})kr|\phi|}, \\
 \text{Gauge Bosons:} & \quad \chi_0^A(\phi) \sim 1,
 \end{aligned} \tag{1.105}$$

where $c_i = M_{i5}/k$ denote the normalized bulk masses for the scalars and fermions, respectively. While the profiles of the KK excitations are peaked towards the IR brane and cannot be changed, the *bulk mass parameters* c_i can be used to localize the zero mode anywhere in the bulk. Note that for the zero mode of the gauge bosons such a freedom is not possible, since gauge-invariance forbids a 5D bulk mass term. In the case of the fermions, which is important for the rest of this discussion here, the (left-handed) zero mode can either be localized near the UV ($c_L < -1/2$) or the IR brane ($c_L > -1/2$).³⁶ This has two appealing effects: The first one is the explanation of the SM fermion masses and mixings. It is obvious that the mass of a particle is directly related to the coupling to the Higgs field or, equivalently, the overlap with the IR brane. This fact together with the observation that the fermion zero modes can be localized anywhere in the bulk can explain why the light quarks and leptons have small, whereas the top quark has large masses. Adjusting the localization parameters in such a way that the light (heavy) particles are localized towards the UV (IR) brane naturally explains the huge differences in the SM fermion masses. The structure of the mixing angles can be explained in a similar way. Although one is still forced to adjust certain input parameters, it is a great achievement of the RS model to allow for $\mathcal{O}(1)$ input parameters which, together with the non-trivial geometry, lead to the hierarchical structure of the SM. The situation is visualized in Figure 1.8. The second benefit of having 5D fermion and gauge boson fields is the suppression of the above-mentioned higher-dimensional operators. Note that the suppression by the (position-dependent) cutoff depends on where the zero modes of the fermions and gauge bosons are localized. The more the involved particles are localized near the UV brane the stronger is the higher-dimensional operator suppressed. This means that the operators involving the light quarks are suppressed by their small masses. This is the so-called *RS-GIM mechanism*. Both the generation of the hierarchies in the fermion sector of the SM and the RS-GIM mechanism will be explained in more detail and more quantitatively in Section 2.2.3.

³⁶The right-handed spinor is UV (IR)-localized for $c_R > 1/2$ ($c_R < 1/2$).

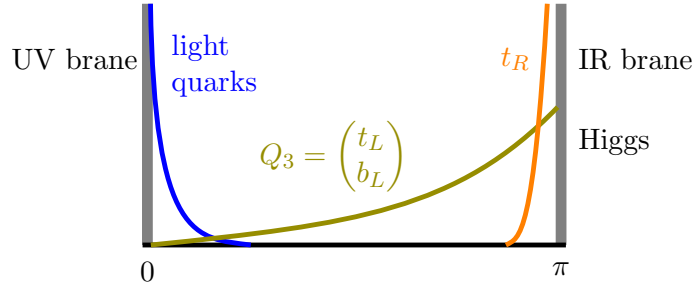


FIGURE 1.8: Visualization of the mechanism that generates the hierarchical structure in the quark sector of the SM. Light quarks are UV-localized and hence have a small overlap with the Higgs field localized on the IR brane. In contrast, the three-generation quarks have larger masses due to their larger overlap with the IR-localized Higgs doublet.

Connection to Strongly-Coupled Theories

We want to close this section with the remark of which scenario (symmetry or strongly-coupled) theories with warped extra dimensions belong to. As a matter of fact, the *AdS/CFT correspondence* conjectured by Maldacena in 1997 [42] states that (weakly-coupled) RS models are dual to strongly-coupled conformal field theories (CFTs) in four dimensions. Thorough discussions of the correspondence and possible applications can be found in [22, 110, 146]. Here we shall briefly explain the dual theory of an RS model with bulk fermions and gauge bosons and an IR-localized Higgs sector. The idea is that each position in the anti-de Sitter space AdS_5 corresponds to an energy scale in the dual 4D theory. For every 5D bulk field Φ living in AdS_5 there is an associated operator \mathcal{O} in the dual theory

$$\Phi(x, x_5) \iff \text{CFT operator } \mathcal{O}, \quad (1.106)$$

where the boundary value of the bulk field

$$\Phi(x, x_5) \Big|_{\text{AdS boundary}} \equiv \phi_0(x) \quad (1.107)$$

acts as a non-dynamical *source field* for the CFT operator \mathcal{O} if the full AdS_5 space ($-\infty \leq x_5 \leq \infty$) is considered. Once one defines a theory in a slice of AdS_5 ($0 \leq x_5 \leq \pi r$), the source field can become dynamical and is part of the 4D Lagrangian. As opposed to the operator \mathcal{O} , which represents composite states in the 4D dual theory, it is regarded as elementary up to energies of Λ_{UV} , which is the scale where in the 4D theory the conformal symmetry is *explicitly* broken. In the 5D theory gravity this scale corresponds to the energy where gravity gets strong at the UV brane.³⁷ In this picture, the holographic interpretation of a UV-localized field is that it is purely elementary, while a field which is completely localized on the IR brane, such as the Higgs boson, is purely composite. The hierarchy problem is then solved in the same way as explained in Section 1.3.2. Bulk fields, on the other hand, are partially elementary, partially composite. The degree of compositeness is determined by the mixing term $\phi_0 \mathcal{O}$, which in turn is dependent on the *scaling dimension* of the operator. To be more precise, let us consider the holographic interpretation of a 5D bulk fermion. As shown in [147], the

³⁷This is actually the reason for the name of the UV and IR branes, respectively.

dual Lagrangian for (left-handed) fermions at scale $M \sim \Lambda_{\text{UV}} = \mathcal{O}(M_{\text{Pl}})$ is given by

$$\mathcal{L} = \mathcal{L}_{\text{el}} + \omega M^{1-|c-\frac{1}{2}|} (\bar{\psi}_L^0 \mathcal{O}_R + \text{h.c.}) + \mathcal{L}_{\text{CFT}}, \quad (1.108)$$

where c is the bulk mass parameter localizing the zero mode in the extra dimension, see (1.105), ω is a dimensionless constant, and $M = \mathcal{O}(M_{\text{Pl}})$ is the fundamental energy scale of the theory. The scaling dimension of operator \mathcal{O}_R is $\dim \mathcal{O}_R = 4 - 3/2 - 1 + |c - 1/2| = 3/2 + |c - 1/2|$. At the compositeness scale Λ_{IR} , where the conformal theory is *spontaneously* broken, the operator $\mathcal{O}_R(x)$ represents a composite bound state in a strongly-coupled theory. Using the notation of Section 1.3.2, the Lagrangian Λ_{IR} can be written as

$$\mathcal{L} = \mathcal{L}_{\text{el}} + \omega M \left(\frac{\Lambda_{\text{IR}}}{M} \right)^{|c-\frac{1}{2}|} (\bar{\psi}_L^0 \mathcal{O}_R + \text{h.c.}) + \mathcal{L}_{\text{CFT}}. \quad (1.109)$$

Comparing this with (1.38), we can identify $|c - 1/2| = 3 - \gamma$ so that the anomalous dimension of the CFT sector is directly related to the localization parameter in the 5D bulk theory. Thus, the degree of compositeness of fermions is given by the localization parameter c . For $c < -1/2$, the mixing is irrelevant and there is almost no mixing between the elementary and the composite state. The massless KK mode is then predominantly given by the elementary source field [148]. For $-1/2 < c < 1/2$, the mixing becomes relevant, which results in a partially composite fermion. For $c > 1/2$, it turns out that the Lagrangian (1.108) does not hold any more [147]. We do not go into detail here, but note that in this case a second elementary field emerges, which couples to the source field via a (Planck) mass term so that both decouple from the theory. The CFT spectrum, on the other hand, contains an ultralight composite state that can be identified with the zero mode. Thus, for $c > 1/2$, the zero mode is almost fully composite.

We finally comment on the holographic description of a bulk gauge field. The dual Lagrangian for the gauge bosons reads (see e.g. [110])

$$\mathcal{L} = -\frac{1}{4} F_{\mu\nu}^a(x) F^{\mu\nu,a}(x) + \omega A_\mu^a(x) \mathcal{O}^{\mu,a}(x) + \mathcal{L}_{\text{CFT}}. \quad (1.110)$$

Since the source fields $A_\mu^a(x)$ represent gauge fields, they couple to conserved currents $\mathcal{O}^{\mu,a}(x)$ of the CFT. From this we can deduce that a bulk gauge group implies a global symmetry of the dual theory, where only a subgroup is gauged, namely that whose gauge fields obey Neumann boundary conditions on the UV brane. Note, however, that the global symmetry is still present in the CFT sector.³⁸

In summary, an RS model with bulk fermions and gauge bosons and a Higgs sector localized on the IR brane is dual to a strongly-coupled 4D theory, where the Higgs boson is fully composite and the duals of the bulk fields (which obey Neumann BCs on the UV brane) are partially elementary and composite. The degree of compositeness of the fermions depends on the bulk mass parameters. The dual of the bulk symmetry is a global symmetry in the strong sector, where only the part of the full gauge group is gauged whose gauge fields obey Neumann UV BCs. The dual theory will become a useful tool to explain certain results in the subsequent chapter.

³⁸The idea of imposing a global symmetry in the CFT sector by choosing the proper bulk symmetry was the motivation for the $SU(2)_L \times SU(2)_R$ bulk gauge group in the RS model with custodial protection, see Section 2.3.

Chapter 2

Models with Warped Extra Dimensions

In this chapter, the two versions of the Randall-Sundrum model the main part of this thesis is based on will be presented. The general RS set-up has already been explained in Section 1.4.4. We have seen that while the Higgs has to be confined on the IR brane in order to cure the fine-tuning problem in the Higgs sector, the matter and gauge fields are desired to propagate in the bulk in order to give an explanation for the fermion hierarchies. The two versions of the RS model differ in the respective gauge group imposed in the bulk. The first one is the so-called *minimal* RS model, whose underlying gauge group is the well-known SM gauge group $\mathcal{G}_{\text{SM}} = SU(3)_c \times SU(2)_L \times U(1)_Y$. As we will see, this set-up leads to generically too large contributions to some of the electroweak precision observables. A viable way to reduce these large contributions is to enlarge the bulk gauge group to $\mathcal{G}_{\text{cust}} = SU(3)_c \times SU(2)_L \times SU(2)_R \times U(1)_X \times P_{LR}$. This so-called *custodial* RS model is able to provide KK particles that could be in reach of direct detection at the LHC and is phenomenologically more viable.

In the following, we will first take into consideration the possibility of having a bulk instead of a brane Higgs in Section 2.1. We will then turn to the minimal version of the RS model in Section 2.2, where we will concentrate on the gauge-boson and fermion sector and the derivation of the corresponding KK profiles and masses. Moreover, it will be shown explicitly how the parameters of the SM quark sector can be generated by $\mathcal{O}(1)$ input parameters and how the RS-GIM mechanism works. Finally, we will check the model for compatibility with electroweak precision tests. Section 2.3 is then dedicated to the custodial model. The proceeding is analogous to the minimal model, where it will be focused on the differences and the compatibility with the electroweak precision measurements.

This chapter is based on [145, 149], but also includes contents of my publications [150, 151] as well as [105, 152].

2.1 Brane-Localized and Bulk-Higgs Scenarios

As in the original version of the Randall-Sundrum model, the extra dimension of the minimal as well as the custodial model is taken to be an S^1/Z_2 orbifold, labeled by the coordinate $\phi \in [-\pi, \pi]$ and bounded by the UV ($\phi = 0$) and the IR brane ($\phi = \pi$). The

RS metric is given by (1.91),

$$ds^2 = e^{-2\sigma(\phi)} \eta_{\mu\nu} dx^\mu dx^\nu - r^2 d\phi^2 = \frac{\epsilon^2}{t^2} \left(\eta_{\mu\nu} dx^\mu dx^\nu - \frac{1}{M_{\text{KK}}^2} dt^2 \right). \quad (2.1)$$

Here, we have introduced the new coordinate

$$t = \epsilon e^{\sigma(\phi)}, \quad \epsilon = e^{-\sigma(\pi)}, \quad (2.2)$$

where $\sigma(\phi) = kr|\phi|$ and $M_{\text{KK}} = k\epsilon$ sets the mass scale for the low-lying KK excitations of the SM particles, as we will see in Section 2.2.1.¹ This notation avoids disturbing exponential factors so that calculations and expressions become more clearly structured and more compact, respectively.

The primary focus of this thesis is put on models where the scalar sector is localized on (or very near) the IR brane at $t = 1$. Not only do these models give a solution to the hierarchy problem but they also define important benchmark scenarios that should be investigated first. Furthermore, we will see in Chapter 4 that only in these cases closed, analytic expressions, e.g. for the production and decay amplitudes of the Higgs boson, can be derived. Nevertheless, several results in the main part of this thesis will also be valid for more involved (but perhaps more natural) models in which the Higgs boson is a 5D field propagating in the extended bulk of the extra dimension. According to the discussion below equation (1.101), the hierarchy problem would still be solved in these models if the Higgs field was localized sufficiently near the IR brane. A comprehensive study of the generic set-up of these models and their potential to address the hierarchy problems of the SM is beyond the scope of this work and can be found in [100, 117, 153–156]. It will, however, be useful to derive certain quantities in these bulk-Higgs models, like the W -boson zero-mode profile or the associated 5D propagator. Therefore, the following two sections do not only contain the presentations of the minimal and the custodial RS model with a brane-localized Higgs sector that follow the discussions of [145, 149], respectively, but there will also be two subsections dedicated to what changes in models with a bulk Higgs. Thereby, it will only be focused on quantities that will be crucial for the main part of this thesis.

In this context, it is useful to make a few comments concerning the definition of a brane-localized Higgs sector, which is general enough to allow for a non-zero width of the Higgs profile, as long as it cannot be resolved by the modes of the theory and hence does not affect any observables. Recall that RS models are effective field theories with an inherent, position-dependent UV cutoff (1.101). As argued in the discussion below (1.103), the scale Λ_{TeV} also provides the effective UV cutoff in loop graphs involving Higgs bosons. The condition that the fermionic modes in the effective theory cannot resolve the width of the Higgs boson can be stated as

$$\eta \ll \frac{v|Y_q|}{\Lambda_{\text{TeV}}} \quad (\text{brane-localized Higgs}), \quad (2.3)$$

where $|Y_q|$ sets the scale for the dimensionless 5D Yukawa couplings of the model, see below. Only when this condition is satisfied, the Higgs field can be regarded as being localized on the IR brane in the sense that any possible extension into the bulk does not give rise to observable effects. This scenario is referred to as the *brane-Higgs* scenario. Relation (2.3) should be considered as a condition on the regulator η at fixed, physical

¹The dimensionless variable $t \in [\epsilon, 1]$ is related to the conformal coordinate z frequently used in the literature by the simple rescaling $z = t/M_{\text{KK}} \equiv R't$.

UV cutoff Λ_{TeV} . For a brane-localized Higgs field one should take the limit $\eta \rightarrow 0$ wherever possible, but the above condition states that keeping η finite but smaller than the bound on the right-hand side would not change the physics.

A Higgs profile with a width $\eta > v|Y_q|/\Lambda_{\text{TeV}}$ must be regarded as a bulk field. The features of the Higgs profile can then be resolved by the fermionic high-momentum states in the effective theory, and indeed we will find in Section 4.1 that high-mass KK fermions make sizable contributions. In the general case, amplitudes in a *bulk-Higgs scenario* of the RS model depend in a complicated way on the shapes of the Higgs and the involved fermion or gauge-boson profiles along the extra dimension. However, we will find that for a narrow Higgs profile, defined by the relation

$$\frac{v|Y_q|}{\Lambda_{\text{TeV}}} \ll \eta \ll \frac{v|Y_q|}{M_{\text{KK}}} \quad (\text{narrow bulk Higgs}), \quad (2.4)$$

sometimes a model-independent expression can be derived. This scenario will be referred to as the *narrow bulk-Higgs* scenario in the following. An important outcome of this work is that it is not always possible to obtain the results in the brane-localized scenario by just taking the limit of the results in the narrow bulk Higgs scenario. Thus, these two variants should be really considered as two different versions of the RS model, where we will not discuss the question which kind of RS model is theoretically most appealing. The overwhelming majority of the RS literature has been based on models in which the scalar sector is localized on the IR brane due to the above-mentioned advantages. These models should therefore be included as a benchmark in any phenomenological study. Yet, having the Higgs as the only brane-localized field is somewhat peculiar, and after realizing that successful models of electroweak symmetry breaking can be constructed with a scalar sector in the bulk one may consider this to be a more appealing scenario. The fact that important one-loop amplitudes such as $gg \rightarrow h$ and $b \rightarrow s\gamma$ (see Chapter 4) are convergent by naive power counting in bulk-Higgs models adds to their attractiveness. However, a bulk-Higgs model featuring a very narrow Higgs profile ($\eta \ll 1$) requires some fine-tuning. The most natural assumption would be that $\eta = \mathcal{O}(1)$.

The discussion above has been made to clarify the nomenclature of the different RS scenarios differing in the localization of the scalar sector. In this thesis, we will predominantly work with models with a Higgs sector which will be fixed on the IR brane via a (regularized) δ -function. When deriving certain quantities, we will also comment on the corresponding results in the bulk-Higgs model. The narrow bulk-Higgs scenario will become important only from Chapter 4 on, although the equality on the right-handed side of (2.4) will already be used in this and the subsequent chapter.

2.2 The Minimal Randall-Sundrum Model

The minimal version of the RS model is just the SM (except for the Higgs) put into the bulk. The complete action of this theory can be split into two parts,

$$S_{\text{minimal}} = S_{\text{gauge}} + S_{\text{matter}}, \quad (2.5)$$

where the gauge sector includes the kinetic terms of the gauge fields, the gauge-fixing as well as the ghost and Higgs Lagrangian. The matter sector consists of the kinetic terms for the fermion fields and the Yukawa interactions. In this section, we will make use of the discussion in Section 1.4.2: Starting from the 5D action, we will derive the

EOMs for the 5D fields, which after inserting the KK decompositions will give us the differential equations for the profiles. Then, with the help of the BCs, the solutions for the profiles and the physical masses of all KK modes will be determined. A special focus will be put on the zero-mode profiles and mass eigenvalues, for which simple, analytical formulas can be derived. It will then be explained in detail how the hierarchies of the SM can be generated and how the RS-GIM mechanism can prevent flavor-changing neutral currents from getting large corrections. Finally, the minimal RS model is checked for compatibility with electroweak precision measurements.

2.2.1 The Gauge Sector

We begin with the gauge sector of the minimal RS model based on the SM gauge group \mathcal{G}_{SM} (1.1), where all gauge fields are allowed to propagate in the bulk. We will see that many of the formulas derived in the following can be immediately recognized as the 5D generalizations of the corresponding SM counterparts.

The 5D Action

As already mentioned above, the 5D action of the gauge sector is a sum of four contributions,

$$S_{\text{gauge}} = \int d^4x \int_{-\pi}^{\pi} d\phi \sqrt{|G|} (\mathcal{L}_{\mathcal{G},\text{W},\text{B}} + \mathcal{L}_{\text{Higgs}} + \mathcal{L}_{\text{GF}} + \mathcal{L}_{\text{FP}}), \quad (2.6)$$

where $\sqrt{|G|} = r e^{4\sigma(\phi)}$ is the square root of the determinant of the metric (2.1). The kinetic Lagrangian $\mathcal{L}_{\mathcal{G},\text{W},\text{B}}$ is given by

$$\mathcal{L}_{\mathcal{G},\text{W},\text{B}} = G^{KM} G^{LN} \left(-\frac{1}{4} \mathcal{G}_{KL}^a \mathcal{G}_{MN}^a - \frac{1}{4} W_{KL}^i W_{MN}^i - \frac{1}{4} B_{KL} B_{MN} \right), \quad (2.7)$$

where the indices at the corresponding fields strength tensors, which are defined analogously to the SM case (1.8) with $\mu, \nu \rightarrow M, N$, run over the generators of the color group $SU(3)_c$ ($a = 1, \dots, 8$) and of $SU(2)_L$ ($i = 1, 2, 3$). The requirement to arrive at the SM as a low-energy theory demands the vector components of the 5D gauge fields to be Z_2 -even functions with Neumann BCs on both branes. According to the discussion in Subsection 1.4.2 the scalar components must be odd and vanish at both branes. As in the SM, the electroweak symmetry is broken by the coupling to the Higgs sector that is confined on the IR brane. The corresponding Lagrangian (1.98) can be written using the more convenient parametrization

$$\mathcal{L}_{\text{Higgs}} = \frac{\delta(|\phi| - \pi)}{r} \left[(D_\mu \Phi)^\dagger (D^\mu \Phi) + \mu^2 \Phi^\dagger \Phi - \lambda (\Phi^\dagger \Phi)^2 \right], \quad (2.8)$$

where the rescaling of the fields and the dimensionful parameters according to (1.99) has already been performed. We will use the following parametrization of the Higgs doublet

$$\Phi(x) = \frac{1}{\sqrt{2}} \begin{pmatrix} -i\sqrt{2}\varphi^+(x) \\ v + h(x) + i\varphi^3(x) \end{pmatrix}, \quad (2.9)$$

where $\varphi^\pm \equiv \varphi^1 \mp \varphi^2$ and φ^3 are the unphysical scalar degrees of freedom, that are eaten by the W and Z boson to give them their masses, and h denotes the physical Higgs

field. Throughout this thesis, v denotes the vev in the RS model, which differs from the SM value $v_{\text{SM}} \approx 246$ GeV by a small amount [157]. The exact relation between v and v_{SM} will be shown at the beginning of Section 5.1. In order to diagonalize the 5D mass terms coming from (2.8) after EWSB, the electroweak gauge fields can be redefined in the conventional way,

$$\begin{aligned} W_M^\pm &= \frac{1}{\sqrt{2}} (W_M^1 \mp iW_M^2), & M_W &= \frac{vg_5}{2}, \\ Z_M &= \frac{1}{\sqrt{g_5^2 + g_5'^2}} (g_5 W_M^3 - g_5' B_M), & M_Z &= \frac{v\sqrt{g_5^2 + g_5'^2}}{2}, \\ A_M &= \frac{1}{\sqrt{g_5^2 + g_5'^2}} (g_5' W_M^3 + g_5 B_M), & M_A &= 0, \end{aligned} \quad (2.10)$$

where g_5 and g_5' are the dimensionful ($[g_5] = [g_5'] = -1/2$) 5D gauge couplings of the $SU(2)_L$ and $U(1)_Y$ subgroups, respectively. In this basis the covariant derivative reads

$$D_M = \partial_M - i\frac{g_5}{\sqrt{2}} (T^+ W_M^+ + T^- W_M^-) - \frac{g_5}{\cos\theta_w} (T^3 - \sin\theta_w) Z_M - ie_5 Q A_\mu, \quad (2.11)$$

where $T^{\pm,3}$ and Q are the group generators. The Weinberg angle θ_w and the 5D electromagnetic gauge coupling e_5 are defined by

$$\cos\theta_w = \frac{g_5}{\sqrt{g_5^2 + g_5'^2}}, \quad \sin\theta_w = \frac{g_5'}{\sqrt{g_5^2 + g_5'^2}}, \quad e_5 = g_5 \sin\theta_w, \quad (2.12)$$

and are again just generalizations of the SM expressions to five dimensions. Note, however, the different mass dimensions of the gauge fields and coupling constants. At this point, some comments are in order. In contrast to the common practice in the literature, e.g. in [145], we do not define a dimensional coupling via $g \equiv g_5/\sqrt{2\pi r}$, and analogously for g' , which is then identified with the SM gauge coupling g_{SM} . The reason is that the coupling to the light fermions, which determines the strength of the weak coupling constants always comes with non-flat profile of the massive gauge bosons derived in (2.31). The only exceptions are the electromagnetic and the strong gauge coupling whose corresponding gauge-boson zero modes have a flat profile, so that [158, 159]

$$e \equiv \frac{e_5}{\sqrt{2\pi r}} \quad \text{and} \quad g_s \equiv \frac{g_{s,5}}{\sqrt{2\pi r}} \quad (2.13)$$

can be identified with the 4D gauge couplings of the SM.

The kinetic term in the Higgs Lagrangian (2.8) includes the square of the covariant derivative acting the Higgs doublet,

$$D_\mu \Phi = \frac{1}{\sqrt{2}} \begin{pmatrix} -i\sqrt{2}(\partial_\mu \varphi^+ + M_W W_\mu^+) \\ \partial_\mu h + i(\partial_\mu \varphi^3 + M_Z Z_\mu) \end{pmatrix} + \text{terms bi-linear in fields}, \quad (2.14)$$

and thus mixes the gauge fields W_μ^\pm and Z_μ with the scalar degrees of freedom φ^\pm and φ^3 . The mixing terms can be removed by appropriate gauge-fixing terms which are

chosen to be

$$\begin{aligned}
\mathcal{L}_{\text{GF}} = & -\frac{1}{2\xi} \left(\partial^\mu A_\mu - \xi \left[M_{\text{KK}} t \partial_t \frac{1}{t} A_5 \right] \right)^2 \\
& -\frac{1}{2\xi} \left(\partial^\mu Z_\mu - \frac{\xi}{2} \left[\delta(t-1) k M_Z \varphi^3 + 2 M_{\text{KK}} t \partial_t \frac{1}{t} Z_5 \right] \right)^2 \\
& -\frac{1}{\xi} \left(\partial^\mu W_\mu^+ - \frac{\xi}{2} \left[\delta(t-1) k M_W \varphi^+ + 2 M_{\text{KK}} t \partial_t \frac{1}{t} W_5^+ \right] \right) \\
& \times \left(\partial^\mu W_\mu^- - \xi \left[\delta(t-1) k M_W \varphi^- + 2 M_{\text{KK}} t \partial_t \frac{1}{t} W_5^- \right] \right),
\end{aligned} \tag{2.15}$$

where we have used the t -notation and redefined the scalar component of the gauge fields

$$A_5(x, t) = \frac{\epsilon}{rt} A_\phi(x, \phi), \tag{2.16}$$

and analogously for W_5^\pm and Z_5 , in order to adjust the mass dimensions. More generally, there could be a different parameter for each term, but we can set all to the same value without loss of generality. The square of the δ -function appearing in (2.15) causes no problems, because these terms cancel out after inserting the KK decomposition of the fields, as we will see later. The Faddeev-Popov Lagrangian \mathcal{L}_{FP} will not be needed for the discussion in this chapter. We will touch on its structure after the KK decomposition, since we need the corresponding Feynman rules in Section 4.2.

As we want to derive the masses and profiles of the physical KK excitations, we will concentrate on the bilinear terms in the following. It is, however, straightforward to incorporate couplings involving three or four gauge bosons. The kinetic terms of the gauge bosons and the Higgs as well as the gauge-fixing terms lead to the bilinear part of the action

$$\begin{aligned}
S_{\text{gauge},2} \ni & \int d^4x \frac{2\pi r}{L} \int_\epsilon^1 \frac{dt}{t} \\
& \left\{ -\frac{1}{4} F_{\mu\nu} F^{\mu\nu} - \frac{1}{2\xi} (\partial^\mu A_\mu)^2 + \frac{1}{2} (\partial_\mu A_5 \partial^\mu A_5 + M_{\text{KK}}^2 \partial_t A_\mu \partial_t A^\mu) \right. \\
& -\frac{1}{4} Z_{\mu\nu} Z^{\mu\nu} - \frac{1}{2\xi} (\partial^\mu Z_\mu)^2 + \frac{1}{2} (\partial_\mu Z_5 \partial^\mu Z_5 + M_{\text{KK}}^2 \partial_t Z_\mu \partial_t Z^\mu) \\
& -\frac{1}{2} W_{\mu\nu}^+ W^{-\mu\nu} - \frac{1}{\xi} (\partial^\mu W_\mu^+) (\partial^\nu W_\nu^-) + (\partial_\mu W_5^+ \partial^\mu W_5^- + M_{\text{KK}}^2 \partial_t W_\mu^+ \partial_t W^{-\mu}) \\
& + \frac{k}{2} \delta(t-1) \left(\frac{1}{2} \partial_\mu h \partial^\mu h - \lambda v^2 h^2 + \partial_\mu \varphi^+ \partial^\mu \varphi^- + \frac{1}{2} \partial_\mu \varphi^3 \partial^\mu \varphi^3 \right. \\
& \qquad \qquad \qquad \left. + \frac{M_Z^2}{2} Z_\mu Z^\mu + M_W^2 W_\mu^+ W^{-\mu} \right) \\
& -\frac{\xi}{2} \left(M_{\text{KK}} t \partial_t \frac{1}{t} A_5 \right)^2 - \frac{\xi}{8} \left(\delta(t-1) k M_Z \varphi^3 + 2 M_{\text{KK}} t \partial_t \frac{1}{t} Z_5 \right)^2 \\
& \left. -\frac{\xi}{4} \left(\delta(t-1) k M_W \varphi^+ + M_{\text{KK}} t \partial_t \frac{1}{t} W_5^+ \right) \left(\delta(t-1) k M_W \varphi^- + M_{\text{KK}} t \partial_t \frac{1}{t} W_5^- \right) \right\}.
\end{aligned} \tag{2.17}$$

The Kaluza-Klein Decomposition

In order to solve the EOMs that follow from the action (2.17), we now decompose the 5D fields into 4D mass eigenstates and choose the following decomposition

$$\begin{aligned}
A_\mu(x, t) &= \frac{1}{\sqrt{r}} \sum_n \chi_n^A(t) A_\mu^{(n)}(x), & A_5(x, t) &= \frac{M_{\text{KK}}}{\sqrt{r}} \sum_n a_n^A \partial_t \chi_n^A(t) \varphi_A^{(n)}(x), \\
Z_\mu(x, t) &= \frac{1}{\sqrt{r}} \sum_n \chi_n^Z(t) Z_\mu^{(n)}(x), & Z_5(x, t) &= \frac{M_{\text{KK}}}{\sqrt{r}} \sum_n a_n^Z \partial_t \chi_n^Z(t) \varphi_Z^{(n)}(x), \\
W_\mu^\pm(x, t) &= \frac{1}{\sqrt{r}} \sum_n \chi_n^W(t) W_\mu^{\pm(n)}(x), & W_5^\pm(x, t) &= \frac{M_{\text{KK}}}{\sqrt{r}} \sum_n a_n^W \partial_t \chi_n^W(t) \varphi_W^{\pm(n)}(x),
\end{aligned} \tag{2.18}$$

where we have used that the profiles $\chi_n^5(t)$ ($B = A, Z, W^\pm$) can be chosen to be $\chi_n^5(t) = a_n^B \partial_t \chi_n^B(t)$ with some coefficients a_n^B that have to be determined [111]. The fields $B_\mu^{(n)}$ are the KK modes of the gauge boson B with masses m_n^B , while the scalar particles $\varphi_a^{(n)}$ ($a = W^\pm, Z$) are the KK modes of the mixture of the fifth component of the gauge field a_5 and the Goldstone bosons arising from the Higgs sector φ^\pm .^{3,2} It is therefore reasonable to expand the latter Goldstone bosons in the same basis of mass eigenstates

$$\varphi^\pm(x) = \sum_n b_n^W \varphi_W^{(n)}(x), \quad \varphi^3(x) = \sum_n b_n^Z \varphi_Z^{(n)}(x). \tag{2.19}$$

Following the discussion below (1.62), we can derive the EOM for the profiles, which in t -notation read

$$-t \partial_t \frac{1}{t} \partial_t \chi_n^B(t) = x_n^2 \chi_n^B(t) - \delta(t-1) \frac{L}{2\pi r} \frac{M_B^2}{M_{\text{KK}}^2} \chi_n^B(t), \tag{2.20}$$

and find that the profiles obey the orthonormality condition

$$\frac{2\pi}{L} \int \frac{dt}{t} \chi_n^B(t) \chi_m^B(t) = \delta_{nm}. \tag{2.21}$$

The difference in the case at hand is the appearance of the δ -function in (2.8) and (2.15). Note that it is only relevant for the massive gauge bosons W^\pm and Z . In order to be in accordance with the boundary conditions of these fields, which guarantee the vanishing of the boundary terms when integrating by parts, we move the δ -function infinitesimally into the bulk and use the 1^- superscript indicating $\delta(t-1^-) \equiv \lim_{\eta \rightarrow 0} \delta(t-1+\eta)$. The δ -function therefore represents a “fake brane” which modifies the BC at $t=1^-$ obtained by integrating the EOM (2.20) over a small interval around the IR brane (in ϕ -notation) or from an infinitesimally displaced point in the bulk to the brane (in t -notation)

$$\partial_t \chi_n^{W,Z}(\epsilon) = 0, \quad \partial_t \chi_n^{W,Z}(1^-) = -\frac{L \tilde{m}_{W,Z}^2}{M_{\text{KK}}^2} \chi_n^{W,Z}(1). \tag{2.22}$$

Here, we have expressed the 5D masses $M_{W,Z}$ in terms of the mass parameters

$$\tilde{m}_W \equiv \frac{g_5}{\sqrt{2\pi r}} \frac{v}{2} \quad \text{and} \quad \tilde{m}_Z \equiv \sqrt{\frac{g_5^2 + g_5'^2}{2\pi r}} \frac{v}{2}, \tag{2.23}$$

²The scalars $\varphi_A^{(n)}$ are just the KK modes of the fifth component A_5 .

which are the leading contributions to the gauge-boson masses in an expansion in powers of v^2/M_{KK}^2 , see (2.30). The photon and the gluon profiles obey Neumann boundary conditions at both branes resulting in a massless zero mode. After inserting the KK decomposition (2.18) into (2.17) and applying the EOM and the orthonormality condition, we arrive at the following effective 4D theory, where the fifth dimension has been integrated out,

$$\begin{aligned}
S_{\text{gauge},2} = & \sum_n \int d^4x \left\{ -\frac{1}{4} F_{\mu\nu}^{(n)} F^{\mu\nu(n)} - \frac{1}{2\xi} \left(\partial^\mu A_\mu^{(n)} \right)^2 + \frac{(m_n^A)^2}{2} A_\mu^{(n)} A^{\mu(n)} \right. \\
& - \frac{1}{4} Z_{\mu\nu}^{(n)} Z^{\mu\nu(n)} - \frac{1}{2\xi} \left(\partial^\mu Z_\mu^{(n)} \right)^2 + \frac{(m_n^Z)^2}{2} Z_\mu^{(n)} Z^{\mu(n)} \\
& - \frac{1}{2} W_{\mu\nu}^{+(n)} W^{-\mu\nu(n)} - \frac{1}{\xi} \partial^\mu W_\mu^{+(n)} \partial^\nu W_\nu^{-(n)} + \frac{(m_n^A)^2}{2} W_\mu^{+(n)} W^{-\mu(n)} \\
& + \frac{1}{2} \partial_\mu \varphi_A^{(n)} \partial^\mu \varphi_A^{(n)} - \frac{\xi(m_n^A)^2}{2} \varphi_A^{(n)} \varphi_A^{(n)} + \frac{1}{2} \partial_\mu \varphi_Z^{(n)} \partial^\mu \varphi_Z^{(n)} - \frac{\xi(m_n^Z)^2}{2} \varphi_Z^{(n)} \varphi_Z^{(n)} \\
& \left. + \partial_\mu \varphi_W^{+(n)} \partial^\mu \varphi_W^{-(n)} - \xi(m_n^W)^2 \varphi_W^{+(n)} \varphi_W^{-(n)} \right\} + \int d^4x \left(\frac{1}{2} \partial_\mu h \partial^\mu h - \lambda v^2 h^2 \right) \\
& + \sum_n \int d^4x \mathcal{L}_{\text{FP}}^{(n)}. \tag{2.24}
\end{aligned}$$

In order to obtain the above structure, we have made the crucial condition that the coefficients in (2.19) must be given by ($a = W, Z$)

$$a_n^a = -\frac{1}{m_n^a}, \quad b_n^a = \frac{\tilde{m}_a}{m_n^a} \sqrt{2\pi} \chi_n^a(1). \tag{2.25}$$

Choosing different coefficients would not lead to the diagonal action (2.24). The latter describes the action of an infinite tower of physical gauge-boson KK modes $B_\mu^{(n)}$ ($B = W^\pm, Z, A$) with masses m_n^B and of the corresponding unphysical Goldstone bosons with masses $\sqrt{\xi} m_n^B$. The zero modes can be identified with the SM gauge bosons. In this approach all mixing effects are implicitly included and the physical zero modes already involves contributions from the KK excitations. This mixing gives rise to different couplings of the gauge-boson zero modes to fermions which we will see below.

Note that in the action (2.24) the Lagrangian for each KK mode has the same form as the SM action. As a consequence, the Faddeev-Popov ghost Lagrangians $\mathcal{L}_{\text{FP}}^{(n)}$ resemble the SM one, with the only generalization that a ghost field is required for every KK mode. Correspondingly, the gauge-boson couplings to their ghosts can be easily deduced from the corresponding SM Feynman rule.

Bulk Profiles and Masses

We now want to obtain the solutions for the bulk profiles χ_n^a . Solving the EOMs (2.20) subject to the BCs (2.22), one finds ($a = W, Z$)

$$\chi_n^a(\phi) = N_n \sqrt{\frac{L}{\pi}} t c_n^+(t), \tag{2.26}$$

where only the UV BC has been used to determine the unspecified coefficient in the general solution, so that

$$\begin{aligned} c_n^+(t) &= Y_0(x_n^a \epsilon) J_1(x_n^a t) - J_0(x_n^a \epsilon) Y_1(x_n^a t), \\ c_n^-(t) &= \frac{1}{x_n^a t} \frac{d}{dt} [t c_n^+(t)] = Y_0(x_n^a \epsilon) J_0(x_n^a t) - J_0(x_n^a \epsilon) Y_0(x_n^a t). \end{aligned} \quad (2.27)$$

The dimensional parameters $x_n^a = m_n^a/M_{\text{KK}}$ are the ratios of the gauge-boson masses normalized to the KK scale. The normalization content N_n is fixed by the orthonormality relation (2.21), and reads

$$N_n^{-2} = [c_n^+(1)]^2 + [c_n^-(1^-)]^2 - \frac{2}{x_n} c_n^+(1) c_n^-(1^-) - \epsilon^2 [c_n^+(\epsilon)]^2. \quad (2.28)$$

The IR BC

$$x_n^a c_n^-(1^-) = -\frac{L \tilde{m}_a^2}{M_{\text{KK}}^2} c_n^+(1), \quad a = W, Z, \quad (2.29)$$

can be used for the determination of the mass eigenvalues x_n^a . The masses of the KK modes ($n \geq 1$) have to be calculated numerically. Since they are determined by the zeroes of Bessel functions they have an approximately equidistant spacing of $\Delta m_a \approx n\pi M_{\text{KK}}$. The masses of the zero modes, on the other hand, can be derived analytically. Expanding (2.29) in powers of v^2/M_{KK}^2 , we find³ ($a = W, Z$)

$$m_a^2 = \tilde{m}_a^2 \left[1 - \frac{\tilde{m}_a^2}{2M_{\text{KK}}^2} \left(L - 1 + \frac{1}{2L} \right) + \mathcal{O} \left(\frac{v^4}{M_{\text{KK}}^4} \right) \right]. \quad (2.30)$$

This equation relates the gauge-boson masses to the SM relation $m_a = g_a v_{\text{SM}}/2$. Direct measurements will determine the mass on the left-hand side of (2.30) and one can therefore absorb the universal RS corrections into m_a . This corresponds to a rescaling of the Higgs vev as discussed in [145]. However, we will use a different determination of the vev shift in Section 5.1. Nevertheless, it is noteworthy that equation (2.30) has to be used in all calculations involving the masses $\tilde{m}_{W,Z}$ in order to obtain results that depend on the physical masses $m_{W,Z}$.

Finally, we can derive analytical expressions for the zero-mode profiles ($a = Z, W$)

$$\sqrt{2\pi} \chi_0^a(t) = 1 - \frac{m_a^2}{2M_{\text{KK}}^2} \left[t^2 \left(L - \frac{1}{2} + \ln t \right) - \frac{1}{2} + \frac{1}{2L} \right] + \mathcal{O} \left(\frac{v^4}{M_{\text{KK}}^4} \right), \quad (2.31)$$

which receive corrections of $\mathcal{O}(v^2/M_{\text{KK}}^2)$ to the flat profile which is the consequence of the mixing with the KK modes. Inserting this result into (2.19) and (2.25) shows that the fields φ^\pm coincide with $\varphi_W^{\pm(0)}$ to leading order and that mixing effects arise at order v^2/M_{KK}^2 or higher. The masses and profiles for the photon and the gluon can be easily adopted from (2.30) and (2.31) with $\tilde{m}_a = 0$, which follows from Neumann boundary conditions at the IR brane, see (2.22). Thus, the zero modes are massless ($m_{A,G} = 0$) and have a flat profile

$$\chi_0^{A,G} = \frac{1}{\sqrt{2\pi}}, \quad (2.32)$$

which, according to the discussion in Section 1.4.2, is crucial for maintaining gauge invariance at zero-mode level.

³Terms of $\mathcal{O}(\epsilon)$ will be neglected in the following.

Modifications for a Bulk Higgs

Up to now, we have treated the Higgs as a brane-localized field. As has been pointed out at the beginning of this chapter, it is also possible and somewhat more natural to allow the Higgs doublet to propagate into the bulk.⁴

Using the orbifold coordinate ϕ , the general action for the Higgs sector, that is given by (2.8) in the case of a brane-localized Higgs sector, now becomes

$$S_h = \int d^4x r \int_{-\pi}^{\pi} d\phi e^{-4\sigma} \left[g^{MN} D_M \Phi^\dagger D_N \Phi - \mu^2 |\Phi|^2 - V_{UV}(\Phi) \delta(|\phi|) - V_{IR}(\Phi) \delta(|\phi| - \pi) \right], \quad (2.33)$$

where μ provides a bulk mass for the scalar field, which can be tachyonic (see below). The potentials localized on the UV and IR branes determine the boundary conditions of the scalar fields and induce electroweak symmetry breaking. They are chosen to be

$$V_{UV}(\Phi) = M_{UV} |\Phi|^2, \quad V_{IR}(\Phi) = -M_{IR} |\Phi|^2 + \lambda_{IR} |\Phi|^4, \quad (2.34)$$

with mass dimensions $[M_{UV}] = [M_{IR}] = 1$ and $[\lambda_{IR}] = -2$. The dimensionful parameters in the 5D action naturally scale with appropriate powers of M_{Pl} , and it will be useful to introduce dimensionless $\mathcal{O}(1)$ parameters by the rescalings

$$m_{UV} \equiv \frac{M_{UV}}{2k}, \quad m_{IR} \equiv \frac{M_{IR}}{2k}, \quad \lambda \equiv \frac{\lambda_{IR} k}{4r}. \quad (2.35)$$

Switching to t -notation, we express the scalar doublet $\Phi(x, \phi)$ in the form

$$\Phi(x, t) = \frac{t}{\epsilon \sqrt{r}} \begin{pmatrix} -i\varphi^+(x, t) \\ \frac{1}{\sqrt{2}} [v(t) + h(x, t) + i\varphi_3(x, t)] \end{pmatrix}, \quad (2.36)$$

where in contrast to (2.9) the Higgs vev profile $v(t)$, the physical Higgs scalar $h(x, t)$, and the Goldstone bosons $\varphi^+(x, t)$, $\varphi_3(x, t)$ are now functions depending on the extra dimension. Being 5D fields, these four scalar degrees of freedom can also be decomposed into KK modes. As a matter of fact, these KK modes mix with the KK modes of the fifth components of the gauge fields. After rotating into the mass basis, there are physical KK excitations of the neutral Higgs boson $h_n(x)$ [161]. Moreover, there are three towers of additional scalars $\phi_n^Z(x)$, $\phi_n^\pm(x)$, which do not possess zero modes. The charged scalars will be important for the discussion in Section 4.2. For the following analysis it is not necessary to consider the Goldstone fields $\varphi^+(x, t)$, $\varphi_3(x, t)$ any further (unitary gauge). Integrating by parts, the Lagrangian corresponding to the action $S_h = \int d^4x \mathcal{L}_h(x)$ in (2.33) can be rewritten in the form

$$\begin{aligned} \mathcal{L}_h = & \frac{2\pi}{L} \int_{\epsilon}^1 \frac{dt}{t} \left\{ \frac{1}{2} \partial_\mu h(x, t) \partial^\mu h(x, t) \right. \\ & + \frac{M_{KK}^2}{2} \left[\frac{v(t) + 2h(x, t)}{t} (t^2 \partial_t^2 + t \partial_t - \beta^2) \frac{v(t)}{t} + \frac{h(x, t)}{t} (t^2 \partial_t^2 + t \partial_t - \beta^2) \frac{h(x, t)}{t} \right] \Big\} \\ & - \frac{\pi M_{KK}^2}{L} \left\{ \left[\frac{v(t) + 2h(x, t)}{t^2} \partial_t [t v(t)] + \frac{h(x, t)}{t^2} \partial_t [t h(x, t)] \right]_{t=\epsilon^+}^{1^-} \right. \\ & \left. + \frac{m_{UV}}{\epsilon^2} [v(\epsilon) + h(x, \epsilon)]^2 - m_{IR} [v(1) + h(x, 1)]^2 + \frac{\lambda}{M_{KK}^2} [v(1) + h(x, 1)]^4 \right\}, \quad (2.37) \end{aligned}$$

⁴ This discussion follows the expositions given in [156, 160] and is part of our publication [150].

where $\beta = \sqrt{4 + \mu^2/k^2}$. Requiring that the terms linear or quadratic in $h(x, t)$ cancel out on the UV and IR branes yields the BCs⁵

$$\begin{aligned} \partial_t [t v(t)]_{t=\epsilon^+} &= m_{\text{UV}} v(\epsilon), & \partial_t [t v(t)]_{t=1^-} &= m_{\text{IR}} v(1) - \frac{2\lambda}{M_{\text{KK}}^2} v^3(1), \\ \partial_t [t h(x, t)]_{t=\epsilon^+} &= m_{\text{UV}} h(x, \epsilon), & \partial_t [t h(x, t)]_{t=1^-} &= m_{\text{IR}} h(x, 1) - \frac{6\lambda}{M_{\text{KK}}^2} v^2(1) h(x, 1). \end{aligned} \quad (2.38)$$

The differential equation for $v(t)$ can be obtained by varying the action with respect to $v(t)$, and we find

$$(t^2 \partial_t^2 + t \partial_t - \beta^2) \frac{v(t)}{t} = 0, \quad \text{with } \beta^2 = 4 + \frac{\mu^2}{k^2}, \quad (2.39)$$

which ensures that the tadpole terms in the Lagrangian (2.37) cancel out. We then obtain

$$\begin{aligned} \mathcal{L}_h(x) &= \frac{2\pi}{L} \int_{\epsilon}^1 \frac{dt}{t} \left[\frac{1}{2} \partial_{\mu} h(x, t) \partial^{\mu} h(x, t) + \frac{M_{\text{KK}}^2}{2} \frac{h(x, t)}{t} (t^2 \partial_t^2 + t \partial_t - \beta^2) \frac{h(x, t)}{t} \right] \\ &\quad - \frac{\pi}{L} \lambda \left[-v^4(1) + 4v(1) h^3(x, 1) + h^4(x, 1) \right]. \end{aligned} \quad (2.40)$$

The general solution to the differential equation (2.39) subject to the boundary conditions (2.38) is

$$v(t) = N_v \left(t^{1+\beta} - r_v t^{1-\beta} \right), \quad \text{with } r_v = \epsilon^{2\beta} \frac{2 + \beta - m_{\text{UV}}}{2 - \beta - m_{\text{UV}}}, \quad (2.41)$$

and

$$N_v^2 = \frac{M_{\text{KK}}^2}{2\lambda} \frac{(m_{\text{IR}} - 2 - \beta) - r_v (m_{\text{IR}} - 2 + \beta)}{(1 - r_v)^3}. \quad (2.42)$$

Before proceeding, let us first discuss which values the parameter β can take. Motivated by the observation that the energy-momentum flux in a pure anti-de Sitter space without an IR brane (which corresponds to taking the limit $r \rightarrow \infty$) vanishes at the boundary only if the 5D scalar field obeys the Breitenlohner-Friedman bound $\mu^2 > -4k^2$ [162], one usually assumes that β must be a real positive number, even though not necessarily larger than 2. Unless β is very close to zero, it follows that the coefficient $r_v \propto \epsilon^{2\beta}$ in (2.41) is extremely small and can be set to zero for all practical purposes. The only exception would be the region where $t \sim \epsilon$ is very near the UV brane, which, however, is irrelevant for the analysis in this thesis. It follows that

$$v(t) = v(1) t^{1+\beta}, \quad \text{with } v(1) = M_{\text{KK}} \sqrt{\frac{m_{\text{IR}} - 2 - \beta}{2\lambda}}. \quad (2.43)$$

The requirement that the Higgs vev be a real number imposes an upper bound on the parameter β , since $\lambda > 0$ is required by vacuum stability. We thus obtain the allowed range

$$0 < \beta < m_{\text{IR}} - 2. \quad (2.44)$$

Note that the parameter $v(1)$ is a function of the 5D input parameters of the theory. It is more convenient to relate it to the physical value v_{SM} of the Higgs vev in the SM. After

⁵As above, these conditions can also be derived by integrating the field equations over infinitesimal intervals about the branes.

electroweak symmetry breaking, the mass terms for the W and Z bosons are generated by the 5D Lagrangian

$$S_m = \int d^4x \frac{2\pi}{L} \int_{\epsilon}^1 \frac{dt}{t} \frac{v^2(t)}{4} \left[g_5^2 W_{\mu}^+(x, t) W^{-\mu}(x, t) + \frac{g_5^2 + g_5'^2}{2} Z_{\mu}(x, t) Z^{\mu}(x, t) \right]. \quad (2.45)$$

Making use of the KK decompositions (2.18), we can identify

$$v_4^2 = \frac{2\pi}{L} \int_{\epsilon}^1 \frac{dt}{t} v^2(t) (\chi_0^W(t) \sqrt{2\pi})^2, \quad (2.46)$$

where the parameter v_4 coincides with the parameter v used elsewhere in this thesis. At lowest order in an expansion in powers of v^2/M_{KK}^2 , it coincides with the SM parameter v_{SM} as defined, e.g. via the value of the Fermi constant, see Section 5. For the determination of the $\mathcal{O}(v^2/M_{\text{KK}}^2)$ corrections to the relation $v_{\text{SM}} = v_4$, one needs to solve the differential equations for the profiles of the gauge-boson zero modes in the presence of the Higgs vev, which will be done in the following. The EOM reads

$$(-t\partial_t \frac{1}{t} \partial_t + \hat{v}^2 t^{2+2\beta}) \chi_0^W(t) = x_0^2 \chi_0^W(t), \quad \hat{v}^2 = \frac{g_5^2}{4r} \frac{v(1)^2}{M_{\text{KK}}^2}, \quad (2.47)$$

and the profiles need to obey Neumann BCs at both branes. Unfortunately, a closed, analytical solution to this equation cannot be derived, but it is possible to find a perturbative solution using the ansatz

$$\chi_0^W(t) = \sum_{n=0}^{\infty} (\hat{v}^2)^n f_n(t), \quad x_0^2 = \sum_{n=1}^{\infty} (\hat{v}^2)^n c_n. \quad (2.48)$$

The sum in the ansatz for x_0^2 starts with $n = 1$, since in the case of no electroweak symmetry breaking the profile is flat $\chi_0^W(t) = f_0(t) \equiv 1/\sqrt{2\pi}$ with eigenvalue $x_0^2 \equiv 0$. Inserting (2.48) into (2.47) and collecting the different orders of \hat{v}^2 we obtain differential equations for the functions $f_n(t)$

$$\begin{aligned} -t\partial_t \frac{1}{t} \partial_t f_0(t) &= 0, \\ -t\partial_t \frac{1}{t} \partial_t f_1(t) &= -t^{2+2\beta} f_0(t) + c_1 f_0(t), \\ -t\partial_t \frac{1}{t} \partial_t f_2(t) &= -t^{2+2\beta} f_1(t) + c_1 f_1(t) + c_2 f_0(t), \end{aligned} \quad (2.49)$$

etc. Using the BCs and the normalization condition (2.21), we obtain

$$f_0(t) = \frac{1}{\sqrt{2\pi}}, \quad (2.50)$$

$$f_1(t) = \frac{1}{\sqrt{2\pi}} \frac{1}{4(1+\beta)} \left[-\frac{1}{2L^2} + \frac{(1+\beta)(3+\beta)}{2L(2+\beta)^2} + t^2 \left(-1 + \frac{t^{2(1+\beta)}}{2+\beta} + \frac{1-2\ln t}{2L} \right) \right],$$

and

$$\begin{aligned} c_1 &= \frac{1}{2L(1+\beta)}, \\ c_2 &= -\frac{1}{4L} \left[\frac{1}{(2+\beta)(3+2\beta)} - \frac{(3+\beta)}{4L(1+\beta)(2+\beta)^2} + \frac{1}{4L^2(1+\beta)^2} \right]. \end{aligned} \quad (2.51)$$

We can now relate $v^2(1)$ to the four-dimensional vev v_4^2 via (2.46) and obtain for the Higgs vev profile at next-to-leading order

$$v(t) = v_4 \sqrt{\frac{L}{\pi}} (1 + \beta) t^{1+\beta} [1 - \hat{v}^2 d_1], \quad (2.52)$$

with

$$d_1 = \frac{1}{4(2 + \beta)} \left[-\frac{2(1 + \beta)}{3 + 2\beta} L + \frac{3 + 2\beta}{2 + \beta} - \frac{1}{2L} \frac{2 + \beta}{1 + \beta} \right]. \quad (2.53)$$

Moreover, the W -mass $m_W^2 = x_0^2 M_{\text{KK}}^2$ is found to be

$$m_W^2 = \tilde{m}_W^2 \left\{ 1 - \frac{\tilde{m}_W^2}{2M_{\text{KK}}^2} \left[\frac{2L(1 + \beta)^2}{(2 + \beta)(3 + 2\beta)} - \frac{(1 + \beta)(3 + \beta)}{(2 + \beta)^2} + \frac{1}{2L} \right] + \mathcal{O}\left(\frac{v^4}{M_{\text{KK}}^4}\right) \right\}, \quad (2.54)$$

where $\tilde{m}_W \equiv v_4 g_5 / (2\sqrt{2\pi r})$. Provided with the above results, it is straightforward to derive the W -boson profile in the background of a bulk-Higgs profile

$$\chi_0^W(t) = \frac{1}{\sqrt{2\pi}} \left\{ 1 + \frac{m_W^2}{2M_{\text{KK}}^2} \left[\frac{Lt^{4+2\beta}}{2 + \beta} + \frac{(1 + \beta)(3 + \beta)}{2(2 + \beta)^2} - \frac{1}{2L} - t^2 \left(L - \frac{1}{2} + \ln t \right) \right] \right\}, \quad (2.55)$$

which is the exact result at $\mathcal{O}(v^2/M_{\text{KK}}^2)$. Note that for $\beta = \mathcal{O}(1)$ the constant terms in (2.54) and (2.55) are reduced with respect to the results (2.30) and (2.31) in the brane-localized scenario, which can be recovered by pushing the Higgs towards the IR brane, i.e. in the limit $\beta \rightarrow \infty$.

We proceed to study the eigenvalue problem for the physical Higgs boson and its KK excitations. Being a 5D field, the 5D Higgs field can be decomposed via

$$h(x, t) = \sum_{n=0}^{\infty} h_n(x) \chi_n^h(t), \quad (2.56)$$

where the zero mode $h(x) \equiv h_0(x)$ corresponds to the SM Higgs boson and the profiles obey the usual orthonormality condition (2.21). In order to obtain canonical mass terms from the Lagrangian (2.40), we must impose the EOM

$$(t^2 \partial_t^2 + t \partial_t + t^2 x_n^2 - \beta^2) \frac{\chi_n(t)}{t} = 0, \quad (2.57)$$

where as usual $x_n = m_n/M_{\text{KK}}$ denote the masses of the KK Higgs bosons in units of M_{KK} . The general solution to this equation is a linear combination of Bessel functions,

$$\chi_n^h(t) = N_n t [J_\beta(x_n t) - r_n Y_\beta(x_n t)], \quad (2.58)$$

where the BC on the UV brane in (2.38) once again implies that $r_n \propto \epsilon^{2\beta}$ is extremely small and can be set to zero for all practical purposes in this thesis. We then obtain

$$\chi_n^h(t) = \sqrt{\frac{L}{\pi}} \frac{t J_\beta(x_n t)}{\sqrt{J_\beta^2(x_n) - J_{\beta+1}(x_n) J_{\beta-1}(x_n)}}. \quad (2.59)$$

For the determination of the physical masses of the KK Higgs bosons, we need the boundary condition on the IR brane

$$\frac{x_n J_{\beta+1}(x_n)}{J_\beta(x_n)} = 2(m_{\text{IR}} - 2 - \beta) \equiv 2\delta. \quad (2.60)$$

From this equation it follows that even the zero mode (the SM Higgs boson) has a mass that is naturally of $\mathcal{O}(M_{\text{KK}})$, which empirically cannot be less than a few TeV. This is the little hierarchy problem, which is not addressed in RS scenarios. In order to obtain a realistic Higgs mass $m_h \ll M_{\text{KK}}$, one has to assume that

$$\delta = m_{\text{IR}} - 2 - \beta \ll 1. \quad (2.61)$$

Once this is done, it is straightforward to obtain a formula for the zero-mode mass in a power series in δ . We find

$$x_0^2 = \frac{m_h^2}{M_{\text{KK}}^2} = 4(1 + \beta) \delta \left[1 - \frac{\delta}{2 + \beta} + \frac{2\delta^2}{(2 + \beta)^2 (3 + \beta)} + \dots \right]. \quad (2.62)$$

Assuming $M_{\text{KK}} = 2 \text{ TeV}$, for example, implies that $(1 + \beta) \delta \approx 10^{-3}$, which corresponds to a fine-tuning of 1 in 1000. For the zero-mode profile, it is now easy to obtain an expansion in powers of x_0^2 . The leading terms are given by

$$\chi_0^h(t) = \sqrt{\frac{L}{\pi}} (1 + \beta) t^{1+\beta} \left[1 - \frac{x_0^2}{4} \left(\frac{t^2}{1 + \beta} - \frac{1}{2 + \beta} \right) + \dots \right]. \quad (2.63)$$

Note that the next-to-leading term is a small correction of $\mathcal{O}(m_h^2/M_{\text{KK}}^2)$ and is even more suppressed by the localization parameter $\beta > 0$. In the limit $\beta \rightarrow \infty$, the profiles of the vev and the Higgs-boson zero mode coincide.

2.2.2 The Matter Sector

We now turn to the matter sector of the action (2.5), where the focus is put on the quark sector. The generalization to the lepton sector is straightforward, but is somewhat more involved: While the RS set-up can address the tiny neutrino masses, without a see-saw mechanism, by means of wave function overlaps [163–165], the localization along the extra dimension does not readily yield the correct mixing angles [166]. Thus, the lepton sector requires some model building. We will come back to the implementation of the lepton sector in Section 4.2, where the loop-induced Higgs decay $h \rightarrow \gamma\gamma$ is analyzed.

The 5D Action

Like the SM, the minimal RS model contains quark fields that are charged under the $SU(3)_c$ gauge group and are doublets and singlets under $SU(2)_L$. The difference to the SM, as pointed out in Section 1.4.2, is that the 5D bulk fermions are now Dirac particles and we need to impose certain BCs to project out the "wrong-chirality" components of the zero modes. The $SU(2)_L$ doublets are denoted as $Q = (U, D)$, whose left-handed component (U_L, D_L) is a Z_2 -even function on the orbifold and fulfills (NN) BCs, while the right-handed component is a Z_2 -odd function and obeys, according to (1.73), the opposite, i.e. (DD) , BCs. This choice accounts for massless left-handed fermions that

can be identified with the $SU(2)_L$ doublet of the SM. Analogously, the $SU(2)_L$ singlet will be denoted by $q = u, d$, where in this case the Z_2 -even right-handed component has to obey (NN) BC in order to arrive at a spectrum that is compatible with the SM. All fields are three-vectors in generation space and we can write down Yukawa interactions that couple to quark fields to the Higgs and give the zero modes their SM masses.

Like in the SM, the action of the matter sector in the minimal RS model consist of two parts,

$$S_{\text{matter}} = S_{\text{kin}}^{\text{ferm}} + S_{\text{Yukawa}} = \int d^4x \int_{-\pi}^{\pi} d\phi \sqrt{G} \left(\mathcal{L}_{\text{kin}}^{\text{ferm}} + \mathcal{L}_{\text{Yukawa}} \right), \quad (2.64)$$

where kinetic action⁶ $S_{\text{kin}}^{\text{ferm}}$ follows from (1.71) with $\Psi = Q, q$ and after evaluating the 5D gamma matrices (1.70) and the vielbein (1.72) reads

$$\begin{aligned} S_{\text{kin}}^{\text{ferm}} = & \sum_{Q,q} \int d^4x r \int_{-\pi}^{\pi} d\phi \\ & \left\{ e^{-3\sigma} (\bar{Q} i \not{\partial} Q + \bar{q} i \not{\partial} q) - e^{-4\sigma} \text{sgn}(\phi) (\bar{Q} \mathbf{M}_Q Q + \bar{q} \mathbf{M}_q q) \right. \\ & \left. - \frac{e^{-2\sigma}}{r} [\bar{Q}_L \partial_\phi (e^{-2\sigma} Q_R) - \bar{Q}_R \partial_\phi (e^{-2\sigma} Q_L) + \bar{q}_L \partial_\phi (e^{-2\sigma} q_R) - \bar{q}_R \partial_\phi (e^{-2\sigma} q_L)] \right\}. \end{aligned} \quad (2.65)$$

The quantities $\mathbf{M}_{Q,q}$ are 3×3 matrices in generation space and the signum in front of the mass terms are due to parity assignments. One can always choose a basis where these matrices are real and diagonal [145], which we will assume from now on. In this basis, the Yukawa interactions read

$$\begin{aligned} S_{\text{Yukawa}} = & \int d^4x \int_{-\pi}^{\pi} d\phi \sqrt{G} \mathcal{L}_{\text{Yukawa}} \\ = & - \int d^4x \int_{-\pi}^{\pi} d\phi \delta(|\phi| - \pi) e^{-4\sigma} \left[\epsilon_{ab} \bar{Q}_{aL} \Phi_b^\dagger \mathbf{Y}_u^{5D,C} u_R + \epsilon_{ab} \bar{Q}_{aR} \Phi_b^\dagger \mathbf{Y}_u^{5D,S} u_L \right. \\ & \left. + \bar{Q}_L \Phi \mathbf{Y}_d^{5D,C} d_R + \bar{Q}_R \Phi \mathbf{Y}_d^{5D,S} d_L + \text{h.c.} \right] \\ \ni & - \int d^4x r \int_{-\pi}^{\pi} d\phi e^{-3\sigma} \frac{v \delta(|\phi| - \pi)}{\sqrt{2}r} \sum_{Q,q} [\bar{Q}_L \mathbf{Y}_q^{5D,C} q_R + \bar{Q}_R \mathbf{Y}_q^{5D,S} q_L + \text{h.c.}], \end{aligned} \quad (2.66)$$

where $\epsilon = i\sigma^2$ and \mathbf{Y}_q^{5D} are the fundamental 5D Yukawa matrices. Due to their mass dimension $[\mathbf{Y}_q^{5D}] = -1$, it is convenient to define [163, 167]

$$\mathbf{Y}_q \equiv \frac{k}{2} \mathbf{Y}_q^{5D}, \quad |(\mathbf{Y}_q)_{ij}| \leq y_\star = \mathcal{O}(1). \quad (2.67)$$

Contrary to the SM, the dimensionless matrices \mathbf{Y}_q are assumed to have anarchical structure, meaning they are non-hierarchical matrices with complex elements bounded from above by y_\star . In order not to clash with the Yukawa perturbativity bound, the typical choice is $y_\star = 3$. In the phenomenological analysis in Chapter 5, we will however also choose different $\mathcal{O}(1)$ values. The perturbativity bound is discussed in Appendix B.

In (2.66) it has been distinguished between the two Yukawa matrices $\mathbf{Y}_q^{5D,C}$ and $\mathbf{Y}_q^{5D,S}$ for the Z_2 -even and Z_2 -odd fields, respectively, where the superscripts refer to the profiles

⁶We only focus on the free kinetic action here. The interactions with the gauge fields can be included by the replacement $\partial_M \rightarrow D_M$, where D_M is the covariant derivative (2.11).

in the KK decomposition of the fermion fields, see below. While this differentiation is possible for a brane-localized Higgs sector, it is forbidden by 5D Lorentz invariance for a bulk Higgs. Thus, the choice $\mathbf{Y}_q^{5D,C} = \mathbf{Y}_q^{5D,S}$ could be motivated by considering a brane-localized Higgs as a limit of a bulk Higgs. We will encounter an example in Section 4.1, however, where it is not always possible to obtain the results in a brane-Higgs scenario as a limit of a bulk Higgs. Therefore, it would be somewhat more natural to impose two different Yukawa matrices for RS models with a brane-localized Higgs sector. On the other hand, we will see that the leading contributions only depend on $\mathbf{Y}_q^{5D,C}$, while the matrices $\mathbf{Y}_q^{5D,S}$ have minor effects. In the following, it will therefore be assumed that $\mathbf{Y}_q^{5D,C} = \mathbf{Y}_q^{5D,S} = \mathbf{Y}_q^{5D}$. We will come back to the possibility of two different Yukawa matrices when necessary. For the generation of hierarchies that will be focused on in the next subsection, the distinction between the two matrices is irrelevant, since they are both structureless and have $\mathcal{O}(1)$ elements.

The Kaluza-Klein Decomposition and the Equations of Motion

In the next step, we decompose the 5D quark fields $Q = (U, D)$ and $q = u, d$. Compared to the gauge-boson case, the decomposition is a little bit more involved due to the flavor degrees of freedom and to the mixing in the Yukawa sector. In fact, the latter leads to diagrams, where a zero mode of the $SU(2)_L$ doublet couples to a KK mode of the $SU(2)_L$ singlets. This shows that the resulting left- and right-handed mass eigenstates $q_{L,R}^{(n)}$ should be part of the KK decomposition of both the 5D doublet and singlet. So, in anticipation of what is happening, we choose the following KK decomposition for the up-type quarks

$$\begin{aligned} U_L(x, t) &= \frac{1}{\sqrt{r}} \frac{t^2}{\epsilon^2} \sum_n \mathbf{C}_n^Q(t) a_n^U u_L^{(n)}(x), & U_R(x, t) &= \frac{1}{\sqrt{r}} \frac{t^2}{\epsilon^2} \sum_n \mathbf{S}_n^Q(t) a_n^U u_R^{(n)}(x), \\ u_L(x, t) &= \frac{1}{\sqrt{r}} \frac{t^2}{\epsilon^2} \sum_n \mathbf{S}_n^u(t) a_n^u u_L^{(n)}(x), & u_R(x, t) &= \frac{1}{\sqrt{r}} \frac{t^2}{\epsilon^2} \sum_n \mathbf{C}_n^u(t) a_n^u u_R^{(n)}(x), \end{aligned} \quad (2.68)$$

and likewise for the down-type quark sector. The superscript n labels the different mass eigenstates in the effective 4D theory such that 1, 2, 3 refer to the SM quarks, while $n = 4, \dots, 9$ label the six quark modes of the first level (due to the doubling of the degrees of freedom at each KK level), and so on. The Z_2 -even and Z_2 -odd quark profiles $\mathbf{C}_n^{Q,u}(t)$ and $\mathbf{S}_n^{Q,u}(t)$ are 3×3 matrices in generation space and correspond to the solutions with (NN) and (DD) BCs, respectively. The 3-component a -vectors $a_n^{(U,u)}$ describe the flavor mixings of the 5D interaction states into 4D mass eigenstates which are generated by the Yukawa interaction on the IR brane. Therefore, while $SU(2)_L$ gauge symmetry implies that the $SU(2)_L$ doublet quark fields have the same profile functions $\mathbf{C}_n^U = \mathbf{C}_n^D \equiv \mathbf{C}_n^Q$ and $\mathbf{S}_n^U = \mathbf{S}_n^D \equiv \mathbf{S}_n^Q$, the vectors $a_n^{U,D}$ do not coincide, since the two components are treated different in the Yukawa interactions. Moreover, the profile functions can be chosen to be diagonal and real, whereas the a -vectors are complex in general. In the limit $v \rightarrow 0$, corresponding to a situation where the Yukawa interactions are switched off, the a -vectors become unit vectors and no flavor mixing occurs.

Although not relevant for the rest of this section, it will be convenient to introduce a compact notation, where the left- and right-handed components of the up- and down-type

states are collected into six-component vectors

$$\mathcal{U}_A(x, t) \equiv \sqrt{\frac{2\pi r}{L\epsilon}} \frac{\epsilon^2}{t^2} \begin{pmatrix} U_A(x, t) \\ u_A(x, t) \end{pmatrix}, \quad \mathcal{D}_A(x, t) \equiv \sqrt{\frac{2\pi r}{L\epsilon}} \frac{\epsilon^2}{t^2} \begin{pmatrix} D_A(x, t) \\ d_A(x, t) \end{pmatrix}, \quad (2.69)$$

with $A = L, R$. They are collectively referred to as $\mathcal{Q}_{L,R}$. The main advantage of this notation is that the factors appearing in integrals are absorbed. The newly-defined vectors $\mathcal{Q}_{L,R}$ have mass dimension 3/2 and can be written as a KK decomposition

$$\mathcal{Q}_A(x, t) = \sum_n \mathcal{Q}_A^{(n)}(t) q_A^{(n)}(x); \quad A = L, R, \quad (2.70)$$

where the functions $\mathcal{Q}_{L,R}^{(n)}$ denote the wave functions of the left- and right-handed components of the n^{th} KK mass eigenstates. From the KK decompositions (2.68) we deduce that the profiles are given by

$$\mathcal{Q}_L^{(n)}(t) \equiv \sqrt{\frac{2\pi}{L\epsilon}} \begin{pmatrix} \mathbf{C}_n^Q(t) a_n^Q \\ \mathbf{S}_n^q(t) a_n^q \end{pmatrix}, \quad \mathcal{Q}_R^{(n)}(t) \equiv \sqrt{\frac{2\pi}{L\epsilon}} \begin{pmatrix} \mathbf{S}_n^Q(t) a_n^Q \\ \mathbf{C}_n^q(t) a_n^q \end{pmatrix}. \quad (2.71)$$

Note that the upper (lower) three components denote the contributions from the 5D doublet (singlet) with corresponding chirality. Using this notation will lead to very compact expressions for overlap integrals, see subsequent subsection, and for the 5D fermion propagator derived in Chapter 3.

We now proceed with the derivation of the EOMs for the profiles functions. Inserting the decomposition (2.68) into the 5D action (2.64) and matching onto the canonical 4D fermion action yields

$$S_{4\text{D}} = \sum_{q=u,d} \sum_n \int d^4x \left[\bar{q}^{(n)}(x) i\not{\partial} q^{(n)} - m_n \bar{q}^{(n)}(x) q^{(n)}(x) \right]. \quad (2.72)$$

While the kinetic term gives rise the orthonormalization relation

$$\begin{aligned} & \int_{\epsilon}^1 dt \mathcal{Q}_{L,R}^{(n)\dagger}(t) \mathcal{Q}_{L,R}^{(n)}(t) \\ &= \frac{2\pi}{L\epsilon} \int_{\epsilon}^1 dt \left\{ a_m^{Q,q\dagger} \mathbf{C}_m^{Q,q}(t) \mathbf{C}_n^{Q,q}(t) a_n^{Q,q} + a_m^{q,Q\dagger} \mathbf{S}_m^{q,Q}(t) \mathbf{S}_n^{q,Q}(t) a_n^{q,Q} \right\} = \delta_{nm}, \end{aligned} \quad (2.73)$$

the mass term leads to the EOMs [145, 149, 163]

$$\begin{aligned} (-t\partial_t - c_Q) \mathbf{S}_n^Q(t) a_n^Q &= -x_n t \mathbf{C}_n^Q(t) a_n^Q + \frac{v\delta(t-1)}{\sqrt{2}M_{\text{KK}}} \mathbf{Y}_q \mathbf{C}_n^q(t) a_n^q, \\ (t\partial_t + c_q) \mathbf{S}_n^q(t) a_n^q &= -x_n t \mathbf{C}_n^q(t) a_n^q + \frac{v\delta(t-1)}{\sqrt{2}M_{\text{KK}}} \mathbf{Y}_q^\dagger \mathbf{C}_n^Q(t) a_n^Q, \\ (t\partial_t - c_Q) \mathbf{C}_n^Q(t) a_n^Q &= -x_n t \mathbf{S}_n^Q(t) a_n^Q + \frac{v\delta(t-1)}{\sqrt{2}M_{\text{KK}}} \mathbf{Y}_q \mathbf{S}_n^q(t) a_n^q, \\ (-t\partial_t + c_q) \mathbf{C}_n^q(t) a_n^q &= -x_n t \mathbf{S}_n^q(t) a_n^q + \frac{v\delta(t-1)}{\sqrt{2}M_{\text{KK}}} \mathbf{Y}_q^\dagger \mathbf{S}_n^Q(t) a_n^Q, \end{aligned} \quad (2.74)$$

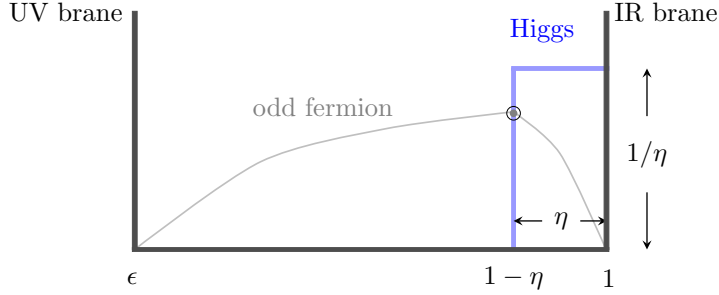


FIGURE 2.1: Visualization of the regularized Higgs profile. The region $t \in [\epsilon, 1 - \eta]$ is called the *bulk* part, whereas the interval $t \in [1 - \eta, 1]$ is referred to as the *sliver* part. The gray curve schematically shows the behavior of the Z_2 -odd fermion profiles in both regions, which are supposed to match at $t = 1 - \eta$.

with the normalized KK masses x_n and the bulk mass parameters $\mathbf{c}_{Q,q} \equiv \pm \mathbf{M}_{Q,q}/k$.⁷ In [145], the terms involving the δ -functions on the right-hand side of the last two lines in (2.74) have been omitted, since the Z_2 -odd profiles vanish at the IR brane. As we will see below, neglecting these terms is not correct. Off the IR brane, i.e. $t \neq 1$, the Yukawa terms do not contribute and the EOMs reduce to the differential equations for the free fermions with the corresponding solutions. One way to find a solution to (2.74) is therefore to take the homogenous solutions in the bulk and consider the Yukawa couplings as perturbations [159, 163, 167–171]. In this way, we obtain the solutions order by order in v^2/M_{KK}^2 . However, we will derive the solution with an exact dependence on the Yukawa matrices which enter through the BCs [145, 149, 167, 172, 173]. Both approaches are equivalent [174], although the latter is more straightforward and will be adopted here.

At this point, we have to come back to the Higgs profile described by a δ -function in the case of a brane-localized Higgs field. In contrast to the boson case, we cannot just move the δ -function infinitesimally into the bulk in order to obtain the corresponding BCs at 1^- . The derived boundary conditions would be in conflict with the EOMs (2.74). For the fermion case, it is therefore important to regularize the δ -function properly. In [149], the authors used an arbitrary regularized profile $\delta^\eta(t - 1)$ with infinitesimal support $[1 - \eta, 1]$ and they showed that in the limit $\eta \rightarrow 0$ the results do not depend on the specific choice of the regularization. Thus, it is justified to use the simple rectangular regularization

$$\delta^\eta(t - 1) = \frac{1}{\eta} \theta(t - 1 + \eta), \quad \text{with } \eta \ll 1, \quad (2.75)$$

which effectively divides the extra dimension into a *bulk* ($t < 1 - \eta$) and a small *sliver* part ($t > 1 - \eta$), as illustrated in Figure 2.1. In these regions of the fifth dimension, the EOMs (2.74) possess independent bulk and sliver solutions.

Continuity requires these two solutions to be equal at $t = 1 - \eta$ and after sending $\eta \rightarrow 0$, this gives a (modified) boundary condition for the bulk profiles at 1^- . If η is small enough, i.e. $\eta \ll v|Y|/M_{\text{KK}}$ (this is the reason for the inequality on the right-hand side of (2.4)), the Yukawa term in (2.74) dominates the remaining mass terms so that

⁷The choice of the sign is such that it is now possible to interpret both left- and right-handed fermions as e.g. UV-localized for $c_{L,R} < -1/2$, and correspondingly for $c_{L,R} > -1/2$. Recall that in (1.105) we have had to distinguish between the two chiralities due to the definition of the bulk mass parameter without the sign.

in the sliver only the following terms in the EOM are relevant⁸

$$\begin{aligned} -\partial_t \mathbf{S}_n^Q(t) a_n^Q &= \frac{v}{\sqrt{2}M_{\text{KK}} \eta} \mathbf{Y}_q \mathbf{C}_n^q(t) a_n^q, & \partial_t \mathbf{S}_n^q(t) a_n^q &= \frac{v}{\sqrt{2}M_{\text{KK}} \eta} \mathbf{Y}_q^\dagger \mathbf{C}_n^Q(t) a_n^Q, \\ -\partial_t \mathbf{C}_n^q(t) a_n^q &= \frac{v}{\sqrt{2}M_{\text{KK}} \eta} \mathbf{Y}_q^\dagger \mathbf{S}_n^Q(t) a_n^Q, & \partial_t \mathbf{C}_n^Q(t) a_n^Q &= \frac{v}{\sqrt{2}M_{\text{KK}} \eta} \mathbf{Y}_q \mathbf{S}_n^q(t) a_n^q. \end{aligned} \quad (2.76)$$

The two equations on the left- and right-hand side can be decoupled at the price of obtaining the second-order differential equations

$$\left[\partial_t^2 - \left(\frac{\mathbf{X}_q}{\eta} \right)^2 \right] \mathbf{S}_n^Q(t) = 0, \quad \left[\partial_t^2 - \left(\frac{\bar{\mathbf{X}}_q}{\eta} \right)^2 \right] \mathbf{S}_n^q(t) = 0, \quad (2.77)$$

where we have introduced the abbreviations

$$\mathbf{X}_q \equiv \frac{v}{\sqrt{2}M_{\text{KK}}} \sqrt{\mathbf{Y}_q \mathbf{Y}_q^\dagger}, \quad \bar{\mathbf{X}}_q \equiv \frac{v}{\sqrt{2}M_{\text{KK}}} \sqrt{\mathbf{Y}_q^\dagger \mathbf{Y}_q}, \quad (2.78)$$

for the positive, hermitian 3×3 matrices that are give entirely by the dimensionless 5D Yukawa matrices. The general solutions to these differential equations are hyperbolic functions. With the help of the boundary conditions $\mathbf{S}_n^{Q,q}(1-\eta)|_{\text{bulk}} = \mathbf{S}_n^{Q,q}(1-\eta)|_{\text{sliver}}$ and $\mathbf{S}_n^{Q,q}(1) = 0$, which follows from the Dirichlet BC for the S -profiles, one obtains the solutions

$$\begin{aligned} \mathbf{S}_n^Q(t) &= \frac{\sinh\left(\frac{\mathbf{X}_q}{\eta}(1-t)\right)}{\sinh(\mathbf{X}_q)} \mathbf{S}_n^Q(1^-), & \mathbf{S}_n^q(t) &= \frac{\sinh\left(\frac{\bar{\mathbf{X}}_q}{\eta}(1-t)\right)}{\sinh(\bar{\mathbf{X}}_q)} \mathbf{S}_n^q(1^-), \\ \mathbf{C}_n^Q(t) &= \frac{\cosh\left(\frac{\mathbf{X}_q}{\eta}(1-t)\right)}{\cosh(\mathbf{X}_q)} \mathbf{C}_n^Q(1^-), & \mathbf{C}_n^q(t) &= \frac{\cosh\left(\frac{\bar{\mathbf{X}}_q}{\eta}(1-t)\right)}{\cosh(\bar{\mathbf{X}}_q)} \mathbf{C}_n^q(1^-). \end{aligned} \quad (2.79)$$

Here, we have used that the solutions for the C -profiles follow from (2.76). Inserting above solutions into the first line of (2.76) and integrating over the small sliver $t \in [1-\eta, 1]$, one finally ends up with a relation between the bulk solutions at the boundary between bulk and sliver ($t = 1^-$)

$$\begin{aligned} \mathbf{S}_n^Q(1^-) a_n^Q &= \frac{v}{\sqrt{2}M_{\text{KK}}} \tilde{\mathbf{Y}}_q \mathbf{C}_n^q(1^-) a_n^q, \\ -\mathbf{S}_n^q(1^-) a_n^q &= \frac{v}{\sqrt{2}M_{\text{KK}}} \tilde{\mathbf{Y}}_q^\dagger \mathbf{C}_n^Q(1^-) a_n^Q. \end{aligned} \quad (2.80)$$

Note that these are conditions for the profiles at $t = 1^-$, not $t = 1$, where the S -profiles vanish. The quantities

$$\tilde{\mathbf{Y}}_q \equiv \frac{\tanh \mathbf{X}_q}{\mathbf{X}_q} \mathbf{Y}_q \quad (2.81)$$

are modified Yukawa matrices that differ from the original Yukawas \mathbf{Y}_q by corrections of the order $\mathcal{O}(v^2/M_{\text{KK}}^2)$. It is straightforward to derive the eigenvalue equation and expressions for the a -vectors from (2.80). Since the diagonal matrices $\mathbf{C}_n^{Q,q}$ and $\mathbf{S}_n^{Q,q}$ are non-singular (otherwise the corresponding SM quark would have no kinetic term),

⁸This discussion follows [149].

they can be inverted and it follows

$$\begin{aligned} \mathbf{S}_n^Q(1^-) a_n^Q &= -\frac{v^2}{2M_{\text{KK}}^2} \tilde{\mathbf{Y}}_q \mathbf{C}_n^q(1^-) [\mathbf{S}_n^q(1^-)]^{-1} \tilde{\mathbf{Y}}_q^\dagger \mathbf{C}_n^Q(1^-) a_n^Q, \\ \mathbf{S}_n^q(1^-) a_n^q &= -\frac{v^2}{2M_{\text{KK}}^2} \tilde{\mathbf{Y}}_q^\dagger \mathbf{C}_n^Q(1^-) [\mathbf{S}_n^Q(1^-)]^{-1} \tilde{\mathbf{Y}}_q \mathbf{C}_n^q(1^-) a_n^q. \end{aligned} \quad (2.82)$$

These relations form a system of $2N_g$ linear equations for the components of the vectors $a_n^{Q,q}$. The mass eigenvalues can be determined by the zeroes of the determinant

$$\det \left(\mathbf{1} - \frac{v^2}{2M_{\text{KK}}^2} [\mathbf{S}_n^Q(1^-)]^{-1} \tilde{\mathbf{Y}}_q \mathbf{C}_n^q(1^-) [-\mathbf{S}_n^q(1^-)]^{-1} \tilde{\mathbf{Y}}_q^\dagger \mathbf{C}_n^Q(1^-) \right) = 0, \quad (2.83)$$

and, with their help, one obtains the eigenvectors $a_n^{Q,q}$ from (2.82).

Before we proceed with the determination of the bulk profiles, it will be convenient for the later analysis to rewrite the EOMs (2.74) and the (modified) BCs (2.80) in the compact notation introduced at the beginning of this subsection. Using (2.71), one finds

$$\begin{aligned} \partial_t \mathcal{Q}_L^{(n)}(t) &= -x_n^q \mathcal{Q}_R^{(n)}(t) + \mathcal{M}_q(t) \mathcal{Q}_L^{(n)}(t), \\ -\partial_t \mathcal{Q}_R^{(n)}(t) &= -x_n^q \mathcal{Q}_L^{(n)}(t) + \mathcal{M}_q(t) \mathcal{Q}_R^{(n)}(t), \end{aligned} \quad (2.84)$$

where

$$\mathcal{M}_q(t) = \frac{1}{t} \begin{pmatrix} \mathbf{c}_Q & 0 \\ 0 & -\mathbf{c}_q \end{pmatrix} + \frac{v}{\sqrt{2}M_{\text{KK}}} \delta^n(t-1) \begin{pmatrix} 0 & \mathbf{Y}_q \\ \mathbf{Y}_q^\dagger & 0 \end{pmatrix} \quad (2.85)$$

is the generalized 6×6 mass matrix with the regularized δ -function. The boundary conditions can be written as

$$(0 \ 1) \mathcal{Q}_L^{(n)}(t_i) = 0, \quad (1 \ 0) \mathcal{Q}_R^{(n)}(t_i) = 0, \quad \text{for } t_i \in \{\epsilon, 1\}. \quad (2.86)$$

One can also drop the Yukawa-dependent term in (2.85) and use the modified BCs at $t = 1^-$ (2.80)

$$\left(\frac{v \tilde{\mathbf{Y}}_q^\dagger}{\sqrt{2}M_{\text{KK}}} \quad 1 \right) \mathcal{Q}_L^{(n)}(1^-) = 0, \quad \left(1 \quad -\frac{v \tilde{\mathbf{Y}}_q}{\sqrt{2}M_{\text{KK}}} \right) \mathcal{Q}_R^{(n)}(1^-) = 0, \quad (2.87)$$

instead. Note that the entries of the vectors on the left-hand side of the obey BCs are 3×3 matrices in generation space.

Bulk Profiles

We now derive solutions for the profile functions in the bulk. Dropping the flavor indices of c_{Q_i, q_i} , one finds the profile functions [163, 168]

$$\begin{aligned} C_n^{(Q,q)}(t) &= \mathcal{N}_n(c_{Q,q}) \sqrt{\frac{Lct}{\pi}} f_n^+(t, c_{Q,q}), \\ S_n^{(Q,q)}(t) &= \pm \mathcal{N}_n(c_{Q,q}) \sqrt{\frac{Lct}{\pi}} f_n^-(t, c_{Q,q}), \end{aligned} \quad (2.88)$$

where the functions f_n^\pm are combinations of Bessel functions

$$f_n^\pm(t, c) = J_{-\frac{1}{2}-c}(x_n \epsilon) J_{\mp\frac{1}{2}+c}(x_n t) \pm J_{\frac{1}{2}+c}(x_n \epsilon) J_{\pm\frac{1}{2}-c}(x_n t). \quad (2.89)$$

Note that, since we have expressed the solution solely by first-order Bessel functions J_α , equation (2.89) is only valid for non-integer $c \pm 1/2$, while for integer values a limiting procedure is necessary. The orthonormality relation (2.73) implies the normalization condition

$$2 \int_\epsilon^1 dt t [f_n^\pm(t, c)]^2 = \frac{1}{\mathcal{N}_n^2(c)} \pm \frac{f_n^+(1, c) f_n^-(1^-, c)}{x_n}, \quad (2.90)$$

which can be used to derive the normalization constant

$$\mathcal{N}_n^{-2}(c) = [f_n^+(1, c)]^2 + [f_n^-(1, c)]^2 - \frac{2c}{x_n} f_n^+(1, c) f_n^-(1, c) - \epsilon^2 [f_n^+(\epsilon, c)]^2. \quad (2.91)$$

As in the boson case, we can derive approximate formulas for the profiles of the SM particles, whose masses m_n^q are much smaller than the KK scale M_{KK} . Expanding the given profiles (2.88) in the limit $x_n \ll 1$, we obtain

$$\begin{aligned} C_n^{(Q,q)}(\phi) &\approx \sqrt{\frac{L\epsilon}{\pi}} F(c_{Q,q}) t^{c_{Q,q}}, \\ S_n^{(Q,q)}(\phi) &\approx \pm \text{sgn}(\phi) \sqrt{\frac{L\epsilon}{\pi}} x_n F(c_{Q,q}) \frac{t^{1+c_{Q,q}} - \epsilon^{1+2c_{Q,q}} t^{-c_{Q,q}}}{1 + 2c_{Q,q}}, \end{aligned} \quad (2.92)$$

which is referred to as the *zero-mode approximation* (ZMA). Accordingly, the function

$$F(c) \equiv \text{sgn}[\cos(\pi c)] \sqrt{\frac{1+2c}{1-\epsilon^{1+2c}}}, \quad (2.93)$$

which determines the overlap of the C -profiles with the IR brane, is called *zero-mode profile*. Note that the S -profiles are proportional to the inverse of the zero-mode profile when approaching the IR brane from the left, i.e. at 1^- . We finish the discussion of the quark profiles with an investigation of the zero-mode profile for different ranges of the bulk mass parameters

$$F(c) \approx \begin{cases} -\sqrt{-1-2c} \epsilon^{-c-1/2}, & -3/2 < c < -1/2, \\ \sqrt{1+2c}, & -1/2 < c < 1/2. \end{cases} \quad (2.94)$$

The crucial point of (2.93) is that small $\mathcal{O}(1)$ differences in the bulk mass parameters c_{Q_i, q_i} could explain large differences in couplings to the Higgs and gauge bosons. This will be the main subject of Subsection 2.2.3.

Modifications in the Yukawa Sector for a Bulk Higgs

Before this will be turned to, we consider what changes in the Yukawa sector in the presence of a bulk-Higgs field. Instead of (2.66), we have in a model with a bulk-Higgs field

$$-\mathcal{L}_{\text{Yuk}}^{\text{bulk}}(x) = \sum_{q=u,d} \int_\epsilon^1 dt \frac{v(t) + h(x, t)}{\sqrt{2}} \bar{Q}_L(x, t) \frac{1}{\sqrt{r}} \begin{pmatrix} 0 & \mathbf{Y}_{q, \text{bulk}}^{5\text{D}} \\ \mathbf{Y}_{q, \text{bulk}}^{5\text{D}\dagger} & 0 \end{pmatrix} Q_R(x, t) + \text{h.c.}, \quad (2.95)$$

where we have used the compact notation for the fermion fields (2.69). The KK decomposition of the 5D Higgs field $h(x, t)$ can be found in (2.56), where only the zero-mode $h_0(x)$ will be relevant for the following discussion. Note that the 5D Yukawa matrices $\mathbf{Y}_{q,\text{bulk}}^{5D}$ now have mass dimension $-1/2$ which leads to a potentially large upper perturbativity bound y_* , see Appendix B. The question we want to address here is how to match the two expressions onto each other so that in the limit $\beta \rightarrow \infty$ we can obtain the brane-Higgs case from a bulk Higgs. For this, we must rewrite the functions $v(t)$ from (2.52) and $\chi_0(t)$ from (2.63) in terms of functions with unit area, which can be mapped onto the normalized distributions $\delta_v^\eta(t-1)$ and $\delta_h^\eta(t-1)$. We obtain

$$\begin{aligned} v(t) &= v_4 \sqrt{\frac{L}{\pi}} \frac{\sqrt{1+\beta}}{2+\beta} \delta_v^{1/\beta}(t-1), \\ \chi_0(t) &= \sqrt{\frac{L}{\pi}} \frac{\sqrt{1+\beta}}{2+\beta} \left[1 + \frac{\beta x_0^2}{4(1+\beta)(2+\beta)(4+\beta)} + \dots \right] \delta_h^{1/\beta}(t-1), \end{aligned} \quad (2.96)$$

with

$$\begin{aligned} \delta_v^{1/\beta}(t-1) &= (2+\beta) t^{1+\beta}, \\ \delta_h^{1/\beta}(t-1) &= (2+\beta) t^{1+\beta} \left[1 - \frac{x_0^2}{4(1+\beta)} \left(t^2 - \frac{2+\beta}{4+\beta} \right) + \dots \right]. \end{aligned} \quad (2.97)$$

Here, $1/\beta$ plays the role of the regulator η that was used in the brane-localized Higgs case. Using the quark bilinear terms as a reference, the corresponding matching relations between the two Yukawa matrices read

$$\mathbf{Y}_q \equiv \frac{k}{2} \mathbf{Y}_q^{5D} = \frac{\sqrt{k(1+\beta)}}{2+\beta} \mathbf{Y}_{q,\text{bulk}}^{5D}. \quad (2.98)$$

The quantities on the left-hand side of the equation are the dimensionless Yukawa matrices introduced in (2.67), whose elements are assumed to be random numbers bounded in magnitude by y_* . If one used the $hq\bar{q}$ couplings instead, the above relation would receive corrections of $\mathcal{O}(x_0^2)$.

We are now in a position to study the limit $\beta \gg 1$ ($\eta \rightarrow 0$), in which the profile functions in (2.97) become strongly localized near the IR brane. The Yukawa matrices of the bulk-Higgs model must be identified with $\mathbf{Y}_q \leftrightarrow \sqrt{k/\beta} \mathbf{Y}_{q,\text{bulk}}^{5D} \approx (k/\sqrt{\mu}) \mathbf{Y}_{q,\text{bulk}}^{5D}$. It would be inappropriate to conclude that the Yukawa matrices \mathbf{Y}_q vanish in the limit $\beta \rightarrow \infty$ from this relation. Rather, one should consider the dimensionless Yukawa couplings as fixed quantities which are related to the observed masses and mixing angles of the SM quarks by means of relations derived in [145]. It then follows that the dimensionful Yukawa matrices $\mathbf{Y}_{q,\text{bulk}}^{5D}$ must scale with $\sqrt{\beta/k} \approx \sqrt{\mu}/k$ (see also the discussion in [175]). Finally, since t is pushed near 1, one can conclude from (2.97) that

$$\frac{\delta_h^{1/\beta}(t-1)}{\delta_v^{1/\beta}(t-1)} = 1 + \mathcal{O}\left(\frac{m_h^2}{\beta^2 M_{\text{KK}}^2}\right), \quad (2.99)$$

and the two profiles become identical.

The discussion shall be finished with the statement that taking the limit of very large β is not particularly natural, since $\beta = \sqrt{4 + \mu^2/k^2}$ is naturally of $\mathcal{O}(1)$. For large β , we have the double hierarchy

$$\frac{1}{r} \ll k \ll \mu \approx \frac{M_{\text{IR}}}{2}, \quad \text{or} \quad \frac{10}{r} \sim k \sim \frac{\mu}{\beta}. \quad (2.100)$$

Large β can be achieved by taking k significantly smaller than the Planck scale (and $1/r$ yet smaller by an order of magnitude), or by assuming that μ and M_{IR} are significantly larger than M_{Pl} . The first possibility, however, appears more plausible.

2.2.3 Fermion Hierarchies and the RS-GIM Mechanism

As already outlined in Section 1.4.4, RS models with gauge and fermion fields allowed to propagate in the bulk have the intriguing feature to give an explanation for the hierarchies in the flavor sector of the SM as well as for the smallness of FCNCs. We will dwell on that in this subsection, where the explanations will be more quantitatively. In particular, we will derive the formulas that will become crucial for the generation of parameter sets used in the numerical analysis later on.

Generating Hierarchies in the Fermion Sector

We first start with the question of how many parameters the minimal RS models possess. It turns out that due to the possibility to incorporate gauge invariant bulk mass terms for fermions, getting along with the hermitian matrices $\mathbf{M}_{Q,u,d}$, we have to deal with 27 new parameters in the flavor sector [176]. To be more precise, there are 27 moduli and ten phases, which have to be compared with the nine moduli (six quark masses and three angles of the CKM matrix) and one CP-violating phase in the SM. Fortunately, these parameters are not completely arbitrary, which would question the predictivity of the RS model, but they have to obey certain relations in order to generate the proper SM masses and Wolfenstein parameters. These relations will now be derived.

The starting point of the generation of the quark zero-mode masses and quark mixings is the similarity between the RS setup of generating hierarchies by different fermion localizations in a slice of AdS_5 and the Froggatt-Nielsen mechanism, explained in Section 1.3.3. To this end, we evaluate the ZMA profiles (2.92) at 1^- , where they couple to the Higgs sector,

$$C_n^{(Q,q)}(\pi) \rightarrow \sqrt{\frac{L\epsilon}{\pi}} F(c_{Q,q}), \quad S_n^{(Q,q)}(\pi^-) \rightarrow \pm \sqrt{\frac{L\epsilon}{\pi}} \frac{x_n}{F(c_{Q,q})}. \quad (2.101)$$

With their help, the BCs can be written to LO in v^2/M_{KK}^2 in the form

$$\frac{\sqrt{2}m_n}{v} \hat{a}_n^Q = \mathbf{Y}_q^{\text{eff}} \hat{a}_n^q, \quad \frac{\sqrt{2}m_n}{v} \hat{a}_n^q = (\mathbf{Y}_q^{\text{eff}})^\dagger \hat{a}_n^Q, \quad (2.102)$$

where the effective Yukawa matrices $\mathbf{Y}_q^{\text{eff}}$ and the rescaled vectors $\hat{a}_n^{Q,q}$ are defined via

$$\mathbf{Y}_q^{\text{eff}} \equiv F(\mathbf{c}_Q) \tilde{\mathbf{Y}}_q F(\mathbf{c}_q) \quad \text{and} \quad \hat{a}_n^{Q,q} \equiv \sqrt{2} a_n^{Q,q}. \quad (2.103)$$

Moreover, we get the important equalities

$$\left(m_n^2 \mathbf{1} - \frac{v^2}{2} \mathbf{Y}_q^{\text{eff}} (\mathbf{Y}_q^{\text{eff}})^\dagger \right) \hat{a}_n^Q = 0, \quad \left(m_n^2 \mathbf{1} - \frac{v^2}{2} (\mathbf{Y}_q^{\text{eff}})^\dagger \mathbf{Y}_q^{\text{eff}} \right) \hat{a}_n^q = 0, \quad (2.104)$$

so that the mass eigenvalues can be obtained from the simple equation

$$\det \left(m_n^2 \mathbf{1} - \frac{v^2}{2} \mathbf{Y}_q^{\text{eff}} (\mathbf{Y}_q^{\text{eff}})^\dagger \right) = 0. \quad (2.105)$$

The hermitian matrices $\mathbf{Y}_q^{\text{eff}} (\mathbf{Y}_q^{\text{eff}})^\dagger$ and $(\mathbf{Y}_q^{\text{eff}})^\dagger \mathbf{Y}_q^{\text{eff}}$ ($q = u, d$) can be diagonalized by the two unitary matrices \mathbf{U}_q and \mathbf{W}_q , whose columns are formed by the eigenvectors $\hat{a}_n^{Q,q}$ ($n = 1, 2, 3$). We can see from (2.104) that the corresponding eigenvalues are m_n^2 , which also appear in the diagonalized matrix of the singular-value decomposition

$$\mathbf{Y}_q^{\text{eff}} = \mathbf{U}_q \boldsymbol{\lambda}_q \mathbf{W}_q^\dagger, \quad (2.106)$$

where

$$\boldsymbol{\lambda}_u = \frac{\sqrt{2}}{v} \mathbf{m}_u \equiv \frac{\sqrt{2}}{v} \text{diag}(m_u, m_c, m_t), \quad \boldsymbol{\lambda}_d = \frac{\sqrt{2}}{v} \mathbf{m}_d \equiv \frac{\sqrt{2}}{v} \text{diag}(m_d, m_s, m_b), \quad (2.107)$$

are diagonal, positive real matrices. The entries m_{q_i} denote the zeroth-order values of the masses of the SM quarks. In Section 4, we will calculate the next-to-leading corrections to these masses. Taking the determinant yields

$$\begin{aligned} m_u m_c m_t &= \frac{v^3}{2\sqrt{2}} |\det(\mathbf{Y}_u)| \prod_{i=1,2,3} |F(c_{Q_i}) F(c_{u_i})|, \\ m_d m_s m_b &= \frac{v^3}{2\sqrt{2}} |\det(\mathbf{Y}_d)| \prod_{i=1,2,3} |F(c_{Q_i}) F(c_{d_i})|. \end{aligned} \quad (2.108)$$

Assuming a hierarchy of the zero-mode profiles

$$|F(c_{A_1})| < |F(c_{A_2})| < |F(c_{A_3})|, \quad (2.109)$$

which is natural in the RS framework due to the small differences in the parameters c_{Q_i, q_i} , one can now apply the findings of Section 1.3.3 and identify

$$(\mathbf{Y}_q^{5D})_{ij} \leftrightarrow (g_q)_{ij}, \quad F(c_{Q_{4-i}}) \leftrightarrow \lambda^{a_j}, \quad F(c_{q_{4-j}}) \leftrightarrow \lambda^{-b_j^q}, \quad (2.110)$$

where $q = u, d$. Thus, the hierarchies of fermion masses and mixings in a warped background result from the Froggatt-Nielsen mechanism without further assumptions. It follows that the SM quark masses can be expressed by

$$\begin{aligned} m_u &= \frac{v}{\sqrt{2}} \frac{|\det(\mathbf{Y}_u)|}{|(M_u)_{11}|} |F(c_{Q_1}) F(c_{u_1})|, & m_d &= \frac{v}{\sqrt{2}} \frac{|\det(\mathbf{Y}_d)|}{|(M_d)_{11}|} |F(c_{Q_1}) F(c_{d_1})|, \\ m_c &= \frac{v}{\sqrt{2}} \frac{|(M_u)_{11}|}{|(Y_u)_{33}|} |F(c_{Q_2}) F(c_{u_2})|, & m_s &= \frac{v}{\sqrt{2}} \frac{|(M_d)_{11}|}{|(Y_d)_{33}|} |F(c_{Q_2}) F(c_{d_2})|, \\ m_t &= \frac{v}{\sqrt{2}} |(Y_u)_{33}| |F(c_{Q_3}) F(c_{u_3})|, & m_b &= \frac{v}{\sqrt{2}} |(Y_d)_{33}| |F(c_{Q_3}) F(c_{d_3})|, \end{aligned} \quad (2.111)$$

where $(M_q)_{ij}$ denotes the minor of \mathbf{Y}_q , i.e. the determinant of the square matrix formed by removing the i^{th} row and the j^{th} column from \mathbf{Y}_q . The diagonalization matrices \mathbf{U}_q

and \mathbf{W}_q , see (2.106), are given to leading order in hierarchies

$$(\mathbf{U}_q)_{ij} = (u_q)_{ij} \begin{cases} \frac{F(c_{Q_i})}{F(c_{Q_j})}, & i \leq j, \\ \frac{F(c_{Q_j})}{F(c_{Q_i})}, & i > j, \end{cases} \quad \mathbf{u}_q = \begin{pmatrix} 1 & \frac{(M_q)_{21}}{(M_q)_{11}} & \frac{(Y_q)_{13}}{(Y_q)_{33}} \\ -\frac{(M_q)_{21}^*}{(M_q)_{11}^*} & 1 & \frac{(Y_q)_{23}}{(Y_q)_{33}} \\ \frac{(M_q)_{31}^*}{(M_q)_{11}^*} & -\frac{(Y_q)_{23}^*}{(Y_q)_{33}^*} & 1 \end{pmatrix}, \quad (2.112)$$

and

$$(\mathbf{W}_q)_{ij} = (w_q)_{ij} e^{i\phi_j} \begin{cases} \frac{F(c_{q_i})}{F(c_{q_j})}, & i \leq j, \\ \frac{F(c_{q_j})}{F(c_{q_i})}, & i > j, \end{cases} \quad \mathbf{w}_q = \begin{pmatrix} 1 & \frac{(M_q)_{12}^*}{(M_q)_{11}^*} & \frac{(Y_q)_{31}^*}{(Y_q)_{33}^*} \\ -\frac{(M_q)_{12}}{(M_q)_{11}} & 1 & \frac{(Y_q)_{32}^*}{(Y_q)_{33}^*} \\ \frac{(M_q)_{13}}{(M_q)_{11}} & -\frac{(Y_q)_{32}}{(Y_q)_{33}} & 1 \end{pmatrix}. \quad (2.113)$$

The diagonal elements $(U_q)_{ii}$ have chosen to be real which is always possible due to the invariance of the singular-value decomposition (2.106) under field redefinitions. This leads to complex-valued elements $(W_q)_{ij}$, whose phase factors $e^{i\phi_j}$ are

$$e^{i\phi_j} = \text{sgn} [F(c_{Q_j})F(c_{q_j})] e^{-i\theta_j}, \quad \boldsymbol{\theta} = \begin{pmatrix} \arg(\det(\mathbf{Y}_q)) - \arg((M_q)_{11}) \\ \arg((M_q)_{11}) - \arg((Y_q)_{33}) \\ \arg((Y_q)_{33}) \end{pmatrix}. \quad (2.114)$$

The CKM matrix in the RS model is given by the SM expression $\mathbf{V}_{\text{CKM}} = \mathbf{U}_u^\dagger \mathbf{U}_d$ and can therefore be directly calculated with the help of (2.112). The Wolfenstein parameters given in (1.27) can then be easily derived at leading order and we obtain

$$\lambda = \frac{|F(c_{Q_1})|}{|F(c_{Q_2})|} \left| \frac{(M_d)_{21}}{(M_d)_{11}} - \frac{(M_u)_{21}}{(M_u)_{11}} \right|, \quad A = \frac{|F(c_{Q_2})|^3}{|F(c_{Q_1})|^2 |F(c_{Q_3})|} \left| \frac{\frac{(Y_d)_{23}}{(Y_d)_{33}} - \frac{(Y_u)_{23}}{(Y_u)_{33}}}{\left[\frac{(M_d)_{21}}{(M_d)_{11}} - \frac{(M_u)_{21}}{(M_u)_{11}} \right]^2} \right|, \\ \bar{\rho} - i\bar{\eta} = \frac{(Y_d)_{33} (M_u)_{31} - (Y_d)_{23} (M_u)_{21} + (Y_d)_{13} (M_u)_{11}}{(Y_d)_{33} (M_u)_{11} \left[\frac{(Y_d)_{23}}{(Y_d)_{33}} - \frac{(Y_u)_{23}}{(Y_u)_{33}} \right] \left[\frac{(M_d)_{21}}{(M_d)_{11}} - \frac{(M_u)_{21}}{(M_u)_{11}} \right]}. \quad (2.115)$$

Note that the CKM matrix does not depend on the diagonalization matrix \mathbf{W}_q and therefore on the right-handed zero-mode profiles $F(c_{q_i})$, as we see explicitly in above relations. It is also explicitly visible that at leading order the Wolfenstein parameters $\bar{\rho}$ and $\bar{\eta}$ do not involve any zero-mode profiles [104]. The RS setup thus predicts that these parameters are of $\mathcal{O}(1)$, while the precise values remain unexplained. The latter relations will be used as the only constraint on the anarchic 3×3 Yukawa matrices when generating parameter sets for the RS model. Details of the generation of parameter sets can be found in e.g. Appendix A of [105].⁹ The hierarchies of the remaining eight parameters (six quark masses, two Wolfenstein parameters λ and A), are determined by

⁹The input parameters, i.e. the values for SM quark masses and Wolfenstein parameters are also given there.

the nine zero-mode profiles $F(c_{Q_i, q_i})$. When deriving the parameter sets, we will reverse this and use the eight SM parameters as an input to fix eight of the nine zero-mode profiles. The remaining zero-mode profile is a free parameter and will be randomly chosen just as the Yukawa matrices. While in [145] the free parameter was chosen to be $F(c_{Q_2})$, we will use $F(c_{u_3})$, since this is the only zero-mode profile that has no exponential dependence on the bulk mass parameter c_{u_3} according to (2.93). Thus, a flat distribution of $F(c_{u_3})$ means a flat distribution for c_{u_3} . The remaining eight zero-mode profiles are then dependent on the Yukawas, the SM input parameters, and the free zero-mode profile $F(c_{u_3})$. Eventually, one finds for the profile functions of the $SU(2)_L$ doublets [105]

$$\begin{aligned} |F(c_{Q_1})| &= \frac{\sqrt{2} m_t}{v} \left(|(Y_u)_{33}| \left| \frac{(Y_d)_{23}}{(Y_d)_{33}} - \frac{(Y_u)_{23}}{(Y_u)_{33}} \right| \left| \frac{(M_d)_{21}}{(M_d)_{11}} - \frac{(M_u)_{21}}{(M_u)_{11}} \right| \right)^{-1} \frac{\lambda^3 A}{|F(c_{u_3})|}, \\ |F(c_{Q_2})| &= \frac{\sqrt{2} m_t}{v} \left(|(Y_u)_{33}| \left| \frac{(Y_d)_{23}}{(Y_d)_{33}} - \frac{(Y_u)_{23}}{(Y_u)_{33}} \right| \right)^{-1} \frac{\lambda^2 A}{|F(c_{u_3})|}, \\ |F(c_{Q_3})| &= \frac{\sqrt{2} m_t}{v} \frac{1}{|(Y_u)_{33}|} \frac{1}{|F(c_{u_3})|}, \end{aligned} \quad (2.116)$$

while the profiles of the up-type and down-type singlets read

$$\begin{aligned} |F(c_{u_1})| &= \frac{m_u}{m_t} \frac{|(Y_u)_{33}| |(M_u)_{11}|}{\det \mathbf{Y}_u} \left| \frac{(Y_d)_{23}}{(Y_d)_{33}} - \frac{(Y_u)_{23}}{(Y_u)_{33}} \right| \left| \frac{(M_d)_{21}}{(M_d)_{11}} - \frac{(M_u)_{21}}{(M_u)_{11}} \right| \frac{|F(c_{u_3})|}{\lambda^3 A}, \\ |F(c_{u_2})| &= \frac{m_u}{m_t} \frac{|(Y_u)_{33}|^2}{|(M_u)_{11}|} \left| \frac{(Y_d)_{23}}{(Y_d)_{33}} - \frac{(Y_u)_{23}}{(Y_u)_{33}} \right| \frac{|F(c_{u_3})|}{\lambda^2 A}, \end{aligned} \quad (2.117)$$

and

$$\begin{aligned} |F(c_{d_1})| &= \frac{m_d}{m_t} \frac{|(Y_u)_{33}| |(M_d)_{11}|}{\det \mathbf{Y}_d} \left| \frac{(Y_d)_{23}}{(Y_d)_{33}} - \frac{(Y_u)_{23}}{(Y_u)_{33}} \right| \left| \frac{(M_d)_{21}}{(M_d)_{11}} - \frac{(M_u)_{21}}{(M_u)_{11}} \right| \frac{|F(c_{u_3})|}{\lambda^3 A}, \\ |F(c_{d_2})| &= \frac{m_s}{m_t} \frac{|(Y_u)_{33}| |(Y_d)_{33}|}{|(M_d)_{11}|} \left| \frac{(Y_d)_{23}}{(Y_d)_{33}} - \frac{(Y_u)_{23}}{(Y_u)_{33}} \right| \frac{|F(c_{u_3})|}{\lambda^2 A}, \\ |F(c_{d_3})| &= \frac{m_b}{m_t} \frac{(Y_u)_{33}}{(Y_d)_{33}} |F(c_{u_3})|, \end{aligned} \quad (2.118)$$

respectively. The hierarchies can now be deduced directly from above expressions. It is not difficult to find

$$\frac{|F(c_{Q_1})|}{|F(c_{Q_2})|} \sim \lambda, \quad \frac{|F(c_{Q_2})|}{|F(c_{Q_3})|} \sim \lambda^2, \quad \frac{|F(c_{Q_1})|}{|F(c_{Q_3})|} \sim \lambda^3, \quad (2.119)$$

for the left-handed profiles and

$$\begin{aligned} \frac{|F(c_{u_1})|}{|F(c_{u_3})|} &\sim \frac{m_u}{m_t} \frac{1}{\lambda^3}, & \frac{|F(c_{u_2})|}{|F(c_{u_3})|} &\sim \frac{m_c}{m_t} \frac{1}{\lambda^2}, \\ \frac{|F(c_{d_1})|}{|F(c_{u_3})|} &\sim \frac{m_d}{m_t} \frac{1}{\lambda^3}, & \frac{|F(c_{d_2})|}{|F(c_{u_3})|} &\sim \frac{m_s}{m_t} \frac{1}{\lambda^2}, & \frac{|F(c_{d_3})|}{|F(c_{u_3})|} &\sim \frac{m_b}{m_t}, \end{aligned} \quad (2.120)$$

for the right-handed ones. These expressions make the hierarchical structure of the rotation matrices (2.112) and (2.113) clearly visible.

At this step, it is worth highlighting what has been achieved. With the help of the $\mathcal{O}(1)$ input parameters of the RS model, it is possible to explain the hierarchies in the fermion sector, as shown in (2.111) and (2.115). The anarchic approach to flavor moreover narrows down many of the new parameters entering the RS setup, making the model more predictive, see (2.116)–(2.118). The relations (2.119) and (2.120) explicitly show how the relative localizations of the different quarks. Note that they are given in terms of observable quantities.

Notice that, due to the fact the above relations only fix ratios of profile functions, there is some freedom in rescaling the profile functions and Yukawa matrices without changing the SM masses and mixing parameters. From (2.111) and (2.115) it is obvious that reparametrizing the profile functions of the doublet and the singlet quarks fields and keeping the Yukawas unchanged

$$F(c_{q_i}) \rightarrow \eta F(c_{Q_i}), \quad F(c_{q_i}) \rightarrow \frac{1}{\eta} F(c_{q_i}), \quad (2.121)$$

or rescaling both the profiles and the Yukawas (but still keeping them of $\mathcal{O}(1)$)

$$F(c_{q_i}) \rightarrow \eta F(c_{Q_i}), \quad F(c_{q_i}) \rightarrow \frac{1}{\eta} F(c_{q_i}), \quad \mathbf{Y}_q \rightarrow \frac{1}{\eta \eta_q} \mathbf{Y}_g \quad (2.122)$$

does not change the physical input parameters. Of course, the transformations (2.121) and (2.122) can be combined in arbitrary ways. For UV localized quarks, which have bulk mass parameters $c_i < 1/2$ and exponentially suppressed profile functions as shown in (2.94), these reparameterizations are equivalent to the shifts $c_{Q_i, q_i} \rightarrow c_{Q_i, q_i} \mp L^{-1} \ln \eta$ and $c_{Q_i, q_i} \rightarrow c_{Q_i, q_i} + L^{-1} \ln \eta_{(q)}$, respectively. This kind of freedom is referred to as *reparametrization invariance* and is a convenient tool to investigate what specific regions in parameter space predict for observables without generating a whole new set of parameters. Note, however, that the Yukawas cannot be too small due to the large top mass and too large due to the perturbativity bound.

Boson Couplings to Fermions and the RS-GIM Mechanism

According to the discussion above, the small masses of the light SM quarks can be explained by the small overlap between the quark profiles and the Higgs fields that is confined on or very close to the IR brane. In Subsection 1.4.4, we have argued qualitatively that the same mechanism is responsible for the smallness of FCNCs and is referred to as the *RS-GIM mechanism* [176–178], in reference to the GIM mechanism, which explains why loop-level FCNCs in the SM are further suppressed [49]. In this subsection, I want to give a somewhat more quantitative explanation for the occurrence of this mechanism. We will briefly discuss the structure of Wilson coefficients belonging to the four-fermion operators that lead to tree-level FCNCs. A detailed discussion of the effective Hamiltonians and their corresponding phenomenology can be found in the literature [176, 177, 179–183]. Only some important results which can explain the suppression of the FCNCs will be presented here.

Crucial ingredients for the following discussion are the boson couplings to fermions. The corresponding Feynman rules can be easily deduced from the 5D Lagrangian. As shown in [184], the interactions have a similar shape as in the SM, but the gauge-boson couplings to the left-handed fermions, which are proportional to V_{nmk} , in general differ

from the couplings to the right-handed fermions, denoted by \tilde{V}_{nmk} .¹⁰ One finds that these overlap integrals read

$$V_{nmk}^{A,\mathcal{G}} = \sqrt{2\pi} \int_{\epsilon}^1 dt \chi_m^{A,\mathcal{G}}(t) \mathcal{Q}_L^{(n)\dagger}(t) \mathcal{Q}_L^{(k)}(t), \quad \tilde{V}_{nmk}^{A,\mathcal{G}} = \sqrt{2\pi} \int_{\epsilon}^1 dt \chi_m^{A,\mathcal{G}}(t) \mathcal{Q}_R^{(n)\dagger}(t) \mathcal{Q}_R^{(k)}(t), \quad (2.123)$$

for the photon and the gluon,

$$\begin{aligned} V_{nmk}^{W^-} &= \sqrt{2\pi} \int_{\epsilon}^1 dt \chi_m^W(t) \mathcal{D}_L^{(n)\dagger}(t) \mathcal{P}_+ \mathcal{U}_L^{(k)}(t), \\ \tilde{V}_{nmk}^{W^-} &= \sqrt{2\pi} \int_{\epsilon}^1 dt \chi_m^W(t) \mathcal{D}_R^{(n)\dagger}(t) \mathcal{P}_+ \mathcal{U}_R^{(k)}(t), \\ V_{nmk}^{W^+} &= \sqrt{2\pi} \int_{\epsilon}^1 dt \chi_m^W(t) \mathcal{U}_L^{(n)\dagger}(t) \mathcal{P}_+ \mathcal{D}_L^{(k)}(t), \\ \tilde{V}_{nmk}^{W^+} &= \sqrt{2\pi} \int_{\epsilon}^1 dt \chi_m^W(t) \mathcal{U}_R^{(n)\dagger}(t) \mathcal{P}_+ \mathcal{D}_R^{(k)}(t), \end{aligned} \quad (2.124)$$

for the W boson,

$$\begin{aligned} V_{nmk}^Z &= \sqrt{2\pi} \int_{\epsilon}^1 dt \chi_m^Z(t) \mathcal{Q}_L^{(n)\dagger}(t) [g_L^q \mathcal{P}_+ + g_R^q \mathcal{P}_-] \mathcal{Q}_L^{(k)}(t), \\ \tilde{V}_{nmk}^Z &= \sqrt{2\pi} \int_{\epsilon}^1 dt \chi_m^Z(t) \mathcal{Q}_R^{(n)\dagger}(t) [g_L^q \mathcal{P}_+ + g_R^q \mathcal{P}_-] \mathcal{Q}_R^{(k)}(t), \end{aligned} \quad (2.125)$$

for the Z boson, and

$$\begin{aligned} g_{mn}^u &= \frac{1}{\sqrt{2}} \int_{\epsilon}^1 dt \delta^\eta(t-1) \mathcal{Q}_L^{\dagger(m)}(t) \begin{pmatrix} 0 & \mathbf{Y}_q \\ \mathbf{Y}_q^\dagger & 0 \end{pmatrix} \mathcal{Q}_R^{(n)}(t), \\ \tilde{g}_{mn}^u &= \frac{1}{\sqrt{2}} \int_{\epsilon}^1 dt \delta^\eta(t-1) \mathcal{Q}_R^{\dagger(m)}(t) \begin{pmatrix} 0 & \mathbf{Y}_q \\ \mathbf{Y}_q^\dagger & 0 \end{pmatrix} \mathcal{Q}_L^{(n)}(t), \end{aligned} \quad (2.126)$$

for the Higgs boson. Here, we have used the compact vector notation (2.71) for the fermion profiles and, $\mathcal{P}_+ \equiv \text{diag}(1, 0)$ and $\mathcal{P}_- \equiv \text{diag}(0, 1)$ are 6×6 matrices in the six-dimensional vector space that project out the $SU(2)_L$ doublet and singlet fields, respectively. As the photon and gluon couple to both doublets and singlets equally, there is no such matrix between the profiles. The W boson only couples to doublets which gives rise to the appearance of \mathcal{P}_+ . The Z boson couples differently, where we abbreviated $g_L^q = T_3^q - Q_q \sin \theta_w$ and $g_R^q = -Q_q \sin \theta_w$. Concerning the Higgs coupling to fermions we have used the regularized δ -function in order to account for the fact that the Z_2 -odd couplings vanish at the IR brane.

In the following, we consider processes that are induced by an exchange of KK photons. Relation (2.123) makes clear that the quark coupling to a massive KK gauge boson is non-diagonal. Only for the photon and gluon zero modes, whose profiles are flat, the overlap integral reduces to δ_{nk} . Thus, FCNCs as shown in Figure 2.2 are possible even at tree-level. These FCNCs, however, suffer from an additional suppression by a factor that is comparable with a loop suppression, as we will see below. The diagram in question can be calculated using the standard techniques, where one however has to

¹⁰The Feynman rules are collected in Appendix C.

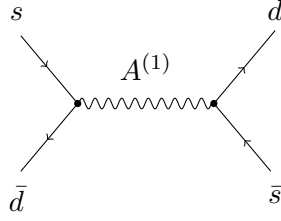


FIGURE 2.2: Tree-level diagram leading to an FCNC. Due to the non-flat profile of the KK photons, there can be flavor changes at both vertices.

include the entire tower of KK particles and encounters the expression (for $p^2 \ll M_{\text{KK}}^2$)

$$\sum_{n=1}^{\infty} \frac{\chi_n^A(t) \chi_n^A(t')}{m_n^2 - p^2} = \frac{1}{4\pi M_{\text{KK}}^2} \left[Lt_{<}^2 - t^2 \left(\frac{1}{2} - \ln t \right) - t'^2 \left(\frac{1}{2} - \ln t' \right) + \frac{1}{2L} \right] + \dots, \quad (2.127)$$

which is equivalent to the 5D propagator function whose derivation will be focused on in Chapter 3. For $p^2 = 0$, which is a good approximation for FCNCs at low energies, it is also possible to derive the term in the square bracket via a recursive procedure [145]. Multiplying the result for the infinite sum with the quark profiles and integrating over the extra dimension then yields integrals of the form ($A, B = L, R$)

$$c_{ijkl} \sim \frac{\alpha}{M_{\text{KK}}^2} \int_{\epsilon}^1 dt \int_{\epsilon}^1 dt' \mathcal{Q}_A^{(i)\dagger}(t) \mathcal{Q}_A^{(j)}(t) \mathcal{Q}_B^{(k)\dagger}(t') \mathcal{Q}_B^{(l)}(t') \times \left[Lt_{<}^2 - t^2 \left(\frac{1}{2} - \ln t \right) - t'^2 \left(\frac{1}{2} - \ln t' \right) + \frac{1}{2L} \right]. \quad (2.128)$$

The orthonormalization condition (2.73) shows that the constant term in (2.128) cannot contribute to a flavor change. Moreover, the terms only depending on t and t' , respectively, can only lead to a flavor change at one vertex, since (2.73) ensures that the coupling at the corresponding second vertex is flavor-diagonal. These processes are called $\Delta F = 1$ transitions. Two flavor changes, i.e. $\Delta F = 2$ transitions shown in Figure 2.2, can only be mediated by the term proportional to $t_{<}^2 \equiv \min[t^2, t'^2]$ in (2.128).

The overlap integral (2.128) demonstrates how the RS-GIM mechanism works. Since there are only non-negative powers of t and t' appearing in the propagator function, it is peaked towards to IR brane, which represents the IR localization of the KK bosons. According to (2.92), the profile functions for the fermions depend on the position in the extra dimension via $t^{c_{Q_i, q_i}}$. This factor only becomes large for the top quarks. For all other fermions, especially for the UV-localized light fermions, at least one of the parameters is $c_{Q_i, q_i} \lesssim -1/2$, so that the overlap between the fermion profiles and the KK gauge bosons becomes small. This is visualized in Figure 2.3. Indeed, one can show that the $\Delta F = 1$ processes are described by quantities like¹¹ [145]

$$(\Delta_{Q, q})_{ij} = \int_{\epsilon}^1 dt t^2 \mathcal{Q}_{L,R}^{(i)\dagger}(t) \mathcal{Q}_{L,R}^{(j)}(t), \quad (\Delta'_{Q, q})_{ij} = \int_{\epsilon}^1 dt t^2 \left(\frac{1}{2} - \ln t \right) \mathcal{Q}_{L,R}^{(i)\dagger}(t) \mathcal{Q}_{L,R}^{(j)}(t), \quad (2.129)$$

¹¹Other quantities contributing to $\Delta F = 1$ transitions will be encountered later.

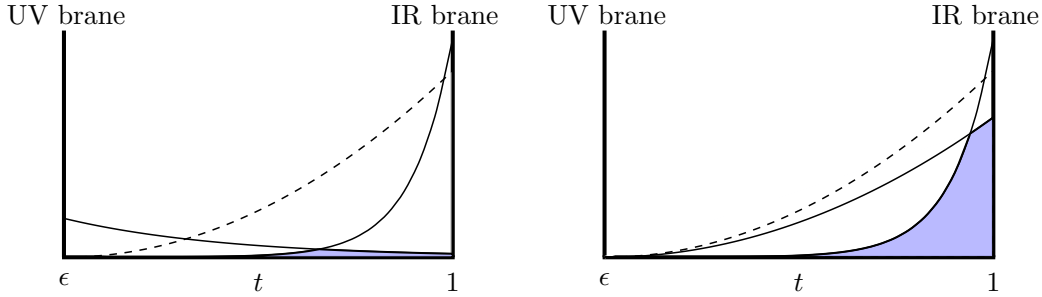


FIGURE 2.3: Visualization of the RS-GIM mechanism according to [105]. The dashed lines represent a t^2 term from the 5D gauge-boson propagator. The solid lines show the profile of a UV and an IR localized fermion zero mode (two IR localized zero modes) in the left (right) panel. The blue shaded area can be interpreted as an indicator of the size of the FCNC coupling resulting from the overlap integral including the three functions.

which scale like (at leading order in hierarchies) [145]

$$(\Delta_{Q,q}^{(i)})_{ij} \sim F(c_{Q_i,q_i}) F(c_{Q_j,q_j}). \quad (2.130)$$

We see that the flavor-changing terms are proportional to the zero-mode profile functions of the external fermions which makes the RS-GIM mechanism explicit. Since the masses are proportional to the zero-mode functions as well, one finds an approximate suppression by [105]

$$\frac{1}{M_{\text{KK}}^2} \times m_f^2 \approx \frac{1}{16\pi^2} \times \frac{m_f^2}{m_W^2}. \quad (2.131)$$

The suppression is thus of the same size as the loop-level suppression of the SM if $M_{\text{KK}} \approx 4\pi m_W$. Remarkably, this is what one hopes to expect from a model, whose goal is to solve the hierarchy problem. Note, however, that for the third-generation quarks the FCNCs are less suppressed and thus significant effects can arise in B physics and top decays. Indeed, as we will see in the next subsection, the RS contributions to the $Zb\bar{b}$ vertex are too large, which can be cured by, for example, an enlarged bulk symmetry.

It shall be stressed that the RS-GIM mechanism is very successful in suppressing FCNCs in the flavor sector and almost all observables can be brought into agreement with a KK scale of a few TeV, which in turn leads to KK modes that are in reach of the LHC. Nevertheless, there are two exceptions, namely the observable ϵ_K in the kaon sector [145, 149, 180, 181, 185] and the neutron electric dipole moment [176, 177], which for generic choices of parameters push the mass of the lightest KK gluon into the $\mathcal{O}(10-20 \text{ TeV})$ range.¹² In order to reduce this strong bound stemming from ϵ_K , one has to use either horizontal symmetries [186, 187], flavor alignment [188], an extended strong sector [189], or one could take the Higgs a little bit off the IR brane [190]. The problem of too large electric dipole moments has been addressed using the idea of spontaneous CP violation in the context of warped extra dimensions [191]. In the following, we will not further focus on these issues. It will be assumed that the techniques and results derived in the main part of this thesis can be extended to these models in a straightforward way.

¹²Moreover, it should be mentioned that the RS-GIM mechanism is not sufficient to suppress proton decay. Nevertheless, the effective suppression scale is several orders higher than the TeV scale so that this issue is not as pressing as the flavor problems above. One way to suppress proton decay even more is to impose discrete symmetries [167, 169].

2.2.4 Compatibility with Electroweak Precision Tests

In this last subsection, we will check the minimal RS model for compatibility with the electroweak precision measurements. We will see that it generically gives too large contributions to some of the precision observables. This results in a lower bound for the mass of the lightest KK gluon which cannot be tested by direct measurements at the LHC. Lowering this bound is the main motivation for the RS model with custodial protection which will be focused on in Section 2.3.

Oblique Parameters

We start with the leading order corrections to the S and T parameter in the minimal RS model. One-loop corrections have been estimated in [192–194] and are part of current work. The tree-level RS contributions originate from the mixing of the electroweak gauge bosons with their KK excitations and one finds [145, 195, 196]

$$S = \frac{2\pi v^2}{M_{\text{KK}}^2} \left(1 - \frac{1}{L}\right), \quad T = \frac{\pi v^2}{2c_w^2 M_{\text{KK}}^2} \left(L - \frac{1}{2L}\right), \quad U = 0. \quad (2.132)$$

The result is illustrated in the left plot of Figure 2.4, which shows the regions of 68% (yellow), 95% (gray) and 99% (blue) probability in the $S - T$ plane.¹³ The black cross denotes the best fit value (1.18), while the star represents the SM prediction. The orange (red) band rising in the direction of large T parameter shows (2.132) for a KK scale of $3 - 10$ ($1 - 3$) TeV. Furthermore, the dependence on the volume of the extra dimension $L \in [5, 33.5]$ is plotted with increasing L in the direction of the arrow.

We can observe that in the minimal RS model the S parameter does not receive large corrections,¹⁴ whereas the T parameter suffers from a large correction, giving rise to a lower bound $M_{\text{KK}} > 4.8$ TeV at 95% CL. This KK scale corresponds to a mass of the lightest KK gluon and photon resonance of

$$M_{g^{(1)}} > 12.0 \text{ TeV} \quad (95\% \text{ CL}). \quad (2.133)$$

The large corrections to the T parameter can be explained with the help of the dual theory of the RS model: Recall that the gauge symmetry in the bulk, which is the SM gauge symmetry in the present case, coincides with a global symmetry of the strongly-coupled sector. Unlike general TC theories, which only receive small corrections $T \sim 1/(4\pi)$, the dual theory of the minimal RS model does not contain a global $SU(2)_L \times SU(2)_R$ symmetry which protects the ρ parameter $\rho = m_W^2/(m_Z^2 c_w^2) = 1 + \alpha T$ and therefore the T parameter. The global $SU(2)_L \times SU(2)_R$ symmetry is the reason for the enlarged bulk gauge group of the custodial RS model which is able to mitigate the large corrections to the T parameter. However, there are two alternative options to obtain a consistent description of the experimental data, while allowing for masses of the first KK gauge-boson modes of the order of 5 TeV. The first possibility is to allow the Higgs to propagate in the bulk. This can be understood if one recalls that the corrections to the gauge-boson masses and profiles (2.54) and (2.55) are mitigated in bulk-Higgs models. The corrections to the S and T parameters (2.132) are determined by the latter quantities, which implies that they are reduced as well. The second possibility is to

¹³This plot has been taken from [105], whose analysis used more recent data than e.g. [145].

¹⁴This can be regarded as an appealing side-effect of bulk fermions [197], see also [105] for further explanations.

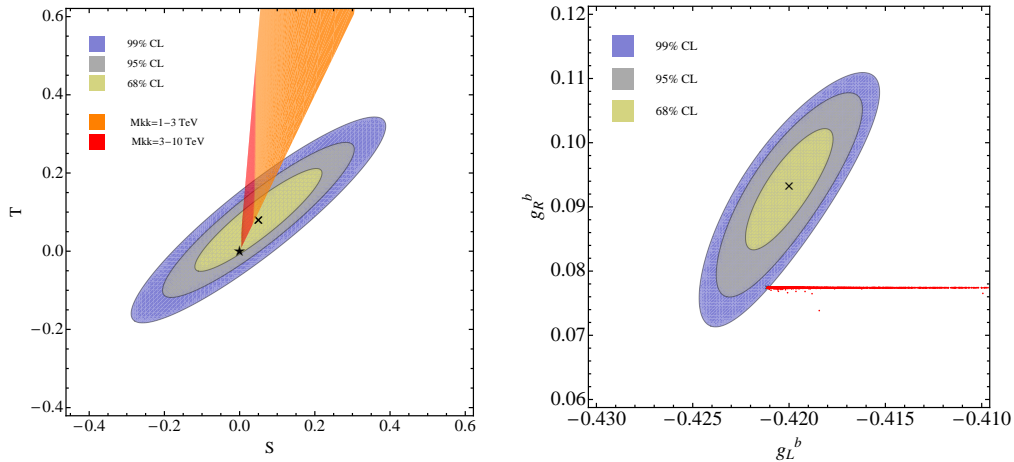


FIGURE 2.4: Left plot: Regions of 68%, 95% and 99% probability in the $S - T$ plane in the case of the minimal RS model. Shaded red (orange) are the accessible regions for $M_{KK} \in [1 - 3]$ TeV ($M_{KK} \in [3 - 10]$ TeV), growing vertically towards large values of T . The black arrow points in the direction of growing volume $L \in [5, 33.5]$. Right plot: Regions of 68%, 95% and 99% probability in the $g_L^b - g_R^b$ plane. The cross and the star denote the best fit value and the experimental value, respectively. The red colored regions indicate the predicted values for a large set of parameter points. Both plots were obtained from the analysis performed in [105].

make the volume L of the extra dimension smaller. This effect is also shown in Figure 2.4, where the value for L is varied between $L = 5$ and $L = 36$ along the black arrows. Note that for these models the hierarchy problem is only solved up to an intermediate scale $\Lambda_{UV} = e^L \text{ TeV} < M_{Pl}$. The UV completion must already set in at this scale. Inspired by little Higgs models, these models are called *little RS* (LRS) models. They however suffer from large corrections to the observable ϵ_K , which are even worse than in the minimal RS model [198]. Note that in [145] two more alternatives - a *heavy Higgs boson* [29, 199–203] and *large brane-localized kinetic terms* [195, 204, 205] - have been considered. However, since also the second option had to rely on a relatively large Higgs mass, both of them are excluded (at least disfavored in the second case) after the discovery of the 126 GeV Higgs boson at the LHC.

Corrections to $Z \rightarrow b\bar{b}$

Another process that should be investigated further is the Z decay into to b quarks. As mentioned earlier, the only electroweak precision observables that have deviations larger than 2σ are associated with this process. In the context of warped extra dimensions, $Z \rightarrow b\bar{b}$ is particularly interesting since the left-handed bottom quark is part of the $SU(2)_L$ doublet $Q_L = (U_L, D_L)$ and hence shares the same bulk mass parameter c_{Q_3} with the left-handed top quark. Due to the large top mass, the doublet field Q_L has a large overlap with the Higgs, which in turn results in a large mixing of the left-handed bottom quark with its KK excitations. Consequentially, we can expect significant effects in observables associated with $Z \rightarrow b\bar{b}$.

The Z -boson coupling to quarks can be derived using the 5D Lagrangian (2.64). It

can be written in the form [145]

$$\mathcal{L}_{4D} \ni \frac{g_5}{\sqrt{2\pi r} c_w} \left[1 + \frac{m_Z^2}{4M_{\text{KK}}^2} \left(1 - \frac{1}{L} \right) \right] Z_\mu^0 \sum_{ij} [(g_L^q)_{ij} \bar{q}_{L,i} \gamma^\mu q_{L,j} + (g_R^q)_{ij} \bar{q}_{R,i} \gamma^\mu q_{R,j}] , \quad (2.134)$$

where $i, j = 1, 2, 3$ denote the flavor indices. The matrices $(g_L^q)_{ij} \equiv V_{i0j}^Z$ and $(g_R^q)_{ij} \equiv \tilde{V}_{i0j}^Z$ can be obtained by evaluating the corresponding integrals (2.125) (with χ_0^Z given in (2.31)). Their exact shape can be found in [145]. For this discussion, it is sufficient to consider the couplings to the bottom quark, which in the ZMA approximation read

$$g_L^b \equiv (g_L^d)_{33} \rightarrow \left(-\frac{1}{2} + \frac{s_w^2}{3} \right) \left[1 - \frac{m_Z^2}{2M_{\text{KK}}^2} \frac{F^2(c_{b_L})}{3 + 2c_{b_L}} \left(L - \frac{5 + 2c_{b_L}}{2(3 + 2c_{b_L})} \right) \right] \quad (2.135)$$

$$+ \frac{m_b^2}{2M_{\text{KK}}^2} \left[\frac{1}{1 - 2c_{b_R}} \left(\frac{1}{F^2(c_{b_R})} - 1 + \frac{F^2(c_{b_R})}{3 + 2c_{b_R}} \right) + \sum_{i=1,2} \frac{|(Y_d)_{3i}|^2}{|(Y_d)_{33}|^2} \frac{1}{1 - 2c_{d_i}} \frac{1}{F^2(c_{b_R})} \right]$$

$$g_R^b \equiv (g_R^d)_{33} \rightarrow \frac{s_w^2}{3} \left[1 - \frac{m_Z^2}{2M_{\text{KK}}^2} \frac{F^2(c_{b_R})}{3 + 2c_{b_R}} \left(L - \frac{5 + 2c_{b_R}}{2(3 + 2c_{b_R})} \right) \right] \quad (2.136)$$

$$+ \frac{m_b^2}{2M_{\text{KK}}^2} \left[\frac{1}{1 - 2c_{b_L}} \left(\frac{1}{F^2(c_{b_L})} - 1 + \frac{F^2(c_{b_L})}{3 + 2c_{b_L}} \right) + \sum_{i=1,2} \frac{|(Y_d)_{i3}|^2}{|(Y_d)_{33}|^2} \frac{1}{1 - 2c_{Q_i}} \frac{1}{F^2(c_{b_L})} \right].$$

Here, we have used the weak isospin and charge for down-type quarks, $T_3^d = -\frac{1}{2}$ and $Q_d = -\frac{1}{3}$, and introduced the notation $c_{b_L} \equiv c_{Q_3}$ and $c_{b_R} \equiv c_{d_3}$. The terms in the second lines in (2.135) and (2.136) are suppressed by m_b/m_Z so that the leading terms are those in the first lines. Note that the latter are determined by the zero-mode profiles $F(c_{b_L})$ and $F(c_{b_R})$.

Provided with that we can compare the RS prediction with experimental data. The latest analysis of the $Z\bar{b}b$ coupling has been done in [105], where three observables were considered: the ratio of the width of the Z -boson decay into two bottom quarks and the total hadronic width R_b^0 , the bottom quark left-right asymmetry parameter A_b , and the forward-backward asymmetry for bottom quarks $A_{\text{FB}}^{0,b}$. While the SM predicts the values [206, 207]

$$R_b^0 = 0.21474, \quad A_b = 0.935, \quad A_{\text{FB}}^{0,b} = 0.1031, \quad (2.137)$$

the corresponding experimental results read [25]

$$\begin{aligned} R_b^0 &= 0.21629 \pm 0.00066, \\ A_b &= 0.923 \pm 0.020 \\ A_{\text{FB}}^{0,b} &= 0.992 \pm 0.0016, \end{aligned} \quad \rho = \begin{pmatrix} 1.00 & -0.08 & -0.10 \\ -0.08 & 1.00 & 0.06 \\ -0.10 & 0.06 & 1.00 \end{pmatrix}, \quad (2.138)$$

where ρ is the correlation matrix. Comparing the experimental values (2.138) with the SM prediction (2.137) immediately reproduces the deviations shown in the right plot of Figure 2.4. It shows that in order to improve the consistency with the experiment, the new-physics corrections to the left-handed coupling should be preferably large and positive, while the corrections to the right-handed couplings should be small or slightly negative.

From the leading contributions in the first lines of (2.135) and (2.136) it is obvious that the RS correction to g_L^d is large and positive, while the correction to g_R^d small and

negative, thus pointing into the opposite direction. The correction to g_R^d is due to the fact that the L -enhanced term is multiplied by $F^2(c_{b_R})$ instead of $F^2(c_{b_L})$, resulting in an suppression of $F^2(c_{b_R})/F^2(c_{b_L}) \approx \mathcal{O}(\text{few})\%$, since the left-handed doublet is more IR localized than the singlet to account for the large top quark (2.111). These corrections are not visible in Figure 2.4, where all parameter points lie entirely in the red band. Most of them therefore fail to agree with the experiment at 3σ . 10% of the scatter points lie within the experimental error ellipse, which translates into a pretty strong lower bound on the KK scale. This bound can be lowered by the custodial RS model, see (2.190) and the corresponding discussion. Another possibility to mitigate the large RS contribution to g_L^b is to reduce the value of the profile function $F(c_{b_L})$ as visible in (2.135). Using the reparametrization invariance (2.121), for $\eta < 1$, we can reshuffle between $F(c_{b_L})$ and $F(c_{b_R})$. For $\eta = 1/2$ ($1/3$), about 35 (45%) of the parameter points lie within the experimental ellipse. This means that scenarios with strongly IR-localized right-handed bottom quarks suffer from less dangerous corrections and thus tend to comply more with the experimental data.

2.3 The Custodial Randall-Sundrum Model

This section focuses on the custodial RS model, whose motivation was to mitigate the just explained large corrections to the T parameter and the $Zb\bar{b}$ coupling and thus allows for the lightest KK particles to be in reach for the direct detection at the LHC [101, 192, 193, 208]. This is achieved by an enlarged gauge group in the bulk of the extra dimension. We will focus on the model with the bulk gauge-symmetry

$$SU(3)_c \times SU(2)_L \times SU(2)_R \times U(1)_X \times P_{LR}, \quad (2.139)$$

where the two $SU(2)$ groups are broken down to the vectorial $SU(2)_V$ on the IR brane. This implements the custodial symmetry and is responsible for the protection of the T parameter [209, 210]. The additional discrete P_{LR} symmetry refers to the exchange of the two $SU(2)$ groups and is important to prevent the left-handed $Zb\bar{b}$ coupling from receiving too large corrections [211] as we will see below. On the UV brane, the symmetry breaking $SU(2)_R \times U(1)_X \rightarrow U(1)_Y$ generates the SM gauge group, which is achieved by an interplay between UV and IR boundary conditions.

In the following, first the set-up of the custodial RS model will be presented and it will be explained how the above-mentioned symmetry breaking is achieved. We will proceed in analogy to the minimal model presented in the previous section. Many technical details of the model considered here can be found in [149, 185]. We will use the notation and conventions of the former reference. It will only be dwelled on the features needed for the main part of this thesis. Subsection 2.3.3 will then give an explanation of how the electroweak precision observables are protected.

2.3.1 The Gauge Sector

We will pursue in the same way as in the minimal model. Starting with the 5D action of the gauge sector, it will be explained how the Higgs sector breaks down the bulk gauge symmetry to the custodial $SU(2)_V$ on the IR brane. The symmetry breaking on the UV brane will only be touched, since the exact mechanism will not be relevant for further discussion. We then perform the KK decomposition, where the KK modes are

the bosonic mass eigenstates, i.e. the mixing among the various weak eigenstates as well as the mixing between the fifth components and the scalar Goldstone boson of the Higgs fields are implicitly taken into account. With the help of the EOMs and BCs for the gauge-boson fields, the profiles and masses of the physical zero modes will be derived. We will confirm that all formulas also include the results in the minimal model in certain limits.

The 5D Action

Since the color sector of the bulk gauge group (2.139) is the same as in the minimal model, we will only consider the electroweak subgroup and explore what changes here. Instead of (2.6), we now deal with the following 5D electroweak gauge action

$$S_{\text{gauge}} = \int d^4x \frac{2\pi r}{L} \int_{\epsilon}^1 \frac{dt}{t} (\mathcal{L}_{L,R,X} + \mathcal{L}_{\text{Higgs}} + \mathcal{L}_{\text{GF}} + \mathcal{L}_{\text{FP}}), \quad (2.140)$$

where the gauge-kinetic terms are given by

$$\mathcal{L}_{L,R,X} = \frac{\sqrt{G}}{r} G^{KM} G^{LN} \left(-\frac{1}{4} L_{KL}^i L_{MN}^i - \frac{1}{4} R_{KL}^i R_{MN}^i - \frac{1}{4} X_{KL} X_{MN} \right). \quad (2.141)$$

The 4-components of the gauge fields L_M^i, R_M^i, X_M ($i = 1, 2, 3$) are chosen to be even under the Z_2 parity, while the fifth components are chosen to be odd, in order to arrive at a low-energy spectrum that is compatible with observation. The gauge-fixing Lagrangian will be presented after inserting the KK decomposition. As it is not relevant for the following discussion, the Faddeev-Popov ghost Lagrangian will not be shown explicitly.

The Higgs Lagrangian

$$\mathcal{L}_{\text{Higgs}} = \frac{L \delta(t-1)}{2\pi r} \left(\frac{1}{2} \text{Tr} |D_\mu \Phi|^2 - V(\Phi) \right) \quad (2.142)$$

is localized on the IR brane, where the Higgs doublet, responsible for breaking $SU(2)_L \times SU(2)_R$ to the diagonal $SU(2)_V$ on the IR brane, transforms as $(\mathbf{2}, \mathbf{2})_0$. In component notation, it is given by

$$\Phi(x) = \frac{1}{\sqrt{2}} \begin{pmatrix} v + h(x) - i\varphi^3(x) & -i\sqrt{2}\varphi^+(x) \\ -i\sqrt{2}\varphi^-(x) & v + h(x) + i\varphi^3(x) \end{pmatrix}, \quad (2.143)$$

where φ^i are real scalar fields, $\varphi^\pm = (\varphi^1 \mp i\varphi^2)/\sqrt{2}$, and v denotes the Higgs vev in the custodial RS model which differs from the value in the SM and minimal RS model. $SU(2)_L$ transformations act from the left on the bi-doublet, while the $SU(2)_R$ transformations act from the right. In order to show how the symmetry breaking is accomplished, we use the covariant derivative

$$D_\mu \Phi = \partial_\mu \Phi - ig_{L,5} L_\mu^a T_L^a \Phi + ig_{R,5} \Phi R_\mu^a T_R^a. \quad (2.144)$$

Here, $g_{L,5}$ and $g_{R,5}$ are the 5D gauge couplings associated with $SU(2)_{L,R}$, and $T_{L,R}^a = \sigma^a/2$ are the corresponding generators. For the evaluation of the kinetic term for the scalar bi-doublet, it is convenient to rotate the gauge bosons L_μ^a and R_μ^a into a new basis

of fields \tilde{A}_μ^a and V_μ^a , such that

$$\begin{pmatrix} \tilde{A}_M^a \\ V_M^a \end{pmatrix} = \begin{pmatrix} \cos \vartheta & -\sin \vartheta \\ \sin \vartheta & \cos \vartheta \end{pmatrix} \begin{pmatrix} L_M^a \\ R_M^a \end{pmatrix} \equiv \mathbf{R}_\vartheta \begin{pmatrix} L_M^a \\ R_M^a \end{pmatrix}, \quad (2.145)$$

where

$$\cos \vartheta = \frac{g_{L,5}}{\sqrt{g_{L,5}^2 + g_{R,5}^2}}, \quad \sin \vartheta = \frac{g_{R,5}}{\sqrt{g_{L,5}^2 + g_{R,5}^2}}. \quad (2.146)$$

In Subsection 2.3.3, we will see that the P_{LR} symmetry enforces that $g_{L,5} = g_{R,5}$, and hence $\cos \vartheta = \sin \vartheta = 1/\sqrt{2}$. For the time being, however, the value of ϑ will be kept as a free parameter. The Higgs vev $\langle \Phi \rangle = (v/\sqrt{2}) \mathbf{1}$ then generates a mass term

$$M_A^2 = \frac{v^2(g_{L,5}^2 + g_{R,5}^2)}{4} \quad (2.147)$$

for the fields \tilde{A}_μ^a , while the fields V_μ^a remain massless. We can also read off the boson coupling to the Higgs boson, once we replace v^2 by $(v+h)^2$. Observe that only the fields \tilde{A}_μ^a couple to the Higgs. This will become important for the derivation of the propagator in the subsequent chapter. Appropriate BCs break the extended electroweak gauge group down to the SM gauge group on the UV boundary $SU(2)_R \times U(1)_X \rightarrow U(1)_Y$, which is accomplished by introducing new fields

$$\begin{pmatrix} Z'_M \\ B_M \end{pmatrix} = \frac{1}{\sqrt{g_{R,5}^2 + g_{X,5}^2}} \begin{pmatrix} g_{R,5} & -g_{X,5} \\ g_{X,5} & g_{R,5} \end{pmatrix} \begin{pmatrix} R_M^3 \\ X_M \end{pmatrix}, \quad (2.148)$$

and giving Dirichlet BCs Z'_μ and $R_\mu^{1,2}$ on the UV brane. Thus, B_μ is the only field that survives on the UV brane and can be identified with the $U(1)_Y$ gauge field. The SM-like neutral electroweak gauge bosons are defined in the standard way through

$$\begin{pmatrix} Z_M \\ A_M \end{pmatrix} = \frac{1}{\sqrt{g_{L,5}^2 + g_{Y,5}^2}} \begin{pmatrix} g_{L,5} & -g_{Y,5} \\ g_{Y,5} & g_{L,5} \end{pmatrix} \begin{pmatrix} L_M^3 \\ B_M^Y \end{pmatrix}, \quad g_{Y,5} = \frac{g_{X,5} g_{R,5}}{\sqrt{g_{R,5}^2 + g_{X,5}^2}}, \quad (2.149)$$

and the definition of the weak-mixing angle

$$\sin \theta_w = \frac{g_{Y,5}}{\sqrt{g_{L,5}^2 + g_{Y,5}^2}}, \quad \cos \theta_w = \frac{g_{L,5}}{\sqrt{g_{L,5}^2 + g_{Y,5}^2}}, \quad (2.150)$$

agrees with the definition in the SM (with $g_{L,5} \rightarrow g$, $g_{Y,5} \rightarrow g'$). Note that from the BCs for the fields on the right-hand side of (2.149) it follows that A_μ and Z_μ obey Neumann boundary conditions, while the corresponding fifth component fulfills Dirichlet BCs on the UV brane. The fields $L_M^\pm \equiv L_M^1 \mp iL_M^2$, Z_M , A_M and R_M^\pm , Z'_M define the so-called *UV basis* with individual BCs on the UV brane, where the vector components of the former three (latter two) obey Neumann (Dirichlet) BCs and thus do (do not) possess a zero mode. Analogously, we can define the so-called *IR basis*, which is given by the fields A_M^\pm , A_M^3 , and V_M^\pm with (modified¹⁵) Neumann BCs for their vector components on the IR boundary. Among the remaining two fields of the IR basis, V_M^3 and X_M , there should be the 5D photon field A_M in order to allow for a massless zero mode for the

¹⁵Due to the mass term (2.147), the fields \tilde{A}_μ must obey $\partial_t \tilde{A}_\mu(x, 1^-) = -L\tilde{m}_W^2/(\cos_\vartheta^2 M_{KK}^2)\tilde{A}_\mu(x, 1)$, with \tilde{m}_W introduced in (2.159), see [149] for details.

photon. We therefore rotate the remaining two fields to the photon field A_M and a state Z_M^H via

$$\begin{pmatrix} Z_M^H \\ A_M \end{pmatrix} = \frac{1}{g_{LRX,5}^2} \begin{pmatrix} g_{L,5} g_{R,5} & -g_{X,5} \sqrt{g_{L,5}^2 + g_{R,5}^2} \\ g_{X,5} \sqrt{g_{L,5}^2 + g_{R,5}^2} & g_{L,5} g_{R,5} \end{pmatrix} \begin{pmatrix} V_M^3 \\ X_M \end{pmatrix}, \quad (2.151)$$

where

$$g_{LRX,5}^2 = \sqrt{g_{L,5}^2 g_{R,5}^2 + g_{L,5}^2 g_{X,5}^2 + g_{R,5}^2 g_{X,5}^2}. \quad (2.152)$$

From now on, we use the notation $\tilde{Z}_M \equiv A_M^3$, since this field it is the linear combination of Z_M and Z'_M that is orthogonal to Z_M^H ,

$$\begin{pmatrix} \tilde{Z}_M \\ Z_M^H \end{pmatrix} = \begin{pmatrix} \cos \vartheta_Z & -\sin \vartheta_Z \\ \sin \vartheta_Z & \cos \vartheta_Z \end{pmatrix} \begin{pmatrix} Z_M \\ Z'_M \end{pmatrix} \equiv \mathbf{R}_{\vartheta_Z} \begin{pmatrix} Z_M \\ Z'_M \end{pmatrix}, \quad (2.153)$$

where we have defined

$$\sin \vartheta_Z = \frac{g_{R,5}^2}{\sqrt{(g_{L,5}^2 + g_{R,5}^2)(g_{R,5}^2 + g_{X,5}^2)}}, \quad \cos \vartheta_Z = \frac{g_{LRX,5}^2}{\sqrt{(g_{L,5}^2 + g_{R,5}^2)(g_{R,5}^2 + g_{X,5}^2)}}. \quad (2.154)$$

The relations (2.145) and (2.153) represent the important connection between the UV basis fields (right) and the IR basis fields (left). The explicit shape of all BCs is not important for the main part of this thesis and can be found in [149]. It should be stressed that there appears only one mass parameter M_A^2 in the IR BCs as opposed to (2.22). This feature will give rise to the protection of the electroweak T parameter. After having defined these two bases with individual BC, the question arises in which basis we define the 5D action. The latter still contains mixing terms between gauge fields and scalars, that can be removed by an appropriate gauge-fixing Lagrangian whose concrete form will be shown below (2.160). As the Higgs sector is localized on the IR brane, it is appropriate to work in the IR basis for that purpose.

The Kaluza-Klein Decomposition

The next step is to perform the KK decomposition of the 5D gauge fields. Defining the vectors

$$\vec{\tilde{Z}}_M \equiv \begin{pmatrix} \tilde{Z}_M \\ Z_M^H \end{pmatrix} = \mathbf{R}_{\vartheta_Z} \begin{pmatrix} Z_M \\ Z'_M \end{pmatrix}, \quad \vec{W}_M^\pm \equiv \begin{pmatrix} \tilde{A}_M^\pm \\ V_M^\pm \end{pmatrix} = \mathbf{R}_\vartheta \begin{pmatrix} L_M^\pm \\ R_M^\pm \end{pmatrix} \quad (2.155)$$

we are able to write the KK decomposition in a form analogous to (2.18), such that

$$\begin{aligned}
A_\mu(x, t) &= \frac{1}{\sqrt{r}} \sum_{n=0}^{\infty} \chi_n^A(t) A_\mu^{(n)}(x), & A_5(x, t) &= -\frac{1}{\sqrt{r}} \sum_{n=0}^{\infty} \frac{M_{\text{KK}}}{m_n^A} \partial_t \chi_n^A(t) \varphi_A^{(n)}(x), \\
\vec{Z}_\mu(x, t) &= \frac{\mathbf{R}_{\vartheta Z}}{\sqrt{r}} \sum_{n=0}^{\infty} \vec{\chi}_n^Z(t) Z_\mu^{(n)}(x), & \vec{Z}_5(x, t) &= -\frac{\mathbf{R}_{\vartheta Z}}{\sqrt{r}} \sum_{n=0}^{\infty} \frac{M_{\text{KK}}}{m_n^Z} \partial_t \vec{\chi}_n^Z(t) \varphi_Z^{(n)}(x), \\
\vec{W}_\mu^\pm(x, t) &= \frac{\mathbf{R}_{\vartheta}}{\sqrt{r}} \sum_{n=0}^{\infty} \vec{\chi}_n^W(t) W_\mu^{\pm(n)}(x), & \vec{W}_5^\pm(x, t) &= -\frac{\mathbf{R}_{\vartheta}}{\sqrt{r}} \sum_{n=0}^{\infty} \frac{M_{\text{KK}}}{m_n^W} \partial_t \vec{\chi}_n^W(t) \varphi_W^{\pm(n)}(x),
\end{aligned} \tag{2.156}$$

where it has already been used that the coefficient of the fifth component is given by $a_n = -1/m_n$. The profiles $\vec{\chi}_n^a(t)$ are even functions on the orbifold and are defined via $\chi_n^A(t) \equiv \chi_n^{A(+)}(t)$ and

$$\vec{\chi}_n^a(t) \equiv \chi_n^a(t) \vec{A}_n^a \equiv \begin{pmatrix} \chi_n^{a(+)}(t) & 0 \\ 0 & \chi_n^{a(-)}(t) \end{pmatrix} \vec{A}_n^a, \quad a = Z, W, \tag{2.157}$$

where the superscripts (+) and (−) label the type of BC we impose on the profiles at the UV brane, i.e., they indicate *untwisted* and *twisted* even functions on the orbifold. Untwisted even functions correspond to ordinary profiles with Neumann boundary conditions on the UV brane, allowing for light zero modes. Twisted even functions obey Dirichlet boundary conditions on the UV brane and are thus not smooth at this orbifold fixed point. The two-component vectors \vec{A}_n^a , with $a = Z, W$, represent the mixings between the different gauge fields and their KK excitations. These vectors are normalized according to $(\vec{A}_n^a)^T \vec{A}_n^a = 1$. Similar to the fermion decomposition in the minimal model (2.73), the profiles $\chi_n^{a(\pm)}(t)$ do not obey exact orthonormality conditions, but the complete vectors (2.157) are orthonormal on each other,

$$\frac{2\pi}{L} \int_\epsilon^1 \frac{dt}{t} \vec{\chi}_n^a(t)^T \vec{\chi}_m^a(t) = \delta_{nm}, \quad a = Z, W. \tag{2.158}$$

The photon obeys the standard orthonormality condition (2.21). Analogously to (2.19), we also expand the 4D Goldstone bosons in the basis of mass eigenstates $\varphi_Z^{(n)}$ and $\varphi_W^{\pm(n)}$

$$\begin{aligned}
\vec{\varphi}^\pm(x) &= \sum_n \frac{\tilde{m}_W}{m_n^W} \sqrt{2\pi} \mathbf{P}_+ \mathbf{R}_{\vartheta} \vec{\chi}_n^W(1) \varphi_W^{\pm(n)}(x); & \tilde{m}_W &= \frac{g_{L,5}}{\sqrt{2\pi r}} \frac{v}{2}, \\
\vec{\varphi}^3(x) &= \sum_n \frac{\tilde{m}_Z}{m_n^Z} \sqrt{2\pi} \mathbf{P}_+ \mathbf{R}_{\vartheta Z} \vec{\chi}_n^Z(1) \varphi_Z^{(n)}(x); & \tilde{m}_Z &= \frac{\sqrt{g_{L,5}^2 + g_{Y,5}^2}}{\sqrt{2\pi r}} \frac{v}{2},
\end{aligned} \tag{2.159}$$

where $\mathbf{P}_+ = \text{diag}(1, 0)$ is a projector on the upper component, and from now on we use the abbreviations $c_{\vartheta_a} \equiv \cos \vartheta_a$ and $s_{\vartheta_a} \equiv \sin \vartheta_a$, with $\vartheta_W \equiv \vartheta$. As in the minimal RS model, the parameters $\tilde{m}_{W,Z}$ are the leading contributions to the gauge-boson masses in an expansion in powers of v^2/M_{KK}^2 , see (2.169). Using the notation introduced above,

the gauge-fixing Lagrangian takes the form (compare with (2.15))

$$\begin{aligned}
\mathcal{L}_{\text{GF}} = & -\frac{1}{2\xi} \left(\partial^\mu A_\mu - \xi \left[M_{\text{KK}} t \partial_t \frac{1}{t} A_5 \right] \right)^2 \\
& - \frac{1}{2\xi} \left(\partial^\mu \vec{Z}_\mu - \frac{\xi}{2} \left[\delta(t-1) k M_{\tilde{A}} \vec{\varphi}^3 + 2M_{\text{KK}} t \partial_t \frac{1}{t} \vec{Z}_5 \right] \right)^2 \\
& - \frac{1}{\xi} \left(\partial^\mu \vec{W}_\mu^+ - \frac{\xi}{2} \left[\delta(t-1) k M_{\tilde{A}} \vec{\varphi}^+ + 2M_{\text{KK}} t \partial_t \frac{1}{t} \vec{W}_5^+ \right] \right)^T \\
& \times \left(\partial^\mu \vec{W}_\mu^- - \xi \left[\delta(t-1) k M_{\tilde{A}} \vec{\varphi}^- + 2M_{\text{KK}} t \partial_t \frac{1}{t} \vec{W}_5^- \right] \right).
\end{aligned} \tag{2.160}$$

We can now insert the KK decompositions (2.156) and the expansions (2.159) into the action to obtain the EOM [149, 158, 159]

$$-t \partial_t \frac{1}{t} \partial_t \vec{\chi}_n^a(t) = x_n^2 \vec{\chi}_n^a(t), \quad a = Z, W, \tag{2.161}$$

which generalizes (2.20) ignoring the δ -function that will be included in the BCs. The profiles $\vec{\chi}_n^a(t)$ are defined in such a way that the upper (lower) component obeys Neumann (Dirichlet) boundary conditions on the UV brane,

$$[\mathbf{P}_+ \partial_t + \mathbf{P}_-] \vec{\chi}_n^a(t) \Big|_{t=\epsilon} = 0, \tag{2.162}$$

with $\mathbf{P}_- = \text{diag}(0, 1)$, while the upper (lower) components of the rotated profiles $\mathbf{R}_{\vartheta_a} \vec{\chi}_n^a(t)$ obey mixed (Neumann) BCs on the IR brane,

$$\mathbf{R}_{\vartheta_a} \partial_t \vec{\chi}_n^a(t) \Big|_{t=1^-} = -\frac{L \tilde{m}_W^2}{c_\vartheta^2 M_{\text{KK}}^2} \mathbf{P}_+ \mathbf{R}_{\vartheta_a} \vec{\chi}_n^a(1). \tag{2.163}$$

Note that for the photon the right-hand side of (2.163) is zero. The IR BCs are used to determine the mass eigenvalues which are the zeroes of

$$\det \left[\partial_t \chi_n^a(1^-) + \frac{L \tilde{m}_W^2}{c_\vartheta^2 M_{\text{KK}}^2} \mathbf{D}_{\vartheta_a} \chi_n^a(1) \right] = 0, \tag{2.164}$$

where we have defined the matrix

$$\mathbf{D}_{\vartheta_a} = \begin{pmatrix} c_a^2 & -s_a c_a \\ -s_a c_a & s_a^2 \end{pmatrix}. \tag{2.165}$$

Once the masses m_n^a are known, the eigenvectors \vec{A}_n^a are determined by (2.163). The equations (2.161)–(2.164) are the generalizations of (2.20), (2.22), and (2.29) in the minimal model, which can be recovered for $\vartheta \rightarrow 0$ (the upper component of $\vec{\chi}_n^a(t)$ can be identified with the profile $\chi_n^a(t)$ of the minimal model).

Bulk Profiles and Masses

We can now solve the EOM (2.161), where the untwisted (twisted) profiles $\chi_n^{(+)}(t)$ ($\chi_n^{(-)}(t)$) need to obey Neumann (Dirichlet) BCs at the UV brane. One then finds the

solutions [149]

$$\chi_n^{(+)}(\phi) = N_n^{(+)} \sqrt{\frac{L}{\pi}} t c_n^{(+)+}(t), \quad \chi_n^{(-)}(\phi) = N_n^{(-)} \sqrt{\frac{L}{\pi}} t c_n^{(-)+}(t), \quad (2.166)$$

with

$$\begin{aligned} c_n^{(+)+}(t) &= Y_0(x_n \epsilon) J_1(x_n t) - J_0(x_n \epsilon) Y_1(x_n t), \\ c_n^{(-)+}(t) &= Y_1(x_n \epsilon) J_1(x_n t) - J_1(x_n \epsilon) Y_1(x_n t), \\ c_n^{(+)-}(t) &= \frac{1}{x_n t} \frac{d}{dt} \left[t c_n^{(+)+}(t) \right] = Y_0(x_n \epsilon) J_0(x_n t) - J_0(x_n \epsilon) Y_0(x_n t), \\ c_n^{(-)-}(t) &= \frac{1}{x_n t} \frac{d}{dt} \left[t c_n^{(-)+}(t) \right] = Y_1(x_n \epsilon) J_0(x_n t) - J_1(x_n \epsilon) Y_0(x_n t). \end{aligned} \quad (2.167)$$

The superscripts a have been dropped for a better readability. The mass eigenvalues are determined by the IR BCs as explained above. It is obvious that the profiles fulfill the UV BCs, since $c_n^{(-)+}(\epsilon) = c_n^{(+)-}(\epsilon) = 0$, which can be explicitly seen in (2.167). The normalization constants $N_n^{(\pm)}$ can be obtained by the orthonormality condition (2.158) and read

$$\begin{aligned} N_n^{(\pm)-2} &= \left[c_n^{(\pm)+}(1) \right]^2 + \left[c_n^{(\pm)-}(1^-) \right]^2 - \frac{2}{x_n} \left(c_n^{(\pm)+}(1) c_n^{(\pm)-}(1^-) - \epsilon c_n^{(\pm)+}(\epsilon) c_n^{(\pm)-}(\epsilon^+) \right) \\ &\quad - \epsilon^2 \left(\left[c_n^{(\pm)+}(\epsilon) \right]^2 + \left[c_n^{(\pm)-}(\epsilon^+) \right]^2 \right). \end{aligned} \quad (2.168)$$

With respect to the corresponding formula in the minimal model (2.28), they contain additional terms due to the different UV BCs. Note that, depending on the type of the UV BCs, some of the terms in (2.168) vanish identically.

We finish the discussion of the boson sector with the calculation of the zero-mode masses and profiles. Expanding (2.164) in powers of v^2/M_{KK}^2 , we arrive at

$$\begin{aligned} m_W^2 &= \tilde{m}_W^2 \left[1 - \frac{\tilde{m}_W^2}{2M_{\text{KK}}^2} \left(\frac{L}{c_\vartheta^2} - 1 + \frac{1}{2L} \right) + \mathcal{O} \left(\frac{v^4}{M_{\text{KK}}^4} \right) \right] \\ m_Z^2 &= \tilde{m}_Z^2 \left[1 - \frac{\tilde{m}_W^2}{2M_{\text{KK}}^2} \left(\frac{L}{c_\vartheta^2} - 1 + \frac{1}{2L} \right) + \frac{\tilde{m}_Z^2}{2M_{\text{KK}}^2} \left(1 - \frac{1}{2L} \right) + \mathcal{O} \left(\frac{v^4}{M_{\text{KK}}^4} \right) \right], \end{aligned} \quad (2.169)$$

which includes additional terms compared to (2.30). Note that the leading corrections to both masses are proportional to $\tilde{m}_W^2/M_{\text{KK}}^2$, with \tilde{m}_W defined in (2.159). This is a consequence of the enlarged bulk gauge symmetry and protects the T parameter. Finally, one can derive the zero-mode profiles that are found to be [149]

$$\begin{aligned} \sqrt{2\pi} \vec{\chi}_0^W(t) &= \left(1 - \frac{m_W^2}{2M_{\text{KK}}^2} \left[t^2 \left(L - \frac{1}{2} + \ln t \right) - \frac{1}{2} + \frac{1}{2L} \right] \right) + \mathcal{O} \left(\frac{v^4}{M_{\text{KK}}^4} \right), \\ &\quad \frac{L s_\vartheta}{2c_\vartheta} \frac{m_W^2}{M_{\text{KK}}^2} t^2 \\ \sqrt{2\pi} \vec{\chi}_0^Z(t) &= \left(1 - \frac{m_Z^2}{2M_{\text{KK}}^2} \left[t^2 \left(L - \frac{1}{2} + \ln t \right) - \frac{1}{2} + \frac{1}{2L} \right] \right) + \mathcal{O} \left(\frac{v^4}{M_{\text{KK}}^4} \right). \\ &\quad \frac{L s_\vartheta c_\vartheta}{2c_\vartheta^2} \frac{m_Z^2}{M_{\text{KK}}^2} t^2 \end{aligned} \quad (2.170)$$

We see that the twisted components are proportional to t^2 and suppressed by the ratio v^2/M_{KK}^2 , while the untwisted components are the same as in the minimal model at this order, see (2.31).

Generalization to a Bulk Higgs

The generalization of the gauge action to a bulk-Higgs sector is equivalent to the case in the minimal model,

$$S_h = \int d^4x r \int_{-\pi}^{\pi} d\phi e^{-4\sigma(\phi)} \left\{ \frac{1}{2} \text{Tr} \left[D_M \Phi^\dagger D^M \Phi \right] - \mu^2 \text{Tr} \Phi^\dagger \Phi - V_{\text{UV}}(\Phi) \delta(|\phi|) - V_{\text{IR}}(\Phi) \delta(|\phi| - \pi) \right\}, \quad (2.171)$$

where the potentials on the UV and IR branes read

$$V_{\text{UV}}(\Phi) = M_{\text{UV}} \text{Tr} \Phi^\dagger \Phi, \quad V_{\text{IR}}(\Phi) = -M_{\text{IR}} \text{Tr} \Phi^\dagger \Phi + \lambda_{\text{IR}} \text{Tr} (\Phi^\dagger \Phi)^2. \quad (2.172)$$

Inserting the Higgs bi-doublet

$$\Phi(x, t) = \frac{1}{\sqrt{2}} \begin{pmatrix} v(t) + h(x, t) - i\varphi^3(x, t) & -i\sqrt{2} \varphi^+(x, t) \\ -i\sqrt{2} \varphi^-(x, t) & v(t) + h(x, t) + i\varphi^3(x, t) \end{pmatrix}, \quad (2.173)$$

and defining

$$m_{\text{UV}} \equiv \frac{M_{\text{UV}}}{k}, \quad m_{\text{IR}} \equiv \frac{M_{\text{IR}}}{k}, \quad \lambda \equiv \frac{\lambda_{\text{IR}} k}{2r}, \quad (2.174)$$

which differ from (2.35) by a factor of 2, we then find that $\mathcal{L}_h(x)$ is given by (2.37) and the following discussion and derivations still hold for the custodial model. In particular, the vev profile at leading order is given by the leading-order term in (2.52), while the Higgs profile can be found in (2.63).

2.3.2 The Matter Sector

Let us now clarify the fermion sector in the model under consideration. Since the bulk gauge group is larger than in the minimal model, we will encounter bi-doublets, triplets, and singlets under the two $SU(2)$ gauge groups. This will result in a much richer quark structure. We will, however, see that by using appropriate defined vectors the formulas of the minimal model can also be used in the custodial RS model.

The 5D Action

Before writing down the 5D fermion action, we have to specify the fermion representations in the custodial model. They are chosen such that they can be embedded into complete $SO(5)$ multiplets used in the context of models with gauge-Higgs unification [101, 193, 212]. As a consequence of the discrete P_{LR} symmetry the left-handed bottom quark has to be embedded in a $SU(2)_L \times SU(2)_R$ bi-doublet with isospin quantum numbers $T_L^3 = -T_R^3 = -1/2$. This fixes the quantum numbers of the other fields uniquely. In particular, the right-handed down-type quarks have to be embedded in an $SU(2)_R$ triplet in order to obtain an $U(1)_X$ -invariant Yukawa coupling. One arrives at the following

multiplet structure for the quark fields with even Z_2 parity:

$$\begin{aligned}
Q_L &= \begin{pmatrix} u_L^{(+)\frac{2}{3}} & \lambda_L^{(-)\frac{5}{3}} \\ d_L^{(+)\frac{-1}{3}} & u_L'^{(-)\frac{2}{3}} \end{pmatrix}_{\frac{2}{3}}, & u_R^c &= \left(u_R^{c(+)\frac{2}{3}} \right)_{\frac{2}{3}}, \\
\mathcal{T}_R &= \mathcal{T}_{1R} \oplus \mathcal{T}_{2R} = \begin{pmatrix} \Lambda_R'^{(-)\frac{5}{3}} \\ U_R'^{(-)\frac{2}{3}} \\ D_R'^{(-)\frac{-1}{3}} \end{pmatrix}_{\frac{2}{3}} \oplus \left(D_R^{(+)\frac{-1}{3}} \quad U_R^{(-)\frac{2}{3}} \quad \Lambda_R^{(-)\frac{5}{3}} \right)_{\frac{2}{3}}.
\end{aligned} \tag{2.175}$$

Q_L is a bi-doublet under $SU(2)_L \times SU(2)_R$, while \mathcal{T}_R transforms as $(\mathbf{3}, \mathbf{1}) \oplus (\mathbf{1}, \mathbf{3})$. The fields with odd Z_2 parity have the opposite chirality. Their profiles are related to those of the Z_2 -even fields by the field equations. The inner and outer subscripts on the various fields denote their $U(1)_{\text{EM}}$ and $U(1)_X$ charges, respectively, which are connected through the relations $Y = -T_R^3 + Q_X$ and $Q = T_L^3 + Y$.

While the IR BCs are understood to be of Neumann type in all cases, the superscripts on the fields specify the type of BCs that they obey on the UV boundary. Fields with superscript (+) obey the usual mixed BCs allowing for a light zero mode, meaning that the Dirichlet condition is imposed on the profile functions of the corresponding Z_2 -odd fields. These zero modes correspond to the SM quarks. Fields with superscripts (−) correspond to heavy, exotic fermions with no counterparts in the SM. For these states, the Dirichlet boundary condition is imposed on the Z_2 -even fields in order to avoid the presence of a zero mode. The remaining UV boundary conditions are of mixed type and follow from the field equations. Note that the same $SU(2)_L \times SU(2)_R$ representations have been chosen for all three quark generations, which is necessary if one wants to consistently incorporate quark mixing in the fully anarchic approach to flavor in warped extra dimensions. Altogether, there are fifteen different quark states in the up sector and nine in the down sector. The boundary conditions give rise to three light modes in each sector, which are identified with the SM quarks. These are accompanied by KK towers consisting of groups of fifteen and nine modes of similar masses in the up and down sectors, respectively. In addition, there is a KK tower of exotic fermion states with electric charge $5/3$, which exhibits nine excitations in each KK level.

In order to simplify the notation as much as possible, it is convenient to introduce the vectors

$$\vec{U} = \begin{pmatrix} u \\ u' \end{pmatrix}, \quad \vec{u} = \begin{pmatrix} u^c \\ U' \\ U \end{pmatrix}, \quad \vec{D} = d, \quad \vec{d} = \begin{pmatrix} D \\ D' \end{pmatrix}, \quad \vec{\Lambda} = \lambda, \quad \vec{\lambda} = \begin{pmatrix} \Lambda' \\ \Lambda \end{pmatrix}, \tag{2.176}$$

which collect the fields with same electric charges ($2/3$, $-1/3$, and $5/3$). Upper-case (lower-case) symbols denote fields whose left-handed (right-handed) components are Z_2 even. Using this notation we can write down the bilinear part of the fermionic 5D action in an analogous way to the minimal model,

$$\begin{aligned}
S_{\text{ferm},2} &= \sum_{Q,q} \int d^4x r \int_{-\pi}^{\pi} d\phi \left\{ e^{-3\sigma} \left(\vec{Q} i \not{\partial} \vec{Q} + \vec{q} i \not{\partial} \vec{q} \right) - e^{-4\sigma} \text{sgn}(\phi) \left(\vec{Q} \mathbf{M}_{\vec{Q}} \vec{Q} + \vec{q} \mathbf{M}_{\vec{q}} \vec{q} \right) \right. \\
&\quad \left. - \frac{e^{-2\sigma}}{r} \left[\vec{Q}_L \partial_{\phi} (e^{-2\sigma} \vec{Q}_R) - \vec{Q}_R \partial_{\phi} (e^{-2\sigma} \vec{Q}_L) + \vec{q}_L \partial_{\phi} (e^{-2\sigma} \vec{q}_R) - \vec{q}_R \partial_{\phi} (e^{-2\sigma} \vec{q}_L) \right] \right\}
\end{aligned}$$

$$- e^{-3\sigma} \frac{v \delta^\eta (|\phi| - \pi)}{\sqrt{2}r} \left[\bar{Q}_L \mathbf{Y}_{\bar{q}}^{5D,C} \vec{q}_R + \bar{Q}_R \mathbf{Y}_{\bar{q}}^{5D,S} \vec{q}_L + \text{h.c.} \right] \Bigg\}, \quad (2.177)$$

where now $(Q, q) = (U, u), (D, d), (\Lambda, \lambda)$. The structure of the matrices of the 5D bulk mass parameters $\mathbf{c}_{\bar{Q}} \equiv \mathbf{M}_{\bar{Q}}/k$ and $\mathbf{c}_{\bar{q}} \equiv -\mathbf{M}_{\bar{q}}/k$ are according to (2.176),

$$\begin{aligned} \mathbf{c}_{\vec{U}} &= \text{diag}(\mathbf{c}_Q, \mathbf{c}_Q), & \mathbf{c}_{\vec{D}} &= \mathbf{c}_Q, & \mathbf{c}_{\vec{\Lambda}} &= \mathbf{c}_Q, \\ \mathbf{c}_{\vec{u}} &= \text{diag}(\mathbf{c}_{u^c}, \mathbf{c}_{\tau_1}, \mathbf{c}_{\tau_2}), & \mathbf{c}_{\vec{d}} &= \text{diag}(\mathbf{c}_{\tau_2}, \mathbf{c}_{\tau_1}), & \mathbf{c}_{\vec{\lambda}} &= \text{diag}(\mathbf{c}_{\tau_1}, \mathbf{c}_{\tau_2}), \end{aligned} \quad (2.178)$$

where each entry is a 3×3 diagonal matrix in generation space. Note that the fields \vec{U} , \vec{D} , and $\vec{\Lambda}$ are governed by the same bulk mass matrix \mathbf{c}_Q , while \vec{u} , \vec{d} , and $\vec{\lambda}$ are associated with three different mass matrices \mathbf{c}_{u^c} , \mathbf{c}_{τ_2} , and \mathbf{c}_{τ_1} . The first two of them, $\mathbf{c}_{u^c} \equiv \mathbf{c}_u$ and $\mathbf{c}_{\tau_2} \equiv \mathbf{c}_d$, can be identified with the mass matrices appearing in the minimal RS model. The three new parameters contained in the matrix \mathbf{c}_{τ_1} can be related to the other ones by extending the P_{LR} symmetry to the part of the quark sector that mixes with the left-handed down-type zero modes, by requiring that the action be invariant under the exchange of the fields D' and D [149]. This extended version of the P_{LR} symmetry implies $\mathbf{c}_{\tau_1} = \mathbf{c}_{\tau_2}$, and hence the number of independent bulk mass parameters is reduced to the same number as in the minimal RS model. As can be seen above, we will work in a basis, where the bulk mass matrices are diagonal so that all flavor mixing is encoded in the 6×9 and 3×6 Yukawa matrices

$$\mathbf{Y}_{\vec{u}} = \begin{pmatrix} \mathbf{Y}_u & \frac{1}{\sqrt{2}} \mathbf{Y}_d & \frac{1}{\sqrt{2}} \mathbf{Y}_d \\ \mathbf{Y}_u & -\frac{1}{\sqrt{2}} \mathbf{Y}_d & -\frac{1}{\sqrt{2}} \mathbf{Y}_d \end{pmatrix}, \quad \mathbf{Y}_{\vec{d}} = \mathbf{Y}_{\vec{\lambda}} = (\mathbf{Y}_d \quad \mathbf{Y}_d). \quad (2.179)$$

Note that the 3×3 block matrices \mathbf{Y}_q appearing in these expressions are the same as in the minimal RS model. Consequently, even though the extended RS model with custodial symmetry has a much richer structure than the minimal model, it features the same number of parameters in the fermion sector once the extended P_{LR} symmetry is imposed.

The Kaluza-Klein Decomposition

Provided with the above definitions, we write the KK decomposition for the up-type quarks as

$$\begin{aligned} \vec{U}_L(x, t) &= \frac{1}{\sqrt{r}} \frac{t^2}{\epsilon^2} \sum_n \mathbf{C}_n^Q(t) \vec{a}_n^U u_L^{(n)}(x), & \vec{U}_R(x, t) &= \frac{1}{\sqrt{r}} \frac{t^2}{\epsilon^2} \sum_n \mathbf{S}_n^Q(t) \vec{a}_n^U u_R^{(n)}(x), \\ \vec{u}_L(x, t) &= \frac{1}{\sqrt{r}} \frac{t^2}{\epsilon^2} \sum_n \mathbf{S}_n^u(t) \vec{a}_n^u u_L^{(n)}(x), & \vec{u}_R(x, t) &= \frac{1}{\sqrt{r}} \frac{t^2}{\epsilon^2} \sum_n \mathbf{C}_n^u(t) \vec{a}_n^u u_R^{(n)}(x). \end{aligned} \quad (2.180)$$

Here, the superscript n labels the different mass eigenstates such that 1, 2, 3 refer to the SM quarks, while $n = 4, \dots, 18$ label the fifteen quark modes of the first level and so on. As mentioned above, the down- and λ -type quark sectors can be decomposed in an analogous way, with the difference that they only possess nine modes in each KK level. The functions $\mathbf{C}_n^A(t)$ and $\mathbf{S}_n^A(t)$ denote the profiles in the custodial model and are given

by

$$\begin{aligned}
\mathbf{C}_n^U &\equiv \text{diag} \left(\mathbf{C}_n^{Q(+)}, \mathbf{C}_n^{Q(-)} \right), & \mathbf{C}_n^u &\equiv \text{diag} \left(\mathbf{C}_n^{u^c(+)}, \mathbf{C}_n^{\mathcal{T}_1(-)}, \mathbf{C}_n^{\mathcal{T}_2(-)} \right), \\
\mathbf{C}_n^D &\equiv \mathbf{C}_n^{Q(+)}, & \mathbf{C}_n^d &\equiv \text{diag} \left(\mathbf{C}_n^{\mathcal{T}_2(+)}, \mathbf{C}_n^{\mathcal{T}_1(-)} \right), \\
\mathbf{C}_n^\Lambda &\equiv \mathbf{C}_n^{Q(-)}, & \mathbf{C}_n^\lambda &\equiv \text{diag} \left(\mathbf{C}_n^{\mathcal{T}_1(-)}, \mathbf{C}_n^{\mathcal{T}_2(-)} \right),
\end{aligned} \tag{2.181}$$

where the analogous expressions hold for the Z_2 -odd profiles \mathbf{S}_n^A with $\mathbf{C} \rightarrow \mathbf{S}$. The 3×3 matrices $\mathbf{C}_n^{A(\pm)}(t)$ ($\mathbf{S}_n^{A(\pm)}(t)$) with $A = Q, u, \mathcal{T}_1, \mathcal{T}_2$ correspond to even (odd) profiles on the orbifold, and the superscript (\pm) indicates the type of BC on the UV brane. The flavor structure is encoded in the three-component vectors

$$\vec{a}_n^U \equiv \begin{pmatrix} a_n^u \\ a_n^{u'} \\ a_n^U \end{pmatrix}, \quad \vec{a}_n^u \equiv \begin{pmatrix} a_n^{u^c} \\ a_n^{U'} \\ a_n^U \end{pmatrix}, \quad \vec{a}_n^D \equiv a_n^d, \quad \vec{a}_n^d \equiv \begin{pmatrix} a_n^D \\ a_n^{D'} \end{pmatrix}, \quad \vec{a}_n^\Lambda \equiv a_n^\lambda, \quad \vec{a}_n^\lambda \equiv \begin{pmatrix} a_n^{\Lambda'} \\ a_n^\Lambda \end{pmatrix}. \tag{2.182}$$

By virtue of the vector notation (2.176), we have reached complete analogy to the decomposition of bulk quark fields in the minimal model. The further analysis can thus be extracted from Section 2.2.2. Explicitly, the equations (2.73)–(2.83) still hold once we make the replacements

$$a_n^A \rightarrow \vec{a}_n^A, \quad \mathbf{Y}_q \rightarrow \mathbf{Y}_{\vec{q}}, \tag{2.183}$$

and the profiles $\mathbf{C}_n^A(t)$ and $\mathbf{S}_n^A(t)$ with $A = U, D, \Lambda, u, d, \lambda$ have the structure given in (2.181). The vectors defined in (2.71) can also be used for the custodial model, once we make latter replacements.

Bulk Profiles

We can therefore directly move on to the solution for the bulk profiles. The explicit form for the Z_2 -even profiles $(C_n^{A(+)}(t))_i$ and $(S_n^{A(+)}(t))_i$ associated with bulk mass parameters M_{A_i} was obtained in [163, 167]. The Z_2 -odd functions $(C_n^{A(-)}(t))_i$ and $(S_n^{A(-)}(t))_i$ can be derived in a similar fashion by requiring a Dirichlet condition for the even mode, $(C_n^{A(-)}(\epsilon))_i = 0$, to account for the additional twist of the non-SM-like fermions at the UV boundary. Dropping the label A and the index i , one finds the bulk profiles [149]

$$\begin{aligned}
C_n^{(\pm)}(t) &= \mathcal{N}_n^{(\pm)}(c) \sqrt{\frac{L\epsilon t}{\pi}} f_n^{(\pm)+}(t, c), \\
S_n^{(\pm)}(t) &= \pm \mathcal{N}_n^{(\pm)}(c) \sqrt{\frac{L\epsilon t}{\pi}} f_n^{(\pm)-}(t, c).
\end{aligned} \tag{2.184}$$

The overall “+” entering the Z_2 -odd profiles holds if $c = c_Q \equiv +M_Q/k$ refers to the bi-doublet, while the “-” sign applies in the case of $c = c_A \equiv -M_A/k$ ($A = u^c, \mathcal{T}_1, \mathcal{T}_2$). The functions $f_n^{(\pm)\pm}(t, c)$ are given by

$$\begin{aligned}
f_n^{(+)\pm}(t, c) &= J_{-\frac{1}{2}-c}(x_n\epsilon) J_{\mp\frac{1}{2}+c}(x_nt) \pm J_{\frac{1}{2}+c}(x_n\epsilon) J_{\pm\frac{1}{2}-c}(x_nt), \\
f_n^{(-)\pm}(t, c) &= J_{+\frac{1}{2}-c}(x_n\epsilon) J_{\mp\frac{1}{2}+c}(x_nt) \mp J_{-\frac{1}{2}+c}(x_n\epsilon) J_{\pm\frac{1}{2}-c}(x_nt).
\end{aligned} \tag{2.185}$$

The normalization constant can be derived analogously to (2.90)

$$\begin{aligned} \left[\mathcal{N}_n^{(a)}(c) \right]^{-2} &= [f_n^{(a)+}(1, c)]^2 + [f_n^{(a)-}(1^-, c)]^2 \\ &\quad - \frac{2c}{x_n} f_n^{(a)+}(1, c) f_n^{(a)-}(1^-, c) - \epsilon^2 \left([f_n^{(a)+}(\epsilon, c)]^2 + [f_n^{(a)+}(\epsilon^+, c)]^2 \right), \end{aligned} \quad (2.186)$$

which extends the result (2.91) to the case of Z_2 -odd profiles with non-zero value at the UV boundary. Finally, one can expand the profiles for $x_n \ll 1$ and finds the ZMA profiles

$$\begin{aligned} C_n^{(+)}(t) &\approx \sqrt{\frac{L\epsilon}{\pi}} F(c) t^c, & S_n^{(+)}(t) &\approx \pm \text{sgn}(\phi) \sqrt{\frac{L\epsilon}{\pi}} x_n F(c) \frac{t^{1+c} - \epsilon^{1+2c} t^{-c}}{1+2c}, \\ C_n^{(-)}(t) &\approx -\sqrt{\frac{L\epsilon}{\pi}} x_n F(-c) \frac{t^{1-c} - \epsilon^{1-2c} t^c}{1-2c}, & S_n^{(-)}(t) &\approx \pm \text{sgn}(\phi) \sqrt{\frac{L\epsilon}{\pi}} F(-c) t^{-c}, \end{aligned} \quad (2.187)$$

with the zero-mode profile defined in (2.93). Note that $C_n^{(+)}(t)$ and $S_n^{(-)}(t)$ are of order one, while $C_n^{(-)}(t)$ and $S_n^{(+)}(t)$ are suppressed by v/M_{KK} .

2.3.3 Compatibility with Electroweak Precision Tests

In this last section on the custodial RS model, we will see that this model is able to mitigate the large RS contributions to the T parameter and to the Zbb vertex. In the following final formulas for the electroweak precision observables, the custodial symmetry will have already been applied. Intermediate steps and the connection to the parameter and couplings of the theory can be found in [149].

Oblique Parameters

The effects of the custodial model on the S , T , and U parameter have been investigated in [149, 196, 209] and they found

$$S = \frac{2\pi v^2}{M_{\text{KK}}^2} \left(1 - \frac{1}{L} \right), \quad T = -\frac{\pi v^2}{4c_w^2 M_{\text{KK}}^2} \frac{1}{L}, \quad U = 0. \quad (2.188)$$

Comparing with the corresponding formulas in the minimal model (2.132), the S parameter remains unaffected, while the L -enhanced term in the T parameter has been cancelled by the extra terms in (2.169) and (2.170) reflecting the underlying custodial symmetry. The only minor corrections to the T parameter can be understood with the help of the dual theory of the custodial RS model as already outlined at the end of Section 1.4.4 [105]: The symmetry breaking of the gauge group $SU(2)_L \times SU(2)_R \times U(1)_X \rightarrow SU(2)_L \rightarrow U(1)_Y$ on the IR brane gives rise the fields L_μ^\pm , L_μ^3 , and B_μ , which correspond to the elementary fields in the dual 4D theory. Thus, the dual gauge sector contains the elementary gauge bosons of the SM gauge group, just as the minimal model, but its composite sector moreover has the (custodial) global symmetry $SU(2)_L \times SU(2)_R$ that is responsible for the protection of the T parameter. The resulting reduction of the RS corrections is depicted in the left plot of Figure 2.5. Requiring the corrections to satisfy the experimental bounds from S and T leads to the lower bound on the KK scale of

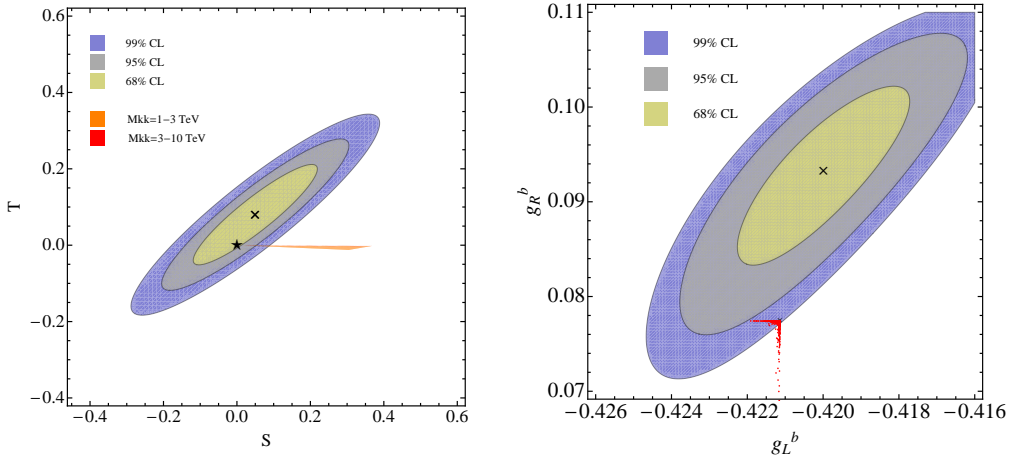


FIGURE 2.5: Regions of 68%, 95% and 99% probability in the $S - T$ (left) and $g_L^b - g_R^b$ (right) plane in the case of the custodial RS model obtained from the analysis performed in [105]. The meaning of the colors, crosses, and stars is the same as in Figure 2.4.

$M_{\text{KK}} > 1.9 \text{ TeV}$ at 95% CL, which is now driven by the S parameter. This KK scale corresponds to a mass of the lightest KK gluon and photon resonance of

$$M_{g^{(1)}} > 4.7 \text{ TeV} \quad (95\% \text{ CL}). \quad (2.189)$$

These KK modes could be detected at a high-luminosity LHC with 3000 fb^{-1} which is sensitive to KK masses of 6.7 TeV [213]. This encourages us to predominantly work on RS models with custodial protection of the enlarged $SU(2)_L \times SU(2)_R$ gauge group.

Corrections to $Zb\bar{b}$

The discrete P_{LR} symmetry has, moreover, the potential to mitigate the large corrections to the $Zb\bar{b}$ vertex. As shown in [149], the result for the Z -boson couplings to bottom quarks in the custodial model, described by the effective Lagrangian (2.134) (with $g_5 \rightarrow g_{L,5}$), reads

$$\begin{aligned} g_L^b &= \left(-\frac{1}{2} + \frac{s_w^2}{3} \right) \left[1 + \frac{m_Z^2}{2M_{\text{KK}}^2} \frac{F^2(c_{b_L})}{3 + 2c_{b_L}} \frac{5 + 2c_{b_L}}{2(3 + 2c_{b_L})} \right] + \frac{m_b^2}{2M_{\text{KK}}^2} \frac{1}{1 - 2c_{b_R}} \left(\frac{F^2(c_{b_R})}{3 + 2c_{b_R}} - 1 \right), \\ g_R^b &= \frac{s_w^2}{3} \left[1 - \frac{m_Z^2}{2M_{\text{KK}}^2} \frac{F^2(c_{b_R})}{3 + 2c_{b_R}} \left(\frac{3c_w^2}{s_w^2} L - \frac{5 + 2c_{b_R}}{2(3 + 2c_{b_R})} \right) \right] \\ &\quad + \frac{m_b^2}{2M_{\text{KK}}^2} \left[\frac{1}{1 - 2c_{b_L}} \left(\frac{1}{F^2(c_{b_L})} - 1 + \frac{F^2(c_{b_L})}{3 + 2c_{b_L}} \right) + \sum_{i=1,2} \frac{|(Y_d)_{i3}|^2}{|(Y_d)_{33}|^2} \frac{1}{1 - 2c_{Q_i}} \frac{1}{F^2(c_{b_L})} \right], \end{aligned} \quad (2.190)$$

where the P_{LR} symmetry has already been applied. The resulting contributions are visualized in the right plot of Figure 2.5. Comparing g_L^b in the custodial model with the corresponding expression in the minimal model (2.135), one notices that the L -enhanced term has been removed. Consequentially, most of the parameter points in Figure 2.5 are in the experimental error band as far as g_L^b is concerned. The L -enhanced term in

the right-handed coupling g_R^b on the other hand, is enlarged by a factor of $3c_w^2/s_w^2 \approx 10$, resulting in parameter points that fall outside the experimental ellipse. Note, however, that still 99% of the parameters are in agreement with the experiment so that there is no new unwanted discrepancy. Interestingly, the corrections to g_L^b seems to improve the situation compared to the SM.

The analysis above has demonstrated that the RS model with an enlarged bulk gauge symmetry is able to ameliorate the situation concerning electroweak precision observables that receive large contributions in the minimal RS model. Equipped with the set-up and most important features of both RS models, we will now turn to the main part of this thesis.

Chapter 3

Warped 5D Propagators

This chapter is dedicated to the calculation of warped 5D propagators which will be a crucial tool for the analysis in Chapter 4. We will work in the mixed momentum-position representation of the 5D propagators [139, 147, 214–216], in which the extra-dimensional coordinate is kept in position space. This is very convenient from a technical point of view, but it is also physically well motivated, as the position along the extra dimension defines the natural scale of the model, see (1.101). Using 5D propagators offers several advantages. Since they implicitly sum over the infinite tower of KK modes, symbolically written as

$$D(t, t'; p) \sim \sum_n \frac{\chi_n(t) \chi_n(t')}{p^2 - m_n^2}, \quad (3.1)$$

its derivation replaces the (numerical) determination of a significant number of KK masses and profiles and is thus less time-consuming especially concerning the fermion sector. It also avoids the necessity to take the limit to infinity which can cause problems, e.g. in Higgs processes generated by fermion loops, see Section 4.1. Moreover, we will in the latter chapter that the calculation of Higgs production via gluon fusion using 5D propagators reveals some interesting new features concerning distinguishable scenarios of the RS model. Furthermore, 5D propagators encode the full 5D theory that can give rise to terms that would not be taken into account when summing up the first few modes. We will encounter an example for that. Finally, we will see that using the 5D propagators it is possible to obtain closed, analytical expressions for amplitudes and hence for Wilson coefficients that include the effect of the complete tower and are exact in an expansion in v^2/M_{KK}^2 .

In the following, it will be focused on the calculation of warped 5D boson and fermion propagators. It will be explained in detail how one can derive the differential equations and obtain the solution for given boundary conditions. Moreover, the low- as well as high-energy behavior of the propagators in question will be presented. These expressions are needed for the analysis in Chapter 4. Section 3.1 deals with the boson propagators, where we will distinguish between the scalar and gauge-boson case. Emphasis will be put on the latter, for which we first derive the solutions for the 5D propagator for arbitrary boundary conditions, before we will then derive the important W -boson propagators for the RS models presented in the previous chapter. It will be distinguished between the minimal and the custodial model, as well as between the bulk and a brane-localized Higgs scenario, where the formulas in the custodial model have been derived for the first time. In Section 3.2, we will then derive the 5D fermion propagators for a brane and a bulk Higgs, where the solution in bulk-Higgs models will be exact only to first

order in the expansion in v^2/M_{KK}^2 . Using the regularized profile of the Higgs boson, which represents scenarios where the Higgs is localized on or very near the IR brane, we will derive results that keep the exact dependence on the Yukawa matrices and the full three-generation flavor structure. Finally, we will present the low- and high-energy limits of the 5D fermion propagator at the end of this section.

3.1 Boson Propagators

This section covers the derivation of the massive scalar and vector boson propagators. We will particularly focus on the gauge-boson case, where the derivations for a brane-localized Higgs field can be found in our publication [151]. The calculation of the 5D propagators in the bulk-Higgs scenario, on the other hand, is unpublished work.

3.1.1 Scalar Boson Propagator

We begin with the simplest case of a real and massive scalar field in the minimal RS model. In t -notation the 5D action reads

$$S_\Phi = \frac{1}{2} \int d^4x \frac{2\pi r}{L\epsilon} \int_\epsilon^1 dt \left(\frac{\epsilon}{t}\right)^3 \Phi(x, t) \left(-\partial_\mu \partial^\mu + M_{\text{KK}}^2 t^3 \partial_t \frac{1}{t^3} \partial_t - \frac{\epsilon^2 m_\Phi^2}{t^2} \right) \Phi(x, t). \quad (3.2)$$

Using $\partial_\mu \rightarrow -ip_\mu$ and rescaling $\Phi \rightarrow \Phi/\sqrt{r}$, which leads to the appropriate mass dimension of the propagator $[D_\Phi] = -2$ when interpreted as an infinite sum (3.1), this translates into the following differential equation for the 5D scalar boson propagator

$$\left(t^3 \partial_t \frac{1}{t^3} \partial_t + \hat{p}^2 - \frac{c^2}{t^2} \right) \frac{D_\Phi(t, t'; p)}{t^2} = -\frac{Lt'}{2\pi} \left(\frac{t'}{\epsilon}\right)^2 \frac{1}{M_{\text{KK}}^2} \delta(t - t'). \quad (3.3)$$

Here we have defined the dimensionless mass parameter $c \equiv \epsilon m_\Phi / M_{\text{KK}}$ and the normalized momentum $\hat{p}^2 = p^2 / M_{\text{KK}}^2$. The general solution to the Bessel differential equation (3.3) can be written as a linear combination of the Bessel functions $J_\alpha(\hat{p}t)$ and $Y_\alpha(\hat{p}t)$ with $\alpha = \sqrt{4 + c^2}$. Upon taking into account the continuity condition at $t = t'$ as well as the *jump condition*

$$\partial_t D_\Phi(t, t'; -p^2) \Big|_{t'-0}^{t'+0} = -\frac{Lt'^3}{2\pi M_{\text{KK}}^2 \epsilon^2}, \quad (3.4)$$

which can be obtained by integrating the differential equation (3.3) over an infinitesimal interval $t \in [t' - 0, t' + 0]$, we find (see the gauge-boson case for a more detailed derivation)

$$D_\Phi(t, t'; p) = -\frac{Lt^2 t'^2}{4M_{\text{KK}}^2 \epsilon^2} \frac{[C_1^> J_\alpha(\hat{p}t_>) + C_2^> Y_\alpha(\hat{p}t_>)] [C_1^< J_\alpha(\hat{p}t_<) + C_2^< Y_\alpha(\hat{p}t_<)]}{C_1^> C_2^< - C_1^< C_2^>}, \quad (3.5)$$

with $t_> = \max(t, t')$, $t_< = \min(t, t')$, where the coefficients $C_{1,2}^{>,<}$ are subject to the BCs. Note that if we had rescaled our scalar field by the factor $\Phi \rightarrow t/\epsilon \Phi$, we would obtain the same propagator solution (3.5), but multiplied with the factor ϵ^2/tt' . We will see in the subsequent section that the gauge-boson propagators have the same structure.

3.1.2 Gauge-Boson Propagator

We now turn to the case of a 5D gauge boson. For the later analysis, it will be important to derive the 5D W -boson propagators in various RS models which will be done in the following. First, however, it will be explained how one obtains the partial differential equations for a general gauge boson out of the Lagrangian. Moreover, the general proceeding to obtain the solution for the propagator for arbitrary BCs will be presented.

General Solutions

The general 5D action for a gauge boson can be written as [139]

$$S = \int d^4x \int_{-\pi}^{\pi} d\phi \sqrt{G} (\mathcal{L}_A + \mathcal{L}_{\text{GF}} + \mathcal{L}_{\text{Mass}}) = \frac{1}{2} \int d^4x \frac{2\pi r}{L} \int_{\epsilon}^1 \frac{dt}{t} A_M K_{\xi}^{MN} A_N, \quad (3.6)$$

where

$$K_{\xi}^{MN} = \begin{pmatrix} (\partial^2 - M_{\text{KK}}^2 t \partial_t^1 \partial_t) \eta^{\mu\nu} - \left(1 - \frac{1}{\xi}\right) \partial^{\mu} \partial^{\nu} + \frac{\epsilon^2}{t^2} M_A^2 \eta^{\mu\nu} & 0 \\ 0 & -\partial^2 + \xi M_{\text{KK}}^2 t \partial_t^1 \partial_t - \frac{\epsilon^2}{t^2} M_A^2 \end{pmatrix} \quad (3.7)$$

is the inverse of the Feynman propagator in general R_{ξ} gauge. In order to study the most general case, we have included a gauge-boson mass term M_A , which could be generated by a bulk Higgs field with profile (2.63). Thus, M_A would be dependent on the extra-dimension parameter t . For the time being, it is assumed to be a constant. Analogously to the scalar boson case, we now rescale the field via $A_M \rightarrow A_M/\sqrt{r}$ in order to interpret the 5D propagator as an infinite tower of 4D propagators, see (3.14). From (3.7) we can now derive the EOMs

$$\left[\left(t \partial_t \frac{1}{t} \partial_t + \hat{p}^2 - \frac{c_A^2}{t^2} \right) \eta^{\mu\nu} - \left(1 - \frac{1}{\xi} \right) \hat{p}^{\mu} \hat{p}^{\nu} \right] D_{\nu\rho}(t, t'; p) = \frac{-Lt'}{2\pi M_{\text{KK}}^2} \delta_{\rho}^{\mu} \delta(t - t'), \quad (3.8)$$

$$\left[t \partial_t \frac{1}{t} \partial_t + \frac{\hat{p}^2}{\xi} - \frac{c_A^2/\xi - 1}{t^2} \right] \xi D_{55}^{\xi}(t, t'; p) = \frac{Lt'}{2\pi M_{\text{KK}}^2} \delta(t - t'), \quad (3.9)$$

where $c_A \equiv \epsilon M_A/M_{\text{KK}}$. For the vector component we make the ansatz [139]

$$D_{\nu\rho}^{\xi}(t, t'; p) = A_{\xi}(t, t'; -p^2) \frac{p_{\nu} p_{\rho}}{p^2} + B(t, t'; -p^2) \left(\eta_{\nu\rho} - \frac{p_{\nu} p_{\rho}}{p^2} \right), \quad (3.10)$$

which after inserting into (3.8) yields the two independent equations

$$\left(t \partial_t \frac{1}{t} \partial_t + \frac{\hat{p}^2}{\xi} - \frac{c_A^2}{t^2} \right) A_{\xi}(t, t'; -p^2) = \left(t \partial_t \frac{1}{t} \partial_t + \hat{p}^2 - \frac{c_A^2}{t^2} \right) B(t, t'; -p^2), \quad (3.11)$$

$$\left(t \partial_t \frac{1}{t} \partial_t + \hat{p}^2 - \frac{c_A^2}{t^2} \right) B(t, t'; -p^2) = -\frac{Lt'}{2\pi M_{\text{KK}}^2} \delta(t - t'). \quad (3.12)$$

From the first equation we can deduce that $A_{\xi}(t, t'; -p^2) = B(t, t'; -p^2/\xi)$ and from (3.9) that

$$D_{55}^{\xi}(t, t'; p) = -\frac{1}{\xi} A_{\xi}(t, t'; -p^2) = -\frac{1}{\xi} B(t, t'; -p^2/\xi) \quad \text{with} \quad c_A \rightarrow \sqrt{c_A^2/\xi - 1}. \quad (3.13)$$

Solving the differential equation (3.12) for $B(t, t'; -p^2)$ is therefore sufficient to compute both propagators and will be the starting point for the following derivations. Note that due to the rescaling of the 5D gauge field A_M , we can identify the propagator function $B(t, t'; -p^2)$ to be

$$B(t, t'; -p^2) \equiv \sum_{n=0}^{\infty} \frac{\chi_n(t) \chi_n(t')}{m_n^2 - p^2}. \quad (3.14)$$

Like the EOM (3.3) for the scalar propagator, equation (3.12) can be rewritten as a Bessel differential equation. The general solution of (3.12) is a linear combination of the Bessel functions J_α and Y_α , where $\alpha \equiv \sqrt{1 + c_A^2}$. The appearance of the δ -function on the right-hand side of (3.12) makes it necessary to split the solution into two parts,

$$\begin{aligned} B_{<}(t, t'; -p^2) &= \hat{p}t [C_1^>(t') J_\alpha(\hat{p}t) + C_2^>(t') Y_\alpha(\hat{p}t)], \quad \text{for } t > t', \\ B_{>}(t, t'; -p^2) &= \hat{p}t [C_1^<(t') J_\alpha(\hat{p}t) + C_2^<(t') Y_\alpha(\hat{p}t)], \quad \text{for } t < t'. \end{aligned} \quad (3.15)$$

Two of the four unknown coefficients can be obtained by using the general UV and IR boundary conditions

$$\left(\partial_t - \frac{b_\epsilon}{\epsilon}\right) B(t, t'; -p^2)|_{t=\epsilon^+} = 0, \quad \left(\partial_t - b_1\right) B(t, t'; -p^2)|_{t=1^-} = 0, \quad (3.16)$$

where b_ϵ and b_1 can be generated by the vevs of some UV- or IR-localized scalars that couple to the 5D vector boson at the boundaries. Note the analogy to the BCs for the gauge-boson profiles stemming from the coupling to the Higgs doublet at the IR brane, see e.g. (2.22). The remaining two coefficients are determined by requiring continuity of the propagator function at $t = t'$

$$B(t, t'; -p^2)|_{t'=0}^{t'+0} = 0, \quad (3.17)$$

and by the jump condition

$$\partial_t B(t, t'; -p^2)|_{t'=0}^{t'+0} = -\frac{Lt'}{2\pi M_{\text{KK}}^2}. \quad (3.18)$$

The general solution can then be written as

$$B(t, t'; -p^2) = \frac{Ltt'}{4M_{\text{KK}}^2} \frac{[C_1^> J_\alpha(\hat{p}t_{>}) + C_2^> Y_\alpha(\hat{p}t_{>})][C_1^< J_\alpha(\hat{p}t_{<}) + C_2^< Y_\alpha(\hat{p}t_{<})]}{C_1^> C_2^< - C_1^< C_2^>}. \quad (3.19)$$

Note the close similarity to the solution of the scalar propagator (3.5). The coefficients depend on the BCs (3.16) and read

$$\begin{aligned} C_1^> &= -\hat{p} Y_{-1+\alpha}(\hat{p}) + (-b_1 - 1 + \alpha) Y_\alpha(\hat{p}), \\ C_2^> &= \hat{p} Y_{-1+\alpha}(\hat{p}) - (-b_1 - 1 + \alpha) Y_\alpha(\hat{p}), \\ C_1^< &= -\hat{p}\epsilon Y_{-1+\alpha}(\hat{p}\epsilon) + (-b_\epsilon - 1 + \alpha) Y_\alpha(\hat{p}\epsilon), \\ C_2^< &= \hat{p}\epsilon Y_{-1+\alpha}(\hat{p}\epsilon) - (-b_\epsilon - 1 + \alpha) Y_\alpha(\hat{p}\epsilon). \end{aligned} \quad (3.20)$$

For certain choices of the BCs it turns out to be appropriate to define linear combinations of Bessel functions in order to compactify (3.19), see e.g. (3.26).

Especially tree-level processes require the knowledge of the low-energy behavior of the 5D propagator function ($\hat{p}_E \ll 1$) in the general set-up described above. In accordance

with [105], we find the solution

$$B(t, t'; 0) = \frac{L}{4\pi M_{\text{KK}}^2} \frac{(tt')^{1-\alpha}}{\alpha} \left[c_1 t_{<}^{2\alpha} + c_2 (tt')^{2\alpha} + c_3 (t^{2\alpha} + t'^{2\alpha}) + c_4 \right], \quad (3.21)$$

where

$$\begin{aligned} c_1 &= 1, \\ c_2 &= \frac{-(b_1 - b_-)(b_\epsilon - b_-)}{(b_1 - b_+)(b_\epsilon - b_-) - (b_1 - b_-)(b_\epsilon - b_+)} \epsilon^{2\alpha} \approx \frac{-(b_1 - b_-)}{b_1 - b_+}, \\ c_3 &= \frac{(b_1 - b_-)(b_\epsilon - b_+) \epsilon^{2\alpha}}{(b_1 - b_+)(b_\epsilon - b_-) - (b_1 - b_-)(b_\epsilon - b_+)} \approx \frac{(b_1 - b_-)(b_\epsilon - b_+)}{(b_1 - b_+)(b_\epsilon - b_-)} \epsilon^{2\alpha}, \\ c_4 &= \frac{-(b_1 - b_+)(b_\epsilon - b_+) \epsilon^{2\alpha}}{(b_1 - b_+)(b_\epsilon - b_-) - (b_1 - b_-)(b_\epsilon - b_+)} \approx \frac{b_1 - b_+}{b_1 - b_-} \epsilon^{2\alpha}, \end{aligned} \quad (3.22)$$

and we have used the abbreviations $b_\pm = 1 \pm \alpha$, for a compact writeup. As explained in [105], the correct way to understand the various terms in (3.21) is to relate them to universal or non-universal diagrams in the dual 4D theory. Universal (non-universal) diagrams give rise to flavor-diagonal (flavor-changing) couplings, when rotated into the mass basis. Consequently, we can attribute the terms which lead to flavor-diagonal, $\Delta F = 1$, or $\Delta F = 2$ transitions to the certain diagrams in the dual theory. For instance, the fact that $c_1 = 1$, irrespective of the certain choice of BCs, can be understood with the help of the dual theory. Since the diagrams with an exchange of composites contribute in all combinations of BCs, this term is universal, whereas the remaining terms, which lead to flavor-changing transitions, vary for the specific choice, see [105] for a detailed discussion. Note also that the expansions (3.21) do not hold in the gauge-boson case ($\alpha = 1$) with Neumann BCs on the UV brane ($b_\epsilon = 0$). In these cases, a limiting procedure necessary.

For completeness, we touch on the special case $b_\epsilon = b_1 = 1 \pm \alpha$, for which we cannot use the expressions given above. This fine-tuning can be enforced by introducing supersymmetry within the AdS space [110]. For the upper branch (+), we obtain

$$\begin{aligned} B(t, t'; -p^2) &= -\frac{L(1+\alpha)}{\pi} \frac{(tt')^{1+\alpha}}{p^2} \\ &+ \frac{L}{4\pi M_{\text{KK}}^2} \frac{(tt')^{1-\alpha}}{\alpha} \left[t_{<}^{2\alpha} - 2\frac{(1+\alpha)^2}{2+\alpha} (tt')^{2\alpha} + \alpha(t^2 + t'^2)(tt')^{2\alpha} \right], \end{aligned} \quad (3.23)$$

which is exact up to $\mathcal{O}(p^2)$ -suppressed terms. Notice that this special case contains a zero mode with a non-flat profile $\chi_0^A(t) = \sqrt{L(1+\alpha)/\pi} t^{1+\alpha}$. The lower branch (-) also admits a pole with additional powers of ϵ and some inverse powers of tt' .

5D W -Boson Propagators

We will now turn to the explicit W -boson propagators needed for the later analysis in Section 4.2. It will be distinguished between the minimal RS model and the RS model with custodial protection as well as a brane-localized and a bulk-Higgs sector. We will see that in the latter case and for arbitrary momenta no closed form can be derived and we are only able to find a solution expanded in powers of $\mathcal{O}(v^2/M_{\text{KK}}^2)$. We will check our bulk-Higgs solutions by sending the Higgs profile to the IR brane and identifying the results with the brane-localized Higgs solutions.

Brane-Localized Higgs Sector, Minimal Model

The calculation of the propagator function B_W in the RS model with a brane-localized Higgs field has been performed, for instance, in [139, 152, 217] and is the solution to the differential equation (3.12) with $B \rightarrow B_W$ and $c_A \equiv 0$ subject to the BCs (3.16) with

$$b_\epsilon = 0 \quad \text{and} \quad b_1 = -\frac{L\tilde{m}_W^2}{M_{\text{KK}}^2}. \quad (3.24)$$

Note the close similarity with the corresponding EOMs and BCs for the gauge-boson profiles $\chi_n^W(t)$ given in relations (2.20) and (2.22). We can thus directly read off the solution from (3.19) with $\alpha = 1$. In the region of time-like momenta ($p^2 \geq 0$), the general solution can be written in the form

$$B_W(t, t'; -p^2) = \frac{Ltt'}{4M_{\text{KK}}^2} \frac{[\hat{p}D_{10}(t_>, 1) - b_1D_{11}(t_>, 1)] D_{10}(t_<, \epsilon)}{\hat{p}D_{00}(1, \epsilon) - b_1D_{10}(1, \epsilon)}, \quad (3.25)$$

where

$$D_{ij}(t, t') = J_i(\hat{p}t) Y_j(\hat{p}t') - Y_i(\hat{p}t) J_j(\hat{p}t'). \quad (3.26)$$

For space-like momenta, we find instead (with $p_E^2 = -p^2 > 0$ and $\hat{p}_E^2 = p_E^2/M_{\text{KK}}^2$)

$$B_W(t, t'; p_E^2) = \frac{Ltt'}{2\pi M_{\text{KK}}^2} \frac{[\hat{p}_E D_{10}(t_>, 1) + b_1 D_{11}(t_>, 1)] D_{10}(t_<, \epsilon)}{\hat{p}_E D_{00}(1, \epsilon) - b_1 D_{10}(1, \epsilon)}, \quad (3.27)$$

with

$$D_{ij}(t, t') = I_i(\hat{p}_E t) K_j(\hat{p}_E t') - (-1)^{i+j} K_i(\hat{p}_E t) I_j(\hat{p}_E t'). \quad (3.28)$$

For the later analysis, it is convenient to expand the propagator function in powers of $1/M_{\text{KK}}^2$ while keeping p^2 and \tilde{m}_W^2 fixed and of order v^2 . This yields

$$B_W(t, t'; -p^2) = \frac{1}{2\pi} \frac{-1}{(p^2 - \tilde{m}_W^2) [1 + \Pi(t, t'; p^2)] + \Sigma(p^2) + i0}, \quad (3.29)$$

where

$$\begin{aligned} \Sigma(p^2) &= \frac{\tilde{m}_W^4}{2M_{\text{KK}}^2} \left(L - \frac{p^2}{\tilde{m}_W^2} + \frac{1}{2L} \frac{p^4}{\tilde{m}_W^4} \right), \\ \Pi(t, t'; p^2) &= \frac{\tilde{m}_W^2}{2M_{\text{KK}}^2} \left\{ Lt_>^2 + \frac{p^2}{\tilde{m}_W^2} \left[Lt_<^2 - t^2 \left(\frac{1}{2} - \ln t \right) - t'^2 \left(\frac{1}{2} - \ln t' \right) \right] \right\}, \end{aligned} \quad (3.30)$$

which are valid up to terms of order v^4/M_{KK}^4 . The zero of the denominator of the propagator in (3.29) defines the physical mass m_W of the ground state, and the residue of the pole determines the corresponding product of profile functions $\chi_0^W(t) \chi_0^W(t')$. Clearly, one must encounter a single pole when replacing \tilde{m}_W^2 by the physical mass m_W^2 (2.30). Indeed, it is possible to show that

$$2\pi B_W(t, t'; -p^2) = \frac{c_1(t, t')}{m_W^2 - p^2} + \frac{c_2(t, t')}{2M_{\text{KK}}^2} + \mathcal{O}\left(\frac{v^2}{M_{\text{KK}}^4}\right), \quad (3.31)$$

where the first term in the bracket represents the pole contribution from the SM W boson, while the second term denotes the tower contribution from the KK excitations.

The t -dependent functions appearing in (3.31) are given by

$$\begin{aligned} c_1(t, t') &= 1 + \frac{m_W^2}{2M_{\text{KK}}^2} \left[1 - \frac{1}{L} - t^2 \left(L - \frac{1}{2} + \ln t \right) - t'^2 \left(L - \frac{1}{2} + \ln t' \right) \right], \\ c_2(t, t') &= Lt_{<}^2 + \frac{1}{2L} + t^2 \left(\ln t - \frac{1}{2} \right) + t'^2 \left(\ln t' - \frac{1}{2} \right). \end{aligned} \quad (3.32)$$

Before we move on to the custodial RS model, it is a fortunate side-effect that we can use (3.29) for an alternative approach to derive explicit expressions for the W -boson mass and profile to any order in v^2/M_{KK}^2 . With the help of (3.30), we find

$$m_W^2 = \tilde{m}_W^2 - \Sigma(m_W^2) = \tilde{m}_W^2 \left[1 - \frac{\tilde{m}_W^2}{2M_{\text{KK}}^2} \left(L - 1 + \frac{1}{2L} \right) + \mathcal{O} \left(\frac{v^4}{M_{\text{KK}}^4} \right) \right], \quad (3.33)$$

which agrees with (2.30). The wave-function renormalization, i.e. the residue of the pole in (3.31), generally reads

$$Z_2(t, t') \equiv 1 - \Pi(t, t'; m_W^2) - \frac{\partial \Sigma(p^2)}{\partial p^2} \Big|_{p^2=m_W^2} = c_1(t, t') + \dots = 2\pi \chi_0^W(t) \chi_0^W(t'), \quad (3.34)$$

from which we can extract the first non-trivial correction to the W -boson profile

$$\chi_0^W(t) = \frac{1}{\sqrt{2\pi}} \left\{ 1 + \frac{m_W^2}{4M_{\text{KK}}^2} \left[1 - \frac{1}{L} + t^2 (1 - 2L - 2 \ln t) \right] + \mathcal{O} \left(\frac{v^4}{M_{\text{KK}}^4} \right) \right\}, \quad (3.35)$$

in accordance with (2.31).

Finally, we explore the asymptotic behavior of the propagator function for small and large momenta. The result for $p^2 = 0$, which will be a key ingredient in Section 5.1, when we derive the vev shift in the RS models under consideration, reads

$$\begin{aligned} 2\pi B_W(t, t', 0) &= \frac{1}{\tilde{m}_W^2} + \frac{L}{2M_{\text{KK}}^2} (1 - t_{>}^2) \\ &= \frac{1}{m_W^2} \left[1 + \frac{m_W^2}{2M_{\text{KK}}^2} \left(-Lt_{>}^2 + 1 - \frac{1}{2L} \right) + \mathcal{O} \left(\frac{v^4}{M_{\text{KK}}^4} \right) \right], \end{aligned} \quad (3.36)$$

where the physical mass has been substituted in the second line. Note that the result in the first line is exact to all orders in the expansion of v^2/M_{KK}^2 . The expression in the second line coincides with formula (33) in [145]. In this reference, the result has been obtained by iterative procedure. For large momenta ($p_E \gg M_{\text{KK}}$), we find

$$\begin{aligned} B_W(t, t', -p^2) &\rightarrow \frac{L}{2\pi \left[\ln \frac{2k}{p_E} - \gamma_E \right] p_E^2}, & p_E t_{<} \ll M_{\text{KK}}, \quad p_E t_{>} \ll M_{\text{KK}}, \\ B_W(1, 1, -p^2) &\rightarrow \frac{L}{2\pi p_E M_{\text{KK}}}, & p_E \gg M_{\text{KK}}, \\ B_W(t, t', -p^2) &\rightarrow e^{-\hat{p}_E(t_{>} - t_{<})} \frac{L\sqrt{t_{>} t_{<}}}{4\pi p_E M_{\text{KK}}}, & p_E t_{<} > M_{\text{KK}}, \quad p_E t_{>} > M_{\text{KK}}. \end{aligned} \quad (3.37)$$

The first limit is valid for $p_E \gg M_{\text{KK}}$, but where the momentum is well below the position-dependent cutoff (1.101). This limit thus does not hold on the IR brane ($t_{>} = t_{<} = 1$), whose result is shown in the second line. Here the $1/p_E^2$ behavior changes to a $1/p_E$ behavior. The last line shows the behavior for the general case $1 \neq t_{>} \neq t_{<}$.

Brane-Localized Higgs Sector, Custodial Model

The exact expression for the 5D gauge-boson propagator in the RS model with custodial symmetry has been derived for the first time in our publication [151]. The differential equation for the propagator function \mathbf{B}_{UV} can be derived analogously to the one in the minimal model. It can also be extracted from the EOM for the profiles (2.161) and is the same as in the minimal model (3.12) (with $c_A \equiv 0$). The BCs, on the other hand, are modified to [149]

$$\begin{aligned} (\mathbf{P}_+ \partial_t + \mathbf{P}_-) \mathbf{B}_W^{\text{UV}}(t, t'; -p^2) \Big|_{t=\epsilon} &= 0, \\ (\partial_t - b_1 \mathbf{D}_\vartheta) \mathbf{B}_W^{\text{UV}}(t, t'; -p^2) \Big|_{t=1^-} &= 0; \quad b_1 = -\frac{L\tilde{m}_W^2}{c_\vartheta^2 M_{\text{KK}}^2}. \end{aligned} \quad (3.38)$$

The first equation follows from the BCs for the UV fields L_M^\pm and R_M^\pm . We have defined $\mathbf{P}_- = \text{diag}(0, 1)$. The second equation is a direct consequence of (2.163). Proceeding as above, we find that, in the region of time-like momenta ($p^2 > 0$), the general solution for the propagator function reads

$$\begin{aligned} \mathbf{B}_W^{\text{UV}}(t, t'; -p^2) &= \frac{Ltt'}{4M_{\text{KK}}^2} \frac{1}{[\hat{p}D_{00}(1, \epsilon) - b_1 D_{10}(1, \epsilon)] D_{01}(1, \epsilon) - b_1 \frac{4s_\vartheta^2}{\pi^2 \hat{p}^2 \epsilon}} \\ &\times \left\{ \left[[\hat{p}D_{10}(t_>, 1) - b_1 D_{11}(t_>, 1)] D_{01}(1, \epsilon) - \frac{2b_1 s_\vartheta^2}{\pi \hat{p}} D_{11}(t_>, \epsilon) \right] D_{10}(t_<, \epsilon) \mathbf{P}_+ \right. \\ &+ \left[[\hat{p}D_{00}(1, \epsilon) - b_1 D_{10}(1, \epsilon)] D_{10}(t_>, 1) + \frac{2b_1 s_\vartheta^2}{\pi \hat{p}} D_{10}(t_>, \epsilon) \right] D_{11}(t_<, \epsilon) \mathbf{P}_- \\ &\left. - b_1 \frac{2s_\vartheta c_\vartheta}{\pi \hat{p}} [D_{10}(t, \epsilon) D_{11}(t', \epsilon) \mathbf{P}_{12} + D_{11}(t, \epsilon) D_{10}(t', \epsilon) \mathbf{P}_{21}] \right\}, \end{aligned} \quad (3.39)$$

with the functions $D_{ij}^\pm(t, t')$ defined in (3.26), and we have introduced the 2×2 matrices \mathbf{P}_{12} and \mathbf{P}_{21} , which have an entry 1 at the corresponding position indicated by the subscripts and entries 0 otherwise. Note that up to irrelevant $\mathcal{O}(\epsilon^2)$ terms we can replace $\hat{p}\epsilon D_{n1}(t, \epsilon) = -\frac{2}{\pi} J_n(\hat{p}t)$ for $n = 0, 1$. This gives rise to a simpler expression, in which the spurious $1/\epsilon$ term in the denominator is removed. In the limit $s_\vartheta \rightarrow 0$, we can identify the coefficient of \mathbf{P}_+ with the result (3.25) obtained in the minimal RS model. Expanding \mathbf{B}_W^{UV} in powers of $1/M_{\text{KK}}^2$, we obtain the result

$$2\pi \mathbf{B}_W^{\text{UV}}(t, t'; -p^2) = \begin{pmatrix} \frac{c_1(t, t')}{m_W^2 - p^2} + \frac{c_2(t, t')}{2M_{\text{KK}}^2} & \frac{Lm_W^2 \tan \vartheta}{2M_{\text{KK}}^2 (m_W^2 - p^2)} t'^2 \\ \frac{Lm_W^2 \tan \vartheta}{2M_{\text{KK}}^2 (m_W^2 - p^2)} t^2 & \frac{Lt_\leq^2}{2M_{\text{KK}}^2} \end{pmatrix} + \mathcal{O}\left(\frac{v^2}{M_{\text{KK}}^4}\right), \quad (3.40)$$

where the functions $c_1(t, t')$ and $c_2(t, t')$ coincide with the expressions in the minimal RS model (3.32). The result for the special case $p^2 = 0$ can easily be read off from (3.40), where the (11) component becomes (3.36), and reduces to equation (54) in [149]. The general results above valid for arbitrary momentum are, however, new. The results for large momenta (at leading order) can be read off from (3.37) multiplied with the 2×2 identity matrix. The off-diagonal elements are further suppressed by v^2/M_{KK}^2 .

Bulk-Higgs Sector, Minimal Model

After having solved the 5D W -boson propagators for RS models with a brane-localized Higgs sector, we will now derive the 5D propagators for RS models with a generic bulk-Higgs field. Like the W -boson profile (see (2.47) and the discussion below), a closed expression for arbitrary momenta cannot be obtained. For the special case $p^2 = 0$, on the other hand, it is possible to arrive at an expression that is exact to all orders in the expansion of v^2/M_{KK}^2 . We will also derive an expression for $p^2 \lesssim \mathcal{O}(v^2)$, which is exact up to corrections suppressed by M_{KK}^4 . The asymptotic behavior for large momenta $p \gg M_{\text{KK}}$ agrees with that of the brane-localized Higgs scenario up to $\mathcal{O}(v^2/M_{\text{KK}}^2)$ corrections, see below.

Starting with the minimal model, we again make use of the partial differential equation (3.12), where the mass parameter comes from the Higgs mechanism with the t -dependent vev (2.52) and reads¹

$$c_A^2(t) \equiv \frac{2\pi\tilde{m}_W^2}{M_{\text{KK}}^2} \frac{t^2 v^2(t)}{v^2} = \frac{L\tilde{m}_W^2}{M_{\text{KK}}^2} (1 + \beta) t^{4+2\beta}, \quad (3.41)$$

with Neumann BCs on both branes and the usual continuity and jump conditions. Note that due to the t -dependence of c_A , we cannot read off the solution from (3.19). For the case of vanishing momentum $p^2 = 0$, we find the exact result

$$B_W(t, t'; 0) = \frac{-L\alpha t t'}{4M_{\text{KK}}^2 \sin(\pi\alpha)} \frac{D_1(t_>, 1) D_1(t_<, \epsilon)}{D_2(1, \epsilon)}, \quad (3.42)$$

where $\alpha \equiv 1/(2 + \beta)$ and we have defined the functions

$$\begin{aligned} D_1(t, t') &= \tilde{I}_\alpha(t) \tilde{I}_{1-\alpha}(t') - \tilde{I}_{-\alpha}(t) \tilde{I}_{\alpha-1}(t'), \\ D_2(t, t') &= \tilde{I}_{\alpha-1}(t) \tilde{I}_{1-\alpha}(t') - \tilde{I}_{-\alpha+1}(t) \tilde{I}_{\alpha-1}(t'), \end{aligned} \quad (3.43)$$

and

$$\tilde{I}_\alpha(t) \equiv I_\alpha \left(\frac{2L\tilde{m}_W^2}{M_{\text{KK}}^2} \frac{1 + \beta}{2 + \beta} t^{\frac{1}{2+\beta}} \right). \quad (3.44)$$

In order to find a general solution for $p^2 = \mathcal{O}(v^2) \ll M_{\text{KK}}^2$, we treat the term on the right-hand side of the differential operator as a perturbation and make the ansatz

$$B_W(t, t', -p^2) = \frac{1}{\tilde{\epsilon}} B_{-1}(t, t', -p^2) + B_0(t, t', -p^2) + \tilde{\epsilon} B_1(t, t', -p^2) + \mathcal{O}(\tilde{\epsilon}^2), \quad (3.45)$$

where $\tilde{\epsilon}$ is a small parameter and counts the orders of v^2/M_{KK}^2 . Analogously to Subsection 2.2.1, we plug the ansatz into the partial differential equation (3.12) and collect all pieces that belong to the different orders of $\tilde{\epsilon}$. The resulting differential equations read

$$t \partial_t \frac{1}{t} \partial_t B_{-1}(t, t'; -p^2) = 0 \quad (3.46)$$

$$t \partial_t \frac{1}{t} \partial_t B_0(t, t'; -p^2) + \left(\hat{p}^2 - \frac{c_A^2(t)}{t^2} \right) B_{-1}(t, t'; -p^2) = -\frac{Lt}{2\pi M_{\text{KK}}^2} \delta(t - t'), \quad (3.47)$$

$$t \partial_t \frac{1}{t} \partial_t B_1(t, t'; -p^2) + \left(\hat{p}^2 - \frac{c_A^2(t)}{t^2} \right) B_0(t, t'; -p^2) = 0, \quad (3.48)$$

¹Here, we use $v_4 \equiv v$ and $\tilde{m}_W = vg_5/(2\sqrt{2\pi r})$.

which shows that the jump condition is only relevant for B_0 , while the derivative of B_{-1} and B_1 is continuous at $t = t'$. Note that for $p^2 \gg M_{\text{KK}}^2$, the vev profile can be neglected and the solution is identical to (3.25) with $b_1 \equiv 0$. Thus, the asymptotic behavior for large momenta does not depend on the brane-localized or bulk-Higgs scenario and is given by (3.37).

Equation (3.46) together with the boundary and continuity conditions can be used to determine

$$B_{-1}(t, t'; -p^2) = C(t'), \quad (3.49)$$

where $C(t')$ is a constant with respect to the dependence on t . From the condition that the propagator is symmetric in t, t' , it follows that $B_{-1} = c$. Note that the constant c cannot be fixed, since the jump condition does not give an additional constraint. For its determination we have to use (3.47) together with the boundary and jump conditions. Similarly, one coefficient of B_0 cannot be fixed completely and we need to make use of (3.47). This is actually the reason why we have taken into account B_1 in the ansatz (3.45). Eventually, one finds the solution (3.29), where the functions are now given by

$$\begin{aligned} \Sigma^\beta(p^2) &= \frac{\tilde{m}_W^4}{2M_{\text{KK}}^2} \left(L \frac{2(1+\beta)^2}{(2+\beta)(3+2\beta)} - \frac{p^2}{\tilde{m}_W^2} \frac{(1+\beta)(3+\beta)}{(2+\beta)^2} + \frac{1}{2L} \frac{p^4}{\tilde{m}_W^4} \right), \\ \Pi^\beta(t, t'; p^2) &= \frac{\tilde{m}_W^2}{2M_{\text{KK}}^2} \left\{ -\frac{L(t^{4+2\beta} + t'^{4+2\beta})}{2+\beta} \right. \\ &\quad \left. + Lt_{>}^2 + \frac{p^2}{\tilde{m}_W^2} \left[Lt_{<}^2 - t^2 \left(\frac{1}{2} - \ln t \right) - t'^2 \left(\frac{1}{2} - \ln t' \right) \right] \right\}. \end{aligned} \quad (3.50)$$

From (3.33) and (3.50) we can deduce the correction to the mass

$$\frac{\tilde{m}_W^2}{m_W^2} = 1 + \frac{m_W^2}{2M_{\text{KK}}^2} \left[\frac{2L(1+\beta)^2}{(2+\beta)(3+2\beta)} - \frac{(1+\beta)(3+\beta)}{(2+\beta)^2} + \frac{1}{2L} \right] + \mathcal{O}\left(\frac{v^4}{M_{\text{KK}}^4}\right), \quad (3.51)$$

which coincides with the result (2.54). Replacing the leading-order mass \tilde{m}_W^2 by the physical one m_W^2 then yields the exact result for the propagator function in the bulk-Higgs model to order v^2/M_{KK}^2 that can be written as (3.31), where now

$$\begin{aligned} c_1^\beta(t, t') &\equiv 1 + \frac{m_W^2}{2M_{\text{KK}}^2} \left[\frac{L(t^{4+2\beta} + t'^{4+2\beta})}{2+\beta} + \frac{(1+\beta)(3+\beta)}{(2+\beta)^2} - \frac{1}{L} \right. \\ &\quad \left. - t^2 \left(L - \frac{1}{2} + \ln t \right) - t'^2 \left(L - \frac{1}{2} + \ln t' \right) \right], \end{aligned} \quad (3.52)$$

while $c_2(t, t')$ remains the same (3.32). We can use $c_1^\beta(t, t') \equiv \chi_0^W(t) \chi_0^W(t')$ to reproduce the correction to the physical W -boson profile $\chi_0^W(t)$, which agrees with the result (2.50).

Finally, we want to present the expansion of the propagator function for $p^2 = 0$,

$$2\pi B(t, t'; 0) = \frac{1}{\tilde{m}_W^2} + \frac{L}{2M_{\text{KK}}^2} \left[\frac{2(1+\beta)^2}{(2+\beta)(3+2\beta)} + \frac{t^{4+2\beta} + t'^{4+2\beta}}{2+\beta} - t_{>}^2 \right] + \mathcal{O}\left(\frac{v^2}{M_{\text{KK}}^4}\right), \quad (3.53)$$

which can be obtained either by expanding (3.42) for large M_{KK}^2 or from (3.31) with (3.52) in the limit $p^2 \rightarrow 0$. Note that in the limit $\beta \rightarrow \infty$ all results above reduce the corresponding results in the brane-localized Higgs case derived in the previous subsection so that there is a smooth transition between the two scenarios.

Bulk-Higgs Sector, Custodial Model

The last propagator to be derived in this section is the 5D W -boson propagator in the custodial RS model. According to Section 2.3.1, it is appropriate to work in the IR basis, which has the advantage to have a decoupled partial differential equation. It reads

$$\left(t \partial_t \frac{1}{t} \partial_t + \hat{p}^2 - \frac{2\pi \tilde{m}_W^2}{c_\vartheta^2 M_{\text{KK}}^2} \frac{v^2(t)}{v^2} \mathbf{P}_+ \right) \mathbf{B}_W^{\text{IR}}(t, t', -p^2) = -\frac{Lt}{2\pi M_{\text{KK}}^2} \delta(t - t'), \quad (3.54)$$

with boundary conditions

$$[\mathbf{P}_+ \partial_t + \mathbf{P}_-] \mathbf{R}_\vartheta^T \mathbf{B}_W^{\text{IR}}(t, t', -p^2) \Big|_{t=\epsilon} = 0, \quad \partial_t \mathbf{B}_W^{\text{IR}}(t, t', -p^2) \Big|_{t=1} = 0, \quad (3.55)$$

where the first one follows from (2.162) after rotating the IR basis fields into the UV basis via \mathbf{R}_ϑ defined in (2.145), while the second one is a direct consequence of (2.163). Performing the same steps as above, we finally end up with the exact solution for the special case $p^2 = 0$

$$\begin{aligned} \mathbf{B}_W^{\text{IR}}(t, t', 0) = \frac{L}{4M_{\text{KK}}^2} & \left\{ \frac{-\pi\alpha tt'}{\sin(\pi\alpha)} \frac{D_1(t_{<}, \epsilon) D_1(t_{>}, 1)}{D_2(1, \epsilon)} \mathbf{P}_+ \right. \\ & + \left[t_{<}^2 - \epsilon^2 - \frac{2s_\vartheta}{c_\vartheta \hat{v}} \frac{D_1(\epsilon, 1)}{D_2(\epsilon, 1)} \right] \mathbf{P}_- \\ & \left. + \frac{2s_\vartheta \epsilon^{1-\frac{1}{\alpha}}}{c_\vartheta \hat{v} D_2(1, \epsilon)} \left[t D_1(t, 1) \mathbf{P}_{12} + t' D_1(t', 1) \mathbf{P}_{21} \right] \right\}, \quad (3.56) \end{aligned}$$

where the functions $D_{1,2}$ have been defined in (3.43) and we have used the abbreviation $\hat{v} \equiv \frac{\tilde{m}_W}{M_{\text{KK}}} \sqrt{2(1-\alpha)/\alpha}$. Notice that the (11) component can be identified to the result of the minimal RS model (3.42). We can now rotate into the UV basis and expand the propagator for large KK scales,

$$\begin{aligned} 2\pi \mathbf{B}_W^{\text{UV}}(t, t'; 0) = \frac{1}{\tilde{m}_W^2} \mathbf{P}_+ + \frac{L}{2M_{\text{KK}}^2} & \left[\left(\frac{2(1+\beta)^2}{c_\vartheta^2 (2+\beta)(3+2\beta)} + \frac{t^{4+2\beta} + t'^{4+2\beta}}{2+\beta} - t_{>}^2 \right) \mathbf{P}_+ \right. \\ & \left. + \frac{s_\vartheta}{c_\vartheta} \left(t'^2 \left(1 - \frac{t'^{2+2\beta}}{2+\beta} \right) \mathbf{P}_{12} + t^2 \left(1 - \frac{t^{2+2\beta}}{2+\beta} \right) \mathbf{P}_{21} \right) + t_{<}^2 \mathbf{P}_- \right], \quad (3.57) \end{aligned}$$

which is exact at order $\mathcal{O}(v^2/M_{\text{KK}}^2)$. For $\beta \rightarrow \infty$ we obtain the same result as for a brane-localized Higgs sector [151]. Moreover, we can identify the (11)-component for $\vartheta \rightarrow 0$ with the result of the minimal RS model (3.53).

3.2 Fermion Propagators

This section deals with the calculation of the 5D fermion propagators in RS models with a brane-localized Higgs sector. Previous analyses of the 5D fermion propagator in warped extra dimensions have been presented in [147, 215, 216]. These results will be generalized by keeping the exact dependence on v^2/M_{KK}^2 and the full three-generation flavor-structure for the first time (see also [152]), and by paying special attention to the effects of the regularized profile of the Higgs boson. The exact 5D fermion propagator will be crucial for the calculation of the loop-induced Higgs production process extensively discussed in Section 4.1. This section includes Section 4 and Appendix A of our publication [150], where some results for the fermion propagator, in particular the propagator functions $\Delta_{LL}^{\vec{q}}$ and $\Delta_{RL}^{\vec{q}}$ with t' in the sliver (see below), have already been published. Moreover, it also contains unpublished work, such as the derivation of the propagator functions for arbitrary chiralities and values of t and t' as well as the final results for the full 5D fermion propagator for both finite η and the case $\eta \rightarrow 0$. Finally, the asymptotic behavior for very small and very large momenta will be examined at the end of this section.

In order to be as general as possible, we focus on the RS model with custodial protection and use the compact notation introduced in (2.69), where profile functions and a -vectors are given by the higher-dimensional objects as defined in (2.181) and (2.182). The corresponding expressions in the minimal version of the RS model can be obtained by simple replacements and will be presented explicitly if necessary. The starting point for the derivation of the 5D propagator is the quark Lagrangian (2.64), which can now be rewritten as

$$S_{\text{ferm},2} = \sum_{Q=\mathcal{U},\mathcal{D},\Lambda} \int d^4x \int_{\epsilon}^1 dt \bar{Q}(x,t) \{i\not{\partial} - M_{\text{KK}}\gamma_5\partial_t - M_{\text{KK}}\mathcal{M}_{\vec{q}}(t)\} Q(x,t). \quad (3.58)$$

The 5D fields $Q(x,t)$ are defined in (2.70) and the generalized mass matrix reads

$$\mathcal{M}_{\vec{q}}(t) = \frac{1}{t} \begin{pmatrix} \mathbf{c}_{\vec{Q}} & 0 \\ 0 & -\mathbf{c}_{\vec{q}} \end{pmatrix} + \frac{v}{\sqrt{2}M_{\text{KK}}} \delta_v^{\eta}(t-1) \begin{pmatrix} 0 & \mathbf{Y}_{\vec{q}} \\ \mathbf{Y}_{\vec{q}}^{\dagger} & 0 \end{pmatrix}, \quad (3.59)$$

with generalized Yukawa matrices $\mathbf{Y}_{\vec{q}}$ defined in (2.179) and an arbitrary vev profile $\delta_v^{\eta}(t-1)$. It is now straightforward to read off the Dirac operator from (3.58)

$$\mathcal{D} = \not{\partial} - M_{\text{KK}}\gamma_5\partial_t - M_{\text{KK}}\mathcal{M}_{\vec{q}}(t),$$

and we can immediately turn to the determination of the 5D fermion propagator in the mixed momentum-position representation. From now on we will use the regularized box profile (2.75) for $\delta_v^{\eta}(t-1)$.

3.2.1 Differential Equations and Boundary Conditions

The grand 15×15 (for up-type quarks) and 9×9 (for down- and λ -type quarks) propagators in the mixed momentum-position representation are given by

$$\begin{aligned} i\mathcal{S}^{\vec{q}}(t, t'; p) &= \int d^4x e^{ipx} \langle 0 | T(\mathcal{Q}_L(x, t) + \mathcal{Q}_R(x, t))(\bar{\mathcal{Q}}_L(x, t) + \bar{\mathcal{Q}}_R(x, t)) | 0 \rangle \\ &= \left[\Delta_{LL}^{\vec{q}}(t, t'; -p^2) \not{p} + \Delta_{RL}^{\vec{q}}(t, t'; -p^2) \right] P_R + (L \leftrightarrow R), \end{aligned} \quad (3.60)$$

with the projectors $P_{L,R} = \frac{1}{2}(1 \pm \gamma_5)$ and the symbol T denoting the time ordering. The objects $\Delta_{AB}^{\vec{q}}$ are referred to as *propagator functions* in the following.² Using the KK decomposition (2.70) it is straightforward to show that

$$\begin{aligned} \Delta_{LL}^{\vec{q}}(t, t'; -p^2) &= \sum_n \frac{1}{p^2 - m_{q_n}^2} \mathcal{Q}_L^{(n)}(t) \mathcal{Q}_L^{(n)\dagger}(t'), \\ \Delta_{RL}^{\vec{q}}(t, t'; -p^2) &= \sum_n \frac{m_{q_n}}{p^2 - m_{q_n}^2} \mathcal{Q}_R^{(n)}(t) \mathcal{Q}_L^{(n)\dagger}(t'), \end{aligned} \quad (3.61)$$

and similarly for the remaining two propagator functions. With the help of the definitions of the vectors $\mathcal{Q}_{L,R}^{(n)}$ (2.71) and their ingredients (2.181) and (2.182), we explicitly see how to interpret the various components of the propagator functions. As an example we consider the (15)-component of $\Delta_{RL}^{\vec{q}}$, which is a 5×5 matrix in representation space. The subscripts denote the handedness of the outgoing and incoming fields, respectively, while the components give information about the charges under the gauge group. In the case in question, the outgoing field is the right-handed field of the bi-doublet whose left-handed component is Z_2 -even, i.e. u_R . The incoming field, on the other hand, is the left-handed field of the triplet whose right-handed component is Z_2 -odd, i.e. U_L . The other components can be interpreted analogously.

With the help of the completeness relation for the bulk profiles

$$\sum_n \mathcal{Q}_A^{(n)}(t) \mathcal{Q}_A^{(n)\dagger}(t') = \delta(t - t'); \quad A = L, R, \quad (3.62)$$

which holds on the interval $t \in [\epsilon, 1]$ once we regularize the Higgs profile, it is easy to show that

$$\mathcal{D}\mathcal{S}^{\vec{q}}(t, t'; p) = \sum_n \left[\mathcal{Q}_L^{(n)}(t) \mathcal{Q}_L^{(n)\dagger}(t') \frac{1 + \gamma_5}{2} + \mathcal{Q}_R^{(n)}(t) \mathcal{Q}_R^{(n)\dagger}(t') \frac{1 - \gamma_5}{2} \right] = \delta(t - t') \mathbf{1}. \quad (3.63)$$

This implies the first-order differential equations

$$\begin{aligned} p^2 \Delta_{LL}^{\vec{q}}(t, t'; -p^2) - M_{\text{KK}} \mathcal{D}_+ \Delta_{RL}^{\vec{q}}(t, t'; -p^2) &= \delta(t - t'), \\ p^2 \Delta_{RR}^{\vec{q}}(t, t'; -p^2) - M_{\text{KK}} \mathcal{D}_- \Delta_{LR}^{\vec{q}}(t, t'; -p^2) &= \delta(t - t'), \end{aligned} \quad (3.64)$$

and

$$\begin{aligned} \Delta_{RL}^{\vec{q}}(t, t'; -p^2) - M_{\text{KK}} \mathcal{D}_- \Delta_{LL}^{\vec{q}}(t, t'; -p^2) &= 0, \\ \Delta_{LR}^{\vec{q}}(t, t'; -p^2) - M_{\text{KK}} \mathcal{D}_+ \Delta_{RR}^{\vec{q}}(t, t'; -p^2) &= 0, \end{aligned} \quad (3.65)$$

²Note that it is principally not necessary to use the superscript \vec{q} instead of q . However, we will use the latter to specify the more special case of the minimal RS model $q = u, d$, while the notation \vec{q} represents $\vec{q} = \vec{u}, \vec{d}, \vec{\lambda}$, i.e. the custodial RS model.

where we have used the shorthand notation $\mathcal{D}_\pm \equiv \pm\partial_t + \mathcal{M}_{\vec{q}}(t)$. These equations can be decoupled at the price of turning first-order into second-order differential equations:

$$\begin{aligned} (\hat{p}^2 - \mathcal{D}_- \mathcal{D}_+) \Delta_{RL}^{\vec{q}}(t, t'; -p^2) &= \frac{1}{M_{\text{KK}}} \mathcal{D}_- \delta(t - t'), \\ (\hat{p}^2 - \mathcal{D}_+ \mathcal{D}_-) \Delta_{LR}^{\vec{q}}(t, t'; -p^2) &= \frac{1}{M_{\text{KK}}} \mathcal{D}_+ \delta(t - t'), \end{aligned} \quad (3.66)$$

and

$$\begin{aligned} (\hat{p}^2 - \mathcal{D}_+ \mathcal{D}_-) \Delta_{LL}^{\vec{q}}(t, t'; -p^2) &= \frac{1}{M_{\text{KK}}^2} \delta(t - t'), \\ (\hat{p}^2 - \mathcal{D}_- \mathcal{D}_+) \Delta_{RR}^{\vec{q}}(t, t'; -p^2) &= \frac{1}{M_{\text{KK}}^2} \delta(t - t'), \end{aligned} \quad (3.67)$$

with the normalized momentum squared $\hat{p}^2 \equiv p^2/M_{\text{KK}}^2$. Integrating (3.64) and (3.65) over an infinitesimal interval $t \in [t' - 0, t' + 0]$ at fixed t' , one obtains the jump conditions

$$\begin{aligned} \Delta_{RL}^{\vec{q}}(t' + 0, t'; -p^2) - \Delta_{RL}^{\vec{q}}(t' - 0, t'; -p^2) &= -\frac{1}{M_{\text{KK}}}, \\ \Delta_{LR}^{\vec{q}}(t' + 0, t'; -p^2) - \Delta_{LR}^{\vec{q}}(t' - 0, t'; -p^2) &= \frac{1}{M_{\text{KK}}}, \\ \Delta_{LL}^{\vec{q}}(t' + 0, t'; -p^2) - \Delta_{LL}^{\vec{q}}(t' - 0, t'; -p^2) &= 0, \\ \Delta_{RR}^{\vec{q}}(t' + 0, t'; -p^2) - \Delta_{RR}^{\vec{q}}(t' - 0, t'; -p^2) &= 0. \end{aligned} \quad (3.68)$$

While the last two equations show the continuity of the propagator functions $\Delta_{LL}^{\vec{q}}$ and $\Delta_{RR}^{\vec{q}}$ (the actual jump occurs in their derivatives), the first two state the discontinuity of $\Delta_{RL}^{\vec{q}}$ and $\Delta_{LR}^{\vec{q}}$.

What is left are the boundary conditions which on the IR brane take the simple form

$$\text{diag}(0 \ 1) \Delta_{LA}^{\vec{q}}(1, t'; -p^2) = 0 = \text{diag}(1 \ 0) \Delta_{RA}^{\vec{q}}(1, t'; -p^2), \quad A = L, R, \quad (3.69)$$

where the entries 0 and 1 are zero and unit matrices of ranks according to the structures (2.71) and (2.181). The UV boundary conditions, on the other hand, differ for the various quark types ($A = L, R$):

$$\begin{aligned} \text{diag}(0, 1, 1, 0, 0) \Delta_{LA}^{\vec{u}}(\epsilon, t'; -p^2) &= 0 = \text{diag}(1, 0, 0, 1, 1) \Delta_{RA}^{\vec{u}}(\epsilon, t'; -p^2), \\ \text{diag}(0, 1, 0) \Delta_{LA}^{\vec{d}}(\epsilon, t'; -p^2) &= 0 = \text{diag}(1, 0, 1) \Delta_{RA}^{\vec{d}}(\epsilon, t'; -p^2), \\ \text{diag}(1, 0, 0) \Delta_{LA}^{\vec{\lambda}}(\epsilon, t'; -p^2) &= 0 = \text{diag}(0, 1, 1) \Delta_{RA}^{\vec{\lambda}}(\epsilon, t'; -p^2). \end{aligned} \quad (3.70)$$

Both UV and IR BCs follow from the respective conditions for the fields embedded in the 15- and 9-component vectors of (2.71). In the minimal model the BCs are given by (3.69) for $t = \epsilon, 1$.

3.2.2 Derivation of the Propagator Functions

We are now able to derive the full propagator for arbitrary t and t' , where we will focus on the determination of the propagator functions $\Delta_{LL}^{\vec{q}}$ and $\Delta_{RL}^{\vec{q}}$. It will be explained that the two propagator functions with reversed chiralities, $\Delta_{RR}^{\vec{q}}$ and $\Delta_{LR}^{\vec{q}}$ can be easily

deduced from the former ones. While deriving the solutions for the propagator functions, one has to distinguish between the cases of whether t is in the bulk or in the sliver and, moreover, whether $t < t'$ or $t > t'$. Having the general solution for $\Delta_{LL}^{\vec{q}}$ at hand, we can easily deduce $\Delta_{RL}^{\vec{q}}$ from the first equation in (3.65). Imposing the boundary as well as the jump conditions, we will have a solution with four independent parameter functions for both the bulk and sliver case. The determination of the unambiguous solution for these coefficient functions will be explained in the next subsection.

Bulk Solution ($t < 1 - \eta$)

In the case of t being in the bulk, $t < 1 - \eta$, the Yukawa matrices do not contribute to the mass matrix and we deal with

$$\mathcal{M}^2(t) \pm \frac{d\mathcal{M}(t)}{dt} = \frac{1}{t^2} \begin{pmatrix} \mathbf{c}_{\vec{Q}}(\mathbf{c}_{\vec{Q}} \mp 1) & 0 \\ 0 & \mathbf{c}_{\vec{q}}(\mathbf{c}_{\vec{q}} \pm 1) \end{pmatrix}, \quad t < 1 - \eta,$$

with $\mathbf{c}_{\vec{Q}}$ and $\mathbf{c}_{\vec{q}}$ having patterns as shown in (2.178). With the help of the ansatz $\sqrt{t}f(\hat{p}Et)$ for each entry in the propagator function $\Delta_{LL}^{\vec{q}}$, where $\hat{p}_E^2 = -p^2/M_{\text{KK}}^2$ denotes the square of the Euclidean momentum normalized to the KK scale, the differential equations become Bessel equations with independent solutions $I_\alpha(\hat{p}Et)$ and $I_{-\alpha}(\hat{p}Et)$ for non-integer α .³ The general solution for $\Delta_{LL}^{\vec{q}}$ is

$$\begin{aligned} \Delta_{LL}^{\vec{q}, \text{bulk}}(t, t'; -p^2) &= \sqrt{t} \begin{pmatrix} I_{\mathbf{c}_{\vec{Q}} - \frac{1}{2}}(\hat{p}Et) & 0 \\ 0 & I_{\mathbf{c}_{\vec{q}} + \frac{1}{2}}(\hat{p}Et) \end{pmatrix} \begin{pmatrix} \mathbf{C}_1(t') & \mathbf{C}_2(t') \\ \mathbf{C}_3(t') & \mathbf{C}_4(t') \end{pmatrix} \\ &+ \sqrt{t} \begin{pmatrix} I_{-\mathbf{c}_{\vec{Q}} + \frac{1}{2}}(\hat{p}Et) & 0 \\ 0 & I_{-\mathbf{c}_{\vec{q}} - \frac{1}{2}}(\hat{p}Et) \end{pmatrix} \begin{pmatrix} \mathbf{C}_5(t') & \mathbf{C}_6(t') \\ \mathbf{C}_7(t') & \mathbf{C}_8(t') \end{pmatrix}, \end{aligned} \quad (3.71)$$

where the zero matrices and the integration functions $\mathbf{C}_i(t')$ are matrices of corresponding rank. It is an easy exercise to derive the solution for $\Delta_{RL}^{\vec{q}}$ from equation (3.65) and we obtain

$$\begin{aligned} \Delta_{RL}^{\vec{q}, \text{bulk}}(t, t'; -p^2) &= -p_E \sqrt{t} \left[\begin{pmatrix} I_{\mathbf{c}_{\vec{Q}} + \frac{1}{2}}(\hat{p}Et) & 0 \\ 0 & I_{\mathbf{c}_{\vec{q}} - \frac{1}{2}}(\hat{p}Et) \end{pmatrix} \begin{pmatrix} \mathbf{C}_1(t') & \mathbf{C}_2(t') \\ \mathbf{C}_3(t') & \mathbf{C}_4(t') \end{pmatrix} \right. \\ &\left. + \begin{pmatrix} I_{-\mathbf{c}_{\vec{Q}} - \frac{1}{2}}(\hat{p}Et) & 0 \\ 0 & I_{-\mathbf{c}_{\vec{q}} + \frac{1}{2}}(\hat{p}Et) \end{pmatrix} \begin{pmatrix} \mathbf{C}_5(t') & \mathbf{C}_6(t') \\ \mathbf{C}_7(t') & \mathbf{C}_8(t') \end{pmatrix} \right]. \end{aligned} \quad (3.72)$$

The general solutions (3.71) and (3.72) hold for arbitrary choices of $t, t' \in [\epsilon, 1 - \eta)$, where the coefficients differ for the solutions for $t < t'$ and $t > t'$. Focusing on the solutions for $t < t'$, we evaluate them at $t = \epsilon$ and make use of the UV BCs (3.70), which lead to relations between the various coefficient functions. Upon rescaling the coefficient functions $\mathbf{C}_i^<(t') \rightarrow \mathbf{K}_i(t')$, one ends up with

$$\begin{aligned} \Delta_{LL}^{\vec{q}, <, \text{bulk}}(t, t'; -p^2) &= \sqrt{t} \begin{pmatrix} \mathbf{D}_1^{\vec{Q}}(\hat{p}_E, t) & 0 \\ 0 & \mathbf{D}_2^{\vec{q}}(\hat{p}_E, t) \end{pmatrix} \begin{pmatrix} \mathbf{K}_1(t') & \mathbf{K}_2(t') \\ \mathbf{K}_3(t') & \mathbf{K}_4(t') \end{pmatrix}, \\ \Delta_{RL}^{\vec{q}, <, \text{bulk}}(t, t'; -p^2) &= -p_E \sqrt{t} \begin{pmatrix} \mathbf{D}_2^{\vec{Q}}(\hat{p}_E, t) & 0 \\ 0 & \mathbf{D}_1^{\vec{q}}(\hat{p}_E, t) \end{pmatrix} \begin{pmatrix} \mathbf{K}_1(t') & \mathbf{K}_2(t') \\ \mathbf{K}_3(t') & \mathbf{K}_4(t') \end{pmatrix}, \end{aligned} \quad (3.73)$$

³For integer α we get the solutions by a limiting procedure.

where the functions $D_1^{\vec{A}}(\hat{p}_E t)$ and $D_2^{\vec{A}}(\hat{p}_E t)$ depend on the specific choice of $\vec{A} = \vec{U}, \vec{D}, \vec{\Lambda}, \vec{u}, \vec{d}, \vec{\lambda}$. They read

$$\begin{aligned}
D_{1,2}^{\vec{U}}(\hat{p}_E, t) &\equiv \text{diag} \left(D_{1,2}^Q(\hat{p}_E, t), D_{3,4}^Q(\hat{p}_E, t) \right), \\
D_{1,2}^{\vec{u}}(\hat{p}_E, t) &\equiv \text{diag} \left(D_{1,2}^{u^c}(\hat{p}_E, t), D_{3,4}^{\tau_1}(\hat{p}_E, t), D_{3,4}^{\tau_2}(\hat{p}_E, t) \right), \\
D_{1,2}^{\vec{D}}(\hat{p}_E, t) &\equiv D_{1,2}^Q(\hat{p}_E, t), \\
D_{1,2}^{\vec{d}}(\hat{p}_E, t) &\equiv \text{diag} \left(D_{1,2}^{\tau_2}(\hat{p}_E, t), D_{3,4}^{\tau_1}(\hat{p}_E, t) \right), \\
D_{1,2}^{\vec{\Lambda}}(\hat{p}_E, t) &\equiv D_{3,4}^Q(\hat{p}_E, t), \\
D_{1,2}^{\vec{\lambda}}(\hat{p}_E, t) &\equiv \text{diag} \left(D_{3,4}^{\tau_1}(\hat{p}_E, t), D_{3,4}^{\tau_2}(\hat{p}_E, t) \right).
\end{aligned} \tag{3.74}$$

The functions $D_i^A(\hat{p}_E, t)$ are defined via

$$D_i^A(\hat{p}_E, t) \equiv D_i^A(\hat{p}_E, t, \epsilon), \tag{3.75}$$

where the latter are linear combinations of Bessel functions defined by

$$\begin{aligned}
D_{1,2}^A(\hat{p}_E, t, t') &\equiv I_{-\mathbf{c}_A - \frac{1}{2}}(\hat{p}_E t') I_{\mathbf{c}_A \mp \frac{1}{2}}(\hat{p}_E t) - I_{\mathbf{c}_A + \frac{1}{2}}(\hat{p}_E t') I_{-\mathbf{c}_A \pm \frac{1}{2}}(\hat{p}_E t), \\
D_{3,4}^A(\hat{p}_E, t, t') &\equiv I_{-\mathbf{c}_A + \frac{1}{2}}(\hat{p}_E t') I_{\mathbf{c}_A \mp \frac{1}{2}}(\hat{p}_E t) - I_{\mathbf{c}_A - \frac{1}{2}}(\hat{p}_E t') I_{-\mathbf{c}_A \pm \frac{1}{2}}(\hat{p}_E t),
\end{aligned}$$

with $A = Q, u^c, \tau_1, \tau_2$. Note that these are 3×3 matrices in generation space. Due to the antisymmetry in the arguments, it is $D_{2,3}^A(\hat{p}_E, t, t) = 0$ and in particular $D_{2,3}^A(\hat{p}_E, \epsilon) = 0$, which has been required by the UV BCs.

Equipped with the solutions $\Delta_{LL}^{\vec{q}, <}$ and $\Delta_{RL}^{\vec{q}, <}$, it is possible to determine $\Delta_{LL}^{\vec{q}, >}$ and $\Delta_{RL}^{\vec{q}, >}$ with the help of the jump conditions. After some algebra we eventually obtain

$$\begin{aligned}
\Delta_{LL}^{\vec{q}, >, \text{bulk}}(t, t'; -p^2) &= \sqrt{t} \begin{pmatrix} D_1^{\vec{Q}}(\hat{p}_E, t) & 0 \\ 0 & D_2^{\vec{q}}(\hat{p}_E, t) \end{pmatrix} \begin{pmatrix} \mathbf{K}_1(t') & \mathbf{K}_2(t') \\ \mathbf{K}_3(t') & \mathbf{K}_4(t') \end{pmatrix} \\
&\quad + \frac{\sqrt{tt'}}{p_E M_{\text{KK}} 1_\eta} \begin{pmatrix} -L_3^{\vec{Q}}(\hat{p}_E, t, t') & 0 \\ 0 & L_2^{\vec{q}}(\hat{p}_E, t, t') \end{pmatrix}, \\
\Delta_{RL}^{\vec{q}, >, \text{bulk}}(t, t'; -p^2) &= -p_E \sqrt{t} \begin{pmatrix} D_2^{\vec{Q}}(\hat{p}_E, t) & 0 \\ 0 & D_1^{\vec{q}}(\hat{p}_E, t) \end{pmatrix} \begin{pmatrix} \mathbf{K}_1(t') & \mathbf{K}_2(t') \\ \mathbf{K}_3(t') & \mathbf{K}_4(t') \end{pmatrix} \\
&\quad + \frac{\sqrt{tt'}}{M_{\text{KK}} 1_\eta} \begin{pmatrix} L_4^{\vec{Q}}(\hat{p}_E, t, t') & 0 \\ 0 & -L_1^{\vec{q}}(\hat{p}_E, t, t') \end{pmatrix}.
\end{aligned} \tag{3.76}$$

In order to avoid clutter, we have used the rescaled quantities

$$L_i^{\vec{A}}(\hat{p}_E, t, t') \equiv \frac{\pi \hat{p}_E 1_\eta}{2 \cos(\pi \mathbf{c}_{\vec{A}})} D_i^{\vec{A}}(\hat{p}_E, t, t'), \quad i = 1, 2, 3, 4, \tag{3.77}$$

where it will turn out to be convenient to include a factor of $1_\eta \equiv 1 - \eta$ in the definition of $L_i^{\vec{A}}$. Having found the solutions for the propagator functions in the bulk, we are now able to turn to the sliver region.

Sliver Solution ($t > 1 - \eta$)

In the sliver region, $t > 1 - \eta$, we start again with the determination of the general solution for $t \neq t'$. Using the regularized profile of the Higgs (2.75), we can approximate

$$\mathcal{M}_q^2(t) + \frac{d\mathcal{M}_q(t)}{dt} = \frac{v^2}{2M_{\text{KK}}^2 \eta^2} \left[\begin{pmatrix} \mathbf{Y}_{\bar{q}} \mathbf{Y}_{\bar{q}}^\dagger & 0 \\ 0 & \mathbf{Y}_{\bar{q}}^\dagger \mathbf{Y}_{\bar{q}} \end{pmatrix} + \mathcal{O}\left(\frac{\eta M_{\text{KK}}}{v|Y_q|}\right) \right], \quad t > 1 - \eta. \quad (3.78)$$

Note that we need to require the relation $\eta \ll v|Y_q|/M_{\text{KK}}$ for the corrections to be small. This is the reason for the right inequality in (2.4). The differential equations (3.67) now take the simple form ($A = L, R$)

$$\left[\partial_t^2 - \left(\hat{p}_E^2 + \frac{\varrho^2}{\eta^2} \begin{pmatrix} \mathbf{Y}_{\bar{q}} \mathbf{Y}_{\bar{q}}^\dagger & 0 \\ 0 & \mathbf{Y}_{\bar{q}}^\dagger \mathbf{Y}_{\bar{q}} \end{pmatrix} \right) \right] \Delta_{AA}^q(t, t'; p^2) = 0, \quad \varrho \equiv \frac{v}{\sqrt{2}M_{\text{KK}}}. \quad (3.79)$$

As in the case of the bulk solution, we first focus on the propagator function $\Delta_{LL}^{\bar{q}, \text{sliver}}$. Using the definitions

$$\mathbf{S}_{\bar{q}} = \sqrt{\mathbf{X}_{\bar{q}}^2 + \eta^2 \hat{p}_E^2}, \quad \bar{\mathbf{S}}_{\bar{q}} = \sqrt{\bar{\mathbf{X}}_{\bar{q}}^2 + \eta^2 \hat{p}_E^2}, \quad (3.80)$$

with $\mathbf{X}_{\bar{q}}, \bar{\mathbf{X}}_{\bar{q}}$ defined in (2.78), the general solution in the sliver region reads

$$\Delta_{LL}^{\bar{q}, \text{sl.}}(t, t'; -p^2) = \begin{pmatrix} \mathcal{C}(t) & 0 \\ 0 & \bar{\mathcal{C}}(t) \end{pmatrix} \begin{pmatrix} \hat{\mathcal{C}}_1(t') & \hat{\mathcal{C}}_2(t') \\ \hat{\mathcal{C}}_3(t') & \hat{\mathcal{C}}_4(t') \end{pmatrix} + \begin{pmatrix} \mathcal{S}(t) & 0 \\ 0 & \bar{\mathcal{S}}(t) \end{pmatrix} \begin{pmatrix} \hat{\mathcal{C}}_5(t') & \hat{\mathcal{C}}_6(t') \\ \hat{\mathcal{C}}_7(t') & \hat{\mathcal{C}}_8(t') \end{pmatrix}, \quad (3.81)$$

where we have appropriately defined

$$\mathcal{S}(t) \equiv [\mathbf{S}_{\bar{q}} \bar{\theta}^\eta(t-1)], \quad \mathcal{C}(t) \equiv [\mathbf{S}_{\bar{q}} \bar{\theta}^\eta(t-1)], \quad (3.82)$$

and analogously $\bar{\mathcal{S}}(t)$ and $\bar{\mathcal{C}}(t)$ with $\mathbf{S}_{\bar{q}}$ replaced by $\bar{\mathbf{S}}_{\bar{q}}$. The dependence on the coordinate t enters via the integral

$$\bar{\theta}^\eta(t-1) \equiv \int_t^1 dt' \delta_v^\eta(t'-1) = \frac{1-t}{\eta}. \quad (3.83)$$

From the differential equation (3.65) we immediately obtain

$$\Delta_{RL}^{\bar{q}, \text{sliver}}(t, t'; -p^2) = \frac{M_{\text{KK}}}{\eta} \left[\begin{pmatrix} \mathbf{S}_{\bar{q}} \mathcal{S}(t) & \varrho \mathbf{Y}_{\bar{q}} \bar{\mathcal{C}}(t) \\ \varrho \mathbf{Y}_{\bar{q}}^\dagger \mathcal{C}(t) & \bar{\mathbf{S}}_{\bar{q}} \bar{\mathcal{S}}(t) \end{pmatrix} \begin{pmatrix} \hat{\mathcal{C}}_1(t') & \hat{\mathcal{C}}_2(t') \\ \hat{\mathcal{C}}_3(t') & \hat{\mathcal{C}}_4(t') \end{pmatrix} \right. \\ \left. + \begin{pmatrix} \mathbf{S}_{\bar{q}} \mathcal{C}(t) & \varrho \mathbf{Y}_{\bar{q}} \bar{\mathcal{S}}(t) \\ \varrho \mathbf{Y}_{\bar{q}}^\dagger \mathcal{S}(t) & \bar{\mathbf{S}}_{\bar{q}} \bar{\mathcal{C}}(t) \end{pmatrix} \begin{pmatrix} \hat{\mathcal{C}}_5(t') & \hat{\mathcal{C}}_6(t') \\ \hat{\mathcal{C}}_7(t') & \hat{\mathcal{C}}_8(t') \end{pmatrix} \right]. \quad (3.84)$$

Again, we need to distinguish between $t > t'$ and $t < t'$. The IR boundary conditions can be used for the former case and we get

$$\begin{aligned}\Delta_{LL}^{\bar{q}>, \text{sliver}}(t, t'; -p^2) &= \begin{pmatrix} \mathcal{C}(t) & 0 \\ 0 & \bar{\mathcal{S}}(t) \end{pmatrix} \begin{pmatrix} \hat{\mathcal{C}}_1^>(t') & \hat{\mathcal{C}}_2^>(t') \\ \hat{\mathcal{C}}_7^>(t') & \hat{\mathcal{C}}_8^>(t') \end{pmatrix}, \\ \Delta_{RL}^{\bar{q}>, \text{sliver}}(t, t'; -p^2) &= \frac{M_{\text{KK}}}{\eta} \begin{pmatrix} \mathbf{S}_{\bar{q}} \mathcal{S}(t) & \varrho \mathbf{Y}_{\bar{q}} \bar{\mathcal{S}}(t) \\ \varrho \mathbf{Y}_{\bar{q}}^\dagger \mathcal{C}(t) & \bar{\mathbf{S}}_{\bar{q}} \bar{\mathcal{C}}(t) \end{pmatrix} \begin{pmatrix} \hat{\mathcal{C}}_1^>(t') & \hat{\mathcal{C}}_2^>(t') \\ \hat{\mathcal{C}}_7^>(t') & \hat{\mathcal{C}}_8^>(t') \end{pmatrix}.\end{aligned}\quad (3.85)$$

The solutions for $t < t'$ can be obtained by taking the employing the jump conditions and read

$$\begin{aligned}\Delta_{LL}^{\bar{q}<, \text{sliver}}(t, t'; -p^2) &= \begin{pmatrix} \mathcal{C}(t) & 0 \\ 0 & \bar{\mathcal{S}}(t) \end{pmatrix} \begin{pmatrix} \hat{\mathcal{C}}_1^>(t') & \hat{\mathcal{C}}_2^>(t') \\ \hat{\mathcal{C}}_7^>(t') & \hat{\mathcal{C}}_8^>(t') \end{pmatrix} + \frac{\eta}{M_{\text{KK}}^2} \begin{pmatrix} \frac{\mathcal{S}(1-t'+t)}{\mathbf{S}_{\bar{q}}} & 0 \\ 0 & \frac{\bar{\mathcal{S}}(1-t'+t)}{\bar{\mathbf{S}}_{\bar{q}}} \end{pmatrix}, \\ \Delta_{RL}^{\bar{q}<, \text{sliver}}(t, t'; -p^2) &= \frac{M_{\text{KK}}}{\eta} \begin{pmatrix} \mathbf{S}_{\bar{q}} \mathcal{S}(t) & \varrho \mathbf{Y}_{\bar{q}} \bar{\mathcal{S}}(t) \\ \varrho \mathbf{Y}_{\bar{q}}^\dagger \mathcal{C}(t) & \bar{\mathbf{S}}_{\bar{q}} \bar{\mathcal{C}}(t) \end{pmatrix} \begin{pmatrix} \hat{\mathcal{C}}_1^>(t') & \hat{\mathcal{C}}_2^>(t') \\ \hat{\mathcal{C}}_7^>(t') & \hat{\mathcal{C}}_8^>(t') \end{pmatrix} \\ &\quad + \frac{1}{M_{\text{KK}}} \begin{pmatrix} \mathcal{C}(1-t'+t) & \varrho \mathbf{Y}_{\bar{q}} \frac{\bar{\mathcal{S}}(1-t'+t)}{\bar{\mathbf{S}}_{\bar{q}}} \\ \varrho \mathbf{Y}_{\bar{q}}^\dagger \frac{\mathcal{S}(1-t'+t)}{\mathbf{S}_{\bar{q}}} & \bar{\mathcal{C}}(1-t'+t) \end{pmatrix}.\end{aligned}\quad (3.86)$$

So far we have achieved to derive the general solution in the bulk ($t < 1 - \eta$) and in the silver ($t > 1 - \eta$) that are both compatible with the boundary as well as the jump conditions. The latter have been used to eliminate 24 of the in total 32 coefficient functions. Thus, there are still eight coefficient matrices unspecified. Their determination will be part of the subsequent subsection.

3.2.3 Determination of the Coefficient Functions and Final Results

The remaining eight coefficient functions are determined by requiring that the solutions are continuous at $t = 1 - \eta$. This matching procedure has to be performed in two steps differing in the position of t' . If t' is in the bulk, the requirement of the functions $\Delta_{LL}^{\bar{q}>}$ and $\Delta_{RL}^{\bar{q}>}$ being continuous yields the bulk part of the coefficient functions. Analogously, $\Delta_{LL}^{\bar{q}<}$ and $\Delta_{RL}^{\bar{q}<}$ have to be continuous in the case of $t' > 1 - \eta$, which determines the corresponding sliver part. At the end of the calculation it will be checked that all coefficient functions are continuous at $t' = 1 - \eta$.

Case of t' Being in the Bulk

For the case $t' < 1 - \eta$, we have to match

$$\Delta_{AL}^{q>, \text{bulk}}(t = (1 - \eta)_-, t'; -p^2) = \Delta_{AL}^{q>, \text{sliver}}(t = (1 - \eta)_+, t'; -p^2) \quad A = L, R. \quad (3.87)$$

The equation with $A = L$ yields the relations

$$\begin{aligned}
-\frac{\sqrt{tt'}}{p_E M_{\text{KK}} 1_\eta} \mathbf{L}_3^{\bar{Q}}(\hat{p}_E, 1_\eta, t') + \sqrt{1_\eta} \mathbf{D}_1^{\bar{Q}}(\hat{p}_E, 1_\eta) \mathbf{K}_1^{\text{bulk}}(t') &= \cosh \mathbf{S}_{\bar{q}} \hat{\mathbf{C}}_1^{>, \text{bulk}}(t'), \\
\sqrt{1_\eta} \mathbf{D}_1^{\bar{Q}}(\hat{p}_E, 1_\eta) \mathbf{K}_2^{\text{bulk}}(t') &= \cosh \mathbf{S}_{\bar{q}} \hat{\mathbf{C}}_2^{>, \text{bulk}}(t'), \\
\sqrt{1_\eta} \mathbf{D}_2^{\bar{q}}(\hat{p}_E, 1_\eta) \mathbf{K}_3^{\text{bulk}}(t') &= \sinh \bar{\mathbf{S}}_{\bar{q}} \hat{\mathbf{C}}_7^{>, \text{bulk}}(t'), \\
\frac{\sqrt{tt'}}{p_E M_{\text{KK}} 1_\eta} \mathbf{L}_2^{\bar{q}}(\hat{p}_E, 1_\eta, t') + \sqrt{1_\eta} \mathbf{D}_2^{\bar{q}}(\hat{p}_E, 1_\eta) \mathbf{K}_4^{\text{bulk}}(t') &= \sinh \bar{\mathbf{S}}_{\bar{q}} \hat{\mathbf{C}}_8^{>, \text{bulk}}(t'),
\end{aligned} \tag{3.88}$$

where the superscript of the coefficients \mathbf{K}_i and $\hat{\mathbf{C}}_i^{>}$ indicates that t' is in the bulk and should not be confused with the superscript of the propagator functions that denote the position of the variable t . Above equations can be used to eliminate the coefficients $\hat{\mathbf{C}}_i^{>, \text{bulk}}(t')$. Note that on the left-hand sides of these equations we could take the limit $\eta \rightarrow 0$ without difficulty, but we will keep the Higgs width η throughout all our calculations. Only when we concentrate on the brane-Higgs case, we will take the limit in question. The remaining four coefficients $\hat{\mathbf{K}}_i^{\text{bulk}}(t')$ can be derived by the equation in (3.87) with $A = R$, where we encounter the ratios

$$\mathbf{R}_{\bar{A}}(\hat{p}_E) \equiv \frac{\mathbf{D}_1^{\bar{A}}(\hat{p}_E, 1_\eta)}{\mathbf{D}_2^{\bar{A}}(\hat{p}_E, 1_\eta)}. \tag{3.89}$$

In order to express the answers in a compact form, we moreover introduce the definitions

$$\begin{aligned}
\mathbf{N}_{\bar{q}}^{\eta,1}(p_E^2) &\equiv 1 + \mathbf{Z}_{\bar{q}}^{\eta,1}(p_E^2) + \eta \hat{p}_E \left[1 + \mathbf{R}_{\bar{Q}}^{-1}(\hat{p}_E) (\mathbf{Y}_{\bar{q}}^\dagger)^{-1} \mathbf{R}_{\bar{q}}(\hat{p}_E) \mathbf{Y}_{\bar{q}}^\dagger \right] \frac{\tanh \mathbf{S}_{\bar{q}}}{\mathbf{S}_{\bar{q}}} \mathbf{R}_{\bar{Q}}(\hat{p}_E), \\
\mathbf{N}_{\bar{q}}^{\eta,2}(p_E^2) &\equiv 1 + \mathbf{Z}_{\bar{q}}^{\eta,2}(p_E^2) + \eta \hat{p}_E \frac{\tanh \mathbf{S}_{\bar{q}}}{\mathbf{S}_{\bar{q}}} \left[\mathbf{R}_{\bar{Q}}(\hat{p}_E) + \mathbf{Y}_{\bar{q}} \mathbf{R}_{\bar{q}}(\hat{p}_E) \mathbf{Y}_{\bar{q}}^{-1} \right],
\end{aligned} \tag{3.90}$$

where

$$\begin{aligned}
\mathbf{Z}_{\bar{q}}^{\eta,1}(p_E^2) &\equiv \varrho^2 \frac{\mathbf{S}_{\bar{q}}^2}{\mathbf{X}_{\bar{q}}^2} \tilde{\mathbf{Y}}_{\bar{q}} \mathbf{R}_{\bar{q}}(\hat{p}_E) \tilde{\mathbf{Y}}_{\bar{q}}^\dagger \mathbf{R}_{\bar{Q}}(\hat{p}_E), \\
\mathbf{Z}_{\bar{q}}^{\eta,2}(p_E^2) &\equiv \varrho^2 \tilde{\mathbf{Y}}_{\bar{q}} \mathbf{R}_{\bar{q}}(\hat{p}_E) \tilde{\mathbf{Y}}_{\bar{q}}^\dagger \frac{\mathbf{S}_{\bar{q}}^2}{\mathbf{X}_{\bar{q}}^2} \mathbf{R}_{\bar{Q}}(\hat{p}_E), \quad \tilde{\mathbf{Y}}_{\bar{q}} \equiv \frac{\tanh \mathbf{S}_{\bar{q}}}{\mathbf{S}_{\bar{q}}} \mathbf{Y}_{\bar{q}}.
\end{aligned} \tag{3.91}$$

After some lengthy algebra, we obtain

$$\begin{aligned}
\mathbf{K}_1^{\text{bulk}}(t') &= \frac{\sqrt{t'}/1_\eta}{p_E M_{\text{KK}} \mathbf{D}_1^{\bar{Q}}(\hat{p}_E, 1_\eta)} \left\{ \mathbf{L}_3^{\bar{Q}}(\hat{p}_E, 1_\eta, t') \right. \\
&\quad \left. - \left[\mathbf{R}_{\bar{Q}} + \eta \hat{p}_E \frac{\coth \mathbf{S}_{\bar{q}}}{\mathbf{S}_{\bar{q}}} \mathbf{Z}_{\bar{q}}^{\eta,1} \right] \frac{1}{\mathbf{N}_{\bar{q}}^{\eta,1}} \frac{\mathbf{D}_1^{\bar{Q}}(\hat{p}_E, t')}{\mathbf{D}_1^{\bar{Q}}(\hat{p}_E, 1_\eta)} \right\}, \\
\mathbf{K}_2^{\text{bulk}}(t') &= \frac{\sqrt{t'}/1_\eta}{p_E M_{\text{KK}} \mathbf{D}_2^{\bar{Q}}(\hat{p}_E, 1_\eta)} \frac{1}{\mathbf{N}_{\bar{q}}^{\eta,2}} \varrho \tilde{\mathbf{Y}}_{\bar{q}} \frac{\mathbf{D}_2^{\bar{q}}(\hat{p}_E, t')}{\mathbf{D}_2^{\bar{q}}(\hat{p}_E, 1_\eta)}, \\
\mathbf{K}_3^{\text{bulk}}(t') &= \frac{\sqrt{t'}/1_\eta}{p_E M_{\text{KK}} \mathbf{D}_2^{\bar{q}}(\hat{p}_E, 1_\eta)} \varrho \tilde{\mathbf{Y}}_{\bar{q}}^\dagger \mathbf{R}_{\bar{Q}} \frac{1}{\mathbf{N}_{\bar{q}}^{\eta,1}} \frac{\mathbf{D}_1^{\bar{Q}}(\hat{p}_E, t')}{\mathbf{D}_1^{\bar{Q}}(\hat{p}_E, 1_\eta)},
\end{aligned} \tag{3.92}$$

$$\mathbf{K}_4^{\text{bulk}}(t') = \frac{-\sqrt{t'}/1_\eta}{p_E M_{\text{KK}} \mathbf{D}_2^{\bar{q}}(\hat{p}_E, 1_\eta)} \left\{ \mathbf{L}_2^{\bar{q}}(\hat{p}_E, 1_\eta, t') \right. \\ \left. + \varrho \tilde{\mathbf{Y}}_{\bar{q}}^\dagger \frac{\mathbf{S}_{\bar{q}}^2}{\mathbf{X}_{\bar{q}}^2} \left[\mathbf{R}_{\bar{Q}} + \eta \hat{p}_E \frac{\coth \mathbf{S}_{\bar{q}}}{\mathbf{S}_{\bar{q}}} \right] \frac{1}{N_{\bar{q}}^{\eta,2}} \varrho \tilde{\mathbf{Y}}_{\bar{q}} \frac{\mathbf{D}_2^{\bar{q}}(\hat{p}_E, t')}{\mathbf{D}_2^{\bar{q}}(\hat{p}_E, 1_\eta)} \right\},$$

where we have dropped the arguments of $\mathbf{R}_{\bar{Q}}$, $\mathbf{Z}_{\bar{q}}^{\eta,i}$, and $N_{\bar{q}}^{\eta,i}$. The coefficients $\mathbf{C}_i^>$ can now be obtained easily with the help of (3.87).

Case of t' Being in the Sliver

For the case $t' > 1 - \eta$, the matching conditions at point $t = 1 - \eta$ read in analogy to (3.87)

$$\Delta_{AL}^{\bar{q}<, \text{bulk}}(t = (1 - \eta)_-, t'; -p^2) = \Delta_{AL}^{\bar{q}<, \text{sliver}}(t = (1 - \eta)_+, t'; -p^2), \quad A = L, R, \quad (3.93)$$

where the equation for $A = L$ leads to the conditions

$$\begin{aligned} \sqrt{1_\eta} \mathbf{D}_1^{\bar{Q}}(\hat{p}_E, 1_\eta) \mathbf{K}_1^{\text{sliver}}(t') &= \cosh \mathbf{S}_{\bar{q}} \hat{\mathbf{C}}_1^{>, \text{sliver}}(t') - \frac{\eta}{M_{\text{KK}}^2} \frac{\mathcal{S}(t' + \eta)}{\mathbf{S}_{\bar{q}}}, \\ \sqrt{1_\eta} \mathbf{D}_1^{\bar{Q}}(\hat{p}_E, 1_\eta) \mathbf{K}_2^{\text{sliver}}(t') &= \cosh \mathbf{S}_{\bar{q}} \hat{\mathbf{C}}_2^{>, \text{sliver}}(t'), \\ \sqrt{1_\eta} \mathbf{D}_2^{\bar{q}}(\hat{p}_E, 1_\eta) \mathbf{K}_3^{\text{sliver}}(t') &= \sinh \bar{\mathbf{S}}_{\bar{q}} \hat{\mathbf{C}}_7^{>, \text{sliver}}(t'), \\ \sqrt{1_\eta} \mathbf{D}_2^{\bar{q}}(\hat{p}_E, 1_\eta) \mathbf{K}_4^{\text{sliver}}(t') &= \sinh \bar{\mathbf{S}}_{\bar{q}} \hat{\mathbf{C}}_8^{>, \text{sliver}}(t') - \frac{\eta}{M_{\text{KK}}^2} \frac{\bar{\mathcal{S}}(t' + \eta)}{\bar{\mathbf{S}}_{\bar{q}}}. \end{aligned} \quad (3.94)$$

Analogously to the previous case, we find the sliver coefficients $\mathbf{K}_i^{\text{sliver}}(t')$ to be

$$\begin{aligned} \mathbf{K}_1^{\text{sliver}}(t') &= -\frac{1}{p_E M_{\text{KK}}} \frac{1}{\sqrt{1_\eta} \mathbf{D}_1^{\bar{Q}}(\hat{p}_E, 1_\eta)} \left[\mathbf{R}_{\bar{Q}} + \eta \hat{p}_E \frac{\coth \mathbf{S}_{\bar{q}}}{\mathbf{S}_{\bar{q}}} \mathbf{Z}_{\bar{q}}^{\eta,1} \right] \frac{1}{N_{\bar{q}}^{\eta,1}(p_E^2)} \frac{\mathcal{C}(t')}{\cosh \mathbf{S}_{\bar{q}}}, \\ \mathbf{K}_2^{\text{sliver}}(t') &= \frac{1}{p_E M_{\text{KK}}} \frac{1}{\sqrt{1_\eta} \mathbf{D}_2^{\bar{Q}}(\hat{p}_E, 1_\eta)} \frac{1}{N_{\bar{q}}^{\eta,2}} \frac{\mathcal{S}(t')}{\sinh \mathbf{S}_{\bar{q}}} \varrho \tilde{\mathbf{Y}}_{\bar{q}}, \\ \mathbf{K}_3^{\text{sliver}}(t') &= \frac{1}{p_E M_{\text{KK}}} \frac{1}{\sqrt{1_\eta} \mathbf{D}_2^{\bar{q}}(\hat{p}_E, 1_\eta)} \varrho \tilde{\mathbf{Y}}_{\bar{q}}^\dagger \mathbf{R}_{\bar{Q}}(\hat{p}_E) \frac{1}{N_{\bar{q}}^{\eta,1}} \frac{\mathcal{C}(t')}{\cosh \mathbf{S}_{\bar{q}}}, \\ \mathbf{K}_4^{\text{sliver}}(t') &= -\frac{1}{p_E M_{\text{KK}}} \frac{\varrho^2}{\sqrt{1_\eta} \mathbf{D}_2^{\bar{q}}(\hat{p}_E, 1_\eta)} \tilde{\mathbf{Y}}_{\bar{q}}^\dagger \frac{\mathbf{S}_{\bar{q}}^2}{\mathbf{X}_{\bar{q}}^2} \left[\mathbf{R}_{\bar{Q}} + \eta \hat{p}_E \frac{\coth \mathbf{S}_{\bar{q}}}{\mathbf{S}_{\bar{q}}} \right] \frac{1}{N_{\bar{q}}^{\eta,2}} \frac{\mathcal{S}(t')}{\sinh \mathbf{S}_{\bar{q}}} \tilde{\mathbf{Y}}_{\bar{q}}. \end{aligned} \quad (3.95)$$

It is straightforward to derive the coefficients $\mathbf{C}_i^{>, \text{sliver}}$ with the help of the relations (3.88). Comparing with (3.92) and recalling that $\mathbf{L}_{2,3}^{\bar{A}}(\hat{p}_E, 1_\eta, 1_\eta) = 0$, we easily see that the coefficients $\mathbf{K}_i(t')$ are continuous at point $t' = 1 - \eta$, which clearly holds for $\mathbf{C}_i^{>, \text{sliver}}$ either.

Results for Finite Width η

We are now ready to present the full solution for the propagator functions. Inserting the coefficient functions \mathbf{K}_i and $\hat{\mathbf{C}}_i^>$ into the solutions (3.73), (3.76), (3.85), and (3.86), we obtain the final results for $\Delta_{LL}^{\vec{q}}$ and $\Delta_{RL}^{\vec{q}}$ for finite η listed in Appendix A. We find that the corresponding results for $\Delta_{RR}^{\vec{q}}$ and $\Delta_{LR}^{\vec{q}}$ can be obtained by applying the replacements

$$\begin{aligned} D_{1,2}^{\vec{A}}(\hat{p}_E, t) &\rightarrow D_{2,1}^{\vec{A}}(\hat{p}_E, t), & \mathcal{S}(t) &\rightarrow \mathcal{C}(t), & \mathcal{S}(t+\eta) &\rightarrow \mathcal{S}(t+\eta), \\ L_{2,3}^{\vec{A}}(\hat{p}_E, 1_\eta, t) &\rightarrow -L_{3,2}^{\vec{A}}(\hat{p}_E, 1_\eta, t), & \mathcal{C}(t) &\rightarrow \mathcal{S}(t), & \mathcal{C}(t+\eta) &\rightarrow \mathcal{C}(t+\eta), \\ L_{1,4}^{\vec{A}}(\hat{p}_E, 1_\eta, t) &\rightarrow -L_{4,1}^{\vec{A}}(\hat{p}_E, 1_\eta, t), & \mathbf{Y}_{\vec{q}} &\rightarrow -\mathbf{Y}_{\vec{q}}. \end{aligned} \quad (3.96)$$

Moreover, one encounters a global minus sign when going from $\Delta_{RL}^{\vec{q}}$ to $\Delta_{LR}^{\vec{q}}$. The above replacements imply that the quantities $\mathbf{Z}_{\vec{q}}^{\eta,i}$ and $\mathbf{N}_{\vec{q}}^{\eta,i}$ transform via

$$\mathbf{Z}_{\vec{q}}^{\eta,i} \rightarrow \mathbf{R}_{\vec{Q}} \frac{1}{\mathbf{Z}_{\vec{q}}^{\eta,i}} \frac{1}{\mathbf{R}_{\vec{Q}}}, \quad \frac{1}{\mathbf{N}_{\vec{q}}^{\eta,1}} \rightarrow \mathbf{R}_{\vec{Q}} \mathbf{Z}_{\vec{q}}^{\eta,1} \frac{1}{\mathbf{N}_{\vec{q}}^{\eta,1}} \frac{1}{\mathbf{R}_{\vec{Q}}}, \quad \frac{1}{\mathbf{N}_{\vec{q}}^{\eta,2}} \rightarrow \mathbf{R}_{\vec{Q}} \frac{1}{\mathbf{N}_{\vec{q}}^{\eta,2}} \mathbf{Z}_{\vec{q}}^{\eta,2} \frac{1}{\mathbf{R}_{\vec{Q}}}. \quad (3.97)$$

3.2.4 The Special Case of the Brane-Localized Higgs Scenario

In this last subsection, we will specialize on the case where t and t' are chosen to be within the bulk region and η is sent to zero. This case is identified with the brane-localized Higgs scenario. After showing the results, we will present an alternative derivation, which is crucial for the generalization to two different Yukawa matrices. Finally, we will dwell on the asymptotic behavior for small and large momenta.

Final Results

We start with the general propagator solutions $\Delta_{LL,RL}^{\vec{q}}(t, t'; -p^2)$, that can be found in Appendix A, for the case of $t, t' \in [\epsilon, 1 - \eta]$. Sending the regulator η to zero implies the relations $\mathbf{S}_{\vec{q}} \rightarrow \mathbf{X}_{\vec{q}}$, $\mathbf{N}_{\vec{q}}^{\eta,i} \rightarrow 1 + \mathbf{Z}_{\vec{q}}$ and $\mathbf{Z}_{\vec{q}}^{\eta,i} \rightarrow \mathbf{Z}_{\vec{q}}$, where

$$\mathbf{Z}_{\vec{q}}(p_E^2) \equiv \frac{v^2}{2M_{\text{KK}}^2} \tilde{\mathbf{Y}}_{\vec{q}} \mathbf{R}_{\vec{q}}(\hat{p}_E) \tilde{\mathbf{Y}}_{\vec{q}}^\dagger \mathbf{R}_{\vec{Q}}(\hat{p}_E). \quad (3.98)$$

Here, $\tilde{\mathbf{Y}}_{\vec{q}}$ is the generalized Yukawa matrix defined in (2.81) and

$$\mathbf{R}_{\vec{A}}(\hat{p}_E) \equiv \frac{D_1^{\vec{A}}(\hat{p}_E, 1)}{D_2^{\vec{A}}(\hat{p}_E, 1)}, \quad (3.99)$$

i.e. (3.89) with $\eta \rightarrow 0$. Note that in the minimal model we just have

$$\mathbf{R}_A(\hat{p}_E) = \mathbf{R}_A^{(+)}(\hat{p}_E) \equiv \frac{D_1^A(\hat{p}_E, 1)}{D_2^A(\hat{p}_E, 1)}, \quad (3.100)$$

while in the custodial model, we also encounter the ratios

$$\begin{aligned} \mathbf{R}_A^{(-)}(\hat{p}_E) &\equiv \frac{D_3^A(\hat{p}_E, 1)}{D_4^A(\hat{p}_E, 1)} = \frac{I_{c_A-\frac{1}{2}}(\epsilon\hat{p}_E) I_{-c_A+\frac{1}{2}}(\hat{p}_E) - I_{-c_A+\frac{1}{2}}(\epsilon\hat{p}_E) I_{c_A-\frac{1}{2}}(\hat{p}_E)}{I_{c_A-\frac{1}{2}}(\epsilon\hat{p}_E) I_{-c_A-\frac{1}{2}}(\hat{p}_E) - I_{-c_A+\frac{1}{2}}(\epsilon\hat{p}_E) I_{c_A+\frac{1}{2}}(\hat{p}_E)} \\ &= \frac{1}{\mathbf{R}_A^{(+)}(\hat{p}_E)} \Big|_{c_A \rightarrow -c_A}. \end{aligned} \quad (3.101)$$

Analogous structures can be found in the ratios $D_{1,2}^A(\hat{p}_E, t)/D_{1,2}^A(\hat{p}_E, 1)$. Provided with the above definitions, we find the quite compact solutions

$$\begin{aligned} \Delta_{LL}^{\bar{q}} \Big|_{11} &= \frac{-\sqrt{tt'}}{p_E M_{\text{KK}}} \left[\frac{D_1^{\bar{Q}}(\hat{p}_E, t)}{D_1^{\bar{Q}}(\hat{p}_E, 1)} \mathbf{R}_{\bar{Q}} \frac{1}{1 + \mathbf{Z}_{\bar{q}}} \frac{D_1^{\bar{Q}}(\hat{p}_E, t')}{D_1^{\bar{Q}}(\hat{p}_E, 1)} - \frac{D_1^{\bar{Q}}(\hat{p}_E, t_{<})}{D_1^{\bar{Q}}(\hat{p}_E, 1)} \mathbf{L}_3^{\bar{Q}}(\hat{p}_E, 1, t_{>}) \right], \\ \Delta_{LL}^{\bar{q}} \Big|_{12} &= \frac{\sqrt{tt'}}{p_E M_{\text{KK}}} \frac{D_1^{\bar{Q}}(\hat{p}_E, t)}{D_1^{\bar{Q}}(\hat{p}_E, 1)} \mathbf{R}_{\bar{Q}} \frac{1}{1 + \mathbf{Z}_{\bar{q}}} \rho \tilde{\mathbf{Y}}_{\bar{q}} \frac{D_2^{\bar{q}}(\hat{p}_E, t')}{D_2^{\bar{q}}(\hat{p}_E, 1)}, \\ \Delta_{LL}^{\bar{q}} \Big|_{21} &= \frac{\sqrt{tt'}}{p_E M_{\text{KK}}} \frac{D_2^{\bar{q}}(\hat{p}_E, t)}{D_2^{\bar{q}}(\hat{p}_E, 1)} \rho \tilde{\mathbf{Y}}_{\bar{q}}^\dagger \mathbf{R}_{\bar{Q}} \frac{1}{1 + \mathbf{Z}_{\bar{q}}} \frac{D_1^{\bar{Q}}(\hat{p}_E, t')}{D_1^{\bar{Q}}(\hat{p}_E, 1)}, \\ \Delta_{LL}^{\bar{q}} \Big|_{22} &= \frac{-\sqrt{tt'}}{p_E M_{\text{KK}}} \left[\frac{D_2^{\bar{q}}(\hat{p}_E, t)}{D_2^{\bar{q}}(\hat{p}_E, 1)} \rho \tilde{\mathbf{Y}}_{\bar{q}}^\dagger \mathbf{R}_{\bar{Q}} \frac{1}{1 + \mathbf{Z}_{\bar{q}}} \rho \tilde{\mathbf{Y}}_{\bar{q}} \frac{D_2^{\bar{q}}(\hat{p}_E, t')}{D_2^{\bar{q}}(\hat{p}_E, 1)} \right. \\ &\quad \left. + \frac{D_2^{\bar{q}}(\hat{p}_E, t_{<})}{D_2^{\bar{q}}(\hat{p}_E, 1)} \mathbf{L}_2^{\bar{q}}(\hat{p}_E, 1, t_{>}) \right], \end{aligned} \quad (3.102)$$

$$\begin{aligned} \Delta_{RL}^{\bar{q}} \Big|_{11} &= \frac{-\sqrt{tt'}}{M_{\text{KK}}} \begin{cases} \frac{D_2^{\bar{Q}}(\hat{p}_E, t)}{D_2^{\bar{Q}}(\hat{p}_E, 1)} \frac{\mathbf{Z}_{\bar{q}}}{1 + \mathbf{Z}_{\bar{q}}} \frac{D_1^{\bar{Q}}(\hat{p}_E, t')}{D_1^{\bar{Q}}(\hat{p}_E, 1)} + \frac{D_2^{\bar{Q}}(\hat{p}_E, t)}{D_2^{\bar{Q}}(\hat{p}_E, 1)} \mathbf{L}_4^{\bar{Q}}(\hat{p}_E, 1, t'), & t < t', \\ \frac{D_2^{\bar{Q}}(\hat{p}_E, t)}{D_2^{\bar{Q}}(\hat{p}_E, 1)} \frac{\mathbf{Z}_{\bar{q}}}{1 + \mathbf{Z}_{\bar{q}}} \frac{D_1^{\bar{Q}}(\hat{p}_E, t')}{D_1^{\bar{Q}}(\hat{p}_E, 1)} + \frac{D_1^{\bar{Q}}(\hat{p}_E, t')}{D_1^{\bar{Q}}(\hat{p}_E, 1)} \mathbf{R}_{\bar{Q}} \mathbf{L}_2^{\bar{Q}}(\hat{p}_E, 1, t), & t > t', \end{cases} \\ \Delta_{RL}^{\bar{q}} \Big|_{12} &= -\frac{\sqrt{tt'}}{M_{\text{KK}}} \frac{D_2^{\bar{Q}}(\hat{p}_E, t)}{D_2^{\bar{Q}}(\hat{p}_E, 1)} \frac{1}{1 + \mathbf{Z}_{\bar{q}}} \rho \tilde{\mathbf{Y}}_{\bar{q}} \frac{D_2^{\bar{q}}(\hat{p}_E, t')}{D_2^{\bar{q}}(\hat{p}_E, 1)}, \\ \Delta_{RL}^{\bar{q}} \Big|_{21} &= -\frac{\sqrt{tt'}}{M_{\text{KK}}} \frac{D_1^{\bar{q}}(\hat{p}_E, t)}{D_1^{\bar{q}}(\hat{p}_E, 1)} \frac{1}{\rho \tilde{\mathbf{Y}}_{\bar{q}}^\dagger} \frac{\mathbf{Z}_{\bar{q}}}{1 + \mathbf{Z}_{\bar{q}}} \frac{D_1^{\bar{Q}}(\hat{p}_E, t')}{D_1^{\bar{Q}}(\hat{p}_E, 1)}, \\ \Delta_{RL}^{\bar{q}} \Big|_{22} &= \frac{\sqrt{tt'}}{M_{\text{KK}}} \begin{cases} \frac{D_1^{\bar{q}}(\hat{p}_E, t)}{D_1^{\bar{q}}(\hat{p}_E, 1)} \frac{1}{\tilde{\mathbf{Y}}_{\bar{q}}^\dagger} \frac{\mathbf{Z}_{\bar{q}}}{1 + \mathbf{Z}_{\bar{q}}} \tilde{\mathbf{Y}}_{\bar{q}} \frac{D_2^{\bar{q}}(\hat{p}_E, t')}{D_2^{\bar{q}}(\hat{p}_E, 1)} + \frac{D_1^{\bar{q}}(\hat{p}_E, t)}{D_1^{\bar{q}}(\hat{p}_E, 1)} \mathbf{R}_{\bar{q}} \mathbf{L}_2^{\bar{q}}(\hat{p}_E, 1, t'), & t < t', \\ \frac{D_1^{\bar{q}}(\hat{p}_E, t)}{D_1^{\bar{q}}(\hat{p}_E, 1)} \frac{1}{\tilde{\mathbf{Y}}_{\bar{q}}^\dagger} \frac{\mathbf{Z}_{\bar{q}}}{1 + \mathbf{Z}_{\bar{q}}} \tilde{\mathbf{Y}}_{\bar{q}} \frac{D_2^{\bar{q}}(\hat{p}_E, t')}{D_2^{\bar{q}}(\hat{p}_E, 1)} + \frac{D_2^{\bar{q}}(\hat{p}_E, t')}{D_2^{\bar{q}}(\hat{p}_E, 1)} \mathbf{L}_4^{\bar{q}}(\hat{p}_E, 1, t), & t > t', \end{cases} \end{aligned} \quad (3.103)$$

where some arguments, like $(t, t'; -p^2)$ of the propagators on the left-hand side, have been neglected to allow for a compact writeup. We can check the jump conditions and can verify that the diagonal components of $\Delta_{RL}^{\bar{q}}$ are discontinuous at $t = t'$ by the amount given in (3.68), while all other components are continuous. Moreover, due to the antisymmetry of D_2^A when exchanging both arguments, one can directly see that the UV boundary conditions in (3.70) are fulfilled. A short calculation also shows that the IR BCs (3.106) (see below) are satisfied as well. Due to the definition of $\Delta_{LL}^{\bar{q}}$ in (3.61), its hermitian conjugate after interchanging t with t' must agree with $\Delta_{LL}^{\bar{q}}$ again. This can be easily checked by using the relation $\mathbf{Z}_{\bar{q}}^\dagger = \mathbf{R}_{\bar{Q}} \mathbf{Z}_{\bar{q}} \mathbf{R}_{\bar{Q}}^{-1}$.

As already mentioned in Section 3.2.3, the solutions $\Delta_{RR}^{\vec{q}}$ and $\Delta_{LR}^{\vec{q}}$ can be obtained from (3.102)–(3.103) by the relations and substitutions given in (3.96). Still, for the upcoming analysis it is convenient to express $\Delta_{RR,LR}^{\vec{q}}$ by the same structures, that are also used in (3.102)–(3.103). In consequence of the transformation rules presented in (3.97), the $\mathbf{Z}_{\vec{q}}$ structure can be formally replaced by $\mathbf{Z}_{\vec{q}} \rightarrow \mathbf{R}_{\vec{Q}} \mathbf{Z}_{\vec{q}}^{-1} \mathbf{R}_{\vec{Q}}^{-1}$ and used to obtain the remaining propagator solutions. They are given by

$$\begin{aligned}
\Delta_{RR}^{\vec{q}} \Big|_{11} &= \frac{-\sqrt{tt'}}{pEM_{\text{KK}}} \left[\frac{D_2^{\vec{Q}}(\hat{p}_E, t)}{D_2^{\vec{Q}}(\hat{p}_E, 1)} \frac{\mathbf{Z}_{\vec{q}}}{1 + \mathbf{Z}_{\vec{q}} \mathbf{R}_{\vec{Q}}} \frac{1}{D_2^{\vec{Q}}(\hat{p}_E, 1)} \frac{D_2^{\vec{Q}}(\hat{p}_E, t')}{D_2^{\vec{Q}}(\hat{p}_E, 1)} + \frac{D_2^{\vec{Q}}(\hat{p}_E, t_{<})}{D_2^{\vec{Q}}(\hat{p}_E, 1)} \mathbf{L}_2^{\vec{Q}}(\hat{p}_E, 1, t_{>}) \right], \\
\Delta_{RR}^{\vec{q}} \Big|_{12} &= \frac{-\sqrt{tt'}}{pEM_{\text{KK}}} \frac{D_2^{\vec{Q}}(\hat{p}_E, t)}{D_2^{\vec{Q}}(\hat{p}_E, 1)} \frac{\mathbf{Z}_{\vec{q}}}{1 + \mathbf{Z}_{\vec{q}} \mathbf{R}_{\vec{Q}}} \frac{1}{\varrho \tilde{\mathbf{Y}}_{\vec{q}}^\dagger} \frac{1}{D_1^{\vec{q}}(\hat{p}_E, 1)} \frac{D_1^{\vec{q}}(\hat{p}_E, t')}{D_1^{\vec{q}}(\hat{p}_E, 1)}, \\
\Delta_{RR}^{\vec{q}} \Big|_{21} &= \frac{-\sqrt{tt'}}{pEM_{\text{KK}}} \frac{D_1^{\vec{q}}(\hat{p}_E, t)}{D_1^{\vec{q}}(\hat{p}_E, 1)} \frac{1}{\varrho \tilde{\mathbf{Y}}_{\vec{q}}^\dagger} \frac{\mathbf{Z}_{\vec{q}}}{1 + \mathbf{Z}_{\vec{q}} \mathbf{R}_{\vec{Q}}} \frac{1}{D_2^{\vec{Q}}(\hat{p}_E, 1)} \frac{D_2^{\vec{Q}}(\hat{p}_E, t')}{D_2^{\vec{Q}}(\hat{p}_E, 1)}, \\
\Delta_{RR}^{\vec{q}} \Big|_{22} &= \frac{-\sqrt{tt'}}{pEM_{\text{KK}}} \left[\frac{D_1^{\vec{q}}(\hat{p}_E, t)}{D_1^{\vec{q}}(\hat{p}_E, 1)} \frac{1}{\varrho \tilde{\mathbf{Y}}_{\vec{q}}^\dagger} \frac{\mathbf{Z}_{\vec{q}}}{1 + \mathbf{Z}_{\vec{q}} \mathbf{R}_{\vec{Q}}} \frac{1}{\varrho \tilde{\mathbf{Y}}_{\vec{q}}^\dagger} \frac{1}{D_1^{\vec{q}}(\hat{p}_E, 1)} \frac{D_1^{\vec{q}}(\hat{p}_E, t')}{D_1^{\vec{q}}(\hat{p}_E, 1)} \right. \\
&\quad \left. - \frac{D_1^{\vec{q}}(\hat{p}_E, t_{<})}{D_1^{\vec{q}}(\hat{p}_E, 1)} \mathbf{L}_3^{\vec{q}}(\hat{p}_E, 1, t_{>}) \right],
\end{aligned} \tag{3.104}$$

$$\begin{aligned}
\Delta_{LR}^{\vec{q}} \Big|_{11} &= \frac{\sqrt{tt'}}{M_{\text{KK}}} \begin{cases} \frac{D_1^{\vec{Q}}(\hat{p}_E, t)}{D_1^{\vec{Q}}(\hat{p}_E, 1)} \mathbf{R}_{\vec{Q}} \frac{1}{1 + \mathbf{Z}_{\vec{q}} \mathbf{R}_{\vec{Q}}} \frac{1}{D_2^{\vec{Q}}(\hat{p}_E, 1)} \frac{D_2^{\vec{Q}}(\hat{p}_E, t')}{D_2^{\vec{Q}}(\hat{p}_E, 1)} - \frac{D_1^{\vec{Q}}(\hat{p}_E, t)}{D_1^{\vec{Q}}(\hat{p}_E, 1)} \mathbf{L}_1^{\vec{Q}}(\hat{p}_E, 1, t'), & t < t', \\ \frac{D_1^{\vec{Q}}(\hat{p}_E, t)}{D_1^{\vec{Q}}(\hat{p}_E, 1)} \mathbf{R}_{\vec{Q}} \frac{1}{1 + \mathbf{Z}_{\vec{q}} \mathbf{R}_{\vec{Q}}} \frac{1}{D_2^{\vec{Q}}(\hat{p}_E, 1)} \frac{D_2^{\vec{Q}}(\hat{p}_E, t')}{D_2^{\vec{Q}}(\hat{p}_E, 1)} - \frac{D_2^{\vec{Q}}(\hat{p}_E, t')}{D_2^{\vec{Q}}(\hat{p}_E, 1)} \mathbf{R}_{\vec{Q}} \mathbf{L}_3^{\vec{Q}}(\hat{p}_E, 1, t), & t > t', \end{cases} \\
\Delta_{LR}^{\vec{q}} \Big|_{12} &= \frac{-\sqrt{tt'}}{M_{\text{KK}}} \frac{D_1^{\vec{Q}}(\hat{p}_E, t)}{D_1^{\vec{Q}}(\hat{p}_E, 1)} \mathbf{R}_{\vec{Q}} \frac{\mathbf{Z}_{\vec{q}}}{1 + \mathbf{Z}_{\vec{q}} \mathbf{R}_{\vec{Q}}} \frac{1}{\varrho \tilde{\mathbf{Y}}_{\vec{q}}^\dagger} \frac{1}{D_1^{\vec{q}}(\hat{p}_E, 1)} \frac{D_1^{\vec{q}}(\hat{p}_E, t')}{D_1^{\vec{q}}(\hat{p}_E, 1)}, \\
\Delta_{LR}^{\vec{q}} \Big|_{21} &= \frac{-\sqrt{tt'}}{M_{\text{KK}}} \frac{D_2^{\vec{Q}}(\hat{p}_E, t)}{D_2^{\vec{Q}}(\hat{p}_E, 1)} \varrho \tilde{\mathbf{Y}}_{\vec{q}}^\dagger \mathbf{R}_{\vec{Q}} \frac{1}{1 + \mathbf{Z}_{\vec{q}} \mathbf{R}_{\vec{Q}}} \frac{1}{D_2^{\vec{Q}}(\hat{p}_E, 1)} \frac{D_2^{\vec{Q}}(\hat{p}_E, t')}{D_2^{\vec{Q}}(\hat{p}_E, 1)}, \\
\Delta_{LR}^{\vec{q}} \Big|_{22} &= \frac{-\sqrt{tt'}}{M_{\text{KK}}} \begin{cases} \frac{D_2^{\vec{q}}(\hat{p}_E, t)}{D_2^{\vec{q}}(\hat{p}_E, 1)} \tilde{\mathbf{Y}}_{\vec{q}}^\dagger \mathbf{R}_{\vec{Q}} \frac{1}{1 + \mathbf{Z}_{\vec{q}} \mathbf{R}_{\vec{Q}}} \frac{1}{\tilde{\mathbf{Y}}_{\vec{q}}^\dagger} \frac{1}{D_1^{\vec{q}}(\hat{p}_E, 1)} \frac{D_1^{\vec{q}}(\hat{p}_E, t')}{D_1^{\vec{q}}(\hat{p}_E, 1)} - \frac{D_2^{\vec{q}}(\hat{p}_E, t)}{D_2^{\vec{q}}(\hat{p}_E, 1)} \mathbf{L}_3^{\vec{q}}(\hat{p}_E, 1, t'), & t < t', \\ \frac{D_2^{\vec{q}}(\hat{p}_E, t)}{D_2^{\vec{q}}(\hat{p}_E, 1)} \tilde{\mathbf{Y}}_{\vec{q}}^\dagger \mathbf{R}_{\vec{Q}} \frac{1}{1 + \mathbf{Z}_{\vec{q}} \mathbf{R}_{\vec{Q}}} \frac{1}{\tilde{\mathbf{Y}}_{\vec{q}}^\dagger} \frac{1}{D_1^{\vec{q}}(\hat{p}_E, 1)} \frac{D_1^{\vec{q}}(\hat{p}_E, t')}{D_1^{\vec{q}}(\hat{p}_E, 1)} - \frac{D_1^{\vec{q}}(\hat{p}_E, t')}{D_1^{\vec{q}}(\hat{p}_E, 1)} \mathbf{L}_1^{\vec{q}}(\hat{p}_E, 1, t), & t > t'. \end{cases}
\end{aligned} \tag{3.105}$$

Alternative Derivation and Generalization to Different Yukawa Matrices

We can also derive the results above via an alternative method, where modified boundary conditions are imposed on the 5D propagator functions. The propagator functions Δ_{AB}^q are now computed by solving the coupled system of equations (3.64) and (3.65) without including the Yukawa term in the generalized mass matrix $\mathcal{M}_q(t)$. Instead, one modifies the boundary conditions on the IR brane according to (2.87), such that

$$\left(\frac{v \tilde{\mathbf{Y}}_{\vec{q}}^\dagger}{\sqrt{2} M_{\text{KK}}} \quad 1 \right) \Delta_{LL}^{\vec{q}}(1^-, t'; -p^2) = \left(1 \quad -\frac{v \tilde{\mathbf{Y}}_{\vec{q}}}{\sqrt{2} M_{\text{KK}}} \right) \Delta_{RL}^{\vec{q}}(1^-, t'; -p^2) = 0 \tag{3.106}$$

instead of condition (3.69). The modified Yukawa matrices are defined in (2.81). The boundary conditions on the UV brane (3.70) and the jump conditions (3.68) remain unchanged. It is a straightforward exercise to derive the propagator functions from these equations and one recovers (3.102)–(3.105).

The alternative derivation will be crucial for the propagator in the brane-localized RS model with two different Yukawa matrices in the Yukawa interactions. To understand this, we consider the equations of motion (3.64) and (3.65) for the propagator functions, which must be generalized to

$$\begin{aligned} p^2 \Delta_{LL}^q(t, t'; -p^2) - M_{\text{KK}} \left(\frac{\partial}{\partial t} + \mathcal{M}_q(t) \right) \Delta_{RL}^q(t, t'; -p^2) &= \delta(t - t'), \\ \Delta_{RL}^q(t, t'; -p^2) - M_{\text{KK}} \left(-\frac{\partial}{\partial t} + \mathcal{M}_q^\dagger(t) \right) \Delta_{LL}^q(t, t'; -p^2) &= 0, \end{aligned} \quad (3.107)$$

where

$$\mathcal{M}_q(t) = \frac{1}{t} \begin{pmatrix} \mathbf{c}_Q & 0 \\ 0 & -\mathbf{c}_q \end{pmatrix} + \frac{v}{\sqrt{2}M_{\text{KK}}} \delta_v^\eta(t-1) \begin{pmatrix} 0 & \mathbf{Y}_q^C \\ \mathbf{Y}_q^{S\dagger} & 0 \end{pmatrix} \quad (3.108)$$

replaces the generalized mass matrix in (3.59). The coupled set of first-order differential equations in (3.107) can be combined to yield the second-order equation

$$\left[\frac{\partial^2}{\partial t^2} - \mathcal{M}_q(t) \mathcal{M}_q^\dagger(t) - \frac{d\mathcal{M}_q^\dagger(t)}{dt} + \left(\mathcal{M}_q(t) - \mathcal{M}_q^\dagger(t) \right) \frac{\partial}{\partial t} - \hat{p}_E^2 \right] \Delta_{LL}^q = \frac{\delta(t-t')}{M_{\text{KK}}^2}. \quad (3.109)$$

In the bulk region $t < 1 - \eta$, where the profile $\delta_v^\eta(t-1)$ of the Higgs vev vanishes and the mass matrix is hermitian, this equation reduces to the original equation with (3.67). However, its structure becomes much more complicated for $t > 1 - \eta$ and it has not been possible to derive a general solution in that region.

In the case of infinitesimal η (at fixed p^2), however, it is consistent to only keep the terms in (3.107) that are enhanced by $1/\eta$ for $1 - \eta < t < 1$. Taking $t' < 1 - \eta$ in the bulk region, squaring the resulting differential operators, and adopting the Higgs profile given in (2.75), we thus need to solve

$$\begin{aligned} \left[\frac{\partial^2}{\partial t^2} - \frac{v^2}{2M_{\text{KK}}^2 \eta^2} \begin{pmatrix} \mathbf{Y}_q^C \mathbf{Y}_q^{S\dagger} & 0 \\ 0 & \mathbf{Y}_q^{S\dagger} \mathbf{Y}_q^C \end{pmatrix} \right] \Delta_{RL}^q(t, t'; -p^2) &= 0 + \dots, \\ \left[\frac{\partial^2}{\partial t^2} - \frac{v^2}{2M_{\text{KK}}^2 \eta^2} \begin{pmatrix} \mathbf{Y}_q^S \mathbf{Y}_q^{C\dagger} & 0 \\ 0 & \mathbf{Y}_q^{C\dagger} \mathbf{Y}_q^S \end{pmatrix} \right] \Delta_{LL}^q(t, t'; -p^2) &= 0 + \dots, \end{aligned} \quad (3.110)$$

where the dots denote subleading terms. The solutions to these equations involve hyperbolic trigonometric functions, whose arguments contain the matrices

$$\mathbf{X}_q = \frac{v}{\sqrt{2}M_{\text{KK}}} \sqrt{\mathbf{Y}_q^C \mathbf{Y}_q^{S\dagger}}, \quad \bar{\mathbf{X}}_q = \frac{v}{\sqrt{2}M_{\text{KK}}} \sqrt{\mathbf{Y}_q^{S\dagger} \mathbf{Y}_q^C}, \quad (3.111)$$

and their hermitian conjugates. It is then not difficult to show that, in the limit $\eta \rightarrow 0$, the boundary conditions given in (3.106) still hold, provided we use \mathbf{X}_q as defined here instead of the original definition in (2.78), and $\tilde{\mathbf{Y}}_q$ now defined by

$$\tilde{\mathbf{Y}}_q = \frac{\tanh \mathbf{X}_q}{\mathbf{X}_q} \mathbf{Y}_q^C \quad (3.112)$$

instead of (2.81). Solving the bulk differential equations for the propagator functions with these boundary conditions, we recover the previous solutions with the substitutions just described. Note that the quantity $\mathbf{Z}_q(p_E^2)$ now becomes

$$\mathbf{Z}_q(p_E^2) = \frac{v^2}{2M_{\text{KK}}^2} \frac{\tanh \mathbf{X}_q}{\mathbf{X}_q} \mathbf{Y}_q^C \mathbf{R}_q(\hat{p}_E) \mathbf{Y}_q^{C\dagger} \frac{\tanh \mathbf{X}_q^\dagger}{\mathbf{X}_q^\dagger} \mathbf{R}_Q(\hat{p}_E). \quad (3.113)$$

The results above will be needed in a subsection of Section 4.1, when we discuss the fermionic contributions to the gluon-fusion amplitude in the brane-localized Higgs scenario with two different Yukawa matrices.

Asymptotic Behavior for Small and Large Momenta

Finally, we derive the asymptotic behavior of the propagator functions, where we will focus on the minimal model here. The results in the custodial model are listed in Appendix A. Considering the minimal model, the corresponding propagator solutions can be obtained from (3.102) and (3.104) by the replacements $\vec{Q} \rightarrow Q$, $\vec{q} \rightarrow q$, implying that one only keeps the (11)-component (3×3 matrix) in the higher-dimensional space. Since we are interested in the low momentum regime $p \rightarrow 0$, we only keep the leading terms. It turns out to be convenient to define the functions

$$F_t(\mathbf{c}_A) \equiv \frac{1 - t^{1+2\mathbf{c}_A}}{1 + 2\mathbf{c}_A}, \quad \tilde{F}_t(\mathbf{c}_A) \equiv \frac{t^{1+2\mathbf{c}_A} - \epsilon^{1+2\mathbf{c}_A}}{1 - \epsilon^{1+2\mathbf{c}_A}}, \quad \hat{F}_t(\mathbf{c}_A) \equiv \frac{t^{1+2\mathbf{c}_A} - \epsilon^{1+2\mathbf{c}_A}}{1 + 2\mathbf{c}_A}, \quad (3.114)$$

which fulfill the relations $F^2(\mathbf{c}_A)\hat{F}_t(\mathbf{c}_A) = \tilde{F}_t(\mathbf{c}_A)$, $F_\epsilon(\mathbf{c}_A) = F^{-2}(\mathbf{c}_A)$ and $F_1(\mathbf{c}_A) = \tilde{F}_\epsilon(\mathbf{c}_A) = \hat{F}_\epsilon(\mathbf{c}_A) = 0$, where $F(\mathbf{c}_A)$ denotes the zero-mode profile function (2.93). Using the definitions in (3.114) we find (up to higher orders in \hat{p}_E)

$$\begin{aligned} \mathbf{R}_A(\hat{p}_E) &\approx \frac{F^2(\mathbf{c}_A)}{\hat{p}_E} + \frac{\hat{p}_E}{1 - 2\mathbf{c}_A} \left[1 - F^2(\mathbf{c}_A) + \frac{F^4(\mathbf{c}_A)}{3 + 2\mathbf{c}_A} \right], \\ \frac{\mathbf{D}_1^A(\hat{p}_E, t)}{\mathbf{D}_1^A(\hat{p}_E)} &\approx t^{-\frac{1}{2} + \mathbf{c}_A}, & \frac{\mathbf{D}_2^A(\hat{p}_E, t)}{\mathbf{D}_2^A(\hat{p}_E)} &\approx \tilde{F}_t(\mathbf{c}_A) t^{-\frac{1}{2} - \mathbf{c}_A}, \\ \mathbf{L}_{2,3}^A(\hat{p}_E, \hat{p}_E, t) &\approx \pm \hat{p}_E F_t(\pm \mathbf{c}_A) t^{-\frac{1}{2} \mp \mathbf{c}_A}, & \mathbf{L}_{1,4}^A(\hat{p}_E, \hat{p}_E, t) &\approx \pm t^{-\frac{1}{2} \mp \mathbf{c}_A}. \end{aligned} \quad (3.115)$$

Equipped with that we expand the propagator solutions (3.102)–(3.105) for small momenta by using (3.115) and we obtain

$$\begin{aligned} \Delta_{LL}^q(t, t'; 0) &= - \begin{pmatrix} t^{c_Q} \left(\frac{1}{\frac{v^2}{2} \tilde{\mathbf{Y}}_q F^2(\mathbf{c}_q) \tilde{\mathbf{Y}}_q^\dagger} + \frac{F_{t>}(-\mathbf{c}_Q)}{M_{\text{KK}}^2} \right) t'^{c_Q} & -t^{c_Q} \frac{1}{\varrho \tilde{\mathbf{Y}}_q^\dagger} \frac{\hat{F}_{t'}(\mathbf{c}_q)}{M_{\text{KK}}^2} \frac{1}{t'^{c_q}} \\ -\frac{1}{t^{c_q}} \frac{\hat{F}_t(\mathbf{c}_q)}{M_{\text{KK}}^2} \frac{1}{\varrho \tilde{\mathbf{Y}}_q} t'^{c_Q} & \frac{1}{t^{c_q}} \frac{\hat{F}_{t<}(\mathbf{c}_q)}{M_{\text{KK}}^2} \frac{1}{t'^{c_q}} \end{pmatrix}, \\ \Delta_{RR}^q(t, t'; 0) &= - \begin{pmatrix} \frac{1}{t^{c_Q}} \frac{\hat{F}_{t<}(\mathbf{c}_Q)}{M_{\text{KK}}^2} \frac{1}{t'^{c_Q}} & -\frac{1}{t^{c_Q}} \frac{\hat{F}_t(\mathbf{c}_Q)}{M_{\text{KK}}^2} \frac{1}{\varrho \tilde{\mathbf{Y}}_q^\dagger} t'^{c_q} \\ -t^{c_q} \frac{1}{\varrho \tilde{\mathbf{Y}}_q} \frac{\hat{F}_{t'}(\mathbf{c}_Q)}{M_{\text{KK}}^2} \frac{1}{t'^{c_Q}} & t^{c_q} \left(\frac{1}{\frac{v^2}{2} \tilde{\mathbf{Y}}_q^\dagger F^2(\mathbf{c}_Q) \tilde{\mathbf{Y}}_q} + \frac{F_{t>}(-\mathbf{c}_q)}{M_{\text{KK}}^2} \right) t'^{c_q} \end{pmatrix}, \\ \Delta_{RL}^q(t, t'; 0) &= - \begin{pmatrix} \frac{\Theta(t-t')}{M_{\text{KK}}} \left(\frac{t'}{t} \right)^{c_Q} & 0 \\ \frac{1}{M_{\text{KK}}} t^{c_q} \frac{1}{\varrho \tilde{\mathbf{Y}}_q} t'^{c_Q} & -\frac{\Theta(t'-t)}{M_{\text{KK}}} \left(\frac{t}{t'} \right)^{c_q} \end{pmatrix} = \Delta_{LR}^{q\dagger}(t', t; 0), \quad (3.116) \end{aligned}$$

where \tilde{Y}_q is defined in (3.98). Here, $\Theta(t - t')$ denotes the Heaviside (step) function defined in this case by

$$\Theta(t - t') = \begin{cases} 1, & t > t' \\ 0, & t \leq t' \end{cases}. \quad (3.117)$$

For the limits of the propagators for large momenta⁴ we can approximate the quantities $R_{\vec{A}}(\hat{p}_E) \approx 1$ and $Z_{\vec{q}}(p_E^2) \approx \tanh^2 \mathbf{X}_{\vec{q}}$ (at leading order in \hat{p}_E) as well as

$$\begin{aligned} \frac{D_{1,4}^{\vec{A}}(\hat{p}_E, t)}{D_{1,4}^{\vec{A}}(\hat{p}_E)} &\approx \frac{e^{\hat{p}_E(t-1)}}{\sqrt{t}} \left(1 + e^{2\hat{p}_E(\epsilon-t)}\right), & \frac{D_{2,3}^{\vec{A}}(\hat{p}_E, t)}{D_{2,3}^{\vec{A}}(\hat{p}_E)} &\approx \frac{e^{\hat{p}_E(t-1)}}{\sqrt{t}} \left(1 - e^{2\hat{p}_E(\epsilon-t)}\right), \\ L_{1,2}(\hat{p}_E, \hat{p}_E, t) &\approx -L_{4,3}(\hat{p}_E, \hat{p}_E, t) \approx \frac{e^{\hat{p}_E(1-t)}}{2\sqrt{t}} \left(1 \pm e^{2\hat{p}_E(t-1)}\right), \end{aligned} \quad (3.118)$$

for $\vec{A} = \vec{Q}, \vec{q}$. Note that the round brackets in (3.118) are only relevant for the special cases of $t = \epsilon$ and $t = 1$, respectively. Applying those relations on the propagator solutions in (3.102), we find ($p_E \gg M_{\text{KK}}$)

$$\begin{aligned} \Delta_{LL}^{\vec{q}} \Big|_{11} &= \begin{cases} \frac{-1}{2p_E M_{\text{KK}}}, \\ \frac{-1}{p_E M_{\text{KK}}} \mathbf{N}_{\vec{Q}}, \\ \frac{-1}{p_E M_{\text{KK}}} \frac{1}{1 + \tanh^2 \mathbf{X}_{\vec{q}}}, \end{cases} & \Delta_{LL}^{\vec{q}} \Big|_{22} &= \begin{cases} \frac{-1}{2p_E M_{\text{KK}}} & t = t' \neq \{\epsilon, 1\}, \\ \frac{-1}{p_E M_{\text{KK}}} \mathbf{N}_{\vec{q}}, & t = t' = \epsilon, \\ \frac{-1}{p_E M_{\text{KK}}} \frac{1}{1 + \tanh^2 \mathbf{X}_{\vec{q}}}, & t = t' = 1, \end{cases} \\ \Delta_{LL}^{\vec{q}} \Big|_{12} &= \frac{1}{p_E M_{\text{KK}}} \frac{1}{1 + \tanh^2 \mathbf{X}_{\vec{q}}} \varrho \tilde{Y}_{\vec{q}}, & \Delta_{LL}^{\vec{q}} \Big|_{21} &= \frac{1}{p_E M_{\text{KK}}} \varrho \tilde{Y}_{\vec{q}}^\dagger \frac{1}{1 + \tanh^2 \mathbf{X}_{\vec{q}}}, \quad t = t' = 1, \\ \Delta_{RL}^{\vec{q}} \Big|_{11} &= \begin{cases} \frac{1}{2M_{\text{KK}}}, \\ \frac{1}{M_{\text{KK}}} \frac{1}{1 + \tanh^2 \mathbf{X}_{\vec{q}}}, \\ \frac{-1}{M_{\text{KK}}} \frac{\tanh^2 \mathbf{X}_{\vec{q}}}{1 + \tanh^2 \mathbf{X}_{\vec{q}}}, \end{cases} & \Delta_{RL}^{\vec{q}} \Big|_{22} &= \begin{cases} \frac{1}{2M_{\text{KK}}}, & t \rightarrow t'^- \neq \{\epsilon, 1\}, \\ \frac{1}{M_{\text{KK}}}, & t \rightarrow t'^+ \neq \{\epsilon, 1\}, \\ \frac{1}{M_{\text{KK}}} \frac{\tanh^2 \mathbf{X}_{\vec{q}}}{1 + \tanh^2 \mathbf{X}_{\vec{q}}}, & t \rightarrow t'^- = 1, \\ \frac{-1}{M_{\text{KK}}} \frac{1}{1 + \tanh^2 \mathbf{X}_{\vec{q}}}, & t' \rightarrow t^- = 1, \end{cases} \\ \Delta_{RL}^{\vec{q}} \Big|_{12} &= \frac{-1}{M_{\text{KK}}} \frac{1}{1 + \tanh^2 \mathbf{X}_{\vec{q}}} \varrho \tilde{Y}_{\vec{q}}, & \Delta_{RL}^{\vec{q}} \Big|_{21} &= \frac{-1}{M_{\text{KK}}} \varrho \tilde{Y}_{\vec{q}}^\dagger \frac{1}{1 + \tanh^2 \mathbf{X}_{\vec{q}}}, \quad t = t' = 1, \end{aligned} \quad (3.119)$$

where we have used the notion $t'^{\pm} = t' \pm 0$, since the diagonal components of $\Delta_{RL}^{\vec{q}}$ are discontinuous at $t = t'$. The relations (3.119) are valid for both the minimal and the custodial model. Concerning the diagonal components of $\Delta_{LL}^{\vec{q}}$, we have needed to make a case distinction in the custodial model and introduced the quantity

$$\mathbf{N}_{\vec{Q}} = \begin{cases} \text{diag}(1, 0), & \vec{Q} = \vec{U}, \\ 1, & \vec{Q} = \vec{D}, \\ 1, & \vec{Q} = \vec{\Lambda}, \end{cases} \quad \mathbf{N}_{\vec{q}} = \begin{cases} \text{diag}(0, 1, 1), & \vec{q} = \vec{u}, \\ \text{diag}(0, 1), & \vec{q} = \vec{d}, \\ \text{diag}(1, 1), & \vec{q} = \vec{\lambda}, \end{cases} \quad (3.120)$$

while in the minimal model we simply replace $\vec{Q}, \vec{q} \rightarrow Q, q$ in the formulas above, where $\mathbf{N}_Q = 1$ and $\mathbf{N}_q = 0$.

⁴Note that $\Delta_{LL}^{\vec{q}}$ and $\Delta_{RR}^{\vec{q}}$ are multiplied within the propagator by an additional momentum power, thus we are actually dealing with the expression $\not{p} \Delta_{LL, RR}^{\vec{q}}$.

Chapter 4

Loop Calculations in Warped Extra Dimensions

In this chapter, which together with Chapter 5 forms the core of this thesis, we will see how the results of the previous chapter can help us to find hints on warped extra dimensions. As will be touched on at the beginning of Chapter 5, the most straightforward way to look for evidence for models with warped extra dimensions is via *direct* detection of KK modes. Finding several KK gluons with equidistant masses would be a clear indication for RS models. However, none of the predicted KK excitations have been observed yet, and, as we have seen in Sections 2.2.4 and 2.3.3, the electroweak precision tests indicate that these particles could be too massive for direct detection at the LHC. Thus, *indirect* searches become more and more attractive. Of special interest are processes that can only be generated at loop level in the SM so that new-physics contributions could give rise to measurable deviations from the SM predictions. Especially the infinite tower of KK modes of extra-dimensional theories are supposed to have a significant effect. In this chapter, we will study some of the most important loop-induced processes, where two of them are associated with the Higgs sector and one with the flavor sector.

This chapter is divided into three sections: In Section 4.1 we will analyze the Higgs production process via gluon fusion before we will then turn to the Higgs decay into two photons in Section 4.2. Section 4.3 then focuses on the flavor-changing neutral current $b \rightarrow s\gamma$, which is affected by two instead of one infinite KK sum, so that its calculation becomes more intricate than the Higgs processes. Another loop-level calculation - the one-loop correction to the Yukawa interactions - is phenomenologically less important and will therefore be discussed in Appendix B.

4.1 Higgs Production via Gluon Fusion

We begin the discussion of loop-induced processes by investigating the Higgs production process via gluon fusion. The corresponding Feynman diagram is shown in Figure 4.1. Before the analysis of gluon fusion in warped dimensions will be presented, it is worth showing a short summary of previous works on this process first. This section complies with our publication [150].

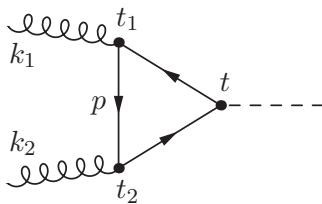


FIGURE 4.1: Gluon-fusion Higgs production process induced by the exchange of 5D quark states. The positions of the vertices along the extra dimension are denoted by $t_{1,2}$ and t . The external momenta k_1, k_2 are assumed to be incoming.

4.1.1 Preliminaries

In the context of warped extra dimensions, Higgs physics has been studied by several authors [144, 149, 157, 218–224]. The effect on the $gg \rightarrow h$ amplitude caused by the heavy b' state, the $SU(2)_R$ partner of the top quark predicted in RS models with custodial symmetry, was investigated in [218]. Models in which the Higgs scalar is a pseudo Nambu-Goldstone boson, such as warped gauge-Higgs unification scenarios, were studied in [219, 223]. In these models, the result for the $gg \rightarrow h$ amplitude only depends on the fundamental parameter v/f , but it is insensitive to the details about the spectrum of the KK quarks. The authors of [157, 220] studied the effect of KK resonances on the loop-induced hgg and $h\gamma\gamma$ couplings by working out the corrections to the top- and bottom-quark Yukawa couplings induced by their mixing with KK states. In these papers, no significant contributions from the heavy KK quark states propagating in the loop were observed, as the Yukawa interactions coupling the Higgs to two Z_2 -odd fermions were implicitly assumed to be zero.¹ The possibly large effect on the Higgs-boson couplings induced by the shift of the Higgs vev relative to its SM value, which can arise in RS models with custodial symmetry, was emphasized in [157]. The first complete calculation of the hgg and $h\gamma\gamma$ couplings, in which both types of Yukawa interactions in (2.126) were included, was performed in [149]. In this paper, both the production of Higgs bosons in the gluon fusion process as well as the main decay channels were studied in the custodial RS model. It was observed that the dominant corrections to the hgg and $h\gamma\gamma$ couplings arise from the towers of KK quark states propagating in the loop. These effects were found to be independent of the masses of the corresponding SM quarks to a very good approximation. The production rate was found to be suppressed in most regions of parameter space, while the branching fraction for the diphoton channel $h \rightarrow \gamma\gamma$ tends to be enhanced with respect to the SM. At about the same time, an independent analysis of the Higgs couplings to gluons and photons appeared [222], which came to the opposite conclusions. In 2012 Carena et. al. [144] showed that the discrepancy between the two sets of results can be traced back to a subtlety in the calculation of the loop-induced Higgs couplings to gluons and photons. As has been explained in Section 2.2.2, for the computation of the relevant overlap integrals of fermion wave functions with the brane-localized Higgs field, it is necessary to regularize the Higgs profile in an intermediate step and give it an infinitesimal width η [175]. When the calculation of the

¹The fact that there are two towers of KK quark states for every massive SM quark, which is deeply connected to the finiteness of the 5D loop amplitude [144], was overlooked in [221]. In order to obtain a finite sum for the infinite KK tower, the authors made the approximation $m_{q_n} = \lambda_{q_n} v/\sqrt{2}$ with $\lambda_{q_n} \approx 1$ for the masses of the KK quarks, see eqs. (8) and (10) of their paper, which is incorrect.

gluon fusion amplitude is performed in a naive way, the limits of sending the regulator to zero ($\eta \rightarrow 0$) and including an infinite number of KK modes ($N \rightarrow \infty$) in the sum over virtual states do not commute. This ambiguity disappears once the loop calculation is performed in the presence of a consistent UV regulator, such as dimensional regularization with $d < 4$ space-time dimensions. This can be seen in their formula

$$\mathcal{A}(gg \rightarrow h) \sim \lim_{N \rightarrow \infty, \eta \rightarrow 0} \sum_{q=u,d} \sum_{n=4}^{3+6N} \frac{v g_{nn}^q}{m_{q_n}} \left(\frac{\mu}{m_{q_n}} \right)^{4-d}, \quad (4.1)$$

where m_{q_n} are the masses of the KK quarks and g_{nn}^q denote their effective 4D Yukawa couplings as defined in (2.126). For $d = 4$, the amplitude above is naively logarithmically divergent and only systematic cancellations within each level of KK quark modes render it finite. The gluon fusion amplitude then receives an unsuppressed “resonance contribution” from high-mass KK states ($m_n \sim M_{\text{KK}}/\eta$), which can resolve the wave function of the Higgs boson (see also [225]). This effect is absent for a brane-localized scalar sector, since it cannot be resolved by these ultra-massive modes. In the presence of the dimensional regulator $d < 4$ the order of limits becomes irrelevant, and one obtains a unique answer for the sum. In the limit $d \rightarrow 4$ taken at the end of the calculation this result coincides with the result found in [149]. The same conclusion can be reached by using a hard UV momentum cutoff on the 4D loop integral. The physical significance of the results found in [222] was not fully elucidated in [144], but the discussion in that paper suggests that they might refer to a certain limit of a model featuring a Higgs boson living in the bulk of the extra dimension.

In this section, we will calculate the $gg \rightarrow h$ amplitude with the help of the 5D fermion propagator derived in the previous chapter. This avoids the very notion of KK states and the infinite sum over KK states is performed implicitly. The only relevant limit to be considered is that of sending the regulator η of the Higgs profile to zero. In the context of dimensional regularization, it will turn out that this limit can be taken either before or after performing the loop integration. In both cases, we will confirm the results obtained in [144, 149]. If the width of the Higgs profile is kept finite according to (2.4), we will recover the findings of [222]. They correspond to the narrow bulk-Higgs scenario. The 5D analysis highlights the relevance of different mass scales. In brane-Higgs models, these are the Higgs vev v , the KK mass scale M_{KK} , and the physical UV cutoff Λ_{TeV} of the RS model near the IR brane. Models in which the Higgs boson is treated as a narrow bulk state additionally contain the scale $v/\eta \gg M_{\text{KK}}$ (the inverse width of the Higgs profile). We will see that it makes an important difference whether this scale lies above or below the cutoff. The relevant loop integrand approaches a first plateau for Euclidean loop momenta $p_E \gg M_{\text{KK}}$ and a second one for $p_E \gg v/\eta$ (see Figure 4.2). While in brane-Higgs models the second plateau is absent, in bulk-Higgs scenarios the $gg \rightarrow h$ amplitude receives an unsuppressed contribution from the high scale v/η , and is thus sensitive to physics on distances shorter than $1/M_{\text{KK}}$.

This section is structured as follows: We will first derive an exact representation of the dimensionally-regularized gluon fusion amplitude in terms of an integral over the mixed-chirality components of the 5D quark propagator in the mixed momentum-position representation, including the contributions of the SM quarks and the full dependence on the Higgs-boson mass. This expression holds for arbitrary Higgs profiles. In Subsection 4.1.3, these results will be used to evaluate the $gg \rightarrow h$ amplitude and we will explicitly show that taking the limit $\eta \rightarrow 0$ commutes with the integration over the 4D loop momentum. We will prove a conjecture made in [144] for the analytic form

of the contribution of the infinite tower of heavy KK quark states. Moreover, an alternative derivation of the same result based on the derivation of the propagator via the modified boundary conditions (3.106) will be presented. In this approach, the notion of an infinitesimal regulator η does not appear, and many of the subtleties related to the $\eta \rightarrow 0$ limit will be avoided from the beginning. This alternative approach will also be used when we consider a generalization of the model in which two different Yukawa matrices enter in the 5D Yukawa interactions. Then, we will discuss the changes that occur in the case of a narrow bulk-Higgs field. Subsection 4.1.4 will address the question of the numerical importance of power-suppressed operators. It will be found that under the assumption that the UV completion of these models is strongly coupled, the corresponding power corrections are likely to be much smaller than the RS loop effects calculated in Subsection 4.1.3. While most of the discussion refers to the minimal RS model with the SM gauge group in the bulk, the results are generalized to the custodial RS model in Subsection 4.1.5.

4.1.2 5D Analysis of the Gluon Fusion Amplitude

The goal of this section is to repeat the calculation of the gluon fusion amplitude using 5D quark propagators derived in Section 3.2. The associated one-loop graph is shown in Figure 4.1, where at each vertex an integral over the fifth coordinate is implied. The results of the calculation will be summarized in terms of two coefficients C_{1g} and C_{5g} defined by the decomposition

$$\mathcal{A}(gg \rightarrow h) = C_{1g} \frac{\alpha_s}{12\pi v} \langle 0 | \mathcal{G}_{\mu\nu}^a \mathcal{G}^{\mu\nu,a} | gg \rangle - C_{5g} \frac{\alpha_s}{8\pi v} \langle 0 | \mathcal{G}_{\mu\nu}^a \tilde{\mathcal{G}}^{\mu\nu,a} | gg \rangle, \quad (4.2)$$

where $\tilde{\mathcal{G}}^{\mu\nu,a} = -\frac{1}{2}\epsilon^{\mu\nu\alpha\beta} \mathcal{G}_{\alpha\beta}^a$ (with $\epsilon^{0123} = -1$) denotes the dual field-strength tensor. Note that the Wilson coefficients C_{1g} and C_{5g} also include the contributions of the SM quarks as opposed to [144].

In order to perform the calculation of the gluon fusion amplitude at one-loop order consistently, it is necessary to introduce two different kinds of regulators. As already stressed several times, it is crucial to regularize the Higgs profile by giving it a small but finite width $\eta \ll 1$. In the following, we will therefore use the notation $\delta_h^\eta(t-1)$ for the regularized Higgs profile given by (2.75). Many of the following results will be independent of the shape of the Higgs profile and would remain valid for the case of a general bulk-Higgs field whose profile is given in (2.52). Only at the end of the analysis it will be specialized to the case of a very narrow Higgs profile, with η satisfying one of the conditions (2.3) or (2.4). At that point, the solutions for the propagator functions derived in the previous chapter become important. Secondly, as has been emphasized above, it is important to introduce a consistent UV regulator in the calculation, even though the final answer for the gluon fusion amplitude is UV finite. This should not be surprising, since even in the 4D case the introduction of a UV regulator is required in order to obtain a gauge-invariant result. To see this, we can consider the loop diagram for a single KK mode, which naively is linearly divergent. Using invariance under $p \rightarrow -p$, only a superficial logarithmic divergence remains. In dimensional regularization, one encounters the integral

$$\int \frac{d^d p}{(2\pi)^d} \left[\frac{4-d}{d} \frac{p^2}{(p^2 - \Delta)^3} + \frac{\Delta}{(p^2 - \Delta)^3} \right] \varepsilon(k_1) \cdot \varepsilon(k_2), \quad (4.3)$$

for $d \neq 4$, where $\Delta = m_{q_n}^2 - xym_h^2$ arises after combining denominator using Feynman parameters. This integral vanishes for $d \neq 4$, but if the calculation was performed naively in four dimensions, then only the second term would be present. Note that this would correspond to a gauge-dependent operator $A_\mu^a A^{\mu,a}$. Thus, a UV regulator is unavoidable in the calculation. In the 5D model, as has been explained above, it has the additional effect of regularizing the infinite sum over KK modes.

With the regulators in place, we can write the gluon fusion amplitude in the form

$$\begin{aligned} \mathcal{A}(gg \rightarrow h) &= ig_s^2 \delta^{ab} \sum_{q=u,d} \int \frac{d^d p}{(2\pi)^d} \int_\epsilon^1 dt_1 \int_\epsilon^1 dt_2 \int_\epsilon^1 dt \delta_h^\eta(t-1) \varepsilon_\nu(k_1) \varepsilon_\mu(k_2) \\ &\times \text{Tr} \left[\frac{1}{\sqrt{2}} \begin{pmatrix} 0 & \mathbf{Y}_q \\ \mathbf{Y}_q^\dagger & 0 \end{pmatrix} \mathbf{S}^q(t, t_2; p - k_2) \gamma^\mu \mathbf{S}^q(t_2, t_1; p) \gamma^\nu \mathbf{S}^q(t_1, t; p + k_1) \right], \end{aligned} \quad (4.4)$$

where k_i denote the incoming momenta of the external gluons, a and b their color indices, and $\varepsilon(k_i)$ their polarization vectors. It would now be straightforward to insert the decomposition of the 5D propagator given in (3.60) with the solutions for the propagator functions Δ_{AB} and try to simplify the result. However, as we explicitly see in the results of Appendix A, the latter are complicated functions of the 4-momentum p and the coordinates t, t' and in order to simplify the calculation, it is convenient to use their representations as sums over KK modes (3.61) in intermediate steps. With the dimensional regulator in place, the 4D loop integral as well as the infinite sums over KK modes converge, and therefore the KK representations provide exact representations of the 5D propagator functions. The advantage of using the representation (3.61) is that we can now perform integrals over the coordinates t_1 and t_2 of the two external gluons using the orthonormality relations (2.70). The latter relations reduce the three infinite sums appearing in the propagator functions Δ_{AB} to a single one, for instance

$$\begin{aligned} \int_\epsilon^1 dt_1 \int_\epsilon^1 dt_2 \Delta_{RR}^q(t, t_2; -(p - k_2)^2) \Delta_{RL}^q(t_2, t_1; -p^2) \Delta_{LL}^q(t_1, t; -(p + k_1)^2) \\ = 2 \int_0^1 dx \int_0^{1-x} dy \Delta_{RL}^q(t, t; -(p^2 + xym_h^2)), \end{aligned} \quad (4.5)$$

where Feynman parameters have been introduced to combine the three denominators. Moreover, it has been used that an on-shell Higgs boson is produced, i.e. $(k_1 + k_2) = k^2 = m_h^2$, where m_h is the Higgs mass. Eventually, we find that the amplitude (4.4) can be reduced to integrals of the regularized Higgs profile with traces of the mixed-chirality components of the 5D propagator evaluated at $t = t'$, which are defined by

$$\begin{aligned} T_+(-p^2) &\equiv \sum_{q=u,d} \frac{-v}{\sqrt{2}} \int_\epsilon^1 dt \delta_h^\eta(t-1) \text{Tr} \left[\begin{pmatrix} 0 & \mathbf{Y}_q \\ \mathbf{Y}_q^\dagger & 0 \end{pmatrix} \frac{\Delta_{RL}^q(t, t; -p^2) + \Delta_{LR}^q(t, t; -p^2)}{2} \right], \\ T_-(-p^2) &\equiv \sum_{q=u,d} \frac{-v}{\sqrt{2}} \int_\epsilon^1 dt \delta_h^\eta(t-1) \text{Tr} \left[\begin{pmatrix} 0 & \mathbf{Y}_q \\ \mathbf{Y}_q^\dagger & 0 \end{pmatrix} \frac{\Delta_{RL}^q(t, t; -p^2) - \Delta_{LR}^q(t, t; -p^2)}{2i} \right]. \end{aligned} \quad (4.6)$$

Matching the resulting expression for the amplitude \mathcal{A} with the two-gluon matrix elements in (4.2), we obtain

$$C_{1g} = 3 \int_0^1 dx \int_0^{1-x} dy (1 - 4xy) I_+(xym_h^2), \quad C_{5g} = 2 \int_0^1 dx \int_0^{1-x} dy I_-(xym_h^2). \quad (4.7)$$

The quantities

$$\begin{aligned}
I_{\pm}(m^2) &\equiv \frac{e^{\hat{\epsilon}\gamma_E}\mu^{2\hat{\epsilon}}}{\Gamma(2-\hat{\epsilon})} \int_0^{\infty} dp_E^2 p_E^{2(1-\hat{\epsilon})} \left(\frac{\partial}{\partial p_E^2} \right)^2 T_{\pm}(p_E^2 - m^2 - i0) \\
&= -\frac{e^{\hat{\epsilon}\gamma_E}\mu^{2\hat{\epsilon}}}{\Gamma(1-\hat{\epsilon})} \int_0^{\infty} dp_E p_E^{-2\hat{\epsilon}} \frac{\partial}{\partial p_E} T_{\pm}(p_E^2 - m^2 - i0)
\end{aligned} \tag{4.8}$$

are the dimensionally regularized loop-momentum integrals (after performing a Wick rotation $p_E^2 \equiv -p^2$) over the functions $T_{\pm}(p_E^2) \equiv T_{\pm}(-p^2)$ in (4.6), shifted by an amount m^2 . We work in the $\overline{\text{MS}}$ scheme with $d = 4 - 2\hat{\epsilon}$ space-time dimensions. In the second step we have integrated by parts, which is justified as long as the quantity $p_E \partial T_{\pm}/\partial p_E$ vanishes at $p_E = 0$ and at $p_E = \infty$. The analysis in the following section will confirm that these conditions are satisfied.

The integral (4.8) can also be expressed using the more intuitive hard UV momentum cutoff regularization. This can be easily implemented once we have the answers in the form given above. Setting $\hat{\epsilon} = 0$ and restricting the loop momentum to the range $0 \leq p_E \leq \Lambda$, we obtain

$$I_{\pm}(m^2) = T_{\pm}(-m^2 - i0) - T_{\pm}(\Lambda^2 - m^2) + \Lambda^2 \frac{\partial}{\partial \Lambda^2} T_{\pm}(\Lambda^2 - m^2), \tag{4.9}$$

where Λ should be identified with the physical UV cutoff Λ_{TeV} of the RS model.

The relations (4.7) are one of the main results of this section. They provide exact expressions for the Wilson coefficients C_{1g} and C_{5g} in terms of a 5D loop integral. The trick of using the KK representation in intermediate steps is legitimate and not different from similar techniques commonly used in 4D loop calculations. In contrast to previous works [144, 149, 157, 218–224] we have not taken the limit $m_h \rightarrow 0$, which provides a good approximation if the mass of the particle in the loop satisfies the inequality $m_{q_n}^2 \gg m_h^2/4$. This approximation is reasonable for the KK excitations, but for the light SM quarks (and to some extent even for the top quark) the Higgs mass must be kept in order to obtain a reliable result. The strategy adopted in the above references was to first evaluate the gluon fusion amplitude in the limit $m_h \rightarrow 0$, then to subtract the contributions of the zero modes by hand, and finally to add back the contributions of the top and bottom quarks using the proper loop functions calculated with the physical value of the Higgs mass. Since in a 5D framework there is no distinction between zero modes and KK excitations, the Higgs mass must be kept finite in order to include the SM contributions in the correct way.

Note that the results (4.6) and (4.7) are valid for an arbitrary Higgs profile along the extra dimension. As long as one succeeds in deriving the mixed-chirality components of the 5D propagator in a generic bulk-Higgs model, one can use (4.7) to compute the corresponding effective ggh couplings. The limit of a brane-localized scalar sector corresponds to taking the limit $\eta \rightarrow 0$ in (4.6). Here we explicitly see the reason for the calculation of the 5D quark propagator performed in the previous chapter. For the case of a brane Higgs, we have to take the limit $\eta \rightarrow 0$, meaning that we could already use the propagator solution shown in Section 3.2.4 and remove the UV regulator. However, we keep the exact dependence on η , since it will be used to point out an important feature of RS models. Before we dwell on this, observe that for a generic bulk Higgs scenario it is $I_{\pm}(m^2) = T_{\pm}(-m^2)$, since the 5D quark propagator vanishes for $p_E \rightarrow \infty$. In this case, we only need to use the propagator at small momentum.

4.1.3 Analysis of the Loop Amplitude

We now calculate the loop integrals $I_{\pm}(m^2)$ for the cases of a brane-localized Higgs boson and a narrow bulk-Higgs field, as defined in (2.3) and (2.4). The calculation is performed in dimensional regularization, but we will first motivate the results in the context of the more intuitive scheme in which a hard UV cutoff is used. We begin by calculating and collecting some general properties of the functions $T_{\pm}(p_E^2)$ defined in (4.6).

Calculation of the Functions $T_{\pm}(p_E^2)$

Equipped with the solutions for the propagator functions derived in the previous chapter, we can easily derive explicit expressions for the quantities $T_{\pm}(p_E^2)$. Using the results of Appendix A, we find that (4.6) can be evaluated to

$$T_+(p_E^2) = \sum_{q=u,d} \int_{\epsilon}^1 dt \delta_h^{\eta}(t-1) \text{Tr} \left\{ \frac{\mathbf{X}_q^2}{\mathbf{S}_q \sinh 2\mathbf{S}_q} \right. \quad (4.10)$$

$$\left. \times \left[\sinh^2 \mathbf{S}_q + \mathcal{C}^2(t) \mathbf{Z}_q^{\eta,1}(p_E^2) \frac{1}{\mathbf{N}_q^{\eta,1}(p_E^2)} - \mathcal{S}^2(t) \frac{\mathbf{N}_q^{\eta,2}(p_E^2) - 1}{\mathbf{N}_q^{\eta,2}(p_E^2)} + \text{h.c.} \right] \right\},$$

and analogously for $T_-(p_E^2)$. The matrix-valued quantities above have been defined in (2.78), (3.80), (3.82), (3.90), and (3.91), respectively. It is now straightforward to perform the integration over the loop momentum. Since (4.8) is essentially a (regularized) integral over the derivative of the functions $T_{\pm}(p_E^2)$, we first study the properties of these functions for small and large momenta.

Properties of the Functions $T_{\pm}(p_E^2)$

In the region of small momenta ($|p_E| \ll M_{\text{KK}}$), the functions $T_{\pm}(p_E^2)$ vary rapidly and in a way that is strongly dependent on the values of the bulk mass parameters c_{Q_i, q_i} . This is expected, because in this momentum range their behavior is dominated by the contributions of the SM quarks. Remarkably, at the special value $p_E = 0$ the results are given by the very simple expressions

$$T_+(0) = \sum_{q=u,d} \text{Tr} [\mathbf{X}_q \coth \mathbf{X}_q] \equiv t_0, \quad T_-(0) = 0, \quad (4.11)$$

which only depend on the 5D Yukawa couplings via the quantity \mathbf{X}_q defined in (2.78). In the neighborhood of this point the behavior is complicated and cannot be described by a simple formula. For larger values of the Euclidean momentum, such that $p_E \gg M_{\text{KK}}$, the function $T_+(p_E^2)$ converges toward a universal limiting value

$$T_+(p_E^2) = \sum_{q=u,d} \text{Tr} \left\{ \mathbf{X}_q \tanh 2\mathbf{X}_q + \frac{1}{2\hat{p}_E} \left[\frac{c_Q \mathbf{X}_q \tanh 2\mathbf{X}_q}{\cosh 2\mathbf{X}_q} + \frac{c_q \bar{\mathbf{X}}_q \tanh 2\bar{\mathbf{X}}_q}{\cosh 2\bar{\mathbf{X}}_q} \right] + \dots \right\}$$

$$\equiv t_1 + \frac{t_2}{\hat{p}_E} + \dots, \quad (M_{\text{KK}} \ll p_E \ll v|Y_q|/\eta) \quad (4.12)$$

while $T_-(p_E^2) = \mathcal{O}(\hat{p}_E^{-2})$ falls off more rapidly. To derive this result, we have taken the limit $\eta\hat{p}_E \rightarrow 0$ and used the asymptotic expansion in (3.115). A dependence on the bulk

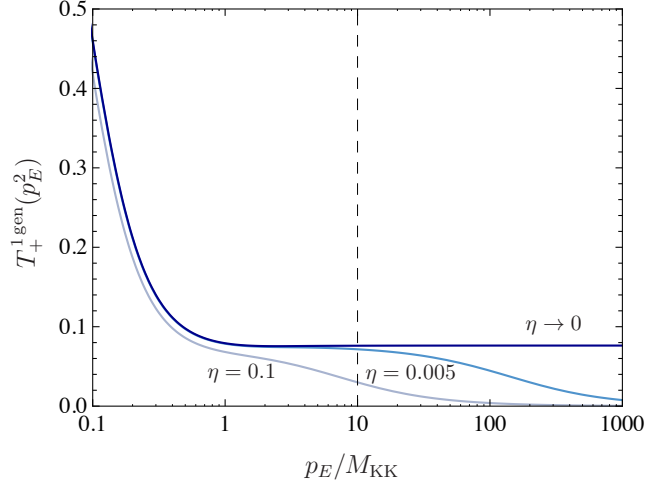


FIGURE 4.2: Momentum dependence of the propagator function $T_+(p_E^2)$ for the case of one fermion generation and parameters corresponding to the top quark. The three curves refer to different values of the regulator η , as indicated. The vertical dashed line indicates the value of the UV cutoff of the RS model (for $\Lambda_{\text{TeV}} = 10 M_{\text{KK}}$).

mass parameters enters only at subleading order. Interestingly, there is a third region of extremely large Euclidean momentum, $p_E \gg v|Y_q|/\eta$, for which the behavior changes once again, and the function $T_+(p_E^2)$ tends to zero according to

$$T_+(p_E^2) = \frac{1}{\eta \hat{p}_E} \sum_{q=u,d} \text{Tr} \mathbf{X}_q^2 + \mathcal{O}(\hat{p}_E^{-2}) \equiv \frac{t_3}{\eta \hat{p}_E} + \dots, \quad (p_E \gg v|Y_q|/\eta) \quad (4.13)$$

while still $T_-(p_E^2) = \mathcal{O}(\hat{p}_E^{-2})$. Note that in this region the loop momentum p_E exceeds the value of the intrinsic UV cutoff of a consistent RS model with a brane-localized Higgs sector, because condition (2.3) implies $\Lambda_{\text{TeV}} \ll v|Y_q|/\eta$. It can therefore only contribute if a bulk-Higgs field as defined in (2.4) is considered.

It is consequential of this discussion that the functions $T_{\pm}(p_E^2)$ have all the properties required for the integration by parts in (4.8). The exact momentum dependence of these functions is rather complicated as can be seen in Appendix A. Hence, we will instead discuss the simpler case of a single fermion generation, which exhibits all the relevant features mentioned above. In this case, the integral (4.10) reduces to the analytic expression

$$T_+^{1 \text{ gen}}(p_E^2) = \sum_{q=u,d} \frac{X_q^2}{S_q} \frac{k_1(\hat{p}_E) S_q \sinh 2S_q + k_2(\hat{p}_E) \eta \hat{p}_E \left(\cosh 2S_q - \frac{\sinh 2S_q}{2S_q} \right)}{k_1(\hat{p}_E) S_q (\cosh 2S_q - 1) + k_2(\hat{p}_E) \eta \hat{p}_E \sinh 2S_q + 2S_q}, \quad (4.14)$$

where S_q has been defined in (3.80), and we have used

$$k_1(\hat{p}_E) = 1 + R_q(\hat{p}_E) R_Q(\hat{p}_E) = 1 + \frac{Z_q(p_E^2)}{\tanh^2 S_q}, \quad k_2(\hat{p}_E) = R_q(\hat{p}_E) + R_Q(\hat{p}_E). \quad (4.15)$$

The function $T_-^{1 \text{ gen}}(p_E^2) = 0$ vanishes trivially. It is a simple exercise to derive the various limiting behaviors shown in (4.11)–(4.13) from (4.14), simplified to the one-generation case. Figure 4.2 shows the behavior of the result (4.14) for the parameter

choices $c_Q = -0.45$, $c_q = 0.395$, and $|Y_q| = 2.3$, which correspond to the physical mass $m_q = 172.6 \text{ GeV}$ of the top quark. The KK scale is set to $M_{\text{KK}} = 2 \text{ TeV}$, such that $X_q \approx 0.2$. The three curves correspond to different values of the regulator η . The three regions of Euclidean momenta mentioned above ($p_E/M_{\text{KK}} \sim 1$, $p_E/M_{\text{KK}} \gg 1$, and $p_E/M_{\text{KK}} \gg X_q/\eta$) are clearly visible from the plot. The dark and light blue curves correspond to models for which $\Lambda_{\text{TeV}}/M_{\text{KK}} \ll X_q/\eta$, and hence condition (2.3) defining a brane-localized Higgs field holds. The gray curve corresponds to the case of a narrow bulk Higgs, as defined in (2.4).

Analysis of the Loop Integrals $I_{\pm}(m^2)$

After we have clarified the properties of the function $T_{\pm}(m^2)$, the final goal is now to calculate the loop integrals $I_{\pm}(m^2)$ defined in (4.8) in the dimensional regularization scheme. For simplicity, however, we first consider the integral $I_+(0)$ at the special point $m^2 = 0$ and work with a hard momentum cutoff $\Lambda = \Lambda_{\text{TeV}}$. For the case of a brane-localized Higgs sector, defined according to condition (2.3), we obtain from (4.9)

$$I_+(0)|_{\text{brane Higgs}} = t_0 - t_1 - \frac{3t_2}{2} \frac{M_{\text{KK}}}{\Lambda_{\text{TeV}}} + \dots, \quad (4.16)$$

with t_0 and $t_{1,2}$ as defined in (4.11) and (4.12), respectively. The last term is a small threshold correction, which is present in a hard-cutoff scheme but will not be visible in the dimensional regularization scheme discussed below. Such power-suppressed terms can be included via higher-dimensional operators in the effective Lagrangian of the RS model. It will be commented more on the structure of power corrections and the role of higher-dimensional operators below.

The difference $(t_0 - t_1)$ coincides with the expression for the quantity $\Sigma_q^{(\text{CGHNP})}$ (summed over $q = u, d$) derived in [144] for the case of a brane-localized Higgs sector. It corresponds to the numerical result first derived in [149], where the authors summed up the first few KK modes. The same result would be obtained if one took the limit $\eta \rightarrow 0$ before performing the integral over the loop momentum. For the opposite case of a narrow bulk-Higgs field, defined according to condition (2.4), the UV cutoff is such that the quantity $T_+(\Lambda^2)$ in (4.9) must be evaluated using (4.13), so that we obtain

$$I_+(0)|_{\text{narrow bulk Higgs}} = t_0 - \frac{3t_3}{2} \frac{M_{\text{KK}}}{\eta \Lambda_{\text{TeV}}} + \dots \quad (4.17)$$

instead of (4.16). The two answers differ by an amount t_1 given by the first term on the right-hand side in (4.12). The term t_0 coincides with the expression for the quantity $\Sigma_q^{(\text{ATZ})}$ (summed over $q = u, d$) derived in [144], which corresponds to the result first obtained in [222]. In the latter reference, the authors summed up all modes (via a completeness relation) before the limit $\eta \rightarrow 0$ was taken. It should be emphasized that the threshold corrections are enhanced by a factor $1/\eta$ in this case. This provides an example of the general behavior for the case of a narrow bulk-Higgs field.

Let us now reproduce the above results in the less intuitive, but more consistent (from a mathematical point of view) dimensional regularization scheme. In this case the limit of a brane-localized Higgs sector can be taken without encountering any ambiguities. In order to demonstrate this, we will perform the integrals over p_E in (4.8) and then take the limit $\eta \rightarrow 0$, and show that this yields the same answer as first setting $\eta \rightarrow 0$ and then integrating over the loop momentum. However, the explicit result in (4.14)

and its generalization to three generations are so complicated that the dimensionally regularized integral cannot be evaluated in closed form. It is therefore more convenient to use a toy model, which captures all important features of the exact result. For this purpose, we study the function

$$T_+^{\text{model}}(p_E^2) = \frac{t_0 - t_1 - t_2}{1 + \hat{p}_E^2} + \frac{t_2}{\sqrt{1 + \hat{p}_E^2}} + \frac{t_3}{\sqrt{(t_3/t_1)^2 + (\eta \hat{p}_E)^2}}, \quad (4.18)$$

which exhibits the same asymptotic behavior in the three regions as the exact result. Evaluating the integrals in (4.8) for this function, we obtain

$$I_+^{\text{model}}(0) = (t_0 - t_1 - t_2) \left(\frac{\mu}{M_{\text{KK}}} \right)^{2\hat{\epsilon}} + t_2 \left(\frac{\mu}{2M_{\text{KK}}} \right)^{2\hat{\epsilon}} + t_1 \left(\frac{t_1}{2t_3} \right)^{2\hat{\epsilon}} \left(\frac{\mu\eta}{M_{\text{KK}}} \right)^{2\hat{\epsilon}} + \mathcal{O}(\hat{\epsilon}^2), \quad (4.19)$$

where $t_1/(2t_3) = 1 + \mathcal{O}(v^2/M_{\text{KK}}^2)$. At this point some comments must be made. While the first two contributions are associated with the scale M_{KK} , i.e. with low-lying KK modes, the third contribution is associated with the super-heavy scale M_{KK}/η , which for a brane-localized Higgs sector is larger than the physical UV cutoff of the RS model. Note that in the limit $\eta \rightarrow 0$ this contribution tends to zero, leaving $I_+^{\text{model}}(0) = (t_0 - t_1)$ as the final result for the integral after the UV regulator $\hat{\epsilon}$ has been removed, in accordance with (4.16). The same result is obtained if the limit $\eta \rightarrow 0$ is taken in (4.18) before the integral is evaluated. The last term in (4.18) then reduces to a constant, which does not contribute to (4.8). In the dimensional regularization scheme, the case of a narrow bulk Higgs, for which the loop momenta, corresponding to the very massive KK modes, can resolve the shape of the Higgs profile and give the very resonance contribution, is obtained by removing the UV regulator $\hat{\epsilon}$ at small but finite value of η . In this case, one finds $I_+^{\text{model}}(0) = t_0$, in accordance with (4.17). The disadvantage of the dimensional regularization is that there are now power corrections that hint on higher-dimensional operators spoiling the predictive power of the RS model.

Power Corrections and Higher-Dimensional Operators

Before we summarize the most important results of this section, it is necessary to comment on the size of generic power corrections, which can be described in terms of higher-dimensional operators added to the Lagrangian of the RS model (with unknown coefficients). In general, higher-dimensional operators can be constructed by inserting one or more (covariant) derivatives acting on the fields.² These operators are suppressed by the fundamental, physical UV cutoff of RS models, which is of order the Planck scale. The leading operators involving a fermion bilinear contain a single derivative, possibly accompanied by a factor $\text{sgn}(\phi)$. It is therefore reasonable to study the object

$$\frac{1}{M_{\text{Pl}}} E_a^M iD_M \gamma^a = \frac{1}{M_{\text{Pl}}} \left(e^{\sigma(\phi)} i\hat{\not{\partial}} - \frac{1}{r} \gamma_5 \partial_\phi \right) + \text{terms containing gauge fields}, \quad (4.20)$$

where $\gamma^a = \{\gamma^\mu, i\gamma_5\}$ are the 5D Dirac matrices and E_a^M denotes the vielbein, already used in (1.70) and (1.72), respectively. From now on, we focus on the derivative terms only. Changing variables from ϕ to t , and using the definition of the warped UV cutoff

²Note that the 5D Lagrangian does not contain any small mass parameters, which could be used to construct non-derivative operators of higher dimension.

in (1.101), we obtain

$$\frac{1}{M_{\text{Pl}}^2} E_a^M iD_M \gamma^a = \frac{1}{\Lambda_{\text{UV}}(t)} (i\cancel{\partial} - \gamma_5 M_{\text{KK}} \partial_t) + \dots \quad (4.21)$$

Operators containing more than one derivative contain similar structures. For example, the 5D d'Alembertian can be written as

$$\frac{1}{M_{\text{Pl}}^2} \square_5 = \frac{e^{2\sigma(\phi)}}{M_{\text{Pl}}^2} \left(\square_4 - \frac{e^{-2\sigma(\phi)}}{r^2} \partial_\phi^2 \right) = \frac{1}{\Lambda_{\text{UV}}^2(t)} \left(\square_4 - M_{\text{KK}}^2 \frac{1}{t} \partial_t t \partial_t \right). \quad (4.22)$$

Several comments are in order. First, we note that higher-derivative operators in the effective Lagrangian are indeed suppressed by the position-dependent UV cutoff $\Lambda_{\text{UV}}(t)$, as stated in Section 2.1. If we consider power corrections to couplings involving the Higgs boson (no matter whether the Higgs field is localized on or near the IR brane), the corresponding cutoff scale is Λ_{TeV} . The 4D derivatives contained in (4.21) and (4.22) will produce powers of external momenta or masses of the various fermion modes, where the corresponding terms scale like $(M_{\text{KK}}/\Lambda_{\text{TeV}})^n$. For models in which the Higgs field is a generic bulk scalar (with width $\eta \sim 1$) or a brane-localized field, derivatives ∂_t acting on the fields near $t = 1$ produce $\mathcal{O}(1)$ factors. This is due to the fact that the wave functions are naturally expressed in terms of the t variable, typically involving Bessel functions of argument $x_n t$ with $x_n = m_n/M_{\text{KK}}$, or powers of t in the case of the SM fermions. (Recall that for a brane-localized Higgs field, these derivatives must be evaluated at $t = 1^-$, i.e. by approaching the IR brane from the left.) Hence, the ∂_t terms in the derivative operators shown above also give rise to $(M_{\text{KK}}/\Lambda_{\text{TeV}})^n$ corrections. The situation changes if we consider a limit of a bulk-Higgs model in which the width η of the Higgs profile becomes parametrically suppressed. Then the Higgs profile itself, as well as the profiles of particles coupling to the Higgs field, change rapidly over a small interval of width η near the IR brane, see Figure 2.1. In such a scenario, a derivative ∂_t acting on the Higgs field or any field coupling to the Higgs boson gives rise to a factor $1/\eta$, and hence the corresponding power corrections scale like $(M_{\text{KK}}/\eta\Lambda_{\text{TeV}})^n$. This is the reason for the appearance of the Higgs width η in (4.17).

Intermediate Summary

At this point, it is convenient to repeat and highlight some important results just derived. We have seen that the results obtained under the two assumptions (2.3) and (2.4) are rather different, both qualitatively and quantitatively. While the low-lying KK modes give the dominate contribution to the gluon-fusion Higgs production process in the former case, a significant contribution stemming from very massive KK modes can be observed in the latter case. Indeed, one should consider the two scenarios as two different, distinguishable realizations of RS models. This fact has also been realized in [226]. This situation resembles that encountered when one compares the original RS model, in which only gravity was allowed to propagate in the extra dimension while all SM fields were confined to the IR brane [115], with the more popular models in which all matter and gauge fields live in the bulk [168]. As already stressed in Subsection 1.4.4, the original model only addressed the hierarchy problem, while the latter models are qualitatively different, since they also provide successful theories of flavor.

Model	bulk Higgs	narrow bulk Higgs	transition region	brane Higgs
Higgs width	$\eta = \mathcal{O}(1)$	$\frac{v Y_q }{\Lambda_{\text{TeV}}} \ll \eta \ll \frac{v Y_q }{M_{\text{KK}}}$	$\eta \sim \frac{v Y_q }{\Lambda_{\text{TeV}}}$	$\eta \ll \frac{v Y_q }{\Lambda_{\text{TeV}}}$
Power cors.	$\left(\frac{M_{\text{KK}}}{\Lambda_{\text{TeV}}}\right)^n$	$\left(\frac{M_{\text{KK}}}{\eta\Lambda_{\text{TeV}}}\right)^n$ $\frac{M_{\text{KK}}}{\Lambda_{\text{TeV}}} \frac{M_{\text{KK}}}{v Y_q } \ll \frac{M_{\text{KK}}}{\eta\Lambda_{\text{TeV}}} \ll \frac{M_{\text{KK}}}{v Y_q }$	$\left(\frac{M_{\text{KK}}}{v Y_q }\right)^n$	$\left(\frac{M_{\text{KK}}}{\Lambda_{\text{TeV}}}\right)^n$
Higgs profile	resolved by all modes	resolved by high-mom. modes	partially resolved by high-mom. modes	not resolved
$\mathcal{A}(gg \rightarrow h)$	enhanced	enhanced	not calculable	suppressed
Result	model-dep.	model-indep.	unreliable	model-indep.

TABLE 4.1: Comparison of the main features of various versions of the RS model (see text for further explanation). The label “model-independent result” means that the corrections to the SM prediction for the Higgs production cross section can be calculated (to excellent approximation) without any reference to the Higgs and fermion bulk profiles.

While the width of the Higgs profile is a physical parameter, which in principle can be adjusted to take any desired value, the transition from the narrow bulk-Higgs scenario (2.4) to the brane-Higgs scenario (2.3) cannot be described in a controlled analytical way. This fact can be understood by investigating the structures of the corresponding effective theories in more detail. Table 4.1 summarizes the main features of the various models as defined by the size of the width parameter η . The second row in the table shows the scaling of power corrections, as represented by higher-dimensional operators in the effective Lagrangian of the RS model. Both in a generic bulk-Higgs model (with $\eta = \mathcal{O}(1)$) and in models where the scalar sector is localized on the IR brane, effects of higher-dimensional operators in Higgs physics are suppressed by powers of the ratio $M_{\text{KK}}/\Lambda_{\text{TeV}}$, since, as explained earlier, the warped Planck scale Λ_{TeV} is the natural UV cutoff of these theories. The situation changes if one considers bulk-Higgs models, in which the width parameter η is parametrically suppressed. Then the effective theory knows about an extra small parameter, and derivatives ∂_t acting on the bulk scalar field can produce powers of $1/\eta$. As we have just seen, this gives rise to a class of enhanced power corrections scaling like $(M_{\text{KK}}/\eta\Lambda_{\text{TeV}})^n$. In the transition region between the narrow bulk-Higgs and brane-localized Higgs scenarios, these enhanced power corrections become of $\mathcal{O}(1)$ or larger, and hence the effective field-theory approach breaks down. In other words, because of the uncontrolled behavior of power-suppressed terms in the transition region, one lacks the analytical control over the theory, which would be required to see how the results interpolate from the bulk-Higgs case to the brane-Higgs scenario as one reduces the value of η . In [222], the authors computed the hgg amplitude in the context of a bulk-Higgs model and took the limit $\eta \rightarrow 0$ at the end of their calculation, stating that the answer corresponds to the case of a brane-localized Higgs. As just argued, such an approach gives the correct result in the model (2.4), and it should be referred to as the result of the narrow bulk-Higgs scenario.

Note that the above remarks describe an idealized case, in which the electroweak scale $v|Y_q|$ and the KK mass scale M_{KK} are of comparable magnitude. In practice, due to the lack of KK modes below the TeV scale, there appears to be a little hierarchy between these scales, such that $v|Y_q|/M_{\text{KK}} \lesssim 0.3$ or less. Then the power corrections in the transition region are even larger than $\mathcal{O}(1)$, and also in the narrow bulk-Higgs case the lower bound on $M_{\text{KK}}/\eta\Lambda_{\text{TeV}}$ cannot be much smaller than 1. In view of this

fact, one must consider the results derived for the narrow bulk-Higgs case with some caution. A more reliable calculation should stay in a regime where $\eta = \mathcal{O}(1)$. This has the disadvantage that the results will depend on the shapes of the Higgs and fermion profiles in a complicated way. If it turns out that this dependence is weak, however, then the results obtained here for the narrow bulk-Higgs scenario might serve as reasonable approximations.

Final Expressions for the Loop Integrals

We are now all set to present the final expressions for the loop integrals. According to the discussion above, it is possible to take the limit $\eta \rightarrow 0$ at the level of the functions $T_{\pm}(p_E^2)$, before the loop integral is performed. Using (4.10) and sending $\eta \rightarrow 0$, we find

$$\begin{aligned} T_+(p_E^2) &= \sum_{q=u,d} \text{Tr} \left\{ \frac{2\mathbf{X}_q}{\sinh 2\mathbf{X}_q} \left[\sinh^2 \mathbf{X}_q + \frac{1}{2} \left(\frac{\mathbf{Z}_q(p_E^2)}{1 + \mathbf{Z}_q(p_E^2)} + \frac{\mathbf{Z}_q^\dagger(p_E^2)}{1 + \mathbf{Z}_q^\dagger(p_E^2)} \right) \right] \right\}, \\ T_-(p_E^2) &= \sum_{q=u,d} \text{Tr} \left\{ \frac{2\mathbf{X}_q}{\sinh 2\mathbf{X}_q} \left[\frac{1}{2i} \left(\frac{\mathbf{Z}_q(p_E^2)}{1 + \mathbf{Z}_q(p_E^2)} - \frac{\mathbf{Z}_q^\dagger(p_E^2)}{1 + \mathbf{Z}_q^\dagger(p_E^2)} \right) \right] \right\}, \end{aligned} \quad (4.23)$$

where the quantity $\mathbf{Z}_q(p_E^2)$ has been defined in (3.98) with the usual Yukawa matrices in the minimal model and the ratio given in (3.99). Any reference to the matrices $\bar{\mathbf{X}}_q$ in the final expressions has been removed by using the identities $\mathbf{Y}_q f(\bar{\mathbf{X}}_q) = f(\mathbf{X}_q) \mathbf{Y}_q$ and $f(\bar{\mathbf{X}}_q) \mathbf{Y}_q^\dagger = \mathbf{Y}_q^\dagger f(\mathbf{X}_q)$, which hold for an arbitrary function $f(\mathbf{X}_q)$ that has a non-singular expansion in powers of \mathbf{X}_q^2 .

The derivation of the final expressions for the loop integrals in (4.8) is now straightforward. The quantities $T_{\pm}(-m^2 - i0)$ computed using (4.23) replace the quantity t_0 in (4.16), (4.17), and (4.19), while t_1 has already been given in (4.12). Removing the UV regulator after the integral over the loop momentum has been performed, we obtain

$$\begin{aligned} I_+(m^2) &= \sum_{q=u,d} \left\{ \text{Tr} g(\mathbf{X}_q) + \frac{1}{2} \text{Tr} \left[\frac{2\mathbf{X}_q}{\sinh 2\mathbf{X}_q} \left(\frac{\mathbf{Z}_q(-m^2)}{1 + \mathbf{Z}_q(-m^2)} + \frac{\mathbf{Z}_q^\dagger(-m^2)}{1 + \mathbf{Z}_q^\dagger(-m^2)} \right) \right] \right\}, \\ I_-(m^2) &= \sum_{q=u,d} \frac{1}{2i} \text{Tr} \left[\frac{2\mathbf{X}_q}{\sinh 2\mathbf{X}_q} \left(\frac{\mathbf{Z}_q(-m^2)}{1 + \mathbf{Z}_q(-m^2)} - \frac{\mathbf{Z}_q^\dagger(-m^2)}{1 + \mathbf{Z}_q^\dagger(-m^2)} \right) \right], \end{aligned} \quad (4.24)$$

where $m^2 \equiv m^2 + i0$, and the function

$$g(\mathbf{X}_q) \Big|_{\text{brane Higgs}} = \mathbf{X}_q \tanh \mathbf{X}_q - \mathbf{X}_q \tanh 2\mathbf{X}_q = -\frac{\mathbf{X}_q \tanh \mathbf{X}_q}{\cosh 2\mathbf{X}_q} = -\mathbf{X}_q^2 + \dots \quad (4.25)$$

obeys a non-singular series expansions in powers of $\mathbf{X}_q^2 = \frac{v^2}{2M_{\text{KK}}^2} \mathbf{Y}_q \mathbf{Y}_q^\dagger$. Note that due to the presence of strong-interaction phases arising from the analytic continuation from a Euclidean momentum p_E^2 to $-m^2 - i0$, the functions $I_{\pm}(m^2)$ cannot simply be written in terms of the real and imaginary parts of a traces over matrices. One may ask what changes in the narrow bulk-Higgs scenario. In this case, the subtraction term t_1 is absent according to the discussion between (4.16) and (4.17). The expressions in (4.24) remain valid also in this case, provided we use

$$g(\mathbf{X}_q) \Big|_{\text{narrow bulk Higgs}} = \mathbf{X}_q \tanh \mathbf{X}_q = \mathbf{X}_q^2 + \dots \quad (4.26)$$

The above equations are the main result of this section. Up to some small corrections to be determined below, the first term on the right-hand side of the equation for $I_+(m^2)$ corresponds to the contribution of the infinite tower of KK quarks to the ggh amplitude. The remaining terms describe the contributions of the SM quarks. For the case of a brane-localized Higgs sector, the function $g(\mathbf{X}_q)$ coincides with an expression first obtained in [144] by means of a conjecture. Here, we have achieved to derive this form. For the case of a narrow bulk-Higgs field, the expansion of $g(\mathbf{X}_q)$ to $\mathcal{O}(\mathbf{X}_q^2)$ reproduces the result derived in [222]. This demonstrates that the ‘‘brane-Higgs limit’’ considered in that paper really corresponds to the case of a narrow bulk scalar, as defined in (2.4).

Note that in the case of a brane-localized scalar sector the dependence on t inside the square brackets in (4.10) disappears, due to the identity $\mathcal{C}^2(t) - \mathcal{S}^2(t) = 1$. This motivates an alternative derivation of the result (4.24), where we derive the functions $T_{\pm}(p_E^2)$ defined in (4.6) in the brane-localized Higgs case via

$$T_+(p_E^2)|_{\text{brane Higgs}} = \sum_{q=u,d} \frac{-v}{\sqrt{2}} \text{Tr} \left[\begin{pmatrix} 0 & \mathbf{Y}_q \\ \mathbf{Y}_q^\dagger & 0 \end{pmatrix} \frac{\Delta_{RL}^q(1^-, 1^-; p_E^2) + \Delta_{LR}^q(1^-, 1^-; p_E^2)}{2} \right], \quad (4.27)$$

and similarly for $T_-(p_E^2)$. The derivation of the corresponding propagator functions Δ_{AB}^q has been shown in Section 3.2.4. Inserting these results into (4.27) reproduces the expressions given in (4.24). This method provides an independent derivation of the result for the brane-localized Higgs case, in which the notion of a regulator η never appears. The important point here is that by using this procedure one finds the result (4.24) without any UV regulation of the momentum integral (4.8). The regulator is only necessary to obtain a gauge-invariant result according to the discussion at the beginning of this section.

Analysis of the Zero-Mode Contributions

We will now analyze the terms involving the matrices \mathbf{Z}_q in (4.24), which include the contributions of the SM quarks, in more detail using results derived in Section 2.2. We first note the eigenvalue equation determining the KK masses (2.83) can be written as

$$\det[1 + \mathbf{Z}_q(-m_n^2)] = 0. \quad (4.28)$$

The asymptotic expansion for \mathbf{R}_A in (3.115) introduces the fermion profiles $F(\mathbf{c}_A)$ next to the modified Yukawa matrices. We can then reexpress the answer in terms of the effective Yukawa matrices defined in (2.103). Including also the subleading terms in the expansion (3.115), we obtain

$$\mathbf{Z}_q(p_E^2) = F^{-1}(\mathbf{c}_Q) \mathbf{U}_q \left[\frac{\mathbf{m}_{q,0}^2}{p_E^2} + \left(\delta_Q + \mathbf{m}_{q,0} \delta_q \mathbf{m}_{q,0}^{-1} \right) + \dots \right] \mathbf{U}_q^\dagger F(\mathbf{c}_Q), \quad (4.29)$$

where

$$\begin{aligned} \delta_Q &= \mathbf{x}_q \mathbf{W}_q^\dagger \left[\frac{1}{1 - 2\mathbf{c}_q} \left(\frac{1}{F^2(\mathbf{c}_q)} - 1 + \frac{F^2(\mathbf{c}_q)}{3 + 2\mathbf{c}_q} \right) \right] \mathbf{W}_q \mathbf{x}_q, \\ \delta_q &= \mathbf{x}_q \mathbf{U}_q^\dagger \left[\frac{1}{1 - 2\mathbf{c}_Q} \left(\frac{1}{F^2(\mathbf{c}_Q)} - 1 + \frac{F^2(\mathbf{c}_Q)}{3 + 2\mathbf{c}_Q} \right) \right] \mathbf{U}_q \mathbf{x}_q \end{aligned} \quad (4.30)$$

with $\mathbf{x}_q = \mathbf{m}_{q,0}/M_{\text{KK}}$ and $\mathbf{U}_q, \mathbf{W}_q$ defined in (2.106), are hermitian matrices giving rise to some small corrections of order v^2/M_{KK}^2 . Except for the two entries proportional

to $m_{u_3}^2 = m_t^2$ they carry an additional strong chiral suppression [145]. Introducing the abbreviation $\boldsymbol{\varepsilon}_q = \boldsymbol{\delta}_Q + \mathbf{m}_{q,0} \boldsymbol{\delta}_q \mathbf{m}_{q,0}^{-1}$, and working to first order in v^2/M_{KK}^2 , the eigenvalue equation (4.28) can be rewritten in the form

$$\det[m_n^2 - \mathbf{m}_{q,0}^2 (1 - \boldsymbol{\varepsilon}_q) + \dots] = 0, \quad (4.31)$$

whereas

$$\frac{\mathbf{Z}_q(p_E^2)}{1 + \mathbf{Z}_q(p_E^2)} = F^{-1}(\mathbf{c}_Q) \mathbf{U}_q \left[\boldsymbol{\varepsilon}_q + \frac{(1 - \boldsymbol{\varepsilon}_q) \mathbf{m}_{q,0}^2 (1 - \boldsymbol{\varepsilon}_q)}{p_E^2 + \mathbf{m}_{q,0}^2 (1 - \boldsymbol{\varepsilon}_q)} + \dots \right] \mathbf{U}_q^\dagger F(\mathbf{c}_Q). \quad (4.32)$$

Only the diagonal elements of the matrices $\boldsymbol{\varepsilon}_q$ contribute when (4.31) and traces of (4.32) are evaluated to first order in v^2/M_{KK}^2 . It is then not difficult to show that the masses of the SM quarks are given by

$$m_{q_i}^2 = m_{q_i,0}^2 (1 - \varepsilon_{q_i} + \dots), \quad \text{with} \quad \varepsilon_{q_i} \equiv (\boldsymbol{\varepsilon}_q)_{ii} = (\boldsymbol{\delta}_Q)_{ii} + (\boldsymbol{\delta}_q)_{ii}, \quad (4.33)$$

where the dots represent terms of order v^4/M_{KK}^4 and higher. Moreover, using (4.32) and $\sinh 2x/2x = 1 + 2x^2/3 + \mathcal{O}(x^4)$, it is straightforward to derive

$$\sum_{q=u,d} \text{Tr} \left[\frac{2\mathbf{X}_q}{\sinh 2\mathbf{X}_q} \frac{\mathbf{Z}_q(p_E^2)}{1 + \mathbf{Z}_q(p_E^2)} \right] = \sum_i \left[\kappa_{q_i} \frac{m_{q_i}^2}{m_{q_i}^2 + p_E^2} + \varepsilon_{q_i} \right] + \dots, \quad (4.34)$$

where

$$\kappa_{q_i} = 1 - \varepsilon_{q_i} - \frac{2}{3} \left[\mathbf{U}_q^\dagger F(\mathbf{c}_Q) \mathbf{X}_q^2 F^{-1}(\mathbf{c}_Q) \mathbf{U}_q \right]_{ii}. \quad (4.35)$$

Note that while the parameters κ_{q_i} are in general complex, the quantities ε_{q_i} are real. Although the sum in (4.34) extends over all six SM quarks, in practice the contributions of the light quarks can safely be neglected. For the third-generation quarks, we find that

$$\kappa_t = 1 - \varepsilon_t - \frac{v^2}{3M_{\text{KK}}^2} \frac{(\mathbf{Y}_u \mathbf{Y}_u^\dagger \mathbf{Y}_u)_{33}}{(\mathbf{Y}_u)_{33}}, \quad (4.36)$$

up to chirally-suppressed terms, and a corresponding formula holds for κ_b . This expression coincides with the result derived in [144].

It is now a simple exercise to evaluate the Wilson coefficients C_{1g} and C_{5g} using (4.7) and we obtain

$$\begin{aligned} C_{1g} &= \sum_{q=u,d} \text{Tr} [g(\mathbf{X}_q) + \boldsymbol{\varepsilon}_q] + \sum_i \text{Re}(\kappa_{q_i}) A_q(\tau_i) + \dots \\ &\approx \text{Tr} g(\mathbf{X}_u) + \text{Tr} g(\mathbf{X}_d) + \left[1 - \frac{v^2}{3M_{\text{KK}}^2} \text{Re} \frac{(\mathbf{Y}_u \mathbf{Y}_u^\dagger \mathbf{Y}_u)_{33}}{(\mathbf{Y}_u)_{33}} \right] A_q(\tau_t) + A_q(\tau_b), \quad (4.37) \\ C_{5g} &= \sum_i \text{Im}(\kappa_{q_i}) B_q(\tau_i) + \dots \approx -\frac{v^2}{3M_{\text{KK}}^2} \text{Im} \left[\frac{(\mathbf{Y}_u \mathbf{Y}_u^\dagger \mathbf{Y}_u)_{33}}{(\mathbf{Y}_u)_{33}} \right] B_q(\tau_t), \end{aligned}$$

where $\tau_i = 4m_{q_i}^2/m_h^2 - i0$, and the parameter integrals evaluate to [227, 228]

$$A_q(\tau) = \frac{3\tau}{2} \left[1 + (1 - \tau) \arctan^2 \frac{1}{\sqrt{\tau - 1}} \right], \quad B_q(\tau) = \tau \arctan^2 \frac{1}{\sqrt{\tau - 1}}. \quad (4.38)$$

For the light SM quarks, these functions must be analytically continued to $\tau < 1$. They both approach 1 for $\tau \rightarrow \infty$. The final results presented in (4.37) are exact up to small corrections of order v^4/M_{KK}^4 , represented by the dots, which are numerically insignificant. The leading effects, which involve traces over functions of Yukawa matrices and thus increase with the number of fermion generations, are exact to all orders in v^2/M_{KK}^2 . The infinite sum over KK quark states contributes the trace term in the expression for C_{1g} , while the second term contains the sum over the contributions of the SM (third-generation) quarks, whose Yukawa interactions are modified with respect to the SM by factors κ_{q_i} .

In the final, approximate expressions it has been used that all ε_{q_i} parameters other than ε_t can be neglected to a very good approximation. For the term proportional to ε_t we can neglect the small deviation of the function $A_q(\tau_t) \approx 1.03$ from 1. Also, for the small b -quark contribution, the small deviation of κ_b from 1 is negligible. Note that, in this approximation, which is accurate to better than 1% for $M_{\text{KK}} \gtrsim 2 \text{ TeV}$, the Wilson coefficients C_{1g} and C_{5g} become independent of the bulk mass parameters c_{Q_i, q_i} . They are entirely given in terms of the 5D Yukawa matrices of the RS model. In the SM, we have $C_{1g}^{\text{SM}} = A_q(\tau_t) + A_q(\tau_b)$ and $C_{5g}^{\text{SM}} = 0$.

Brane-Localized Higgs Sector with Different Yukawa Matrices

Before closing this section, we return to the generalization of the RS model with a brane-localized Higgs sector in which one allows for different Yukawa matrices \mathbf{Y}_q^C and $\mathbf{Y}_q^{S\dagger}$ in the Yukawa interactions, see (2.126) and (3.108). We will refer to this model as *type-II brane-Higgs* scenario. Recall that this generalization is only allowed if the Higgs boson is localized on the IR brane due to 5D Poincaré invariance. At the level of the gluon fusion amplitude (4.4), the above modification is implemented by the substitution

$$\frac{1}{\sqrt{2}} \begin{pmatrix} 0 & \mathbf{Y}_q \\ \mathbf{Y}_q^\dagger & 0 \end{pmatrix} \rightarrow \frac{1}{\sqrt{2}} \begin{pmatrix} 0 & \mathbf{Y}_q^C \\ \mathbf{Y}_q^{S\dagger} & 0 \end{pmatrix} P_R + \frac{1}{\sqrt{2}} \begin{pmatrix} 0 & \mathbf{Y}_q^S \\ \mathbf{Y}_q^{C\dagger} & 0 \end{pmatrix} P_L, \quad (4.39)$$

and we have to use the propagator solution derived in Section 3.2.4. Since the new matrices (3.111) are now non-hermitian, the master formulae (4.24) must be generalized to read

$$\begin{aligned} I_+(m^2) &= \sum_{q=u,d} \left\{ \text{Re Tr } g(\mathbf{Y}_q^C, \mathbf{Y}_q^S) \right. \\ &\quad \left. + \frac{1}{2} \text{Tr} \left[\frac{2\mathbf{X}_q}{\sinh 2\mathbf{X}_q} \frac{\mathbf{Z}_q(-m^2)}{1 + \mathbf{Z}_q(-m^2)} + \frac{2\mathbf{X}_q^\dagger}{\sinh 2\mathbf{X}_q^\dagger} \frac{\mathbf{Z}_q^\dagger(-m^2)}{1 + \mathbf{Z}_q^\dagger(-m^2)} \right] \right\}, \\ I_-(m^2) &= \sum_{q=u,d} \left\{ \text{Im Tr } g(\mathbf{Y}_q^C, \mathbf{Y}_q^S) \right. \\ &\quad \left. + \frac{1}{2i} \text{Tr} \left[\frac{2\mathbf{X}_q}{\sinh 2\mathbf{X}_q} \frac{\mathbf{Z}_q(-m^2)}{1 + \mathbf{Z}_q(-m^2)} - \frac{2\mathbf{X}_q^\dagger}{\sinh 2\mathbf{X}_q^\dagger} \frac{\mathbf{Z}_q^\dagger(-m^2)}{1 + \mathbf{Z}_q^\dagger(-m^2)} \right] \right\}, \end{aligned} \quad (4.40)$$

where

$$g(\mathbf{Y}_q^C, \mathbf{Y}_q^S) \Big|_{\text{brane Higgs}}^{\text{type-II}} = -\frac{2\mathbf{X}_q}{\sinh 2\mathbf{X}_q} \frac{\frac{v^2}{2M_{\text{KK}}^2} \tilde{\mathbf{Y}}_q \tilde{\mathbf{Y}}_q^\dagger}{1 + \frac{v^2}{2M_{\text{KK}}^2} \tilde{\mathbf{Y}}_q \tilde{\mathbf{Y}}_q^\dagger} = -\frac{v^2}{2M_{\text{KK}}^2} \mathbf{Y}_q^C \mathbf{Y}_q^{C\dagger} + \dots \quad (4.41)$$

Finally, in the formulae for κ_t in (4.36) one must replace the combination

$$\frac{(\mathbf{Y}_u \mathbf{Y}_u^\dagger \mathbf{Y}_u)_{33}}{(\mathbf{Y}_u)_{33}} \rightarrow \frac{(\mathbf{Y}_u^C \mathbf{Y}_u^{S\dagger} \mathbf{Y}_u^C)_{33}}{(\mathbf{Y}_u^C)_{33}}. \quad (4.42)$$

Note that because \mathbf{X}_q is no longer a positive hermitian matrix, traces of \mathbf{X}_q^n can now have arbitrary phases. However, at leading order in the expansion in v^2/M_{KK}^2 the trace of the function $g(\mathbf{Y}_q^C, \mathbf{Y}_q^S)$ is a negative real number. Indeed, at this order there is no difference between the result (4.41) and the original result in (4.25) valid for the brane-Higgs scenario with $\mathbf{Y}_q^C = \mathbf{Y}_q^S$.

An interesting special case is that where $\mathbf{Y}_q^S = 0$, meaning that the Yukawa couplings involving a product of two Z_2 -odd fields, given by the second term in the last line of (2.66), is put to zero. This choice was frequently adopted in the literature. It corresponds to taking the limit $\mathbf{X}_q \rightarrow 0$ in the results above, in which case $\tilde{\mathbf{Y}}_q \rightarrow \mathbf{Y}_q^C$, and the quantities κ_{q_i} in (4.35) reduce to $\kappa_{q_i} = 1 - \varepsilon_{q_i}$. It follows that in this particular model one obtains

$$\begin{aligned} C_{1g} &= \sum_{q=u,d} \text{Tr} [g(\mathbf{Y}_q^C, 0) + \varepsilon_q] + \sum_i (1 - \varepsilon_{q_i}) A_q(\tau_i) + \dots \\ &\approx C_{1g}^{\text{SM}} + [1 - A_q(\tau_t)] \varepsilon_t + \varepsilon_b - \frac{v^2}{2M_{\text{KK}}^2} \text{Tr} [\mathbf{Y}_u^C \mathbf{Y}_u^{C\dagger} + \mathbf{Y}_d^C \mathbf{Y}_d^{C\dagger}], \end{aligned} \quad (4.43)$$

whereas $C_{5g} = 0$. The first term in the first line is the result of the summation over the KK tower of quark states, while the second term gives the contributions of the SM quarks, whose Yukawa couplings are modified with respect to their values in the SM by factors $(1 - \varepsilon_{q_i})$. It suffices for all practical purposes to keep only the terms shown in the second line. Apart from the last term, they agree with a corresponding result presented in [157]. The first two corrections to the SM result are numerically very small, because $1 - A_q(\tau_t) \approx -0.03$ and the quantity ε_b is chirally suppressed. The third correction, which arises from the infinite sum over KK states, gives the most dominant contribution by far. This effect was not found in [222], because in this paper the brane-Higgs case was derived by taking a limit of a bulk-Higgs result. If one formally introduces two different Yukawa matrices in the narrow bulk-Higgs scenario, one indeed finds that $g(\mathbf{X}_q)$ defined in (4.26) vanishes in the limit where $\mathbf{Y}_q^S \rightarrow 0$. However, in the context of a bulk Higgs model taking \mathbf{Y}_q^S different from \mathbf{Y}_q^C violates 5D Lorentz invariance, and moreover (as explained several times) the brane-Higgs case cannot be derived by taking a limit of the bulk-Higgs results.

In practice, the corrections to the gluon fusion amplitude found in the type-II brane-Higgs scenario are numerically very similar to those obtained in the original brane-Higgs model. The main difference is a slightly larger spread of the distribution of points obtained when one scans the parameter space of the model. In the phenomenological analysis in Chapter 5, we will thus restrict ourselves to study the case where $\mathbf{Y}_q^C = \mathbf{Y}_q^S$.

4.1.4 Impact of Higher-Dimensional $|\Phi|^2(G_{\mu\nu}^a)^2$ Operators

Recall that RS models must be considered as effective field theories, valid below a (position-dependent) UV cutoff given by the warped Planck scale. The UV completion of these models may be strongly coupled, for instance due to effects of quantum gravity. As explained in Subsection 1.4.2, short-distance contributions from physics above the

cutoff scale give rise to higher-dimensional operators, such as those studied briefly in Subsection 4.1.3. Two particularly interesting higher-dimensional operators relevant for Higgs production are $\Phi^\dagger \Phi \mathcal{G}_{MN}^a \mathcal{G}^{MN,a}$ and $\Phi^\dagger \Phi \mathcal{G}_{MN}^a \tilde{\mathcal{G}}^{MN,a}$, which mediate effective hgg couplings at tree level. This subsection will address the question of how important the contributions of these operators are in the low-energy effective theory. We will focus on the first operator for concreteness.

In the RS model with the scalar sector localized on the IR brane, the relevant effective action is

$$S_{\text{eff}} = \int d^4x r \int_{-\pi}^{\pi} d\phi c_{\text{eff}} \delta(|\phi| - \pi) \frac{\Phi^\dagger \Phi}{\Lambda_{\text{TeV}}^2} \frac{g_{s,5}^2}{4} \mathcal{G}_{\mu\nu}^a \mathcal{G}^{\mu\nu,a} + \dots, \quad (4.44)$$

where terms involving $\mathcal{G}_{\mu 5}^a$ will be ignored. Here, $g_{s,5}$ is the five-dimensional strong coupling, which is related to the coupling g_s of the SM by (2.13). The natural UV cutoff governing the suppression of the brane-localized higher-dimensional operator is Λ_{TeV} . NDA suggests that the dimensionless coupling c_{eff} could be as large as $\mathcal{O}(1)$ if the UV completion above the cutoff of the RS model is strongly coupled. In the absence of a complete model, it is impossible to say how c_{eff} might depend on other parameters, such as the Yukawa couplings or the number of fermion generations. Even in a strongly-coupled theory, it is possible that c_{eff} could be significantly smaller than 1,³ for instance because the effective degrees of freedom coupling the Higgs boson to two gluons can only be pair-produced, or because they have suppressed couplings to the operators $\Phi^\dagger \Phi$ or $\mathcal{G}_{\mu\nu}^a \mathcal{G}^{\mu\nu,a}$. Following common practice, it shall be assumed that taking $c_{\text{eff}} = \mathcal{O}(1)$ provides a conservative upper bound for the effect of the brane-localized operators on the gluon fusion amplitude.

Using the KK decomposition of the gluon field,

$$\mathcal{G}_{\mu\nu}^a(x, \phi) = \frac{1}{\sqrt{r}} \sum_n G_{\mu\nu}^{(n)a}(x) \chi_n^G(\phi) = \frac{1}{\sqrt{2\pi r}} G_{\mu\nu}^a(x) + \text{KK modes}, \quad (4.45)$$

where the zero mode (the SM gluon $G_{\mu\nu}^a \equiv G_{\mu\nu}^{(0)a}$) has a flat profile along the extra dimension, and writing the scalar doublet in the standard form (2.9), we find that the relevant terms in the action (4.44) give rise to the effective Lagrangian

$$\mathcal{L}_{\text{eff}} = \frac{c_{\text{eff}}}{\Lambda_{\text{TeV}}^2} \mathcal{O}_{\text{eff}}, \quad (4.46)$$

where

$$\mathcal{O}_{\text{eff}} = \Phi^\dagger \Phi \frac{g_s^2}{4} G_{\mu\nu}^a G^{\mu\nu,a} \ni \frac{g_s^2 v^2}{8} \left(1 + \frac{h(x)}{v}\right)^2 G_{\mu\nu}^a G^{\mu\nu,a}. \quad (4.47)$$

We now repeat this analysis for an RS model in which the Higgs field lives in the bulk of the extra dimension. In this case the higher-dimensional operator can be localized on both the IR and UV branes, or it can live in the bulk. We thus consider the general action

$$S_{\text{eff}} = \int d^4x r \int_{-\pi}^{\pi} d\phi \left[c_1 + c_2 \delta(|\phi| - \pi) + c_3 \delta(\phi) \right] \frac{\Phi^\dagger \Phi}{M_{\text{Pl}}^2} \frac{g_{s,5}^2}{4} \mathcal{G}_{\mu\nu}^a \mathcal{G}^{\mu\nu,a} + \dots, \quad (4.48)$$

where the coupling c_1 is dimensionless, while $c_{2,3} \sim 1/M_{\text{Pl}}$. Since all fields live in the bulk, the natural cutoff suppressing the operator is set by the Planck scale. Also, the

³An example is provided by the $\pi^0 \rightarrow \gamma\gamma$ decay amplitude, which is loop suppressed in the SM despite the fact that QCD is strongly coupled in the low-energy regime.

scalar field now takes the form shown in relation (2.36). Using the KK decomposition of the Higgs field given in (2.56), we find that

$$S_{\text{eff}} = \int d^4x \frac{g_s^2}{4} G_{\mu\nu}^a(x) G^{\mu\nu,a}(x) \frac{2\pi}{L} \int_\epsilon^1 \frac{dt}{t} \frac{v^2(t)}{2\Lambda_{\text{UV}}^2(t)} \left(1 + h(x) \frac{\chi_0(t)}{v(t)}\right)^2 \times \left\{ c_1 + \frac{k}{2} [c_2 \delta(t-1) + \epsilon c_3 \delta(t-\epsilon)] \right\} + \dots, \quad (4.49)$$

where $\Lambda_{\text{UV}}(t) = M_{\text{Pl}} \epsilon/t$ is the warped Planck scale as introduced in (1.101), and $v(t)$ and $\chi_0^h(t)$ are the profiles of the Higgs vev and the physical SM Higgs boson along the extra dimension derived in Subsection 2.2.1. We can now use the leading-order result for the profile of the Higgs vev given in (2.52), as well as the fact that according to (2.63) we have $\chi_0(t)/v(t) = 1/v$ (with $v \approx 246$ GeV) up to corrections of order v^2/M_{KK}^2 , which will be neglected here. It is then straightforward to perform the integration over t in the above result. Matching the answer onto the effective Lagrangian given in (4.46), we obtain

$$c_{\text{eff}} = \frac{1+\beta}{2+\beta} c_1 + (1+\beta) k c_2 \xrightarrow{\beta \gg 1} c_1 + |\mu| c_2. \quad (4.50)$$

Recall that the parameter $\beta \sim 1/\eta$ appearing in the solutions for the vev and the Higgs profile is related to the width of the profile of the scalar field. NDA suggests that c_1 and $k c_2$ can be as large as $\mathcal{O}(1)$ if the UV completion of the RS model is strongly coupled. The contribution of the operator localized on the UV brane is of $\mathcal{O}(\epsilon^{4+2\beta}) c_3$, which results from a factor $1/M_{\text{Pl}}^2$ times $v^2(\epsilon) \sim \epsilon^{2+2\beta}$ reflecting the smallness of the Higgs vev profile on the UV brane, and is therefore entirely negligible. Note that in the limit of a very narrow bulk-Higgs field, corresponding to $\beta \gg 1$ (or $\eta \ll 1$), the largest mass scale in the model is the Higgs mass parameter $|\mu| \approx \beta k = \mathcal{O}(M_{\text{Pl}})$ in (2.33) and (2.39), and hence it is more appropriate to assume that $c_2 \sim 1/|\mu| \sim 1/M_{\text{Pl}}$. Once again, this leads to $c_{\text{eff}} = \mathcal{O}(1)$. The structure of the result (4.50) is completely analogous to the corresponding expression in (4.46) valid for a brane-localized Higgs boson. In both cases the results for c_{eff} , and hence the magnitude of the contributions of higher-dimensional operators, are expected to be of the same order.

One may ask what is the effect of the effective Lagrangian (4.46) to the Wilson coefficient C_{1g} . Matching (4.46) onto the effective amplitude according to (4.2) yields the contribution

$$\Delta C_{1g} = \frac{3c_{\text{eff}}}{4} \left(\frac{4\pi v}{\Lambda_{\text{TeV}}} \right)^2 \approx c_{\text{eff}} \left(\frac{2.7 \text{ TeV}}{\Lambda_{\text{TeV}}} \right)^2. \quad (4.51)$$

In order for this contribution to be much smaller than the SM value $C_1 = 1$, we need to assume that either the cutoff scale is much larger than about 3 TeV or that $|c_{\text{eff}}| \ll 1$ for some reason. With $\Lambda_{\text{TeV}} \sim 10 M_{\text{KK}} \sim 20\text{--}50$ TeV, the first criterion is satisfied in realistic RS models even if $c_{\text{eff}} = \mathcal{O}(1)$. The expected contribution to the Wilson coefficient C_{1g} is then in the percent range, which is negligible in view of the current experimental uncertainty in the measurements of the Higgs-boson couplings. The more interesting question is under which assumptions the contribution (4.51) is much smaller than the loop corrections to the SM result $C_{1g} = 1$, which are approximately given by

$$|C_{1g} - 1| \approx \frac{v^2}{2M_{\text{KK}}^2} \sum_{q=u,d} \text{Tr} \left(\mathbf{Y}_q \mathbf{Y}_q^\dagger \right) \approx \frac{v^2}{2M_{\text{KK}}^2} 2N_g^2 |Y_q|^2, \quad (4.52)$$

where $N_g = 3$ is the number of fermion generations, and $|Y_q|$ is the typical size of an element of the anarchic 5D Yukawa matrices, defined by

$$|Y_q|^2 \equiv \langle |(\mathbf{Y}_q)_{ij}|^2 \rangle = \frac{y_\star^2}{2}. \quad (4.53)$$

The equality on the right-hand side comes from the fact that we work with anarchic 5D Yukawa matrices and assume that the entries $(\mathbf{Y}_q)_{ij}$ are random complex numbers, which with equal probability can take any value in the complex plane inside a circle of radius y_\star , see also (2.67). It follows that the power-suppressed contribution (4.51) can be neglected as long as

$$c_{\text{eff}} \left(\frac{M_{\text{KK}}}{\Lambda_{\text{TeV}}} \right)^2 \ll \frac{N_g^2 y_\star^2}{24\pi^2}, \quad (4.54)$$

which for $\Lambda_{\text{TeV}} \approx 10M_{\text{KK}}$ can be rewritten as $c_{\text{eff}} \ll 3.8 y_\star^2$. In the custodial RS model studied in the next section, the expression on the right-hand side of this relation is multiplied by 4, yielding the weaker condition $c_{\text{eff}} \ll 15.2 y_\star^2$. In the phenomenological analysis in Chapter 5 we will consider values of y_\star between 3 and 0.5. In order to neglect the power-suppressed contributions for $y_\star = 0.5$ in the minimal RS model, one would need to rely on the assumption that $|c_{\text{eff}}| \ll 1$.

Relation (4.54) makes it clear that, in comparing the contributions from higher-dimensional operators with the contribution from virtual KK states, we are comparing a power-suppressed effect with a loop effect. Since we treat the dimensionless Yukawa couplings as $\mathcal{O}(1)$ random complex parameters, it would follow that in the formal limit $\Lambda_{\text{TeV}} \rightarrow \infty$ the higher-dimensional operator contribution tends to zero, while the loop contribution remains as the dominant effect.⁴ However, since by construction the RS model is free of large hierarchies, the ratio $M_{\text{KK}}/\Lambda_{\text{TeV}}$ cannot be made arbitrarily small. We therefore do not expect a strong hierarchy between the contribution from virtual KK states and those from higher-dimensional operators. In practice, which of the effect dominates is more of a numerical question than a parametric one. In Chapter 5, the contribution ΔC_1 in (4.51) is included by treating c_{eff} as a random number with magnitude less than 1.

For the loop calculation (4.37) to be trustable, we should impose an upper bound on the size of y_\star by requiring that the Yukawa interactions remain perturbative up to the cutoff of the RS model under consideration (see e.g. [160, 180]). Following common practice, it will be assumed that $y_\star < y_{\text{max}} = 3$. A detailed discussion of different estimates of the perturbativity bound and also of an exact calculation (using 5D fermion propagators) of y_{max} is presented in Appendix B.

4.1.5 Extension to the RS Model with Custodial Symmetry

In this last subsection, we will now generalize the analysis presented in the previous sections to the extended RS model with custodial symmetry. With the help of the compact notation introduced in (2.71) and already used in Section 3.2, where the 5D fermion propagators have been derived, this is a very straightforward exercise. We just have to make the replacements

$$\mathbf{X}_q \rightarrow \mathbf{X}_{\vec{q}}, \quad \mathbf{R}_q \rightarrow \mathbf{R}_{\vec{q}}, \quad \mathbf{Z}_q \rightarrow \mathbf{Z}_{\vec{q}}, \quad (4.55)$$

⁴Since for too large values of the cutoff the Yukawa sector becomes strongly coupled (see below), the result in such an academic limit could at best be taken as a rough estimate of the KK loop contributions.

where the latter matrices can be found in (2.78), (3.98), and (3.99). Hence, the central results (4.24) remain valid if we extend the sum over flavors appropriately, i.e.

$$I_+(m^2) = \sum_{q=u,d,\lambda} \left\{ \text{Tr} g(\mathbf{X}_{\bar{q}}) + \frac{1}{2} \text{Tr} \left[\frac{2\mathbf{X}_{\bar{q}}}{\sinh 2\mathbf{X}_{\bar{q}}} \left(\frac{\mathbf{Z}_{\bar{q}}(-m^2)}{1 + \mathbf{Z}_{\bar{q}}(-m^2)} + \frac{\mathbf{Z}_{\bar{q}}^\dagger(-m^2)}{1 + \mathbf{Z}_{\bar{q}}^\dagger(-m^2)} \right) \right] \right\}, \quad (4.56)$$

and similarly for $I_-(m^2)$. The relevant squared Yukawa matrices entering the quantities $\mathbf{X}_{\bar{q}}$ in (4.56) are given by the 6×6 matrix

$$\mathbf{Y}_{\bar{u}} \mathbf{Y}_{\bar{u}}^\dagger = \begin{pmatrix} \mathbf{Y}_u \mathbf{Y}_u^\dagger + \mathbf{Y}_d \mathbf{Y}_d^\dagger & \mathbf{Y}_u \mathbf{Y}_u^\dagger - \mathbf{Y}_d \mathbf{Y}_d^\dagger \\ \mathbf{Y}_u \mathbf{Y}_u^\dagger - \mathbf{Y}_d \mathbf{Y}_d^\dagger & \mathbf{Y}_u \mathbf{Y}_u^\dagger + \mathbf{Y}_d \mathbf{Y}_d^\dagger \end{pmatrix} = \mathbf{V} \begin{pmatrix} 2\mathbf{Y}_d \mathbf{Y}_d^\dagger & 0 \\ 0 & 2\mathbf{Y}_u \mathbf{Y}_u^\dagger \end{pmatrix} \mathbf{V}^\dagger, \\ \text{with } \mathbf{V} = \mathbf{V}^\dagger = \frac{1}{\sqrt{2}} \begin{pmatrix} -1 & 1 \\ 1 & 1 \end{pmatrix}, \quad (4.57)$$

and the 3×3 matrices $\mathbf{Y}_{\bar{d}} \mathbf{Y}_{\bar{d}}^\dagger = \mathbf{Y}_{\bar{\lambda}} \mathbf{Y}_{\bar{\lambda}}^\dagger = 2\mathbf{Y}_d \mathbf{Y}_d^\dagger$. It follows that

$$\sum_{q=u,d,\lambda} \text{Tr} g(\mathbf{X}_{\bar{q}}) = \text{Tr} g(\sqrt{2}\mathbf{X}_u) + 3 \text{Tr} g(\sqrt{2}\mathbf{X}_d), \quad (4.58)$$

where the final answer is now expressed in terms of traces over the same 3×3 matrices \mathbf{X}_q as in the minimal RS model.

The next task is to reduce also the second term in (4.56) to traces over 3×3 matrices. From the definition (3.98), it is straightforward to derive that

$$\mathbf{Z}_{\bar{u}}(p_E^2) = \frac{v^2}{2M_{\text{KK}}^2} \mathbf{V} \begin{pmatrix} \tilde{\mathbf{Y}}_d [\mathbf{R}_{\tau_1}^{(-)} + \mathbf{R}_{\tau_2}^{(-)}] \tilde{\mathbf{Y}}_d^\dagger & 0 \\ 0 & 2\tilde{\mathbf{Y}}_u \mathbf{R}_{u^c}^{(+)} \tilde{\mathbf{Y}}_u^\dagger \end{pmatrix} \mathbf{V}^\dagger \begin{pmatrix} \mathbf{R}_Q^{(+)} & 0 \\ 0 & \mathbf{R}_Q^{(-)} \end{pmatrix}, \\ \mathbf{Z}_{\bar{d},\bar{\lambda}}(p_E^2) = \frac{v^2}{2M_{\text{KK}}^2} \tilde{\mathbf{Y}}_d [\mathbf{R}_{\tau_2}^{(\pm)} + \mathbf{R}_{\tau_1}^{(-)}] \tilde{\mathbf{Y}}_d^\dagger \mathbf{R}_Q^{(\pm)}, \quad (4.59)$$

where again we have omitted the argument \hat{p}_E of the $\mathbf{R}_A^{(\pm)}$ matrices on the right-hand side of the equations. In the custodial model, the modified Yukawa matrices appearing in (4.59) are defined as

$$\tilde{\mathbf{Y}}_q \Big|_{\text{cust}} \equiv \frac{\tanh(\sqrt{2}\mathbf{X}_q)}{\sqrt{2}\mathbf{X}_q} \mathbf{Y}_q, \quad (4.60)$$

with an extra factor of $\sqrt{2}$ inserted compared with the minimal model.⁵ In (4.7), we need to evaluate the result (4.56) for values $|p_E^2| \ll M_{\text{KK}}^2$. Using the expansion in (3.115), we obtain (again with $\mathbf{x}_q = \mathbf{m}_{q,0}/M_{\text{KK}}$)

$$\mathbf{V}^\dagger \mathbf{Z}_{\bar{u}} \mathbf{V} = F^{-1}(\mathbf{c}_Q) \mathbf{U}_u \left\{ \left[\frac{\mathbf{m}_{u,0}^2}{p_E^2} + (\Phi_U + \mathbf{m}_{u,0} \Phi_u \mathbf{m}_{u,0}^{-1}) + \dots \right] \begin{pmatrix} 0 & 0 \\ -1 & 1 \end{pmatrix} \right. \\ \left. + \mathbf{V}_{\text{CKM}} \mathbf{x}_d \mathbf{W}_d^\dagger \frac{1}{2F^2(\mathbf{c}_{\tau_2})} \left[\frac{1}{F^2(-\mathbf{c}_{\tau_1})} + \frac{1}{F^2(-\mathbf{c}_{\tau_2})} \right] \mathbf{W}_d \mathbf{x}_d \mathbf{V}_{\text{CKM}}^\dagger \begin{pmatrix} 1 & -1 \\ 1 & -1 \end{pmatrix} \right. \\ \left. + \mathbf{x}_u^2 \mathbf{U}_u^\dagger \frac{2}{F^2(\mathbf{c}_Q) F^2(-\mathbf{c}_Q)} \mathbf{U}_u \begin{pmatrix} 0 & 0 \\ 1 & 0 \end{pmatrix} + \dots \right\} \mathbf{U}_u^\dagger F(\mathbf{c}_Q), \quad (4.61)$$

⁵Note that $\tilde{\mathbf{Y}}_q \Big|_{\text{cust}} \neq \tilde{\mathbf{Y}}_{\bar{q}} \equiv [\tanh(\mathbf{X}_{\bar{q}})/(\mathbf{X}_{\bar{q}})] \mathbf{Y}_{\bar{q}}$.

and

$$\mathbf{Z}_{\bar{d}}(p_E^2) = F^{-1}(\mathbf{c}_Q) \mathbf{U}_d \left[\frac{\mathbf{m}_{d,0}^2}{p_E^2} + \left(\Phi_D + \mathbf{m}_{d,0} \Phi_d \mathbf{m}_{d,0}^{-1} \right) + \dots \right] \mathbf{U}_d^\dagger F(\mathbf{c}_Q), \quad (4.62)$$

after a straightforward calculation, where $\mathbf{V}_{\text{CKM}} = \mathbf{U}_u^\dagger \mathbf{U}_d$ is the CKM mixing matrix and the dependence on \hat{p}_E^2 has been dropped for a compact writeup. The terms shown explicitly above are of leading and subleading order in v^2/M_{KK}^2 . To this order, the quantity $\mathbf{Z}_{\bar{\chi}}(p_E^2)$ vanishes. The quantities Φ_A are generalizations of the matrices δ_A given in (4.30). In ZMA approximation, they read [149]

$$\begin{aligned} \Phi_U &= \mathbf{x}_u \mathbf{W}_u^\dagger \left[\frac{1}{1-2\mathbf{c}_u} \left(\frac{1}{F^2(\mathbf{c}_u)} - 1 + \frac{F^2(\mathbf{c}_u)}{3+2\mathbf{c}_u} \right) \right] \mathbf{W}_u \mathbf{x}_u \\ &\quad + \mathbf{V}_{\text{CKM}} \mathbf{x}_d \mathbf{W}_d^\dagger \frac{1}{2F^2(\mathbf{c}_{\tau_2})} \left[\frac{1}{F^2(-\mathbf{c}_{\tau_1})} + \frac{1}{F^2(-\mathbf{c}_{\tau_2})} \right] \mathbf{W}_d \mathbf{x}_d \mathbf{V}_{\text{CKM}}^\dagger, \\ \Phi_u &= \mathbf{x}_u \mathbf{U}_u^\dagger \left[\frac{1}{1-2\mathbf{c}_Q} \left(\frac{1}{F^2(\mathbf{c}_Q)} \left[1 + \frac{1-2\mathbf{c}_Q}{F^2(-\mathbf{c}_Q)} \right] - 1 + \frac{F^2(\mathbf{c}_Q)}{3+2\mathbf{c}_Q} \right) \right] \mathbf{U}_u \mathbf{x}_u, \\ \Phi_D &= \mathbf{x}_d \mathbf{W}_d^\dagger \left[\frac{1}{1-2\mathbf{c}_{\tau_2}} \left(\frac{1}{F^2(\mathbf{c}_{\tau_2})} \left[1 + \frac{1-2\mathbf{c}_{\tau_2}}{F^2(-\mathbf{c}_{\tau_1})} \right] - 1 + \frac{F^2(\mathbf{c}_{\tau_2})}{3+2\mathbf{c}_{\tau_2}} \right) \right] \mathbf{W}_d \mathbf{x}_d, \\ \Phi_d &= \mathbf{x}_d \mathbf{U}_d^\dagger \left[\frac{1}{1-2\mathbf{c}_Q} \left(\frac{1}{F^2(\mathbf{c}_Q)} - 1 + \frac{F^2(\mathbf{c}_Q)}{3+2\mathbf{c}_Q} \right) \right] \mathbf{U}_d \mathbf{x}_d. \end{aligned} \quad (4.63)$$

After a lengthy calculation, we find that in analogy with (4.34)

$$\sum_{q=u,d,\lambda} \text{Tr} \left[\frac{2\mathbf{X}_{\bar{q}}}{\sinh 2\mathbf{X}_{\bar{q}}} \frac{\mathbf{Z}_{\bar{q}}(p_E^2)}{1 + \mathbf{Z}_{\bar{q}}(p_E^2)} \right] = \sum_i \left[\kappa_{q_i} \frac{m_{q_i}^2}{m_{q_i}^2 + p_E^2} + \varepsilon_{q_i} \right] + \dots, \quad (4.64)$$

where

$$\kappa_{q_i} = 1 - \varepsilon_{q_i} - \frac{2}{3} \left[\mathbf{U}_q^\dagger F(\mathbf{c}_Q) 2\mathbf{X}_q^2 F^{-1}(\mathbf{c}_Q) \mathbf{U}_q \right]_{ii} \quad (4.65)$$

now contains an extra factor of 2 in the last term compared with the result (4.35) for the minimal model, while

$$\varepsilon_{q_i} = (\Phi_Q)_{ii} + (\Phi_q)_{ii}. \quad (4.66)$$

We are now all set for presenting the final expressions for the Wilson coefficients C_{1g} and C_{5g} in the RS model with custodial symmetry. To an excellent approximation, we obtain (instead of (4.37))

$$\begin{aligned} C_{1g} &\approx \left[1 - \frac{2v^2}{3M_{\text{KK}}^2} \text{Re} \frac{(\mathbf{Y}_u \mathbf{Y}_u^\dagger \mathbf{Y}_u)_{33}}{(\mathbf{Y}_u)_{33}} \right] A_q(\tau_t) + A_q(\tau_b) + \text{Tr} g(\sqrt{2}\mathbf{X}_u) + 3\text{Tr} g(\sqrt{2}\mathbf{X}_d), \\ C_{5g} &\approx -\frac{2v^2}{3M_{\text{KK}}^2} \text{Im} \left[\frac{(\mathbf{Y}_u \mathbf{Y}_u^\dagger \mathbf{Y}_u)_{33}}{(\mathbf{Y}_u)_{33}} \right] B_q(\tau_t), \end{aligned} \quad (4.67)$$

which once again is independent of the bulk mass parameters c_{Q_i, q_i} . This approximation is accurate to better than 2% for $M_{\text{KK}} \gtrsim 2\text{TeV}$. Whereas the small corrections parameterized by κ_{q_i} and ε_{q_i} have only a minor impact, the main difference between the minimal and the custodial RS models consists in the different multiplicity factors in the trace terms in (4.37) and (4.67). Since the functions $g(\mathbf{X}_q)$ start with a quadratic term, we must compare $\mathbf{X}_u^2 + \mathbf{X}_d^2$ in the minimal model with the combination $2\mathbf{X}_u^2 + 6\mathbf{X}_d^2$ in

the custodial model. Since it is assumed that the 5D Yukawa matrices in the up- and down-type quark sectors are random matrices of similar magnitude, it follows that the effect of the KK modes in the custodial model is approximately four times as large as in the minimal model.⁶

4.2 Higgs Decay into Two Photons

After the gluon-fusion process has been discussed extensively, we will now address the loop-induced Higgs decay into two photons. This decay is also affected by the KK quark tower, but moreover receives contributions from KK boson loops, as shown in Figure 4.3. This section is based on our publication [151].

4.2.1 Preliminaries

In the context of warped extra dimensions, the Higgs decay $h \rightarrow \gamma\gamma$ was investigated in the same works that focused on Higgs production via gluon fusion [149, 157, 220–222]. While these papers mainly focused on the contribution stemming from the fermionic KK states, a detailed analysis of the bosonic loop contributions to the $h \rightarrow \gamma\gamma$ amplitude, which in unitary gauge stem from the W bosons and their KK excitations, will be provided in this section. The advantages of the approach here are that it is possible to derive an exact result, which includes the full dependence on the Higgs-boson mass and holds to all orders in v^2/M_{KK}^2 , similar to the corresponding formula for the gluon fusion amplitude (4.7). It is straightforward to extend the final results to the case where the Higgs boson lives in the bulk of the extra dimension. We will also carefully study the effects of the fifth components of the gauge fields, whose profiles are discontinuous on the IR brane, similar to the Z_2 -odd fermion profiles, which indeed require a careful treatment as has been discussed several times.

The rest of this section is subdivided into two subsections: In Subsection 4.2.2 the general structure of the $h \rightarrow \gamma\gamma$ amplitude will be discussed and the results for the fermionic contributions from charged quarks and leptons propagating in the loop summarized. We will then focus on the bosonic loop contributions, calculate them in the KK-decomposed theory and show that the result for the contributions of each individual KK mode is gauge invariant. In the next step we will resum the KK towers and derive an exact formula for the $h \rightarrow \gamma\gamma$ amplitude in terms of an overlap integral over the Higgs-boson profile and the transverse part of the 5D gauge-boson propagator, including the exact dependence on the Higgs-boson mass, which has not been obtained before. The further proceeding will be analogous to that in the previous section: By expanding the results in powers of v^2/M_{KK}^2 , we will be able to identify the contributions from the W bosons (with modified couplings to the Higgs boson) and their KK towers, confirming the results of [157]. Finally, in Subsection 4.2.3 we will generalize the findings to the custodial RS model that are consistent with those of [149] when expanded to order v^2/M_{KK}^2 .

⁶Based on a naive counting of degrees of freedom, this factor was estimated as 11/4 (instead of 4) in [224].

4.2.2 5D Analysis of the $h \rightarrow \gamma\gamma$ Amplitude

The goal is to calculate the $h \rightarrow \gamma\gamma$ decay amplitude entirely in terms of the 5D propagators for both gauge bosons and fermions. While the contributions from quarks and charged leptons can be easily deduced from the corresponding results for the $gg \rightarrow h$ amplitude derived in Section 4.1, a detailed consideration of the gauge-boson contribution has not been performed in 5D language yet. The approach we take here is the following: First, we will calculate the bosonic contributions to the $h \rightarrow \gamma\gamma$ amplitude in the KK-decomposed effective theory and show that at each KK level the sum of all diagrams is gauge-invariant. The only contributing diagrams in unitary gauge are those with vector bosons propagating in the loop. This observation can be used to rewrite the amplitude as an expression involving the 5D gauge-boson propagator derived in Section 3.1.2. We will see that in the limit of a very narrow Higgs profile the amplitude approaches an unambiguous value, which is insensitive to the details of the Higgs localization mechanism. At the end of this subsection, we employ the exact results to derive expressions for the contributions of the zero modes (the standard W bosons) and their infinite towers of KK excitations to the $h \rightarrow \gamma\gamma$ amplitude.

We begin with the calculation in the minimal RS model. The results in the custodial model can be easily deduced from those derived here, which we will see in the next subsection. The one-loop Feynman diagrams contributing to the $h \rightarrow \gamma\gamma$ decay amplitude are shown in Figure 4.3 for a general R_ξ gauge. Below, we will demonstrate that the full amplitude is gauge invariant. In the unitary gauge only the diagrams (a)–(c) contribute. Analogously to (4.2), the $h \rightarrow \gamma\gamma$ amplitude, including the contributions from SM particles, is parametrized by means of two Wilson coefficients $C_{1\gamma}$ and $C_{5\gamma}$ defined via

$$\mathcal{A}(h \rightarrow \gamma\gamma) = C_{1\gamma} \frac{\alpha}{6\pi v} \langle \gamma\gamma | F_{\mu\nu} F^{\mu\nu} | 0 \rangle - C_{5\gamma} \frac{\alpha}{4\pi v} \langle \gamma\gamma | F_{\mu\nu} \tilde{F}^{\mu\nu} | 0 \rangle, \quad (4.68)$$

where $\tilde{F}^{\mu\nu} = -\frac{1}{2}\epsilon^{\mu\nu\alpha\beta} F_{\alpha\beta}$ with $\epsilon^{0123} = -1$. As opposed to (4.2), each Wilson coefficient now consists of three terms,

$$C_i = C_i^W + C_i^g + C_i^l, \quad (4.69)$$

where in a general gauge C_i^W includes the bosonic contributions from gauge bosons, scalar bosons, and ghosts. The calculation of these bosonic contributions is the main subject of this subsection. The fermionic loop contributions due to virtual quarks and leptons shown in diagram (a) can be readily deduced from (4.37) and will be summarized in (4.73).

We will also discuss the (narrow) bulk-Higgs scenario. As already mentioned at the end of Section (2.2.1), this scenario gives rise to a tower of *physical* scalar particles $\phi_W^{\pm(n)}$, which in some sense are the KK excitations of the charged components of the Higgs doublet. They are defined in terms of a gauge-invariant superposition of W_5^\pm and φ^\pm . The effect of these heavy scalar particles on the $h \rightarrow \gamma\gamma$ amplitude is [161]

$$C_{1\gamma}^\phi = \frac{1}{8} \sum_{n=1}^{\infty} \frac{v g_{h\phi\phi}^{(n,n)}}{(m_n^\phi)^2} A_\phi(\tau_n^\phi), \quad C_{5\gamma}^\phi = 0, \quad (4.70)$$

where $\tau_n^\phi = 4(m_n^\phi)^2/m_h^2$, and the function

$$A_\phi(\tau) = 3\tau \left[\tau \arctan^2 \frac{1}{\sqrt{\tau-1}} - 1 \right] \quad (4.71)$$

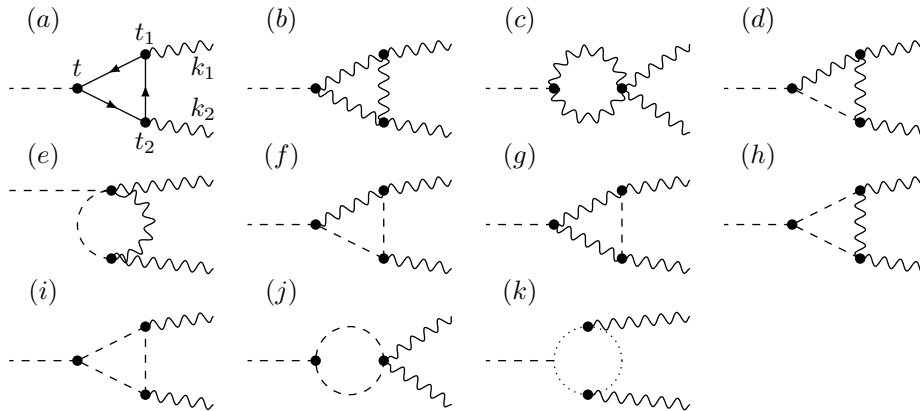


FIGURE 4.3: One-loop Feynman diagrams for the process $h \rightarrow \gamma\gamma$. Diagram (a) contains the fermion loops, while diagrams (b)–(k) show the contributions from the gauge sector in a general R_ξ gauge. Solid lines represent fermion mass eigenstates, wavy lines vector-boson mass eigenstates $W_\mu^{\pm(n)}$, dashed lines scalar mass eigenstates $\varphi_W^{\pm(n)}$, and dotted lines ghost mass eigenstates $c_W^{\pm(n)}$. The ghost masses and profiles are the same as for the W bosons and their KK excitations [161].

approaches 1 for $\tau \rightarrow \infty$. In the limit of a very narrow Higgs profile, the couplings $g_{h\phi\phi}^{(n,n)}$ scale like $1/\eta$, while the masses of the heavy scalar particles scale like M_{KK}/η . It follows that $C_{1\gamma}^\phi = \mathcal{O}(\eta)$, and hence this contribution decouples in the limit $\eta \rightarrow 0$, as expected. Consequently, the corresponding Feynman diagrams are not considered in the following analysis.

Fermionic Contributions to the Wilson Coefficients

The one-loop contributions to the $h \rightarrow \gamma\gamma$ amplitude stemming from the quarks and leptons can be derived in a straightforward way from analogous results for the quark contributions to the $gg \rightarrow h$ amplitude. We only need to include appropriate factor of color and electric charges. According to the discussion in 4.1.3 the exact result can be written in the form

$$\begin{aligned}
 C_{1\gamma}^q &= 3N_c \sum_{f=u,d} Q_q^2 \int_0^1 dx \int_0^{1-x} dy (1-4xy) [T_+^q(-xym_h^2) - T_+^q(\Lambda_{\text{TeV}}^2)], \\
 C_{5\gamma}^q &= 2N_c \sum_{f=u,d} Q_q^2 \int_0^1 dx \int_0^{1-x} dy [T_-^q(-xym_h^2) - T_-^q(\Lambda_{\text{TeV}}^2)],
 \end{aligned}
 \tag{4.72}$$

where $Q_u = 2/3$ and $Q_d = -1/3$ are the electric charges of the quarks, and $N_c = 3$ is the number of colors. The functions $T_\pm^q(-p^2)$ are given in (4.23). An analogous expression with N_c replaced by 1 and Q_q replaced by $Q_e = -1$ holds for the charged-lepton contribution. Neglecting some terms of order v^4/M_{KK}^4 and chirally-suppressed

$\mathcal{O}(v^2/M_{\text{KK}}^2)$ terms then leads to the explicit expressions (compare with (4.37))

$$C_{1\gamma}^q \approx \left[1 - \frac{v^2}{3M_{\text{KK}}^2} \text{Re} \frac{(\mathbf{Y}_u \mathbf{Y}_u^\dagger \mathbf{Y}_u)_{33}}{(\mathbf{Y}_u)_{33}} \right] N_c Q_u^2 A_q(\tau_t) + N_c Q_d^2 A_q(\tau_b) + \sum_{q=u,d} N_c Q_q^2 \text{Re Tr } g(\mathbf{X}_q), \quad (4.73)$$

$$C_{5\gamma}^q \approx -\frac{v^2}{3M_{\text{KK}}^2} \text{Im} \left[\frac{(\mathbf{Y}_u \mathbf{Y}_u^\dagger \mathbf{Y}_u)_{33}}{(\mathbf{Y}_u)_{33}} \right] N_c Q_u^2 B_q(\tau_t) + \sum_{q=u,d} N_c Q_q^2 \text{Im Tr } g(\mathbf{X}_q),$$

and

$$C_{1\gamma}^l + iC_{5\gamma}^l \approx Q_e^2 \text{Tr } g(\mathbf{X}_e), \quad (4.74)$$

where the contributions from the SM fermions and the KK excitations can now readily be identified. The loop functions $A_q(\tau_i)$ and $B_q(\tau_i)$ (with $\tau_i = 4m_i^2/m_h^2$) and the matrices \mathbf{X}_f can be found in (4.38) and (2.78), respectively. Note that with the hermitian matrices \mathbf{X}_f the traces over matrix-valued functions $g(\mathbf{X}_f)$ are real, so that $C_{5\gamma}^l = 0$ and the only contribution to the coefficient $C_{5\gamma}^q$ arises from the top-quark contribution given by the first term on the right-hand side of (4.73). The function $g(\mathbf{X}_f)$ itself depends on the details of the localization of the scalar sector on or near the IR brane and is shown in (4.25) for the brane-localized and in (4.26) for the narrow bulk-Higgs scenario. The function in the type-II brane-Higgs model is defined in (4.41). As already mentioned in the gluon-fusion case, the matrices \mathbf{X}_f are no longer hermitian, but to leading order it is still a hermitian matrix. The type-II brane-Higgs scenario is thus rather similar to the original brane-Higgs model with identical Yukawa matrices $\mathbf{Y}_f^C = \mathbf{Y}_f^S = \mathbf{Y}_f$ and it is therefore convenient to restrict ourselves to a study of the two cases shown in (4.25) and (4.26).

Gauge Invariance of the Amplitude

Having clarified the fermion contribution to the $h \rightarrow \gamma\gamma$ amplitude, we now turn to the bosonic contribution. In the SM, Ref. [229] has thoroughly discussed the ξ independence of the $h \rightarrow \gamma\gamma$ amplitude in dimensional regularization and has shown that the calculation can be performed consistently in the unitary gauge $\xi \rightarrow \infty$. In the case of the RS model, it is useful to first work in the KK-decomposed theory, where 4D Feynman propagators have the same structure as in the SM. The Feynman rules required to evaluate the one-loop diagrams shown in Figure 4.3 are summarized in Appendix C.⁷ From these rules, it follows that:

- All vertices involving one or two external photons but no Higgs boson are diagonal in KK number after one integrates over the extra-dimensional coordinate of the vertex with measure $\int_{-\pi}^{\pi} d\phi = (2\pi/L) \int_{\epsilon}^1 dt/t$. The Feynman rules for these vertices have the same form as in the SM after one identifies the 4D electromagnetic coupling as $e = e_5/\sqrt{2\pi r}$, see (2.13). For the mass-dependent vertex connecting a photon to $W_\mu^{\pm(n)} \varphi_W^{\mp(n)}$, one must replace $m_W \rightarrow m_n^W$.

⁷The Feynman rules can be easily deduced from the relevant terms in the 5D action (2.6). Details of the derivation of Feynman rules in the RS model can be found in [184, 230–233].

- As a result, all one-loop diagrams contributing to the $h \rightarrow \gamma\gamma$ amplitude involve a single KK particle in the loop. Hence, only KK-diagonal Higgs couplings are required in the calculation.
- All KK-diagonal Higgs couplings have the same structure as in the SM but come with an overall prefactor

$$\frac{v}{2} \frac{g_5^2}{2\pi r} 2\pi [\chi_n^W(1)]^2 = \frac{2\tilde{m}_W^2}{v} 2\pi [\chi_n^W(1)]^2, \quad (4.75)$$

which replaces the corresponding factor $gm_W = 2m_W^2/v_{\text{SM}}$ in the SM. In addition, for each scalar boson $\varphi_W^{\pm(n)}$ a factor $1/m_n^W$ appears, which replaces $1/m_W$ in the corresponding SM Feynman rule for vertices involving the Goldstone bosons φ^\pm .

From these observations it follows that, diagram by diagram and in a general R_ξ gauge, the bosonic loop contributions obtained in the RS model resemble those of the SM up to trivial substitutions, such that

$$\mathcal{A}_{\text{RS}}^W(h \rightarrow \gamma\gamma) = \frac{\tilde{m}_W^2}{v} \sum_{n=0}^{\infty} 2\pi [\chi_n^W(1)]^2 \left[\frac{v_{\text{SM}}}{m_W^2} \mathcal{A}_{\text{SM}}^W(h \rightarrow \gamma\gamma) \right]_{m_W \rightarrow m_n^W}. \quad (4.76)$$

For vertices involving a photon and a pair of vector bosons, fermions or ghosts, the statement that the interactions are diagonal in KK number (first bullet) is a direct consequence of the flatness of the photon profile and the orthogonality of the relevant vector-boson and fermion profiles. For interactions involving the scalar bosons $\varphi_W^{\pm(n)}$, however, which according to (2.18) and (2.19) receive contributions from W_5^\pm and φ^\pm , the vertices become diagonal only after one adds up these two contributions. Consider, for instance, the vertex (h) needed for diagram (j) in Figure 4.3.⁸ After integrating over the coordinate of this vertex, we obtain the Feynman rule

$$2ie^2\eta_{\mu\nu} \left[\frac{M_{\text{KK}}^2}{m_m^W m_n^W} \frac{2\pi}{L} \int_\epsilon^1 \frac{dt}{t} [\partial_t \chi_m^W(t)] [\partial_t \chi_n^W(t)] + \frac{\tilde{m}_W^2}{m_m^W m_n^W} 2\pi \chi_m^W(1) \chi_n^W(1) \right], \quad (4.77)$$

where the first contribution originates from the $W_5 W_5 A_\mu A^\mu$ term contained in the Yang-Mills action for the W -boson fields using the KK decomposition (2.18), while the second contribution arises from the $\varphi^+ \varphi^- A_\mu A^\mu$ term contained in the kinetic term for the Higgs doublet using the KK decomposition (2.19). We now integrate by parts in the first term use the equations of motion for the gauge-boson profiles (2.20) (for $t < 1$) taking into account the boundary conditions (2.22). In this way, we obtain the Feynman rule

$$2ie^2\eta_{\mu\nu} \left[\frac{m_n^W}{m_m^W} \frac{2\pi}{L} \int_\epsilon^1 \frac{dt}{t} \chi_m^W(t) \chi_n^W(t) \right] = 2ie^2\eta_{\mu\nu} \delta_{mn}, \quad (4.78)$$

where the boundary term cancels the contribution arising from the $\varphi^+ \varphi^- A_\mu A^\mu$ term. In the last step the orthonormality relation (2.21) for the gauge-boson profiles has been used.

Let us now explore the consequences of the general result (4.76). Obviously, this relation implies that for each single KK mode the $h \rightarrow \gamma\gamma$ amplitude in the RS model is gauge invariant provided the amplitude is gauge invariant in the SM. Since, as will be demonstrated, the sum over KK modes is convergent, it follows that gauge invariance

⁸The remaining vertices can be derived analogously, see [232, 233] for details.

is maintained also in the 5D theory. We recall that to show gauge invariance in the SM one divides the W -boson propagator in R_ξ gauge into two parts,

$$\frac{i}{p^2 - m_W^2} \left[\frac{(1 - \xi) p^\mu p^\nu}{p^2 - \xi m_W^2} - \eta^{\mu\nu} \right] = \frac{i}{p^2 - m_W^2} \left(\frac{p^\mu p^\nu}{m_W^2} - \eta^{\mu\nu} \right) - \frac{i}{p^2 - \xi m_W^2} \frac{p^\mu p^\nu}{m_W^2}, \quad (4.79)$$

where the first part coincides with the propagator in unitary gauge and the second part has the same structure as the scalar-boson and ghost propagators. It has been shown in [229] that, after adding up all diagrams, many intricate cancellations occur, and at the end only the diagrams (b) and (c) in Figure 4.3 with the W -boson propagators in unitary gauge, as well as the fermion loop contributions shown in diagram (a), remain.

5D Analysis of the Bosonic Loop Contributions to $h \rightarrow \gamma\gamma$

We now repeat the calculation of the bosonic loop contributions to the $h \rightarrow \gamma\gamma$ amplitude using a 5D approach. Based on the findings of the previous section we adopt unitary gauge and consider only the contributions of diagrams (b) and (c) in Figure 4.3. We employ the 5D gauge-boson propagator $D_{W,\mu\nu}^\xi(t, t'; p)$ derived in Section 3.1.2. Like in the gluon-fusion case, we introduce a dimensional regulator $d = 4 - 2\hat{\epsilon}$ on the loop integral in intermediate steps in order to preserve gauge-invariance. This regulator can be removed at the end of the calculation. We also regularize the Higgs profile by replacing the δ -function profile of the brane-localized Higgs field by a smooth function $\delta^\eta(t - 1)$ of width $\eta \ll 1$. As we have seen, such a regularization is important in the calculation of the fermionic loop contributions to the $gg \rightarrow h$ and $h \rightarrow \gamma\gamma$ amplitudes. However, we will find that in the calculation of the bosonic loop contributions the limit $\eta \rightarrow 0$ can be taken without encountering any ambiguities.

Diagrams (b) and (c) give rise to the amplitude

$$\begin{aligned} i\mathcal{A}(h \rightarrow \gamma\gamma) = & -\frac{2\tilde{m}_W^2}{v} 2\pi e^2 \epsilon_\mu^*(k_1) \epsilon_\nu^*(k_2) \eta^{\alpha\beta} \int \frac{d^d p}{(2\pi)^d} \int_\epsilon^1 dt \delta^\eta(t - 1) \frac{2\pi}{L} \int_\epsilon^1 \frac{dt_1}{t_1} \\ & \times \left[\frac{2\pi}{L} \int_\epsilon^1 \frac{dt_2}{t_2} 2V^{\gamma\mu\lambda\rho\nu\delta} D_{W,\alpha\gamma}^{\xi \rightarrow \infty}(t, t_1, p + k_1) D_{W,\lambda\rho}^{\xi \rightarrow \infty}(t_1, t_2, p) D_{W,\delta\beta}^{\xi \rightarrow \infty}(t_2, t, p - k_2) \right. \\ & \left. + \left(2\eta^{\gamma\delta} \eta^{\mu\nu} - \eta^{\delta\nu} \eta^{\gamma\mu} - \eta^{\nu\gamma} \eta^{\mu\delta} \right) D_{W,\alpha\gamma}^{\xi \rightarrow \infty}(t, t_1, p + k_1) D_{W,\beta\delta}^{\xi \rightarrow \infty}(t_1, t, p - k_2) \right], \quad (4.80) \end{aligned}$$

where $V^{\gamma\mu\lambda\rho\nu\delta} = V^{\gamma\mu\lambda}(p + k_1, -k_1, -p) V^{\rho\nu\delta}(p, -k_2, -p + k_2)$ arises from the product of two triple gauge-boson vertices, with $V^{\mu\nu\rho}(k, p, q) = \eta^{\mu\nu}(k - p)^\rho + \eta^{\nu\rho}(p - q)^\mu + \eta^{\rho\mu}(q - k)^\nu$. The goal is to rewrite this result as a Feynman parameter integral over a *single* 5D gauge-boson propagator, which should be possible, since in the KK-decomposed theory only a single KK mode propagates in the loops. In order to simplify the answer, we decompose the 5D propagator as (3.10) and use the KK decomposition (3.14) in an intermediate step. The use of the KK representation is justified because all expressions are finite and the KK sum converges. At the end of the calculation we will obtain an expression without any reference to KK modes.

Again, we can perform the integration over t_1 and t_2 using the orthonormality relation for the gauge-boson profiles (2.21). Working out the Dirac algebra and making use of Passarino-Veltman reductions, the answer reduces to a simple Feynman parameter integral [232]. After the contributions from the various diagrams have been combined,

the dimensional regulator $\hat{\epsilon}$ can be set to 0. We find (with $m_h^2 \equiv m_h^2 + i0$)

$$C_{1\gamma}^W = -3\pi\tilde{m}_W^2 \int_{\epsilon}^1 dt \delta^\eta(t-1) \sum_{n=0}^{\infty} [\chi_n^W(t)]^2 \left[\frac{1}{(m_n^W)^2} + 6 \int_0^1 dx \int_0^{1-x} dy \frac{1-2xy}{(m_n^W)^2 - xym_h^2} \right] \quad (4.81)$$

and $C_{5\gamma}^W = 0$. It is now a simple exercise to recast the answer in terms of the 5D propagator function $B_W(t, t'; -p^2)$ defined in (3.14). We obtain

$$C_{1\gamma}^W = -3\pi\tilde{m}_W^2 \left[T_W(0) + 6 \int_0^1 dx \int_0^{1-x} dy (1-2xy) T_W(-xym_h^2) \right], \quad (4.82)$$

where $T_W(-p^2)$ denotes the overlap integral of the Higgs profile with the transverse part of the 5D W -boson propagator evaluated at $t = t'$,

$$T_W(-p^2) = \int_{\epsilon}^1 dt \delta^\eta(t-1) B_W(t, t; -p^2 - i0) = B_W(1, 1; -p^2 - i0) + \mathcal{O}(\eta). \quad (4.83)$$

At this step we need the propagator function $B_W(t, t; -p^2)$ in the brane-localized Higgs scenario, which has been derived in Section 3.1.2. As we have seen in the latter section, the W -boson propagator function can be obtained from the propagator in the RS model with a bulk Higgs in the limit $\eta \rightarrow 0$ ($\beta \rightarrow \infty$). Thus, the integral above exhibits a smooth behavior in the limit of small η , so that the last identity holds and the regulator on the Higgs profile can be taken to zero without encountering any ambiguities.

Relation (4.82) is one of the main results of this section. It shows the exact result for the Wilson coefficient $C_{1\gamma}$ in dependence of overlap integrals of the Higgs profile and the 5D gauge-boson propagator. It can be shown that this relation also holds for an arbitrary bulk-Higgs profile $\chi_h(t)$, if one uses the corresponding 5D gauge-boson propagator in the bulk-Higgs model [161]. Then the regularized δ -function in (4.83) must be replaced by

$$\delta^\eta(t-1) \rightarrow \frac{2\pi}{Lt} \frac{v(t)}{v} \chi_0^h(t) = 2(1+\beta) t^{1+2\beta} + \dots, \quad (4.84)$$

with the profiles given in (2.52) and (2.63). Note, however, that in this case it is necessary to also include the contribution (4.70) due to the physical scalar excitations of the bulk Higgs field. In the region where $\beta \gg 1$, the function on the right-hand side indeed approaches a regularized δ -distribution, with a characteristic width given by $\eta = 1/(3+2\beta)$.

Note that relation (4.81) results after integrating a Feynman loop integrand of the type $1/[p_E^2 + (m_n^W)^2 - xym_h^2]^3$ over d^4p_E (after the Wick rotation), analogously to (4.8). In order for this integral to exist, we again have to require that both $T_W(p_E^2)$ and $p_E \partial_{p_E} T_W(p_E^2)$ vanish for very large Euclidean momenta. We will show that this is indeed the case below. The vanishing behavior of $T_W(p_E^2)$ is also the reason why in (4.82) there is no boundary term $T_W(\Lambda_{\text{TeV}}^2)$ as in (4.72). Recall that this plateau stemming from the non-zero value of the fermion propagator at $t = t' = 1^-$ in the limit $\hat{p}_E \rightarrow \infty$ was the reason for the different results in the brane-localized and the narrow bulk-Higgs scenario.

We now evaluate the result (4.83) and insert the propagator in the time-like region (3.25), evaluated at $t = t' = 1$, into (4.83). We obtain (with $\hat{p} \equiv p/M_{\text{KK}} + i0$)

$$T_W(-p^2) = \frac{1}{2\pi\tilde{m}_W^2} \left[1 + \frac{\hat{p}M_{\text{KK}}^2}{L\tilde{m}_W^2} \frac{J_0(\hat{p}) Y_0(\hat{p}\epsilon) - Y_0(\hat{p}) J_0(\hat{p}\epsilon)}{J_1(\hat{p}) Y_0(\hat{p}\epsilon) - Y_1(\hat{p}) J_0(\hat{p}\epsilon)} \right]^{-1} \equiv \frac{1}{2\pi\tilde{m}_W^2} \hat{T}_W(-p^2), \quad (4.85)$$

which is exact to all orders in v^2/M_{KK}^2 .⁹ It follows from this expression that $\hat{T}_W(0) = 1$. We have thus succeeded in deriving a closed analytic expression for the Wilson coefficient $C_{1\gamma}^W$ in (4.82), valid for the minimal RS model with a Higgs sector localized on the IR brane. The quantity \tilde{m}_W , which is the leading-order contribution to the mass of the physical W boson, has been kept in the prefactor above, since it will cancel against a corresponding factor in the definition of the Wilson coefficient (4.82). Indeed, the final result for this coefficient takes the form

$$C_{1\gamma}^W = -\frac{3}{2} \left[1 + 6 \int_0^1 dx \int_0^{1-x} dy (1 - 2xy) \hat{T}_W(-xym_h^2) \right]. \quad (4.86)$$

Before we proceed, we will briefly study the behavior of the propagator function in the region of large space-like momenta. For large Euclidean momenta $p_E \gg M_{\text{KK}}$, this function approaches an inverse power-law behavior given by

$$T_W(p_E^2) = \frac{L}{2\pi M_{\text{KK}}} \frac{1}{p_E} + \mathcal{O}(p_E^{-2}), \quad (4.87)$$

which can be easily read off from (3.37). It follows that both $T_W(p_E^2)$ and $p_E \partial_{p_E} T_W(p_E^2)$ vanish for large Euclidean momenta $p_E^2 = -p^2 \rightarrow \infty$, and hence the conditions required for the validity of relation (4.82) are indeed satisfied. This holds for both the brane-localized and the (narrow-) bulk Higgs scenario.

Analysis of the Zero-Mode and KK Contributions

The exact expression for the overlap integral $T_W(-p^2)$ in (4.85) contains the contribution of the zero mode – the standard W boson with its modified coupling to the Higgs field – as well as the infinite tower of KK excitations. It is instructive to isolate the contribution from the zero mode and the KK tower explicitly. To this end, we expand the exact formula in powers of v^2/M_{KK}^2 , using that we need this function for values $p^2 = \mathcal{O}(m_h^2)$ much smaller than the KK scale M_{KK}^2 . We find

$$\hat{T}_W(-p^2) = \frac{m_W^2}{m_W^2 - p^2 - i0} \left[1 - \frac{m_W^2}{2M_{\text{KK}}^2} \left(\frac{L}{c_\vartheta^2} - 1 + \frac{1}{2L} \right) \right] + \frac{m_W^2}{2M_{\text{KK}}^2} \left(\frac{L}{c_\vartheta^2} - 1 + \frac{1}{2L} \right), \quad (4.88)$$

where $c_\vartheta = 1$ in the minimal RS model and we have neglected terms of $\mathcal{O}(v^4/M_{\text{KK}}^4)$. We will show below that the same result holds in the custodial RS model, where however the parameter $c_\vartheta = 1/\sqrt{2}$ takes a different value. In the above result the parameter \tilde{m}_W has been replaced by the physical W -boson mass m_W using relation (2.30).

Based on the formulas above, we can perform the integration over the Feynman parameters in (4.82) and find the Wilson coefficient

$$C_{1\gamma}^W = -\frac{21}{4} \left[\kappa_W A_W(\tau_W) + \nu_W \right] + \mathcal{O}\left(\frac{v^4}{M_{\text{KK}}^4}\right), \quad C_{5\gamma}^W = 0, \quad (4.89)$$

where $\tau_W = 4m_W^2/m_h^2$, and the W -boson loop function

$$A_W(\tau) = \frac{1}{7} \left[2 + 3\tau + 3\tau(2 - \tau) \arctan^2 \frac{1}{\sqrt{\tau - 1}} \right] \quad (4.90)$$

⁹We can simplify the result using that $J_0(\hat{p}\epsilon) = 1 + \mathcal{O}(\epsilon^2)$ and $Y_0(\hat{p}\epsilon) = (2/\pi)(\gamma_E + \ln(\hat{p}/2) - L) + \mathcal{O}(\epsilon^2)$.

approaches 1 for $\tau \rightarrow \infty$ [228]. Analogously to (4.37), we can interpret the two terms in (4.89): The first contribution to $C_{1\gamma}$ arises from the standard W boson, whose coupling to the Higgs boson is modified, compared with the SM, by a factor κ_W times v_{SM}/v . The last factor is accounted for by using the Higgs vev in the RS model in the definition of the effective operators in (4.68). The term ν_W in (4.89) is due to the KK excitations. Explicitly, we obtain

$$\kappa_W = 1 - \frac{m_W^2}{2M_{\text{KK}}^2} \left(\frac{L}{c_\vartheta^2} - 1 + \frac{1}{2L} \right), \quad \nu_W = \frac{m_W^2}{2M_{\text{KK}}^2} \left(\frac{L}{c_\vartheta^2} - 1 + \frac{1}{2L} \right). \quad (4.91)$$

Note that at this order $\nu_W = (1 - \kappa_W)$, such that the RS corrections to $C_{1\gamma}$ in (4.89) would cancel in the limit $\tau_W \rightarrow \infty$. This simple relation is, however, not preserved in higher orders. The result for $C_{1\gamma}$ agrees with a corresponding expression derived in [157]. Notice also that the value of κ_W is consistent with relation (4.75), which gives $\kappa_W = \frac{\tilde{m}_W^2}{m_W^2} 2\pi[\chi_0^W(1)]^2$.

We close this subsection by returning briefly to the case of a (narrow) bulk-Higgs model, in which the scalar sector is localized not on but near the IR brane. As a concrete model, we adopt the scenario discussed at the end of Subsection 2.2.1. As discussed earlier, relation (4.83) still holds in this model provided one makes the replacement (4.84) and calculated the gauge-boson propagator in the background of a bulk-Higgs field. The latter propagator has been derived in the previous chapter and the result can be found in (3.31) with (3.52). We then find

$$\begin{aligned} \kappa_W^{\text{bulk}} &= 1 - \frac{m_W^2}{2M_{\text{KK}}^2} \left[\frac{2L(1+\beta)^2}{(2+\beta)(3+2\beta)} - \frac{(1+\beta)(3+\beta)}{(2+\beta)^2} + \frac{1}{2L} \right] = \kappa_W + \frac{3Lm_W^2}{2M_{\text{KK}}^2} \eta + \dots, \\ \nu_W^{\text{bulk}} &= \frac{m_W^2}{2M_{\text{KK}}^2} \left[\frac{L(1+\beta)}{(2+\beta)} - \frac{(1+\beta)(3+\beta)}{(2+\beta)^2} + \frac{1}{2L} \right] = \nu_W - \frac{Lm_W^2}{M_{\text{KK}}^2} \eta + \dots, \end{aligned} \quad (4.92)$$

instead of (4.91). In the last step we have identified $\eta = 1/(3+2\beta)$ and taken the limit $\eta \ll 1$. This demonstrates that the result for the bosonic loop contributions to the $h \rightarrow \gamma\gamma$ amplitude interpolates smoothly from the narrow bulk-Higgs scenario into a scenario with a brane-localized scalar sector. Note also that the largest effect is obtained for the brane-localized Higgs scenario, since the corrections for a bulk Higgs ($\nu > 0$) point in the direction of the SM prediction $\kappa_W^{\text{SM}} = 1$ and $\nu_W^{\text{SM}} = 0$. This can be traced back to the smaller overlap integrals of the Higgs-boson profile with the profiles of the W -boson zero mode and its KK excitations.

4.2.3 Extension to the RS Model with Custodial Symmetry

The above results will now be generalized to the RS model with custodial protection. First the fermionic loop contributions to the $h \rightarrow \gamma\gamma$ amplitude are presented, where it is distinguished between the quark and the lepton contribution. Since the lepton sector has not been discussed in Section 2.3, it will be shortly introduced here as well. Then, the focus will be put on the W -boson loop contribution, where we will confirm the results (4.89) and (4.91), where c_ϑ is now an additional parameter.

Quark Contributions to the Wilson Coefficients

The loop contributions from the quarks to the $h \rightarrow \gamma\gamma$ amplitude in the custodial RS model are generalizations of relations (4.73) and read

$$\begin{aligned}
C_{1\gamma}^q &\approx \left[1 - \frac{2v^2}{3M_{\text{KK}}^2} \text{Re} \frac{(\mathbf{Y}_u \mathbf{Y}_u^\dagger \mathbf{Y}_u)_{33}}{(\mathbf{Y}_u)_{33}} \right] N_c Q_u^2 A_q(\tau_t) + N_c Q_d^2 A_q(\tau_b) \\
&\quad + N_c Q_u^2 \text{Re Tr } g(\sqrt{2}\mathbf{X}_u) + N_c (Q_u^2 + Q_d^2 + Q_\lambda^2) \text{Re Tr } g(\sqrt{2}\mathbf{X}_d), \\
C_{5\gamma}^q &\approx -\frac{2v^2}{3M_{\text{KK}}^2} \text{Im} \left[\frac{(\mathbf{Y}_u \mathbf{Y}_u^\dagger \mathbf{Y}_u)_{33}}{(\mathbf{Y}_u)_{33}} \right] N_c Q_u^2 B_q(\tau_t) \\
&\quad + N_c Q_u^2 \text{Im Tr } g(\sqrt{2}\mathbf{X}_u) + N_c (Q_u^2 + Q_d^2 + Q_\lambda^2) \text{Im Tr } g(\sqrt{2}\mathbf{X}_d),
\end{aligned} \tag{4.93}$$

where the explicit forms of the function $g(\mathbf{X}_f)$ are given in (4.25), (4.26), and (4.41). Recall that the Taylor expansion of these functions starts with \mathbf{X}_f^2 , and thus the factors of $\sqrt{2}$ arising in the quark contributions in the custodial model approximately double the contribution arising in the minimal model. Combined with the large electric charge of the λ -type quarks, one finds that due to the higher multiplicity of KK quark states the contribution in the custodial RS model is much larger than in the minimal model [150, 224], by approximately a factor 68/5.

Charged-Lepton Contributions to the Wilson Coefficients

The result for the loop contributions to the $h \rightarrow \gamma\gamma$ amplitude involving charged leptons depends on the way in which the lepton fields are embedded into the extended gauge symmetry of the custodial RS model. A first possibility is a model in which the lepton multiplets are chosen in analogy to the quark multiplets in (2.175). This choice was adopted in [185]. In component notation, the corresponding fields are

$$\begin{aligned}
\xi_{1L} &= \begin{pmatrix} \nu_L^{(+)} & \psi_L^{(-)} \\ \begin{pmatrix} + \\ - \end{pmatrix} & \begin{pmatrix} 1 \\ 0 \end{pmatrix} \\ e_L & \nu_L' \end{pmatrix}_0, & \xi_{2R} &= \begin{pmatrix} \nu_R^{c(+)} \\ 0 \end{pmatrix}_0, \\
\xi_{3R} = \mathcal{T}_{3R} \oplus \mathcal{T}_{4R} &= \begin{pmatrix} \Psi_R'^{-} \\ \begin{pmatrix} - \\ 0 \end{pmatrix} \\ N_R' \\ E_R' \end{pmatrix}_0 \oplus \begin{pmatrix} E_R^{(+)} & N_R^{(-)} & \Psi_R^{(-)} \\ -1 & 0 & 1 \end{pmatrix}_0.
\end{aligned} \tag{4.94}$$

There are fifteen different lepton states in the neutrino sector and nine in the charged-lepton sector. The boundary conditions give rise to three light modes in each sector, which are identified with the SM neutrinos and charged leptons. These are accompanied by KK towers consisting of groups of fifteen and nine modes in the two sectors, respectively. In addition, there is a KK tower of exotic lepton states with electric charge $Q_\psi = +1$, which exhibits nine excitations in each KK level. This is the analog to the exotic λ -type quarks in the quark sector. The gauge-invariant Yukawa interactions for these fields are constructed in complete analogy with the quark Yukawa interactions [149, 185]. They can be expressed in terms of two dimensionless 3×3 Yukawa matrices \mathbf{Y}_ν and \mathbf{Y}_e , having an anarchic structure as always. When dressed with the fermion profiles on the IR brane, these matrices give masses to the SM leptons. The resulting contributions to the Wilson coefficients have the same structure as in (4.93), except that there are no zero-mode contributions (they are proportional to m_l^2/m_h^2 and thus can be

neglected) and that we must replace $\mathbf{Y}_u \rightarrow \mathbf{Y}_\nu$, $\mathbf{Y}_d \rightarrow \mathbf{Y}_e$, $N_c \rightarrow 1$, and $Q_u \rightarrow Q_\nu = 0$, $Q_d \rightarrow Q_e = -1$, $Q_\lambda \rightarrow Q_\psi = +1$. We thus obtain

$$C_{1\gamma}^l + iC_{5\gamma}^l \approx (Q_e^2 + Q_\psi^2) \text{Tr} g(\sqrt{2}\mathbf{X}_e). \quad (4.95)$$

It follows that the leptonic contribution in the custodial RS model is approximately 4 times larger than in the minimal model.

A second possibility is a model with a more minimal embedding of the leptons into the extended gauge group. Note that there are no such constraints from $Z\tau\bar{\tau}$ as in the case of the quarks from $Zb\bar{b}$. Thus, it is not necessary to embed the left-handed neutrino and the left-handed charged lepton in the same $SU(2)_L \times SU(2)_R$ bidoublet. The simplest assignment is to put the left-handed neutrino and electron into an $SU(2)_L$ doublet (as in the SM) and the right-handed electron along with a new, exotic neutral particle N_R into an $SU(2)_R$ doublet. The lepton fields with even Z_2 parity are then chosen as

$$L_L = \begin{pmatrix} \nu_L^{(+)} \\ (+) \\ e_L \end{pmatrix}_{-\frac{1}{2}}, \quad L_R^c = \begin{pmatrix} e_R^{c(+)} \\ (-) \\ N_R \end{pmatrix}_{-\frac{1}{2}}, \quad (4.96)$$

and they transform as $(\mathbf{2}, \mathbf{1})$ and $(\mathbf{1}, \mathbf{2})$, respectively. The choice of the boundary conditions is such that the zero modes correspond to the light leptons of the SM, without a right-handed neutrino. The gauge-invariant Yukawa interaction that can be built using these fields is

$$\mathcal{L}_Y = \frac{v}{\sqrt{2}} \int_{-\pi}^{\pi} d\phi \delta(|\phi| - \pi) e^{-3\sigma(\phi)} \frac{2}{k} (Y_e)_{ij} (\bar{L}_L^i \Phi \varepsilon L_R^{cj} + \bar{L}_R^i \Phi \varepsilon L_L^{cj}) + \text{h.c.}, \quad (4.97)$$

where $\varepsilon = i\sigma^2$. Upon electroweak symmetry breaking this generates a mass term for the zero modes of the charged leptons. The SM neutrinos remain massless at this order. Their masses can be explained by means of higher-dimensional operators [234–236]. The only additional lepton field is the right-handed neutrino, which is charged under $SU(2)_R$ but electrically neutral, so that it does not affect the $h \rightarrow \gamma\gamma$ decay amplitude. The lepton contribution is therefore the same as in the minimal version of the RS model, namely $C_{1\gamma}^l + iC_{5\gamma}^l \approx Q_e^2 \text{Tr} g(\mathbf{X}_e)$ as in (4.74).

Bosonic Contribution to the Wilson Coefficients

Finally, we turn to the bosonic contribution to the $h \rightarrow \gamma\gamma$ amplitude in the custodial RS model. For this, we first deduce the Feynman rules from the ones in the minimal model compiled in Appendix C. Using (2.158), we can convince ourselves that the W_M^\pm couplings to the photon are not changed at all. This statement is independent of the basis, since the rotation matrix \mathbf{R}_ϑ in the KK decomposition (2.156) drops out in the orthonormalization condition. In contrast, as mentioned in the discussion below (2.147) the Higgs only couples to the IR basis fields \tilde{A}_μ^\pm with a strength proportional to $(g_{L,5}^2 + g_{R,5}^2)$. This can be taken into account with the help of the projection operator \mathbf{P}_+ rotated into the IR basis and accompanied by a factor $1/c_\vartheta^2$. It follows that, compared with the SM, all KK-diagonal Higgs couplings in the custodial RS model come with a prefactor

$$\frac{2\tilde{m}_W^2}{c_\vartheta^2 v} 2\pi \vec{\chi}_n^W(1)^T \mathbf{R}_\vartheta^T \mathbf{P}_+ \mathbf{R}_\vartheta \vec{\chi}_n^W(1) \equiv \frac{2\tilde{m}_W^2}{c_\vartheta^2 v} 2\pi \vec{\chi}_n^W(1)^T \mathbf{D}_\vartheta \vec{\chi}_n^W(1), \quad (4.98)$$

which replaces the corresponding factor (4.75) in the minimal model. The matrix \mathbf{D}_ϑ has been introduced in (2.165). In analogy with expression (4.76) valid in minimal RS model, we then find that the $h \rightarrow \gamma\gamma$ amplitude in the custodial RS model can be written as

$$\mathcal{A}_{\text{cust. RS}}^W(h \rightarrow \gamma\gamma) = \frac{\tilde{m}_W^2}{c_\vartheta^2 v} \sum_{n=0}^{\infty} 2\pi \vec{\chi}_n^W(1)^T \mathbf{D}_\vartheta \vec{\chi}_n^W(1) \left[\frac{v_{\text{SM}}}{m_W^2} \mathcal{A}_{\text{SM}}^W(h \rightarrow \gamma\gamma) \right]_{m_W \rightarrow m_n^W}. \quad (4.99)$$

It follows that expression (4.82) for the Wilson coefficient $C_{1\gamma}^W$ remains valid, provided we replace the quantity $T_W(-p^2)$ defined in (4.83) with

$$T_W(-p^2) = \text{Tr} \left[\frac{\mathbf{D}_\vartheta}{c_\vartheta^2} \mathbf{B}_W^{\text{UV}}(1, 1; -p^2 - i0) \right]. \quad (4.100)$$

With the help of the solution for the propagator function \mathbf{B}_W^{UV} shown in (3.39), it is now straightforward to calculate the quantity $T_W(-p^2)$ in (4.100), which we need for the calculation of the Wilson coefficient $C_{1\gamma}^W$ in (4.82). Expanding this answer in powers of v^2/M_{KK}^2 and for $p^2 = \mathcal{O}(m_h^2)$, i.e. using (3.40), we recover expression (4.88). With respect to the minimal RS model, the only modification concerns the coefficient of the leading L -enhanced correction terms, which is enhanced by $1/c_\vartheta^2$. This affects both the contributions from the W boson and the KK tower. In the custodial RS model with P_{LR} symmetry, this enhancement factor is equal to 2. With $c_\vartheta^2 = 1/2$ the expressions in (4.91) are compatible with corresponding results obtained in [149]. In this reference the Wilson coefficient $C_{1\gamma}^W$ belonged to the operator $vhF_{\mu\nu}F^{\mu\nu}$ instead of the one in (4.68), and hence $\kappa_W^{\text{Ref. [19]}} = \kappa_W/\kappa_v^2$.

4.3 The Flavor-Changing Neutral Current $b \rightarrow s\gamma$

This section focuses on the flavor-changing neutral current $b \rightarrow s\gamma$. This transition is the underlying quark-level process of the B decays discussed in the phenomenological Chapter 5. As in the previous sections, it is assumed that the reader is familiar with the SM calculation of $b \rightarrow s\gamma$ and, moreover, with the associated RG evolution [4, 237–240]. This section includes unpublished work and is a continuation of my diploma thesis [184]. Detailed calculations of the required Feynman rules and the amplitudes (in terms of infinite KK sums) can be found there. Here, it will be focused on deriving compact formulas for the corresponding Wilson coefficients. As opposed to the results derived in the previous two sections, they will, however, only be valid at leading order in the expansion in v^2/M_{KK}^2 .

4.3.1 Preliminaries

Like the loop-induced processes in the Higgs sector analyzed in the previous sections, the $b \rightarrow s\gamma$ transition only occurs at loop-level in the SM, illustrated in Figure 4.4, and is one of the most interesting processes in flavor physics. This is for two reasons: Besides being suppressed by a loop factor, this FCNC is moreover suppressed by the GIM mechanism [49], which results in a high sensitivity of the process to high-scale physics. On the other hand, it is dominated by perturbative QCD effects which replace

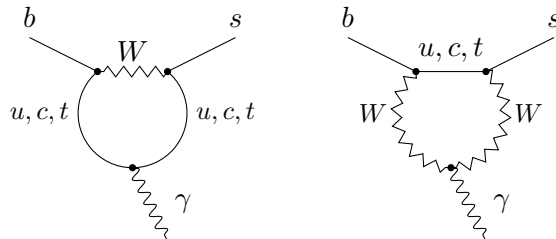


FIGURE 4.4: The two leading-order diagrams contributing to the $b \rightarrow s\gamma$ in the SM (in unitary gauge). In a general R_ξ gauge, there are four further diagrams, where at least one W -boson line is replaced by the scalar propagator of the Goldstone boson.

the power-like GIM suppression by a logarithmic one [241]. The mild suppression of the QCD corrected amplitude reduces the sensitivity to new physics, but enhances the branching ratio for e.g. $\bar{B} \rightarrow X_s\gamma$ with respect to the purely electroweak prediction by a factor of around three and is therefore experimentally accessible.¹⁰ The logarithmic GIM cancellation originates from operator mixing and the non-conservation of the tensor current which is generated at the electroweak scale by loop diagrams involving W -boson and top-quark exchange. The associated large logarithms $L = \log(m_W/m_b)$ have to be resummed at each order in α_s , using techniques of the RG improved perturbation theory, see e.g. [238–240].

A convenient framework to achieve the resummation is to describe the process $b \rightarrow s\gamma$ via an effective Lagrangian with five active quarks, photons, and gluons, whereas the electroweak gauge bosons and the top quark are integrated out. Including terms of dimension up to six in the local operator product expansion the effective Lagrangian at a scale $\mu \lesssim m_W$ reads [239, 242, 243]

$$\mathcal{L}_{\text{eff}} = \mathcal{L}_{\text{QCD} \times \text{QED}} + \frac{4G_F}{\sqrt{2}} V_{ts}^* V_{tb} \sum_{k=1}^{6,7\gamma,8g} C_k(\mu) Q_k(\mu). \quad (4.101)$$

Here, the first term is the conventional QCD and QED Lagrangian for the light SM particles. The second term includes the Fermi constant G_F , the elements of the CKM matrix V_{ij} and the Wilson coefficients $C_k(\mu)$ of the corresponding operators Q_k built out of the light fields. Due to operator mixing effects all operators can contribute to the $b \rightarrow s\gamma$ transition. They can be written as

$$\begin{aligned} Q_{1,2} &= (\bar{s}\Gamma_i c)(\bar{c}\Gamma'_i b), & Q_{7\gamma} &= \frac{em_b}{16\pi^2} \bar{s}\sigma_{\mu\nu} F^{\mu\nu} P_R b, \\ Q_{3-6} &= \bar{s}\Gamma_i b \sum_q \bar{q}\Gamma'_i q, & Q_{8g} &= \frac{g_s m_b}{16\pi^2} \bar{s}\sigma_{\mu\nu} \mathcal{G}_a^{\mu\nu} t_a P_R b, \end{aligned} \quad (4.102)$$

where the quantities Γ_i and Γ'_i , which enter both the current-current operators $Q_{1,2}$ and the QCD penguin operators Q_{3-6} , stand for various products of Dirac and color matrices [242, 243]. In the definition of the *dipole* operators $Q_{7\gamma}$ and Q_{8g} , the fields $q_{L,R} \equiv P_{L,R} q$ denote the chiral quarks, $F^{\mu\nu}$ and $\mathcal{G}_a^{\mu\nu}$ are the electromagnetic and gluonic field strength tensors, and t_a are the color generators. The most important operators for the $b \rightarrow s\gamma$ transition are given by the dipole operators $Q_{7\gamma}$ and Q_{8g} , whose Wilson coefficients evaluated at scale μ_b contribute to the observables that will be studied in Chapter 5. Due to the already mentioned QCD effects, the initial conditions $C_k(\mu_W)$ of

¹⁰In fact, the branching ratio $\text{Br}(\bar{B} \rightarrow X_s\gamma)$ is a well-measured observable, see Section 5.2.

the remaining Wilson coefficients at the matching scale $\mu_W = \mathcal{O}(m_W)$ (where the heavy SM particles are integrated out) also give a non-negligible contribution to $C_{7\gamma}(\mu_b)$ and hence have to be determined as well.

In order to determine the impact of the RS model on $b \rightarrow s\gamma$ we also make use of an EFT approach and use the effective Lagrangian ($\mu \lesssim \mu_{\text{KK}} \equiv \mathcal{O}(M_{\text{KK}})$)

$$\begin{aligned} \mathcal{L}_{\text{eff}} = & \frac{4G_F}{\sqrt{2}} V_{ts}^* V_{tb} \left[C_{7\gamma}(\mu) Q_{7\gamma}(\mu) + \tilde{C}_{7\gamma}(\mu) \tilde{Q}_{7\gamma}(\mu) + C_{8g}(\mu) Q_{8g}(\mu) + \tilde{C}_{8g}(\mu) \tilde{Q}_{8g}(\mu) \right] \\ & + \text{non-dipole operators}, \end{aligned} \quad (4.103)$$

where the prefactors have been extracted according to (4.101). We will touch on the non-dipole operators which can contribute to the dipole operators through operator mixing in Subsection 4.3.4. The Wilson coefficients $\tilde{C}_{7\gamma,8g}$ belong to the *chirality-flipped* operators $\tilde{Q}_{7\gamma,8g}$, defined by

$$\tilde{Q}_{7\gamma} = \frac{em_b}{16\pi^2} \bar{s} \sigma_{\mu\nu} F^{\mu\nu} P_L b, \quad \tilde{Q}_{8g} = \frac{g_s m_b}{16\pi^2} \bar{s} \sigma_{\mu\nu} G_a^{\mu\nu} t_a P_L b, \quad (4.104)$$

which are suppressed by m_s/m_b in the SM and therefore negligible. We will see that they receive large contributions in the RS model. In (4.103), all KK modes are integrated out, whereas all SM particles including the top quark as well as the electroweak gauge bosons are still active degrees of freedom.

The main goal of this section is the derivation of compact, analytic expressions for the Wilson coefficients

$$C_{7\gamma,8g}^{\text{KK}} \equiv C_{7\gamma,8g}(\mu_{\text{KK}}) \quad \text{and} \quad \tilde{C}_{7\gamma,8g}^{\text{KK}} \equiv \tilde{C}_{7\gamma,8g}(\mu_{\text{KK}}), \quad (4.105)$$

which after the RG evolution down to the hadron scale μ_b , represent the RS corrections to the SM predictions. There are several differences with respect to the previous two sections: Higgs processes take place at scales of $\mathcal{O}(m_h)$, whereas B meson decays which are based on the $b \rightarrow s\gamma$ amplitude occur at much smaller scales $\mu_b = \mathcal{O}(m_b) \ll m_h, M_{\text{KK}}$. Thus, while in the Higgs processes mixing effects are small, they have to be taken into account in the present case. Furthermore, again due to the RG running, we need to distinguish between the contributions stemming from the KK modes and those from the zero modes. Recall that in the final results (4.7) and (4.82) both contributions have been included implicitly. Finally, we will see that there are two (instead of one) infinite KK towers contributing to this process. It has not been achieved yet to obtain closed formulas like (4.7) and (4.82) for the corresponding Wilson coefficients which are integrals of the 5D propagators with the Higgs profile over the fifth dimension and exact to all orders in v^2/M_{KK}^2 . However, we will find that at leading order in the latter expansion the final results can be well approximated in terms of simple expressions that have already been encountered in the tree-level processes discussed in [145, 149, 183].

The influence of the RS model with a brane-localized Higgs sector on loop-induced FCNCs like $b \rightarrow s\gamma$ was firstly estimated and discussed in various works [169, 176, 177, 244], claiming the amplitudes to be logarithmically divergent at one-loop level and thus UV sensitive at all orders. Putting a special focus on the counting of superficial degrees of freedom, the authors of [216] showed that all diagrams describing the leptonic decay $\mu \rightarrow e\gamma$ are finite at one-loop order, including the diagrams with a brane-localized Higgs field, that are superficially logarithmically divergent. Likewise, the process $b \rightarrow s\gamma$ was investigated in the 5D formalism in [245]. In the latter references, the authors used free 5D propagators in mixed position/momentum space and treated the Yukawa

interactions as perturbations. We will take a different approach: We will perform a complete calculation in the 4D KK formalism and provide a careful discussion concerning convergence behavior and the relative magnitudes of the various types of diagrams. The results will then be compared to those of [245]. The calculation of this process using the 5D propagators derived in Chapter 3, which in principle is possible but in reality causes some subtleties, is left for future work. Also, only the effects of the minimal RS model will be focused on here.

This section is structured as follows: In Subsection 4.3.2, we will recapitulate the calculation of all diagrams contributing to the $b \rightarrow s\gamma$ amplitude in the minimal RS model. A thorough analysis of the results will be provided in Section 4.3.3, which forms the main part of this section. Using the equations of motion for the fermion profiles, one can derive analytic formulas for the Wilson coefficients, which are valid at leading order in the expansion in v^2/M_{KK}^2 . Being calculable with small numerical effort, these formulas facilitate to study the RS effects on observables related to the dipole operators. In Subsection 4.3.4, the RG evolution of the Wilson coefficients down to the hadronic scale μ_b will be presented. Finally, we will comment on the structure of the RS corrections to the Wilson coefficients at μ_b . The phenomenological consequences will be discussed in Section 5.2 of the next chapter.

4.3.2 Calculation of the $b \rightarrow s\gamma$ Amplitude

We begin with a repetition of the calculation of the $b \rightarrow s\gamma$ amplitude in the minimal RS model [184, 230]. Due to the variety of flavor-changing couplings in the RS model, there are many more one-loop diagrams contributing at leading order than in the SM. They are shown in Figure 4.5, where the diagonal coupling of the photon zero mode $\gamma \equiv A^{(0)}$ has already been taken into account. Note that in a general R_ξ gauge, each gauge-boson diagram has an additional diagram where the gauge boson is replaced by the corresponding Goldstone boson. In the case of the W -boson emitting the photon, i.e. diagram (f), there are three more diagrams. Then, there are in total thirteen diagrams contributing to the amplitude. They are explicitly shown in Appendix D. Due to the gauge-invariance of the diagrams, however, it will be sufficient to consider only the six diagrams of Figure 4.5 (in unitary gauge).

Analogously to the Higgs processes, we parametrize the $b \rightarrow s\gamma$ amplitude by means of the two Wilson coefficients defined via (at scale $\mu = \mu_{\text{KK}}$)

$$\mathcal{A}(b \rightarrow s\gamma) = \frac{4G_F}{\sqrt{2}} V_{ts}^* V_{tb} \left\{ C_{7\gamma}^{\text{KK}} \langle s\gamma | Q_{7\gamma} | b \rangle + \tilde{C}_{7\gamma}^{\text{KK}} \langle s\gamma | \tilde{Q}_{7\gamma} | b \rangle \right\}. \quad (4.106)$$

The Wilson coefficients contributing to $b \rightarrow sg$, i.e. C_{8g}^{KK} and $\tilde{C}_{8g}^{\text{KK}}$, can be easily extracted from the corresponding ones contributing to $b \rightarrow s\gamma$ once the factors are adjusted properly. The Feynman diagrams are essentially given by the ones shown in Figure 4.5, where the outgoing photon has to be replaced by a gluon $g \equiv \mathcal{G}^{(0)}$. The only difference is the three-gluon diagram having a different topology compared to the $WW\gamma$ -vertex diagram (f) in Figure 4.5. We will treat this diagram separately.

For the time being, we focus on the RS corrections $C_{7\gamma}^{\text{KK}}$ and $\tilde{C}_{7\gamma}^{\text{KK}}$, i.e. the contributions from diagrams with at least one KK mode in the loop. The zero-mode contributions, i.e. diagrams with quark and gauge-boson zero modes or the Higgs-boson, are included later. The goal is to calculate these Wilson coefficients, which, as mentioned

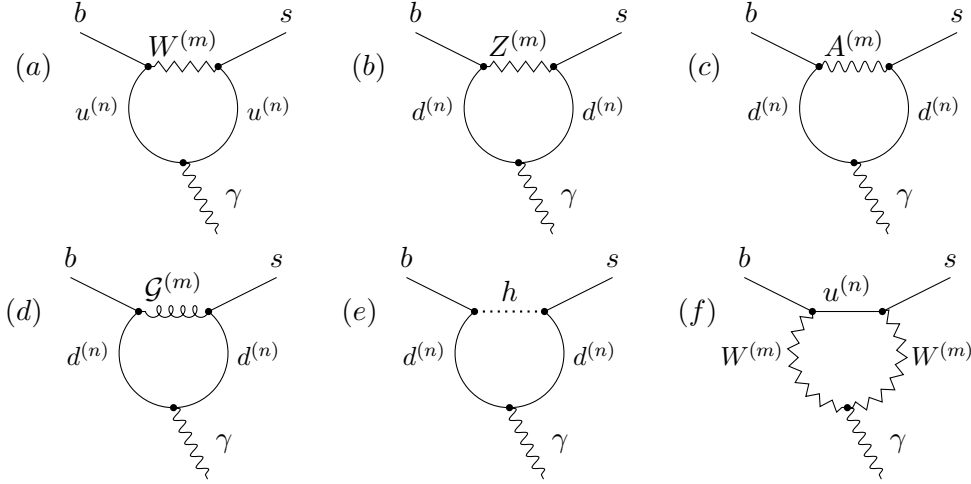


FIGURE 4.5: Feynman diagrams contributing to $b \rightarrow s\gamma$ in the minimal RS model at leading order and in unitary gauge. In general R_ξ gauge, there are additional diagrams, where the respective gauge boson $B_\mu^{(m)} = A_\mu^{(m)}, \mathcal{G}_\mu^{(m)}, W_\mu^\pm(m), Z_\mu^{(m)}$ is replaced by the associated scalar degree of freedom $\varphi_B^{(m)}$, see Appendix D.

above, consist of five parts

$$C_i^{\text{KK}} = C_i^W + C_i^{\mathcal{G}} + C_i^\gamma + C_i^Z + C_i^h, \quad i = 7\gamma, 8g. \quad (4.107)$$

An analogous formulas holds for \tilde{C}_i^{KK} . Note that $C_{8\gamma}^W$ ($C_{8g}^{\mathcal{G}}$) includes both diagrams (a) and (f) (the three-gluon vertex in the case of $C_{8g}^{\mathcal{G}}$). Similarly to Section 4.2, the calculation of the $b \rightarrow s\gamma$ amplitude is performed in the KK-decomposed theory and the gauge invariance of the amplitude is shown. As an example, we consider the W -boson exchange diagram (a). The remaining diagrams can be studied analogously.

Feynman Rules and Gauge Invariance

As opposed to the diagrams contributing to the $gg \rightarrow h$ and $h \rightarrow \gamma\gamma$ amplitudes, the diagrams depicted in Figure 4.5 involve gauge-boson couplings to fermions. The derivation of the corresponding Feynman rules can be found in [184, 230] and a summary of all Feynman rules crucial for the following analysis is listed in Appendix C. They all have the same general form illustrated at the example of the W^+ -exchange:

$$\begin{array}{c} d^{(k)} \\ \xrightarrow{p} \bullet \\ \swarrow \quad \searrow \\ q \quad k \\ \gamma \quad \gamma \\ W_\alpha^{+(m)} \end{array} \quad \bar{u}^{(n)} = i \frac{g_5}{\sqrt{2}} \frac{1}{\sqrt{2\pi r}} \gamma^\alpha \left(V_{nmk}^{W^+} P_L + \tilde{V}_{nmk}^{W^+} P_R \right).$$

The superscript at the gauge boson denotes the incoming charge, while the bar above the quark field stands for an outgoing up-type quark. The overlap integrals V_{nmk} and \tilde{V}_{nmk} are integrals of the fermion and boson profiles over the extra dimension and determine the strength of the respective boson coupling to left-handed (right-handed) quarks. Their explicit form can be found in (2.123)–(2.125). The factors in front of the parenthesis are similar to those of the SM if one identifies with the SM gauge coupling $g_{\text{SM}} \equiv g_5/\sqrt{2\pi r}$, where g_5 is the five-dimensional $SU(2)_L$ gauge coupling in the RS model. As before, we

rewrite the 5D coupling constant as

$$\frac{g_5}{\sqrt{2\pi r}} = \frac{2\tilde{m}_W}{v}, \quad (4.108)$$

where v denotes the vev in the RS model and \tilde{m}_W is related to the physical W -boson mass via (2.30).

Working in Feynman-'t Hooft gauge ($\xi = 1$), we also have to derive the fermion couplings to the Goldstone bosons $\varphi_W^{\pm(n)}$. Similar to the Feynman rule explicitly derived in (4.77), according to (2.18) and (2.19) the coupling gets contributions from the fermion coupling to the fifth component of the gauge field W_5^\pm and of the charged degree of freedom of the Higgs doublet φ^\pm .¹¹ It turns out that summing up these two contributions leads to a very simple relation between the couplings to the Goldstone bosons and to the corresponding gauge bosons. As an example we consider the coupling to $\varphi_W^{+(m)}$ characterized by $V_{nmk}^{\varphi_W^+}$ and $\tilde{V}_{nmk}^{\varphi_W^+}$:

$$\begin{array}{c} d^{(k)} \\ \xrightarrow{p} \bullet \\ \swarrow \quad \searrow \\ q \quad k \\ \varphi_W^{+(m)} \end{array} \quad \bar{u}^{(n)} = \frac{g_5}{\sqrt{4\pi r}} \left(V_{nmk}^{\varphi_W^+} P_L + \tilde{V}_{nmk}^{\varphi_W^+} P_R \right).$$

The explicit formulas for the overlap integrals, which contain both contributions, can be found in [184, 230]. Since the contribution from W_5^\pm contains a derivative of the gauge-boson profile, see (2.18), one can use the same techniques as in (4.77) and show that these two overlap integrals can be expressed as [184, 230]

$$V_{nmk}^{\varphi_W^+} = \frac{m_n^u}{m_m^W} V_{nmk}^{W^+} - \frac{m_k^d}{m_m^W} \tilde{V}_{nmk}^{W^+}, \quad \tilde{V}_{nmk}^{\varphi_W^+} = \frac{m_n^u}{m_m^W} \tilde{V}_{nmk}^{W^+} - \frac{m_k^d}{m_m^W} V_{nmk}^{W^+}. \quad (4.109)$$

The analogous expressions for the fermion couplings to the Goldstone bosons $\varphi_W^{-(m)}$, $\varphi_Z^{(m)}$, $\varphi_A^{(m)}$, and $\varphi_G^{(m)}$ are listed in Appendix C. It is now easy to sum up the two contributions of the vector and the scalar exchange in order to derive at a gauge-invariant result. In [184, 230] it has been verified by an explicit calculation in R_ξ that the gluon exchange is ξ -independent. Since all Feynman rules have the identical structure, one can deduce that this is also true for the massive gauge bosons. Note that in the case at hand the results for the W and Z boson exchanges include the diagrams of [245] with a scalar 4D (Goldstone) boson from the Higgs doublet and KK fermions, which are supposed to give the most significant contributions to the Wilson coefficients. We will return to this issue later.

Calculation and Result of the Amplitude in the KK-Decomposed Theory

According to the discussion in Section 4.1, a UV regulator has been needed for two reasons: firstly, for ensuring gauge-invariance of the amplitude and, secondly, for regulating the momentum integral as well as the infinite sum over KK states. For the calculation of the Wilson coefficients $C_{7\gamma}$ and $\tilde{C}_{7\gamma}$ gauge-invariance is not an issue, since we do not encounter structures such as (4.3), and the (finite) result of each single diagram is

¹¹This also holds for the Z boson, whereas there is no Higgs doublet contribution to the scalars $\varphi_{A,G}^{(m)}$. The latter are just the KK modes of the fifth component of the 5D gluon (photon) field, see (2.18).

unambiguous. We have also argued that in the brane-localized Higgs scenario, we could have used the 5D fermion propagator with modified BCs and remove the regulator right from the beginning. In 4D language, this means that we can calculate the Feynman rules with a regularized Higgs profile, take the limit $\eta \rightarrow 0$, and then sum up the entire tower. No regulator is necessary because the sum over the KK modes is finite as we will see below. Thus, the evaluation of the diagrams can be performed analogously to the SM calculation [237], when using the corresponding Feynman rules [184, 230, 231]. A summary of the results for all amplitudes is given in Appendix D. Taking into account all valid values of n and m , one finds for the W -boson exchange (including the scalars $\varphi_W^{(n)}$) in the full (RS) theory [184, 230]

$$\begin{aligned}
i\mathcal{A}_W^{b \rightarrow s\gamma} &= i \frac{-2Q_u}{v^2} \sum_{n,m} \left(\frac{\tilde{m}_W}{m_m^W} \right)^2 \left[\frac{m_n^u}{m_b} I_A(x_{nm}^{uW}) V_{2mn}^{W-} \tilde{V}_{nm3}^{W+} + I_B(x_{nm}^{uW}) V_{2mn}^{W-} V_{nm3}^{W+} \right] \langle Q_{7\gamma} \rangle \\
&+ i \frac{-2Q_u}{v^2} \sum_{n,m} \left(\frac{\tilde{m}_W}{m_m^W} \right)^2 \left[\frac{m_n^u}{m_b} I_A(x_{nm}^{uW}) \tilde{V}_{2mn}^{W-} V_{nm3}^{W+} + I_B(x_{nm}^{uW}) \tilde{V}_{2mn}^{W-} \tilde{V}_{nm3}^{W+} \right] \langle \tilde{Q}_{7\gamma} \rangle,
\end{aligned} \tag{4.110}$$

where the functions I_A and I_B stem from the integration over Feynman parameters [246]. They are defined as

$$\begin{aligned}
I_A(x) &= - \frac{-4 + 3x + x^3 - 6x \log(x)}{2(x-1)^3} && \in [-2, -1/2], \\
I_B(x) &= \frac{8 - 38x + 39x^2 - 14x^3 + 5x^4 - 18x^2 \log(x)}{12(x-1)^4} && \in [5/12, 2/3],
\end{aligned} \tag{4.111}$$

and depend on the ratio of the squared masses of the internal fermions and bosons $x_{nm}^{uW} \equiv (m_n^u/m_m^W)^2$ in this particular case. Note that they are bounded on the interval $x \in [0, \infty)$, which is indicated by the intervals on the right-hand side. The left (right) value represents the value for $I_{A,B}(x)$ for $x \rightarrow 0$ ($x \rightarrow \infty$). The matrix element $\langle Q_{7\gamma} \rangle$ represents

$$\langle Q_{7\gamma} \rangle \equiv \langle s\gamma | Q_{7\gamma} | b \rangle = \frac{em_b}{8\pi^2} \bar{u}_s i\sigma^{\mu\nu} q_\nu \epsilon_\mu^* P_R u_b, \tag{4.112}$$

where $u_{s,b}$ are the Dirac spinors of the external quarks. Writing the amplitude in this way allows for an easy matching onto the effective Lagrangian (4.106). The analogous expression with $P_R \rightarrow P_L$ holds for $\langle \tilde{Q}_{7\gamma} \rangle$.

4.3.3 Analysis of the Radiative Wilson Coefficients

The result (4.111) shows that the diagrams do not only lead to contributions to $C_{7\gamma}^{\text{KK}}$, but also to the chirality flipped Wilson coefficient $\tilde{C}_{7\gamma}^{\text{KK}}$. This can be traced back to the fact that the W -boson coupling to the right-handed quarks \tilde{V}_{nmk} is non-zero in the RS model. Furthermore, each Wilson coefficient receives contributions from two terms. The second term contributes a factor m_b to the operator and is suppressed by a factor of $\mathcal{O}(1/M_{\text{KK}}^2)$. It will be referred to as the *dimension-six* contribution $C_{7\gamma}^6$. The first term, however, is proportional to m_n^u/m_b , i.e. the ratio of the mass of the n -th KK quark and the b -quark mass, and thus seems to be only suppressed by a factor of $\mathcal{O}(1/M_{\text{KK}})$. Analogously, this *dimension-five* contribution is denoted by $C_{7\gamma}^5$. NDA now tells us that this would result in the logarithmic divergent behavior of the sum as claimed in [216]. The observation of a possibly enhanced dimension-5 contribution in NP models

is not new, see e.g. [247]. If they indeed occurred, the six-dimensional operators could be neglected and we would only deal with the operators

$$Q_{7\gamma}^{5D} = \frac{e}{16\pi^2} \bar{s} \sigma_{\mu\nu} F^{\mu\nu} P_R b \quad \text{and} \quad Q_{8g}^{5D} = \frac{g_s}{16\pi^2} \bar{s} \sigma_{\mu\nu} G_a^{\mu\nu} t_a P_R b, \quad (4.113)$$

where the b -quark mass has been dropped. Analogous definitions hold for $\tilde{Q}_{7\gamma}^{5D}$ and \tilde{Q}_{8g}^{5D} . As there are no further five-dimensional operators in the theory, this would mean that only the operators $Q_{7\gamma}$ and Q_{8g} can mix, which in turn would result in a very easy RG-evolution down to the scale μ_b . However, we will argue that there are non-trivial cancellations among the KK modes like in the Higgs production [144, 150], so that the contributions above are not enhanced after all and the sum is convergent. Another surprising observation is the fact that no brane effects occur at first sight, since the overlap integrals V_{nmk}^B are usual integrals of the fermion and gauge profiles. This is the first hint that the contributions are finite as for the argumentation in [216]. However, we will find these brane-localized terms again when investigating the dimension-5 term more carefully. We will thus tackle the following three problems:

- Do the double sums in (4.110) converge, therefore leading to a well-defined result?
- Are there really dimension-5 contributions or is there a hidden suppression by $1/M_{\text{KK}}$?
- Which of the various diagrams contribute most to the Wilson coefficients?

The approach is the following: In order to confirm the finiteness, we perform a numerical calculation of the double sum (4.110) ranging from $n = 1$ to $3+6\cdot 5 = 33$ and $m = 0$ to 5 , i.e. we sum up the first five KK levels.¹² We then fit a function of the type $f(x) = a+b/x^c$. Figure 4.6 shows the behavior of convergence of five randomly selected parameter points for the real parts of $C_{7\gamma}^{\mathcal{G},5}$ and $C_{7\gamma}^{W,5}$. The plots for the imaginary parts as well as for the remaining coefficients look similar. The fact that all other points show the same feature confirms that the assumed function $f(x)$ has been a convenient choice.¹³ For each parameter set it is found that $c \approx \mathcal{O}(1)$. Consequentially, the sum converges to a limit value a and we verify the convergence of all Wilson coefficients. It is an interesting observation that the first few modes almost give the entire contribution, while the heavier KK modes decouple quickly. Having shown the finiteness of all diagrams numerically, we will now study the Wilson coefficients analytically with the help of the EOMs and BCs for the fermion profiles as well as the boson propagator functions at $p = 0$. We will see that expressing the infinite sums (4.110) in terms of simple quantities is a very good approximation. After having done this, the third bullet above can be easily addressed.

We will first focus on the gluon exchange. The photon exchange is implicitly included in this discussion, since gluons and photons have the same profiles and KK masses and thus the two results just differ by a factor. The W - and Z -boson diagrams, which additionally include a gauge-boson zero-mode, will be investigated afterwards. The Higgs diagram turns out to be completely negligible and is therefore not included in this discussion. Moreover, it will be focused on the contributions to $C_{7\gamma}$ in the following. As we will explain explicitly, almost all results for the contributions to C_{8g} as well as the

¹²The case $n = 1, 2, 3$ and $m = 0$ is, however, not included here. This case contributes to the Wilson coefficient at scale m_W , where the top quark, the electroweak gauge bosons, and the Higgs are integrated out.

¹³For the sake of clarity we refrain from showing all parameter points in Figure 4.6.

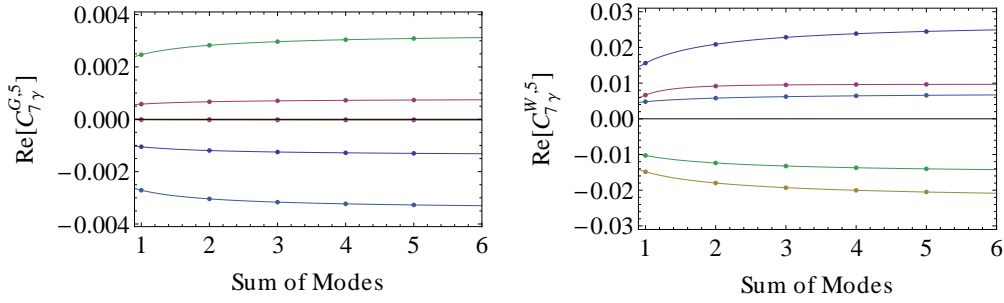


FIGURE 4.6: The real parts of the dimension-five contributions to the Wilson coefficients $C_{7\gamma}^G$ and $C_{7\gamma}^W$ as a function of the number of modes for five arbitrarily chosen parameter points. The plots for all other coefficients, the imaginary parts, and the dimension-six contributions look similar. In each case the fit function reads $f(x) = a + b/x^c$, with $c \approx \mathcal{O}(1)$ for each parameter set. These plots substantiate the finiteness of all Wilson coefficients contributing to $b \rightarrow s\gamma$.

chirality-flipped Wilson coefficients can then be deduced easily from the contributions to $C_{7\gamma}$. An exception is given by the three-gluon vertex, which will be investigated further in its own subsection. It is supposed to give the main contribution to C_{8g} and \tilde{C}_{8g} [245]. Then the analytical results for the various contributions to all aforementioned Wilson coefficients will be presented and we will discuss their orders of magnitude and the associated importance for observables.

Contributions from Gluon Exchange

In the case of the gluon contribution $C_{7\gamma}^G$, all possible combinations of n, m contribute and one finds [184, 230]

$$C_{7\gamma}^G = \sum'_{n,m} \left(\frac{\tilde{m}_W}{m_m^G} \right)^2 \left(\frac{Q_d C_F \alpha_s s_w^2}{\kappa_v^2 \alpha \lambda_t} \right) \left\{ \frac{m_n^d}{m_b} V_{2mn}^G \tilde{V}_{nm3}^G I_A(x_{nm}^{dG}) + V_{2mn}^G V_{nm3}^G I_B(x_{nm}^{dG}) \right\}, \quad (4.114)$$

where $\sum'_{n,m} = \sum_{n=1, m=1}^{\infty}$, $\lambda_t = V_{tb} V_{ts}^*$, $x_{nm}^{dG} = (m_n^d/m_m^G)^2$, and the overlap integrals V_{nmk}^G and \tilde{V}_{nmk}^G are given in (2.123). The vev shift κ_v must be taken into account, since in the matching procedure the Fermi constant ($G_F/\sqrt{2} = 1/(2v_{SM}^2)$ at tree-level) has been extracted out, see (4.106).¹⁴ The corrections to $\tilde{C}_{7\gamma}$ are obtained from the expressions given above by simply interchanging the overlap integrals V_{nmk}^G with \tilde{V}_{nmk}^G .

Owing to the fact that the functions I_A and I_B appearing in (4.114) link the two sums over the fermion and boson towers, the latter cannot be treated independently. However, as already noticed in (4.111), both loop functions are bounded on the interval $x \in [0, \infty)$. It seems to be appropriate to replace the x -dependent functions $I_A(x)$ and $I_B(x)$ by some constant, e.g. their means $I_A(x) \rightarrow c_A = -5/4$ and $I_B(x) \rightarrow c_B = 13/24$. It will turn out that a more suitable choice is to take the values $x \gg 1$ for the W and Z boson and $x \approx 1$ for the gluon and the photon. The reason is that in the former case the RS contribution is dominated by the loop with a zero-mode boson and KK fermions (and hence $x = (m_n^q)^2/m_{W,Z}^2 \gg 1$), whereas in the latter case the dominant contribution stems from the lowest lying KK fermions and KK bosons (and hence $x = (m_n^q/m_m^G)^2 \approx 1$).

¹⁴When working at leading in v^2/M_{KK}^2 , we can however neglect this correction.

Using this approximation the calculation becomes very easy. Neglecting all prefactors we can rewrite the dimension-6 contribution $C_{7\gamma}^{\mathcal{G},6}$

$$\begin{aligned}
C_{7\gamma}^{\mathcal{G},6} &\sim \sum'_{n,m} \left(\frac{1}{m_m^{\mathcal{G}}} \right)^2 V_{2mn}^{\mathcal{G}} V_{nm3}^{\mathcal{G}} \\
&= 2\pi \int_{\epsilon}^1 dt \int_{\epsilon}^1 dt' \sum'_m \frac{\chi_m^{\mathcal{G}}(t) \chi_m^{\mathcal{G}}(t')}{(m_m^{\mathcal{G}})^2} \mathcal{D}_L^{(2)\dagger}(t) \sum_n \mathcal{D}_L^{(n)}(t) \mathcal{D}_L^{(n)\dagger}(t') \mathcal{D}_L^{(3)}(t') \\
&= \frac{1}{2M_{\text{KK}}^2} \int_{\epsilon}^1 dt \int_{\epsilon}^1 dt' \left[Lt_{<}^2 - t^2 \left(\frac{1}{2} - \ln t \right) - t'^2 \left(\frac{1}{2} - \ln t' \right) + \frac{1}{2L} \right] \\
&\quad \times \delta(t-t') \mathcal{D}_L^{(2)\dagger}(t) \mathcal{D}_L^{(3)}(t') \\
&= \frac{1}{2M_{\text{KK}}^2} \int_{\epsilon}^1 dt \left[Lt^2 - 2t^2 \left(\frac{1}{2} - \ln t \right) \right] \mathcal{D}_L^{(2)\dagger}(t) \mathcal{D}_L^{(3)}(t),
\end{aligned} \tag{4.115}$$

where the definitions of the overlap integrals $V_{nmk}^{\mathcal{G}}$ have been used in the second step. In the third step, we have inserted the result for the infinite sum over the gluon profiles divided by the KK masses squared (2.127). Moreover, the completeness relation for the fermion profiles (3.62) has been employed. In the last step, the $1/2L$ term in the square bracket gives no contribution due to the orthonormality condition (2.73). Upon taking into account the prefactor, the complete expression for $C_{7\gamma}^{\mathcal{G},6}$ finally reads

$$C_{7\gamma}^{\mathcal{G},6} \approx c_B \left(\frac{Q_d C_F \alpha_s s_w^2}{2\alpha \lambda_t} \right) \frac{m_W^2}{M_{\text{KK}}^2} \left\{ L(\Delta_D)_{23} - 2(\Delta'_D)_{23} \right\}, \tag{4.116}$$

where $c_B = \mathcal{O}(1)$ is a constant and we have neglected terms of order $\mathcal{O}(v^4/M_{\text{KK}}^4)$.¹⁵ The matrices $\Delta_D^{(j)}$ have already been encountered in tree-level $\Delta F = 1$ transitions, see e.g. [189], and are explicitly given in (2.129). With the help of these easy recasts, we find that the completeness relation is responsible for a well-defined, finite result. Physically, this means that the contributions coming from the Z_2 -even and Z_2 -odd fermions within a given KK level approximately cancel each other, similar to the gluon fusion process, as discussed in [144].

Recall that the dimension-6 contribution has been expected to be finite right from the beginning. One may ask if one can derive an analogous formula for the more intricate dimension-5 contribution. Its calculation requires a closer examination. Again, we concentrate on the overlap integral and consider

$$\begin{aligned}
C_{7\gamma}^{\mathcal{G},5} &\sim 2\pi \int_{\epsilon}^1 dt \int_{\epsilon}^1 dt' \sum'_m \frac{\chi_m^{\mathcal{G}}(t) \chi_m^{\mathcal{G}}(t')}{(m_m^{\mathcal{G}})^2} \mathcal{D}_L^{(2)\dagger}(t) \sum_n m_n^d \mathcal{D}_L^{(n)}(t) \mathcal{D}_R^{(n)\dagger}(t') \mathcal{D}_R^{(3)}(t') \\
&= \frac{1}{2M_{\text{KK}}^2} \int_{\epsilon}^1 dt \int_{\epsilon}^1 dt' \left[-Lt_{>}^2 + t^2 \left(L - \frac{1}{2} + \ln t \right) + t'^2 \left(L - \frac{1}{2} + \ln t' \right) + \frac{1}{2L} \right] \\
&\quad \times \mathcal{D}_L^{(2)\dagger}(t) \sum_n m_n^d \mathcal{D}_L^{(n)}(t) \mathcal{D}_R^{(n)}(t') \mathcal{D}_R^{(3)}(t'),
\end{aligned} \tag{4.117}$$

where we have used $t_{<}^2 = -t_{>}^2 + t^2 + t'^2$. The completeness relation cannot be applied due to the appearance of m_n^d in the sum. Nevertheless, the last three terms in the square bracket can be evaluated easily using the orthonormality condition (3.62). While the t -

¹⁵This is the reason why the vev shift has been dropped.

and t' -independent contribution to (4.117) vanishes and the t' -dependent contribution is suppressed by m_s/m_b , the t -dependent correction evaluates to

$$\begin{aligned} & \frac{1}{2M_{\text{KK}}^2} \sum_n m_n^d \int_{\epsilon}^1 dt t^2 \left(L - \frac{1}{2} + \ln t \right) \mathcal{D}_L^{(2)\dagger}(t) \mathcal{D}_L^{(n)}(t) \int_{\epsilon}^1 dt' \mathcal{D}_R^{(n)\dagger}(t') \mathcal{D}_R^{(3)}(t') \quad (4.118) \\ & = \frac{1}{2M_{\text{KK}}^2} \sum_n m_n^d \left[L(\Delta_D)_{2n} - (\Delta'_D)_{2n} \right] \delta_{n3} = \frac{m_b}{2M_{\text{KK}}^2} \left[L(\Delta_D)_{23} - (\Delta'_D)_{23} \right]. \end{aligned}$$

The contribution depending on $t_{>}^2$ is somewhat more involved. In order to get rid of the mass x_n^d , we make use of the EOMs (2.84) (twice) including the BCs (2.87) and get

$$\begin{aligned} & \int_{\epsilon}^1 dt \int_{\epsilon}^1 dt' t_{>}^2 \mathcal{D}_L^{(2)\dagger}(t) \sum_n x_n^d \mathcal{D}_L^{(n)}(t) \mathcal{D}_R^{(n)\dagger}(t') \mathcal{D}_R^{(3)}(t') \\ & = x_2^d \int_{\epsilon}^1 dt t^2 \mathcal{D}_R^{(2)\dagger}(t) \mathcal{D}_R^{(3)}(t) + \mathcal{D}_L^{(2)\dagger}(1^-) \sum_n \mathcal{D}_R^{(n)}(1^-) \int_{\epsilon}^1 dt' \mathcal{D}_R^{(n)\dagger}(t') \mathcal{D}_R^{(3)}(t') \\ & = x_2^d \int_{\epsilon}^1 dt t^2 \mathcal{D}_R^{(2)\dagger}(t) \mathcal{D}_R^{(3)}(t) + \mathcal{D}_L^{(2)\dagger}(1^-) \mathcal{D}_R^{(3)}(1^-) \approx 0, \quad (4.119) \end{aligned}$$

where the completeness and the orthonormality relations have been used again. In the last step, we have neglected m_s/m_b -suppressed terms and made use of the fact that the boundary term on the right-hand side vanishes [149]. Hence, we end up with the following result

$$C_{7\gamma}^{\mathcal{G},5} \approx c_A \left(\frac{Q_d C_F \alpha_s s_w^2}{2\alpha \lambda_t} \right) \frac{m_W^2}{M_{\text{KK}}^2} \left\{ L(\Delta_D)_{23} - (\Delta'_D)_{23} \right\}, \quad (4.120)$$

up to v^4/M_{KK}^4 and m_s/m_b suppressed terms.¹⁶ It shall be stressed that, with the help of the above recasts, we have shown that also $C_{7\gamma}^{\mathcal{G},5}$ is suppressed by two orders of the KK scale and the second question at the beginning of this section is answered. Thus, we only deal with dimension-6 contributions which will get important for the RG running discussed in the subsequent section. Note also that at leading order in small parameters the Δ' matrices [189] can be neglected, hence $C_{7\gamma}^{\mathcal{G},5}$ and $C_{7\gamma}^{\mathcal{G},6}$ only differ in the constants c_A and c_B . Consequently, we expect a constant ratio of $C_{7\gamma}^{\mathcal{G},5}/C_{7\gamma}^{\mathcal{G},6} \approx c_A/c_B \approx -2$, which has been verified numerically [184, 230].

Comparing the limit values with the analytic results (4.116) and (4.120) with the above derived analytical expressions gives an idea of whether the original assumption of replacing the functions $I_{A,B}$ by constants has been justified. For this, we define the ratios

$$R_{\text{Re}}^{\mathcal{G}} \equiv \frac{\text{Re} \left[C_{7\gamma}^{\mathcal{G},a} \right]}{\text{Re} \left[C_{7\gamma}^{\mathcal{G},n} \right]}, \quad R_{\text{Im}}^{\mathcal{G}} \equiv \frac{\text{Im} \left[C_{7\gamma}^{\mathcal{G},a} \right]}{\text{Im} \left[C_{7\gamma}^{\mathcal{G},n} \right]}, \quad (4.121)$$

where $C_{7\gamma}^{\mathcal{G},n}$ denotes the numerically determined limit value and $C_{7\gamma}^{\mathcal{G},n}$ represents the analytical formulas derived above. The constants are chosen to be $c_A = -1$ and $c_B = 13/24$, i.e. the value of $I_{A,B}$ evaluated at $x_{nm} = 1$. This reflects the fact the dominant contribution stems from the diagram with the first KK excitation of both the fermions and the bosons. Figure 4.7 shows a stunning agreement between the analytical and numerical approach of this problem. The plots show the distributions for $R_{\text{Re}}^{\mathcal{G},5}$ (left

¹⁶In the following, we will refer to these corrections as “subdominant terms”.

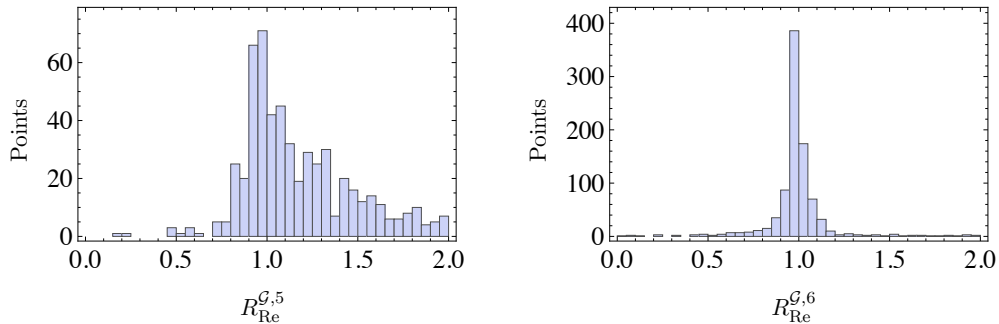


FIGURE 4.7: Distributions of the ratios $R_{\text{Re}}^{\mathcal{G},5}$ (left) and $R_{\text{Re}}^{\mathcal{G},6}$ (right) for 1000 parameter points. The constants are chosen to be $c_A = -1$ and $c_B = 13/24$. The plots for the imaginary parts look similar. See text for details.

plot) and $R_{\text{Re}}^{\mathcal{G},6}$ (right plot) for 1000 parameter points. We see that the majority of the numerical limit values can be well described by the analytical formulas (4.116) and (4.120) with properly chosen constants c_A and c_B . Consequently, we have been able to show that the RS gluon contribution to the Wilson coefficient $C_{7\gamma}$ is suppressed by two orders of M_{KK} and finite. The final results for $C_{7\gamma}^{\mathcal{G}}$ and $C_{7\gamma}^A$ read

$$\begin{aligned}
 C_{7\gamma}^{\mathcal{G}} &\approx \frac{Q_d C_F \alpha_s s_W^2}{2\alpha \lambda_t} \frac{m_W^2}{M_{\text{KK}}^2} \left\{ (c_A + c_B) L (\Delta_D)_{23} - (c_A - 2c_B) (\Delta'_D)_{23} \right\} \\
 &\approx \frac{\pi \alpha_s}{10 \lambda_t} \frac{Lv^2}{M_{\text{KK}}^2} (\Delta_D)_{23} , \tag{4.122}
 \end{aligned}$$

$$\begin{aligned}
 C_{7\gamma}^A &\approx \frac{Q_d^3 s_W^2}{\lambda_t} \frac{m_W^2}{M_{\text{KK}}^2} \left\{ (c_A + c_B) L (\Delta_D)_{23} - (c_A - 2c_B) (\Delta'_D)_{23} \right\} \\
 &\approx \frac{\pi}{200} \frac{\alpha}{\lambda_t} \frac{Lv^2}{M_{\text{KK}}^2} (\Delta_D)_{23} , \tag{4.123}
 \end{aligned}$$

where in the last lines subdominant terms have been neglected and we have evaluated all constants except for $|\lambda_t| \approx 0.04$. Observe that numerically, $C_{7\gamma}^{\mathcal{G}}$ is a factor of around $20\alpha_s/\alpha \approx 200$ bigger than $C_{7\gamma}^A$, so the latter can be safely neglected due to the much smaller gauge coupling. Furthermore, note that the corrections to $C_{7\gamma}^{\mathcal{G}}$ and $C_{7\gamma}^A$ are both L -enhanced and proportional to the same flavor-breaking term $(\Delta_D)_{23}$, which also appears in the $\Delta B = 1$ Hamiltonian giving rise to $b \rightarrow s$ transitions [189]. The results for the chirality-flipped Wilson coefficients $\tilde{C}_{7\gamma}^{\mathcal{G}}$ and $\tilde{C}_{7\gamma}^A$ are obtained from (4.122) and (4.123), respectively, by the interchange $D \leftrightarrow d$. This implies that to leading order in the volume L the effects are proportional to $(\Delta_d)_{23}$. Recall that the matrices $\Delta_{D,d}$ scale with the product of two zero-mode profiles, see (2.130). Since $|F(c_{Q_3})| \gg |F(c_{d_3})|$ due to the large top-quark mass, the contribution to $\tilde{C}_{7\gamma}^{\mathcal{G},A}$ is more than one order of magnitude smaller.

Contributions from W and Z Bosons

We now turn to the analysis of the W - and Z -boson contributions which additionally include the exchange of a gauge-boson zero mode. In the case of the W boson, the contribution moreover includes the two diagrams (a) and (f) in Figure 4.5. Note that

the latter fact does not affect the following considerations, since both contributions are identical despite the functions I_i , which are set to a constant in both cases. As stated above, the numerical approach of summing up the first five modes demonstrates that both contributions are finite and dominated by the lowest-lying KK modes. We thus proceed analogously to the gluon case, where we will encounter subtleties which have not appeared before.

In the following, we only focus on the interesting dimension-5 contributions to the Wilson coefficients. The dimension-6 contributions can be derived analogously to (4.115), where we use the solution for the propagator function (3.36). The results will be given (4.132) and (4.134). Performing the same steps as above, we find for the dimension-5 contribution in the Z -boson case

$$\begin{aligned}
C_{7\gamma}^{Z,5} &\sim \sum_{n,m} \left(\frac{\tilde{m}_Z}{m_m^Z} \right)^2 \frac{m_n^d}{m_b} V_{2mn}^Z \tilde{V}_{nm3}^Z & (4.124) \\
&\approx \frac{1}{x_3^d} \sum_n \int_\epsilon^1 dt \int_\epsilon^1 dt' \left(1 + \frac{Lm_Z^2}{2M_{\text{KK}}^2} [1 - t_{>}^2] \right) \mathcal{D}_L^{(2)\dagger}(t) [g_L^d \mathcal{P}_+ + g_R^d \mathcal{P}_-] \mathcal{D}_L^{(n)}(t) \\
&\quad \times x_n^d \mathcal{D}_R^{(n)}(t') [g_L^d \mathcal{P}_+ + g_R^d \mathcal{P}_-] \mathcal{D}_R^{(3)}(t') \\
&\approx -\frac{1}{x_3^d} \left(g_L^d - g_R^d \right)^2 I_{++}^Z - g_L^d \left(g_L^d - g_R^d \right) (\boldsymbol{\delta}_D)_{23} - (g_L^d)^2 \frac{Lm_Z^2}{2M_{\text{KK}}^2} (\boldsymbol{\Delta}_D)_{23},
\end{aligned}$$

where we have defined

$$I_{++}^Z \equiv \sum_n \int_\epsilon^1 dt \mathcal{D}_L^{(2)\dagger}(t) \mathcal{P}_+ \mathcal{D}_L^{(n)}(t) \mathcal{D}_L^{(n)\dagger}(1^-) \mathcal{P}_+ \mathcal{D}_R^{(3)}(1^-), \quad (4.125)$$

and neglected subleading terms.¹⁷ Note that we cannot apply the completeness relation in (4.125), due to the appearance of the projection operators. For the general case of three generations, it is not possible to obtain a closed, analytic expression. Therefore, we calculate it for the special case of one generation, whose bulk mass parameters vanish, i.e. $c_Q = c_u = c_d = 0$, and then conjecture that this result can be generalized to the more general case of three dimensions and non-vanishing bulk mass parameters.¹⁸ For this special case, the EOMs for the profile functions become very easy and are solved in terms of simple trigonometrical functions, which can be evaluated in the limit $\epsilon \rightarrow 0$. The KK masses $x_n = m_{q_n}/M_{\text{KK}}$ are the solutions to the eigenvalue equation [144]

$$\tan^2 x_n = \tanh^2 X_q, \quad X_q = \frac{v}{\sqrt{2}M_{\text{KK}}} Y_q, \quad (4.126)$$

where without loss of generality it is assumed that Y_q is real and positive. This equation can be solved to give

$$x_n = \begin{cases} \frac{n-1}{2} \pi + x_1, & n = 1, 3, 5, \dots, \\ \frac{n}{2} \pi - x_1, & n = 2, 4, 6, \dots, \end{cases} \quad (4.127)$$

¹⁷Besides omitting terms suppressed by v^4/M_{KK}^4 and m_s/m_b , we have also neglected terms proportional to $(\boldsymbol{\varepsilon}_{D,d})_{23}$. The matrices $\boldsymbol{\varepsilon}_{D,d}$ are given by the left integral in (2.129), where the projection operators \mathcal{P}_\mp are inserted between the fermion profiles. In other words, they are defined as the matrices $\boldsymbol{\Delta}_{D,d}$, where the C -profiles are omitted [145].

¹⁸This idea was used in [144] to conjecture formula (4.25) for the KK contribution to the gluon-fusion amplitude.

where $x_1 = \arctan(\tanh X_q)$ denotes the mass of the SM quark in units of the KK scale. The corresponding even and odd profile functions are

$$\begin{aligned} \sqrt{\frac{2\pi}{L\epsilon}} C_n^{(Q)}(t) a_n^{(Q)} &= \cos(x_n t), & \sqrt{\frac{2\pi}{L\epsilon}} C_n^{(q)}(t) a_n^{(q)} &= \pm \cos(x_n t), \\ \sqrt{\frac{2\pi}{L\epsilon}} S_n^{(Q)}(t) a_n^{(Q)} &= \sin(x_n t), & \sqrt{\frac{2\pi}{L\epsilon}} S_n^{(q)}(t) a_n^{(q)} &= \mp \sin(x_n t), \end{aligned} \quad (4.128)$$

where the upper (lower) signs hold for odd (even) values of n . It is now an easy exercise to evaluate (4.125) for this special case,

$$\begin{aligned} I_{++}^{Z,1\text{gen}} &= \sum_n \int_0^1 dt \cos(x_1^d t) \cos(x_n^d t) \cos(x_n^d) \sin(x_1^d) \\ &= \cos(x_1^d) \sin(x_1^d) \left\{ \int_0^1 dt \cos^2(x_1^d t) + 2 \sum_n (-1)^n \int_0^1 dt \cos^2(x_1^d t) \cos(n\pi t) \right\} \\ &= \cos(x_1^d) \cos^2(x_1^d) \sin(x_1^d) \\ &= \cos(x_1^d) \frac{1}{1 + \tanh^2 X_d} \sin(x_1^d), \end{aligned} \quad (4.129)$$

where relation (4.126) has been used in the last step. It is reasonable to conjecture that I_{++}^Z in the more general case of three dimensions and non-vanishing bulk mass parameters reads

$$\begin{aligned} I_{++}^Z &= \frac{\sqrt{2\pi}}{L\epsilon} \frac{v}{M_{\text{KK}}} a_2^{(D)\dagger} \mathbf{C}_2^{(Q)}(1^-) \frac{1}{1 + \tanh^2 \mathbf{X}_d} \tilde{\mathbf{Y}}_d \mathbf{C}_3^{(d)}(1^-) a_3^{(d)} \\ &= \frac{\sqrt{2\pi}}{L\epsilon} \frac{v}{M_{\text{KK}}} a_2^{(D)\dagger} \mathbf{C}_2^{(Q)}(1^-) \left(1 - \frac{v^2}{2M_{\text{KK}}^2} \mathbf{Y}_d \mathbf{Y}_d^\dagger + \dots \right) \tilde{\mathbf{Y}}_d \mathbf{C}_3^{(d)}(1^-) a_3^{(d)} \quad (4.130) \\ &= -x_3^d (\boldsymbol{\delta}_D)_{23} - \frac{3}{2} \frac{v}{M_{\text{KK}}} (\Delta \tilde{\mathbf{g}}_h^d)_{23} + \dots, \end{aligned}$$

up to terms suppressed by m_s/m_b . In the last step, we have employed the ZMA approximation and defined [149]

$$\Delta \tilde{\mathbf{g}}_h^d = \frac{\sqrt{2}v^2}{6M_{\text{KK}}^2} \mathbf{U}_d^\dagger F(c_Q) \mathbf{Y}_d \mathbf{Y}_d^\dagger \mathbf{Y}_d F(c_d) \mathbf{W}_d, \quad (4.131)$$

with the zero-mode profiles and the diagonalization matrices defined in (2.93) and (2.106), respectively. This chirally unsuppressed contribution, which arises from the Z_2 -odd Yukawa couplings,¹⁹ is the dominant source of flavor violation in the Higgs sector [149]. It can be assigned to the diagram with KK fermions and the longitudinal degrees of freedom, i.e. the Goldstone bosons of the Higgs doublet (2.9), running in the loop, see Figure 1(a) in [245]. Consequentially, this term is missing in the gluon and photon case (note that the corresponding prefactor in (4.124) vanishes for $g_L^d = g_R^d = 1$).

Although this procedure turned out to be successful in the case of the Higgs production process via gluon fusion [144], it is not obvious why the quantity (4.125) is supposed to be independent of the bulk mass parameters. In fact, the 5D fermion propagator has a complicated structure which depends non-trivially on the bulk masses. One can show numerically that (4.130) still holds in the case of one generation and $c_Q = c_q \neq 0$. In

¹⁹Note that for $\mathbf{Y}_d^\dagger \equiv \mathbf{Y}_d^{S,\dagger} \rightarrow 0$ this term vanishes.

the case of $c_Q \neq c_q$, the conjecture (4.130) is not correct any more. However, we will see that (4.130) is still a very good approximation for (4.125). A derivation of a formula including the dependence of c_{Q_i, q_i} is left for future work.

We are now all set to write down the final, approximate results for the Wilson coefficients

$$\begin{aligned} C_{7\gamma}^{Z,5} &\approx \frac{-c_A Q_d}{\lambda_t} \left\{ (g_L^d)^2 \frac{Lm_Z^2}{2M_{\text{KK}}^2} (\Delta_D)_{23} + g_R(g_L^d - g_R^d)(\delta_D)_{23} - (g_L^d - g_R^d)^2 \frac{3v}{2m_b} (\Delta\tilde{g}_h^d)_{23} \right\}, \\ C_{7\gamma}^{Z,6} &\approx \frac{-c_B Q_d}{\lambda_t} \left\{ (g_L^d)^2 \frac{Lm_Z^2}{2M_{\text{KK}}^2} (\Delta_D)_{23} + \left((g_L^d)^2 - (g_R^d)^2 \right) (\delta_D)_{23} \right\}. \end{aligned} \quad (4.132)$$

The results for the W -boson contribution can be directly read off from (4.132), keeping in mind that in this case $g_L \equiv 1$, $g_R \equiv 0$. Defining

$$\Delta\tilde{g}_h^{ud} = \frac{\sqrt{2}v^2}{6M_{\text{KK}}^2} \mathbf{U}_d^\dagger F(c_Q) \mathbf{Y}_u \mathbf{Y}_u^\dagger \mathbf{Y}_d F(c_d) \mathbf{W}_d, \quad (4.133)$$

which accounts for the fact that the term $1/(1 + \tanh^2 \mathbf{X}_u)$ replaces the corresponding term in (4.130), we find

$$\begin{aligned} C_{7\gamma}^{W,5} &\approx -\frac{1}{2\lambda_t} \left(c_A \frac{Q_u}{2} + c_C \right) \left\{ \frac{Lm_Z^2}{2M_{\text{KK}}^2} (\Delta_D)_{23} - \frac{3v}{2m_b} (\Delta\tilde{g}_h^{ud})_{23} \right\}, \\ C_{7\gamma}^{W,6} &\approx -\frac{1}{2\lambda_t} \left(c_B \frac{Q_u}{2} + c_D \right) \left\{ \frac{Lm_Z^2}{2M_{\text{KK}}^2} (\Delta_D)_{23} + (\delta_D)_{23} \right\}. \end{aligned} \quad (4.134)$$

Both contributions from the W -boson exchange diagram (c_A , c_B) and the three-boson vertex diagram (c_C , c_D) have been taken into account. Neglecting the chirally-suppressed terms $(\Delta_D)_{23}$ and $(\delta_D)_{23}$ we arrive at

$$C_{7\gamma}^Z \approx c_A \frac{3Q_d}{2\lambda_t} (T_3^d)^2 \frac{v}{m_b} (\Delta\tilde{g}_h^d)_{23} \approx \frac{1}{16\lambda_t} \frac{v}{m_b} (\Delta\tilde{g}_h^d)_{23}, \quad (4.135)$$

$$C_{7\gamma}^W \approx \frac{3}{4\lambda_t} \left(c_A \frac{Q_u}{2} + c_C \right) \frac{v}{m_b} (\Delta\tilde{g}_h^{ud})_{23} \approx -\frac{5}{16\lambda_t} \frac{v}{m_b} (\Delta\tilde{g}_h^{ud})_{23}, \quad (4.136)$$

where we have assumed $c_A = -1/2$ and $c_C = -1/4$, i.e. the functions evaluated for values for $M_{\text{KK}}^2 \gg m_{W,Z}^2$. The (approximate) results for the chirally-flipped Wilson coefficients $\tilde{C}_{7\gamma}^Z$ and $\tilde{C}_{7\gamma}^W$ are given by the above results with $\Delta\tilde{g}_h^d \rightarrow (\Delta\tilde{g}_h^d)^\dagger$ and $\Delta\tilde{g}_h^{ud} \rightarrow (\Delta\tilde{g}_h^{ud})^\dagger$.

The results (4.122), (4.123), (4.135), and (4.136) are the main results of this section. They provide approximate expressions for the infinite double sum in terms of simple quantities. Except for $\Delta\tilde{g}_h^{ud}$ all of them have already been encountered in tree-level FCNCs. In order to validate the above results, we compare these analytical expressions with the numerical limit values. Figure 4.8 shows a pretty good agreement, so it is justified to use the results in question for the following analyses. The enhancement in (4.134) and (4.132) by a factor of v/m_b compared to the corrections due to KK gluon and photon exchange will render the W -boson contribution the most important one.²⁰

²⁰The Z -boson contribution is suppressed by the small factor $(g_L^d - g_R^d)^2 = 1/4$.

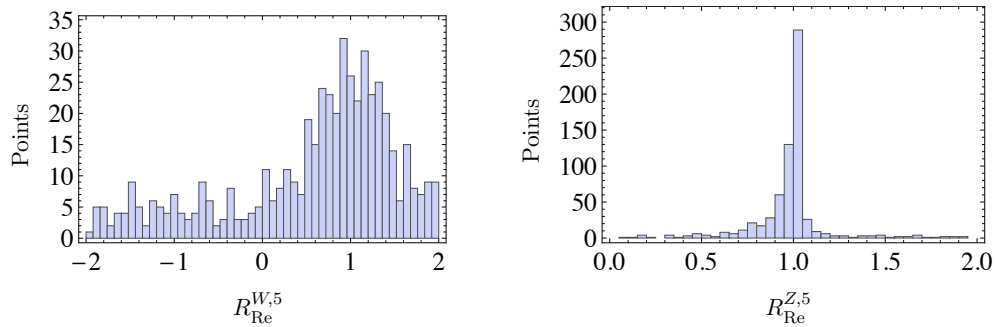


FIGURE 4.8: Distribution of the ratios $R_{\text{Re}}^{W,5}$ and $R_{\text{Re}}^{Z,5}$, which are defined according to (4.121) with $c_A = -0.5$. The plots for the imaginary part as well as for the dimension-six contributions look similar.

Contribution from the Three-Gluon Vertex

So far, we have only investigated contributions to the Wilson coefficients $C_{7\gamma}$ and its chirality-flipped counterpart and stated that the ones for C_{8g} and \tilde{C}_{8g} can be simply obtained by exchanging the prefactors. However, the three-boson vertex differs in both cases. While it is the emission of the photon by the W boson in the former case (diagram (f) in Figure 4.5), it is the three-gluon vertex (see Figure D.6 in the appendix) in the latter. Let us check if the three-boson vertex indeed gives the main contribution to C_{8g} and \tilde{C}_{8g} , as claimed in [245].

The result for the three gluon contribution differs from the one stemming from the gluon exchange just by the functions I_i . While I_A (I_B) are strictly positive (negative), the situation changes in the present case. The functions I_E and I_F range from

$$\begin{aligned}
 I_E(x) &= \frac{1 + 9x - 13x^2 + 3x^3 + 8x \log(x)}{2(-1+x)^3} && \in [-1/2, 3/2], \\
 I_F(x) &= \frac{4 + 40x - 99x^2 + 68x^3 - 13x^4 - 6x(-6+5x) \log(x)}{12(-1+x)^4} && \in [-13/12, 1/3].
 \end{aligned}
 \tag{4.137}$$

Due to the fact that the sign changes for a certain mass ratio, it is not as nicely motivated as in the previous cases to replace the functions by a constant. However, doing the same analysis, we find that the constants can be chosen $c_E = 5/6$ and $c_F = -5/8$. Again, these values agree with the function values at 1, representing the main contribution originating from both fermion and boson KK modes ($x_{mn}^G \approx 1$). Being able to replace the function by a constant means, on the other hand, that the two contributions from the gluon exchange and the three-gluon vertex are comparably big. However, the gluon contribution to both C_{8g} and \tilde{C}_{8g} is still negligible compared to the one stemming from the W -boson exchange, which we will see in the following subsection. This observation stands in contradiction with the findings of [245].

Final Results and Relative Magnitudes of the Diagrams

It is now possible to write down the final results for the Wilson coefficients at leading order in small parameters. They read

$$\begin{aligned} C_{7\gamma}^{\text{KK}} &\approx \frac{1}{\lambda_t} \left[-\frac{5}{16} \frac{v}{m_b} (\Delta \tilde{\mathbf{g}}_h^{ud})_{23} + \frac{1}{16} \frac{v}{m_b} (\Delta \tilde{\mathbf{g}}_h^d)_{23} + \frac{\pi\alpha_s}{10} \frac{Lv^2}{M_{\text{KK}}^2} (\Delta_D)_{23} \right], \\ \tilde{C}_{7\gamma}^{\text{KK}} &\approx \frac{1}{\lambda_t} \left[-\frac{5}{16} \frac{v}{m_b} (\Delta \tilde{\mathbf{g}}_h^{ud\dagger})_{23} + \frac{1}{16} \frac{v}{m_b} (\Delta \tilde{\mathbf{g}}_h^{d\dagger})_{23} + \frac{\pi\alpha_s}{10} \frac{Lv^2}{M_{\text{KK}}^2} (\Delta_d)_{23} \right], \end{aligned} \quad (4.138)$$

and

$$\begin{aligned} C_{8g}^{\text{KK}} &\approx \frac{1}{\lambda_t} \left[\frac{3}{16} \frac{v}{m_b} (\Delta \tilde{\mathbf{g}}_h^{ud})_{23} + \frac{3}{16} \frac{v}{m_b} (\Delta \tilde{\mathbf{g}}_h^d)_{23} + \frac{\pi\alpha_s}{11} \frac{Lv^2}{M_{\text{KK}}^2} (\Delta_D)_{23} \right], \\ \tilde{C}_{8g}^{\text{KK}} &\approx \frac{1}{\lambda_t} \left[\frac{3}{16} \frac{v}{m_b} (\Delta \tilde{\mathbf{g}}_h^{ud\dagger})_{23} + \frac{3}{16} \frac{v}{m_b} (\Delta \tilde{\mathbf{g}}_h^{d\dagger})_{23} + \frac{\pi\alpha_s}{11} \frac{Lv^2}{M_{\text{KK}}^2} (\Delta_d)_{23} \right], \end{aligned} \quad (4.139)$$

where the W -boson (Z -boson, gluon) contributions are given by the first (second, third) terms. These relations also hold for the $b \rightarrow d\gamma$ transition, provided that the indices are adjusted properly ($2 \rightarrow 1$).

Addressing the question about the relative magnitudes of the various contributions is now any easy task. For this, we evaluate the three contributions in the final results (4.138) and (4.139) numerically. It turns out that the relative magnitudes are generically

$$\begin{aligned} C_{7\gamma}^W : C_{7\gamma}^Z : C_{7\gamma}^G &\sim 1 : \mathcal{O}(10^{-1}) : \mathcal{O}(10^{-2}), \\ \tilde{C}_{7\gamma}^W : \tilde{C}_{7\gamma}^Z : \tilde{C}_{7\gamma}^G &\sim 1 : \mathcal{O}(10^{-1}) : \mathcal{O}(10^{-3}), \\ C_{8g}^W : C_{8g}^Z : C_{8g}^G &\sim 1 : \mathcal{O}(1) : \mathcal{O}(10^{-2}), \\ \tilde{C}_{8g}^W : \tilde{C}_{8g}^Z : \tilde{C}_{8g}^G &\sim 1 : \mathcal{O}(1) : \mathcal{O}(10^{-3}). \end{aligned} \quad (4.140)$$

We see that in all cases the W -boson diagrams give the largest contributions. In the case of $C_{7\gamma}$ and $\tilde{C}_{7\gamma}$, they dominate over the Z -boson contributions due to the larger prefactor and due to the fact that $(\Delta \tilde{\mathbf{g}}_h^{ud\dagger})_{23}$ turns out to a factor of approximately twice as large as $(\Delta \tilde{\mathbf{g}}_h^d)_{23}$. The gluon contribution only has a minor effect, since $(\Delta_{D,d})_{23}$ are chirally suppressed which cannot be compensated by the enhancement from the larger gauge coupling. The significance of the Z -boson contribution increases in the case of C_{8g} and \tilde{C}_{8g} , since in that case the three- (W) -boson vertex diagram is not contributing. The three-gluon vertex diagram rather increases the gluon contribution by a factor of roughly 5. Although the W -boson contribution is decreased and the gluon contribution increased, we see that the latter is still subdominant, which is due to the smallness of $(\Delta_{D,d})_{23}$.

To conclude, we have succeeded in answering all questions at the beginning of this subsection. For the further analysis, we will use the results (4.138) and (4.139). Before we can turn to the phenomenological implications in Section 5, we will first discuss the RG evolution of the Wilson coefficients.

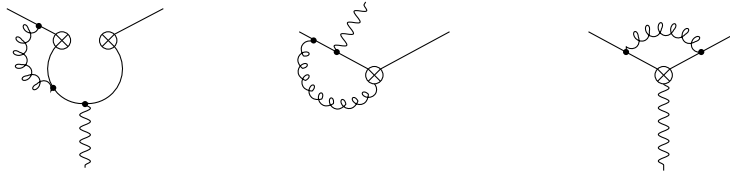


FIGURE 4.9: The diagram on the left (in the middle) shows how current-current operators (the dipole operator \mathcal{O}_{8g}) can contribute to $\mathcal{O}_{7\gamma}$, whereas the diagram on the right shows how $\mathcal{O}_{7\gamma}$ mixes into itself.

4.3.4 Renormalization Group Evolution and Final Results

Equipped with final expressions for the Wilson coefficients at M_{KK} , we will now investigate the QCD effects for which the operator mixing of all contributing dimension-6 operators, in particular the four-fermion operators that can be contributed through the diagram shown on the left-hand side in Figure 4.9, have to be considered. What concerns the neutral current-current operators, this has been done in [247]. Upon taking into account also the charged current-current operators, the complete effective Lagrangian reads

$$\begin{aligned} \mathcal{L}_{\text{eff}} = & -\frac{4G_F}{\sqrt{2}} \left[\sum_{u=c,t} \sum_{i=1,2} \lambda_u C_i^{(u)} Q_i^{(u)} - \lambda_t \sum_{i=3,\dots,6,7\gamma,8g} C_i Q_i \right. \\ & + \sum_{i=1,2} \sum_{A=L,R} \left\{ \sum_{q=u,c,t,d,s,b} C_i^{(q),LA} Q_i^{(q)}(L,A) + \hat{C}_i^{(d),LA} \hat{Q}_i^{(d)}(L,A) \right\} \\ & \left. + \{C \rightarrow \tilde{C}, Q \rightarrow \tilde{Q}, L \leftrightarrow R\} \right], \end{aligned} \quad (4.141)$$

where all Wilson coefficients are evaluated at M_{KK} . The charged current-current operators $Q_i^{(u)}$ are defined as in the SM, where the corresponding operators with right-left or left-right chirality do not mix into the other operators and thus do not have to be taken into account here. The definitions of all neutral current-current operators can be found in [247] and we have adopted the nomenclature of this reference. One finds that their effect is negligible in the RS model, so it is not necessary to show them explicitly.

We will now go through the basic steps of how to find the phenomenologically relevant Wilson coefficients at the meson scale μ_b . In order to derive the evolution matrix $U(\mu_b, M_{\text{KK}})$, one has to determine the ADM $\hat{\gamma}$ of the operator basis which has been already done in [247]. Using these anomalous dimensions, the evolution matrices of the form $U(\mu_1, \mu_2)$ can be derived via the relation

$$U(\mu_1, \mu_2) = \hat{V} \left(\left[\frac{\alpha_s(\mu_2)}{\alpha_s(\mu_1)} \right]^{\frac{\vec{\gamma}^{(0)}}{2\beta_0}} \right)_D \hat{V}^{-1}, \quad (4.142)$$

with $\beta_0 = (33 - 2f)/3$, where f denotes the number of flavors integrated out. The matrix \hat{V} diagonalizes $\hat{\gamma}^{(0)T}$, while $\vec{\gamma}^{(0)}$ represents the vector containing the eigenvalues of $\hat{\gamma}^{(0)T}$. We integrate out the top quark at $\mu_t = 172.6 \text{ GeV}$ separately, so that the evolution matrix $U(\mu_W, M_{\text{KK}})$ splits into two parts:

$$U(\mu_W, M_{\text{KK}}) = U^{(f=5)}(\mu_W, \mu_t) U^{(f=6)}(\mu_t, M_{\text{KK}}). \quad (4.143)$$

M_{KK}	1 TeV	2 TeV	5 TeV	10 TeV
a_7	0.505	0.480	0.450	0.430
a_8	0.120	0.123	0.126	0.128
b_8	0.550	0.526	0.497	0.478

TABLE 4.2: The coefficients for the Wilson coefficients (4.149) and (4.150) depending on different KK scales.

Note that not only β_0 , but also the ADM depends on f . Arrived at μ_W , we add the zero-mode contributions $C_i^{(0)}(\mu_W)$ stemming from the diagrams with zero-mode of the fermions and the massive gauge bosons, which can be split into of two parts:

$$\vec{C}^{(0)}(\mu_W) = \vec{C}^{\text{SM}}(\mu_W) + \vec{C}^{\text{RS}(0)}(\mu_W). \quad (4.144)$$

The vector $\vec{C} \equiv \{C_i\}_i$ comprises all Wilson coefficients of (4.141). The coefficients $C_i^{\text{RS}(0)}(\mu_W)$ include the contributions from the Z -boson zero mode as well as the RS corrections due the non-unitarity of the CKM matrix and the differences in the masses \tilde{m}_W^2 and m_W^2 . While the SM value is added at the end of the calculation, i.e. at the scale μ_b , we have to let the additional RS contributions

$$\vec{C}^{\text{RS}}(\mu_W) = U(\mu_W, M_{\text{KK}}) \vec{C}^{\text{KK}}(M_{\text{KK}}) + \vec{C}^{\text{RS}(0)}(\mu_W) \quad (4.145)$$

run down to the hadron scale μ_b via the matrix $U(\mu_b, \mu_W)$. This matrix is obtained in same way as $U(\mu_W, \mu_t)$. We finally obtain the formula for the RS contributions at μ_b :

$$\begin{aligned} \vec{C}^{\text{RS}}(\mu_b) &= U(\mu_b, \mu_W) \vec{C}^{\text{RS}}(\mu_W) \\ &= U(\mu_b, M_{\text{KK}}) \vec{C}^{\text{KK}}(M_{\text{KK}}) + U(\mu_b, \mu_W) \vec{C}^{\text{RS}(0)}(\mu_W). \end{aligned} \quad (4.146)$$

After adding the SM contribution the final Wilson coefficients read

$$\vec{C}^{\text{fin}}(\mu_b) = \vec{C}^{\text{SM}}(\mu_b) + \vec{C}^{\text{RS}}(\mu_b), \quad (4.147)$$

where $\vec{C}^{(\text{SM})}(\mu_b)$ includes the NNLO SM results for $C_{7\gamma}$ and C_{8g} [248–250]

$$C_{7\gamma}^{\text{SM}}(\mu_b) = -0.353, \quad C_{8g}^{\text{SM}}(\mu_b) = -0.150. \quad (4.148)$$

The RS contributions at LO are given by

$$\begin{aligned} C_{7\gamma}^{\text{RS}}(\mu_b) &= a_7 C_{7\gamma}^{\text{RS}}(M_{\text{KK}}) + a_8 C_{8g}^{\text{RS}}(M_{\text{KK}}) \\ &\quad + 0.630 C_{7\gamma}^{\text{RS}(0)}(\mu_W) + 0.100 C_{8g}^{\text{RS}(0)}(\mu_W) - 0.196 \sum_{u=u,c} C_2^{(u)}(\mu_W), \end{aligned} \quad (4.149)$$

$$C_{8g}^{\text{RS}}(\mu_b) = b_8 C_{8g}^{\text{RS}}(M_{\text{KK}}) + 0.067 C_{8g}^{\text{RS}(0)}(\mu_W) - 0.090 \sum_{u=u,c} C_2^{(u)}(\mu_W). \quad (4.150)$$

Depending on the KK scale M_{KK} we get different values for the coefficients a_i and b_i shown in Table 4.2, where we have chosen $\mu_b = 2.5$ GeV and $\mu_t = 172.6$ GeV. These formulas also hold for $\tilde{C}_{7\gamma}^{\text{RS}}$ as QCD is blind to the fermion chirality.²¹ We see that, just as in the SM, the Wilson coefficients of the dipole operators are suppressed by QCD

²¹The corresponding SM values for $\tilde{C}_{7\gamma}$ and \tilde{C}_{8g} are set to zero due to the already mentioned m_s/m_b -suppression.

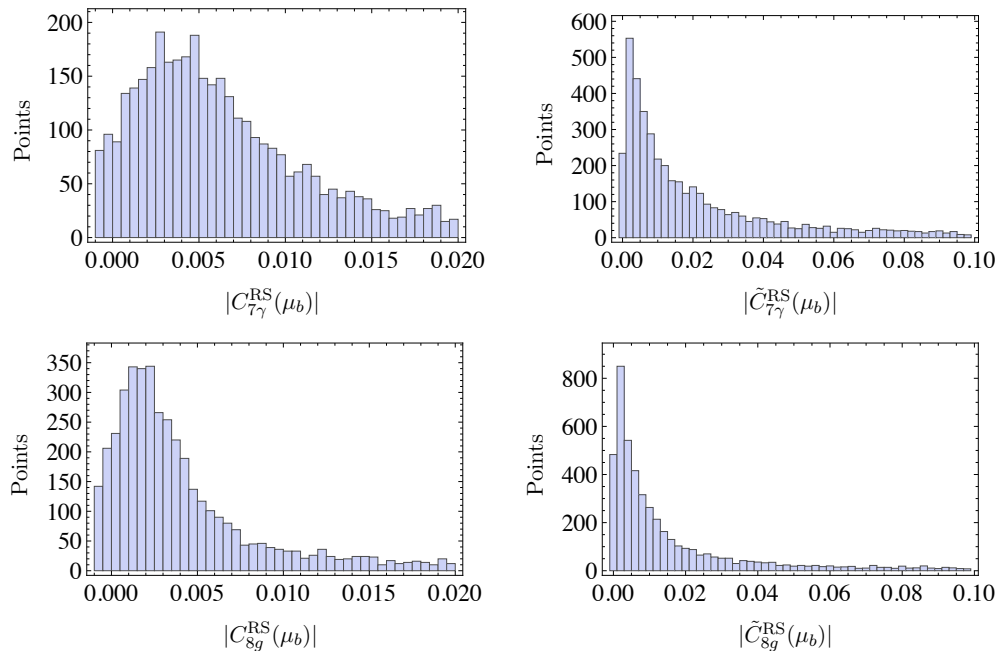


FIGURE 4.10: Distribution of the absolute values of the RS contributions to the Wilson coefficients $C_{7\gamma}$ (upper left), $\tilde{C}_{7\gamma}$ (upper right), C_{8g} (lower left), and \tilde{C}_{8g} (lower right), evaluated at the scale $\mu_b = 2.5$ GeV. Note the different scaling of the diagrams on the left and right-hand side.

effects. Furthermore, contributions can arise from the charged current-current operators

$$C_2^{(u,c)}(\mu_W) \approx \frac{2\pi\alpha v^2}{s_w^2 M_{\text{KK}}^2}, \quad (4.151)$$

which originate from the universal corrections to the W -boson profile and are roughly in the same order of magnitude as the radiative Wilson coefficients. However, they are multiplied by -0.196 , so they do not give significant effects.

The equations (4.149) and (4.150) together with (4.138) and (4.139) provide the final results for the RS contributions to the Wilson coefficients $C_{7\gamma}$, $\tilde{C}_{7\gamma}$, C_{8g} , and \tilde{C}_{8g} , including the effects of the RG evolution down to the hadron scale μ_b . The general pattern of these corrections is illustrated in Figure 4.10, which shows a distribution of their absolute values for 5000 parameter points. Comparing the corrections to $C_{7\gamma}$ and $\tilde{C}_{7\gamma}$, shown in the first row, we observe that the chirality-flipped operator receives about one order of magnitude larger contributions. This can be understood by having a closer look at the dominating quantities (4.131) and (4.133), respectively. Recall that $C_{7\gamma}$ ($\tilde{C}_{7\gamma}$) depends on $F(c_{b_R})$ ($F(c_{b_L})$), where $c_{b_L} \equiv c_{Q_3}$ and $c_{b_R} \equiv c_{q_3}$. Consequentially, the dominance of $\tilde{C}_{7\gamma}$ can be traced back to the fact that $|F(c_{b_L})| \gg |F(c_{b_R})|$, which is due to the large mass difference between the top and bottom quark. The same effect can be observed in the second row, where the corrections to C_{8g} and \tilde{C}_{8g} are depicted. The fact that the corrections are of the same order of magnitude stands in contraction to the findings of [245] claiming that the corrections to C_{8g} and \tilde{C}_{8g} are about one order of magnitude larger due to the three-gluon vertex diagram. Nevertheless, the effects are still significant, especially for the chirality-flipped Wilson coefficients. Since the phases are not fixed, there can be large imaginary parts leading to CP-violating effects. The resulting phenomenological consequences will be examined in the subsequent chapter.

Chapter 5

Phenomenological Implications

A clear indication for models with warped extra dimensions would be the direct detection of KK modes. Unfortunately, none of these predicted particles have been observed yet, and the electroweak precision measurements indicate that their masses could be too large for direct detection at the LHC, as discussed in Sections 2.2.4 and 2.3.3. Indeed, the current limit on the mass of the lightest KK gluon $g^{(1)}$ via searches for resonances in the invariant mass spectrum of $t\bar{t}$ production by the ATLAS Collaboration is reported to be (see Figure 5.1) [251]

$$M_{g^{(1)}} > 2.0 \text{ TeV} \quad \text{at 95\% confidence level (CL)}. \quad (5.1)$$

Thus, indirect searches for warped extra dimensions become a more and more attractive alternative. One possibility is given by precision measurements of the Higgs-boson couplings to SM particles, which are accessible via studies of both the Higgs production cross section and its decay rates. Another viable framework to look for deviations from the SM predictions is given by the investigation of flavor processes which are loop-suppressed in the SM and hence allow for NP to be reflected in significant effects. In this chapter, we will make use of the findings of Chapter 4 and examine their phenomenological implications on both Higgs and flavor processes. While Section 5.1 is based on our publications [150, 151, 252], Section 5.2 includes unpublished work.

5.1 Higgs Physics in Warped Extra Dimensions

In this section, we study the phenomenological implication of the findings of Section 4.1 and 4.2. In the context of Higgs physics, new-physics deviations from the SM can be searched for by the signal rates

$$R_X \equiv \frac{(\sigma \cdot \text{BR})(pp \rightarrow h \rightarrow X)_{\text{NP}}}{(\sigma \cdot \text{BR})(pp \rightarrow h \rightarrow X)_{\text{SM}}} = \frac{\sigma(pp \rightarrow h)_{\text{NP}}}{\sigma(pp \rightarrow h)_{\text{SM}}} \frac{\Gamma(h \rightarrow X)_{\text{NP}}}{\Gamma(h \rightarrow X)_{\text{SM}}} \frac{\Gamma_h^{\text{SM}}}{\Gamma_h^{\text{NP}}}, \quad (5.2)$$

for the production of the Higgs boson in pp collisions and its subsequent inclusive decay into an arbitrary final state X . This section includes a detailed discussion of the signal rates R_X for the Higgs production and the most relevant decays into $X = b\bar{b}$, $\tau^+\tau^-$, WW^* , ZZ^* , and $\gamma\gamma$ at the LHC in different incarnations of the RS model. From (5.2) we can read off that new physics can show up in three different ways. Firstly,

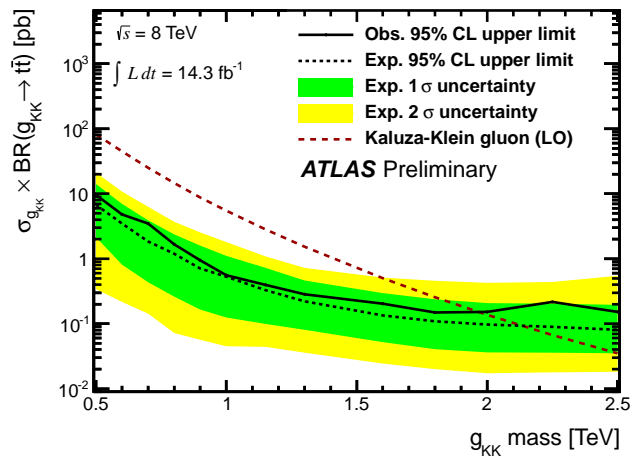


FIGURE 5.1: Exclusion plot for the mass of the first KK gluon obtained from an analysis of the invariant mass spectrum of $t\bar{t}$ production by the ATLAS Collaboration [251].

it can lead to deviations in the Higgs production cross section $\sigma(pp \rightarrow h)$, which can be decomposed into the Higgs production via gluon fusion, vector-boson fusion, Higgs-strahlung, and the Higgs production associated with an emission of a $t\bar{t}$ pair, where relative contributions read (for $m_h = 125$ GeV) [253]

$$\sigma(pp \rightarrow h) = 0.872\sigma_{ggh} + 0.070\sigma_{VVh} + 0.033\sigma_{Wh} + 0.020\sigma_{Zh} + 0.005\sigma_{t\bar{t}h}. \quad (5.3)$$

Secondly, we can investigate the new-physics contributions to the Higgs decay rates $\Gamma(h \rightarrow X)$, and, thirdly, to the total Higgs width Γ_h . Via the latter quantity the rates are sensitive to non-standard or invisible Higgs decays. The following analysis will take into account all three possibilities. While the gluon-fusion process has already been discussed in Section 4.1, we will analyze the effects of the exchange of virtual KK resonances in the Higgs-strahlung and vector boson-fusion production processes. Moreover, we will take a closer look at the Higgs decays into pairs of W and Z bosons, including their subsequent decays into leptons. This allows for a thorough discussion of the implications of the latest LHC results on the RS parameter space.

In the context of various RS models, the couplings of all tree- and loop-induced Higgs couplings to fermions and gauge bosons, as well as the Higgs self-couplings will be summarized and discussed. It has been reported in [254] that the LHC at $\sqrt{s} = 14$ TeV and with an integrated luminosity of 300 fb^{-1} has the potential to probe deviations of Higgs couplings to fermions in the range of $\sim 30\%$ and to gauge bosons in the range of $\sim 16\%$, both at 95% confidence level (CL), in a model-independent way. At future lepton colliders like the *International Linear Collider* (ILC) [255–258] the sensitivity to deviations can be improved by almost one order of magnitude (assuming $\sqrt{s} = 1$ TeV and an integrated luminosity of 1000 fb^{-1}). In order to explore to which extent it is possible to obtain evidence for models with warped extra dimensions by indirect measurements, it will be illustrated which regions of parameter space could be probed at these facilities. This analysis will be performed for both the minimal and the custodial RS model, taking into account the distinction between the brane-localized and the narrow bulk-Higgs scenario. Although the findings of the Sections 3.1.2 and 4.2.2 could be used to extent parts of the following analysis to the more general case of a bulk Higgs sector, this is beyond the scope of this thesis and is part of future work [259].

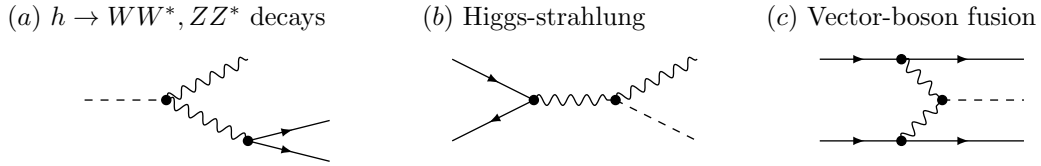


FIGURE 5.2: Tree-level Feynman diagrams for the off-shell Higgs decays to pairs of W and Z bosons, and Higgs production in the Higgs-strahlung and vector-boson fusion processes.

This section is structured as follows: In Section 5.1.1 we will calculate the cross sections for the Higgs production processes via Higgs-strahlung and vector-boson fusion as well as the decay rates for the Higgs decay into pairs of electroweak gauge bosons. Section 5.1.2 will then summarize the main Higgs couplings to fermions and gauge bosons in the RS model, including the loop-induced couplings to two gluons and photons. All expressions will be exact at first order in the expansion in v^2/M_{KK}^2 . A numerical study of these couplings will be performed in Section 5.1.3, where a discussion of the CP-odd couplings and of the anti-correlation between the hgg and $h\gamma\gamma$ couplings will be included as well. It will moreover be commented on the possibility to detect deviations from the SM values of the Higgs couplings at the LHC operating at $\sqrt{s} = 14$ TeV and with an integrated luminosity of 300 fb^{-1} , and an ILC operating at $\sqrt{s} = 1$ TeV with an integrated luminosity of 1000 fb^{-1} . In Section 5.1.4 the RS predictions for $pp \rightarrow h \rightarrow b\bar{b}$, $\tau^+\tau^-$, WW^* , ZZ^* , $\gamma\gamma$ will then be compared with the current data from the LHC, which can be used to deduce bounds on the relevant parameters of the RS models. An overview of the bounds coming from all five decay channels will be given at the end of this section.

5.1.1 Higgs Production and Decay via W, Z Bosons

We begin with the detailed discussion of the structure of new physics effects in the couplings of the Higgs boson to pair of electroweak gauge bosons. These couplings are probed in the off-shell Higgs decays $h \rightarrow WW^*$ and $h \rightarrow ZZ^*$ with subsequent decays into four fermions, as well as in the production of the Higgs boson in vector-boson fusion or in the Higgs-strahlung process, see Figure 5.2. All these three tree-level processes have in common that they involve the exchange of virtual vector bosons, which implies that in addition to the SM W and Z bosons we must consider the effect of the infinite towers of KK resonances. It is often assumed in the literature that the main effect of new physics on these processes arises from a rescaling of the on-shell hVV couplings. It will be shown that there are also several other effects that need to be accounted for, namely a possible rescaling of the Higgs vev, a modification of the couplings of the W and Z bosons to light fermions, and the exchange of new heavy particles in the off-shell propagators. In RS models all of these effects are indeed present, and accounting for them correctly will be important for a general definition of the signal strength in terms of the Higgs couplings to fermions and vector bosons in Section 5.1.4. To good approximation, however, we will find that the main effects can be accounted for by a multiplicative rescaling of the SM decay rates and production cross sections.

Higgs Decay into Vector Bosons

We will now study the decay of the Higgs boson to a pair of electroweak gauge bosons, taking $h \rightarrow WW^*$ as a concrete example. Since $m_h < 2m_W$, this decay is only allowed if at least one of the W bosons is produced off-shell. We thus need to consider the process $h \rightarrow W^- W^{+*} \rightarrow W^- f_i \bar{f}'_j$, where the off-shell boson decays into a pair of light fermions f_i and \bar{f}'_j with generation indices i, j . In the SM, the corresponding differential decay rate is given by [260]

$$\frac{d\Gamma}{ds} = \frac{1}{16\pi^2 m_h^3} \frac{\Gamma(W^+ \rightarrow f_i \bar{f}'_j)}{m_W} \frac{m_W^2}{v^2} \frac{\lambda^{\frac{1}{2}}(m_h^2, m_W^2, s)}{(m_W^2 - s)^2} \left[(m_h^2 - m_W^2)^2 + 2s(5m_W^2 - m_h^2) + s^2 \right], \quad (5.4)$$

where s is the invariant mass squared of the fermion pair, and $\lambda(x, y, z) = (x - y - z)^2 - 4yz$. The result has been expressed in terms of the on-shell decay rate for the process $W^+ \rightarrow f_i \bar{f}'_j$,

$$\Gamma(W^+ \rightarrow f_i \bar{f}'_j) = N_c^f m_W \frac{g^2}{24\pi} |g_{ij,L}|^2, \quad (5.5)$$

where g denotes the $SU(2)_L$ gauge coupling, the color factor $N_c^f = 1$ for leptons and 3 for quarks, and $g_{ij,L} = \delta_{ij}/\sqrt{2}$ for leptons and $V_{ij}^{\text{CKM}}/\sqrt{2}$ for quarks. Performing the remaining integration over s in the interval $0 \leq s \leq (m_h - m_W)^2$ and neglecting fermion-mass effects, one obtains

$$\Gamma(h \rightarrow W^- W^{+*} \rightarrow W^- f_i \bar{f}'_j) = \frac{m_h^3}{32\pi v^2} \frac{\Gamma(W^+ \rightarrow f_i \bar{f}'_j)}{\pi m_W} g\left(\frac{m_W^2}{m_h^2}\right), \quad (5.6)$$

where the first factor is one half of the (would-be) on-shell $h \rightarrow WW$ width in the limit $m_h \gg m_W$, the second factor accounts for the suppression due to the fact that one of the W bosons in the decay $h \rightarrow WW^*$ is produced off-shell, and the phase-space function is given by

$$g(x) = \frac{6x(1 - 8x + 20x^2)}{\sqrt{4x - 1}} \arccos\left(\frac{3x - 1}{2x^{3/2}}\right) - 3x(1 - 6x + 4x^2) \ln x - (1 - x)(2 - 13x + 47x^2). \quad (5.7)$$

The off-shell decay considered here arises if $x > 1/4$. It is common practice to define the off-shell $h \rightarrow WW^*$ decay rate as

$$\Gamma(h \rightarrow WW^*) \equiv 2 \sum_{f_i, f'_j} \Gamma(h \rightarrow W^+ f_i \bar{f}'_j), \quad (5.8)$$

where the sum includes all fermion pairs with total mass lighter than m_W . The factor 2 accounts for the charge-conjugated decays $h \rightarrow W^- \bar{f}_i f'_j$. In the SM the expression for $\Gamma(h \rightarrow WW^*)$ has the same form as in (5.6), but with the partial decay rate $\Gamma(W^+ \rightarrow f_i \bar{f}'_j)$ replaced by twice the total decay width Γ_W of the W boson.

Analogous formulas hold for the decays based on $h \rightarrow ZZ^*$, where we must replace $W \rightarrow Z$ everywhere and use the corresponding expression

$$\Gamma(Z \rightarrow f \bar{f}) = N_c^f m_Z \frac{g^2}{24\pi c_w^2} (g_{f,L}^2 + g_{f,R}^2), \quad (5.9)$$

for the partial decay rates of the Z boson in the SM, where $g_{f,L} = T_3^f - s_w^2 Q_f$ and $g_{f,R} = -s_w^2 Q_f$ are the left-handed and right-handed couplings of the various fermion species, and $s_w = \sin \theta_w$ and $c_w = \cos \theta_w$ are the sine and cosine of the weak mixing angle, see below. In this case the total off-shell decay rate is defined as

$$\Gamma(h \rightarrow ZZ^*) \equiv \sum_f \Gamma(h \rightarrow Zf\bar{f}), \quad (5.10)$$

where the sum includes all fermions lighter than $m_Z/2$. It follows from this definition that for the golden channel

$$\Gamma(h \rightarrow ZZ^* \rightarrow l^+l^-l^+l^-) = \Gamma(h \rightarrow ZZ^*) [\text{Br}(Z \rightarrow l^+l^-)]^2. \quad (5.11)$$

After the description of the Higgs decay into two gauge bosons in the SM, we now discuss in detail how the above results must be modified in the context of the minimal RS model. For the purposes of this discussion it is convenient to define the weak mixing angle s_w^2 via the structure of the neutral current, which can be studied experimentally via the Z -pole polarization asymmetries observed at LEP. Alternative definitions are related to this one through the electroweak precision variables S , T and U ; see e.g. [161] for a detailed discussion. In the context of RS models one has $s_w^2 = g_5^2/(g_5^2 + g_5^{\prime 2})$ in terms of the 5D gauge couplings, see also (2.12). If this ratio is extracted from experiment there are no new physics corrections to the branching ratios $\text{Br}(W \rightarrow f_i\bar{f}_j')$ and $\text{Br}(Z \rightarrow f\bar{f})$. Modifications arise for the Higgs couplings to vector bosons, the electroweak gauge couplings entering the partial decay rates (5.5) and (5.9), and due to the contributions of heavy KK resonances, which change the momentum-dependent gauge boson propagator. For concreteness the decay $h \rightarrow W^-W^{+*}$ will be considered to study the impact of these corrections in the context of the minimal RS model. In the Feynman diagram in Figure 5.2(a) the off-shell gauge-boson propagator now contains the SM gauge boson and its infinite tower of KK excitations. The Feynman rule for the $W^{+(0)}W^{-(n)}h$ vertex is (with $n = 0$ for the zero mode and $n > 0$ for the KK excitations, see (C.1), diagram b))

$$\begin{aligned} \text{minimal RS:} & \quad \frac{2i\tilde{m}_W^2}{v} \eta_{\mu\nu} 2\pi \chi_0^W(1) \chi_n^W(1), \\ \text{custodial RS:} & \quad \frac{2i\tilde{m}_W^2}{vc_\vartheta^2} \eta_{\mu\nu} 2\pi \vec{\chi}_0^W(1)^T \mathbf{D}_\vartheta \vec{\chi}_n^W(1), \end{aligned} \quad (5.12)$$

where the leading order W -boson masses \tilde{m}_W^2 and profiles $\chi_0^W(t)$, $\vec{\chi}_0^W(t)$ are given in (2.30), (2.169) and (2.31), (2.170). The matrix \mathbf{D}_ϑ with the angle ϑ defined in (2.146) can be found in (2.165). As mentioned several times, the vev v in the RS model differs from the Higgs vev v_{SM} . It is determined by the shift to the Fermi constant derived in the RS model by considering (at tree level) the effect of the exchange of the infinite tower of KK modes of the W boson on the rate for muon decay.¹ Employing the results for the 5D boson propagator functions at vanishing momenta, given in (3.36) and (3.40),

¹If one uses instead the shift on the value of the W -boson mass, one finds some additional contributions not enhanced by a factor of L , which are numerically insignificant [145].

one obtains

$$\begin{aligned} \frac{G_F}{\sqrt{2}} &= \frac{1}{2v_{\text{SM}}^2} \stackrel{\text{min}}{=} \frac{1}{8} \frac{g_5^2}{2\pi r} B_W(\epsilon, \epsilon, 0) = \frac{1}{2v^2} \left[1 + \frac{Lm_W^2}{2M_{\text{KK}}^2} + \dots \right], \\ &\stackrel{\text{cust}}{=} \frac{1}{8} \frac{g_{L,5}^2}{2\pi r} (1 \ 0) \mathbf{B}_W^{\text{UV}}(\epsilon, \epsilon, 0) \begin{pmatrix} 1 \\ 0 \end{pmatrix} = \frac{1}{2v^2} \left[1 + \frac{Lm_W^2}{2c_\vartheta^2 M_{\text{KK}}^2} + \dots \right], \end{aligned} \quad (5.13)$$

where the first (second) line holds for the minimal (custodial) RS model. Here and in the following, the ellipsis stands for terms of order v^4/M_{KK}^4 . We can combine the above results via

$$\kappa_v \equiv \frac{v}{v_{\text{SM}}} = 1 + \frac{Lm_W^2}{4c_\vartheta^2 M_{\text{KK}}^2} + \dots, \quad (5.14)$$

where $c_\vartheta^2 = 1$ in the minimal RS model, while it can take non-trivial values and may therefore be enhanced in the RS model with custodial symmetry. In particular, the correction is twice as large if the P_{LR} symmetry is at work.

Combining the Feynman rule (5.12) with the vev shift, one finds correction factors for the Higgs coupling to two W -boson zero modes of

$$\begin{aligned} c_W|_{\text{min}} &= \frac{v_{\text{SM}}}{v} \frac{\tilde{m}_W^2}{m_W^2} 2\pi \chi_0^W(1) \chi_0^W(1) = 1 - \frac{m_W^2}{2M_{\text{KK}}^2} \left(\frac{3L}{2} - 1 + \frac{1}{2L} \right) + \dots, \\ c_W|_{\text{cust}} &= \frac{v_{\text{SM}}}{v} \frac{\tilde{m}_W^2}{m_W^2 c_\vartheta^2} 2\pi \vec{\chi}_0^W(1)^T \mathbf{D}_\vartheta \vec{\chi}_0^W(1) = 1 - \frac{m_W^2}{2M_{\text{KK}}^2} \left(3L - 1 + \frac{1}{2L} \right) + \dots \end{aligned} \quad (5.15)$$

These correction factors are just $c_W \equiv \kappa_W/\kappa_v$, where κ_W and the vev shift κ_v are given in (4.91) and (5.14) respectively. Notice that in the custodial model the dominant term in the round bracket on the right-hand side involves a factor of 2.

The Feynman rule for the $W_\mu^{+(n)} \bar{u}_A^{(i)} d_A^{(j)}$ vertex, where $A = L, R$ is a chirality label and i, j labels the flavors of the SM quarks, has already been needed in the previous chapter, when we discussed the $b \rightarrow s\gamma$ transition. While the corresponding Feynman rule in the minimal model is given in (C.2), it reads in the custodial model

$$i \frac{g_{L,5}}{\sqrt{2}} \frac{1}{\sqrt{2\pi r}} \int_\epsilon^1 dt \sqrt{2\pi} \mathcal{U}_A^{(i)}(t) \left(\Omega_1 \frac{g_{R,5}}{g_{L,5}} \Omega_2 \right) \vec{\chi}_n^W(t) \gamma^\mu \mathcal{D}_A^{(j)}(t) P_A, \quad (5.16)$$

with the chirality projector $P_{R,L} = \frac{1}{2}(1 \pm \gamma_5)$ and the matrices

$$\Omega_1 = \begin{pmatrix} 1 & 0 & 0 \\ 0 & 0 & 0 \\ 0 & 0 & 0 \\ 0 & 0 & 1 \\ 0 & 0 & 0 \end{pmatrix}, \quad \Omega_2 = \begin{pmatrix} 0 & 0 & 0 \\ 1 & 0 & 0 \\ 0 & 0 & 0 \\ 0 & 0 & 0 \\ 0 & 1 & 0 \end{pmatrix}. \quad (5.17)$$

Note that for the W boson the leading contribution to the CKM matrix is given by the (11)-component of Ω_1 . Corrections coming from the non-universality of the KK gauge bosons as well as from the admixture of the U' and D' are chirally suppressed and can be neglected for the components that couple light fermions [149]. This feature extends to the case of the KK excitations of the W boson. Effectively this means that only the universal contribution of the W profiles, which are given by $\vec{\chi}_n^W(\epsilon)$, need to be kept. It

turns out that it is an excellent approximation for the light SM quarks to use

$$\begin{aligned} \text{minimal RS:} & \quad i \frac{g_5}{\sqrt{2}} \frac{1}{\sqrt{2\pi r}} \sqrt{2\pi} \chi_n^W(\epsilon) V_{ij}^{\text{CKM}} \gamma^\mu P_L, \\ \text{custodial RS:} & \quad i \frac{g_{L,5}}{\sqrt{2}} \frac{1}{\sqrt{2\pi r}} \sqrt{2\pi} \begin{pmatrix} 1 & 0 \end{pmatrix} \vec{\chi}_n^W(\epsilon) V_{ij}^{\text{CKM}} \gamma^\mu P_L. \end{aligned} \quad (5.18)$$

Corrections to this result, including the couplings to right-handed fermions, are strongly chirality suppressed. Note, in particular, that for the zero mode one encounters correction factors

$$\begin{aligned} c_{\Gamma_W}^{1/2}|_{\text{min}} & \equiv \frac{g_5}{\sqrt{2\pi r g}} \sqrt{2\pi} \chi_0^W(\epsilon) = c_{\Gamma_W}^{1/2}, \\ c_{\Gamma_W}^{1/2}|_{\text{cust}} & \equiv \frac{g_{L,5}}{\sqrt{2\pi r g}} \sqrt{2\pi} \begin{pmatrix} 1 & 0 \end{pmatrix} \vec{\chi}_0^W(\epsilon) = c_{\Gamma_W}^{1/2}, \end{aligned} \quad (5.19)$$

relative to the SM, which will affect all decay amplitudes of the W boson into light fermions. We see that this correction factor is the same for both the minimal and the custodial RS model and reads

$$c_{\Gamma_W}^{1/2} = 1 - \frac{m_W^2}{2M_{\text{KK}}^2} \frac{1}{4L} + \dots \quad (5.20)$$

It follows that, relative to the SM, we must make the following replacements in the SM decay amplitude for $h \rightarrow W^+ W^{-*} \rightarrow W^+ \bar{u}_i d_j$:

$$\begin{aligned} \frac{1}{m_W^2 - s} & \xrightarrow{\text{min}} \frac{v_{\text{SM}}}{v} \frac{\tilde{m}_W^2}{m_W^2} \sqrt{2\pi} \chi_0^W(1) \frac{g_5}{\sqrt{2\pi r g}} 2\pi B_W(1, \epsilon; -s), \\ & \xrightarrow{\text{cust}} \frac{v_{\text{SM}}}{v} \frac{\tilde{m}_W^2}{m_W^2 c_\beta^2} \sqrt{2\pi} \chi_0^W(1)^T \frac{g_{L,5}}{\sqrt{2\pi r g}} 2\pi \mathbf{B}_W^{\text{UV}}(1, \epsilon; -s) \begin{pmatrix} 1 \\ 0 \end{pmatrix}, \end{aligned} \quad (5.21)$$

with the 5D gauge-boson propagators $B_W(t, t'; -p^2)$ and $\mathbf{B}_W^{\text{UV}}(t, t'; -p^2)$. Using the expansions for $p^2 \lesssim m_W^2$ (3.31) and (3.40), we can now rewrite the right-hand side of (5.21) in the form

$$\frac{1}{m_W^2 - s} \rightarrow c_{\Gamma_W}^{1/2} c_W \left[\frac{1}{m_W^2 - s} - \frac{1}{4M_{\text{KK}}^2} \left(1 - \frac{1}{L} + \dots \right) \right]. \quad (5.22)$$

This result has an intuitive form. The factor $c_{\Gamma_W}^{1/2}$ rescales the W -boson decay amplitudes of the SM in a uniform way, the factor c_W rescales the Higgs-boson coupling to a $W^+ W^-$ pair, and the last term in brackets is the contribution of heavy KK resonances. Substituting (5.22) into (5.4) and performing the integration over s , we obtain the final result

$$\Gamma(h \rightarrow WW^*) = \frac{m_h^3}{16\pi v_{\text{SM}}^2} \frac{c_{\Gamma_W} \Gamma_W^{\text{SM}}}{\pi m_W} c_W^2 \left[g \left(\frac{m_W^2}{m_h^2} \right) - \frac{m_h^2}{2M_{\text{KK}}^2} \left(1 - \frac{1}{L} \right) h \left(\frac{m_W^2}{m_h^2} \right) + \dots \right], \quad (5.23)$$

where the new function is given by

$$h(x) = -(1 - 4x + 12x^2) \sqrt{4x - 1} \arccos\left(\frac{3x - 1}{2x^{3/2}}\right) - \frac{1}{2}(1 - 6x + 36x^2) \ln x + \frac{1}{6}(1 - x)(11 - 61x + 38x^2). \quad (5.24)$$

The analysis of new physics effects on the $h \rightarrow ZZ^*$ decay rate proceeds analogously. Instead of c_W in (5.15) one then finds the correction factors

$$\begin{aligned} c_Z|_{\min} &= \frac{v_{\text{SM}}}{v} \frac{\tilde{m}_Z^2}{m_Z^2} 2\pi \chi_0^Z(1) \chi_0^Z(1) = 1 - \frac{m_Z^2}{2M_{\text{KK}}^2} \left(L - 1 + \frac{1}{2L}\right) - \frac{Lm_W^2}{4M_{\text{KK}}^2} + \dots, \\ c_Z|_{\text{cust}} &= \frac{v_{\text{SM}}}{v} \frac{\tilde{m}_W^2}{m_Z^2 c_\vartheta^2} 2\pi \vec{\chi}_0^Z(1)^T \mathbf{D}_{\vartheta_Z} \vec{\chi}_0^Z(1) = 1 - \frac{m_W^2}{2M_{\text{KK}}^2} \left(3L + 1 - \frac{1}{2L}\right) + \dots \end{aligned} \quad (5.25)$$

for the hZZ coupling. The fact that the L -enhanced terms in the effective couplings c_W in (5.15) and c_Z in (5.25) in the minimal model are different is problematic from a phenomenological point of view, as this amounts to a breaking of custodial symmetry in the effective couplings of the Higgs to electroweak gauge bosons. Indeed, the difference ($c_W - c_Z$) is related to the T parameter, which receives dangerously large corrections in the minimal RS model as we have seen in Section 2.2.4. Recall that taming these effects has been the main motivation for the construction of RS models with a custodial symmetry in the bulk as discussed in Section 2.3. The custodial protection ensures that the leading, L -enhanced term is the same for both hWW and hZZ couplings [149], see (5.15) and (5.25), whereas the subleading terms are different.

Moreover, the $Zf\bar{f}$ couplings entering (5.9) get replaced by

$$\begin{aligned} \frac{g}{c_w} g_{f,A}(s_w^2) &\xrightarrow{\min} \frac{g_5}{\sqrt{2\pi r} c_w} \sqrt{2\pi} \chi_0^Z(\epsilon) g_{f,A}(s_w^2), \\ &\xrightarrow{\text{cust}} \frac{g_{L,5}}{\sqrt{2\pi r} c_w} \sqrt{2\pi} \begin{pmatrix} 1 & 0 \end{pmatrix} \vec{\chi}_0^Z(\epsilon) g_{f,A}(s_w^2). \end{aligned} \quad (5.26)$$

Here, we have used the Feynman rule for the couplings of the Z boson and its KK excitations to quarks, the $Z_\mu^{(n)} \bar{q}_A^{(i)} q_A^{(i)}$ vertex (with $A = L, R$), shown in (C.2) for the minimal model, while in the custodial model it reads

$$\frac{i}{\sqrt{2}} \frac{g_{L,5}}{\sqrt{2\pi r} c_w} \int_\epsilon^1 dt \sqrt{2\pi} \mathcal{Q}_A^{\dagger(i)}(t) \left(Q_Z^q \quad \frac{g_{Z',5}^q}{g_{Z,5}^q} Q_{Z'}^q \right) \vec{\chi}_n^Z(t) \gamma^\mu \mathcal{Q}_A^{(i)}(t) P_A. \quad (5.27)$$

The couplings are given by

$$\frac{g_Z^{\prime 2}}{g_Z^2} = \frac{\cos^2 \theta_w \tan^4 \vartheta}{\tan^2 \vartheta - \tan^2 \theta_w}, \quad Q_Z^q = T_L^{q3} - s_w^2 Q_q, \quad Q_{Z'}^q = -T_R^{q3} - \frac{\tan^2 \theta_w}{\tan^2 \vartheta} Y^q, \quad (5.28)$$

where $T_{L,R}^{q3}$ denotes the eigenvalue under the third generator of $SU(2)_{L,R}$, Y^q is the hyper- and Q_q the electromagnetic charge of the quark. Analogously to the W -boson vertex we only need to keep the universal contributions so that (5.26) is justified. If the weak mixing angle now is defined via the structure of the couplings $g_{f,A}(s_w^2)$, then the

only difference with regard to the SM is a factor

$$\begin{aligned} c_{\Gamma_Z}^{1/2}|_{\min} &\equiv \frac{g_5}{\sqrt{2\pi r g}} \sqrt{2\pi} \chi_0^Z(\epsilon) = c_{\Gamma_Z}^{1/2}, \\ c_{\Gamma_Z}^{1/2}|_{\text{cust}} &\equiv \frac{g_{L,5}}{\sqrt{2\pi r g}} \sqrt{2\pi} (1 \ 0) \vec{\chi}_0^Z(\epsilon) = c_{\Gamma_Z}^{1/2}, \end{aligned} \quad (5.29)$$

with

$$c_{\Gamma_Z}^{1/2} = c_{\Gamma_W}^{1/2} \left[1 + \frac{m_Z^2 - m_W^2}{4M_{\text{KK}}^2} \left(1 - \frac{1}{L} \right) + \dots \right]. \quad (5.30)$$

Thus, also the correction factor for the $Zf\bar{f}$ coupling remains unchanged in the custodial RS model.

It then follows that we must make the replacements (5.21), where now $W \rightarrow Z$. The propagator functions $B_Z(t, t'; -p^2)$ and $\mathbf{B}_Z^{\text{UV}}(t, t'; -p^2)$ can be easily obtained from (3.31) and (3.40), making the replacements $W \rightarrow Z$ and $\vartheta \rightarrow \vartheta_Z$ as well as $c_1(t, t') \rightarrow c_1^Z(t, t') = 2\pi \chi_0^Z(t) \chi_0^Z(t')$, where $\chi_0^Z(t)$ denotes the zero mode profile of the Z boson (2.31). Hence, the final result for the decay width $\Gamma(h \rightarrow ZZ)$ is given by (5.23) with $W \rightarrow Z$ and multiplied with a factor 1/2.

Higgs-Strahlung

We now move on to study the cross section for the Higgs-strahlung process, in which the Higgs boson is produced in pp collisions in association with a W or Z boson, see Figure 5.2(b). Since the Feynman diagram for Higgs-strahlung is identical to that for the Higgs-boson decay into a pair of electroweak gauge bosons, it follows that the amplitude at the quark level receives exactly the same corrections as the Higgs decay amplitude discussed in the previous section. If the invariant mass squared of the hV pair in the final state is denoted by s , one immediately obtains from (5.22) (for $V = W, Z$)

$$\frac{d\sigma(pp \rightarrow hV)}{ds} = c_{\Gamma_V} c_V^2 \left[1 + \frac{s - m_V^2}{2M_{\text{KK}}^2} \left(1 - \frac{1}{L} \right) + \dots \right] \frac{d\sigma(pp \rightarrow hV)_{\text{SM}}}{ds}. \quad (5.31)$$

Because the s dependence of the SM cross section is sensitive to the shapes of the parton distribution functions, it is not possible to derive a simple analytic formula for the corrections to the total Higgs-strahlung cross sections. However, the leading correction terms enhanced by L are universal and independent of s . When only these terms are kept, one obtains

$$\sigma(pp \rightarrow hV) \approx c_V^2 \sigma(pp \rightarrow hV)_{\text{SM}}. \quad (5.32)$$

This approximation has been frequently used in the literature. In RS models it is accurate up to small corrections not enhanced by L .

Higgs Production in Vector-Boson Fusion

We finally consider the vector-boson fusion process shown in Figure 5.2(c). It involves two gauge-boson propagators, whose momenta we denote by $p_{1,2}$. In analogy with the discussion in the previous sections, we find that in order to account for new physics

effects one must replace

$$\begin{aligned}
& \frac{1}{(m_V^2 - p_1^2)(m_V^2 - p_2^2)} \\
& \xrightarrow{\min} \frac{v_{\text{SM}}}{v} \frac{\tilde{m}_V^2}{m_V^2} \left(\frac{g_5}{\sqrt{2\pi r g}} \right)^2 (2\pi)^2 B_V(\epsilon, 1; -p_1^2) B_V(1, \epsilon; -p_2^2) \\
& \xrightarrow{\text{cust}} \frac{v_{\text{SM}}}{v} \frac{\tilde{m}_W^2}{m_V^2 c_\vartheta^2} \left(\frac{g_{L,5}}{\sqrt{2\pi r g}} \right)^2 (2\pi)^2 \begin{pmatrix} 1 & 0 \end{pmatrix} \mathbf{B}_V^{\text{UV}}(\epsilon, 1; -p_1^2) \mathbf{D}_{\vartheta_V} \mathbf{B}_V^{\text{UV}}(1, \epsilon; -p_2^2) \begin{pmatrix} 1 \\ 0 \end{pmatrix} \\
& = \frac{c_{\Gamma_V} c_V}{(m_V^2 - p_1^2)(m_V^2 - p_2^2)} \left[1 - \frac{2m_V^2 - p_1^2 - p_2^2}{4M_{\text{KK}}^2} \left(1 - \frac{1}{L} \right) + \dots \right] \quad (5.33)
\end{aligned}$$

in the expression for the scattering amplitude. Once again the integrations over the virtual momenta flowing through the propagators cannot be performed in closed form, because they involve convolutions with parton distribution functions. However, the leading correction terms enhanced by L are universal. When only these terms are kept, one obtains

$$\sigma(pp \rightarrow hq\bar{q}') \approx c_V^2 \sigma(pp \rightarrow hq\bar{q}')_{\text{SM}}, \quad (5.34)$$

which is an approximation often adopted in the literature.

5.1.2 Higgs Couplings in RS Models

In this section, we summarize the RS contributions to the various Higgs couplings. In order to parameterize them, we use an effective Lagrangian defined at the electroweak scale $\mu \approx v$. For simplicity, the effects of RG running from the new physics scale $\mu \approx M_{\text{KK}}$ down to the electroweak scale is neglected, as their numerical impact is of minor importance. The phenomenologically most relevant Higgs couplings can be described using the following Lagrangian in the broken electroweak phase:

$$\begin{aligned}
\mathcal{L}_{\text{eff}} = & c_W \frac{2m_W^2}{v_{\text{SM}}} h W_\mu^+ W^{-\mu} + c_Z \frac{m_Z^2}{v_{\text{SM}}} h Z_\mu Z^\mu - \sum_{f=t,b,\tau} \frac{m_f}{v_{\text{SM}}} h \bar{f} (c_f + c_{f5} i\gamma_5) f \\
& - c_{3h} \frac{m_h^2}{2v_{\text{SM}}} h^3 - c_{4h} \frac{m_h^2}{8v_{\text{SM}}^2} h^4 + c_g \frac{\alpha_s}{12\pi v_{\text{SM}}} h G_{\mu\nu}^a G^{a,\mu\nu} - c_{g5} \frac{\alpha_s}{8\pi v_{\text{SM}}} h G_{\mu\nu}^a \tilde{G}^{a,\mu\nu} \\
& + c_\gamma \frac{\alpha}{6\pi v_{\text{SM}}} h F_{\mu\nu} F^{\mu\nu} - c_{\gamma 5} \frac{\alpha}{4\pi v_{\text{SM}}} h F_{\mu\nu} \tilde{F}^{\mu\nu} + \dots \quad (5.35)
\end{aligned}$$

It should be emphasized that this is not a complete list of operators. For instance, we have not included the operators $h Z_\mu \bar{f} \gamma^\mu f$ and $h Z_\mu \bar{f} \gamma^\mu \gamma_5 f$ contributing to the $h \rightarrow ZZ^* \rightarrow Z \bar{f} f$ decay rate, since as shown in Section 5.1.1 their contribution is subdominant. Furthermore, we will not consider the Higgs decay $h \rightarrow Z\gamma$ here. Both the CP-even couplings c_i and the CP-odd coefficients c_{i5} are real. In the SM $c_W = c_Z = c_f = c_{3h} = c_{4h} = 1$ and $c_{f5} = c_g = c_{g5} = c_\gamma = c_{\gamma 5} = 0$.

Tree-Level Higgs Couplings to Fermions and Electroweak Gauge Bosons

In the SM, the Higgs boson couples to fermions and electroweak gauge bosons at tree level, with coupling strengths proportional to the masses of these particles. The non-universality of these couplings is the most distinguished feature of the Higgs mechanism.

In RS models, modifications of the couplings arise from two effects: genuine corrections to the hVV (with $V = W, Z$) and hff vertices, and an overall rescaling of all couplings due to the shift of the Higgs vev, which appears because the SM vev v_{SM} is used in the effective Lagrangian (5.35). Note that the c_i differ from the couplings κ_i previously used in this thesis, in (4.36) and (4.91) for example, via

$$c_i = \frac{\kappa_i}{\kappa_v}, \quad i = t, t5, b, b5, \tau, \tau5, W, Z. \quad (5.36)$$

The loop-induced Higgs couplings will be somewhat more involved, since we have to distinguish between the zero-mode and the KK tower corrections. In the following, explicit expressions for the various c_i parameters to (at least) first order in v^2/M_{KK}^2 will be presented. Wherever possible, the differences between the minimal and the custodial RS model (from now on we will assume the P_{LR} to be at work) will be parameterized by means of a parameter ξ , which equals 1 in the minimal model and 2 in the custodial model.²

The Higgs couplings to W and Z bosons in RS models have been derived in (5.15) and (5.25) and read (at order v^2/M_{KK}^2)

$$\begin{aligned} c_W|_{\text{min}} &= 1 - \frac{m_W^2}{2M_{\text{KK}}^2} \left(\frac{3L}{2} - 1 + \frac{1}{2L} \right), & c_W|_{\text{cust}} &= 1 - \frac{m_W^2}{2M_{\text{KK}}^2} \left(3L - 1 + \frac{1}{2L} \right), \\ c_Z|_{\text{min}} &= 1 - \frac{m_Z^2}{2M_{\text{KK}}^2} \left(L - 1 + \frac{1}{2L} \right) - \frac{Lm_W^2}{4M_{\text{KK}}^2}, & c_Z|_{\text{cust}} &= 1 - \frac{m_W^2}{2M_{\text{KK}}^2} \left(3L + 1 - \frac{1}{2L} \right). \end{aligned} \quad (5.37)$$

With $L \approx 33-34$, the L -enhanced contributions are by far dominant numerically. Future precise measurements of c_W and c_Z would thus provide a direct tool to determine the ratio M_{KK}/\sqrt{L} in the RS model.

The couplings of the Higgs boson to the third-generation fermions have been studied in detail in Section 4.1, where it was found that flavor-changing couplings are strongly suppressed. For the CP-even and CP-odd flavor-diagonal couplings, it follows from (4.36) that (with $f = t, b, \tau$ on the left-hand side and $f = u, d, e$ on the right-hand side)

$$\begin{aligned} c_f &= 1 - \varepsilon_f - \frac{\xi L m_W^2}{4M_{\text{KK}}^2} - \frac{\xi v^2}{3M_{\text{KK}}^2} \text{Re} \frac{(\mathbf{Y}_f \mathbf{Y}_f^\dagger \mathbf{Y}_f)_{33}}{(\mathbf{Y}_f)_{33}} + \dots, \\ c_{f5} &= -\frac{\xi v^2}{3M_{\text{KK}}^2} \text{Im} \frac{(\mathbf{Y}_f \mathbf{Y}_f^\dagger \mathbf{Y}_f)_{33}}{(\mathbf{Y}_f)_{33}} + \dots, \end{aligned} \quad (5.38)$$

where the real-valued quantities ε_f are given by³

$$\varepsilon_f = \begin{cases} (\boldsymbol{\delta}_F)_{33} + (\boldsymbol{\delta}_f)_{33}; & \text{minimal RS model,} \\ (\boldsymbol{\Phi}_F)_{33} + (\boldsymbol{\Phi}_f)_{33}; & \text{custodial RS model.} \end{cases} \quad (5.39)$$

The matrices $\boldsymbol{\delta}_{F,f}$ and $\boldsymbol{\Phi}_{F,f}$ can be found in (4.30) and (4.63), respectively. Recall that for all practical purposes, one can retain $\varepsilon_u = (\boldsymbol{\delta}_U)_{33} + (\boldsymbol{\delta}_u)_{33}$, with $(\boldsymbol{\delta}_{Q,q})$ given in (4.30), but $\varepsilon_d \approx (\boldsymbol{\delta}_D)_{33}$, $(\varepsilon_e)_{33} \approx 0$, and similarly for the custodial RS model. Numerically, the

²Note that in the formulas for the boson couplings ξ can be identified with $\xi = 1/c_g^2 = 2$, while this is not true for the Higgs couplings to fermions, which is why we introduce a new variable here.

³In this section we use the subscripts $f = u, d, e$ instead of t, b, τ in order to be able to summarize the couplings c_f as shown in (5.38).

ε_f parameters turn out to play a numerically subleading role compared with the “three-Yukawa terms” in c_f .

In contrast to the Higgs couplings to the massive vector bosons, the couplings to the fermions do not only depend on the KK scale but also in a complicated manner on the dimensionless 5D Yukawa matrices \mathbf{Y}_f . However, it is possible to simplify the Yukawa-dependent terms using that for a large set of random complex matrices on average

$$\left\langle \frac{(\mathbf{Y}_f \mathbf{Y}_f^\dagger \mathbf{Y}_f)_{33}}{(\mathbf{Y}_f)_{33}} \right\rangle = (2N_g - 1) \frac{y_\star^2}{2}, \quad (5.40)$$

where $N_g = 3$ is the number of fermion generations. It follows that the Higgs couplings to fermions are rather insensitive to the individual entries of the Yukawa matrices, but they do scale with y_\star^2 . Hence, we encounter a similar situation as in the gauge-boson case, where the relevant parameter is now given by M_{KK}/y_\star . One should add at this point that in practice relation (5.40) is subject to some flavor-dependent corrections, which arise when the scan over random Yukawa matrices is performed subject to the constraint that one obtains acceptable values for the quark and lepton masses and for the CKM matrix in the quark sector. When this is done, one finds numerically that the expectation value (5.40) is slightly enhanced for the top quark and somewhat reduced for the bottom quark.⁴

In the type-II brane-Higgs scenarios, the Yukawa-dependent terms in (5.40) change according to (4.42), while the remaining terms are unaffected at leading order in the expansion in v^2/M_{KK}^2 . For the special case $\mathbf{Y}_f^S = 0$, which was sometimes adopted in the literature, this term vanishes and gives no contribution to the Higgs couplings to fermions. There is then no contribution to the CP-odd couplings c_{f5} .

Higgs Self-Couplings

One of the predictions of the SM is that the trilinear and quartic Higgs couplings can be expressed in terms of the Higgs-boson mass and the vev of the Higgs field, such that $c_{3h} = c_{4h} = 1$ in (5.35). In RS models these coefficients receive calculable corrections, which happen to be described by the same formula for the minimal and the custodial RS models. As long as the Higgs sector is localized on or near the IR brane, one obtains

$$c_{3h} = \frac{v_{\text{SM}}}{v} = 1 - \frac{\xi L m_W^2}{4M_{\text{KK}}^2} + \dots, \quad c_{4h} = \frac{v_{\text{SM}}^2}{v^2} = 1 - \frac{\xi L m_W^2}{2M_{\text{KK}}^2} + \dots \quad (5.41)$$

For a KK mass scale of $M_{\text{KK}} = 1.5$ TeV, one finds a 2.4% (4.8%) reduction of the trilinear coupling and a 4.8% (9.6%) reduction of the quartic coupling in the minimal (custodial) RS model. Moving the Higgs field into the bulk would attenuate these deviations and move the couplings closer to their SM values [259]. Such small deviations will not be measurable by the LHC, and even for a future linear collider like the ILC this is probably out of reach. Therefore, it is refrained from presenting a detailed numerical analysis of the Higgs self-couplings in the subsequent section.

⁴For $y_\star = 1$, one finds numerically that the expectation value (5.40) is equal to 2.5 (as expected) for anarchic matrices, while it is 2.7 in the up-quark sector and 2.2 in the down-quark sector. The neutrino masses or the PMNS matrix are not considered in this analysis, since this would require the specification of the neutrino sector, which is both model dependent and of little relevance to Higgs physics.

Loop-Induced Higgs Couplings to Two Gluons

The loop-induced couplings to gluons and photons have been extensively discussed in Sections 4.1 and 4.2. We begin with a discussion of the loop-induced Higgs couplings to gluons, which are relevant for the calculation of the gluon-fusion cross section $\sigma(gg \rightarrow h)$, which is the main Higgs production channel at high-energy hadron colliders such as the LHC. In the limit where we neglect $\mathcal{O}(v^2/M_{\text{KK}}^2)$ corrections which in addition are strongly chirality suppressed, the expressions for the induced Higgs couplings to two gluons read (see (4.37))⁵

$$c_g + ic_{g5} = \begin{cases} \text{Tr } g(\mathbf{X}_u) + \text{Tr } g(\mathbf{X}_d) + \varepsilon_u + \varepsilon_d; & \text{minimal RS model,} \\ \text{Tr } g(\sqrt{2}\mathbf{X}_u) + 3 \text{Tr } g(\sqrt{2}\mathbf{X}_d) + \varepsilon_u + \varepsilon_d; & \text{custodial RS model,} \end{cases} \quad (5.42)$$

where the quantities \mathbf{X}_f are defined in (2.78). The functions $g(\mathbf{X}_f)$ differ for the brane-localized and narrow bulk-Higgs scenario and are given in (4.25) and (4.26), respectively. Recall that $g(\mathbf{X}_f) = \mp \frac{v^2}{2M_{\text{KK}}^2} \mathbf{Y}_f \mathbf{Y}_f^\dagger + \dots$ so that the effect from the KK tower is approximately equal but of opposite sign in the two scenarios. For a large ensemble of random matrices, one obtains on average

$$\langle \text{Tr } \mathbf{Y}_f \mathbf{Y}_f^\dagger \rangle = N_g^2 \frac{y_*^2}{2}. \quad (5.43)$$

Due to the additional factors $\sqrt{2}$ and 3 in the second case in (5.42), the quark KK tower contribution in the custodial RS model is roughly four times larger than in the minimal RS model. Note also that with the hermitian matrices \mathbf{X}_f the traces over the matrix-valued functions $g(\mathbf{X}_f)$ are real, so that

$$c_{g5} = 0, \quad (5.44)$$

irrespective of the Higgs localization or the type of RS model (minimal or custodial). For the type-II brane-Higgs model, the function $g(\mathbf{X}_f)$ is given by the function (4.41) starting with the term $-\frac{v^2}{2M_{\text{KK}}^2} \mathbf{Y}_f^C \mathbf{Y}_f^{C\dagger} + \dots$, and hence to leading order there is no difference with the result shown above. In this model, the CP-odd coupling c_{g5} receives contributions starting at $\mathcal{O}(v^4/M_{\text{KK}}^4)$, which are however too small to be of any phenomenological significance. In the subsequent sections it will be therefore restricted to a study of the two cases shown in (4.25) and (4.26).

When the top-quark is integrated out from the effective Lagrangian (5.35), additional contributions to the effective hgg couplings are induced at one-loop order. They can be accounted for by using the effective couplings

$$c_g^{\text{eff}} = \frac{c_g + A_q(\tau_t) c_t}{A_q(\tau_t)}, \quad c_{g5}^{\text{eff}} = \frac{c_{g5} + B_q(\tau_t) c_{t5}}{A_q(\tau_t)}, \quad (5.45)$$

where we have normalized such that $c_g^{\text{eff}} = 1$ in the SM. The explicit expressions for the top-quark loop functions $A_q(\tau_t) \approx 1.03$ and $B_q(\tau_t) \approx 1.05$ (with $\tau_t = 4m_t^2/m_h^2$) are given in (4.38). Both approach 1 for $\tau \rightarrow \infty$, and it is an excellent approximation to use the asymptotic values for the small new-physics corrections to the Wilson coefficients. It then follows that the terms proportional to ε_u , which in c_g^{eff} combine to $\varepsilon_u [1 - A_q(\tau_t)]$, can be safely neglected. Note also that to a very good approximation $c_{g5}^{\text{eff}} \approx c_{t5}$.

⁵Since we work at leading order in v^2/M_{KK}^2 the effect of κ_v does not need to be considered here.

Loop-Induced Higgs Couplings to Two Photons

We finally turn our attention to the couplings of the Higgs boson to two photons, which play a crucial role for the $h \rightarrow \gamma\gamma$ decay channel, in which the Higgs boson has been discovered in 2012. Neglecting as before $\mathcal{O}(v^2/M_{\text{KK}}^2)$ corrections which in addition are strongly chirality suppressed, the expressions for the induced Higgs couplings to two photons in the minimal RS model have been derived in Section 4.2 and read (see (4.73) and (4.89))

$$c_\gamma + ic_{\gamma 5} = N_c Q_u^2 [\text{Tr} g(\mathbf{X}_u) + \varepsilon_u] + N_c Q_d^2 [\text{Tr} g(\mathbf{X}_d) + \varepsilon_d] + Q_e^2 \text{Tr} g(\mathbf{X}_e) - \frac{21}{4} \nu_W, \quad (5.46)$$

while in the custodial model one obtains (see (4.93) and (4.89))

$$\begin{aligned} c_\gamma + ic_{\gamma 5} &= N_c Q_u^2 \text{Tr} g(\sqrt{2}\mathbf{X}_u) + N_c (Q_u^2 + Q_d^2 + Q_\lambda^2) \text{Tr} g(\sqrt{2}\mathbf{X}_d) + Q_e^2 \text{Tr} g(\mathbf{X}_e) \\ &\quad + N_c Q_u^2 \varepsilon_u + N_c Q_d^2 \varepsilon_d - \frac{21}{4} \nu_W. \end{aligned} \quad (5.47)$$

Recall that they receive KK contributions from the quark and lepton loops as well as from loops of W bosons and scalar Goldstone fields. Here $Q_{u,d,e}$ denote the electric charges of the SM fermions, and $Q_\lambda = \frac{5}{3}$ is the charge of a new exotic, heavy fermion species encountered in the custodial RS model. The infinite tower of the KK excitations of the W bosons (including the Goldstone fields) contributes (see (4.91))

$$\nu_W = \frac{m_W^2}{2M_{\text{KK}}^2} \left(\xi L - 1 + \frac{1}{2L} \right) + \dots \quad (5.48)$$

Like in the case of the gluon-fusion channel $gg \rightarrow h$, effective coefficients can be obtained after the heavy particles t , W , and Z of the SM are integrated out. They are related to the above coefficients by

$$c_\gamma^{\text{eff}} = \frac{c_\gamma + N_c Q_u^2 A_q(\tau_t) c_t - \frac{21}{4} A_W(\tau_W) c_W}{N_c Q_u^2 A_q(\tau_t) - \frac{21}{4} A_W(\tau_W)}, \quad c_{\gamma 5}^{\text{eff}} = \frac{c_{\gamma 5} + N_c Q_u^2 B_q(\tau_t) c_{t5}}{N_c Q_u^2 A_q(\tau_t) - \frac{21}{4} A_W(\tau_W)}, \quad (5.49)$$

where again we have chosen the normalization such that c_γ^{eff} in the SM. The W -boson loop function A_W (with $\tau_W = 4m_W^2/m_h^2$) can be found in (4.90). From the fact that the coefficient $c_{\gamma 5}$ in (5.46) and (5.47) vanishes, it follows that to a very good approximation

$$c_{\gamma 5}^{\text{eff}} \approx -0.28 c_{t5}. \quad (5.50)$$

5.1.3 Numerical Analysis of the Higgs Couplings

We now study the structure of new physics effects to both tree-level and loop-induced Higgs couplings to fermions and gauge bosons in the context of the RS model with custodial symmetry, for which the bounds derived from electroweak precision tests allow for KK masses in the few TeV range. Recall that the tree-level analysis of the S and T parameters yields $M_{g(1)} > 4.7 \text{ TeV}$ (at 95% CL) for the mass of the lightest KK gluon and photon resonances, see (2.189). Somewhat lighter masses are possible for the KK fermion resonances. We will see that these bounds still allow for sizable effects in the Higgs sector. On the other hand, the corresponding bound $M_{g(1)} > 12.0 \text{ TeV}$ (at 95% CL) obtained in the minimal model, see (2.133), is so high that the resulting corrections

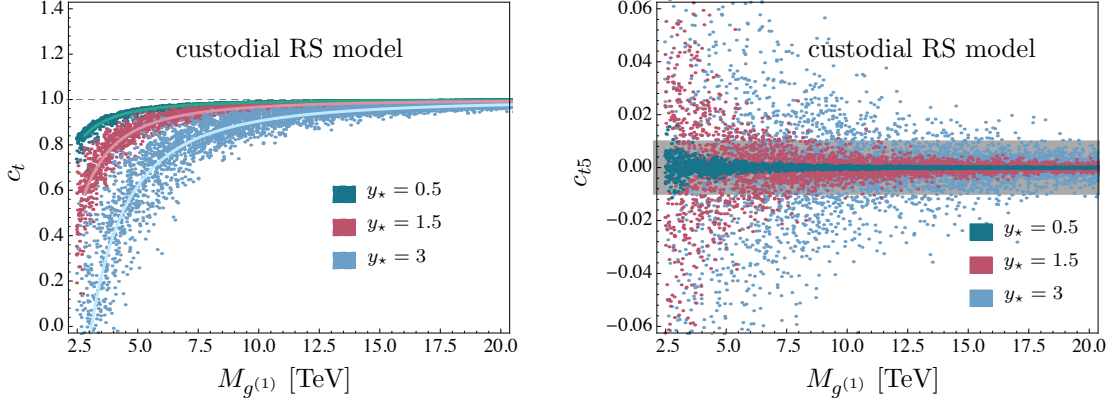


FIGURE 5.3: Predictions for the Higgs coupling to top quarks as a function of the KK gluon mass $M_{g(1)}$ in the custodial RS model. The green, red, and blue scatter points correspond to model points obtained using $y_\star = 0.5$, 1.5, and 3, respectively. The overlaid lines in the left plot show fits to the various distributions as explained in the text. The gray band in the right plot shows the experimental bound on $|c_{t5}|$ derived from the electron EDM (at 90% CL).

to the Higgs couplings are generally below the sensitivity level of present and planned collider experiments. In the following analysis we take $m_h = 125.6$ GeV for the Higgs mass, as well as the pole mass $m_t = 172.6$ GeV. The RS volume is chosen to be $L = 33.5$.

Tree-Level Higgs Couplings

In the custodial RS model, the corrections to the tree-level Higgs couplings to W and Z bosons in (5.37) are identical up to very small corrections not enhanced by L . Numerically, we obtain

$$c_W \approx c_Z \approx 1 - 0.078 \left(\frac{5 \text{ TeV}}{M_{g(1)}} \right)^2. \quad (5.51)$$

Realistically, with KK masses not in conflict with electroweak precision tests, we might thus expect corrections of a few up to a maximum of 10%. The corrections to the Higgs self-couplings in (5.41) are even smaller; the coefficients in front of the correction term are 0.026 for c_{3h} and 0.052 for c_{4h} .

Next we study the corrections to the CP-even and CP-odd Higgs couplings c_f and c_{f5} to the third generation fermions, as obtained from (5.38). For the analysis, three sets of 5000 random and anarchic 5D Yukawa matrices are generated, whose entries satisfy $|(\mathbf{Y}_q)_{ij}| \leq y_\star$ with $y_\star = 0.5$, 1.5, and 3, and which correctly reproduce the Wolfenstein parameters $\bar{\rho}$ and $\bar{\eta}$ of the unitarity triangle, see Subsection 2.2.3. Furthermore, the bulk mass parameters are chosen to be in the range $c_{Q_i, q_i} \leq 1$ and, together with the generated Yukawa matrices, to reproduce the correct values for the SM quark masses evaluated at the scale $\mu = 1$ TeV.⁶ The left plot of Figure 5.3 shows the Higgs coupling to top quarks as a function of the lightest KK gluon state $M_{g(1)} \approx 2.45 M_{\text{KK}}$ and for different values of y_\star . In accordance with (5.38) we observe that c_t is reduced compared to the SM value 1 for almost all parameter points, where the depletion increases with

⁶ The parameter c_{Q_3} is restricted to be $c_{Q_3} < 0.5$, since otherwise the ZMA approximation (4.63) is not valid.

y_\star	0.5	1.5	3	y_\star	0.5	1.5	3
a_t	3.4	9.0	26.3	b_t	0.96	1.24	1.33
a_b	2.3	5.9	16.7	b_b	0.96	0.89	0.89
a_τ	2.1	5.2	15.4	b_τ	0.96	0.89	0.89

TABLE 5.1: Fit coefficients a_f and b_f for the Higgs couplings to the third-generation fermions for different values of y_\star .

larger values for the Yukawa scale y_\star . The corresponding plots for c_b and c_τ look very similar, with the magnitude of the corrections somewhat reduced. The main differences are due to the chiral contributions coming from the overlap integrals in (5.38) and due to the constrained structure of the Yukawa matrices as explained in the text below (5.40). The solid lines in the left plot show simple polynomial fits of the form $c_f = 1 - 0.015 a_f (5 \text{ TeV}/M_{g(1)})^2$ to the scatter points, with coefficients $a_f = a_f(y_\star)$ given in Table 5.1. At this point, a comment must be added to the case of the type-II brane Higgs model. While the effects of the quantities ε_q and of the Higgs vev shift still give rise to small negative corrections, the corresponding scatter plots would show points scattered more or less around the central value $c_i = 1$, and which can become larger than 1 for not too small values for y_\star due to the indefinite sign of the three-Yukawa terms. Although they are not as pronounced as in the conventional brane-Higgs scenarios, significant effects on the Higgs coupling to the top quark are still possible. For example, with $y_\star = 3$ a modification of c_t by 20% is possible for KK excitations as heavy as 7.5 TeV.

The CP-odd couplings of the Higgs to two fermions c_{f5} are given by the second expression in (5.38). For random complex Yukawa matrices \mathbf{Y}_f bounded by $\langle |(\mathbf{Y}_f)_{ij}| \rangle \leq y_\star$, we expect to obtain an approximately Gaussian distribution with zero mean and a standard deviation

$$\sigma_{c_{f5}} \approx 0.005 b_f y_\star^2 \left(\frac{5 \text{ TeV}}{M_{g(1)}} \right)^2, \quad (5.52)$$

with $b_f = 1$. Due to the constraint that we must obtain realistic values of the quark masses and CKM mixing angles the actual results differ slightly from this result and we obtain the value shown in Table 5.1. It has been argued in [261] that present experimental bounds on electric dipole moments (EDMs) of the electron, neutron, and mercury impose non-trivial bounds on the CP-odd Higgs couplings to the third-generation fermions. The strongest constraint exists for the magnitude on c_{t5} and comes from the EDM of the electron, which is sensitive to the $ht\bar{t}$ couplings via two-loop Barr-Zee diagrams. Using the present 90% CL upper limit $d_e < 8.7 \cdot 10^{-29} e \text{ cm}$ [262] and assuming that the Higgs coupling to electrons is not changed with respect to its SM value, one obtains $|c_{t5}| \leq 0.01$ [261]. In the RS models considered in this thesis this assumption is valid to high accuracy, since corrections to the he^+e^- coupling are strongly chirality suppressed. This resulting bound is shown by the gray band in the right plot in Figure 5.3. Interestingly, we find that for $y_\star \gtrsim 1.5$ there are many points in the RS parameter space for which $|c_{t5}|$ takes values of the same order of magnitude as the experimental bound. Hence, in the context of RS models it is conceivable that first hints of a non-zero electron EDM might be seen in the next round of experiments.

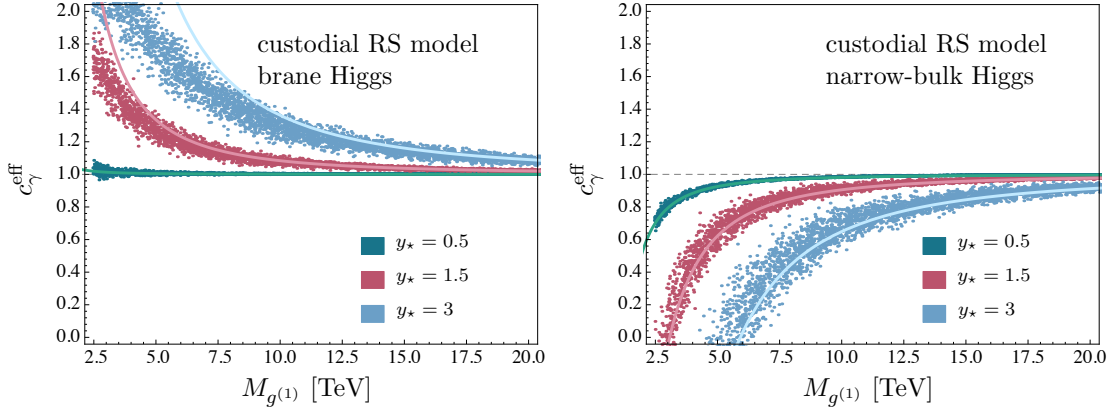


FIGURE 5.4: Predictions for the CP-even effective Higgs coupling to two photons as a function of the KK gluon mass $M_{g(1)}$ in the custodial RS model, for the scenarios with a brane-localized scalar sector (left) and a narrow bulk-Higgs field (right). The meaning of the colors and lines is the same as in Figure 5.3.

Loop-Induced Higgs Couplings

We move on to study the RS corrections to the loop-induced hgg and $h\gamma\gamma$ couplings. They are of special interest, since they are very sensitive probes of virtual KK excitations. We concentrate on the CP-even couplings c_g^{eff} and c_γ^{eff} , since current measurements are not sensitive enough to probe the CP-odd couplings.⁷ Using the analytic expressions for c_g^{eff} and c_γ^{eff} given in (5.45) and (5.49), it is straightforward to derive approximate expressions for these coefficients which help to understand the interplay of the various contributions. To this end, we expand the fermion KK tower contributions in (5.42), (5.46), and (5.47) to first order in v^2/M_{KK}^2 and employ (5.40) and (5.43). We also approximate the top-quark loop function $A_q(\tau_t)$ by its asymptotic value 1 and neglect subleading terms not enhanced by L in the bosonic contributions. This yields

$$\begin{aligned}
 c_g^{\text{eff}} &\approx 1 + \frac{v^2}{2M_{\text{KK}}^2} \left[\left(\mp 36 - \frac{10}{3} \right) y_*^2 - \frac{Lm_W^2}{v^2} \right] \approx 1 + \frac{v^2}{2M_{\text{KK}}^2} [(\mp 36.0 - 3.3) y_*^2 - 3.6], \\
 c_\gamma^{\text{eff}} &\approx 1 + \frac{v^2}{2M_{\text{KK}}^2} \left[\frac{1}{|C_{1\gamma}^{\text{SM}}|} \left(\pm \frac{213}{2} + \frac{40}{9} \right) y_*^2 - \frac{21(A_W(\tau_W) - 1)}{4|C_{1\gamma}^{\text{SM}}|} \frac{2Lm_W^2}{v^2} - \frac{Lm_W^2}{v^2} \right] \\
 &\approx 1 + \frac{v^2}{2M_{\text{KK}}^2} [(\pm 21.7 + 0.9) y_*^2 - 5.1]. \tag{5.53}
 \end{aligned}$$

Here the upper sign holds for the brane-Higgs case, while the lower one corresponds to the narrow bulk-Higgs scenario. We have kept the dependence on the one-loop SM amplitude $C_{1\gamma}^{\text{SM}} = \frac{4}{3} - \frac{21}{4}A_W(\tau_W) \approx -4.9$ explicit. In each square bracket, the first term is due to the effects of KK fermion resonances, while the second term accounts for the vev shift and the contribution of bosonic KK states (for c_γ^{eff}). The fermionic contributions enter the two coefficients with opposite signs and are larger in magnitude in the case of c_g^{eff} . Figure 5.4 shows the predictions for the coefficient c_γ^{eff} as a function

⁷There exist proposals for how to probe $c_{\gamma 5}^{\text{eff}}$ in $h \rightarrow \gamma\gamma$ decays in which both photons undergo nuclear conversion, by measuring certain kinematic distributions of the electron-positron pairs [263]. Unfortunately, however, the level of sensitivity one can achieve does not allow one to probe the small effects (5.50) predicted in RS models, where the CP-odd $ht\bar{t}$ coupling is the only source of the effect.

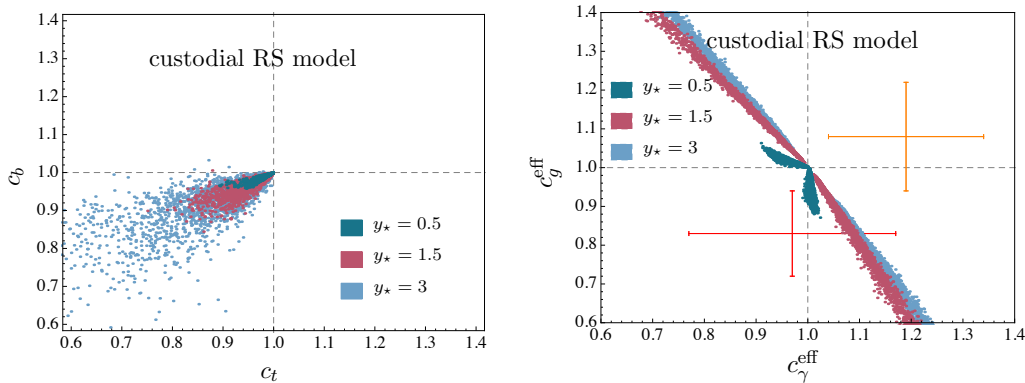


FIGURE 5.5: Correlation between the Higgs couplings c_t and c_b (left) and the effective Higgs couplings c_γ^{eff} and c_g^{eff} (right) in the custodial RS model. All points obey the constraint $M_{g(1)} > 4.7$ TeV imposed by the tree-level analysis of the S and T parameters at 95% CL. In the right plot, the orange (red) cross represents the experimental values (with 1σ errors) obtained by ATLAS (CMS).

of $M_{g(1)}$ and for different values of y_\star . We clearly see that large deviations from the SM prediction are possible, where the results exhibit a large sensitivity to the precise nature of the localization of the scalar sector on or near the IR brane. On average, the distribution of scatter points follows the approximate formulas shown in (5.53). The corresponding information on how c_g^{eff} depends on $M_{g(1)}$ and y_\star can be deduced from the correlation between the two loop-induced couplings, to which we turn now.

Correlations between Higgs Couplings

We have explained earlier that, to good approximation, the average results for the various Higgs couplings in RS models can be expressed in terms of only two parameters M_{KK} and y_\star with some relatively narrow distribution of model points about these average predictions. As a result, in these models there are strong correlations between various Higgs couplings. This important fact is illustrated in Figure 5.5, where we display the predictions in the $c_b - c_t$ and $c_g^{\text{eff}} - c_\gamma^{\text{eff}}$ planes. In the right plot, scatter points below $c_g^{\text{eff}} = 1$ (lower right plane) correspond to the brane-Higgs scenario, while points above $c_g^{\text{eff}} = 1$ (upper left plane) refer to the narrow bulk-Higgs scenario. All points included in these plots obey the constraint $M_{g(1)} > 4.7$ TeV implied by electroweak precision tests, see (2.189) derived in Subsection 2.3.3. In the case of the couplings c_t and c_b we observe a clear correlation in the sense that both couplings are smaller than 1 by approximately equal amounts. On the other hand, we see a clear anti-correlation between c_γ^{eff} and c_g^{eff} , which is due to the fermion KK contributions as explained above. This implies that there are no regions of parameter space where both couplings are smaller or larger than 1. Thus, a precise measurement of such values could rule out all RS scenarios considered in this thesis. The orange and red crosses denote the 1σ fit values $c_g^{\text{eff,exp}} = 1.08_{-0.13}^{+0.15}$, $c_\gamma^{\text{eff,exp}} = 1.19_{-0.12}^{+0.15}$ [264] and $c_g^{\text{eff,exp}} = 0.83_{-0.10}^{+0.11}$, $c_\gamma^{\text{eff,exp}} = 0.97_{-0.20}^{+0.17}$ [265] reported by the ATLAS and CMS Collaborations. Those fit values have a slight tendency to values larger (smaller) than 1 for both couplings in case of ATLAS (CMS), but they are compatible with the predictions within the error bars. Note that we have to be cautious when comparing the theoretical predictions with the fit values in question, because they have been obtained by varying c_g^{eff} and c_γ^{eff} so as to obtain the best fit values

c_i	W	Z	t	b
LHC 14 TeV, 300 fb ⁻¹	(-0.069, 0)	(-0.077, 0)	(-0.154, 0.147)	(-0.231, 0.041)
ILC 1 TeV, 1000 fb ⁻¹	(-0.004, 0)	(-0.006, 0)	(-0.044, 0.035)	(-0.003, 0.011)

c_i	τ	g	γ
LHC 14 TeV, 300 fb ⁻¹	(-0.093, 0.132)	(-0.078, 0.10)	(-0.096, 0.059)
ILC 1 TeV, 1000 fb ⁻¹	(-0.013, 0.017)	(-0.014, 0.014)	(-0.032, 0.035)

TABLE 5.2: Experimental sensitivities on the Higgs couplings expressed as 1σ confidence intervals calculated in [254].

to the experimental data assuming that the tree-level Higgs couplings at their SM values. It would be much preferable - and the clearest way to test any new physics model - to compare the theoretical predictions with future results from *model-independent* analyses of the Higgs couplings, which as of today have not been performed by ATLAS and CMS due to the limited statistics of the data.

Future Sensitivities on Higgs Couplings of LHC and ILC

In the last part of this subsection, we illustrate the potential for constraining relevant parameters of the RS models by a future, model-independent couplings analysis. It has been reported in [254] that the LHC operating at 14 TeV and with an integrated luminosity of 300 fb⁻¹ has the potential to probe deviations of Higgs couplings to fermions in the range of 14% – 46% and to gauge bosons in the range of 14% – 30%, both at 95% CL. At future lepton colliders like the ILC [255–258] the sensitivity to deviations can be improved by almost one order of magnitude. In the following analysis, we focus on the LHC at 14 TeV with 300 fb⁻¹ and on the ILC at 1 TeV with 1000 fb⁻¹.

The goal is to derive exclusion bounds for the first KK gluon mass $M_{g(1)}$ for each of the Higgs couplings in the custodial model. To obtain these bounds, we plot the couplings c_i as in Figure 5.3, fit a Gaussian distribution to the model points for each pair of y_\star and $M_{g(1)}$, and determine the mean values \bar{c}_i with the standard deviations σ_{c_i} . The experimental couplings are assumed to be SM-like $c_i^{\text{exp}} = 1$ with the 1σ errors given in Table 5.2. We then consider the ratio $\bar{c}_i/c_i^{\text{exp}} = \bar{c}_i$, and calculate the corresponding standard deviation by combining the theoretical and experimental errors in quadrature. Finally, we test at which confidence level \bar{c}_i is compatible with 1. The results are compiled in Figure 5.6 for two representative values of y_\star . The colored regions are the 95% CL excluded regions for the mass of the lightest KK gluon resonance. To obtain exclusion bounds for arbitrary values of y_\star , one can make use of the fact that the exclusion limits depend linearly on y_\star to good approximation. We see that the strongest bounds emerge from the loop-induced Higgs couplings, for which we distinguish between the brane-Higgs (b.) and narrow bulk-Higgs (n.b.) scenarios. The results imply for the LHC analysis that $M_{g(1)} > 21 \text{ TeV} \times (y_\star/3)$ ($M_{g(1)} > 13 \text{ TeV} \times (y_\star/3)$) in the brane (narrow bulk) Higgs scenario. For the ILC one expects to rule out KK gluons of even $M_{g(1)} > 43 \text{ TeV} \times (y_\star/3)$ in both scenarios.⁸ Note also that, independent of the realization of the Yukawa sector (and hence the parameter y_\star), the analysis of the Higgs couplings to W bosons at the ILC is expected to be sensitive to KK gluon masses of up to $M_{g(1)} \approx 15 \text{ TeV}$.

⁸The different limits in the case of the LHC are due to the asymmetric error margins for c_g , see Table 5.2.

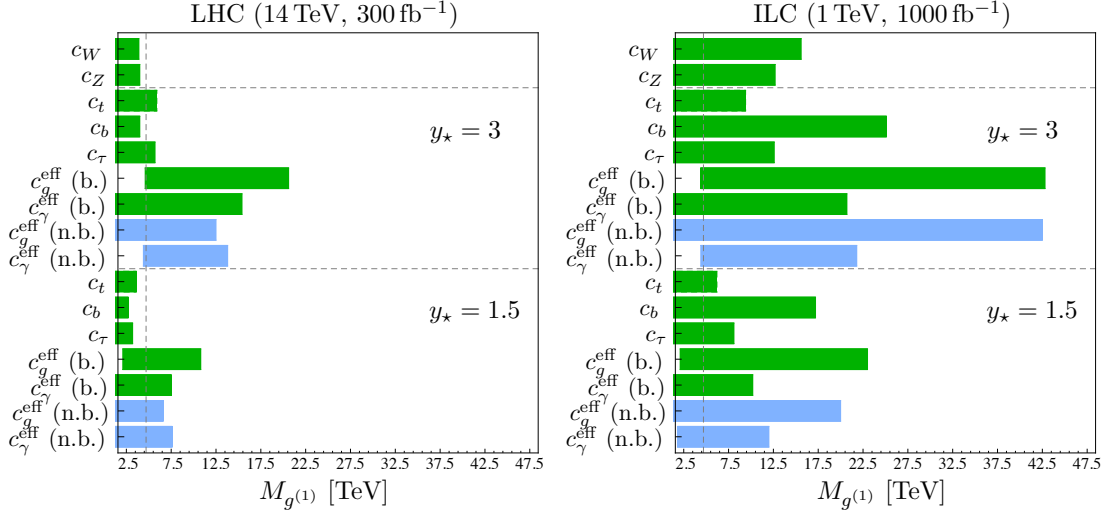


FIGURE 5.6: Summary of the exclusion limits (at 95% CL) on the mass of the first KK gluon resonance in the custodial RS model, which could be derived from SM-like measurements of the Higgs couplings at the high-luminosity LHC (left) and the ILC (right), for two representative values of y_* . For the loop-induced couplings c_g^{eff} and c_γ^{eff} we distinguish between the brane (green) and the narrow bulk-Higgs (blue) scenarios. The dashed lines show the lower bounds on $M_{g(1)}$ obtained from electroweak precision measurements.

5.1.4 Analysis of the Signal Rates: $h \rightarrow b\bar{b}$, $\tau^+\tau^-$, WW^* , ZZ^* , $\gamma\gamma$

Finally, we will investigate the Higgs decays into two b quarks, τ leptons, W or Z bosons, and photons. In order to directly compare the predictions with experimental measurements we study the signal rates R_X defined in (5.2), which can be expressed in terms of the modified couplings c_i derived in Section 5.1.2 via ($X = \tau^+\tau^-$, WW^* , ZZ^* , $\gamma\gamma$)

$$R_X \equiv \frac{(\sigma \cdot \text{BR})(pp \rightarrow h \rightarrow X)_{\text{RS}}}{(\sigma \cdot \text{BR})(pp \rightarrow h \rightarrow X)_{\text{SM}}} = \frac{[(|c_g^{\text{eff}}|^2 + |c_{g5}^{\text{eff}}|^2) f_{\text{GF}} + c_W^2 f_{\text{VBF}}] [|c_X|^2 + |c_{X5}|^2]}{c_h}. \quad (5.54)$$

The correction to the total Higgs width relative to the SM total width $\Gamma_h^{\text{SM}} = 4.14 \text{ MeV}$ [266] (for $m_h = 125.5 \text{ GeV}$) can be accounted for by the parameter

$$c_h = \frac{\Gamma_h^{\text{RS}}}{\Gamma_h^{\text{SM}}} = 0.57 |c_b|^2 + 0.22 |c_W|^2 + 0.09 (|c_g^{\text{eff}}|^2 + |c_{g5}^{\text{eff}}|^2) + 0.12, \quad (5.55)$$

where the corrections to the decays $h \rightarrow \tau^+\tau^-$, $c\bar{c}$, ZZ^* , \dots have a numerically insignificant effect and therefore can be neglected (their combined branching ratio is 12% in the SM). In (5.54) we have taken into account the probabilities to produce a Higgs via gluon fusion ($f_{\text{GF}} \approx 0.9$) or vector-boson fusion ($f_{\text{VBF}} \approx 0.1$) for inclusive decays at the LHC. Concerning the latter production process, we have implemented the findings of Section 5.1.1, showing that the significant corrections are given by c_W^2 in both cases for W - and Z -boson fusion in both the minimal (for points in the parameter space that fulfill the constraints from the electroweak precision tests) and the custodial RS model. Other Higgs production channels, such as the associated Higgs production with a $t\bar{t}$ pair or a vector boson, can be neglected to good approximation. The only exception in this work is the signal rate for $X = b\bar{b}$. In this case, Higgs-strahlung is an experimentally

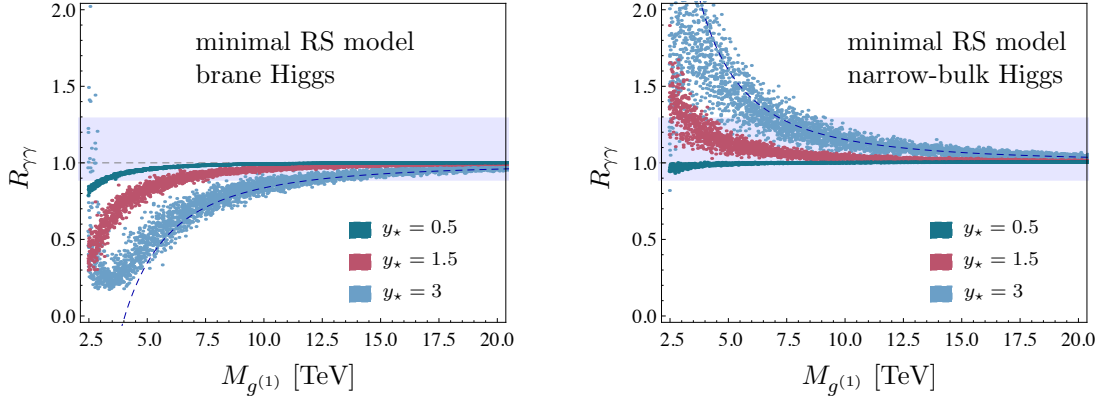


FIGURE 5.7: Predictions for the ratio $R_{\gamma\gamma}$ as a function of the lightest KK gluon mass $M_{g(1)}$ and for different values of the parameter y_* in the minimal RS model, for the cases of a brane-localized Higgs boson (left) and a narrow bulk-Higgs field (right). The dashed curves show the approximation (5.56) for $y_* = 3$.

more feasible Higgs production channel than gluon fusion, since the latter suffers from an overwhelming QCD background [267]. As we have seen in Section 5.1.1, the dominant correction to the Higgs-strahlung production process is also given by c_W^2 in both RS models. So, for the signal rate R_{bb} we just have to set $f_{GF} = 0$ and $f_{VBF} = 1$ in (5.54). Some further comment has to be given on the Higgs decays into a pair of W or Z bosons. According to the discussion of Subsection 5.1.1, we have to use the result $\Gamma(h \rightarrow VV^*)/\Gamma(h \rightarrow VV^*)_{SM}$ derived in (5.23) (instead of c_V^2) for the Higgs decays into VV^* ($V = W, Z$) with a subsequent decay of the off-shell vector boson into fermions.

Analysis of the Signal Rate $R_{\gamma\gamma}$

We start the discussion with the decay into two photons. Although the main focus is again put on the custodial RS model, it is worth presenting some of the results in the minimal model as well, in order to compare the effects in both models. Figure 5.7 shows the predictions for $R_{\gamma\gamma}$ as a function of the lightest KK gluon state $M_{g(1)}$ and for three different values for y_* obtained in the minimal RS model with a brane-localized Higgs sector (left plot) and a narrow bulk-Higgs state (right plot). The blue band represents the 1σ error band corresponding to the latest experimental values for $R_{\gamma\gamma}$ given in Table 5.3, where the naively averaged value has been used. Model points falling outside these bands are excluded at 68% CL. It is interesting to observe that for relatively large values for y_* the data already disfavor KK gluon masses in the low TeV range. The tensions between the theoretical predictions and the experimental data are stronger for the brane-Higgs model due to the mild tendency of an enhanced cross section seen in the data, which is in conflict with the suppression of the predicted cross section in this case. It shall be emphasized, however, that using the individual values for $R_{\gamma\gamma}$ reported by ATLAS and CMS one would obtain different conclusions.

The shape of the various bands of scatter points shown in the plots can be understood as follows. For not too small Yukawa couplings, the largest RS corrections are those arising from fermionic loop contributions. In the brane-localized Higgs (narrow bulk-Higgs) scenario, they suppress (enhance) the gluon-fusion cross section and enhance (suppress) the decay rate into photons. Since the dominant SM contribution to $h \rightarrow \gamma\gamma$

R_X	bb	$\tau\tau$	WW	ZZ	$\gamma\gamma$
ATLAS [264]	$0.2^{+0.7}_{-0.6}$	$1.4^{+0.5}_{-0.4}$	$1.00^{+0.32}_{-0.29}$	$1.44^{+0.40}_{-0.35}$	$1.57^{+0.33}_{-0.28}$
CMS [265]	$1.0^{+0.5}_{-0.5}$ [268]	$0.78^{+0.27}_{-0.27}$ [269]	$0.68^{+0.20}_{-0.20}$	$0.92^{+0.28}_{-0.28}$	$0.77^{+0.27}_{-0.27}$
average	$0.7^{+0.4}_{-0.4}$	$0.92^{+0.24}_{-0.22}$	$0.77^{+0.17}_{-0.16}$	$1.09^{+0.23}_{-0.22}$	$1.09^{+0.21}_{-0.19}$

TABLE 5.3: Experimental values for the signal rates measured by the ATLAS and CMS Collaborations including the 1σ errors, where the assumed Higgs masses are $m_h = 125.5$ GeV in [264], $m_h = 125.7$ GeV in [265] and $m_h = 125$ GeV in [268, 269].

involves W -boson loops and acts in the opposite direction as the fermionic contributions, the RS corrections to the Higgs production cross section dominate over those to the decay rate. Hence, we find a suppression (an enhancement) of $R_{\gamma\gamma}$ in the brane-Higgs (narrow bulk-Higgs) scenario. To see this more explicitly, we expand the various expressions in (5.54) in powers of v^2/M_{KK}^2 , exploiting the anarchy of the 5D Yukawa matrices and making the same approximations as for c_g^{eff} and c_γ^{eff} in (5.53). One then obtains

$$\begin{aligned}
R_{\gamma\gamma} \approx 1 + \frac{v^2}{2M_{\text{KK}}^2} & \left[\left(f_{\text{GF}} - \frac{4}{3|C_{1\gamma}^{\text{SM}}|} \right) \left(\mp 18 - \frac{10}{3} \right) y_\star^2 \right. \\
& - \left(f_{\text{VBF}} + \frac{21[A_W(\tau_W) - 1]}{4|C_{1\gamma}^{\text{SM}}|} \right) \frac{2m_W^2}{v^2} \left(L - 1 + \frac{1}{2L} \right) \\
& \left. - \frac{Lm_W^2}{v^2} + 0.57 \frac{10}{3} y_\star^2 + 0.22 \frac{2m_W^2}{v^2} \left(L - 1 + \frac{1}{2L} \right) - 0.09 \left(\mp 18 - \frac{10}{3} \right) y_\star^2 \right], \quad (5.56)
\end{aligned}$$

where the first two lines contain the corrections to the production and decay rates, with corrections to the $h \rightarrow \gamma\gamma$ rate being accompanied by a factor of $1/|C_{1\gamma}^{\text{SM}}|$. The third line shows the corrections to the Higgs vev and total width, as parameterized by c_h in (5.55). The upper sign holds for the brane-localized Higgs scenario, while the lower sign corresponds to the narrow bulk-Higgs case. We explicitly see from the first term on the right-hand side of (5.56) that the fermionic contributions to the $gg \rightarrow h$ production process dominate over those to the $h \rightarrow \gamma\gamma$ decay rate and come with opposite sign. Evaluating all terms in (5.56) yields

$$R_{\gamma\gamma} \approx 1 - \frac{v^2}{2M_{\text{KK}}^2} [(\pm 9.7 - 0.1) y_\star^2 + 4.1]. \quad (5.57)$$

For the case where $y_\star = 3$ this result is shown by the dashed lines in the figure. Note that due to the contribution of the production process via vector-boson fusion the observable $R_{\gamma\gamma}$ is bounded from below in the brane-Higgs case. This explains the behavior for very small KK scales seen in the left plot in Figure 5.7. For $y_\star = 3$, the $gg \rightarrow h$ production cross section vanishes for $M_{g(1)} \approx 3.5$ TeV, because the new-physics contribution cancels the SM amplitude. However, due to the vector-boson fusion production process a non-zero value of $R_{\gamma\gamma}$ remains.

Even at the present level of precision, the existing measurements of the observable $R_{\gamma\gamma}$ already provide some interesting constraints on the parameter space of the RS models under consideration. Figure 5.8 shows the regions in the $M_{g(1)} - y_\star$ parameter space that are excluded by the current data at various confidence levels. For instance, for the particular choice $y_\star = 3$ one finds $M_{g(1)} > 8.5$ TeV at 95% CL for the brane-Higgs model

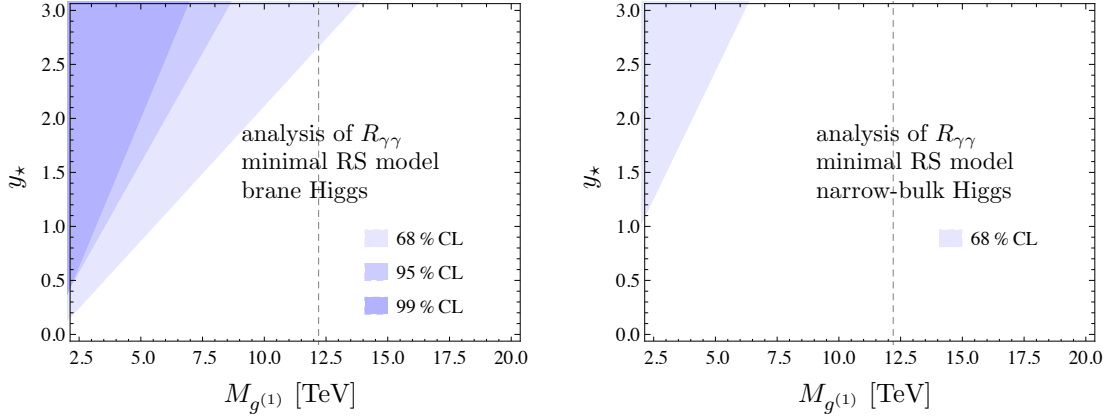


FIGURE 5.8: Excluded regions of parameter space derived from the analysis of $R_{\gamma\gamma}$ in the minimal RS model, for the brane-localized Higgs scenario (left) and the narrow bulk-Higgs model (right). The vertical dashed line denotes the lower bound on $M_{g(1)}$ obtained from a tree-level analysis of electroweak precision observables.

and $M_{g(1)} > 6.4$ TeV at 68% CL for the narrow bulk-Higgs model. Weaker constraints are obtained for smaller values for y_* . These bounds can be compared with the bound from electroweak precision measurements, indicated by the vertical dashed line in the figure. We see that, at present, this bound is still stronger than the constraints derived from $R_{\gamma\gamma}$.

Softening the constraints from electroweak precision observables by means of a symmetry has been the main motivation for custodial RS model whose effects on the quantity $R_{\gamma\gamma}$ are studied in Figure 5.9. In analogy with (5.56), it is possible to derive an approximate formula. For the model with the minimal lepton sector shown in (4.96), one finds

$$\begin{aligned}
 R_{\gamma\gamma} \approx 1 + \frac{v^2}{2M_{\text{KK}}^2} & \left[\mp \left(72f_{\text{GF}} - \frac{213}{|C_{1\gamma}^{\text{SM}}|} \right) y_*^2 - \frac{20}{3} \left(f_{\text{GF}} - \frac{4}{3|C_{1\gamma}^{\text{SM}}|} \right) y_*^2 \right. \\
 & - \left(f_{\text{VBF}} + \frac{21[A_W(\tau_W) - 1]}{4|C_{1\gamma}^{\text{SM}}|} \right) \frac{2m_W^2}{v^2} \left(2L - 1 + \frac{1}{2L} \right) - \frac{2Lm_W^2}{v^2} \\
 & \left. + 0.57 \frac{20}{3} y_*^2 + 0.22 \frac{2m_W^2}{v^2} \left(2L - 1 + \frac{1}{2L} \right) - 0.09 \left(\mp 72 - \frac{20}{3} \right) y_*^2 \right]. \quad (5.58)
 \end{aligned}$$

If instead the extended lepton sector shown in (4.94) is employed, then the coefficient 213 inside the parenthesis in the first term must be replaced by 240. Note that the individual corrections due to fermion loops are huge, however significant cancellations take place when one adds the corrections to the $gg \rightarrow h$ and $h \rightarrow \gamma\gamma$ rates. Altogether, one obtains for the model with the minimal lepton sector

$$R_{\gamma\gamma} \approx 1 - \frac{v^2}{2M_{\text{KK}}^2} [(\pm 15.0 - 0.2) y_*^2 + 8.3]. \quad (5.59)$$

In the model with the extended lepton sector the coefficient ± 15.0 in the first term must be replaced by ± 9.5 . Observe that in linearized form the corrections are only moderately larger than in the minimal model, see (5.57). Once again, for $y_* = 3$ this result is shown by the dashed lines in the figure, where we show results for the custodial model with

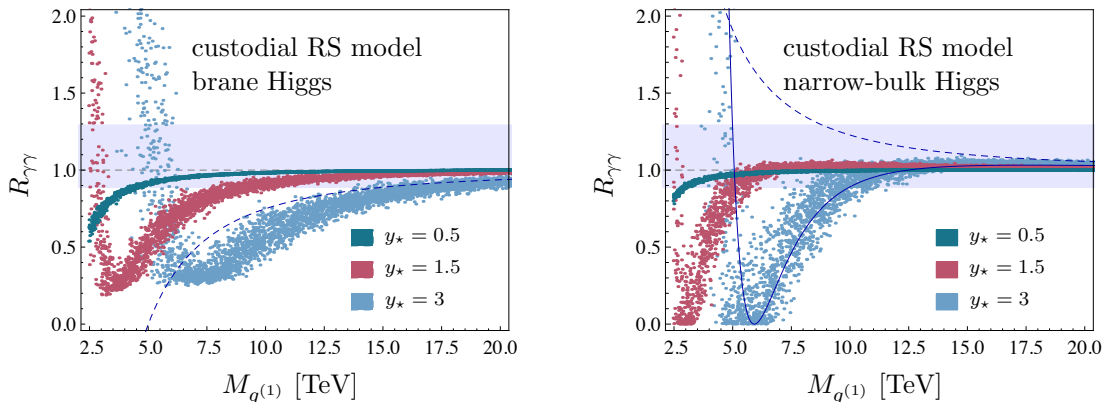


FIGURE 5.9: Predictions for the ratio $R_{\gamma\gamma}$ as a function of the KK gluon mass $M_{g(1)}$ in the custodial RS model with minimal lepton sector (4.96), for the cases of a brane-localized Higgs boson (left) and a narrow bulk-Higgs field (right). See text for details.

the minimal lepton sector. If instead the model with an extended lepton sector is considered, the distribution of scatter points looks very similar. For the brane-localized Higgs scenario, Figure 5.9 shows a similar behavior as in the minimal model, but the new-physics effects are slightly larger. For $y_* = 1.5$ and 3, the $gg \rightarrow h$ production cross section vanishes near $M_{g(1)} \approx 3.5$ TeV and 7 TeV, respectively, and the vector-boson fusion process remains as the only production mechanism. This explains the minimum values for $R_{\gamma\gamma}$ at these points. For even smaller masses the ratio $R_{\gamma\gamma}$ increases and can even exceed 1. In the narrow bulk-Higgs case, on the other hand, the linearized approximation (5.58) breaks down for large values y_* , as is evident from the discrepancy between the dashed curve and the blue band of scatter points. A reasonable approximation, shown by the solid line, is obtained by linearizing the expressions for the various c_i parameters but not further expanding expression (5.54). It turns out that the negative corrections to the $h \rightarrow \gamma\gamma$ decay rate are so significant in this model that they compensate the large positive corrections to the gluon-fusion rate in the region of large $M_{g(1)}$. For smaller KK masses, these negative corrections become dominant and drive the ratio $R_{\gamma\gamma}$ toward values significantly less than 1. Eventually, for $M_{g(1)} \approx 3$ TeV (for $y_* = 1.5$) and 5.5 TeV (for $y_* = 3$), the di-photon decay rate even vanishes. It is obvious that in regions of parameter space where such dramatic cancellations occur the RS predictions are highly model dependent. Given the preliminary pattern of Higgs couplings seen in experiment, which within errors agree with the SM predictions, it appears unlikely (but not impossible) that there could be $\mathcal{O}(1)$ corrections to the $gg \rightarrow h$ and $h \rightarrow \gamma\gamma$ production and decay rates, which cancel each other in the result for the observable $R_{\gamma\gamma}$.

Figure 5.10 shows the excluded regions of RS parameter space derived from the analysis of the observable $R_{\gamma\gamma}$ in the custodial RS model. In the scenario with a brane-localized Higgs sector, one can exclude the ranges $6.0 \text{ TeV} < M_{g(1)} < 13.4 \text{ TeV}$ and $M_{g(1)} < 3.5 \text{ TeV}$ for $y_* = 3$, while in the narrow bulk-Higgs model the exclusion range reads $5.1 \text{ TeV} < M_{g(1)} < 8.4 \text{ TeV}$, both at 95% CL. Note that there is a small region in the upper left corner (at small $M_{g(1)}$ and large y_*) of the left plot, which is allowed by both $R_{\gamma\gamma}$ and the S parameter constraint (2.189). On the other hand, these plots allow one to impose bounds on y_* if one wants to have the first KK gluon resonance to be in reach for direct production at the LHC. For instance, in the minimal RS model with a hypothetical KK gluon mass $M_{g(1)} = 5$ TeV, the results imply an upper bound of

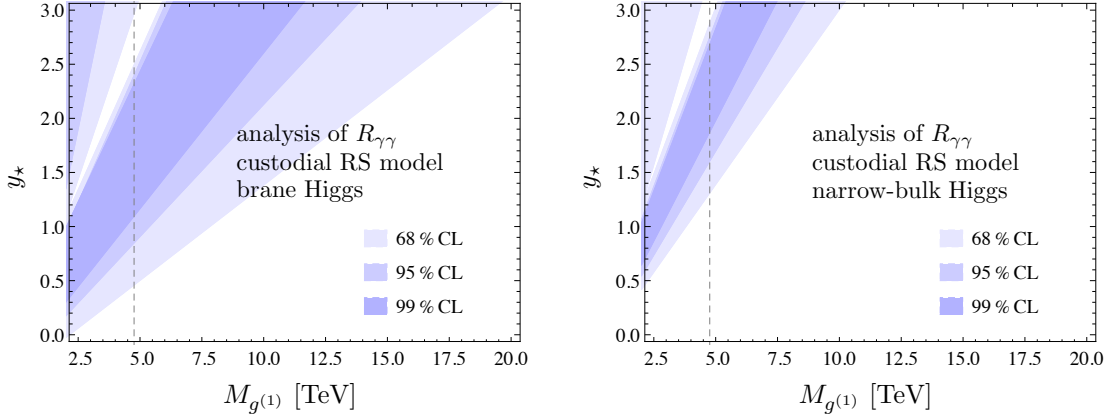


FIGURE 5.10: Excluded regions of parameter space derived from the analysis of $R_{\gamma\gamma}$ in the custodial RS model with minimal lepton sector (4.96), for the brane-localized Higgs scenario (left) and the narrow bulk-Higgs model (right). The vertical dashed line denotes the bound obtained from a tree-level analysis of electroweak precision observables.

$y_* < 1.5$ at 95% CL in the brane-Higgs model, and $y_* < 2.4$ at 68% CL in the narrow bulk-Higgs scenario. In the custodial RS model, those bounds are tightened to $y_* < 0.9$ for a brane Higgs and $y_* < 1.7$ for a narrow bulk Higgs, both at 95% CL.

Analysis of the Signal Rates R_{ZZ} and R_{WW}

The next analysis focuses on the Higgs decay into a pair of electroweak gauge bosons. The previous analysis has shown that in the minimal (custodial) RS model the bounds derived from Higgs physics are weaker (stronger) than those from electroweak precision tests. It turns out that this is not only true for $R_{\gamma\gamma}$, but also for all other signal rates (except for R_{bb}). In the following analyses, we will therefore restrict ourselves on the RS model with custodial protection.

The upper row of Figure 5.11 shows the results for the ratio R_{ZZ} in the custodial RS model for the scenarios with a brane-localized Higgs boson (left plot) and a narrow bulk-Higgs field (right plot), in dependence of $M_{g(1)}$. The scatter points also represent the results for the observable R_{WW} , since at the level of the L -enhanced terms the Higgs decays into a pair of W and Z bosons are expressed by the same modification factor $c_W^2 \approx c_Z^2$, see (5.23) and (5.37).⁹ The effects are stronger than in the case of $R_{\gamma\gamma}$, since in the present case there is no compensation between the production via gluon fusion and the decay into two electroweak gauge bosons. Recall that the loop-induced decay into photons is highly affected by the infinite tower of KK fermions, whose effect works in the opposite direction with respect to the modifications to the gluon fusion, whereas the tree-level Higgs couplings to massive vector bosons only receive moderate corrections. Correspondingly, we obtain larger exclusion regions than derived via $R_{\gamma\gamma}$. This is shown in the lower two rows of Figure 5.11. In the brane-Higgs scenario, we obtain the exclusion range $4.6 \text{ TeV} < M_{g(1)} < 19.9 \text{ TeV}$ (from the analysis of R_{ZZ}) and $5.0 \text{ TeV} < M_{g(1)} < 13.0 \text{ TeV}$ (from R_{WW}) for $y_* = 3$, while in the narrow bulk-Higgs

⁹We only show the experimental error band of the observable R_{ZZ} and refrain from including the corresponding error band of R_{WW} for the sake of clarity.

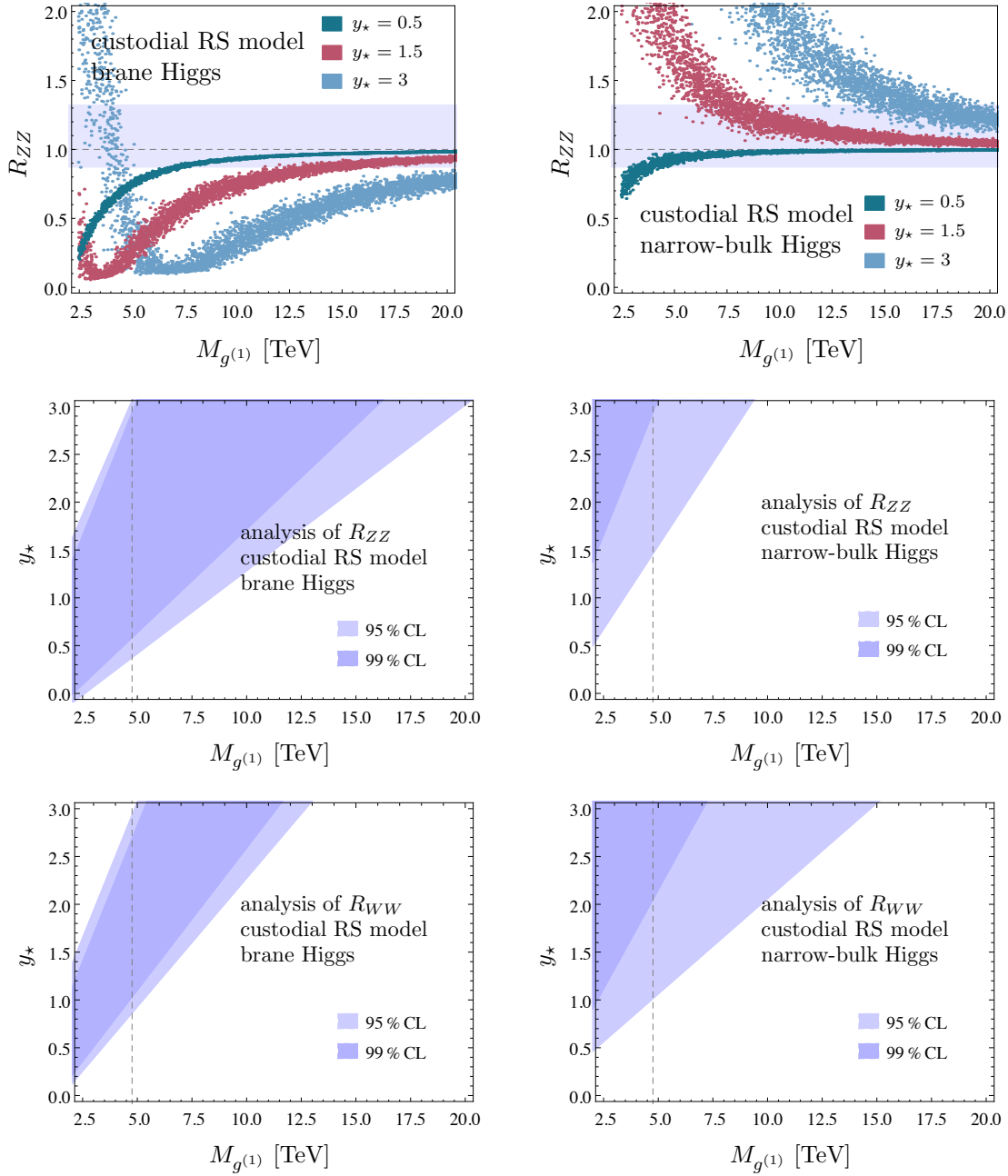


FIGURE 5.11: Predictions for the ratio R_{ZZ} (and R_{WW}) (upper row) and excluded regions of parameter space in the custodial RS model derived from the analysis of R_{ZZ} (middle row) and R_{WW} (lower row), for the cases of a brane-localized Higgs boson (left) and a narrow bulk-Higgs field (right). The meaning of the colors and lines is the same as in Figures 5.7 and 5.8. See text for details.

model we find the lower bounds $M_{g(1)} > 9.1$ TeV (from R_{ZZ}) and $M_{g(1)} > 14.9$ TeV (from R_{WW}), both at 95% CL. Note that the allowed region in the upper left corner (at small $M_{g(1)}$ and large y_*) of the first plot in the middle row is one in which the new-physics contribution to the gluon fusion amplitude is larger than the SM contribution by about a factor 2 and interferes destructively, which appears somewhat unnatural. Moreover, it has been argued that most models in which the gluon fusion amplitude has the opposite sign than in the SM have problems with fine-tuning and vacuum stability [270].

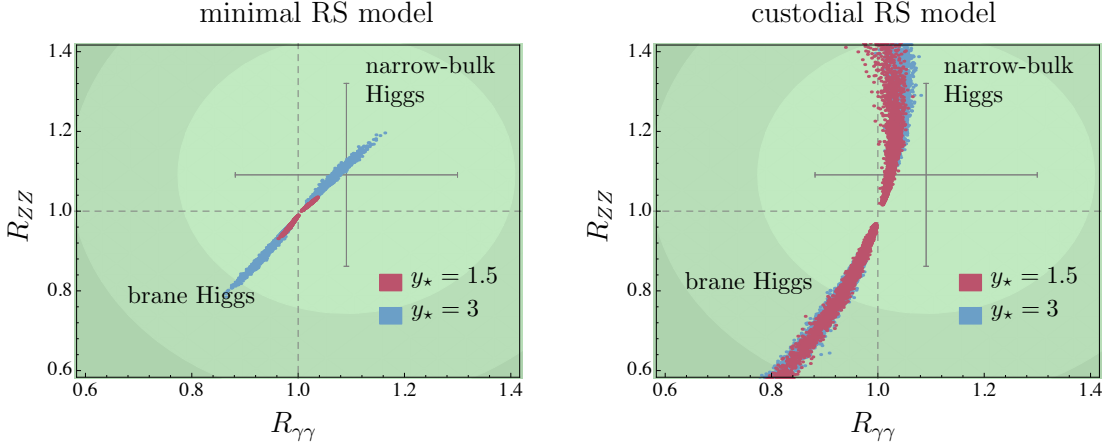


FIGURE 5.12: Predictions for the signal rates R_{ZZ} and $R_{\gamma\gamma}$ in the minimal (left) and custodial (right) RS model for the cases of a brane-localized Higgs boson and a narrow bulk-Higgs field. All scatter points fulfill the constraints from electroweak precision tests. The black dashed lines denote the SM predictions. The cross shows the experimental 1σ -errors for the signal rates measured.

Comparing the bounds shown in Figure 5.11 with those derived from the analysis of the observable $R_{\gamma\gamma}$, we observe that the small region in the upper left corner of the left plot in Figure 5.10 can be excluded by the current measurement of the observable R_{ZZ} . Furthermore, the strongest bounds on the parameter space of the narrow bulk-Higgs scenario are those coming from the analysis of R_{WW} . The constraints implied by Higgs physics are also much stronger than those derived from the analysis of electroweak precision observables indicated by the dashed line in the lower row of Figure 5.11. Again, the bounds on $M_{g(1)}$ can be attenuated for regions in parameter space where y_* is very small. For example, if one would like to have a KK gluon mass of $M_{g(1)} = 5$ TeV, the bounds on the parameter y_* are $y_* < 0.4$ (R_{ZZ}) and $y_* < 0.9$ (R_{WW}) in the brane-Higgs model, and $y_* < 1.5$ (R_{ZZ}) and $y_* < 1.1$ (R_{WW}) in the narrow bulk-Higgs scenario (both at 95% CL).

Correlation between R_{ZZ} and $R_{\gamma\gamma}$

We now continue the discussion in Subsection 5.1.3 between the two loop-induced Higgs couplings to photons and gluons, but now at the level of the corresponding signal rates. Figure 5.12 shows the predictions in the $R_{ZZ} - R_{\gamma\gamma}$ plane in the minimal (left plot) and custodial RS model (right plot) for the brane-localized and narrow bulk-Higgs scenarios. The SM predicts the values $R_{ZZ,\gamma\gamma}^{\text{SM}} = 1$ denoted by the black dashed lines. Scatter points below the horizontal dashed line belong to the brane-localized Higgs scenario, while the points above the line belong to the narrow bulk-Higgs scenario.¹⁰ All scatter points fulfill the bounds imposed by the measurements of the oblique parameters S and T . The cross shows the experimental values given in Table 5.3, while the green ellipses present the 68%, 95%, and 99% confidence regions of the combined measurements. In the case of the minimal RS model, we observe a strong linear correlation between R_{ZZ} and $R_{\gamma\gamma}$. This can be traced back to the fact that both signal rates are dominated by

¹⁰We only show the points for $y_* = 1.5$ and 3 here. For the choice $y_* = 0.5$, both R_{ZZ} and $R_{\gamma\gamma}$ are reduced in both scenarios, see Figures 5.9 and 5.11.

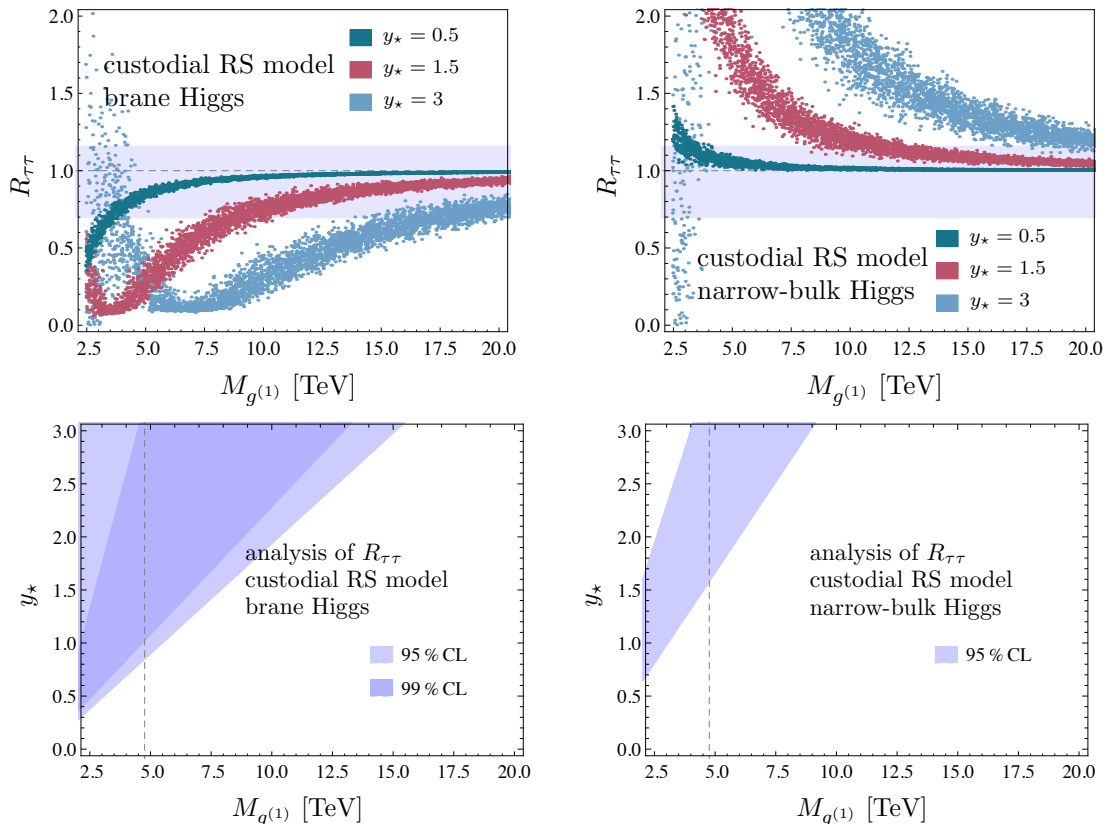


FIGURE 5.13: Predictions for $R_{\tau\tau}$ as a function of the KK gluon mass $M_{g^{(1)}}$ (upper row) and the derived excluded regions of the parameter space (lower row) in the custodial RS model, for the cases of a brane-localized Higgs boson (left) and a narrow bulk-Higgs field (right).

the Higgs production process of gluon fusion, while the decay only receives moderate corrections. It is also noteworthy that the parameter space is strongly constrained by the requirement to pass the electroweak precision measurements. In the custodial RS model the corrections to the signal rates can be much larger, due to the enlarged fermion content of the model and due to the reduced bound on M_{KK} from electroweak precision tests. We can also see a correlation between both signal rates, but it is not as marked as in the minimal RS model. This is due to the fact that the KK excitations for the Higgs decay process $h \rightarrow \gamma\gamma$ are enhanced by the factor $\sim 71/8 \approx 8.9$ compared to the minimal RS model, while the ones for the gluon-fusion process $gg \rightarrow h$ are only enhanced by the factor 4. As explained in Section 5.1.3 both couplings are working in opposite directions, from which it follows that the shape of the scatter points in the right plot is characterized by a larger slope. Notice that in both RS models, current experimental data slightly favor the narrow bulk-Higgs over the brane-localized Higgs scenario.

Analysis of the Signal Rates $R_{\tau\tau}$ and R_{bb}

Finally, we touch on the predictions for $R_{\tau\tau}$ and R_{bb} in the custodial RS model. The observable $R_{\tau\tau}$ is shown as a function of $M_{g^{(1)}}$ in the upper row of Figure 5.13. As in the previous cases, the shape of the curves for KK gluon masses larger than 5 TeV

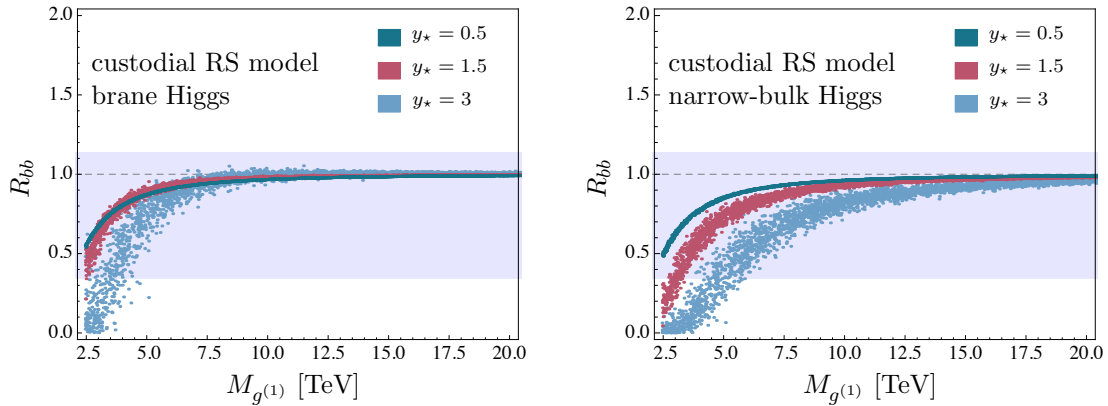


FIGURE 5.14: Predictions for R_{bb} as a function of the KK gluon mass $M_{g(1)}$ in the custodial RS model, for the cases of a brane-localized Higgs boson (left) and a narrow bulk-Higgs field (right).

are due to the Higgs-boson production process, which is dominated by the gluon-fusion production channel. Particularly for small KK scales, these effects are quite large and have the potential to compensate and even exceed the SM contribution, so that only the vector-boson fusion production channel contributes. This can be clearly seen in the brane-localized Higgs case, where the observable $R_{\tau\tau}$ is bounded from below due to finite fraction of the vector-boson fusion in the production process. For very small KK scales ($M_{g(1)} \lesssim 3$ TeV), on the other hand, it can even drop to zero. This can be traced back to the vanishing $h\tau\tau$ couplings, see Figure 5.3 and the discussion that follows.

The lower row of Figure 5.13 shows the regions in the $M_{g(1)} - y_*$ parameter space that are excluded by the current LHC data. We see that in both versions of the custodial RS model portions of the model parameter space can be excluded. Assuming the conventional choice $y_* = 3$, for example, one finds $M_{g(1)} \geq 15.1$ TeV for the brane-Higgs and $M_{g(1)} \geq 8.9$ TeV or $M_{g(1)} \leq 4.0$ TeV for the narrow bulk-Higgs model, both at 95% CL. Weaker constraints are obtained for smaller values for y_* . For instance, a mass of $M_{g(1)} = 5$ TeV leads to an upper bound of $y_* < 0.9$ ($y_* < 1.6$) in the brane-Higgs (narrow bulk-Higgs) scenario. For larger values the bounds from $h \rightarrow \tau^+\tau^-$ are stronger than those from electroweak precision observables, indicated in the lower row of Figure 5.13 by the vertical line. However, they cannot compete with the bounds coming from the latest measurements of R_{ZZ} and R_{WW} , respectively.

Compared to the remaining ratios, the observable R_{bb} only suffers from moderate effects in the RS model, since it only includes the minor affected production process via Higgs-strahlung. This is shown in Figure 5.14. Although there is no need to distinguish between the brane-localized and narrow bulk-Higgs scenario in the Higgs production cross section and the decay width, the plots differ due to the effect of $h \rightarrow gg$ in the modified Higgs width. This modification leads to suppression which is larger in the narrow bulk-Higgs scenario, which can be understood with the help of Figure 5.16, discussed below. Note that it is refrained from showing the exclusion plots derived from the analysis of R_{bb} , since the current experimental accuracy is worse than for the remaining channels, as can be seen in Table 5.3.

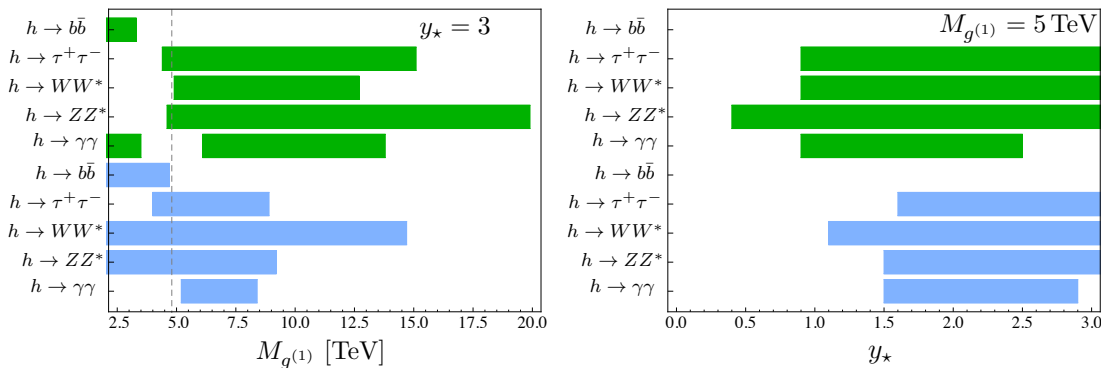


FIGURE 5.15: Summary of the bounds on the mass of the lightest KK gluon (left) and the parameter y_* (right) obtained from the exclusion plots in the custodial RS model for the brane-localized (green) and narrow bulk-Higgs scenario (blue). The shaded regions are excluded at 95% CL for each corresponding decay channel. We have assumed $y_* = 3$ ($M_{g^{(1)}} = 5 \text{ TeV}$) in the left (right) plot. The dashed line shows the bound obtained from a tree-level analysis of electroweak precision observables.

Summary of Exclusion Bounds for $M_{g^{(1)}}$ and y_*

In the last part of this section, we summarize the current LHC bounds on the relevant parameter space of the custodial RS model obtained from all relevant Higgs decays at 95% CL. The derived exclusion limits on the mass of the lightest KK gluon are shown in the left plot of Figure 5.15. The green (blue) bars stand for the brane-localized (narrow bulk-Higgs) scenario. The most stringent bounds emerge from the decays into ZZ^* and WW^* . The former yields tighter constraints in the brane-localized Higgs scenario and the latter in the narrow bulk-Higgs scenario. This is due to the fact that the mild tendency of the enhanced (suppressed) signal rate seen in the data is in conflict with the suppression (enhancement) predicted in the case of $pp \rightarrow h \rightarrow ZZ^*$ ($pp \rightarrow h \rightarrow WW^*$).

Taking the most stringent bounds from Figure 5.15, we see that the bounds on the mass of the first KK excitation of the gluon from Higgs physics read

$$M_{g^{(1)}} \Big|_{\text{brane Higgs}}^{\text{custodial RS}} \geq 19.9 \text{ TeV} \quad \text{and} \quad M_{g^{(1)}} \Big|_{\text{narrow bulk Higgs}}^{\text{custodial RS}} \geq 14.9 \text{ TeV}. \quad (5.60)$$

It shall be stressed that, since the bounds in (5.60) are much stronger than those stemming from electroweak precision measurements, there is not much gained by custodial protection. While it can protect tree-level effects in RS models, it suffers from generically too large contributions to loop-induced processes. This observation has also been made in loop-induced flavor processes like $b \rightarrow s\gamma$ [245], see subsequent section. However, we will see that the effects found there are less pronounced.

A possible way out, aside from gauge-Higgs unification models [100, 117], where the Higgs is the fifth component of a 5D gauge field, is to lower the maximum allowed value of the 5D Yukawa elements y_* . The right plot of Figure 5.15 summarizes the upper bounds on y_* , where a KK gluon mass of $M_{g^{(1)}} = 5 \text{ TeV}$ has been assumed. Moreover, the analysis has been restricted to values for y_* below the perturbativity bound $y_* \leq y_{\text{max}} \equiv 3$. Again, the most stringent bounds come from the processes $h \rightarrow ZZ^*$ and $h \rightarrow WW^*$ and can be combined to give the constraints

$$y_* \Big|_{\text{brane Higgs}}^{\text{custodial RS}} < 0.4 \quad \text{and} \quad y_* \Big|_{\text{narrow bulk Higgs}}^{\text{custodial RS}} < 1.1. \quad (5.61)$$

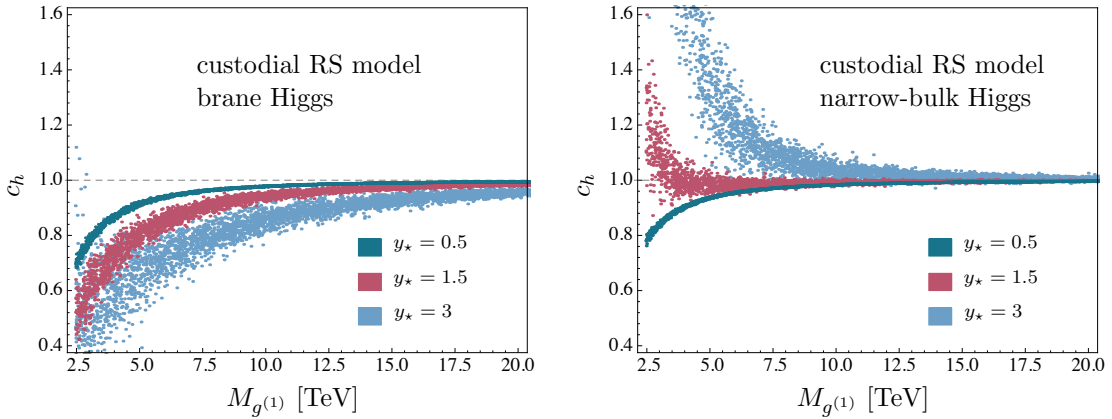


FIGURE 5.16: Predictions for $c_h = \Gamma_h^{\text{RS}}/\Gamma_h^{\text{SM}}$ as a function of $M_{g(1)}$ in the custodial RS model, for the cases of a brane-localized (left) and a narrow bulk-Higgs field (right).

We see that in particular in the brane-Higgs scenario small values are preferred. However, too small Yukawa couplings would give rise to enhanced corrections to ϵ_K [180] and hence they would reinforce the RS flavor problem.

The above analysis has shown that Higgs physics provides sensitive probes of the virtual KK excitations in the context of various RS models. In particular the Higgs decays into two massive gauge bosons, which are dominated by the Higgs-boson production rate in gluon-fusion, could be used to either explain possible deviations in the corresponding cross sections or to derive strong bounds on the RS parameter space. These bounds are complementary to and sometimes stronger than those from electroweak precision observables and rare flavor-changing processes. In the custodial RS model, the indirect effect of KK states on the Higgs processes are strongly enhanced compared with the minimal model, and hence the current experimental Higgs-physics results provide the strongest constraints in this case. The strongest bounds emerge from $h \rightarrow ZZ^*$ in the brane-localized Higgs, and $h \rightarrow WW^*$ in the narrow bulk-Higgs scenario. Even under the pessimistic assumption that the direct detection of KK excitations is out of reach at the LHC, one may still see sizable modifications of the $pp \rightarrow h \rightarrow \tau^+\tau^-, WW^*, ZZ^*, \gamma\gamma$ cross sections. For example, even for $M_{g(1)} = 10$ TeV or 15 TeV, significant deviations from the SM predicted value $R_{\tau\tau, WW, ZZ} = 1$ are still possible. For $R_{\gamma\gamma}$ the effects are less strong, since a reduction (enhancement) in the Higgs production cross section is partially compensated by an enhancement (reduction) in the $h \rightarrow \gamma\gamma$ decay rate.

It is noteworthy that, while the signal rate R_{bb} only implies very weak bounds for the RS parameter space, the Higgs coupling to bottom quarks c_b is important, since it is one of the significant corrections to the Higgs width (5.55), that enters all of the signal rates. Figure 5.16 shows the total Higgs width normalized to the SM value $c_h = \Gamma_h^{\text{RS}}/\Gamma_h^{\text{SM}}$, defined in (5.55), in the custodial RS model, including the corrections from the Higgs decays $h \rightarrow b\bar{b}, WW^*, gg$. We see that in the brane-Higgs scenario the Higgs width can be reduced by $\sim 30\%$ (15%) for a KK gluon mass $M_{g(1)} \approx 5$ TeV (10 TeV) and maximal Yukawa value $y_* = 3$. The dominant correction comes from the decay into two bottom quarks, which leads to an enhancement of all branching ratios. This differs from the case of the narrow bulk-Higgs scenario, where a large contribution comes from the Higgs decaying into two gluons, which enhances the Higgs width and counteracts the suppression through c_b . This effect dominates for $y_* \gtrsim 1.5$ leading to a Higgs width larger than in the SM and consequentially reducing all branching ratios.

5.2 $\bar{B} \rightarrow X_s \gamma$ Decays in Warped Extra Dimensions

In the last section of the main part of this thesis, we will investigate the phenomenological implications of the RS contributions derived in Section 4.3 on the following physical observables most directly related to the parton-level transition $b \rightarrow s\gamma$: the branching ratio (BR) $\text{Br}(\bar{B} \rightarrow X_s \gamma)$, the time-dependent CP asymmetry $S_{K^* \gamma}$ in the decay $\bar{B} \rightarrow \bar{K}^* \gamma$, and the photon polarization parameter λ_γ , measured via the angular distribution in the $\bar{B} \rightarrow \bar{K}_1(\bar{K} \rightarrow \pi\pi)\gamma$ decay. Recall that especially the chirality-flipped Wilson coefficients can receive large corrections and are expected to give rise to significant deviations from the SM prediction.¹¹ So the latter observables are particularly viable to look for RS effects. While CP asymmetries were discussed in previous works [176, 177, 245], this section will moreover add a discussion of the photon polarization parameter λ_γ , which have gained importance after it has been clarified how it is experimentally accessible. Note also that the Wilson coefficients related to the $b \rightarrow s\gamma$ transition affect observables associated with the semi-leptonic decay $\bar{B} \rightarrow X_s \mu \bar{\mu}$ [272, 273], which will, however, not be discussed here. A discussion of this process in the RS model can be found in [245].

5.2.1 The Branching Ratio $\bar{B} \rightarrow X_s \gamma$

We begin with the branching ratio of the inclusive decay $\bar{B} \rightarrow X_s \gamma$. The current experimental value reads [274, 275]

$$\text{Br}(\bar{B} \rightarrow X_s \gamma) = (3.43 \pm 0.22) \times 10^{-4},$$

while the SM prediction at NNLO is [250, 276]

$$\text{Br}(\bar{B} \rightarrow X_s \gamma) = (3.15 \pm 0.23) \times 10^{-4}.$$

Since these two values agree very nicely at the moment, the measured branching ratio will be used as a constraint on the parameter sets of the RS model. For this, we simply require the RS corrections to fulfill the constraint

$$\Delta \text{Br}(\bar{B} \rightarrow X_s \gamma) = \text{Br}(\bar{B} \rightarrow X_s \gamma)_{\text{exp}} - \text{Br}(\bar{B} \rightarrow X_s \gamma)_{\text{SM}} = (0.28 \pm 0.64) \cdot 10^{-4}, \quad (5.62)$$

which represents the 2σ ranges when combining experimental and theoretical uncertainties in quadrature. The effect of the RS model can be estimated with the help of the formula of [245]

$$\text{Br}(\bar{B} \rightarrow X_s \gamma) = \text{Br}(\bar{B} \rightarrow X_s \gamma)_{\text{SM}} + 0.00247 \left[|C_{7\gamma}^{\text{RS}}|^2 + |\tilde{C}_{7\gamma}^{\text{RS}}|^2 - 0.706 \text{Re}(C_{7\gamma}^{\text{RS}}) \right], \quad (5.63)$$

where the RS corrections are evaluated at μ_b and all known SM non-perturbative contributions are taken into account. The RS corrections are included only at LO neglecting uncertainties which is accurate enough to estimate the possible RS effects. Note that a positive RS correction to $\text{Br}(\bar{B} \rightarrow X_s \gamma)_{\text{SM}}$ is favorable to get a theoretical value which is closer to the data. With the help of (4.147), (4.148), and (4.149) we derive the branching ratio in the minimal RS model, which is depicted in Figure 5.17 as a function of the

¹¹See [271] for a review of possible measurements of $\tilde{C}_{7\gamma}$.

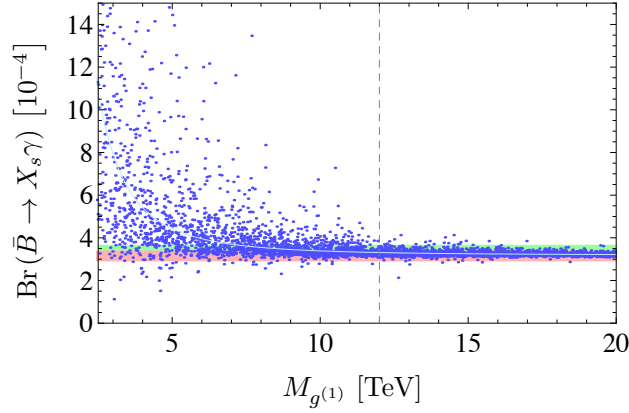


FIGURE 5.17: Branching ratio of the decay $\bar{B} \rightarrow X_s \gamma$ depending on the mass of the first KK gluon $M_{g(1)}$ in the minimal RS model. The light blue line denotes a fit function of the parameter points, while the green (red) band shows the experimental value (SM prediction). The vertical dashed line denotes the T parameter bound.

mass of the lightest KK gluon resonance.¹² The green (red) band shows the current experimental value (SM prediction) including the corresponding error margin, while the blue points represent possible RS scenarios. The light blue line denotes a fit function of the parameter points. As in the previous section, 5000 parameter sets are generated, where the Yukawa matrices and bulk mass parameters correctly reproduce the SM quark masses and Wolfenstein parameters. In order to obtain the maximally possible RS effects, the upper bound $|(\mathbf{Y}_q)_{ij}| \leq y_\star = 3$ has been imposed. We see that for large values of the first KK gluon mass the parameter points are centered around the SM value due to the decoupling of the RS effects, whereas a large enhancement is observed for small KK scales. This has been expected due to the contribution of the chirality-flipped operators. Note, however, that the majority of parameter points lies within the experimental error band and obeys the BR constraint (5.62), in particular those points which obey the T parameter constraint $M_{g(1)} > 12$ TeV indicated by the vertical dashed line.

5.2.2 The Time-Dependent CP Asymmetry in $\bar{B} \rightarrow \bar{K}^* \gamma$

Due to the fact that the RS model induces large CP violating phases, it is of great interest to study CP asymmetries in B decays based on the $b \rightarrow s \gamma$ transition. One possible observable is the direct CP asymmetry in the inclusive decay $\bar{B} \rightarrow X_s \gamma$ [275], which in principle is highly sensitive to NP contributions [277]. In practice, however, the perturbative SM prediction is spoiled by large non-perturbative long-distance effects leaving not much room for new physics [278]. Therefore, a theoretically more clean observable will be considered, namely the time-dependent CP asymmetry in the exclusive decay $\bar{B} \rightarrow \bar{K}^* \gamma$. As opposed to the corresponding branching ratio, this CP asymmetry does not depend on the theoretical uncertainty of the $\bar{B} \rightarrow \bar{K}^*$ form factors [279–281]. It is defined by

$$\frac{\Gamma(\bar{B}^0 \rightarrow \bar{K}^{*0} \gamma) - \Gamma(B^0 \rightarrow K^{*0} \gamma)}{\Gamma(\bar{B}^0 \rightarrow \bar{K}^{*0} \gamma) + \Gamma(B^0 \rightarrow K^{*0} \gamma)} = S_{K^* \gamma} \sin(\Delta M_d t) - C_{K^* \gamma} \cos(\Delta M_d t), \quad (5.64)$$

¹²Note that we mix the NLO SM values with the LO RS corrections which is actually somewhat inconsistent. However, for our goal, i.e. the estimation of the possible effects of the RS model, it is justified to use the above relation.

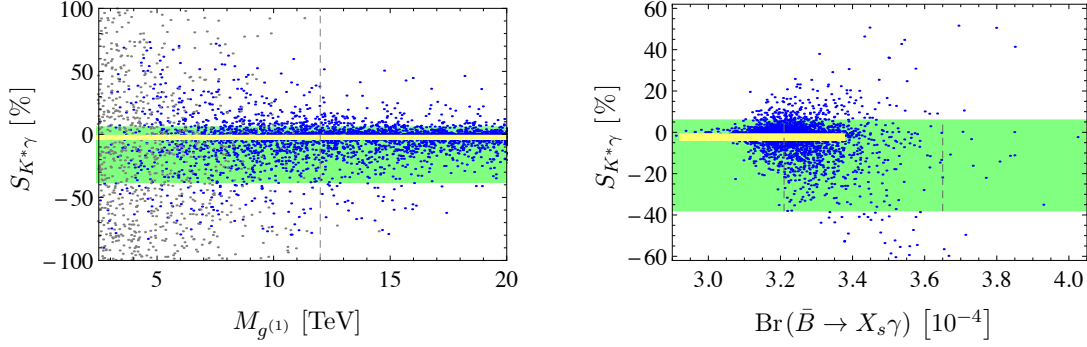


FIGURE 5.18: The time-dependent CP asymmetry $S_{K^*\gamma}$ as a function of the KK gluon mass $M_{g^{(1)}}$ (left) and the branching ratio $\text{Br}(\bar{B} \rightarrow X_s \gamma)$ (right). The experimental 1σ error margins are given by the green bands and black vertical lines (in the right plot), while the SM predictions are represented by the yellow bars. In the left plot, the blue (gray) points obey (do not obey) the BR constraint and the vertical line represents the bound from electroweak precision tests. In the right plot, all points fulfill both the BR constraint and the T parameter bound. See text for details.

where $S_{K^*\gamma}$ at leading order is given by [280, 282]

$$S_{K^*\gamma} \simeq \frac{2}{|C_{7\gamma}|^2 + |\tilde{C}_{7\gamma}|^2} \text{Im} \left[e^{-i\phi_d} C_{7\gamma} \tilde{C}_{7\gamma} \right]. \quad (5.65)$$

The Wilson coefficients are given in (4.147) and contain both SM and RS contributions. The angle ϕ_d is the phase of $B^0 - \bar{B}^0$ mixing and has been measured in $B \rightarrow J/\psi K_S$ decays to be $\sin \phi_d = 0.67 \pm 0.02$ [275]. Due to the occurrence of the Wilson coefficient $\tilde{C}_{7\gamma}$ in the numerator, the SM prediction for $S_{K^*\gamma}$ is m_s/m_b -suppressed and reads

$$S_{K^*\gamma}^{\text{SM}} = (-2.3 \pm 1.6)\%. \quad (5.66)$$

The current experimental value [275, 283, 284]

$$S_{K^*\gamma}^{\text{exp}} = (-16 \pm 22)\% \quad (5.67)$$

has the potential to reveal possible NP effects, but still suffers from large uncertainties, so that more precise measurements would be desirable. Figure 5.18 shows the RS contributions to $S_{K^*\gamma}$ depending on KK gluon mass $M_{g^{(1)}}$ (left plot) and the branching ratio $\text{Br}(\bar{B} \rightarrow X_s \gamma)$ (right plot). The green bands denote the experimental 1σ error margin for $S_{K^*\gamma}$ and the yellow bars include the corresponding SM predictions. In the left plot, the blue (gray) parameter points fulfill the BR constraint (5.62) and the dashed gray line represents the T parameter bound. In the right plot, all points are compatible with both the BR constraint and the bounds stemming from electroweak precision tests. The black dashed lines represent the 1σ error margin of the current measurement of $\text{Br}(\bar{B} \rightarrow X_s \gamma)$. Note that due to the uncertainty in the SM prediction, all points on the left and on the right-hand side of the dashed lines are still compatible with the BR constraint. We observe that large deviations from the SM prediction for $S_{K^*\gamma}$ are still possible for very heavy KK gluon excitations. 33% of the parameter points can lead to deviations by $|\Delta S_{K^*\gamma}| = |S_{K^*\gamma} - S_{K^*\gamma}^{\text{SM}}| > 5\%$. It is reported in [285] that the expected sensitivity on $S_{K^*\gamma}$ at the SuperB-factories is about 2%, so a precise measurement of this observable could give us a first indication of the RS model in the future.

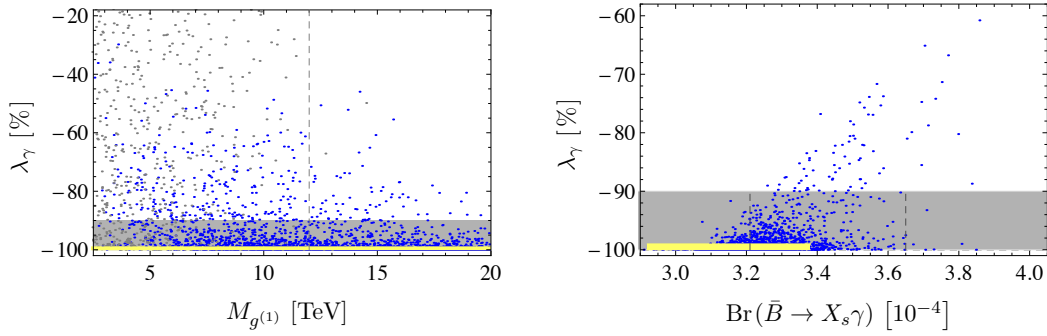


FIGURE 5.19: The photon polarization parameter λ_γ as a function of $M_{g^{(1)}}$ (left) and $\text{Br}(\bar{B} \rightarrow X_s \gamma)$ (right). The meaning of the colors, lines, bars, and dots is the same as in Figure 5.18. The gray band represents the future sensitivity at LHCb. See text for details.

5.2.3 The Photon Polarization Parameter λ_γ

Finally, we discuss the polarization of the emitted photon. This observable allows us to disentangle the relative contributions to $b \rightarrow s \gamma$ from the operators $Q_{7\gamma}$ and $\tilde{Q}_{7\gamma}$. A detailed consideration of how to measure the photon polarization can be found in [286–288]. Here, the proposal of [287] will be considered, which suggests to study the angular distribution of the decay products in the $\bar{B} \rightarrow \bar{K}_1(\rightarrow \bar{K} \pi \pi) \gamma$ decay and extract the polarization parameter

$$\lambda_\gamma = \frac{|\mathcal{A}(\bar{B} \rightarrow \bar{K}_1 \gamma_R)|^2 - |\mathcal{A}(\bar{B} \rightarrow \bar{K}_1 \gamma_L)|^2}{|\mathcal{A}(\bar{B} \rightarrow \bar{K}_1 \gamma_R)|^2 + |\mathcal{A}(\bar{B} \rightarrow \bar{K}_1 \gamma_L)|^2} = \frac{|\tilde{C}_{7\gamma}|^2 - |C_{7\gamma}|^2}{|\tilde{C}_{7\gamma}|^2 + |C_{7\gamma}|^2} \quad (5.68)$$

via a measurement of the observable of the so-called up-down asymmetry.¹³ The indices L and R in the matrix elements denote the polarization of the external photon. The SM prediction for this quantity is $\lambda_\gamma^{\text{SM}} \approx -1$, where small deviations are caused by the m_s/m_b -suppression and hadronization effects. As stressed several times, it is possible in the RS model to have a very large coefficient $\tilde{C}_{7\gamma}$. One expects to observe this fact in the polarization parameter resulting in values far above $\lambda_\gamma = -1$. We can indeed find such scenarios, illustrated in Figure 5.19, where λ_γ is shown as a function of $M_{g^{(1)}}$ (left plot) and $\text{Br}(\bar{B} \rightarrow X_s \gamma)$ (right plot). The yellow bars show the SM predictions, which are approached by the parameter points for large choices of the KK scale. Note that even for these, it is possible to get significant effects from the RS model. Precision measurements of this quantity could therefore give rise to a clear indication for new physics. On the other hand, the future sensitivities are reported to be $\sim 20\%$ (with integrated luminosity of 75 ab^{-1}) at the B-factories and $\sim 10\%$ at LHCb (with integrated luminosity of only 2 fb^{-1}) [271, 288], represented by the gray bands in Figure 5.19. Since only 3% of the parameter points can give rise to contributions larger than 10%, the future experiments are probably not sensitive enough to verify the deviations induced by the minimal RS model.

¹³It is also possible and even more feasible (since it increases the experimental sensitivity on λ_γ) to measure λ_γ via a method which takes into account information on the Dalitz distribution, see [288] for details.

Summary

The above analysis has shown that also B decays mediated by the loop-induced parton-level transition $b \rightarrow s\gamma$ can provide sensitive probes of virtual effects of KK excitations. The time-dependent CP asymmetry $S_{K^*\gamma}$ and the polarization parameter λ_γ generically receive large corrections, even under the assumption that the bounds from the branching ratio of $\bar{B} \rightarrow X_s\gamma$ and the electroweak precision measurements are fulfilled. In the former case, the corrections are in the ballpark of the expected future experimental sensitivities. Hence, in the context of the minimal RS model it is possible that a deviation of the SM prediction for $S_{K^*\gamma}$ might be seen in the future experiments. One may ask what order of magnitude one can expect for the effects in the RS model with custodial protection. According to analysis performed in [245] the contributions to the Wilson coefficients are supposed to be larger than in the minimal model due to the much richer fermion content which was introduced to reconcile the model with the $Zb\bar{b}$ constraint. This can lead to modifications of the CP asymmetry $S_{K^*\gamma}$ and also of the polarization parameter λ_γ , which are more pronounced than in the minimal model. Moreover, the relatively low S and T parameter bound of $M_{g^{(1)}} > 4.7 \text{ TeV}$ in the custodial model allows for many more parameter points in the left plots of Figures 5.18 and 5.19 to be considered. Note, however, that the BR constraint is likely to exclude more parameter points due to the larger corrections to the Wilson coefficients. In any case, it will be interesting to observe what the future measurements will tell us about the radiative Wilson coefficients and in particular $\tilde{C}_{7\gamma}$.

Conclusions

The first run of the LHC was both a success and a disappointment. On the one hand, it verified the existence of the Higgs boson, the last missing piece of the SM, which made the question of what stabilizes the Higgs mass around the electroweak scale more pressing than ever. On the other hand, it did not reveal any evidence for new physics which could answer that question. This in turn has kept alive plenty of new-physics models, few of which have been introduced in Chapter 1. One possibility with promising characteristics is given by Randall-Sundrum models. Not only can these models explain the hierarchy problem, but they, moreover, provide the currently best explanation for the hierarchies in the flavor sector of the SM. However, the predicted particles are probably too heavy for direct detection at the LHC, as explained extensively in Chapter 2. For this reason, the intention of this thesis has been to point out possibilities how to look for the heavy KK partners of the SM particles indirectly, in particular via measurements of observables which are loop-suppressed and hence very sensitive to additional virtual degrees of freedom in the loop. Chapters 4 and 5, which have formed the core of this thesis, have focused on the Higgs production channel via gluon fusion, the Higgs decay into two photons, and the flavor-changing neutral current $b \rightarrow s\gamma$ in various incarnations of the RS model, in which the Higgs sector is localized on or near the IR brane.

In the case of the loop-induced Higgs processes, it has been achieved to derive exact expressions for the $gg \rightarrow h$ and $h \rightarrow \gamma\gamma$ amplitudes in terms of integrals of the 5D fermion and boson propagators with the Higgs-boson profile along the extra dimension has been derived. Both expressions can be used to calculate the effective CP-even and CP-odd ggh and $h\gamma\gamma$ couplings, as long as one succeeds in deriving an explicit expression for the respective 5D propagator. The advantage of this approach is that one avoids the notion of KK modes from the beginning, since the infinite sum over KK modes is performed implicitly. In Chapter 3, we have derived both the warped-space 5D fermion propagator with the full three-generation flavor structure and the gauge-boson propagators in the minimal and custodial model, which are valid to all orders in v^2/M_{KK}^2 . In contrast to the procedure commonly used in the literature, all calculations have been performed by keeping the exact dependence on the Higgs-boson mass. At the end of the calculation the contributions of the SM particles and the fermion and boson KK towers to the effective ggh and $h\gamma\gamma$ couplings have been identified.

The 5D analysis of the ggh amplitude has pointed the relevance of different mass scales. While in models with a brane-localized Higgs sector the gluon fusion amplitude receives the dominant new-physics contributions from states with masses of order several times M_{KK} , in a narrow bulk-Higgs scenario there is another equally important contribution arising from (fermionic) states with masses of order v/η , which can resolve the “bulky nature” of the Higgs boson. The various versions of RS models according to the parametric relation of the characteristic width η of the Higgs-boson profile with respect to the two ratios $v|Y_q|/M_{\text{KK}}$ and $v|Y_q|/\Lambda_{\text{TeV}}$, where Λ_{TeV} is the value of the inherent

UV cutoff near the IR brane, have been classified in Table 4.1.

An important outcome of this thesis is that there is no controllable interpolation between bulk-Higgs and brane-Higgs models. In RS models in which the scalar sector is localized on the IR brane, we have found that the gluon fusion cross section is reduced compared with its SM value, whereas in models in which the Higgs-boson is described in terms of a narrow bulk field localized near the IR brane, the cross section is generally enhanced. The results have confirmed the contradictory calculations of [149] and [222]. It has been demonstrated that when trying to interpolate between the bulk-Higgs and brane-Higgs scenarios, i.e. taking the limit $\eta \rightarrow 0$ in a bulk-Higgs model, one enters a transition region with $\eta \sim v|Y_q|/\Lambda_{\text{TeV}}$, in which the contributions from certain higher-dimensional operators involving additional derivatives of the Z_2 -odd fermion profiles become unsuppressed, so that the effective field-theory approach breaks down. Such an operator is not present for the bosonic degrees of freedom, so that one obtains no resonance contribution from bosons and the W -boson contribution to the $h\gamma\gamma$ amplitude is unambiguous. Furthermore, we have addressed the question of the numerical impact of power-suppressed $|\Phi|^2(G_{\mu\nu}^a)^2$ operators, which contribute to the $gg \rightarrow h$ amplitude at tree level. It has been shown that, irrespective of whether the Higgs sector is localized on the IR brane or lives in the bulk, one expects power corrections of similar size. We have argued that the resulting power corrections are likely to be numerically smaller than the RS loop effects. The analogous argumentation holds for $|\Phi|^2(F_{\mu\nu})^2$ operators contributing to the $h\gamma\gamma$ amplitude.

While most of the calculations have been performed in the minimal RS model, we have also generalized the findings to the RS model with custodial symmetry. Analytical expressions for the effective ggh and $h\gamma\gamma$ couplings in terms of the same input parameters that appear in the minimal model have been derived. Due to the higher multiplicity of particles running in the loop, the contribution from the infinite KK tower of virtual quark states to the ggh ($h\gamma\gamma$) amplitude has turned out to be four ($68/5$) times larger than in the minimal model. The boson contribution is only twice as large.

In the phenomenological section, we have first studied the tree-level processes of Higgs decays into two electroweak gauge bosons as well as the Higgs production processes via Higgs-strahlung and vector-boson fusion. The analysis has included the effects from the virtual KK gauge bosons, which have been found to be subleading with respect to the L -enhanced contributions stemming from the modified hVV couplings.

The analysis of all tree- and loop-induced Higgs couplings has shown that the corrections of the custodial RS model to the $h f \bar{f}$ coupling scale like $\sim y_\star^2 v^2 / M_{\text{KK}}^2$ and can be affected by $\mathcal{O}(10\%)$ for small KK scales ($M_{g(1)} \lesssim 5 \text{ TeV}$) and not too small values for the maximal Yukawa value $y_\star \gtrsim 1$. It has further been pointed out that the CP-odd coupling of the top quark c_{t5} receives corrections that are already in the ballpark of the measurements of the electric dipole moment of the electron. The largest RS corrections appear in the loop-induced Higgs couplings to gluons and photons due to the high multiplicity of virtual KK particles running in the loop. Even for a KK gluon mass of $M_{g(1)} = 10 \text{ TeV}$, modifications of the Higgs couplings to gluons and photons in the custodial model can reach up to 53 % and 32 %, respectively. In order to show the potential of future measurements in the Higgs sector for the search after warped extra dimensions all relevant couplings have been compared with the sensitivities that can be reached by the LHC operating at $\sqrt{s} = 14 \text{ TeV}$ (with integrated luminosity 300 fb^{-1}) and the ILC operating at $\sqrt{s} = 1 \text{ TeV}$ (with 1000 fb^{-1}). We have derived strong exclusion bounds at 95% CL in the custodial RS model, which are summarized in Figure 5.6. Particularly the ILC has turned out to be very sensitive to KK gluons, being able to rule out KK gluon masses of $M_{g(1)} \geq 43 \text{ TeV} \times (y_\star/3) \text{ TeV}$ deduced from an analysis of the loop-induced

Higgs couplings to gluons. The analysis of the Higgs couplings to W bosons at the ILC has been used to expect a sensitivity on KK gluon masses of $M_{g(1)} \approx 15.0$ TeV, which is independent of the realization of the Yukawa sector and hence the parameter y_* .

We have finally compared the predictions of the measured signal rates for the processes $pp \rightarrow h \rightarrow b\bar{b}, \tau^+\tau^-, WW^*, ZZ^*, \gamma\gamma$ with the latest experimental data from the LHC. The strongest exclusion bounds originate from the Higgs decay into a pair of electroweak gauge bosons. In the custodial RS model KK gluon masses lighter than $19.9 \text{ TeV} \times (y_*/3)$ in the brane-Higgs and $14.9 \text{ TeV} \times (y_*/3)$ in the narrow bulk-Higgs scenario are excluded at 95% CL, which has been illustrated in the left plots of Figure 5.15. These bounds derived from Higgs physics are already much stronger than those obtained from electroweak precision tests. A possible way to lower these bounds is to reduce the values for the maximal Yukawa matrix entry y_* . Assuming a KK gluon with mass of $M_{g(1)} = 5$ TeV in the custodial RS model would require values of $y_* \leq 0.4$ in the brane-localized and $y_* \leq 1.1$ in the narrow bulk-Higgs scenario, shown in the right plot in Figure 5.15. As too small values for y_* would create a tension with other observables, such as the parameter ϵ_K in the kaon system, this analysis has shown that the direct detection of KK particles of the custodial RS model is disfavored by the current LHC data.

This thesis has also provided an analysis of the FCNC $b \rightarrow s\gamma$ in the minimal Randall-Sundrum model. We have argued that the relevant contributions to the $b \rightarrow s\gamma$ amplitude from the bosonic degree of freedom add up to a gauge-invariant result and that the summation of the first five modes leads to a finite result. We have achieved to derive approximate analytic formulas for the radiative Wilson coefficients. Importantly, it has been observed that the completeness relation for the fermion profiles is responsible for the elimination of one infinite sum, from which one can deduce that systematic cancellations within every KK mode leads to the finite result. It has been shown that in particular the chirality-flipped Wilson coefficients receive large corrections from the minimal RS model.

In the phenomenological analysis, we have investigated the impact of the potentially large corrections to the chirality-flipped Wilson coefficients. While the well-measured branching ratio of the decay $\bar{B} \rightarrow X_s\gamma$ has been used as an additional constraint besides the T parameter bound, we have focused on observables which are more sensitive on $\tilde{C}_{\tau\gamma}$, namely the time-dependent CP asymmetry $S_{K^*\gamma}$ in the decay $\bar{B} \rightarrow \bar{K}^*\gamma$ and the polarization parameter λ_γ in the decay $\bar{B} \rightarrow \bar{K}_1\gamma$. We have pointed out the fact the latter observable can receive up to 10%–20% corrections, but suffers from a limited sensitivity of future experiments. On the other hand, the time-dependent CP asymmetry can receive corrections of larger than 5% (even for parameter points that obey both the BR constraint and the T parameter bound), which the future experiments are expected to be sensitive to. The effect of the custodial RS model is expected to be even more pronounced, but has not been addressed in the analysis of $b \rightarrow s\gamma$ and is left for future work.

It will be exciting to compare the predictions derived in this thesis with future, more precise experimental results. Even if no KK particles are to be discovered at the LHC, we might hope that the measurements of the Higgs couplings and the time-dependent CP asymmetry in $\bar{B} \rightarrow \bar{K}^*\gamma$ either at the LHC or at a future linear collider could provide a hint of the possible existence of warped extra dimensions.

Appendix A

Compendium of Results for the Propagator Functions

Here the results for the propagator functions $\Delta_{LL}^{\vec{q}}$ and $\Delta_{RL}^{\vec{q}}$ for small, but finite Higgs width η are shown. The corresponding results for the $\Delta_{RR}^{\vec{q}}$ and $\Delta_{LR}^{\vec{q}}$ can be obtained with the help of the replacements shown at the end of Section 3.2.3. The limit $\eta \rightarrow 0$ has been discussed in Section 3.2.4. Keeping the η dependency, the propagator solutions depend on the region where t and t' take their values. We use a subscript b (s) for t , t' when the fifth coordinate lives in the bulk (sliver) region. The final results read

$$\begin{aligned}
\Delta_{LL}^{\vec{q}} \Big|_{11} &= \left\{ \begin{aligned} &\frac{-\sqrt{tt'}}{p_E M_{KK} 1_\eta} \left[\frac{D_1^{\vec{Q}}(t)}{D_1^{\vec{Q}}(1_\eta)} \left(\eta \hat{p}_E \frac{\coth S_{\vec{q}}}{S_{\vec{q}}} Z_{\vec{q}}^{\eta 1} + R_{\vec{Q}} \right) \frac{1}{N_{\vec{q}}^{\eta 1}} \frac{D_1^{\vec{Q}}(t')}{D_1^{\vec{Q}}(1_\eta)} + \frac{D_1^{\vec{Q}}(\hat{p}_E, t_{<})}{D_1^{\vec{Q}}(\hat{p}_E, 1_\eta)} L_3^{\vec{Q}}(\hat{p}_E, t_{>}, 1_\eta) \right] \\ &\frac{-1}{p_E M_{KK}} \sqrt{\frac{t}{1_\eta}} \frac{D_1^{\vec{Q}}(\hat{p}_E, t)}{D_1^{\vec{Q}}(\hat{p}_E, 1_\eta)} \left(\eta \hat{p}_E \frac{\coth S_{\vec{q}}}{S_{\vec{q}}} Z_{\vec{q}}^{\eta 1} + R_{\vec{Q}} \right) \frac{1}{N_{\vec{q}}^{\eta 1}} \frac{C(t')}{C(1_\eta)} \\ &\frac{-1}{p_E M_{KK}} \sqrt{\frac{t'}{1_\eta}} \frac{C(t)}{C(1_\eta)} \left(\eta \hat{p}_E \frac{\coth S_{\vec{q}}}{S_{\vec{q}}} Z_{\vec{q}}^{\eta 1} + R_{\vec{Q}} \right) \frac{1}{N_{\vec{q}}^{\eta 1}} \frac{D_1^{\vec{Q}}(\hat{p}_E, t')}{D_1^{\vec{Q}}(\hat{p}_E, 1_\eta)} \\ &\frac{-1}{p_E M_{KK}} \left[\frac{C(t)}{C(1_\eta)} \left(\eta \hat{p}_E \frac{\coth S_{\vec{q}}}{S_{\vec{q}}} Z_{\vec{q}}^{\eta 1} + R_{\vec{Q}} \right) \frac{1}{N_{\vec{q}}^{\eta 1}} \frac{C(t')}{C(1_\eta)} - \eta \hat{p}_E \frac{C(t_{>})}{C(1_\eta)} \frac{S(t_{<} + \eta)}{S_{\vec{q}}} \right] \end{aligned} \right. \\
\Delta_{LL}^{\vec{q}} \Big|_{12} &= \left\{ \begin{aligned} &\frac{\sqrt{tt'}}{p_E M_{KK} 1_\eta} \frac{D_1^{\vec{Q}}(\hat{p}_E, t)}{D_1^{\vec{Q}}(\hat{p}_E, 1_\eta)} R_{\vec{Q}} \frac{1}{N_{\vec{q}}^{\eta 2}(\hat{p}_E)} \varrho \tilde{Y}_{\vec{q}} \frac{D_2^{\vec{q}}(\hat{p}_E, t')}{D_2^{\vec{q}}(\hat{p}_E, 1_\eta)} \\ &\frac{\sqrt{tt'}}{p_E M_{KK} 1_\eta} \frac{D_1^{\vec{Q}}(\hat{p}_E, t)}{D_1^{\vec{Q}}(\hat{p}_E, 1_\eta)} R_{\vec{Q}} \frac{1}{N_{\vec{q}}^{\eta 2}(\hat{p}_E)} \varrho \tilde{Y}_{\vec{q}} \frac{D_2^{\vec{q}}(\hat{p}_E, t')}{D_2^{\vec{q}}(\hat{p}_E, 1_\eta)} \\ &\frac{1}{p_E M_{KK}} \sqrt{\frac{t'}{1_\eta}} \frac{C(t)}{C(1_\eta)} R_{\vec{Q}} \frac{1}{N_{\vec{q}}^{\eta 2}} \varrho \tilde{Y}_{\vec{q}} \frac{D_2^{\vec{q}}(\hat{p}_E, t')}{D_2^{\vec{q}}(\hat{p}_E, 1_\eta)} \\ &\frac{1}{p_E M_{KK}} \frac{C(t)}{C(1_\eta)} R_{\vec{Q}} \frac{1}{N_{\vec{q}}^{\eta 2}} \frac{S(t')}{S(1_\eta)} \varrho \tilde{Y}_{\vec{q}} \end{aligned} \right. \\
\Delta_{LL}^{\vec{q}} \Big|_{21} &= \left\{ \begin{aligned} &\frac{\sqrt{tt'}}{p_E M_{KK} 1_\eta} \frac{D_2^{\vec{q}}(\hat{p}_E, t)}{D_2^{\vec{q}}(\hat{p}_E, 1_\eta)} \varrho \tilde{Y}_{\vec{q}}^\dagger R_{\vec{Q}} \frac{1}{N_{\vec{q}}^{\eta 1}} \frac{D_1^{\vec{Q}}(\hat{p}_E, t')}{D_1^{\vec{Q}}(\hat{p}_E, 1_\eta)} \\ &\frac{1}{p_E M_{KK}} \sqrt{\frac{t}{1_\eta}} \frac{D_2^{\vec{q}}(\hat{p}_E, t)}{D_2^{\vec{q}}(\hat{p}_E, 1_\eta)} \varrho \tilde{Y}_{\vec{q}}^\dagger R_{\vec{Q}} \frac{1}{N_{\vec{q}}^{\eta 1}} \frac{C(t')}{C(1_\eta)} \\ &\frac{1}{p_E M_{KK}} \sqrt{\frac{t'}{1_\eta}} \varrho \tilde{Y}_{\vec{q}}^\dagger \frac{S(t)}{S(1_\eta)} R_{\vec{Q}} \frac{1}{N_{\vec{q}}^{\eta 1}} \frac{D_1^{\vec{Q}}(\hat{p}_E, t')}{D_1^{\vec{Q}}(\hat{p}_E, 1_\eta)} \\ &\frac{1}{p_E M_{KK}} \varrho \tilde{Y}_{\vec{q}}^\dagger \frac{S(t)}{S(1_\eta)} R_{\vec{Q}}(\hat{p}_E) \frac{1}{N_{\vec{q}}^{\eta 1}} \frac{C(t')}{C(1_\eta)} \end{aligned} \right. \\
\Delta_{LL}^{\vec{q}} \Big|_{22} &= \left\{ \begin{aligned} &\frac{-\sqrt{tt'}}{p_E M_{KK} 1_\eta} \left[\frac{D_2^{\vec{q}}(t)}{D_2^{\vec{q}}(1_\eta)} \tilde{Y}_{\vec{q}}^\dagger \frac{S_{\vec{q}}^2}{X_{\vec{q}}^2} \left(\eta \hat{p}_E \frac{\coth S_{\vec{q}}}{S_{\vec{q}}} + R_{\vec{Q}} \right) \frac{\varrho^2}{N_{\vec{q}}^{\eta 2}} \tilde{Y}_{\vec{q}} \frac{D_2^{\vec{q}}(t')}{D_2^{\vec{q}}(1_\eta)} - \frac{D_2^{\vec{q}}(t_{<})}{D_2^{\vec{q}}(1_\eta)} L_2^{\vec{q}}(t_{>}, 1_\eta) \right] \\ &\frac{-1}{p_E M_{KK}} \sqrt{\frac{t}{1_\eta}} \frac{D_2^{\vec{q}}(\hat{p}_E, t)}{D_2^{\vec{q}}(\hat{p}_E, 1_\eta)} \varrho \tilde{Y}_{\vec{q}}^\dagger \frac{S_{\vec{q}}^2}{X_{\vec{q}}^2} \left(\eta \hat{p}_E \frac{\coth(S_{\vec{q}})}{S_{\vec{q}}} + R_{\vec{Q}} \right) \frac{1}{N_{\vec{q}}^{\eta 2}} \frac{S(t')}{S(1_\eta)} \tilde{Y}_{\vec{q}} \\ &\frac{-1}{p_E M_{KK}} \sqrt{\frac{t'}{1_\eta}} \varrho \tilde{Y}_{\vec{q}}^\dagger \frac{S_{\vec{q}}^2}{X_{\vec{q}}^2} \frac{S(t)}{S(1_\eta)} \left(\eta \hat{p}_E \frac{\coth S_{\vec{q}}}{S_{\vec{q}}} + R_{\vec{Q}} \right) \frac{1}{N_{\vec{q}}^{\eta 2}} \varrho \tilde{Y}_{\vec{q}} \frac{D_2^{\vec{q}}(\hat{p}_E, t')}{D_2^{\vec{q}}(\hat{p}_E, 1_\eta)} \\ &\frac{-1}{p_E M_{KK}} \varrho \tilde{Y}_{\vec{q}}^\dagger \frac{S_{\vec{q}}^2}{X_{\vec{q}}^2} \left[\frac{S(t)}{S(1_\eta)} \left(\eta \hat{p}_E \frac{\coth S_{\vec{q}}}{S_{\vec{q}}} + R_{\vec{Q}} \right) \frac{1}{N_{\vec{q}}^{\eta 2}} \frac{S(t')}{S(1_\eta)} - \eta \hat{p}_E \frac{S(t_{>})}{S(1_\eta)} \frac{S(t_{<} + \eta)}{S_{\vec{q}} \tanh^2 S_{\vec{q}}} \right] \varrho \tilde{Y}_{\vec{q}} \end{aligned} \right.
\end{aligned}$$

$$\begin{aligned}
\Delta_{RL}^{\bar{q}} \Big|_{11} &= \left\{ \begin{aligned} & \frac{\sqrt{tt'}}{M_{KK}1_\eta} \left[\frac{D_2^{\bar{q}}(\hat{p}_E, t)}{D_2^{\bar{q}}(\hat{p}_E, 1_\eta)} \left(1 + \frac{\eta \hat{p}_E \coth S_{\bar{q}}}{R_{\bar{Q}}} Z^{\eta 1} \right) \frac{1}{N_{\bar{q}}^{\eta 1}} \frac{D_1^{\bar{q}}(\hat{p}_E, t')}{D_1^{\bar{q}}(\hat{p}_E, 1_\eta)} \right. \\ & \qquad \qquad \qquad \left. + \begin{cases} \frac{D_1^{\bar{q}}(\hat{p}_E, t')}{D_1^{\bar{q}}(\hat{p}_E, t)} L_4^{\bar{Q}}(\hat{p}_E, t, 1_\eta), & t_b > t'_b \\ \frac{D_2^{\bar{q}}(\hat{p}_E, t)}{D_1^{\bar{q}}(\hat{p}_E, 1_\eta)} L_3^{\bar{Q}}(\hat{p}_E, t', 1_\eta), & t_b < t'_b \end{cases} \right] \\ & \frac{1}{M_{KK}} \sqrt{\frac{t}{1_\eta}} \frac{D_2^{\bar{q}}(\hat{p}_E, t)}{D_2^{\bar{q}}(\hat{p}_E, 1_\eta)} \left(1 + \frac{\eta \hat{p}_E \coth S_{\bar{q}}}{R_{\bar{Q}}} Z^{\eta 1} \right) \frac{1}{N_{\bar{q}}^{\eta 1}} \frac{C(t')}{C(1_\eta)} \\ & \frac{-1}{M_{KK}} \sqrt{\frac{t'}{1_\eta}} \frac{S(t)}{S(1_\eta)} \left(Z^{\eta 1} + \eta \hat{p}_E \frac{\tanh S_{\bar{q}}}{S_{\bar{q}}} R_{\bar{Q}} \right) \frac{1}{N_{\bar{q}}^{\eta 1}} \frac{D_1^{\bar{q}}(\hat{p}_E, t')}{D_1^{\bar{q}}(\hat{p}_E, 1_\eta)} \\ & \frac{-1}{M_{KK}} \left[\frac{S(t)}{S(1_\eta)} \left(Z^{\eta 1} + \eta \hat{p}_E \frac{\tanh S_{\bar{q}}}{S_{\bar{q}}} R_{\bar{Q}} \right) \frac{1}{N_{\bar{q}}^{\eta 1}} \frac{C(t')}{C(1_\eta)} - \begin{cases} \frac{S(t)S(t'+\eta)}{C(1_\eta)}, & t_s > t'_s \\ \frac{C(t+\eta)C(t')}{C(1_\eta)}, & t_s < t'_s \end{cases} \right] \end{aligned} \right. \\
\Delta_{RL}^{\bar{q}} \Big|_{12} &= \left\{ \begin{aligned} & \frac{-\sqrt{tt'}}{M_{KK}1_\eta} \frac{D_2^{\bar{q}}(\hat{p}_E, t)}{D_2^{\bar{q}}(\hat{p}_E, 1_\eta)} \frac{1}{N_{\bar{q}}^{\eta 2}} \varrho \tilde{Y}_{\bar{q}} \frac{D_2^{\bar{q}}(\hat{p}_E, t')}{D_2^{\bar{q}}(\hat{p}_E, 1_\eta)} \\ & \frac{-1}{M_{KK}} \sqrt{\frac{t}{1_\eta}} \frac{D_2^{\bar{q}}(\hat{p}_E, t)}{D_2^{\bar{q}}(\hat{p}_E, 1_\eta)} \frac{1}{N_{\bar{q}}^{\eta 2}} \frac{S(t')}{S(1_\eta)} \varrho \tilde{Y}_{\bar{q}}^\eta \\ & \frac{-1}{M_{KK}} \sqrt{\frac{t'}{1_\eta}} \frac{S(t)}{S(1_\eta)} \frac{1}{N_{\bar{q}}^{\eta 2}} \varrho \tilde{Y}_{\bar{q}} \frac{D_2^{\bar{q}}(\hat{p}_E, t')}{D_2^{\bar{q}}(\hat{p}_E, 1_\eta)} \\ & \frac{-1}{M_{KK}} \left(\frac{S(t)}{S(1_\eta)} \frac{1}{N_{\bar{q}}^{\eta 2}} \frac{S(t')}{S(1_\eta)} - \frac{S(t_{>})}{S(1_\eta)} \frac{S(t_{<+\eta})}{\tanh S_{\bar{q}}} \right) \varrho \tilde{Y}_{\bar{q}} \end{aligned} \right. \\
\Delta_{RL}^{\bar{q}} \Big|_{21} &= \left\{ \begin{aligned} & \frac{-\sqrt{tt'}}{M_{KK}1_\eta} \frac{D_1^{\bar{q}}(\hat{p}_E, t)}{D_1^{\bar{q}}(\hat{p}_E, 1_\eta)} \frac{1}{\varrho \tilde{Y}_{\bar{q}}} \frac{X_{\bar{q}}^2}{S_{\bar{q}}^2} Z^{\eta 1} \frac{1}{N_{\bar{q}}^{\eta 1}} \frac{D_1^{\bar{q}}(\hat{p}_E, t')}{D_1^{\bar{q}}(\hat{p}_E, 1_\eta)} \\ & \frac{-1}{M_{KK}} \sqrt{\frac{t}{1_\eta}} \frac{D_1^{\bar{q}}(\hat{p}_E, t)}{D_1^{\bar{q}}(\hat{p}_E, 1_\eta)} \frac{1}{\varrho \tilde{Y}_{\bar{q}}^\eta} \frac{X_{\bar{q}}^2}{S_{\bar{q}}^2} Z^{\eta 1} \frac{1}{N_{\bar{q}}^{\eta 1}} \frac{C(t')}{C(1_\eta)} \\ & \frac{-1}{M_{KK}} \sqrt{\frac{t'}{1_\eta}} \frac{1}{\varrho \tilde{Y}_{\bar{q}}^\eta} \frac{X_{\bar{q}}^2}{S_{\bar{q}}^2} \frac{C(t)}{C(1_\eta)} Z^{\eta 1} \frac{1}{N_{\bar{q}}^{\eta 1}} \frac{D_1^{\bar{q}}(\hat{p}_E, t')}{D_1^{\bar{q}}(\hat{p}_E, 1_\eta)} \\ & \frac{-1}{M_{KK}} \frac{1}{\varrho \tilde{Y}_{\bar{q}}} \frac{X_{\bar{q}}^2}{S_{\bar{q}}^2} \left(\frac{C(t)}{C(1_\eta)} Z^{\eta 1} \frac{1}{N_{\bar{q}}^{\eta 1}} \frac{C(t')}{C(1_\eta)} - \frac{C(t_{>})}{C(1_\eta)} \frac{S(t_{<+\eta})}{\coth S_{\bar{q}}} \right) \end{aligned} \right. \\
\Delta_{RL}^{\bar{q}} \Big|_{22} &= \left\{ \begin{aligned} & \frac{\sqrt{tt'}}{M_{KK}1_\eta} \left[\frac{D_1^{\bar{q}}(\hat{p}_E, t)}{D_1^{\bar{q}}(\hat{p}_E, 1_\eta)} \frac{1}{\tilde{Y}_{\bar{q}}} Z^{\eta 2} \left(1 + \frac{\eta \hat{p}_E \coth S_{\bar{q}}}{R_{\bar{Q}}} \right) \frac{1}{N_{\bar{q}}^{\eta 2}} \tilde{Y}_{\bar{q}} \frac{D_2^{\bar{q}}(\hat{p}_E, t')}{D_2^{\bar{q}}(\hat{p}_E, 1_\eta)} \right. \\ & \qquad \qquad \qquad \left. - \begin{cases} \frac{D_2^{\bar{q}}(\hat{p}_E, t')}{D_2^{\bar{q}}(\hat{p}_E, 1_\eta)} L_1^{\bar{q}}(\hat{p}_E, t, 1_\eta), & t_b > t'_b \\ \frac{D_1^{\bar{q}}(\hat{p}_E, t)}{D_2^{\bar{q}}(\hat{p}_E, 1_\eta)} L_2^{\bar{q}}(\hat{p}_E, t', 1_\eta), & t_b < t'_b \end{cases} \right] \\ & \frac{1}{M_{KK}} \sqrt{\frac{t}{1_\eta}} \frac{D_1^{\bar{q}}(\hat{p}_E, t)}{D_1^{\bar{q}}(\hat{p}_E, 1_\eta)} \frac{1}{\tilde{Y}_{\bar{q}}} Z^{\eta 2} \left(1 + \frac{\eta \hat{p}_E \coth S_{\bar{q}}}{R_{\bar{Q}}} \right) \frac{1}{N_{\bar{q}}^{\eta 2}} \frac{S(t')}{S(1_\eta)} \tilde{Y}_{\bar{q}} \\ & \frac{-1}{M_{KK}} \sqrt{\frac{t'}{1_\eta}} \frac{1}{\tilde{Y}_{\bar{q}}} \frac{C(t)}{C(1_\eta)} \left(1 + \eta \hat{p}_E \frac{\tanh S_{\bar{q}}}{S_{\bar{q}}} R_{\bar{Q}} \right) \frac{1}{N_{\bar{q}}^{\eta 2}} \tilde{Y}_{\bar{q}} \frac{D_2^{\bar{q}}(\hat{p}_E, t')}{D_2^{\bar{q}}(\hat{p}_E, 1_\eta)} \\ & \frac{-1}{M_{KK}} \frac{1}{\tilde{Y}_{\bar{q}}} \left[\frac{C(t)}{C(1_\eta)} \left(1 + \eta \hat{p}_E \frac{\tanh S_{\bar{q}}}{S_{\bar{q}}} R_{\bar{Q}} \right) \frac{1}{N_{\bar{q}}^{\eta 2}} \frac{S(t')}{S(1_\eta)} - \begin{cases} \frac{C(t)S(t'+\eta)}{S(1_\eta)}, & t_s > t'_s \\ \frac{C(t+\eta)S(t')}{S(1_\eta)}, & t_s < t'_s \end{cases} \right] \tilde{Y}_{\bar{q}}, \end{aligned} \right.
\end{aligned}$$

where the four lines correspond to the cases ($A, B = L, R$ and $i, j = 1, 2$)

$$\Delta_{AB}^{\bar{q}} \Big|_{ij} = \begin{cases} \dots & t_b, t'_b \\ \dots & t_b < t'_s \\ \dots & t_s > t'_b \\ \dots & t_s, t'_s \end{cases}. \quad (\text{A.1})$$

The propagator functions have been written down in such a way that one can immediately notice their continuity at point $1 - \eta$ for both t and t' . Using

$$\begin{aligned}
L_{1,4}^{\bar{A}}(\hat{p}_E 1_\eta, \hat{p}_E 1_\eta) &= \pm 1, & S(1_\eta) &= \sinh S_{\bar{q}}, & S(1) &= C(1) = 0, \\
L_{2,3}^{\bar{A}}(\hat{p}_E 1_\eta, \hat{p}_E 1_\eta) &= 0, & C(1_\eta) &= \cosh S_{\bar{q}}, & & \end{aligned} \quad (\text{A.2})$$

the continuity becomes obvious in almost all cases. For the (11)- and (22)-elements of the propagator function $\Delta_{RL}^{\bar{q}}$, one moreover needs the relations (3.90).

Appendix B

The Yukawa Perturbativity Bound

In this appendix, we will discuss the Yukawa perturbativity bound. As pointed out in Section 2.2.2, the Yukawa matrix elements \mathbf{Y}_{ij} are expected to be anarchic, complex $\mathcal{O}(1)$ numbers, i.e. they are assumed not to be too small and too large, respectively. In fact, we must impose an upper bound on the size of the 5D Yukawa couplings, since they otherwise do not remain perturbative up to the cutoff of the RS models under consideration. Here we will first recall the NDA estimates for the Yukawa perturbativity bound in RS models with a brane-localized and a bulk-Higgs sector. These estimates will be somewhat more refined than those done in the literature, e.g. in [160, 180], taking into account the dependence on the number of generations N_g . After that, the perturbativity bound will be calculated explicitly using the exact 5D fermion propagators derived in Section 3.2. We will find that the explicit calculation leads to stronger bounds than the conventional NDA estimates. The first part of this appendix is based on Appendix D of our publication [150], while the second part is unpublished work.

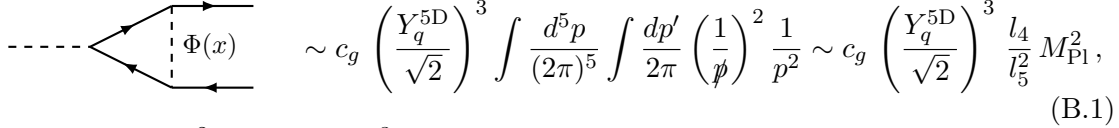
B.1 NDA Estimates

We begin with the NDA estimates, which build the basis for what is the upper bound for the Yukawa matrix elements $|(\mathbf{Y}_q)_{ij}| \leq y_\star$ is usually adopted in the literature. As we will see, they will depend on whether the scalar sector is a bulk or an IR-localized field. We will also derive the value of β , for which the NDA estimate for the bulk scenario has to be replaced by the corresponding one for the brane-Higgs scenario.

Brane-Localized Higgs Scenario

In an RS model with a brane-localized Higgs sector, we have to take into account the fact that the scalar field is localized on a brane (fixed by the δ -function). This in turn implies that the momentum is not conserved in certain directions due to the breaking of translational invariance and hence some of the dp_5 integrals coming from the $\int d^5p \dots$ representation of the propagators cannot be eliminated and remain part of the loop integration. Neglecting external momenta as well as the scalar and fermion masses, one

finds the following the NDA estimate for the one-loop correction to the Yukawa coupling [111, 150],¹



$$\sim c_g \left(\frac{Y_q^{5D}}{\sqrt{2}} \right)^3 \int \frac{d^5 p}{(2\pi)^5} \int \frac{dp'}{2\pi} \left(\frac{1}{\not{p}} \right)^2 \frac{1}{p^2} \sim c_g \left(\frac{Y_q^{5D}}{\sqrt{2}} \right)^3 \frac{l_4}{l_5^2} M_{\text{Pl}}^2, \quad (\text{B.1})$$

where $l_4 = 16\pi^2$ and $l_5 = 24\pi^3$ are the 4D and 5D loop factors defined in (1.58) and M_{Pl} is the physical UV cutoff Λ_{UV} of the RS model. The coefficient $c_g = 2N_g - 1$ accounts for the multiplicity of fermion generations and is determined by the relation (5.40). The corresponding typical size of an element of the anarchic 5D Yukawa matrices is given by $|Y_q^{5D}| = 2|Y_q|/k$, where $|Y_q|$ is related to the maximal value y_* via (4.53). Requiring that the above one-loop correction is smaller than the tree-level Yukawa coupling yields the condition

$$c_g \left(\frac{|Y_q^{5D}|}{\sqrt{2}} \right)^3 \frac{l_4}{l_5^2} M_{\text{Pl}}^2 = \frac{c_g |Y_q|^2}{18\pi^4} \left(\frac{\Lambda_{\text{TeV}}}{M_{\text{KK}}} \right)^2 \stackrel{!}{<} 1, \quad (\text{B.2})$$

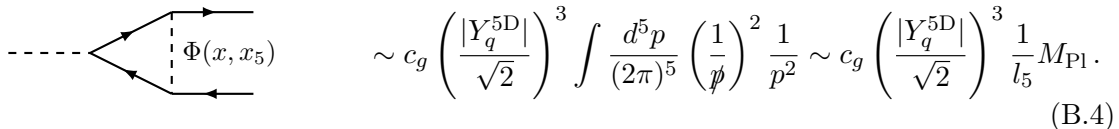
where we have used that $\Lambda_{\text{TeV}} = M_{\text{Pl}}\epsilon$ and $M_{\text{KK}} = k\epsilon$. A similar estimate can be obtained in the KK picture, where the quadratic behavior on the cutoff arises from a double sum over N_{KK} levels of states with masses below the cutoff Λ_{TeV} [180]. We then find

$$c_g \left(\frac{|Y_q|}{\sqrt{2}} \right)^3 \frac{1}{l_4} N_{\text{KK}}^2 \approx \frac{c_g |Y_q|^2}{32\pi^4} \left(\frac{\Lambda_{\text{TeV}}}{M_{\text{KK}}} \right)^2 \stackrel{!}{<} 1, \quad (\text{B.3})$$

where it has been used that the masses of the KK modes are determined by the zeroes of some Bessel functions, see (2.29). This in turn means that the states in the N^{th} KK level have masses approximately given by $N\pi M_{\text{KK}}$ (valid for large N), and therefore $N_{\text{KK}} \approx \Lambda_{\text{TeV}}/(\pi M_{\text{KK}})$. Note that the two estimates (B.2) and (B.3) are equivalent up to a harmless $\mathcal{O}(1)$ factor. Employing (4.53) and solving for y_* , we find the condition $y_* < y_{\text{max}}$, with the upper bounds $y_{\text{max}} = (6\pi^2/\sqrt{c_g}) M_{\text{KK}}/\Lambda_{\text{TeV}}$ derived from (B.2) and $y_{\text{max}} = (6\pi^2/\sqrt{c_g}) M_{\text{KK}}/\Lambda_{\text{TeV}}$ derived from (B.3). Assuming $\Lambda_{\text{TeV}} \approx 10 M_{\text{KK}}$, which reflects the proper balance between several KK modes below the UV cutoff without reintroducing a large hierarchy, one finds that $y_{\text{max}} \approx 2.6$ in the first case and $y_{\text{max}} \approx 3.5$ in the second. These estimates are somewhat more refined than those presented elsewhere in the literature (since the dependence on the number of generations N_g is included), but they are compatible with the conventional choice $y_{\text{max}} = 3$ adopted in most phenomenological analyses of RS models.

Bulk-Higgs Scenario

For a bulk scalar we do not need to account for brane-localized vertices and the one-loop corrections to the Yukawa interaction can be estimated as



$$\sim c_g \left(\frac{|Y_q^{5D}|}{\sqrt{2}} \right)^3 \int \frac{d^5 p}{(2\pi)^5} \left(\frac{1}{\not{p}} \right)^2 \frac{1}{p^2} \sim c_g \left(\frac{|Y_q^{5D}|}{\sqrt{2}} \right)^3 \frac{1}{l_5} M_{\text{Pl}}. \quad (\text{B.4})$$

¹Note that the factor of $\sqrt{2}$ in the denominator has been included, as this factor appears in the Feynman rule (2.126).

It follows in this case that

$$c_g \left(\frac{|Y_q^{5D}|}{\sqrt{2}} \right)^2 \frac{1}{l_5} M_{\text{Pl}} = \frac{c_g |Y_q|^2 (2 + \beta)^2 \Lambda_{\text{TeV}}}{48\pi^3 (1 + \beta) M_{\text{KK}}} \stackrel{!}{<} 1, \quad (\text{B.5})$$

where we have used relation (2.98) for the dimensionless Yukawa matrix. This translates into $y_\star < y_{\text{max}}$ with $y_{\text{max}} = \sqrt{96\pi^3/c_g} \frac{\sqrt{1+\beta}}{2+\beta} \sqrt{M_{\text{KK}}/\Lambda_{\text{TeV}}}$. Note that in the bulk-Higgs case the suppression in the ratio $M_{\text{KK}}/\Lambda_{\text{TeV}}$ is parametrically weaker than in the case of a brane-localized Higgs field. In practice, with $\Lambda_{\text{TeV}} \sim 10M_{\text{KK}}$, this effect is not too important, however. Even for a very broad bulk Higgs with $\beta \rightarrow 0$, we obtain $y_{\text{max}} \approx 3.9$, which is of the same order as the bound in the brane-Higgs case. In a narrow bulk-Higgs scenario, for which $\eta = 1/\beta \ll 1$ is a small parameter (see Table 4.1), one can simplify $y_{\text{max}} = \sqrt{96\pi^3/c_g} \sqrt{\eta M_{\text{KK}}/\Lambda_{\text{TeV}}} \approx 7.7\sqrt{\eta}$. This formula can only be trusted as long as $\eta \gtrsim M_{\text{KK}}/\Lambda_{\text{TeV}} \approx 0.1$. For smaller η , the relevant bound is that found in the brane-Higgs case, $y_{\text{max}} \approx 2.6$. From a practical point of view, there is no significant difference between the two bounds.

B.2 Calculation Using the Exact 5D Fermion Propagator

Let us now derive the Yukawa perturbativity bound at one-loop order by a calculation via the exact 5D fermion propagator in the minimal RS model. The calculation for the custodial model can be performed analogously. We consider the diagram shown in (B.1), where the incoming momentum are denoted by k , while k_1 and k_2 are the outgoing momenta for the two quarks, i.e. $k_\mu = k_{1\mu} + k_{2\mu}$. The Lagrangian of the Yukawa interactions can be generally written as

$$\begin{aligned} \mathcal{L}_{\text{Yuk}}(x) = & - \sum_{q=u,d} \int_\epsilon^1 dt \int_\epsilon^1 dt' \delta_h^\eta(t-1) h(x) \bar{\mathcal{Q}}_L(t, x) \frac{1}{\sqrt{2}} \begin{pmatrix} 0 & \mathbf{Y}_q^C \\ \mathbf{Y}_q^{S\dagger} & 0 \end{pmatrix} \\ & \times \left[\delta(t-t') + I(k_1, k_2, t, t') \right] \mathcal{Q}_R(t', x) + \text{h.c.}, \end{aligned} \quad (\text{B.6})$$

where the integral $I(k_1, k_2, t, t')$ represents the one-loop correction and we distinguish between the Yukawa matrices for the Z_2 -even and Z_2 -odd fermion profiles. Considering the amplitude for an outgoing left-handed and an incoming right-handed quark, we find

$$\begin{aligned} i\mathcal{A}_{RL} = & \frac{1}{2\sqrt{2}\varrho^3} \int \frac{d^d p}{(2\pi)^d} \int_\epsilon^1 dt \int_\epsilon^1 dt' \int_\epsilon^1 dt'' \frac{\delta_h^\eta(t-1) \delta_h^\eta(t'-1) \delta_h^\eta(t''-1)}{(p+k_1)^2 - m_h^2} \\ & \times \bar{u}_L^{(n)}(k_1) \mathcal{Q}_L^{(n)\dagger}(t) \mathcal{M}_q \mathbf{S}_q(t, t''; p) \mathcal{M}_q^\dagger \mathbf{S}_q(t'', t'; p+k) \mathcal{M}_q \mathcal{Q}_R^{(n')}(t') u_R^{(n')}(k_2), \end{aligned} \quad (\text{B.7})$$

where $\mathcal{Q}_{L,R}^{(n)}$ are the fermion profiles in the vector representation (2.71), \mathbf{S}_q is the fermion propagator derived in Section 3.2 and \mathcal{M}_q denotes the 6×6 Yukawa matrix shown in the first line of (B.6) (with an additional factor of $\varrho = v/(\sqrt{2}M_{\text{KK}})$). Matching the amplitude on the effective Lagrangian (B.6), we obtain

$$I(k_1, k_2, t, t') = \frac{i}{2} \int \frac{d^d p}{(2\pi)^d} \frac{\not{p}(\not{p} + \not{k}) \left[\mathbf{T}_{RL}^q(p, p+k, t, t') + \mathbf{T}_{LR}^q(p, p+k, t, t') \right]}{(p+k_1)^2 - m_h^2}, \quad (\text{B.8})$$

where

$$\mathbf{T}_{AB}^q(p, q, t, t') \equiv \frac{1}{\varrho^2} \delta_h^\eta(t' - 1) \int_\epsilon^1 dt'' \delta_h^\eta(t'' - 1) \Delta_{RA}^q(t, t''; -p^2) \mathcal{M}_q^\dagger \Delta_{BL}^q(t'', t'; -q^2) \mathcal{M}_q \quad (\text{B.9})$$

is the interesting quantity to be calculated. We now distinguish between the brane-localized and the bulk-Higgs scenario.

In the former case, the solutions for the propagator functions are shown in Section 3.2.4. Evaluating them at $t = t' = 1^-$, we find

$$\begin{aligned} \mathbf{T}_{RL}^q(p, q, 1^-, 1^-) &= \frac{1}{p_E q_E M_{\text{KK}}^2} \begin{pmatrix} -\varrho^2 \mathbf{W}_q(p, q) \tilde{\mathbf{Y}}_q \mathbf{Y}_q^{S\dagger} & \varrho \mathbf{W}_q(p, q) \mathbf{Y}_q^C \\ -\varrho \frac{1}{\tilde{\mathbf{Y}}_q} \mathbf{W}_q(p, q) \tilde{\mathbf{Y}}_q \mathbf{Y}_q^{S\dagger} & \frac{1}{\tilde{\mathbf{Y}}_q} \mathbf{W}_q(p, q) \mathbf{Y}_q^C \end{pmatrix}, \\ \mathbf{T}_{LR}^q(p, q, 1^-, 1^-) &= \frac{1}{M_{\text{KK}}^2} \begin{pmatrix} \varrho^2 \mathbf{V}_q(p, q) \tilde{\mathbf{Y}}_q \mathbf{Y}_q^{S\dagger} & \varrho \mathbf{V}_q(p, q) \mathbf{Z}_q \mathbf{Y}_q^C \\ \varrho \frac{1}{\tilde{\mathbf{Y}}_q} \mathbf{V}_q(p, q) \tilde{\mathbf{Y}}_q \mathbf{Y}_q^{S\dagger} & \frac{1}{\tilde{\mathbf{Y}}_q} \mathbf{V}_q(p, q) \mathbf{Z}_q \mathbf{Y}_q^C \end{pmatrix}, \end{aligned} \quad (\text{B.10})$$

with the defined quantities

$$\begin{aligned} \mathbf{W}_q(p, q) &\equiv \frac{\mathbf{Z}_q(p_E^2)}{1 + \mathbf{Z}_q(p_E^2)} \frac{1}{\mathbf{R}_Q(p_E)} \left(\frac{1}{\varrho^2} \frac{\mathbf{X}_q}{\tanh \mathbf{X}_q} - \mathbf{Y}_q^S \tilde{\mathbf{Y}}_q^\dagger \right) \mathbf{R}_Q(q_E) \frac{1}{1 + \mathbf{Z}_q(q_E^2)}, \\ \mathbf{V}_q(p, q) &\equiv \frac{1}{1 + \mathbf{Z}_q(p_E^2)} \left(\tilde{\mathbf{Y}}_q \mathbf{Y}_q^{C\dagger} + \frac{1}{\varrho} \mathbf{Z}_q(p_E^2) \mathbf{Y}_q^S \frac{1}{\varrho \tilde{\mathbf{Y}}_q} \right) \frac{1}{1 + \mathbf{Z}_q(q_E^2)}. \end{aligned} \quad (\text{B.11})$$

The integral (B.8) could in principle be evaluated in order to obtain the correction to the Yukawa coupling. However, it turns out to be more appropriate to first expand the terms in $\mathcal{O}(v^2/M_{\text{KK}}^2)$. Working at leading order in v^2/M_{KK}^2 , we can send $\varrho \rightarrow 0$ for the propagator solutions, in which case they drastically simplify to

$$\Delta_{LL}^q(1^-, 1^-; -p^2) = -\frac{\mathbf{R}_Q(\hat{p}_E)}{p_E M_{\text{KK}}} \begin{pmatrix} 1 & 0 \\ 0 & 0 \end{pmatrix}, \quad \Delta_{RR}^q(1^-, 1^-; -p^2) = -\frac{\mathbf{R}_Q(\hat{p}_E)}{p_E M_{\text{KK}}} \begin{pmatrix} 0 & 0 \\ 0 & 1 \end{pmatrix}, \quad (\text{B.12})$$

while $\Delta_{RL}^q(1^-, 1^-; -p^2) = 0 = \Delta_{LR}^q(1^-, 1^-; -p^2)$ completely vanish. Consequentially, it is $\mathbf{T}_{LR}(p, q, 1^-, 1^-) \approx 0$ in this limit and

$$\mathbf{T}_{RL}^q(p, q, 1^-, 1^-) \approx \frac{1}{p_E q_E M_{\text{KK}}^2} \begin{pmatrix} 0 & 0 \\ 0 & \mathbf{R}_q(\hat{p}_E) \mathbf{Y}_q^{C\dagger} \mathbf{R}_Q(\hat{q}_E) \mathbf{Y}_q^C \end{pmatrix}. \quad (\text{B.13})$$

Note that $p_E q_E$ is not meant to be a euclidean scalar product, but as the product $\sqrt{-p^2} \sqrt{-q^2}$. Inserting (B.13) into (B.8) gives

$$I(k_1, k_2, t, t') = \frac{1}{2M_{\text{KK}}^2} \frac{1}{l_4} \int_0^\infty dp_E^2 p_E^{d-2} \frac{\mathbf{R}_q(\hat{p}_E) \mathbf{Y}_q^{C\dagger} \mathbf{R}_Q((\hat{p} + \hat{k})_E) \mathbf{Y}_q^C}{(p_E + k_{1E})^2 + m_h^2} \begin{pmatrix} 0 & 0 \\ 0 & 1 \end{pmatrix}. \quad (\text{B.14})$$

Notice the appearance of the loop factor $l_4 = (4\pi)^2$. Note further that the correction is exact up to higher orders in v^3/M_{KK}^3 . At this step, another simplification is necessary, since the integrand is quite complicated and the momentum integral cannot be performed easily. Being interested in large momenta $k_{1E, 2E} \ll p_E \lesssim \Lambda_{\text{TeV}}$, we can approximate the integrand using the expansion $\mathbf{R}_{q, Q} \approx 1$. In this limit, the corrections to the Yukawa

sector are given by (sending $d \rightarrow 4$)

$$I_1 \approx \frac{1}{2M_{\text{KK}}^2 l_4} \int_0^{\Lambda_{\text{TeV}}} dp_E^2 \begin{pmatrix} 0 & 0 \\ 0 & \mathbf{Y}_q^{C\dagger} \mathbf{Y}_q^C \end{pmatrix} = \frac{1}{2l_4} \left(\frac{\Lambda_{\text{TeV}}}{M_{\text{KK}}} \right)^2 \begin{pmatrix} 0 & 0 \\ 0 & \mathbf{Y}_q^{C\dagger} \mathbf{Y}_q^C \end{pmatrix}, \quad (\text{B.15})$$

and we recover the quadratic sensitivity on the UV cutoff already shown up in the NDA estimate. Thus, the Yukawa coupling is indeed quadratically divergent in the RS model. Employing (5.40), we find that the leading correction only affects \mathbf{Y}_q^C by

$$(\mathbf{Y}_q^C)_{ij} \rightarrow (\mathbf{Y}_q^C)_{ij} \left[1 + \frac{1}{2l_4} \left(\frac{\Lambda_{\text{TeV}}}{M_{\text{KK}}} \right)^2 (2N_g - 1) |Y_q|^2 \right], \quad (\text{B.16})$$

and with the help of (4.53) this translates into maximal value when the Yukawa sector gets strongly coupled

$$y_\star < y_{\text{max}} < 2 \sqrt{\frac{l_4}{2N_g - 1} \frac{M_{\text{KK}}}{\Lambda_{\text{TeV}}}} \approx 1.1. \quad (\text{B.17})$$

As before, it has been used in the second step that practically $\Lambda_{\text{TeV}} \approx 10 M_{\text{KK}}$. We see that this bound is very tight and much stronger than the NDA estimate. However, the actual value for y_\star has to be determined by measurement of observables that are sensitive on the value of y_\star , like the loop-induced Higgs processes analyzed in the previous sections. In fact, as shown in Section 5.1, the current LHC data prefer small values for y_\star to be compatible with KK boson mass that are in reach of direct detection at the LHC. Nevertheless, the value for y_{max} derived above should be kept in mind when discussing possible ranges of allowed Yukawa matrix elements. Note also that y_\star is the upper bound imposed for the elements of the Yukawa matrices. A typical element is $|Y_q| \sim y_\star / \sqrt{2}$ according to (4.53) and hence even smaller.

In the bulk-Higgs scenario, the exact solution for the 5D fermion propagator has not been derived yet and it is therefore necessary to work at leading order in the expansion of v^2/M_{KK}^2 right from the beginning. However, one does not even need the propagator solutions at v^2/M_{KK}^2 , since the corrections to (B.6) at that order come from the Yukawa matrices \mathcal{M}_q , see (B.7). Thus, one can make use of the solutions for the free 5D fermion propagator, which can be deduced from the results in Section 3.2.4 in the limit $\mathbf{Y}_q \rightarrow 0$. Provided with these solutions and the Higgs profile (2.63) one could in principle calculate the function \mathbf{T}_{AB} (B.9). The result is exact in v^2/M_{KK}^2 . However, for a generic bulk-Higgs profile it is not possible to get a compact, analytical result after the integration over the extra dimension. For the case of a very localized Higgs profile ($\beta \gg 1$), on the other hand, some simplifications can be made allowing us to show that the brane result is recovered in the limit $\beta \rightarrow \infty$. As the Higgs profile is IR-localized and the localization increases for larger β , only values for t , t' , and t'' that are $\mathcal{O}(1)$ have to be considered. If one furthermore takes into account that the propagator functions fall off exponentially for values $t, t', t'' \neq 1$ and high momenta (see (3.118)), the functions \mathbf{T} can be written as

$$\mathbf{T}_{RL}(p, q, t, t') = \frac{\chi_0^h(t')}{r_{PEQE} M_{\text{KK}}^2} \begin{pmatrix} 0 & 0 \\ 0 & \mathbf{Y}_q^{C,5D\dagger} \mathbf{Y}_q^{C,5D} \end{pmatrix} \int_\epsilon^1 dt'' \chi_0^h(t''). \quad (\text{B.18})$$

Upon evaluating the integral over t'' and redefining the Yukawas via (2.98), we finally get

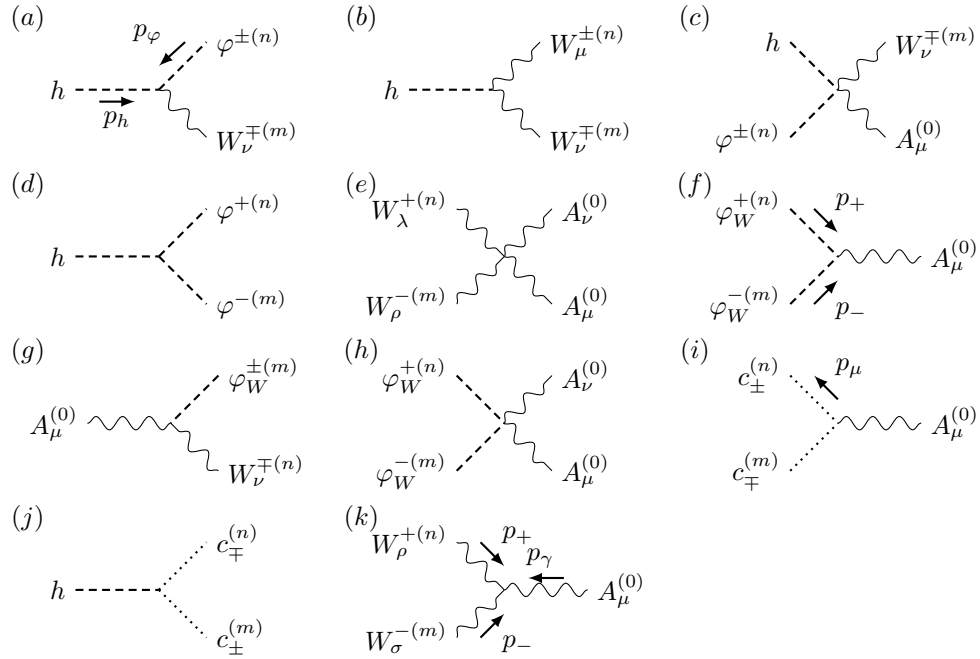
$$\mathbf{T}_{RL}(p, q, t, t') = \frac{\delta_h^{1/\beta}(t' - 1)}{p_{EQE} M_{\text{KK}}^2} \begin{pmatrix} 0 & 0 \\ 0 & \mathbf{Y}_q^{C\dagger} \mathbf{Y}_q^C \end{pmatrix}, \quad (\text{B.19})$$

where $\delta_h^{1/\beta}(t-1) = (2+\beta)t^{1+\beta}$ has been used, see (2.97). This is equivalent to the corresponding formula in the brane-localized Higgs case (B.13) and consequently, concerning the Yukawa perturbativity bound, there exists no difference between the two cases.

Appendix C

Feynman Rules in the 4D Effective Theory

Couplings within the Boson Sector



Here the Feynman rules needed for the calculation of the one-loop gauge-boson, scalar, and ghost contributions to the $h \rightarrow \gamma\gamma$ decay amplitude in the KK-decomposed version of the minimal RS model are listed. We work in a general R_ξ gauge and use mass eigenstates of all SM particles and their KK excitations. The Feynman rules for the

vertices shown above are:

$$\begin{aligned}
(a): & \quad \frac{\tilde{m}_W^2}{vm_W^2} 2\pi \chi_m^W(1) \chi_n^W(1) (p_\varphi - p_h)_\nu, & (b): & \quad \frac{2i\tilde{m}_W^2}{v} 2\pi \chi_m^W(1) \chi_n^W(1) \eta_{\mu\nu}, \\
(c): & \quad \pm e \frac{\tilde{m}_W^2}{vm_W^2} 2\pi \chi_m^W(1) \chi_n^W(1) \eta_{\mu\nu}, & (d): & \quad \frac{-im_h^2}{v} \frac{2\pi \tilde{m}_W^2}{m_m^W m_n^W} \chi_m^W(1) \chi_n^W(1), \\
(e): & \quad -ie^2 (2\eta_{\lambda\rho} \eta_{\mu\nu} - \eta_{\lambda\mu} \eta_{\rho\nu} - \eta_{\lambda\nu} \eta_{\rho\mu}) \delta_{mn}, & (f): & \quad ie (p_+ - p_-)_\mu \delta_{mn}, \\
(g): & \quad \pm e m_m^W \eta_{\mu\nu} \delta_{mn}, & (h): & \quad 2ie^2 \eta_{\mu\nu} \delta_{mn}, \\
(i): & \quad \pm ie p_\mu \delta_{mn}, & (j): & \quad -\xi \frac{i\tilde{m}_W^2}{v} 2\pi \chi_m^W(1) \chi_n^W(1), \\
(k): & \quad ie \delta_{mn} V_{\rho\mu\sigma}(p_+, p_\gamma, p_-), & &
\end{aligned} \tag{C.1}$$

where v is the Higgs vev in the RS model, the parameter \tilde{m}_W has been defined in (2.30), and the structure $V_{\rho\mu\sigma}$ of the three-boson vertex has been given in the text after (4.80).

Fermion Coupling to Bosons

The Feynman rules for the fermion coupling to vector bosons have been derived in [184, 230] and can be summarized as

$$i\mathcal{M} = ig_B \gamma^\alpha \left(V_{nmk}^B P_L + \tilde{V}_{nmk}^B P_R \right), \tag{C.2}$$

where α denotes the boson polarization and the g_B 's are the respective couplings, i.e. $g/\sqrt{2}$ for the W^- and W^+ , $g_s t^a$ for the gluon, eQ_f for the photon, and $g/\cos\theta_w$ for the Z boson exchange. The subscripts denote the outgoing (n) and the incoming (k) fermion modes, whereas the boson mode is represented by m . The specific form of the overlap integrals can be found in (2.123)–(2.125).

The couplings to the scalar bosons are given by

$$i\mathcal{M} = g_B \left(V_{nmk}^{\varphi_B} P_L + \tilde{V}_{nmk}^{\varphi_B} P_R \right). \tag{C.3}$$

While g_B is just the same as above, the coupling to the Higgs is chosen to be $g_H = i$, with $V_{nk} = g_{nk}$ given in (2.126). The overlap integrals $V_{nmk}^{\varphi_B}$ and $\tilde{V}_{nmk}^{\varphi_B}$ can be written as ($B = \gamma, \mathcal{G}, Z$)

$$V_{nmk}^{\varphi_B} = \frac{m_n^d}{m_m^B} V_{nmk}^B - \frac{m_k^d}{m_m^B} \tilde{V}_{nmk}^B, \quad \tilde{V}_{nmk}^{\varphi_B} = \frac{m_n^d}{m_m^B} \tilde{V}_{nmk}^B - \frac{m_k^d}{m_m^B} V_{nmk}^B$$

and

$$\begin{aligned}
V_{nmk}^{\varphi_W^+} &= \frac{m_n^u}{m_m^W} V_{nmk}^{W^+} - \frac{m_k^d}{m_m^W} \tilde{V}_{nmk}^{W^+}, & \tilde{V}_{nmk}^{\varphi_W^+} &= \frac{m_n^u}{m_m^W} \tilde{V}_{nmk}^{W^+} - \frac{m_k^d}{m_m^W} V_{nmk}^{W^+}, \\
V_{nmk}^{\varphi_W^-} &= \frac{m_n^d}{m_m^W} V_{nmk}^{W^-} - \frac{m_k^u}{m_m^W} \tilde{V}_{nmk}^{W^-}, & \tilde{V}_{nmk}^{\varphi_W^-} &= \frac{m_n^d}{m_m^W} \tilde{V}_{nmk}^{W^-} - \frac{m_k^u}{m_m^W} V_{nmk}^{W^-}.
\end{aligned}$$

Appendix D

Results for the $b \rightarrow s\gamma$ and $b \rightarrow sg$ Amplitudes

In this appendix, the results for the amplitudes of the diagrams shown in Figure 4.5 and the corresponding ones for $b \rightarrow sg$ are shown. The radiative Wilson coefficients can be read off with the help of (4.106). Only the sums of scalar and vector-boson contributions are presented for reasons of gauge invariance. The underlying Feynman rules can be found in Appendix C. The functions from the integrals over Feynman parameters are given by

$$\begin{aligned} I_3(x) &= \frac{3 - 4x + x^2 + 2 \log(x)}{2(x-1)^3}, \\ I_4(x) &= \frac{2 + 3x - 6x^2 + x^3 + 6x \log(x)}{12(x-1)^4}, \\ I_A(x) &= -\frac{-4 + 3x + x^3 - 6x \log(x)}{2(x-1)^3}, \\ I_B(x) &= \frac{8 - 38x + 39x^2 - 14x^3 + 5x^4 - 18x^2 \log(x)}{12(x-1)^4}, \\ I_C(x) &= \frac{1 - 12x + 15x^2 - 4x^3 - 6x \log(x)}{4(x-1)^3}, \\ I_D(x) &= \frac{4 - 49x + 78x^2 - 43x^3 + 10x^4 - 18x \log(x)}{24(x-1)^4}, \\ I_E(x) &= \frac{1 + 9x - 13x^2 + 3x^3 + 8x \log(x)}{2(-1+x)^3}, \\ I_F(x) &= \frac{4 + 40x - 99x^2 + 68x^3 - 13x^4 - 6x(-6+5x) \log(x)}{12(-1+x)^4}. \end{aligned}$$

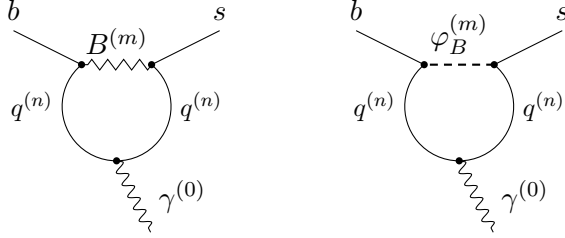
Results for the $b \rightarrow s\gamma$ Amplitude

FIGURE D.1: Gauge-boson exchange. It is $q = u$ and $x_{nm}^{qB} = (m_n^u)^2 / (m_m^W)^2$ for $B = W$ and $q = d$ and $x_{nm}^{qB} = (m_n^d)^2 / (m_m^B)^2$ for the neutral bosons.

$$i\mathcal{A}_B = i \frac{-2}{v^2} \kappa_B \sum_{n,m} \left(\frac{\tilde{m}_W}{m_m^B} \right)^2 \left[\frac{m_n^q}{m_b} I_A(x_{nm}^{qB}) V_{2mn}^B \tilde{V}_{nm3}^B + I_B(x_{nm}^{qB}) V_{2mn}^B V_{nm3}^B \right] \langle Q_{7\gamma} \rangle$$

The values for κ_B read: $\kappa_W = Q_u/2$, $\kappa_Z = Q_d/c_w^2$, $\kappa_A = Q_d^3 s_w^2$, and $\kappa_G = Q_d C_F \alpha_s s_w^2 / \alpha$.

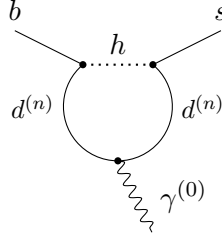


FIGURE D.2: Higgs exchange, $x_n^{dh} = (m_n^d)^2 / (m_h)^2$.

$$i\mathcal{A}_h = i \frac{-2}{v^2} \sum_{n=1}^{\infty} \left(\frac{\tilde{m}_W}{m_h} \right)^2 \left(\frac{-Q_d s_w^2}{8\pi\alpha} \right) \left[\frac{m_n^d}{m_b} I_3(x_n^{dh}) \tilde{V}_{2n}^h \tilde{V}_{n3}^h + I_4(x_n^{dh}) \tilde{V}_{2n}^h V_{n3}^h \right] \langle Q_{7\gamma} \rangle$$

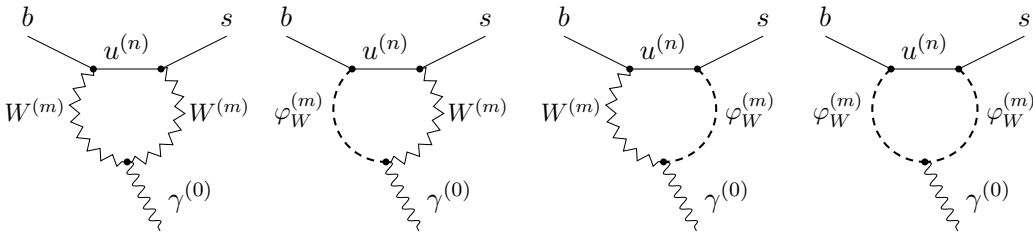


FIGURE D.3: W boson emits photon, $x_{mn}^{Wu} = (m_m^W)^2 / (m_n^u)^2$.

$$i\mathcal{A}_{WW} = i \frac{-2}{v^2} \sum_{n,m} \left(\frac{\tilde{m}_W}{m_m^W} \right)^2 \left[\frac{m_n^u}{m_b} I_C(x_{mn}^{Wu}) V_{2mn}^{W-} \tilde{V}_{nm3}^{W+} + I_D(x_{mn}^{Wu}) V_{2mn}^{W-} V_{nm3}^{W+} \right] \langle Q_{7\gamma} \rangle$$

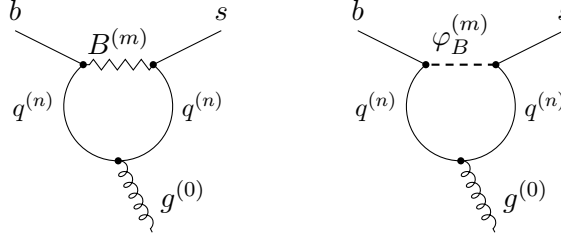
Results for the $b \rightarrow sg$ Amplitude


FIGURE D.4: Gauge-boson exchange. It is $q = u$ and $x_{nm}^{qB} = (m_n^u)^2/(m_m^W)^2$ for $B = W$ and $q = d$ and $x_{nm}^{qB} = (m_n^d)^2/(m_m^B)^2$ for the neutral bosons.

$$i\mathcal{A}_B = i\frac{-2}{v^2}\frac{\kappa'_B}{Q_q}\sum_{n,m}\left(\frac{\tilde{m}_W}{m_m^B}\right)^2\left[\frac{m_n^q}{m_b}I_A(x_{nm}^{qB})V_{2mn}^B\tilde{V}_{nm3}^B + I_B(x_{nm}^{qB})V_{2mn}^B V_{nm3}^B\right]\langle Q_{8g}\rangle$$

The values for κ'_B read: $\kappa'_W = \kappa_W$, $\kappa'_Z = \kappa_Z$, $\kappa'_A = \kappa_A$, and $\kappa'_G = -Q_d\alpha_s s_w^2/2\alpha N_c$.

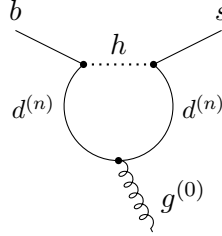


FIGURE D.5: Higgs exchange, $x_n^{dh} = (m_n^d)^2/(m_h)^2$.

$$i\mathcal{A}_h = i\frac{-2}{v^2}\sum_{n=1}^{\infty}\left(\frac{\tilde{m}_W}{m_h}\right)^2\left(-\frac{s_w^2}{8\pi\alpha}\right)\left[\frac{m_n^d}{m_b}I_3(x_n^{dh})\tilde{V}_{2n}^h\tilde{V}_{n3}^h + I_4(x_n^{dh})\tilde{V}_{2n}^h V_{n3}^h\right]\langle Q_{8g}\rangle$$

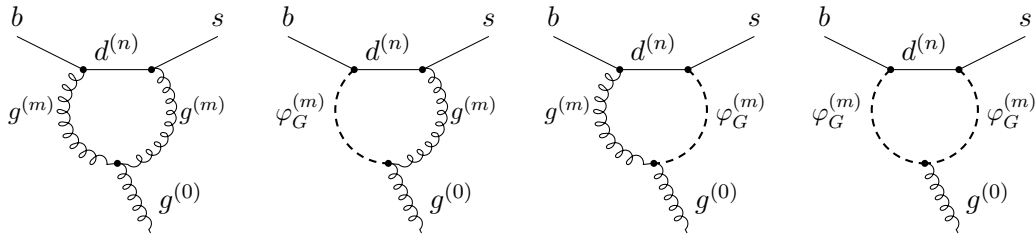


FIGURE D.6: Three-gluon vertex, $x_{mn}^{Gd} = (m_m^G)^2/(m_n^d)^2$.

$$i\mathcal{A}_{GG} = i\frac{-2}{v^2}\sum_{n,m}\left(\frac{\tilde{m}_W}{m_m^G}\right)^2\frac{3\alpha_s s_w^2}{2\alpha}\left[\frac{m_n^d}{m_b}I_E(x_{mn}^{Gd})V_{2mn}^G\tilde{V}_{nm3}^G + I_F(x_{mn}^{Gd})V_{2mn}^G V_{nm3}^G\right]\langle Q_{8g}\rangle$$

Bibliography

- [1] M. E. Peskin and D. V. Schroeder, *An Introduction to Quantum Field Theory* (Westview Press, 1995).
- [2] S. Weinberg, *The Quantum Theory of Fields. Vol. 1: Foundations* (Cambridge, UK: University Press, 1995).
- [3] S. Weinberg, *The Quantum Theory of Fields: Vol. 2: Modern Applications* (Cambridge, UK: University Press, 1996).
- [4] A. J. Buras, “Weak Hamiltonian, CP violation and rare decays,” (1998), arXiv:hep-ph/9806471 [hep-ph] .
- [5] M. Neubert, “Effective field theory and heavy quark physics,” (2005), arXiv:hep-ph/0512222 [hep-ph] .
- [6] S. Glashow, Nucl.Phys. **22**, 579 (1961).
- [7] S. Weinberg, Phys.Rev.Lett. **19**, 1264 (1967).
- [8] A. Salam, Conf.Proc. **C680519**, 367 (1968).
- [9] D. J. Gross and F. Wilczek, Phys.Rev.Lett. **30**, 1343 (1973).
- [10] D. Gross and F. Wilczek, Phys.Rev. **D8**, 3633 (1973).
- [11] D. Gross and F. Wilczek, Phys.Rev. **D9**, 980 (1974).
- [12] H. D. Politzer, Phys.Rept. **14**, 129 (1974).
- [13] G. Arnison *et al.* (UA1 Collaboration), Phys.Lett. **B122**, 103 (1983).
- [14] S. Herb, D. Hom, L. Lederman, J. Sens, H. Snyder, *et al.*, Phys.Rev.Lett. **39**, 252 (1977).
- [15] F. Abe *et al.* (CDF Collaboration), Phys.Rev.Lett. **74**, 2626 (1995), arXiv:hep-ex/9503002 [hep-ex] .
- [16] S. Abachi *et al.* (D0 Collaboration), Phys.Rev.Lett. **74**, 2422 (1995), arXiv:hep-ex/9411001 [hep-ex] .
- [17] G. Aad *et al.* (ATLAS Collaboration), Phys.Lett. **B716**, 1 (2012), arXiv:1207.7214 [hep-ex] .
- [18] S. Chatrchyan *et al.* (CMS Collaboration), Phys.Lett. **B716**, 30 (2012), arXiv:1207.7235 [hep-ex] .

- [19] J. Donoghue, E. Golowich, and B. R. Holstein, *Dynamics of the Standard Model* (Cambridge University Press, 1992).
- [20] G. 't Hooft and M. Veltman, Nucl.Phys. **B44**, 189 (1972).
- [21] Y. Fukuda *et al.* (Super-Kamiokande Collaboration), Phys.Rev.Lett. **81**, 1562 (1998), arXiv:hep-ex/9807003 [hep-ex] .
- [22] R. Contino, “The Higgs as a Composite Nambu-Goldstone Boson,” (2010), arXiv:1005.4269 [hep-ph] .
- [23] N. Cabibbo, Phys.Rev.Lett. **10**, 531 (1963).
- [24] M. Kobayashi and T. Maskawa, Prog.Theor.Phys. **49**, 652 (1973).
- [25] S. Schael *et al.* (ALEPH Collaboration, DELPHI Collaboration, L3 Collaboration, OPAL Collaboration, SLD Collaboration, LEP Electroweak Working Group, SLD Electroweak Group, SLD Heavy Flavour Group), Phys.Rept. **427**, 257 (2006), arXiv:hep-ex/0509008 [hep-ex] .
- [26] C. Campagnari and M. Franklin, Rev.Mod.Phys. **69**, 137 (1997), arXiv:hep-ex/9608003 [hep-ex] .
- [27] M. Baak, M. Goebel, J. Haller, A. Hoecker, D. Kennedy, *et al.*, Eur.Phys.J. **C72**, 2205 (2012), arXiv:1209.2716 [hep-ph] .
- [28] M. E. Peskin and T. Takeuchi, Phys.Rev.Lett. **65**, 964 (1990).
- [29] M. E. Peskin and T. Takeuchi, Phys.Rev. **D46**, 381 (1992).
- [30] M. Li, X.-D. Li, S. Wang, and Y. Wang, Commun.Theor.Phys. **56**, 525 (2011), arXiv:1103.5870 [astro-ph.CO] .
- [31] N. Arkani-Hamed, D. P. Finkbeiner, T. R. Slatyer, and N. Weiner, Phys.Rev. **D79**, 015014 (2009), arXiv:0810.0713 [hep-ph] .
- [32] A. Sakharov, Pisma Zh.Eksp.Teor.Fiz. **5**, 32 (1967).
- [33] J. Ellis, J. Espinosa, G. Giudice, A. Hoecker, and A. Riotto, Phys.Lett. **B679**, 369 (2009), arXiv:0906.0954 [hep-ph] .
- [34] P. Hernandez, “Neutrino physics,” (2010), arXiv:1010.4131 [hep-ph] .
- [35] I. Low, “TASI 2013: Particles Beyond the Standard Model,” (2013).
- [36] J. Polchinski, “Effective field theory and the Fermi surface,” (1992), arXiv:hep-th/9210046 [hep-th] .
- [37] P. A. Dirac, Nature **139**, 323 (1937).
- [38] P. A. Dirac, Proc.Roy.Soc.Lond. **A165**, 199 (1938).
- [39] G. 't Hooft, C. Itzykson, A. Jaffe, H. Lehmann, P. Mitter, *et al.*, NATO Adv.Study Inst.Ser.B Phys. **59**, pp.1 (1980).
- [40] M. Tegmark *et al.* (SDSS Collaboration), Phys.Rev. **D69**, 103501 (2004), arXiv:astro-ph/0310723 [astro-ph] .

- [41] G. Giudice and R. Rattazzi, Nucl.Phys. **B757**, 19 (2006), arXiv:hep-ph/0606105 [hep-ph] .
- [42] J. M. Maldacena, Adv.Theor.Math.Phys. **2**, 231 (1998), arXiv:hep-th/9711200 [hep-th] .
- [43] M. Luty and T. Okui, JHEP **0609**, 070 (2006), arXiv:hep-ph/0409274 [hep-ph] .
- [44] R. Rattazzi, V. S. Rychkov, E. Tonni, and A. Vichi, JHEP **0812**, 031 (2008), arXiv:0807.0004 [hep-th] .
- [45] P. F. Bedaque and U. van Kolck, Ann.Rev.Nucl.Part.Sci. **52**, 339 (2002), arXiv:nucl-th/0203055 [nucl-th] .
- [46] S. J. Brodsky and S. Drell, Phys.Rev. **D22**, 2236 (1980).
- [47] D. Hanneke, S. Fogwell, and G. Gabrielse, Phys.Rev.Lett. **100**, 120801 (2008), arXiv:0801.1134 [physics.atom-ph] .
- [48] V. Weisskopf, Phys.Rev. **56**, 72 (1939).
- [49] S. Glashow, J. Iliopoulos, and L. Maiani, Phys.Rev. **D2**, 1285 (1970).
- [50] J. Beringer *et al.* (Particle Data Group), Phys.Rev. **D86**, 010001 (2012).
- [51] J. Wess and J. Bagger, *Supersymmetry and Supergravity* (Princeton University Press, 1983).
- [52] S. Martin, “A Supersymmetry primer,” (1997), arXiv:hep-ph/9709356 [hep-ph] .
- [53] S. R. Coleman and J. Mandula, Phys.Rev. **159**, 1251 (1967).
- [54] B. Sakita, Phys.Rev. **136**, B1756 (1964).
- [55] R. Haag, J. T. Lopuszanski, and M. Sohnius, Nucl.Phys. **B88**, 257 (1975).
- [56] S. Dimopoulos and H. Georgi, Nucl.Phys. **B193**, 150 (1981).
- [57] N. Seiberg, Phys.Lett. **B318**, 469 (1993), arXiv:hep-ph/9309335 [hep-ph] .
- [58] P. Fayet, Phys.Lett. **B64**, 159 (1976).
- [59] R. Barbier, C. Berat, M. Besancon, M. Chemtob, A. Deandrea, *et al.*, Phys.Rept. **420**, 1 (2005), arXiv:hep-ph/0406039 [hep-ph] .
- [60] E. Nikolidakis and C. Smith, Phys.Rev. **D77**, 015021 (2008), arXiv:0710.3129 [hep-ph] .
- [61] C. Csaki, Y. Grossman, and B. Heidenreich, Phys.Rev. **D85**, 095009 (2012), arXiv:1111.1239 [hep-ph] .
- [62] S. Ferrara, L. Girardello, and F. Palumbo, Phys.Rev. **D20**, 403 (1979).
- [63] A. H. Chamseddine, R. L. Arnowitt, and P. Nath, Phys.Rev.Lett. **49**, 970 (1982).
- [64] R. Barbieri, S. Ferrara, and C. A. Savoy, Phys.Lett. **B119**, 343 (1982).
- [65] H. P. Nilles, M. Srednicki, and D. Wyler, Phys.Lett. **B120**, 346 (1983).

- [66] E. Cremmer, P. Fayet, and L. Girardello, *Phys.Lett.* **B122**, 41 (1983).
- [67] L. J. Hall, J. D. Lykken, and S. Weinberg, *Phys.Rev.* **D27**, 2359 (1983).
- [68] S. K. Soni and H. A. Weldon, *Phys.Lett.* **B126**, 215 (1983).
- [69] M. Dine, W. Fischler, and M. Srednicki, *Nucl.Phys.* **B189**, 575 (1981).
- [70] S. Dimopoulos and S. Raby, *Nucl.Phys.* **B192**, 353 (1981).
- [71] M. Dine and W. Fischler, *Phys.Lett.* **B110**, 227 (1982).
- [72] C. R. Nappi and B. A. Ovrut, *Phys.Lett.* **B113**, 175 (1982).
- [73] L. Alvarez-Gaume, M. Claudson, and M. B. Wise, *Nucl.Phys.* **B207**, 96 (1982).
- [74] M. Dine and A. E. Nelson, *Phys.Rev.* **D48**, 1277 (1993), arXiv:hep-ph/9303230 [hep-ph] .
- [75] M. Dine, A. E. Nelson, Y. Nir, and Y. Shirman, *Phys.Rev.* **D53**, 2658 (1996), arXiv:hep-ph/9507378 [hep-ph] .
- [76] G. Giudice and R. Rattazzi, *Phys.Rept.* **322**, 419 (1999), arXiv:hep-ph/9801271 [hep-ph] .
- [77] L. E. Ibanez and G. G. Ross, *Phys.Lett.* **B110**, 215 (1982).
- [78] G. Aad *et al.* (ATLAS Collaboration), (2014), arXiv:1405.7875 [hep-ex] .
- [79] G. Aad *et al.* (ATLAS Collaboration), *JHEP* **1405**, 071 (2014), arXiv:1403.5294 [hep-ex] .
- [80] M. Papucci, J. T. Ruderman, and A. Weiler, *JHEP* **1209**, 035 (2012), arXiv:1110.6926 [hep-ph] .
- [81] L.-T. Wang and I. Yavin, *Int.J.Mod.Phys.* **A23**, 4647 (2008), arXiv:0802.2726 [hep-ph] .
- [82] R. Jackiw and K. Johnson, *Phys.Rev.* **D8**, 2386 (1973).
- [83] S. Weinberg, *Phys.Rev.* **D19**, 1277 (1979).
- [84] L. Susskind, *Phys.Rev.* **D20**, 2619 (1979).
- [85] A. Manohar and H. Georgi, *Nucl.Phys.* **B234**, 189 (1984).
- [86] S. Dimopoulos and L. Susskind, *Nucl.Phys.* **B155**, 237 (1979).
- [87] E. Eichten and K. D. Lane, *Phys.Lett.* **B90**, 125 (1980).
- [88] B. Holdom, *Phys.Rev.* **D24**, 1441 (1981).
- [89] B. Holdom, *Phys.Lett.* **B150**, 301 (1985).
- [90] K. Yamawaki, M. Bando, and K.-i. Matumoto, *Phys.Rev.Lett.* **56**, 1335 (1986).
- [91] T. W. Appelquist, D. Karabali, and L. Wijewardhana, *Phys.Rev.Lett.* **57**, 957 (1986).
- [92] T. Appelquist and L. Wijewardhana, *Phys.Rev.* **D35**, 774 (1987).

- [93] T. Appelquist and L. Wijewardhana, *Phys.Rev.* **D36**, 568 (1987).
- [94] A. Delgado, K. Lane, and A. Martin, *Phys.Lett.* **B696**, 482 (2011), arXiv:1011.0745 [hep-ph] .
- [95] E. Gildener and S. Weinberg, *Phys.Rev.* **D13**, 3333 (1976).
- [96] W. D. Goldberger, B. Grinstein, and W. Skiba, *Phys.Rev.Lett.* **100**, 111802 (2008), arXiv:0708.1463 [hep-ph] .
- [97] S. Abel and A. Mariotti, (2013), arXiv:1312.5335 [hep-ph] .
- [98] D. B. Kaplan and H. Georgi, *Phys.Lett.* **B136**, 183 (1984).
- [99] D. B. Kaplan, H. Georgi, and S. Dimopoulos, *Phys.Lett.* **B136**, 187 (1984).
- [100] K. Agashe, R. Contino, and A. Pomarol, *Nucl.Phys.* **B719**, 165 (2005), arXiv:hep-ph/0412089 [hep-ph] .
- [101] R. Contino, L. Da Rold, and A. Pomarol, *Phys.Rev.* **D75**, 055014 (2007), arXiv:hep-ph/0612048 [hep-ph] .
- [102] N. Arkani-Hamed, A. G. Cohen, T. Gregoire, and J. G. Wacker, *JHEP* **0208**, 020 (2002), arXiv:hep-ph/0202089 [hep-ph] .
- [103] M. Schmaltz, *JHEP* **0408**, 056 (2004), arXiv:hep-ph/0407143 [hep-ph] .
- [104] C. Froggatt and H. B. Nielsen, *Nucl.Phys.* **B147**, 277 (1979).
- [105] M. Bauer, *On Flavor in Strongly Coupled Theories*, Ph.D. thesis, Johannes Gutenberg-Universität Mainz (2012).
- [106] R. S. Chivukula and H. Georgi, *Phys.Lett.* **B188**, 99 (1987).
- [107] C. Csaki, “TASI lectures on extra dimensions and branes,” (2004), arXiv:hep-ph/0404096 [hep-ph] .
- [108] R. Sundrum, “Tasi 2004 lectures: To the fifth dimension and back,” (2005), arXiv:hep-th/0508134 [hep-th] .
- [109] G. D. Kribs, “TASI 2004 lectures on the phenomenology of extra dimensions,” (2006), arXiv:hep-ph/0605325 [hep-ph] .
- [110] T. Gherghetta, “TASI Lectures on a Holographic View of Beyond the Standard Model Physics,” (2010), arXiv:1008.2570 [hep-ph] .
- [111] E. Ponton, “TASI 2011: Four Lectures on TeV Scale Extra Dimensions,” (2012), arXiv:1207.3827 [hep-ph] .
- [112] G. Nordström, *Phys. Z.* **15**, 504 (1914).
- [113] T. Kaluza, *Sitzungsbr. Preuss. Akad. Wiss. Berlin (Math. Phys.)* **1921**, 966 (1921).
- [114] O. Klein, *Z. Phys.* **37**, 895 (1926).
- [115] L. Randall and R. Sundrum, *Phys.Rev.Lett.* **83**, 3370 (1999), arXiv:hep-ph/9905221 [hep-ph] .

- [116] C. Csaki, C. Grojean, and H. Murayama, Phys.Rev. **D67**, 085012 (2003), arXiv:hep-ph/0210133 [hep-ph] .
- [117] R. Contino, Y. Nomura, and A. Pomarol, Nucl.Phys. **B671**, 148 (2003), arXiv:hep-ph/0306259 [hep-ph] .
- [118] N. Arkani-Hamed, S. Dimopoulos, and G. Dvali, Phys.Lett. **B429**, 263 (1998), arXiv:hep-ph/9803315 [hep-ph] .
- [119] D. Kapner, T. Cook, E. Adelberger, J. Gundlach, B. R. Heckel, *et al.*, Phys.Rev.Lett. **98**, 021101 (2007), arXiv:hep-ph/0611184 [hep-ph] .
- [120] N. Arkani-Hamed and M. Schmaltz, Phys.Rev. **D61**, 033005 (2000), arXiv:hep-ph/9903417 [hep-ph] .
- [121] E. A. Mirabelli, M. Perelstein, and M. E. Peskin, Phys.Rev.Lett. **82**, 2236 (1999), arXiv:hep-ph/9811337 [hep-ph] .
- [122] G. Aad *et al.* (ATLAS Collaboration), JHEP **1304**, 075 (2013), arXiv:1210.4491 [hep-ex] .
- [123] S. Cullen and M. Perelstein, Phys.Rev.Lett. **83**, 268 (1999), arXiv:hep-ph/9903422 [hep-ph] .
- [124] T. Appelquist, H.-C. Cheng, and B. A. Dobrescu, Phys.Rev. **D64**, 035002 (2001), arXiv:hep-ph/0012100 [hep-ph] .
- [125] T. Appelquist and H.-U. Yee, Phys.Rev. **D67**, 055002 (2003), arXiv:hep-ph/0211023 [hep-ph] .
- [126] H.-C. Cheng, K. T. Matchev, and M. Schmaltz, Phys.Rev. **D66**, 036005 (2002), arXiv:hep-ph/0204342 [hep-ph] .
- [127] K. Kong and K. T. Matchev, JHEP **0601**, 038 (2006), arXiv:hep-ph/0509119 [hep-ph] .
- [128] D. Spergel *et al.* (WMAP Collaboration), Astrophys.J.Suppl. **148**, 175 (2003), arXiv:astro-ph/0302209 [astro-ph] .
- [129] C. Bennett *et al.* (WMAP Collaboration), Astrophys.J.Suppl. **148**, 1 (2003), arXiv:astro-ph/0302207 [astro-ph] .
- [130] I. Gogoladze and C. Macesanu, Phys.Rev. **D74**, 093012 (2006), arXiv:hep-ph/0605207 [hep-ph] .
- [131] K. Agashe, N. Deshpande, and G. Wu, Phys.Lett. **B514**, 309 (2001), arXiv:hep-ph/0105084 [hep-ph] .
- [132] A. J. Buras, A. Poschenrieder, M. Spranger, and A. Weiler, Nucl.Phys. **B678**, 455 (2004), arXiv:hep-ph/0306158 [hep-ph] .
- [133] H.-C. Cheng, K. T. Matchev, and M. Schmaltz, Phys.Rev. **D66**, 056006 (2002), arXiv:hep-ph/0205314 [hep-ph] .
- [134] A. Datta, K. Kong, and K. T. Matchev, Phys.Rev. **D72**, 096006 (2005), arXiv:hep-ph/0509246 [hep-ph] .

- [135] The ATLAS Collaboration, “Differential cross sections of the Higgs boson measured in the diphoton decay channel using 8 TeV pp collisions,” (2013).
- [136] G. Belanger, A. Belyaev, M. Brown, M. Kakizaki, and A. Pukhov, EPJ Web Conf. **28**, 12070 (2012), arXiv:1201.5582 [hep-ph] .
- [137] W. D. Goldberger and M. B. Wise, Phys.Rev. **D60**, 107505 (1999), arXiv:hep-ph/9907218 [hep-ph] .
- [138] W. D. Goldberger and M. B. Wise, Phys.Rev.Lett. **83**, 4922 (1999), arXiv:hep-ph/9907447 [hep-ph] .
- [139] L. Randall and M. D. Schwartz, JHEP **0111**, 003 (2001), arXiv:hep-th/0108114 [hep-th] .
- [140] A. Pomarol, Phys.Rev.Lett. **85**, 4004 (2000), arXiv:hep-ph/0005293 [hep-ph] .
- [141] K.-w. Choi, H. D. Kim, and I.-W. Kim, JHEP **0211**, 033 (2002), arXiv:hep-ph/0202257 [hep-ph] .
- [142] W. D. Goldberger and I. Z. Rothstein, Phys.Rev.Lett. **89**, 131601 (2002), arXiv:hep-th/0204160 [hep-th] .
- [143] K. Agashe, A. Delgado, and R. Sundrum, Nucl.Phys. **B643**, 172 (2002), arXiv:hep-ph/0206099 [hep-ph] .
- [144] M. Carena, S. Casagrande, F. Goertz, U. Haisch, and M. Neubert, JHEP **1208**, 156 (2012), arXiv:1204.0008 [hep-ph] .
- [145] S. Casagrande, F. Goertz, U. Haisch, M. Neubert, and T. Pfoh, JHEP **0810**, 094 (2008), arXiv:0807.4937 [hep-ph] .
- [146] O. Aharony, S. S. Gubser, J. M. Maldacena, H. Ooguri, and Y. Oz, Phys.Rept. **323**, 183 (2000), arXiv:hep-th/9905111 [hep-th] .
- [147] R. Contino and A. Pomarol, JHEP **0411**, 058 (2004), arXiv:hep-th/0406257 [hep-th] .
- [148] B. Batell and T. Gherghetta, Phys.Rev. **D76**, 045017 (2007), arXiv:0706.0890 [hep-th] .
- [149] S. Casagrande, F. Goertz, U. Haisch, M. Neubert, and T. Pfoh, JHEP **1009**, 014 (2010), arXiv:1005.4315 [hep-ph] .
- [150] R. Malm, M. Neubert, K. Novotny, and C. Schmell, JHEP **1401**, 173 (2014), arXiv:1303.5702 .
- [151] J. Hahn, C. Hörner, R. Malm, M. Neubert, C. Schmell, *et al.*, Eur.Phys.J. **C74**, 2857 (2014).
- [152] F. Goertz, “Warped Extra Dimensions: Flavor, Precision Tests and Higgs Physics,” (2011), arXiv:1112.6387 [hep-ph] .
- [153] B. Batell, T. Gherghetta, and D. Sword, Phys.Rev. **D78**, 116011 (2008), arXiv:0808.3977 [hep-ph] .

- [154] J. A. Cabrer, G. von Gersdorff, and M. Quiros, *New J.Phys.* **12**, 075012 (2010), arXiv:0907.5361 [hep-ph] .
- [155] J. A. Cabrer, G. von Gersdorff, and M. Quiros, *Phys.Lett.* **B697**, 208 (2011), arXiv:1011.2205 [hep-ph] .
- [156] P. R. Archer, *JHEP* **1209**, 095 (2012), arXiv:1204.4730 [hep-ph] .
- [157] C. Bouchart and G. Moreau, *Phys.Rev.* **D80**, 095022 (2009), arXiv:0909.4812 [hep-ph] .
- [158] H. Davoudiasl, J. Hewett, and T. Rizzo, *Phys.Lett.* **B473**, 43 (2000), arXiv:hep-ph/9911262 [hep-ph] .
- [159] A. Pomarol, *Phys.Lett.* **B486**, 153 (2000), arXiv:hep-ph/9911294 [hep-ph] .
- [160] G. Cacciapaglia, C. Csaki, G. Marandella, and J. Terning, *JHEP* **0702**, 036 (2007), arXiv:hep-ph/0611358 [hep-ph] .
- [161] P. R. Archer, M. Carena, A. Carmona, and M. Neubert, “Higgs Production and Decay in Models of a Warped Extra Dimension with a Bulk Higgs,” (2014), arXiv:1408.5406 [hep-ph] .
- [162] P. Breitenlohner and D. Z. Freedman, *Annals Phys.* **144**, 249 (1982).
- [163] Y. Grossman and M. Neubert, *Phys.Lett.* **B474**, 361 (2000), arXiv:hep-ph/9912408 [hep-ph] .
- [164] K. Agashe, T. Okui, and R. Sundrum, *Phys.Rev.Lett.* **102**, 101801 (2009), arXiv:0810.1277 [hep-ph] .
- [165] M. Carena, A. D. Medina, N. R. Shah, and C. E. Wagner, *Phys.Rev.* **D79**, 096010 (2009), arXiv:0901.0609 [hep-ph] .
- [166] C. Csaki, C. Delaunay, C. Grojean, and Y. Grossman, *JHEP* **0810**, 055 (2008), arXiv:0806.0356 [hep-ph] .
- [167] T. Gherghetta and A. Pomarol, *Nucl.Phys.* **B586**, 141 (2000), arXiv:hep-ph/0003129 [hep-ph] .
- [168] S. J. Huber and Q. Shafi, *Phys.Lett.* **B498**, 256 (2001), arXiv:hep-ph/0010195 [hep-ph] .
- [169] S. J. Huber, *Nucl.Phys.* **B666**, 269 (2003), arXiv:hep-ph/0303183 [hep-ph] .
- [170] F. del Aguila and J. Santiago, *Phys.Lett.* **B493**, 175 (2000), arXiv:hep-ph/0008143 [hep-ph] .
- [171] J. Hewett, F. Petriello, and T. Rizzo, *JHEP* **0209**, 030 (2002), arXiv:hep-ph/0203091 [hep-ph] .
- [172] C. Csaki, C. Grojean, J. Hubisz, Y. Shirman, and J. Terning, *Phys.Rev.* **D70**, 015012 (2004), arXiv:hep-ph/0310355 [hep-ph] .
- [173] J. A. Bagger, F. Feruglio, and F. Zwirner, *Phys.Rev.Lett.* **88**, 101601 (2002), arXiv:hep-th/0107128 [hep-th] .

- [174] F. Goertz and T. Pfoh, JHEP **0810**, 035 (2008), arXiv:0809.1378 [hep-ph] .
- [175] A. Azatov, M. Toharia, and L. Zhu, Phys.Rev. **D80**, 035016 (2009), arXiv:0906.1990 [hep-ph] .
- [176] K. Agashe, G. Perez, and A. Soni, Phys.Rev. **D71**, 016002 (2005), arXiv:hep-ph/0408134 [hep-ph] .
- [177] K. Agashe, G. Perez, and A. Soni, Phys.Rev.Lett. **93**, 201804 (2004), arXiv:hep-ph/0406101 [hep-ph] .
- [178] K. Agashe, M. Papucci, G. Perez, and D. Pirjol, (2005), arXiv:hep-ph/0509117 [hep-ph] .
- [179] S. Chang, C. Kim, and J. Song, Phys.Rev. **D77**, 075001 (2008), arXiv:0712.0207 [hep-ph] .
- [180] C. Csaki, A. Falkowski, and A. Weiler, JHEP **0809**, 008 (2008), arXiv:0804.1954 [hep-ph] .
- [181] M. Blanke, A. J. Buras, B. Duling, S. Gori, and A. Weiler, JHEP **0903**, 001 (2009), arXiv:0809.1073 [hep-ph] .
- [182] M. Blanke, A. J. Buras, B. Duling, K. Gemmler, and S. Gori, JHEP **0903**, 108 (2009), arXiv:0812.3803 [hep-ph] .
- [183] M. Bauer, S. Casagrande, U. Haisch, and M. Neubert, JHEP **1009**, 017 (2010), arXiv:0912.1625 [hep-ph] .
- [184] C. Schmell, *The Inclusive Radiative Decay $\bar{B} \rightarrow X_s \gamma$ in the Randall-Sundrum model*, Master's thesis, Johannes Gutenberg-Universität Mainz (2011).
- [185] M. E. Albrecht, M. Blanke, A. J. Buras, B. Duling, and K. Gemmler, JHEP **0909**, 064 (2009), arXiv:0903.2415 [hep-ph] .
- [186] J. Santiago, JHEP **0812**, 046 (2008), arXiv:0806.1230 [hep-ph] .
- [187] C. Csaki, A. Falkowski, and A. Weiler, Phys.Rev. **D80**, 016001 (2009), arXiv:0806.3757 [hep-ph] .
- [188] C. Csaki, G. Perez, Z. Surujon, and A. Weiler, Phys.Rev. **D81**, 075025 (2010), arXiv:0907.0474 [hep-ph] .
- [189] M. Bauer, R. Malm, and M. Neubert, Phys.Rev.Lett. **108**, 081603 (2012), arXiv:1110.0471 [hep-ph] .
- [190] K. Agashe, A. Azatov, and L. Zhu, Phys.Rev. **D79**, 056006 (2009), arXiv:0810.1016 [hep-ph] .
- [191] C. Cheung, A. L. Fitzpatrick, and L. Randall, JHEP **0801**, 069 (2008), arXiv:0711.4421 [hep-th] .
- [192] M. S. Carena, E. Ponton, J. Santiago, and C. E. Wagner, Nucl.Phys. **B759**, 202 (2006), arXiv:hep-ph/0607106 [hep-ph] .
- [193] M. S. Carena, E. Ponton, J. Santiago, and C. Wagner, Phys.Rev. **D76**, 035006 (2007), arXiv:hep-ph/0701055 [hep-ph] .

- [194] G. Burdman and L. Da Rold, *JHEP* **0811**, 025 (2008), arXiv:0809.4009 [hep-ph] .
- [195] M. S. Carena, A. Delgado, E. Ponton, T. M. Tait, and C. Wagner, *Phys.Rev.* **D68**, 035010 (2003), arXiv:hep-ph/0305188 [hep-ph] .
- [196] A. Delgado and A. Falkowski, *JHEP* **0705**, 097 (2007), arXiv:hep-ph/0702234 [hep-ph] .
- [197] G. Cacciapaglia, C. Csaki, C. Grojean, and J. Terning, *Phys.Rev.* **D71**, 035015 (2005), arXiv:hep-ph/0409126 [hep-ph] .
- [198] M. Bauer, S. Casagrande, L. Grunder, U. Haisch, and M. Neubert, *Phys.Rev.* **D79**, 076001 (2009), arXiv:0811.3678 [hep-ph] .
- [199] B. A. Dobrescu and C. T. Hill, *Phys.Rev.Lett.* **81**, 2634 (1998), arXiv:hep-ph/9712319 [hep-ph] .
- [200] R. S. Chivukula and N. J. Evans, *Phys.Lett.* **B464**, 244 (1999), arXiv:hep-ph/9907414 [hep-ph] .
- [201] M. E. Peskin and J. D. Wells, *Phys.Rev.* **D64**, 093003 (2001), arXiv:hep-ph/0101342 [hep-ph] .
- [202] D. Choudhury, T. M. Tait, and C. Wagner, *Phys.Rev.* **D65**, 115007 (2002), arXiv:hep-ph/0202162 [hep-ph] .
- [203] R. Barbieri, L. J. Hall, and V. S. Rychkov, *Phys.Rev.* **D74**, 015007 (2006), arXiv:hep-ph/0603188 [hep-ph] .
- [204] H. Davoudiasl, J. Hewett, and T. Rizzo, *Phys.Rev.* **D68**, 045002 (2003), arXiv:hep-ph/0212279 [hep-ph] .
- [205] M. S. Carena, E. Ponton, T. M. Tait, and C. Wagner, *Phys.Rev.* **D67**, 096006 (2003), arXiv:hep-ph/0212307 [hep-ph] .
- [206] J. Field, *Mod.Phys.Lett.* **A13**, 1937 (1998), arXiv:hep-ph/9801355 [hep-ph] .
- [207] A. Freitas and Y.-C. Huang, *JHEP* **1208**, 050 (2012), arXiv:1205.0299 [hep-ph] .
- [208] G. Cacciapaglia, C. Csaki, G. Marandella, and J. Terning, *Phys.Rev.* **D75**, 015003 (2007), arXiv:hep-ph/0607146 [hep-ph] .
- [209] K. Agashe, A. Delgado, M. J. May, and R. Sundrum, *JHEP* **0308**, 050 (2003), arXiv:hep-ph/0308036 [hep-ph] .
- [210] C. Csaki, C. Grojean, L. Pilo, and J. Terning, *Phys.Rev.Lett.* **92**, 101802 (2004), arXiv:hep-ph/0308038 [hep-ph] .
- [211] K. Agashe, R. Contino, L. Da Rold, and A. Pomarol, *Phys.Lett.* **B641**, 62 (2006), arXiv:hep-ph/0605341 [hep-ph] .
- [212] A. D. Medina, N. R. Shah, and C. E. Wagner, *Phys.Rev.* **D76**, 095010 (2007), arXiv:0706.1281 [hep-ph] .
- [213] ATLAS Collaboration, “Physics at a High-Luminosity LHC with ATLAS,” (2013), arXiv:1307.7292 [hep-ex] .

- [214] M. Puchwein and Z. Kunszt, *Annals Phys.* **311**, 288 (2004), arXiv:hep-th/0309069 [hep-th] .
- [215] M. S. Carena, A. Delgado, E. Ponton, T. M. Tait, and C. Wagner, *Phys.Rev.* **D71**, 015010 (2005), arXiv:hep-ph/0410344 [hep-ph] .
- [216] C. Csaki, Y. Grossman, P. Tanedo, and Y. Tsai, *Phys.Rev.* **D83**, 073002 (2011), arXiv:1004.2037 [hep-ph] .
- [217] C. Csaki, J. Erlich, and J. Terning, *Phys.Rev.* **D66**, 064021 (2002), arXiv:hep-ph/0203034 [hep-ph] .
- [218] A. Djouadi and G. Moreau, *Phy.Let.* **B660**, 67 (2008), arXiv:0707.3800 [hep-ph] .
- [219] A. Falkowski, *Phys.Rev.* **D77**, 055018 (2008), arXiv:0711.0828 [hep-ph] .
- [220] G. Cacciapaglia, A. Deandrea, and J. Llodra-Perez, *JHEP* **0906**, 054 (2009), arXiv:0901.0927 [hep-ph] .
- [221] G. Bhattacharyya and T. S. Ray, *Phys.Lett.* **B675**, 222 (2009), arXiv:0902.1893 [hep-ph] .
- [222] A. Azatov, M. Toharia, and L. Zhu, *Phys.Rev.* **D82**, 056004 (2010), arXiv:1006.5939 [hep-ph] .
- [223] A. Azatov and J. Galloway, *Phys.Rev.* **D85**, 055013 (2012), arXiv:1110.5646 [hep-ph] .
- [224] F. Goertz, U. Haisch, and M. Neubert, *Phys.Lett.* **B713**, 23 (2012), arXiv:1112.5099 [hep-ph] .
- [225] C. Delaunay, J. F. Kamenik, G. Perez, and L. Randall, *JHEP* **1301**, 027 (2013), arXiv:1207.0474 [hep-ph] .
- [226] M. Beneke, P. Dey, and J. Rohrwild, *JHEP* **1308**, 010 (2013), arXiv:1209.5897 [hep-ph] .
- [227] M. Beneke and M. Neubert, *Nucl.Phys.* **B651**, 225 (2003), arXiv:hep-ph/0210085 [hep-ph] .
- [228] A. Djouadi, *Phys.Rept.* **459**, 1 (2008), arXiv:hep-ph/0503173 [hep-ph] .
- [229] W. J. Marciano, C. Zhang, and S. Willenbrock, *Phys.Rev.* **D85**, 013002 (2012), arXiv:1109.5304 [hep-ph] .
- [230] J. Mutschall, *Radiative B-Meson Decays in Warped Extra Dimensions*, Master's thesis, Johannes Gutenberg-Universität Mainz (2011).
- [231] T. Pfoh, *Grundlagen der Flavorphysik in fünfdimensionaler Anti-de Sitter-Raumzeit*, Master's thesis, Johannes Gutenberg-Universität Mainz.
- [232] J. Hahn, *Higgs Decay to Two Photons in Warped Extra Dimensions*, Master's thesis, Johannes Gutenberg-Universität Mainz (2013).
- [233] C. Hörner, *Higgs Decay into Two Photons in a Small and Warped Extra Dimension*, Master's thesis, Johannes Gutenberg-Universität Mainz (2014).

- [234] S. J. Huber and Q. Shafi, Phys.Lett. **B512**, 365 (2001), arXiv:hep-ph/0104293 [hep-ph] .
- [235] S. J. Huber and Q. Shafi, Phys.Lett. **B583**, 293 (2004), arXiv:hep-ph/0309252 [hep-ph] .
- [236] G. Burdman, Phys.Rev. **D66**, 076003 (2002), arXiv:hep-ph/0205329 [hep-ph] .
- [237] A. J. Buras, M. Jamin, M. Lautenbacher, and P. H. Weisz, Nucl.Phys. **B370**, 69 (1992).
- [238] A. Buras, M. Misiak, M. Munz, and S. Pokorski, Nucl.Phys. **B424**, 374 (1994), arXiv:hep-ph/9311345 [hep-ph] .
- [239] G. Buchalla, A. J. Buras, and M. E. Lautenbacher, Rev.Mod.Phys. **68**, 1125 (1996), arXiv:hep-ph/9512380 [hep-ph] .
- [240] C. Greub, T. Hurth, and D. Wyler, Phys.Rev. **D54**, 3350 (1996), arXiv:hep-ph/9603404 [hep-ph] .
- [241] U. Haisch, “ $\bar{B} \rightarrow X_s \gamma$: Standard Model and Beyond,” (2008), arXiv:0805.2141 [hep-ph] .
- [242] K. G. Chetyrkin, M. Misiak, and M. Munz, Phys.Lett. **B400**, 206 (1997), arXiv:hep-ph/9612313 [hep-ph] .
- [243] A. J. Buras, A. Czarnecki, M. Misiak, and J. Urban, Nucl.Phys. **B631**, 219 (2002), arXiv:hep-ph/0203135 [hep-ph] .
- [244] C. Kim, J. Kim, and J.-h. Song, Phys.Rev. **D67**, 015001 (2003), arXiv:hep-ph/0204002 [hep-ph] .
- [245] M. Blanke, B. Shakya, P. Tanedo, and Y. Tsai, JHEP **1208**, 038 (2012), arXiv:1203.6650 [hep-ph] .
- [246] T. Inami and C. Lim, Prog.Theor.Phys. **65**, 297 (1981).
- [247] A. J. Buras, L. Merlo, and E. Stamou, JHEP **1108**, 124 (2011), arXiv:1105.5146 [hep-ph] .
- [248] M. Misiak, H. Asatrian, K. Bieri, M. Czakon, A. Czarnecki, *et al.*, Phys.Rev.Lett. **98**, 022002 (2007), arXiv:hep-ph/0609232 [hep-ph] .
- [249] P. Gambino and M. Misiak, Nucl.Phys. **B611**, 338 (2001), arXiv:hep-ph/0104034 [hep-ph] .
- [250] M. Misiak and M. Steinhauser, Nucl.Phys. **B764**, 62 (2007), arXiv:hep-ph/0609241 [hep-ph] .
- [251] *A search for $t\bar{t}$ resonances in the lepton plus jets final state with ATLAS using 14 fb^{-1} of pp collisions at $\sqrt{s} = 8 \text{ TeV}$* , Tech. Rep. ATLAS-CONF-2013-052 (CERN, Geneva, 2013) not published in the proceedings.
- [252] R. Malm, M. Neubert, and C. Schmell, “Higgs Couplings and Phenomenology in a Warped Extra Dimension,” (2014), arXiv:1408.4456 [hep-ph] .

- [253] S. Heinemeyer *et al.* (LHC Higgs Cross Section Working Group), (2013), 10.5170/CERN-2013-004, arXiv:1307.1347 [hep-ph] .
- [254] M. E. Peskin, “Comparison of LHC and ILC Capabilities for Higgs Boson Coupling Measurements,” (2012), arXiv:1207.2516 [hep-ph] .
- [255] H. Baer, T. Barklow, K. Fujii, Y. Gao, A. Hoang, *et al.*, “The International Linear Collider Technical Design Report - Volume 2: Physics,” (2013), arXiv:1306.6352 [hep-ph] .
- [256] M. Klute, R. Lafaye, T. Plehn, M. Rauch, and D. Zerwas, *Europhys.Lett.* **101**, 51001 (2013), arXiv:1301.1322 [hep-ph] .
- [257] D. Asner, T. Barklow, C. Calancha, K. Fujii, N. Graf, *et al.*, (2013), arXiv:1310.0763 [hep-ph] .
- [258] J. Tian and K. Fujii, “Measurement of Higgs couplings and self-coupling at the ILC,” (2013), arXiv:1311.6528 [hep-ph] .
- [259] C. Hörner, R. Malm, M. Neubert, and C. Schmell, “Higgs Physics in Randall-Sundrum Models with a Bulk Higgs,” In preparation.
- [260] W.-Y. Keung and W. J. Marciano, *Phys.Rev.* **D30**, 248 (1984).
- [261] J. Brod, U. Haisch, and J. Zupan, *JHEP* **1311**, 180 (2013), arXiv:1310.1385 [hep-ph] .
- [262] J. Baron *et al.* (ACME Collaboration), *Science* **343**, 269 (2014), arXiv:1310.7534 [physics.atom-ph] .
- [263] F. Bishara, Y. Grossman, R. Harnik, D. J. Robinson, J. Shu, *et al.*, *JHEP* **1404**, 084 (2014), arXiv:1312.2955 [hep-ph] .
- [264] The ATLAS Collaboration, “Updated coupling measurements of the Higgs boson with the ATLAS detector using up to 25 fb^{-1} of proton-proton collision data,” (2014).
- [265] The CMS Collaboration, “Combination of standard model Higgs boson searches and measurements of the properties of the new boson with a mass near 125 GeV,” (2013).
- [266] V. Barger, M. Ishida, and W.-Y. Keung, *Phys.Rev.Lett.* **108**, 261801 (2012), arXiv:1203.3456 [hep-ph] .
- [267] The ATLAS Collaboration, “Search for the bb decay of the Standard Model Higgs boson in associated W/ZH production with the ATLAS detector,” (2013).
- [268] S. Chatrchyan *et al.* (CMS Collaboration), *Phys.Rev.* **D89**, 012003 (2014), arXiv:1310.3687 [hep-ex] .
- [269] S. Chatrchyan *et al.* (CMS Collaboration), *JHEP* **1405**, 104 (2014), arXiv:1401.5041 [hep-ex] .
- [270] M. Reece, *New J.Phys.* **15**, 043003 (2013), arXiv:1208.1765 [hep-ph] .
- [271] D. Becirevic, E. Kou, A. Le Yaouanc, and A. Tayduganov, *JHEP* **1208**, 090 (2012), arXiv:1206.1502 [hep-ph] .

- [272] U. Egede, T. Hurth, J. Matias, M. Ramon, and W. Reece, *JHEP* **1010**, 056 (2010), arXiv:1005.0571 [hep-ph] .
- [273] D. Becirevic and E. Schneider, *Nucl.Phys.* **B854**, 321 (2012), arXiv:1106.3283 [hep-ph] .
- [274] J. Lees *et al.* (BaBar Collaboration), *Phys.Rev.* **D86**, 112008 (2012), arXiv:1207.5772 [hep-ex] .
- [275] Y. Amhis *et al.* (Heavy Flavor Averaging Gr.), “Averages of B-Hadron, C-Hadron, and tau-lepton properties as of early 2012,” (2012), arXiv:1207.1158 [hep-ex] .
- [276] L. Lavoura, *Eur.Phys.J.* **C29**, 191 (2003), arXiv:hep-ph/0302221 [hep-ph] .
- [277] T. Hurth, E. Lunghi, and W. Porod, *Nucl.Phys.* **B704**, 56 (2005), arXiv:hep-ph/0312260 [hep-ph] .
- [278] M. Benzke, S. J. Lee, M. Neubert, and G. Paz, *Phys.Rev.Lett.* **106**, 141801 (2011), arXiv:1012.3167 [hep-ph] .
- [279] D. Atwood, M. Gronau, and A. Soni, *Phys.Rev.Lett.* **79**, 185 (1997), arXiv:hep-ph/9704272 [hep-ph] .
- [280] P. Ball and R. Zwicky, *Phys.Lett.* **B642**, 478 (2006), arXiv:hep-ph/0609037 [hep-ph] .
- [281] P. Ball, G. W. Jones, and R. Zwicky, *Phys.Rev.* **D75**, 054004 (2007), arXiv:hep-ph/0612081 [hep-ph] .
- [282] W. Altmannshofer, P. Paradisi, and D. M. Straub, *JHEP* **1204**, 008 (2012), arXiv:1111.1257 [hep-ph] .
- [283] Y. Ushiroda *et al.* (Belle Collaboration), *Phys.Rev.* **D74**, 111104 (2006), arXiv:hep-ex/0608017 [hep-ex] .
- [284] B. Aubert *et al.* (BaBar Collaboration), *Phys.Rev.* **D78**, 071102 (2008), arXiv:0807.3103 [hep-ex] .
- [285] M. Bona *et al.* (SuperB Collaboration), “SuperB: A High-Luminosity Asymmetric e^+e^- Super Flavor Factory. Conceptual Design Report,” (2007), arXiv:0709.0451 [hep-ex] .
- [286] Y. Grossman and D. Pirjol, *JHEP* **0006**, 029 (2000), arXiv:hep-ph/0005069 [hep-ph] .
- [287] M. Gronau, Y. Grossman, D. Pirjol, and A. Ryd, *Phys.Rev.Lett.* **88**, 051802 (2002), arXiv:hep-ph/0107254 [hep-ph] .
- [288] E. Kou, A. Le Yaouanc, and A. Tayduganov, *Phys.Rev.* **D83**, 094007 (2011), arXiv:1011.6593 [hep-ph] .